Bounds on the Maximum Attainable Equilibrium Spin Polarization of Protons at High Energy in HERA

Dissertation
zur Erlangung des Doktorgrades
des Fachbereichs Physik
der Universität Hamburg

Vorgelegt von
Mathias Vogt
aus Hamburg

2000

Gutachter der Dissertation:	Dr. D. P. Barber Prof. Dr. G. Kramer Prof. Dr. J. Bartels
Gutachter der Disputation:	Prof. Dr. G. Kramer Dr. habil. J. Roßbach
Datum der Disputation:	20.06.2000
Dekan des Fachbereichs Physik und Vorsitzender des Promotionsausschusses:	Prof. Dr. F.–W. Büßer

Abstract

For some years HERA has been supplying longitudinally spin polarised electron and positron ($e^{\pm}$) beams to the HERMES experiment and in the future longitudinal polarisation will be supplied to the H1 and ZEUS experiments. As a result there has been a development of interest in complementing the polarised $e^{\pm}$ beams with polarised protons. In contrast to the case of $e^{\pm}$ where spin flip due to synchrotron radiation in the main bending dipoles leads to self polarisation owing to an up–down asymmetry in the spin flip rates (Sokolov–Ternov effect), there is no convincing self polarisation mechanism for protons at high energy. Therefore protons must be polarised almost at rest in a source and then accelerated to the working energy.

At HERA, if no special measures are adopted, this means that the spins must cross several thousand "spin–orbit resonances". Resonance crossing can lead to loss of polarisation and at high energy such effects are potentially strong since spin precession is very pronounced in the very large magnetic fields needed to contain the proton beam in HERA–p. Moreover simple models which have been successfully used to describe spin motion at low and medium energies are no longer adequate. Instead, careful numerical spin–orbit tracking simulations are needed and a new, mathematically rigorous look at the theoretical concepts is required.

This thesis describes the underlying theoretical concepts, the computational tools (`SPRINT`) and the results of such a study. In particular strong emphasis is put on the concept of the invariant spin field and its non–perturbative construction. The invariant spin field is then used to define the amplitude dependent spin tune and to obtain numerical non–perturbative estimates of the latter. By means of these two key concepts the nature of higher order resonances in the presence of snakes is clarified and their impact on the beam polarisation is analysed. We then go on to discuss the special aspects of the HERA–p ring and measures for minimising the perturbations to the spin motion ($\rightarrow$ depolarisation) and thereby obtain first upper bounds on the permissible beam emittances needed to maintain polarisation up to high energy in HERA–p.

Current `e-mail` address of the author: `vogtm@math.unm.edu`

Zusammenfassung

Seit einigen Jahren stellt HERA dem Experiment HERMES longitudinal polarisierte Elektronen oder Positronen ($e^{\pm}$) zur Verfügung und in Zukunft werden auch den Experimente ZEUS und H1 longitudinale Polarisation zur Verfügung stehen. Als Konsequenz daraus ist Interesse gewachsen, den polarisierten $e^{\pm}$ Strahl durch polarisierten Protonen zu ergänzen. Im Unterschied zu $e^{\pm}$ wo eine Asymmetrie der Übergangsraten zwischen parallelen und antiparallelen Spinzuständen bei der Synchrotronstrahlung in den Hauptdipolen (Sokolov–Ternov Effekt) zu einer Selbstpolarisation führt, gibt es für hochenergetische Protonen keinen realistischen Mechanismus zur Erzeugung von Polarisation in Speicherringen. Deshalb müssen Protonen quasi bei Ruhenergie in der Quelle polarisiert und dann auf die gewünschte Energie beschleunigt werden.

Wenn in HERA keine speziellen Maßnahmen ergriffen werden, bedeutet das, dass mehrere tausend Spin–Orbit Resonanzen gekreuzt werden müssen. Das Kreuzen einer solchen Resonanz kann zu Verlusten bei der Polarisation führen. Speziell bei hoher Energie ist dieser Effekte potentiell stark, da die Präzessionsfrequenz der Spins in den starken Magnetfelder, die benötigt werden um den Strahl zu fokussieren, sehr hoch ist. Hinzu kommt, dass die simplen Modelle, die lange Zeit erfolgreich benutzt wurden, um Spindynamik bei geringer und mittlerer Energie zu beschreiben, bei hoher Energie inadäquat werden. Statt dessen werden präzise numerische Spin–Orbit tracking Simulationen und eine neue, mathematisch rigorose Herangehensweise an die physikalischen Konzepte erforderlich.

Diese Dissertation beschreibt die theoretischen Konzepte, die der Spindynamik in Beschleunigern zugrunde liegt, die numerischen Werkzeuge (`SPRINT`) und die Resultate einer Studie führ den Beschleuniger und Speicherring HERA–p. Im besonderen wird das Konzept des invarianten Spinfeldes und seine nicht–störungstheoretische Berechnung betont. Mit Hilfe des invarianten Spinfeldes wird der amplituden–abhängige “spin tune” definiert und es werden nicht–störungstheoretische Methoden zur Berechnung desselben eingeführt. Im weiteren wird unter Zuhilfenahme dieser beiden wesentlichen Konzepte der Mechanismus, der zum Entstehen von Resonanzen höherer Ordnung im Beisein von “snakes” führt, sowie der der Einfluss dieser Resonanzen auf die Spinbewegung erklärt. Im Anschluss werden die spezielle Aspekte der Spindynamik in HERA–p sowie Maßnahmen zur Minimierung der Störung der Spinbewegung (Depolarisation) diskutiert. In diesem Zusammenhang werden sich unter anderem auch erste Abschätzungen für die maximalen Strahlemittanzen, bis zu denen Polarisation bei hoher Energie gewährleistet werden kann, ergeben.

Contents

Chapter 1

Introduction

HERA is the "Hadron Elektron Ring Anlage" at "Deutsches Elektronen–Synchrotron" (DESY) in Hamburg. It consists of a proton (p) ring, currently operated at 920 GeV, and a concentric electron/positron ($e^{\pm}$) ring, operated at 27.5 GeV. $e^{\pm}$–p collisions from the counter rotating beams are studied in the North and South interaction regions by the H1 and ZEUS experiments. The HERMES experiment in the East has an internal target in the $e^{\pm}$ ring and the HERA–B experiment in the West studies CP–violation using an internal target in the p ring.

The HERA $e^{\pm}$ ring was designed with a view to obtaining longitudinal spin polarisation via the Sokolov–Ternov effect [ST64] and with the help of spin rotators [BB95]. A pair of rotators was brought into operation in 1994 and since then HERA has been supplying up to 60% longitudinal polarisation to the HERMES experiment [HC93]. The HERMES experiment is dedicated to providing a deeper understanding of the spin structure of nucleons by studying collisions of polarised electrons and positrons with polarised nucleons in an internal gas target. The total spin of the proton $s_p = {}^1\!/_2$ can be decomposed into the sum of partonic contributions and the orbital angular momentum

$$\frac{1}{2} = \Delta q + \Delta g + L_{\mathrm{orb}}$$

where Δq and Δg are given by differences of the parton densities of positive and negative helicity quarks and gluons respectively. Here Δq includes contributions from the valence quarks ("$p^+ = uud$"), as well as the sea quarks, mainly u, $\bar{u}$, d, $\bar{d}$, s, $\bar{s}$. It was found experimentally in 1988 by the European Muon Collaboration (EMC) at CERN [EMC88] that the quark contribution to the proton spin is much smaller, namely about 30%, than that predicted in the quark parton model. This has then been confirmed by later measurements [ID96, BN95]. Therefore the major contribution to the proton spin must come either from Δg [HC00] or L_{orb}.

The partonic helicity distributions are functions of the kinematic variables x_B which is the fractional part of the momentum of the proton carried by the current quark and measured in the centre of mass system, and Q^2 which is the negative square of the 4–momentum transfer. To extract the gluon contribution with sufficient accuracy one needs data in a kinematic region with low x_B but with Q^2 still high enough to allow application of perturbative QCD. The latter constraint means that Q^2 should be much bigger than Λ^2_{QCD} where $\Lambda_{\mathrm{QCD}} \approx 200$ MeV is the position of the Landau pole of the running coupling. This is given in one–loop approximation by $\alpha_s(Q^2) = \frac{12\pi}{(33-2N_{\mathrm{flv}})\log(Q^2/\Lambda^2_{\mathrm{QCD}})}$ where N_{flv} is the number of quark flavours active at Q^2. The scattering parameters are related to the centre of mass energy $\sqrt{s} \equiv \sqrt{(p_e + p_p)^\mu (p_e + p_p)_\mu}$ via

$$Q^2 = x_B\, y_B\, s$$

where y_B is the normalised energy transfer of the lepton in the laboratory frame. Since $y_B < 1$ the kinematic region of an experiment is bounded by $Q^2/x_B < s$. In other words, increase of s

implies the ability to measure Δg in regions of lower x_B without decreasing Q^2. For a reference momentum of the $e^{\pm}$ beam of 27.5 GeV the centre of mass energy for the HERMES experiment is little more than 7 GeV whereas in the collider experiments ZEUS and H1 we obtain $\sqrt{s} \approx 300$ GeV with a reference momentum of the proton beam of 820 GeV. It would therefore be very useful if the high energy protons in HERA were polarised and indeed there is a strong interest in this possibility [BN95, BD97, DG98, BR99b]. This thesis describes part of a study of the feasibility of providing such polarised protons. The references just given contain reviews of a whole range of investigations that could be undertaken with polarised protons.

An $e^{\pm}$ beam in a storage ring polarises itself by the Sokolov–Ternov (S–T) effect. This effect is based on the spin flip rates due to synchrotron radiation being slightly different for up→down and down→up in the main dipole fields. Neglecting possible depolarisation due to spin diffusion driven by the stochastic nature of quantum emission, the S–T effect leads to an equilibrium polarisation in a uniform magnetic field of

$$P_{\text{ST}} = \frac{8}{5\sqrt{3}} \approx 92.38\%$$

on a typical time scale of

$$\tau_{\text{ST}} = \frac{8}{5\sqrt{3}} \frac{m_e^2|\rho|^3}{e^2\gamma^5} \quad ,$$

where $|\rho|$ is the bending radius of the magnetic field and rationalised units[1] have been used. This value for P_{ST} is valid only in the case $|g/2-1| \ll 1$ which is the case for electrons ($\approx 0.115\ 10^{-3}$) but not for protons (≈ 1.79). In fact for protons P_{ST} is closer to 100% than for $e^{\pm}$ [JJ76]. However, since the time scale for the build up of polarisation is proportional to m^7/E^5, even at high energy in HERA the build up time is *many* orders of magnitude bigger for protons than for $e^{\pm}$ where it is of the order of 36 min. Two other methods have been considered for generating proton polarisation at high energy, namely via spin exchange with a polarised internal target [RM93, CM93, HM94] or electron beam or via resonant use of the relativistic Stern–Gerlach force. See for example [CP95, CP95, YD90a, YD90b, KH96]. But neither of them acts quickly enough or is practical in the real world of accelerator physics. Therefore protons have to be polarised in the p or H^- source of the accelerator complex and then accelerated through the whole pre–accelerator chain up to the final working energy.

As we will see below, preservation of polarisation during acceleration to high energy is far from trivial and concepts applicable in low energy rings are no longer adequate. Thus in this thesis a formalism which is capable of describing the non–linear spin dynamics at high energy is introduced and this is then employed to evaluate methods for overcoming loss of polarisation. Furthermore this thesis provides an initial specification of the conditions needed to attain and maintain proton polarisation at high energy in HERA.

The motion of the spin expectation value of a particle in electromagnetic fields is governed by a classical precession equation of the form

$$\mathrm{D}_t\,\widehat{S} = \vec{\Omega} \times \widehat{S}$$

where the vector $\vec{\Omega}$, which was given by Thomas, Bargmann, Michel and Telegdi (T–BMT) [JF26, LT27, MC55, BM59], depends on the electromagnetic fields at the particle and on its velocity and energy. The implications of the T–BMT equation will be explained in some detail in chapter 2. See appendix B for the mathematical notation.

If accelerators only had dipole magnets bending the orbit in one, generally horizontal, plane, then spins would precess around the (vertical) direction normal to the plane exactly $G\gamma + 1$ times in one revolution around the ring where $G = g/2 - 1 \approx 1.79$ is the gyromagnetic anomaly of the proton and γ is the Lorentz–factor. In particular in magnetic fields perpendicular to the tangent vector of

[1]Throughout this thesis rationalised units, i.e. units in which $c = \hbar = 1$, will be used.

the trajectory the spin precesses $G\gamma$ times more than the orbital deflection angle around the constant field direction. For protons this precession enhancement factor $G\gamma$ is increased by one integer each 523 MeV. As we will see later for protons at 820 GeV, 1 mrad of orbital deflection leads to about 90° of spin precession — in the high magnetic fields of the HERA–p ring spin motion is very sensitive to the fields! However vertical spins would stay vertical. In other words the equilibrium polarisation direction would also be vertical.

Even if an accelerator could be built with dipoles only, small spin perturbations due to small errors in the field directions of the bending magnets could add up coherently to produce large deviations from the vertical if the spin precession frequency were in resonance with the revolution frequency around the accelerator

$$f_{\text{spin}} = k_0 f_{\text{rev}}, \quad k_0 \in \mathbb{Z} \ .$$

Such so–called imperfection resonances can be understood as follows: Normally the unperturbed rotation around the vertical dominates spin motion, but if the precession frequency is an integer multiple of the revolution frequency, the unperturbed spin transport map for one turn is the identity. Then in that case even tiny perturbations will control the spin motion.

In a real accelerator with the radial magnetic fields in the vertically focusing and defocusing quadrupoles the spin of a proton oscillating around the ideal orbit (design orbit) experiences oscillating radial field components. These radial fields tilt the spins away from the vertical. On the design orbit of a perfectly aligned ring the radial field components vanish. In a small domain around the design orbit perturbations due to the radial fields can be treated as small. In this domain the tilt of the spin w.r.t. the vertical direction acquired during traversal of a focusing quadrupole is small and might be almost completely cancelled during traversal of the next defocusing quadrupole. But perturbations can build up coherently to produce large deviations from the vertical when the spin precession frequency is in resonance with the orbital oscillation frequencies of the particle at the so–called intrinsic resonances

$$f_{\text{spin}} = k' f_{\text{rev}} + k\, f_{\text{orbit}}, \quad k', k \in \mathbb{Z},\ k \neq 0 \ .$$

In a real misaligned ring with a distorted closed orbit the quadrupoles also contribute to the field errors seen by the spins and thereby also drive imperfection resonances.

During acceleration up to 820 GeV several thousand spin–orbit resonances must be crossed and by analogy with the nuclear magnetic resonance (NMR) technique mentioned below, it is clear that the polarisation can easily be destroyed. So measures must be taken to preserve the beam polarisation during acceleration. These primarily involve the inclusion of sets of magnetic devices called "Siberian Snakes". Furthermore one one must check beforehand that, independently of the acceleration process, an acceptable level of polarisation can exist *in principle* at the final constant high energy.

The quickly oscillating radial fields experienced by spins together with the piecewise constant perpendicular "holding" fields are analogous to the field configurations met in NMR techniques. In the NMR case the effect on spin precession of an oscillating electromagnetic field perpendicular to a constant magnetic holding field is described by decomposing the oscillating field into two counter rotating constant fields with frequencies κ and $-\kappa$. In NMR only one of these rotating fields can be in resonance with the spin precession frequency

$$f = geB/2m \ .$$

The influence of the other component is neglected. As we will see in chapter 2 the equations of spin motion for such a system can then be solved analytically. NMR experiments exploit the fact that when either the holding field or the frequency of the oscillating field are scanned through the resonance condition, spins in a sample can flip and the resultant change in magnetisation can be detected electronically. This tendency for spin flip when traversing a resonance is also the origin of the depolarisation that can occur during acceleration mentioned above. In the case of an accelerator with complete mid–plane symmetry any deviation of a spin away from the vertical results from the coherent build up of small perturbations due to the radial fields in the focusing quadrupoles. This build up happens if the spin precession frequency is close to a frequency in the Fourier spectrum of the radial field components evaluated on a synchro–betatron trajectory. The corresponding Fourier component describes a rotating field. In low and medium energy *proton* accelerators this so–called single resonance model (SRM) [CR80, FS60] has been very successful in describing depolarisation effects as well as in suggesting cures for depolarisation.

For the SRM to be applicable the separation of adjacent excited harmonics must be large compared to their "strength", i.e. the resonances should not overlap. But the Fourier spectrum of the spin perturbations of HERA–p at high energy contains such a large number of sufficiently strong harmonics that the validity of the SRM must be questioned. Indeed tracking simulations at high energy in HERA–p show that spins on betatron orbits with realistic amplitudes are in general far away from the vertical even if the unperturbed spin precession frequency is kept away from frequencies with strongly spin perturbing harmonics. In the high energy regime of HERA–p and for representative orbital amplitudes, resonances can never be treated as isolated. Therefore in general many harmonics influence the spin at a given precession frequency. The failure of the SRM for HERA–p is not only due to the high working energy but is also due to the fact that even the unperturbed proton ring has *no* mid–plane symmetry. Instead it has vertical bend sections around three of the four straight sections so that the ring has a marked azimuthal asymmetry. When taking into account the positions of the vertical bend sections as well as the different lattice layouts of the straight sections, HERA–p has only the trivial superperiodicity of 1.

The study described in this thesis of how to maintain polarisation in HERA–p from injection at 40 GeV up to high energy covers three main aspects:

- Concepts describing the equilibrium polarisation state, already in use for $e^{\pm}$ polarisation but new to the analysis of proton polarisation, are introduced and employed to derive structural properties of proton spin dynamics at high energy.

- Computational tools have been developed in order to apply these concepts to real accelerator lattices. The computer code `SPRINT` which was developed for this purpose is based mainly on single particle multi–turn tracking using symplectic 6–dimensional orbit maps and orthogonal 3–dimensional spin maps. It offers a wide range of methods for the analysis of spin motion in accelerators.

- Various simulations for diverse HERA modifications were made in order to find optimal settings and Siberian Snake layouts that allow acceleration of polarised protons with minimal losses during acceleration and maximum equilibrium polarisation at the top energy.

Owing to the complexity of spin dynamics in HERA–p, even with an unperturbed machine, the simulations in this thesis will exclude all effects of misalignment. In order to guarantee consistency between different simulations I limit myself to studying the 1996 set of optics for HERA–p, so that the effects of an "upgraded" lattice are ignored. In this context it should be noted that this type of simulation typically takes days or even weeks "per run" even on modern fast workstations. Therefore, and because the `SPRINT` code has been continuously extended and refined, some of the simulation data produced at earlier stages might look less skillfully prepared than later data. — One does not jettison the output of a month of CPU time just because one has found a more elegant way of producing more data points with similar effort! The physics content of data coming from different stages of the program development will always be consistent.

The starting point for the theoretical and numerical description of a polarised beam in a storage ring is the finding of the stationary state of the beam. By definition, at equilibrium the phase space density at a point in phase space and at a fixed azimuth in the ring is constant from turn to turn. Of course "equilibrium" is an idealisation but it nevertheless represents a very useful starting point for the discussion. If a corresponding stationary polarisation exists and is non–zero, then the value of the polarisation and its direction at each point in phase space must be an invariant of the "one–turn map" of coupled spin–orbit motion. This notion leads to the concept of the *invariant spin field* and the *static polarisation limit* which describes a history independent bound on the equilibrium polarisation. It also leads to the concept of the *amplitude dependent spin tune* and to an action–angle representation for spin variables. In the past many (even most) attempts to define the equilibrium polarisation directions, spin tune and spin–orbit resonance on synchro–betatron orbits were misleading and inconsistent. For example the spin tune has very often been taken to be the rate of spin rotation around the field over the phase space of unit eigenvectors with eigenvalue 1 of the one–turn spin map. Each of these eigenvectors is reproduced under application of the one–turn map, but is generally not an eigenvector at the new point in phase space and, seen as a function of the position in the ring, not a solution of the T–BMT equation. Conclusions drawn from this erroneous premise have to be viewed with suspicion, although they sometimes *qualitatively* reflect the reality. Thus in this thesis I will start from mathematically clean definitions and only then derive the crucial properties for spin dynamics useful in high energy accelerators. In particular, using the invariant spin field and the amplitude dependent spin tune at constant reference energy, a periodic coordinate system can be assigned to each point in phase space. In this coordinate system the spin precesses uniformly with constant projection on one of the base vectors.

In chapter 2 I will review the basics of relativistic spin motion needed for the understanding of the later chapters. Chapter 3 is devoted to the basic behaviour of spins in the presence of Siberian Snakes. In chapter 4 I will introduce the concepts of the invariant spin field and the amplitude dependent spin tune, relate them to the SRM and describe some computational methods. In particular, section 4.10 describes the effect of acceleration on a polarised beam using the concept of adiabatic invariance. If the acceleration process were an adiabatic evolution through stationary polarisation states, then almost no polarisation would be lost and the polarisation at the top energy would be very close to the static polarisation limit. In chapter 5 the simulations made for HERA–p are presented. They cover the consequences of various snake schemes and orbital tunes for fixed reference momenta and for accelerated motion.

The most advanced project in the field of polarised protons to be approved so far is the RHIC–SPIN[TR99] project at the Relativistic Heavy Ion Collider (RHIC) at Brookhaven National Laboratory. At RHIC, collisions of polarised protons on polarised protons at 2×250 GeV are planned for 2001. During the preparation of this thesis I have performed simulations for RHIC. Although these simulations cannot be discussed here due to time limitations, it should be noted that under the assumptions of linear unperturbed orbital motion, attaining polarisation in RHIC is likely to be much less problematic than at HERA. The main reasons for this are: the lower energy, the absence of vertical bending magnets and the higher superperiodicity of RHIC compared to HERA–p.

Owing to the finite length of the Latin and Greek alphabets it will sometimes be necessary to use the same symbol for different physical and mathematical quantities. However the meaning will always be clear from the context.

Chapter 2

Introduction to spin motion in circular accelerators

This chapter is devoted to a discussion of the basics of spin motion. We define the notion of beam polarisation, present the equation of spin motion in electromagnetic fields and describe various ways to parametrise spin vectors and spin transport maps. In particular we will introduce a coordinate system in which spin precession restricted to the closed orbit is especially simple and discuss the effect of small perturbations w.r.t. the periodic spin trajectory in this coordinate system.

In particle accelerators the phase space densities are small compared to the densities where restrictions imposed by the uncertainty principle and the Pauli Exclusion Principle become significant and in all existing proton rings radiation effects can be neglected. Moreover, the wave packets are very narrow compared to the typical spatial scales of the external electromagnetic fields. Then, by applying Ehrenfest's theorem to the expectation values of the orbital operators, the particle motion can be treated as being classical and governed by a classical Hamiltonian which, for electromagnetic fields, leads to the Lorentz force. It is not necessary to appeal to wave equations.

Although in accelerator physics one is always interested in a large ensemble of typically 10^{10} to 10^{13} particles, one usually begins calculations in the "single particle picture", i.e. one neglects the interaction between particles. That this is a realistic starting point is clear since the collective forces from space charge are at most of order $1/\gamma^2$ and can be neglected at very high energy. Moreover, the collective effects arising from wake fields can normally be neglected up to a certain beam intensity. The beam–beam effect can in general not be neglected under collision conditions but to leading order it merely produces a tune shift which can be compensated by an adequate setting of the correction quadrupoles. Therefore in this thesis only *external* fields, i.e. fields from the magnetic beam line elements and cavities will be taken into account. Of course, at a later stage noise, non–linear beam–beam effects and other collective effects will have to be investigated.

The spin of a particle is an intrinsically quantum mechanical property but for a particle following a classical trajectory, the expectation value $\langle | \widehat{\mathfrak{S}} | \rangle$ of the Pauli spin operator $\widehat{\mathfrak{S}}$ representing the spin observable in the instantaneous rest frame of a charged particle with spin $^1/_2$ satisfies the T–BMT equation to be given in the next section.

At high energy the Stern–Gerlach force in inhomogeneous magnetic fields exerted by the magnetic moment

$$\vec{\mu} = \frac{ge}{4m} \langle | \widehat{\mathfrak{S}} | \rangle \quad , \tag{2.1}$$

on the trajectory of the particle is very small [KH96] compared to the Lorentz force. Here e, m are the charge and the rest mass of the particle respectively, g is the Landé factor and we have introduced the Gothic font for operators in this and the next paragraphs. Thus the effects of the Stern–Gerlach force are not considered to fall within the scope of this thesis. Therefore the orbital equations of motion (EOM) can be integrated before including spin dynamics. This means that the spin of a particle is treated as a "spectator/passenger" experiencing varying electromagnetic fields as the particle propagates through the accelerator on its trajectory. The effect of the orbital motion on the dynamics of spin precession is called spin–orbit coupling and leads to the phenomena which are the subject of this thesis.

The instantaneous polarisation $\vec{P}(t) = \sum_{i=1}^{N} \rho_{(i)} \langle i | \widehat{\mathfrak{S}} | i \rangle$ is the ensemble average of the expectation values of the Pauli spin operator $\widehat{\mathfrak{S}}$, where $|i\rangle$ is i-th single particle state with statistical weight $\rho_{(i)}$. Alternatively we can write as usual [MS70] $\vec{P} = \text{trace}\left(\mathfrak{h}\widehat{\mathfrak{S}}\right)$, where $\mathfrak{h} = {}^1\!/_2(1 + \vec{P}\cdot\widehat{\mathfrak{S}})$ is the spin density operator.

If $\vec{P}(t) \neq \vec{0}$ we may transform to a coordinate system in which e.g. $\hat{y} = \vec{P}/\|\vec{P}\|$. In this coordinate system one can write the projection of the spin operator on the $\hat{y}$–axis $\mathfrak{S}_y$ as the difference of two projectors $\mathfrak{P}_+$ for "spin up" and $\mathfrak{P}_-$ for "spin down" (see equation (2.56h) for a matrix representation $\underline{P}_\pm$ of the projector $\mathfrak{P}_\pm$), so that $\mathfrak{S}_y = \mathfrak{P}_+ - \mathfrak{P}_-$ and $\mathfrak{P}_+ + \mathfrak{P}_- \equiv 1$. Taking the expectation with $|i\rangle$ and summing up over i we obtain the commonly used expression $P_y = (N_+ - N_-)/(N_+ + N_-)$ where the $N_\pm$ are the summed expectations of $\mathfrak{P}_\pm$. If the single particle states $|i\rangle$ are eigenstates of the $\mathfrak{P}_\pm$, i.e. $\mathfrak{P}_\pm|i\rangle =$ either 0 or $|i\rangle$, then the $N_\pm$ can be interpreted as *numbers* of particles with spin up/down w.r.t. the axis $\hat{y}$. In chapter 4 we will see that for proton beams in high energy accelerators a *global* axis $\hat{y}$, so that the $|i\rangle$ are eigenstates of $\mathfrak{P}_\pm$, does *not* exist in general but that usually a *local* axis $\hat{n}(\vec{q},\vec{p})$ in phase space can be found at least to a very good approximation.

The spin expectation value $\langle i | \widehat{\mathfrak{S}} | i \rangle$ evolves through the T–BMT equation as a classical dynamical vector variable, whose length is conserved. Therefore in the remainder of this work we will treat spin in classical terms and define a classical spin viewed in the instantaneous particle rest frame:

Definition 2.1 (Classical spin) *A (classical) spin $\widehat{S}$ is a unit vector in $\mathbb{R}^3$. The 2-dimensional (real) manifold of spin vectors is the unit-sphere $\mathcal{S}_\mathbb{R} \equiv \mathcal{S}_2(\mathbb{R})$. $\mathcal{S}_\mathbb{R}$, if viewed as a subset of $\mathbb{R}^3$ can be written as $\mathcal{S}_\mathbb{R} = \{\widehat{S} \in \mathbb{R}^3 : \|\widehat{S}\| = 1\}$ where we have used the Euclidean norm on $\mathbb{R}^3$: $\|\hat{x}\| \equiv \sqrt{x_1^2 + x_2^2 + x_3^3}$. A spin trajectory is a continuously differentiable (i.e. $\mathcal{C}^1$) map $\widehat{S} : \mathbb{R} \to \mathcal{S}_\mathbb{R}$, $t \mapsto \widehat{S}(t)$.*

With this definition the instantaneous polarisation of an ensemble of N particles is

$$\vec{P}_{\text{ens}}(t) \equiv P(t)\hat{P}(t) \equiv \frac{1}{N}\sum_{i=1}^{N} \widehat{S}_i(t) = \left\langle \widehat{S} \right\rangle_{\text{ens}} \quad , \tag{2.2}$$

where we have introduced the degree of polarisation P and the polarisation direction $\hat{P}$. Throughout this thesis variable length vectors are symbolised by an "arrow" ($\vec{x}$) whereas unit vectors are symbolised by a "hat" ($\hat{x}$). In chapter 4 spin *fields* on phase space $\times$ ring azimuth will be defined so that the discrete ensemble average is replaced by an integral over phase space.

It should be noted that instead of describing the evolution of the expectation value of the spin operator in electromagnetic fields in terms of the evolution of a real unit 3–vector, it can as well be described by the evolution of a complex 2 component spinor. This will be covered in greater detail in section 2.2.1. Some of the literature which describes spin in accelerators in terms of spinors gives the impression that the spinors are wavefunctions. Of course, in quantum mechanics where interference of states and the Pauli principle are issues this the only adequate description. However, a classical treatment of spin–orbit coupling with classical dynamical orbit variables does *not* become quantum mechanical just by introducing spinors and calling the precession equation "Schrödinger equation"! The classical precession equation for $\widehat{S}$ describes the expectation value of $\widehat{\mathfrak{S}}$ in a coupled spin–orbit system. An equivalent spinor representation still only describes this expectation value and *not* the evolution of wave functions.

2.1 The T–BMT equation

The motion of the spin expectation value of a particle moving in electromagnetic fields and evaluated in the instantaneous particle rest frame is described by the T–BMT equation [JF26, LT27, MC55, BM59] (see also [JJ83, BM84, SL97, BH98c]), which in terms of our classical spin vector reads as

$$
\begin{aligned}
\mathrm{D}_t \widehat{S} &= \vec{\Omega}_{\mathrm{BMT}}(\vec{r}, \vec{\beta}, t) \times \widehat{S} \\
\vec{\Omega}_{\mathrm{BMT}} &\equiv -\frac{e}{m\gamma}\left[(1+G\gamma)\vec{B}_{\perp} + (1+G)\vec{B}_{||} - \left(G\gamma + \frac{\gamma}{1+\gamma}\right)\vec{\beta}\times\vec{E}\right] \quad , \qquad (2.3)
\end{aligned}
$$

with the position $\vec{r}(t)$ and velocity $\vec{\beta}(t)$ of the particle and the magnetic and electric fields $\vec{B}(\vec{r}, t)$, $\vec{E}(\vec{r}, t)$ evaluated in the laboratory frame. Here we have introduced the gyromagnetic anomaly $G \equiv {}^{g}/_{2} - 1$, which is approximately [pdg94] 1.79284739 for protons and $1.15965212\,10^{-3}$ for electrons and positrons, and the magnetic field vectors parallel and perpendicular to the particle velocity $\vec{B}_{||} \equiv \vec{\beta}\cdot\vec{B}\vec{\beta}/||\vec{\beta}||^2$ and $\vec{B}_{\perp} \equiv \vec{B} - \vec{B}_{||}$ respectively. Note that usually the gyromagnetic anomaly for leptons is called a rather than G. In an accelerator one can normally apply the paraxial approximation, since the transverse momenta are small compared to the momentum in the beam direction. Then in transverse magnetic fields $\vec{B}_{||} \ll \vec{B}_{\perp}$ and a significant contribution to $\vec{B}_{||}$ can only arise from the longitudinal fields in solenoids. Moreover the electric field in conventional accelerators is non–zero only in the RF–cavities where its main component is longitudinal. Therefore the term in 2.3 which contains $\vec{B}_{\perp}$ is the strongest contribution to the spin precession outside the solenoids. Since $\vec{B}\times\vec{\beta} = \vec{B}_{\perp}\times\vec{\beta}$, the Lorentz force in purely magnetic fields can be rewritten with the kinetic momentum $\vec{\pi} = m\gamma\vec{\beta}$ as

$$
\mathrm{D}_t\,\vec{\pi} = -\frac{e}{m\gamma}\vec{B}_{\perp}\times\vec{\pi} \quad . \qquad (2.4)
$$

This formal similarity with the T–BMT equation leads to the following conclusions for spin motion in purely transverse magnetic fields:

1. Since the norms of both $\widehat{S}$ and $\vec{\pi}$ stay constant we get, with $\hat{\pi} \equiv \vec{\pi}/||\vec{\pi}||$, the relation $d\widehat{S} = (G\gamma + 1)d\hat{\pi}$.

2. Let $\widetilde{S}$ be the spin vector measured in a coordinate system rotating with $\hat{\pi}$. Then $d\widetilde{S} = G\gamma d\hat{\pi}$ where $\hat{\pi}$ is evaluated in the laboratory frame. In other words if the orbit is deflected by ϕ in a transverse magnetic field with constant direction $\widehat{B}$ then the spin is rotated by $G\gamma\phi$ w.r.t. the orbit. For protons with $||\vec{\pi}|| = 820$ GeV a deflection angle of 1 mrad causes about 90° of spin rotation. For electrons/positrons at $||\vec{\pi}|| = 27.5$ GeV 1 mrad corresponds to about 3.6° of spin rotation. If a proton in an accelerator sees only vertical magnetic fields on its trajectory and the paraxial approximation is valid, then in one turn around the ring the spin performs $G\gamma$ full revolutions relative to the particle's direction of flight. For a proton in a flat HERA–p at a momentum of 820 (920) GeV this means about 1567 (1758) spin revolutions. For $e^{\pm}$ at a momentum of 27.5 GeV in HERA–e without spin rotators a spin performs 62.5 revolutions. Therefore we will occasionally call $G\gamma$ the *spin enhancement factor.*

3. Whenever the energy of a proton or an electron/positron is increased by about 523 MeV $= {}^{m_p}/_{G}$ or about 441 MeV $= {}^{m_e}/_{a}$ respectively, the spin performs one more revolution per turn around the ring.

4. In the limit $\gamma \to \infty$ the (spin precession rate)/(field integral) saturates. Asymptotically a field integral of about 5.48 (4.62) Tm produces a 180° spin rotation for protons (electrons/positrons).

Ring–like accelerators are always built so that, no matter what bending field orientations are involved, there is a closed orbit, i.e. a trajectory $\vec{Z}(t) \equiv (\vec{R}(t), \vec{p}(t))^{\mathrm{T}}$ in phase space so that $\vec{Z}(t +$

$1/f_0) = \vec{Z}(t)$ where f_0 is the revolution frequency of the synchronous particle. In a perfectly aligned ring this *design orbit* is defined by the holding fields of the bending magnets. The closed orbit trajectory $\vec{Z}$ can be parametrised [VW97] by the *generalised machine azimuth*

$$\theta \equiv \frac{2\pi l}{L} \quad , \quad \mathrm{D}_t\, l = ||\mathrm{D}_t\, \vec{R}|| \quad , \quad L \equiv \int_{t_0}^{t_0+1/f_0} ||\mathrm{D}_t\, \vec{R}(t)|| dt \quad , \tag{2.5}$$

so that it is 2π–periodic $\vec{Z}(\theta + 2\pi) = \vec{Z}(\theta)$.

In order to allow an expansion in small parameters the EOM are transformed to a curvilinear coordinate system [HR87, MB90, BH94a, GH94, GH99b, CW98] w.r.t. the reference trajectory $\vec{R}(\theta)$. An actual trajectory in configuration space $\mathbb{R}^3$ is given by $\vec{r}(\theta) = \vec{R}(\theta) + x(\theta)\hat{x}(\theta) + y(\theta)\hat{y}(\theta)$ where $\hat{x}$ and $\hat{y}$ are unit vectors and form together with $\hat{z} \equiv \mathrm{D}_\theta\, \vec{R}/||\mathrm{D}_\theta\, \vec{R}||$ an orthonormal base of the $\mathbb{R}^3$. The $\hat{x}$ and $\hat{y}$ differ from the normal and conormal unit vectors of the Frenet–Serret coordinate system [VW97] by being wound back by the integral torsion around $\hat{z}$ which is the tangent vector of the Frenet–Serret system. The actual trajectory in momentum space is then $\vec{p}(\theta) = p_x(\theta)\hat{x} + p_y(\theta)\hat{y} + p_z(\theta)\hat{z}$. The last step is to introduce the scaled variables

$$x \ , \ a \equiv \frac{p_x}{p_0} \ , \ y \ , \ b \equiv \frac{p_y}{p_0} \ , \ \tau \equiv (t_0 - t)\frac{K_0}{p_0} \ , \ \delta \equiv \frac{K - K_0}{K_0} \ , \ \vec{z} \equiv (x, a, y, b, \tau, \delta)^{\mathrm{T}} \ , \ \vec{z}_0 \equiv \vec{0} \tag{2.6}$$

where $K = \sqrt{m^2 + p^2} - m$ is the "kinetic energy", $t_0 - t$ is the time–of–flight difference w.r.t. the synchronous particle and the index 0 has been used to indicate evaluation on the reference trajectory. These pairs (x, a), (y, b) and (τ, δ) are canonically conjugate pairs [CS58, HR87, MB90, BH94a, HM96] and are in general small. Note that δ as defined above is small only when the momentum difference $p - p_0$ is small compared to p_0 whereas the perhaps more familiar looking $\delta_E \equiv (E - E_0)/(E_0)$ with $E \equiv \sqrt{m^2 + p^2}$ can be small even for finite $p - p_0$ in the limit $p_0 \to 0$. Also note that in the literature the independent parameter is usually *not* chosen to be θ but l as from 2.5.

We now introduce the canonical transformation $\vec{f} : \mathbb{R}^6 \to \mathbb{R}^6$, $\vec{z} \mapsto (\vec{r}, \vec{p}) \equiv \vec{f}(\vec{z})$ and the transformation $\vec{g} : \mathbb{R}^6 \to \mathbb{R}^6$, $(\vec{r}, \vec{p}) \mapsto (\vec{r}, \vec{\beta}) \equiv \vec{g}(\vec{r}, \vec{p})$ that acts as an identity on configuration space but transforms the canonical momenta to the Lagrangian velocities. We also need

$$\vec{\kappa} \equiv \frac{\hat{x}\cos\lambda + \hat{y}\sin\lambda,}{\rho} \quad , \quad h \equiv 1 + x\kappa_x + y\kappa_y \quad , \quad \tilde{\beta} \equiv ||\mathrm{D}_\theta\, \vec{r}|| \quad . \tag{2.7}$$

Here $\vec{\kappa}$ and ρ are the vector of curvature and the instantaneous radius of curvature of the reference trajectory respectively, λ is its torsion integrated from some reference θ_0 to θ and $\tilde{\beta}$ is the "particle velocity" in terms of the generalised azimuth. Then one finds [BH94a, GH94, GH99b, CW98] for the transformed T–BMT equation

$$\begin{aligned} \mathrm{D}_\theta\, \widehat{S} &= \vec{\Omega}(\vec{z}, \theta) \times \widehat{S} \\ \vec{\Omega}(\vec{z}, \theta) &\equiv \left(\vec{\Omega}_{\mathrm{BMT}}(\,\cdot\,, \theta)\frac{h||\vec{p}||}{\tilde{\beta}p_z} - \vec{\kappa} \times \hat{z}\right) \circ \vec{g} \circ \vec{f}\,(\vec{z}) \end{aligned} \tag{2.8}$$

Finally we split $\vec{\Omega}(\vec{z}, \theta)$ into the part arising from closed orbit motion and the part from synchro–betatron motion

$$\vec{\Omega}(\vec{z}, \theta) = \vec{\Omega}_0(\theta) + \vec{\omega}(\vec{z}, \theta) \quad . \tag{2.9}$$

Then the off–orbit part $\vec{\omega}(\vec{z}, \theta)$ is "origin preserving" in the sense that $\vec{\omega}(\vec{0}_6, \theta) = \vec{0}_3$ where $\vec{0}_i$ is the zero in $\mathbb{R}^i$.

In chapter 4 we will derive parameters for spin motion which can be considered as action–angle variables. Therefore it is useful to find a Hamiltonian for the T–BMT equation. A completely Hamiltonian treatment of spin motion is discussed in [DK73, KY86, BH94a, BH94b, BG98a]. Here we will only mention two principle difficulties.

1. Strictly speaking, the 2–dimensional manifold $\mathcal{S}_{\mathbb{R}}$ needs an atlas of at least 2 charts $\hat{\xi}_{1,2} : \mathcal{U} \subset \mathbb{R}^2 \to \mathcal{S}_{\mathbb{R}}$ with $\mathcal{U}$ open [BG80, VW97, BG98a]. As an example the standard polar parametrisation of $\mathcal{S}_{\mathbb{R}}$ interpreted as a subset of $\mathbb{R}^3$, $\hat{\xi}_1 : (\varphi, \vartheta) \mapsto (\sin\vartheta\sin\varphi, \cos\vartheta, \sin\vartheta\cos\varphi)$, $(\varphi, \vartheta) \in [0, 2\pi) \times [0, \pi)$ of the whole unit sphere has 2 singular points, namely the North- and the South–pole *and* the domain of (φ, ϑ) is *not* an open set. One can of course restrict (φ, ϑ) to $(0, 2\pi) \times (0, \pi)$ which excludes the two poles w.r.t. the $\hat{y}$–axis as well as the meridian $\varphi = 0$ through $(0, 0, 1)$. Then one needs another chart which can be easily constructed by e.g. $\hat{\xi}_2 : (\varphi, \vartheta) \mapsto (\cos\vartheta, \sin\vartheta\sin\varphi, -\sin\vartheta\cos\varphi)$ over the same domain but which excludes the two poles w.r.t. the $\hat{x}$–axis and the meridian $\varphi = 0$ through $(0, 0, -1)$. Nevertheless in order to describe spin motion on the *whole* unit sphere one must be ready to switch between $\hat{\xi}_1$ and $\hat{\xi}_2$ (or some equivalent charts) backwards and forwards. In [BG98a] this inconvenience is avoided by a Hamiltonian description with a degenerate Poisson bracket in which all *three* dependent coordinates on $\mathcal{S}_{\mathbb{R}}$ embedded in $\mathbb{R}^3$ are used. But we will in general use a non–Hamiltonian description with unit 3–vectors as dynamical variables. Wherever the symplectic structure of $\mathcal{S}_{\mathbb{R}}$ is treated we will sacrifice mathematical rigour for a more comprehensible *global* 2–dimensional parametrisation so that the behaviour in some neighbourhoods around the unavoidable singular points of the parametrisation has to be discussed explicitly.

2. The T–BMT equation contains the orbital phase space coordinates. We neglect the Stern–Gerlach force. Therefore the orbital Hamiltonian $H^{(\mathrm{orb.})}(\vec{z}, \theta)$ does *not* contain the spin variables. If one constructs a spin Hamiltonian $H^{(\mathrm{sp.})}(\vec{z}, q^{(\mathrm{sp.})}, p^{(\mathrm{sp.})}, \theta)$ so that the complete Hamiltonian is $H(\vec{z}, q^{(\mathrm{sp.})}, p^{(\mathrm{sp.})}, \theta) = H^{(\mathrm{or.})}(\vec{z}, \theta) + H^{(\mathrm{sp.})}(\vec{z}, q^{(\mathrm{sp.})}, p^{(\mathrm{sp.})}, \theta)$ and so that $\mathrm{D}_\theta\, q^{(\mathrm{sp.})} = \partial_{p^{(\mathrm{sp.})}} H$ and $\mathrm{D}_\theta\, p^{(\mathrm{sp.})} = -\partial_{q^{(\mathrm{sp.})}} H$ resemble the T–BMT precession equation, then one automatically obtains a kind of Stern–Gerlach back reaction $\mathrm{D}_\theta\, \vec{z} = \underline{J}\partial_{\vec{z}}\,(H^{(\mathrm{or.})} + H^{(\mathrm{sp.})})$. (See appendix A for an explanation on this notation.) This can be circumvented by introducing the *triangular system* [BG98a]: One solves the orbital EOM $\mathrm{D}_\theta\, \vec{z} = \underline{J}\partial_{\vec{z}}\, H^{(\mathrm{or.})}$ first and then obtains a 6 parameter family of spin Hamiltonians $\widetilde{H}^{(\mathrm{sp.})}_{\vec{z}_0}(q^{(\mathrm{sp.})}, p^{(\mathrm{sp.})}, \theta)$, i.e. one spin Hamiltonian for each set of orbital initial conditions $\vec{z}(\theta_0) = \vec{z}_0$.

We will briefly mention now two sets of canonical spin coordinates and the corresponding spin Hamiltonians. Assume we have some orthonormal basis $(\hat{x}, \hat{y}, \hat{z})$ of $\mathbb{R}^3$ and represent every 3–vector $\vec{v}$ and every spin $\widehat{S}$ by its coordinate triple w.r.t. this basis, i.e. (v_x, v_y, v_z) and (S_x, S_y, S_z) respectively. Furthermore we choose one base vector, say $\hat{y}$, to be distinguished from the other two. One canonical pair (α, β) is [BH92, BH94a, BH94b]

$$\alpha = S_z\sqrt{\frac{2}{1+S_y}}\ ,\ \beta = S_x\sqrt{\frac{2}{1+S_y}}\ ,\ \widehat{S} = \left(\beta\sqrt{1-\frac{\alpha^2+\beta^2}{4}},\ 1-\frac{\alpha^2+\beta^2}{2},\ \alpha\sqrt{1-\frac{\alpha^2+\beta^2}{4}}\right) \tag{2.10}$$

and with the Hamiltonian

$$H^{(\mathrm{sp.})}_{\vec{z}_0}(\alpha, \beta, \theta) \equiv \vec{\Omega}(\vec{z}(\theta; \vec{z}_0), \theta) \cdot \widehat{S}(\alpha, \beta) = \sqrt{1-\frac{\alpha^2+\beta^2}{4}}(\Omega_z\alpha + \Omega_x\beta) + \left(1-\frac{\alpha^2+\beta^2}{2}\right)\Omega_y \tag{2.11}$$

the canonical equations $\mathrm{D}_\theta\, \alpha = \partial_\beta\, H^{(\mathrm{sp.})}$ and $\mathrm{D}_\theta\, \beta = -\partial_\alpha\, H^{(\mathrm{sp.})}$ lead to the T–BMT equation $\mathrm{D}_\theta\, \widehat{S} = \vec{\Omega} \times \widehat{S}$ [BH92]. The only singular point of this parametrisation is $S_y = -1$. If analogous coordinates are used to describe deviations of T–BMT solutions from the periodic vector $\hat{n}_0$, to be treated later, then in the limit $\alpha^2 + \beta^2 \ll 1$ they reduce to those used in perturbation theory [AC80, SM86a, SM86b, BH92, BH94a, BH94b]. See equation (2.99).

Another pair of canonically conjugate coordinates [KY86, BH94a, BH94b] can be found using the generating function $F(\alpha, \varphi) = \frac{\alpha^2}{2}\tan\varphi - \varphi$. Then solving $\beta = \partial_\alpha\, F$, $K = -\partial_\varphi\, F$ for K and φ one finds

$$K = S_y = 1 - \frac{\alpha^2+\beta^2}{2} \quad , \quad \varphi = \arctan\frac{S_x}{S_z} = \arctan\frac{\beta}{\alpha} \tag{2.12}$$

and

$$(\alpha, \beta) = \sqrt{2(1-K)}(\cos\varphi, \sin\varphi) \quad , \quad \widehat{S} = \left(\sqrt{1-K^2}\cos\varphi, K, \sqrt{1-K^2}\sin\varphi\right) \quad . \tag{2.13}$$

With the Hamiltonian

$$H^{(\mathrm{sp.})}_{\vec{z}_0}(\varphi, K, \theta) \equiv \vec{\Omega}(\vec{z}(\theta; \vec{z}_0), \theta) \cdot \widehat{S}(\varphi, K) = \sqrt{1-K^2}(\Omega_z \cos\varphi + \Omega_x \sin\varphi) + \Omega_y K \tag{2.14}$$

the T–BMT equation can again be derived [KY86, BH94a, BH94b] from $\mathrm{D}_\theta\, \varphi = \partial_K\, H^{(\mathrm{sp.})}$ and $\mathrm{D}_\theta\, K = -\partial_\varphi\, H^{(\mathrm{sp.})}$. The chart defined by (2.13) has two singular points at $S_y = \pm 1$. But if a phase space dependent rotation of the coordinate system $(\hat{x}, \hat{y}, \hat{z})$ to another system $(\hat{u}_1, \hat{n}, \hat{u}_2)$ exists so that the rotation vector $\widetilde{\Omega}$ of the T–BMT equation in the $(\hat{u}_1, \hat{n}, \hat{u}_2)$ system has the coordinate vector $(0, \nu, 0)$, then a canonical change of coordinates $(K, \varphi) \mapsto (I, \Phi)$ can be found [KY86] so that $\mathrm{D}_\theta\, I = 0$, $\mathrm{D}_\theta\, \Phi = \nu = \text{const.}$ and the map $(I, \Phi) \mapsto \widehat{S}$ is 2π–periodic in Φ. Thus (I, Φ) are the spin action–angle variables (see appendix A) of the spin system. In chapter 4 we will construct such a local basis $(\hat{u}_1, \hat{n}, \hat{u}_2)$.

If the orbital motion is integrable with the action–angle variables $\vec{J}, \vec{\Psi} \in \mathbb{R}^3$, then (see section A.1.3) $\vec{\Omega}_{\vec{J},\vec{\Psi}_0}(\theta) \equiv \vec{\Omega}_{\vec{J}}(\Psi_0 + \vec{Q}\theta, \theta)$ is pseudo–periodic over the orbital tunes $\vec{Q}$. Thus the precession vector $\vec{\Omega}(\vec{z}, \theta)$ can be expanded in a generalised Fourier series that contains only the "frequencies" $k + \vec{k}\cdot\vec{Q}$ with $k \in \mathbb{Z}$, $\vec{k} \in \mathbb{Z}^3$. In particular $\vec{\Omega}_0(\theta)$ from equation (2.9) is 2π–periodic and $\vec{\omega}_{\vec{J},\vec{\Psi}_0}(\theta)$ (also from (2.9)) contains only "frequencies" $k + \vec{k}\cdot\vec{Q}$ with, $\vec{k} \in \mathbb{Z}^3 - \{\vec{0}\}$.

2.2 The T–BMT flow

An intrinsic property of a precession equation $\mathrm{D}_\theta\, \widehat{S} = \vec{\Omega} \times \widehat{S}$ is that the scalar product of two solutions is an invariant of motion.

$$\begin{aligned}
\mathrm{D}_\theta\, \widehat{S}_1 \cdot \widehat{S}_2 &= (\vec{\Omega} \times \widehat{S}_1) \cdot \widehat{S}_2 + \widehat{S}_1 \cdot (\vec{\Omega} \times \widehat{S}_2) \\
&= (\vec{\Omega} \times \widehat{S}_1) \cdot \widehat{S}_2 + (\vec{\Omega} \times \widehat{S}_2) \cdot \widehat{S}_1 \\
&= (\vec{\Omega} \times \widehat{S}_1) \cdot \widehat{S}_2 + (\widehat{S}_1 \times \vec{\Omega}) \cdot \widehat{S}_2 \\
&= (\vec{\Omega} \times \widehat{S}_1) \cdot \widehat{S}_2 - (\vec{\Omega} \times \widehat{S}_1) \cdot \widehat{S}_2 = 0
\end{aligned} \tag{2.15}$$

As a consequence not only the angle between $\widehat{S}_1$ and $\widehat{S}_2$ defined by $\angle(\widehat{S}_1, \widehat{S}_2) \equiv \arccos \widehat{S}_1 \cdot \widehat{S}_2$ but also the Euclidean norm $\|\widehat{S}\| \equiv \sqrt{\widehat{S}\cdot\widehat{S}}$ is an invariant of motion. Additionally the T–BMT equation in the form $\mathrm{D}_\theta\, \widehat{S} = \vec{f}(\widehat{S}, \theta)$ with $\vec{f}(\widehat{S}, \theta) \equiv \vec{\Omega}(\vec{z}(\theta), \theta) \times \widehat{S}$ and with $\|\vec{\Omega}\|$ bounded fulfils a global Lipschitz condition, i.e. there is a real positive constant L such that for all $\widehat{S}_1, \widehat{S}_2 \in \mathcal{S}_{\mathbb{R}}$ the condition $\|\vec{f}(\widehat{S}_1, \theta) - \vec{f}(\widehat{S}_2, \theta)\| \le L\|\widehat{S}_1 - \widehat{S}_2\|$ holds, where the difference $\widehat{S}_1 - \widehat{S}_2$ is a bounded vector of $\mathbb{R}^3$ rather than a unit vector. In accelerators the external fields are bounded inside the acceptance of the machine and if the orbital motion is stable, then $\vec{z}$ is bounded too. Therefore in all realistic cases the global Lipschitz condition is fulfilled by the T–BMT equation. We assume that $\vec{\Omega}$ is piecewise continuous w.r.t. θ. Hence [ems1, OF84] a solution of the T–BMT equation always exists at least locally and is unique.

The T–BMT equation can be rewritten in the standard form of a linear ordinary differential equation (ODE)

$$\mathrm{D}_\theta\, \widehat{S} = \underline{\Omega}(\vec{z}, \theta)\widehat{S} \quad , \quad \underline{\Omega} \equiv \begin{pmatrix} 0 & -\Omega_z & \Omega_y \\ \Omega_z & 0 & -\Omega_x \\ -\Omega_y & \Omega_x & 0 \end{pmatrix} \quad , \tag{2.16}$$

where we have introduced the anti–symmetric real matrix $\underline{\Omega}$ to represent $\vec{\Omega}$. The flow of a linear ODE in d dimensions $\mathrm{D}_\theta\, \vec{x} = \underline{C}(\theta)\vec{x}$ is a linear map $\vec{M}_{\theta_f,\theta_i} : \mathbb{R}^d \to \mathbb{R}^d$, $\vec{x} \mapsto \vec{M}_{\theta_f,\theta_i}(\vec{x}) \equiv \underline{M}_{\theta_f,\theta_i}\vec{x}$, so that $\vec{x}(\theta) \equiv \underline{M}_{\theta,\theta_i}\vec{x}_i$ is a solution to the initial value problem (IVP) defined by the linear ODE and $\vec{x}(\theta_i) = \vec{x}_i$ for all $\vec{x}_i$. Therefore, and since $\widehat{S} \in \mathcal{S}_{\mathbb{R}} \subset \mathbb{R}^3$, the flow of the T–BMT equation must be an orthogonal real map. The group $\mathbf{O(3)}$ of orthogonal real 3×3–maps consists of two distinct connected domains i.e. the maps can have a determinant of ±1. The flow of a linear ODE is continuous w.r.t. θ_f, the determinant is a continuous map from the space of linear real maps to $\mathbb{R}$ and the T–BMT flow for $\theta_f = \theta_i$ is the identity. Therefore the T–BMT flow must be in the group of special orthogonal maps $\mathbf{SO(3)}$.

The Lie algebra of anti–symmetric real 3×3–matrices is abbreviated as $\mathbf{so(3)}$ and generates the $\mathbf{SO(3)}$ in the sense that for every $\underline{R} \in \mathbf{SO(3)}$ there is an $\underline{\Omega} \in \mathbf{so(3)}$ and a $\theta \in \mathbb{R}$ so that $\underline{R} = \exp(\theta\,\underline{\Omega})$. We note that since the precession vector of the "triangular system" can be written as $\vec{\Omega}(\vec{z},\theta) = \vec{\Omega}_{\vec{z}_0}(\theta)$ the T–BMT flow in general depends on the initial phase space coordinate of the trajectory along which we integrate the T–BMT equation.

Definition 2.2 (T–BMT flow) *The flow of the T-BMT equation or just the T-BMT flow is a map* $\hat{R}_{\theta_f,\theta_i,\vec{z}_i} : \mathcal{S}_{\mathbb{R}} \to \mathcal{S}_{\mathbb{R}},\ \widehat{S}_i \mapsto \hat{R}_{\theta_f,\theta_i,\vec{z}_i}(\widehat{S}_i) \equiv \underline{R}(\theta_f,\theta_i;\vec{z}_i)\widehat{S}_i$, *with* $\underline{R}$ *being the realisation of* $\hat{R}$ *in a given orthonormal basis of* $\mathbb{R}^3$ *so that* $\underline{R}(\theta_f,\theta_i;\vec{z}_i) \in \mathbf{SO(3)}\ \forall \theta_f,\theta_i,\vec{z}_i$ *and so that the spin trajectory* $\widehat{S}_{\theta_i,\vec{z}_i,\widehat{S}_i}(\theta) \equiv \hat{R}_{\theta,\theta_i,\vec{z}_i}(\widehat{S}_i)$ *fulfils*

1. $\mathrm{D}_\theta\, \widehat{S}_{\theta_i,\vec{z}_i,\widehat{S}_i}(\theta) = \vec{\Omega}(\vec{z}_{\theta_i,\vec{z}_i}(\theta),\theta) \times \widehat{S}_{\theta_i,\vec{z}_i,\widehat{S}_i}(\theta)$ *or equivalently* $\partial_\theta\ \underline{R}(\theta,\theta_i;\vec{z}_i) = \underline{\Omega}(\vec{z}_{\theta_i,\vec{z}_i}(\theta),\theta)\,\underline{R}(\theta,\theta_i;\vec{z}_i)$,
2. $\widehat{S}_{\theta_i,\vec{z}_i,\widehat{S}_i}(\theta_i) = \widehat{S}_i$ *or equivalently* $\underline{R}(\theta_i,\theta_i;\vec{z}_i) = \underline{1}$.

If it is clear which θ_i, $\vec{z}_i$ and $\widehat{S}_i$ are meant we will often omit these labels on the spin trajectory.

In the following we will in general perform calculations in some given basis of the $\mathbb{R}^3$ and identify the map $\hat{R}$ with the matrix $\underline{R}$. The fundamental properties of the T–BMT equation are independent of the particular basis chosen but for a properly chosen basis the coordinate vector $(\Omega_x,\Omega_y,\Omega_z)$ and the matrix realization $\underline{R}$ can sometimes be drastically simplified. It therefore seems worthwhile to discuss the change of the T–BMT equation under an orthogonal change of coordinates. Let $\widehat{S}' = \underline{A}(\vec{z},\theta)\widehat{S}$ with some possibly azimuth and phase space dependent $\underline{A} \in \mathbf{SO(3)}$, then the EOM for $\widehat{S}'$ is

$$\mathrm{D}_\theta\,\widehat{S}' = \left(\underline{A}\,\underline{\Omega}\,\underline{A}^{\mathrm{T}} + (\mathrm{D}_\theta\ \underline{A})\,\underline{A}^{\mathrm{T}}\right)\ \widehat{S}' \tag{2.17}$$

with $\mathrm{D}_\theta\ \underline{A} = (\mathrm{D}_\theta\,\vec{z})^{\mathrm{T}}\partial_{\vec{z}}\ \underline{A} + \partial_\theta\ \underline{A}$.

2.2.1 Orthogonal and unitary representations

Although we treat spin motion classically, i.e. spins are represented by 3–dimensional unit vectors $\widehat{S}$ and the T–BMT flow is an $\mathbf{SO(3)}$ map, it is sometimes more convenient to use other representations — in particular concerning the flow.

We begin by just mentioning some key properties of $\mathbf{SO(3)}$ maps. The *special orthogonal group of real* 3×3 *matrices*, $\mathbf{SO(3)}$ is the set of regular matrices $\underline{R} \in \mathbb{R}^{3\times3}$ which fulfil $\underline{R}^{\mathrm{T}}\,\underline{R} = \underline{R}\,\underline{R}^{\mathrm{T}} = \underline{1}$ and $\det(\underline{R}) = +1$. They can be parametrised by the Euler angles (α,β,γ) via the elementary rotations

$$\underline{R}_1(\psi) \equiv \begin{pmatrix} 1 & 0 & 0 \\ 0 & \cos\psi & -\sin\psi \\ 0 & \sin\psi & \cos\psi \end{pmatrix} \quad , \quad \underline{R}_3(\psi) \equiv \begin{pmatrix} \cos\psi & -\sin\psi & 0 \\ \sin\psi & \cos\psi & 0 \\ 0 & 0 & 1 \end{pmatrix} \quad . \tag{2.18}$$

One can show [WH90] that the mapping of the Euler angles to the $\mathbf{SO(3)}$ matrices defined by $[0,2\pi)\times[0,\pi]\times[0,2\pi) \to \mathbf{SO(3)}$, $(\alpha,\beta,\gamma) \mapsto \underline{R}_3(\alpha)\,\underline{R}_1(\beta)\,\underline{R}_3(\gamma)$ is surjective.

However, a more intuitive parametrisation of an $\mathbf{SO(3)}$ map is via its rotation axis $\hat{r}$ and the angle of rotation ψ. Unfortunately this parametrisation is not one–to–one since a rotation around $\hat{r}$ by ψ is equivalent to a rotation around $-\hat{r}$ by $-\psi$. Nevertheless a similar parametrisation is quite handy in analytical calculations as well as in numerical evaluation. This leads us to the group of the

Definition 2.3 (Unit–quaternions) *We will call the unit sphere in* $\mathbb{R}^4$, $\mathbf{S}_{\mathbb{H}} \equiv \mathcal{S}_3(\mathbb{R}) = \{\bar{q} \in \mathbb{R}^4 : \|\bar{q}\| = 1\}$, $\bar{q} \equiv (q_0, \vec{q})$ *with the product*

$$\bar{a}\bar{b} = (a_0 b_0 - \vec{a}\cdot\vec{b},\ a_0\vec{b} + \vec{a}b_0 + \vec{a}\times\vec{b}) \quad , \quad \bar{a}, \bar{b} \in \mathbf{S}_{\mathbb{H}} \quad , \tag{2.19}$$

the set (or as we will see later: the group) of unit–quaternions. We introduce the following notation for $\bar{q} \in \mathbf{S}_{\mathbb{H}} : \bar{q} \equiv (q_0, \vec{q}) \equiv (q_0, q_1, q_2, q_3) \equiv (\cos\frac{\psi}{2}, \sin\frac{\psi}{2}\hat{q})$.

Note that the "base quaternions" $(1,0,0,0)$, $(0,1,0,0)$, $(0,0,1,0)$ and $(0,0,0,1)$ fulfil $(1,0,0,0)^2 = (1,0,0,0)$ and $(0,1,0,0)^2 = (0,0,1,0)^2 = (0,0,0,1)^2 = -(1,0,0,0)$.

Theorem 2.1 *Let* $\bar{a} = (a_0, \vec{a})$, $\bar{b} = (b_0, \vec{b})$, $\bar{c} = (b_0, \vec{c})$ *be arbitrary unit–quaternions and* $\bar{1} \equiv (1, \vec{0})$, *then*

$$\begin{aligned} \|\bar{a}\bar{b}\| &= 1 && (2.20\text{a})\\ \bar{a}(\bar{b}\bar{c}) &= (\bar{a}\bar{b})\bar{c} && (2.20\text{b})\\ \bar{1}\bar{a} = \bar{a}\bar{1} &= \bar{a} && (2.20\text{c})\\ (a_0, \vec{a})(a_0, -\vec{a}) = (a_0, -\vec{a})(a_0, \vec{a}) &= \bar{1} \quad \textit{(an inverse } \bar{a}^{-1} \equiv (a_0, -\vec{a}) \textit{ exists)}. && (2.20\text{d}) \end{aligned}$$

In other words: the product, as defined in definition 2.3 is an inner operation ($\bar{a}, \bar{b} \in \mathbf{S}_{\mathbb{H}} \Rightarrow \bar{a}\bar{b} \in \mathbf{S}_{\mathbb{H}}$) *and* $\mathbf{S}_{\mathbb{H}}$ *with this product is a group.*

The parts (2.20c) and (2.20d) obviously follow immediately from definition 2.3, so that we only have to show (2.20a) and (2.20b). Starting with

$$\begin{aligned} \|\bar{a}\bar{b}\|^2 &= \left(a_0 b_0 - \vec{a}\cdot\vec{b}\right)^2 + \left\|a_0\vec{b} + \vec{a}b_0 + \vec{a}\times\vec{b}\right\|^2 \\ &= (a_0 b_0)^2 + (\vec{a}\cdot\vec{b})^2 + a_0^2\|\vec{b}\|^2 + b_0^2\|\vec{a}\|^2 + \|\vec{a}\times\vec{b}\|^2 \end{aligned} \tag{2.21}$$

and introducing $a_0 \equiv \cos\frac{\alpha}{2}$, $b_0 \equiv \cos\frac{\beta}{2}$, $\vec{a} = \sin\frac{\alpha}{2}\hat{a}$ and $\vec{b} = \sin\frac{\beta}{2}\hat{b}$ we obtain

$$\|\bar{a}\bar{b}\|^2 = \cos^2\frac{\alpha}{2}\cos^2\frac{\beta}{2} + \cos^2\frac{\alpha}{2}\sin^2\frac{\beta}{2} + \sin^2\frac{\alpha}{2}\cos^2\frac{\beta}{2} + \sin^2\frac{\alpha}{2}\cos^2\frac{\beta}{2}\left((\hat{a}\cdot\hat{b})^2 + \|\hat{a}\times\hat{b}\|^2\right) \tag{2.22}$$

which finally yields $\|\bar{a}\bar{b}\| = 1$ since $(\hat{a}\cdot\hat{b})^2 = \cos^2\phi$ and $\|\hat{a}\times\hat{b}\|^2 = \sin^2\phi$ with $\phi \equiv \angle(\hat{a}, \hat{b})$. To prove (2.20b) we have to handle many terms and therefore define

$$\begin{aligned} \bar{d}_a &\equiv (a_0, \vec{a})(b_0 c_0 - \vec{b}\cdot\vec{c},\ b_0\vec{c} + \vec{b}c_0 + \vec{b}\times\vec{c}) \\ \bar{d}_c &\equiv (a_0 b_0 - \vec{a}\cdot\vec{b},\ a_0\vec{b} + \vec{a}b_0 + \vec{a}\times\vec{b})(c_0, \vec{c}) \quad , \end{aligned} \tag{2.23}$$

and show $d_{a,0} = d_{c,0}$ and $\vec{d}_a = \vec{d}_c$ separately. After evaluating the quaternion products for $\bar{d}_a$ and $\bar{d}_c$ and cancelling the trivially identical terms in both expressions we obtain

$$\begin{aligned} d_{a,0} = d_{c,0} \quad &\Leftrightarrow \quad (\vec{a}\times\vec{b})\cdot\vec{c} = \vec{a}\cdot(\vec{b}\times\vec{c}) && (2.24\text{a})\\ \vec{d}_a = \vec{d}_c \quad &\Leftrightarrow \quad (\vec{a}\times\vec{b})\times\vec{c} - (\vec{a}\cdot\vec{b})\vec{c} = \vec{a}\times(\vec{b}\times\vec{c}) - \vec{a}(\vec{b}\cdot\vec{c}) \quad , && (2.24\text{b}) \end{aligned}$$

where the r.h.s. of the equivalence (2.24a) is true because the "hybrid" product $(\vec{x}\times\vec{y}\cdot\vec{z})$ is invariant under cyclic permutations and the r.h.s. of (2.24b) is true since of $(\vec{a}\times\vec{b})\times\vec{c} = \vec{b}(\vec{a}\cdot\vec{c}) - \vec{a}(\vec{b}\cdot\vec{c})$ and $\vec{a}\times(\vec{b}\times\vec{c}) = \vec{b}(\vec{a}\cdot\vec{c}) - \vec{c}(\vec{a}\cdot\vec{b})$. Thus the theorem is proved. □

Note that for the proof of part (2.20b) we did *not* use the constraint that the norms of the quaternions involved are unity. So with the standard vector sum and the product from definition 2.3, $\mathbb{R}^4$ can be identified as the *skew–field* $\mathbb{H}$ of the quaternions.

Definition 2.4 *For all $\bar{r} \in \mathbf{S}_{\mathbb{H}}$ we define $\underline{F}: \mathbf{S}_{\mathbb{H}} \to \mathbb{R}^{3\times 3}$, $\bar{r} \mapsto \underline{F}(\bar{r})$ so that for $\underline{R} \equiv \underline{F}(\bar{r})$ we have*

$$R_{ij} = (2r_0^2 - 1)\delta_{ij} + 2r_i r_j - 2r_0 \epsilon_{ijk} r_k \quad , \tag{2.25}$$

where ϵ_{ijk} are the components of the totally anti–symmetric Levi–Civita tensor in 3 dimensions and Einstein's sum convention has been used.

Obviously $\underline{F}$ is a quadratic form in the r_i so that $\bar{r}$ and $-\bar{r}$ map to the same matrix $\underline{R}$.

Theorem 2.2 *For all $\bar{r} \in \mathbf{S}_{\mathbb{H}}$ the matrix $\underline{R} = \underline{F}(\bar{r}) \in \mathbf{SO(3)}$.*

We first prove $\underline{R}\,\underline{R}^{\mathrm{T}} = \underline{1}$ which is equivalent to $R_{ik}R_{jk} = \delta_{ij}$. Introducing the abbreviation $f \equiv 2r_0^2 - 1$ we obtain

$$\begin{aligned}
R_{ik}R_{jk} &= (f\delta_{ik} + 2r_i r_k - 2r_0\epsilon_{ikl}r_l)(f\delta_{jk} + 2r_j r_k - 2r_0\epsilon_{jkm}r_m) \\
&= f^2\delta_{ij} + 4(f + \|\vec{r}\|^2)r_i r_j + 4r_0^2\epsilon_{ikl}\epsilon_{jkm}r_l r_m \\
&= f^2\delta_{ij} + 4(f + 1 - r_0^2)r_i r_j + 4r_0^2(\delta_{ij}\delta_{lm} - \delta_{im}\delta_{jl})r_l r_m \\
&= (f^2 + 4r_0^2(1 - r_0^2))\delta_{ij} + 4(f + 1 - 2r_0^2)r_i r_j \;=\; \delta_{ij} \quad ,
\end{aligned} \tag{2.26}$$

where we have omitted many terms that vanish due to the anti–symmetry of the Levi–Civita tensor. The map $\underline{R}$ is given explicitly by

$$\underline{R} = 2\begin{pmatrix} r_0^2 + r_1^2 - \frac{1}{2} & r_1 r_2 - r_0 r_3 & r_1 r_3 + r_0 r_2 \\ r_2 r_1 + r_0 r_3 & r_0^2 + r_2^2 - \frac{1}{2} & r_2 r_3 - r_0 r_1 \\ r_3 r_1 - r_0 r_2 & r_3 r_2 + r_0 r_1 & r_0^2 + r_3^2 - \frac{1}{2} \end{pmatrix} \quad . \tag{2.27}$$

By using the constraint $r_0^2 + r_1^2 + r_2^2 + r_3^2 = 1$ one easily verifies that $\det(\underline{R}) = +1$. $\square$

Theorem 2.3 *The map $\underline{F}$ from definition 2.4 is surjective.*

We prove that for each $\underline{R} \in \mathbf{SO(3)}$ we can find a $\bar{r}^+ \in \mathbf{S}_{\mathbb{H}}$. We first compute the trace of $\underline{R}$

$$\mathrm{trace}\,(\underline{R}) = 3(2r_0^2 - 1) + 2\|\vec{r}\|^2 = 4r_0^2 - 1 \quad \Rightarrow \quad r_0^+ = +\frac{1}{2}\sqrt{\mathrm{trace}\,(\underline{R}) + 1} \tag{2.28}$$

and contract $\underline{R}$ with the Levi–Civita tensor

$$\epsilon_{ijk}R_{jk} = -2r_0\epsilon_{ijk}\epsilon_{jkl}r_l = -4r_0 r_i \quad . \tag{2.29}$$

If $\mathrm{trace}\,(\underline{R}) \neq -1$, then we obtain for r_i^+, $i = 1, 2, 3$

$$r_i^+ = -\frac{\epsilon_{ijk}R_{jk}}{2\sqrt{\mathrm{trace}\,(\underline{R}) + 1}} \quad . \tag{2.30}$$

If $\mathrm{trace}\,(\underline{R}) = -1$ so that $r_0 = 0$, then $R_{jk} = 2r_j r_k - \delta_{jk}$ and we find $r_i^2 = (R_{\underline{ii}} + 1)/2$ so that for $\mathrm{trace}\,(\underline{R}) = -1$ we have a non–vanishing

$$r_m^+ = +\sqrt{\frac{R_{\underline{mm}} + 1}{2}} \quad , \tag{2.31}$$

for some $m \in \{1, 2, 3\}$. Here underlined indices indicate that they are not subject to contraction. We then obtain

$$r_i^+ = \frac{R_{\underline{m}i}}{2r_{\underline{m}}^+} \quad , i \neq m \quad . \tag{2.32}$$

Therefore for every $\underline{R} \in \mathbf{SO(3)}$ there is a $\bar{r} \in \mathbf{S}_{\mathbb{H}}$.$\square$

Recall that $\bar{r}^- = -\bar{r}^+$ is a also solution of $\underline{R} = \underline{F}(\bar{r})$. Moreover we find that if $\mathrm{trace}\,(\underline{R}) = -1$ the numerator of equation (2.30) vanishes as well as the denominator so that the singularity is possibly manageable. We show now that $\vec{r}$ is always an eigenvector with eigenvalue 1 of $\underline{R}$ so that the singularity is indeed manageable.

Theorem 2.4 *Let $\bar{r} \equiv (\cos\frac{\psi}{2}, \sin\frac{\psi}{2}\hat{r}) \in \mathbf{S}_{\mathbb{H}}$ and $\underline{R} = \underline{F}(\bar{r})$, then $\underline{R}$ describes a rotation around $\hat{r}$ by the angle $+\psi$.*

In the trivial case of $\sin\frac{\psi}{2} = 0$ we have $\underline{R} = \underline{1}$ and there is nothing to show. If $\psi \neq 0 \mod 2\pi$ then $\vec{r} = \sin\frac{\psi}{2}\hat{r}$ is a non–zero vector and

$$\begin{aligned} R_{ij}r_j &= ((2r_0^2-1)\delta_{ij} + 2r_ir_j - 2r_0\epsilon_{ijk}r_k)\, r_j \\ &= ((2r_0^2-1) + 2\|\vec{r}\|^2)r_i = r_i \quad , \end{aligned} \tag{2.33}$$

so that $\underline{R}\hat{r} = \hat{r}$ and $\hat{r}$ is an eigenvector of $\underline{R}$ with eigenvalue 1. Now we choose two unit vectors $\hat{v}\perp\vec{r}$ and $\hat{r}\times\hat{v}$ so that $(\hat{r}, \hat{v}, \hat{r}\times\hat{v})$ is a right–handed orthonormal basis of $\mathbb{R}^3$ and obtain

$$\begin{aligned} \hat{v}\cdot(\underline{R}\hat{v}) &= v_i((2r_0^2-1)\delta_{ij} + 2r_ir_j - 2r_0\epsilon_{ijk}r_k)v_i \\ &= v_i((2r_0^2-1)v_i - 2r_0(\hat{v}\times\hat{r})_i) \\ &= 2r_0^2 - 1 = 2\cos\frac{\psi}{2} - 1 = \cos\psi \end{aligned} \tag{2.34a}$$

$$\begin{aligned} \hat{r}\times\hat{v}\cdot(\underline{R}\hat{v}) &= \frac{1}{\sin\frac{\psi}{2}}\epsilon_{ilm}r_lv_m((2r_0^2-1)\delta_{ij} + 2r_ir_j - 2r_0\epsilon_{ijk}r_k)v_i \\ &= \frac{-2r_0}{\sin\frac{\psi}{2}}(\delta_{lj}\delta_{mk} - \delta_{lk}\delta_{mj})r_lv_mv_jr_k \\ &= \frac{2r_0}{\sin\frac{\psi}{2}}\|\vec{r}\|^2 = 2\cos\frac{\psi}{2}\sin\frac{\psi}{2} = \sin\psi \quad . \end{aligned} \tag{2.34b}$$

Therefore each vector in the plane perpendicular to $\hat{r}$ is rotated by ψ. The theorem now follows from $(\hat{r}, \hat{v}, \hat{r}\times\hat{v})$ being a basis of $\mathbb{R}^3$ and the linearity of $\underline{R}$. □

In fact this also shows that the apparent singularity in equation (2.30) is manageable and that for every $\underline{R} \in \mathbf{SO(3)}$ we can find a $\bar{r} \in \mathbf{S}_{\mathbb{H}}$ by solving the eigenproblem for $\underline{R}$, diagonalising $\underline{R}$ in a right–handed system of eigenvectors and identifying the positive rotation angle from the eigenvalues $(1, e^{i\psi}, e^{-i\psi})$. The corresponding unit–quaternion is then just given by $(\cos\frac{\psi}{2}, \sin\frac{\psi}{2}\hat{r})$ or $-(\cos\frac{\psi}{2}, \sin\frac{\psi}{2}\hat{r})$, where $\hat{r}$ is the normalised eigenvector with eigenvalue 1. Degeneracy occurs in the case of the unit transformation $\underline{R} = \underline{1}$ where every $\vec{a} \in \mathbb{R}^3$ is an invariant of $\underline{R}$ but since the angle is zero we then obtain $\bar{r} = \pm(1,0,0,0)$. The case $\text{trace}\,(\underline{R}) = -1$ corresponds to $\psi = \pi$.

There is a nice geometrical interpretation of $\underline{R}$ seen as a function of the rotation axis $\hat{r}$ and the angle ψ. An arbitrary vector $\vec{v}$ can be decomposed into a vector $\hat{r}(\hat{r}\cdot\vec{v})$ parallel to $\hat{r}$ and a vector $\vec{v} - \hat{r}(\hat{r}\cdot\vec{v})$ perpendicular to $\hat{r}$. The parallel component is invariant under $\underline{R}$ and the perpendicular component is rotated by ψ in the plane spanned by $\vec{v} - \hat{r}(\hat{r}\cdot\vec{v})$ and $\hat{r}\times(\vec{v} - \hat{r}(\hat{r}\cdot\vec{v})) = \hat{r}\times\vec{v}$. Therefore $\vec{v}$ is transformed by $\underline{R}$ into

$$\vec{v}' = \hat{r}(\hat{r}\cdot\vec{v}) + (\vec{v} - \hat{r}(\hat{r}\cdot\vec{v}))\cos\psi + \hat{r}\times\vec{v}\sin\psi \quad . \tag{2.35}$$

Then by introducing $r_0 = \cos\frac{\psi}{2}$ and $\vec{r} = \sin\frac{\psi}{2}\hat{r}$ one arrives at definition 2.4 rather naturally.

Theorem 2.5 *$\underline{F}$ as from definition 2.4 is a group homomorphism, in other words for $\bar{a}, \bar{b} \in \mathbf{S}_{\mathbb{H}}$*

$$\underline{F}(\bar{a}\bar{b}) = \underline{F}(\bar{a})\,\underline{F}(\bar{b}) \tag{2.36}$$

We define $\underline{A} \equiv \underline{F}(\bar{a})$, $\underline{B} \equiv \underline{F}(\bar{b})$, $f_a = (2a_0^2 - 1)$, $f_b = (2b_0^2 - 1)$ and $c_0 = a_0b_0 - \vec{a}\cdot\vec{b}$. It suffices to show that $\text{trace}\,(\underline{A}\,\underline{B}) = 4c_0^2 - 1$ and $\epsilon_{lij}A_{ik}B_{kj} = -4c_0(a_0b_l + b_la_0 + (\vec{a}\times\vec{b})_l)$.

$$\begin{aligned} A_{ik}B_{kj} &= (f_a\delta_{ik} + 2a_ia_k - 2a_0\epsilon_{ikl}a_l)(f_b\delta_{kj} + 2b_kb_j - 2b_0\epsilon_{kjm}b_m) \\ &= (f_af_b - 4a_0b_0\vec{a}\cdot\vec{b})\delta_{ij} + 2f_ab_ib_j + 2f_ba_ia_j + 4\vec{a}\cdot\vec{b}a_ib_j + 4a_0b_0a_ib_j \\ &\quad + 4a_0(\vec{a}\times\vec{b})_ib_j + 4b_0a_i(\vec{a}\times\vec{b})_j - 2a_0f_b\epsilon_{ijl}a_l - 2b_0f_a\epsilon_{ijl}b_l \end{aligned} \tag{2.37}$$

Therefore by using the anti–symmetry of the Levi–Civita tensor we obtain

$$\begin{aligned}\mathrm{trace}\,(\underline{A}\,\underline{B}) &= (f_a f_b - 4a_0b_0\vec{a}\cdot\vec{b})\,\mathrm{trace}\,(\underline{\delta}) + 2f_a\|\vec{b}\|^2 + 2f_b\|\vec{a}\|^2 + 4(\vec{a}\cdot\vec{b})^2 + 4a_0b_0\vec{a}\cdot\vec{b} \\ &= 3\left((2a_0^2-1)(2b_0^2-1) - 4a_0b_0\vec{a}\cdot\vec{b}\right) + 2(2a_0^2-1)(1-b_0^2) + 2(2b_0^2-1)(1-a_0^2) \\ &\quad +4a_0b_0\vec{a}\cdot\vec{b} + 4(\vec{a}\cdot\vec{b})^2 \\ &= 4(a_0b_0 - \vec{a}\cdot\vec{b})^2 - 1 \equiv 4c_0^2 - 1 \quad , \end{aligned} \tag{2.38}$$

and

$$\begin{aligned}\epsilon_{lij}A_{ik}B_{kj} &= -4(a_0b_0 - \vec{a}\cdot\vec{b})(\vec{a}\times\vec{b})_l \\ &\quad +4a_0\,\epsilon_{lij}\,\epsilon_{ikn}\,a_kb_nb_j + 4b_0\,\epsilon_{lij}\,\epsilon_{jkn}\,a_ia_kb_n - 4a_0f_ba_l - 4b_0f_ab_l \\ &= -4c_0(\vec{a}\times\vec{b})_l \\ &\quad +4a_0(\vec{a}\cdot\vec{b}b_l - \|\vec{b}\|^2a_l) + 4b_0(\vec{a}\cdot\vec{b}b_l - \|\vec{a}\|^2b_l) - (8a_0b_0^2 - 4a_0)a_l - (8b_0a_0^2 - 4b_0)b_l \\ &= -4c_0(a_0b_l + b_la_0 + (\vec{a}\times\vec{b})_l) \quad . \end{aligned} \tag{2.39}$$

□

Note that $\underline{F}$ seen as $\mathbf{S}_{\mathbb{H}} \to \mathbf{GL}(\mathbb{R}^3)$ is a representation of $\mathbf{S}_{\mathbb{H}}$ on $\mathbb{R}^3$. It is certainly not faithful since $\underline{F}(\bar{r}) = \underline{F}(-\bar{r})$ but it is an irreducible representation since the only subspaces of $\mathbb{R}^3$ which are invariant under the $\mathbf{SO(3)}$ are $\{\vec{0}\}$ and $\mathbb{R}^3$.

We will now derive an equation of motion for the spin transport map in quaternion notation [GH96]. We start from

$$\mathrm{D}_\theta\, R_{ij} = \epsilon_{ilk}\Omega_l R_{kj} \quad , \tag{2.40}$$

and by using (2.28), (2.29) and the convention ($\underline{R} \leftrightarrow \bar{r}$) from definition 2.4 we find

$$\mathrm{trace}\,(\mathrm{D}_\theta\,\underline{R}) = \epsilon_{ilk}\,\Omega_l\,R_{ki} = -2r_0\epsilon_{lki}\,\epsilon_{nki}\,\Omega_l\,r_n = -4r_0(\vec{\Omega}\cdot\vec{r}) \tag{2.41a}$$

$$\begin{aligned}\epsilon_{nij}\,\mathrm{D}_\theta\,R_{ij} &= -\epsilon_{inj}\,\epsilon_{ilk}\,\Omega_l\,R_{kj} \\ &= (\delta_{nk}\delta_{jl} - \delta_{nl}\delta_{jk})\Omega_l\,R_{kj} \\ &= R_{nl}\,\Omega_l - \Omega_n\ \mathrm{trace}\,(\underline{R}) \\ &= ((2r_0^2-1)\delta_{nl} + 2r_n\,r_l - 2r_0\,\epsilon_{nlk}\,r_k)\Omega_l - \Omega_n\,(4r_0^2-1) \\ &= -4r_0^2\,\Omega_n + 2(1-\|\vec{r}\|^2)\Omega_n + 2(\vec{\Omega}\cdot\vec{r})r_n - 2r_0\epsilon_{nlk}\,\Omega_l\,r_k \\ &= -2r_0^2\,\Omega_n + 2(\vec{\Omega}\cdot\vec{r})r_n - 2r_0\epsilon_{nlk}\,\Omega_l\,r_k \quad . \end{aligned} \tag{2.41b}$$

Then we take the derivatives w.r.t. θ of the trace and the contraction of $\underline{R}$ with the Levi–Civita tensor according to equations (2.28) and (2.29)

$$\mathrm{D}_\theta\ \mathrm{trace}\,(\underline{R}) = 8r_0\mathrm{D}_\theta\,r_0 \tag{2.42a}$$

$$\mathrm{D}_\theta\,\epsilon_{nij}R_{ij} = -4(r_n\mathrm{D}_\theta\,r_0 + r_0\mathrm{D}_\theta\,r_n) \quad . \tag{2.42b}$$

Comparing (2.41a) with (2.42a) and (2.41b) with (2.42b) we have to distinguish between two cases : $r_0 \neq 0$ and $r_0 = 0$. If $r_0 \neq 0$ we immediately obtain

$$\mathrm{D}_\theta\,r_0 = \frac{\mathrm{D}_\theta\ \mathrm{trace}\,(\underline{R})}{8r_0} = -\frac{1}{2}\vec{\Omega}\cdot\vec{r} \tag{2.43a}$$

$$\mathrm{D}_\theta\,r_n = \frac{\epsilon_{nij}\ \mathrm{D}_\theta\,R_{ij} + 4r_n\mathrm{D}_\theta\,r_0}{-4r_0} = \frac{1}{2}(r_0\Omega_n + (\vec{\Omega}\times\vec{r})_n) \quad . \tag{2.43b}$$

If $r_0 = 0$ we obtain from (2.41b) and (2.42b)

$$-4r_n\mathrm{D}_\theta\,r_0 = \epsilon_{nij}\mathrm{D}_\theta\,R_{ij} = 2(\vec{\Omega}\cdot\vec{r})r_n \quad , \tag{2.44}$$

for all $1 \leq n \leq 3$. There is at least one $1 \leq k \leq 3$ with $r_k \neq 0$ and hence we find again equation (2.43a). Moreover

$$\mathrm{D}_\theta\, R_{ij}\big|_{r_0=0} = 2r_i \mathrm{D}_\theta\, r_j + 2r_j \mathrm{D}_\theta\, r_i - 2\epsilon_{ijk}\, r_k \mathrm{D}_\theta\, r_0 \quad . \tag{2.45}$$

Therefore we find with $1 = r_0^2 + \|\vec{r}\|^2 = \|\vec{r}\|^2$ and $0 = r_0 \mathrm{D}_\theta\, r_0 + r_i \mathrm{D}_\theta\, r_i = r_i \mathrm{D}_\theta\, r_i$

$$r_j \mathrm{D}_\theta\, R_{ij}\big|_{r_0=0} = 2\mathrm{D}_\theta\, r_i \tag{2.46}$$

Using equation (2.40) and the fact that $\vec{r}$ is an eigenvector of $\underline{R}$ with eigenvalue 1, we obtain

$$r_j \mathrm{D}_\theta\, R_{ij}\big|_{r_0=0} = \epsilon_{ikl}\Omega_k R_{lj} r_j = \epsilon_{ikl}\Omega_k r_l = (\vec{\Omega} \times \vec{r})_i \quad . \tag{2.47}$$

We equate the right hand sides of (2.46) and (2.47) and adding $0 = r_0\vec{\Omega}$ we have reproduced equation (2.43b) in the case $r_0 = 0$. Finally we can rewrite equations (2.43a) and (2.43b) in terms of 4–vectors and obtain

$$\mathrm{D}_\theta\, \bar{r} = \underline{\Omega}_{4\times 4}\bar{r} \quad , \quad \underline{\Omega}_{4\times 4} \equiv \frac{1}{2}\begin{pmatrix} 0 & -\Omega_1 & -\Omega_2 & -\Omega_3 \\ +\Omega_1 & 0 & -\Omega_3 & +\Omega_2 \\ +\Omega_2 & +\Omega_3 & 0 & -\Omega_1 \\ +\Omega_3 & -\Omega_2 & +\Omega_1 & 0 \end{pmatrix} \tag{2.48}$$

independently of the value of r_0. We have explicitly constructed an EOM for $\bar{r}$ that leads to a T–BMT equation for $\underline{F}(\bar{r})$ and have therefore proved the

Theorem 2.6 *If $\bar{r}(\theta)$ is a solution of equation (2.48) with initial conditions $\bar{r}(0) = \bar{1}$, then $\underline{R}(\theta) \equiv \underline{F}(\bar{r}(\theta))$ is a solution of $\mathrm{D}_\theta\, \underline{R} = \underline{\Omega}\,\underline{R}$ with initial conditions $\underline{R}(0) = \underline{1}$.*

The theorems 2.2 to 2.6 show that the description of classical spin motion via unit–quaternions is equivalent to the use of $\mathbf{SO(3)}$ matrices in the sense that every quaternion has an equivalent $\mathbf{SO(3)}$ matrix and that the quaternionic product is compatible with matrix multiplication. We will later see that the usage of unit–quaternions is indeed much simpler for analytical and numerical purposes. As an application we will now give explicit formulae for a rotation that transforms an arbitrary unit vector $\hat{a}$ into an other arbitrary unit vector $\hat{b}$, the group commutator and the similarity transform. For $|\hat{a}\cdot\hat{b}| \neq 1$ the rotation that transforms $\hat{a}$ into $\hat{b}$ describes a rotation around $\hat{a}\times\hat{b}$ by the angle $\arccos \hat{a}\cdot\hat{b}$. Since $(\hat{a}, \hat{b}, \hat{a}\times\hat{b})$ is a right handed basis of $\mathbb{R}^3$ for $|\hat{a}\cdot\hat{b}| \neq 1$ the unit–quaternion must take the form

$$\bar{q}(\hat{b}, \hat{a}) \equiv \left(\cos\left(\frac{1}{2}\arccos \hat{a}\cdot\hat{b}\right), \sin\left(\frac{1}{2}\arccos \hat{a}\cdot\hat{b}\right)\frac{\hat{a}\times\hat{b}}{\|\hat{a}\times\hat{b}\|}\right) \quad . \tag{2.49}$$

It is easily verified that $\bar{b} = \bar{q}\bar{a}$.

The group commutator [WH90, HN91][1] $\bar{C}$ is defined so that $\bar{a}\bar{b} = \bar{C}(\bar{a}, \bar{b})\bar{b}\bar{a}$. Therefore

$$\bar{C}(\bar{a}, \bar{b}) = \bar{a}\bar{b}\bar{a}^{-1}\bar{b}^{-1} \quad . \tag{2.50}$$

Since $\bar{a}^{-1}\bar{b}^{-1} = (a_0 b_0 - \vec{a}\cdot\vec{b},\, -a_0\vec{b} - \vec{a}b_0 + \vec{a}\times\vec{b})$ and setting $\cos\Phi = \hat{a}\cdot\hat{b}$, $\bar{a} \equiv (\cos\frac{\alpha}{2}, \sin\frac{\alpha}{2}\hat{a})$ and $\bar{b} \equiv (\cos\frac{\beta}{2}, \sin\frac{\beta}{2}\hat{b})$ we obtain

$$\begin{aligned} C_0(\bar{a}, \bar{b}) &= a_0^2 b_0^2 + a_0^2\|\vec{b}\|^2 + b_0^2\|\vec{a}\|^2 + (\vec{a}\cdot\vec{b})^2 - \|\vec{a}\times\vec{b}\|^2 && \text{(2.51a)} \\ &= \cos^2\frac{\alpha}{2}\cos^2\frac{\beta}{2} + \cos^2\frac{\alpha}{2}\sin^2\frac{\beta}{2} + \sin^2\frac{\alpha}{2}\cos^2\frac{\beta}{2} + \sin^2\frac{\alpha}{2}\sin^2\frac{\beta}{2}\cos 2\Phi && \text{(2.51b)} \\ \frac{1}{2}\vec{C}(\bar{a}, \bar{b}) &= (a_0 b_0 - \vec{a}\cdot\vec{b})\vec{a}\times\vec{b} + (a_0\vec{b} + b_0\vec{a})\times(\vec{a}\times\vec{b}) && \text{(2.51c)} \\ &= \left(a_0\|\vec{b}\|^2 + b_0\vec{a}\cdot\vec{b}\right)\vec{a} - \left(b_0\|\vec{a}\|^2 + a_0\vec{a}\cdot\vec{b}\right)\vec{b} + (a_0 b_0 - \vec{a}\cdot\vec{b})\vec{a}\times\vec{b} && \text{(2.51d)} \end{aligned}$$

[1]Not to be confused with the Lie–algebra commutator $[a, b] = ab - ba$.

$$\begin{aligned} = \quad & \left(\cos\frac{\alpha}{2}\sin\frac{\alpha}{2}\sin^2\frac{\beta}{2} + \cos\frac{\beta}{2}\sin\frac{\beta}{2}\sin^2\frac{\alpha}{2}\cos\Phi\right)\hat{a} \\ & -\left(\cos\frac{\beta}{2}\sin\frac{\beta}{2}\sin^2\frac{\alpha}{2} + \cos\frac{\alpha}{2}\sin\frac{\alpha}{2}\sin^2\frac{\beta}{2}\cos\Phi\right)\hat{b} \\ & +\sin\frac{\alpha}{2}\sin\frac{\beta}{2}\left(\cos\frac{\alpha}{2}\cos\frac{\beta}{2} - \sin\frac{\alpha}{2}\sin\frac{\beta}{2}\cos\Phi\right)\hat{a}\times\hat{b} \quad . \end{aligned} \tag{2.51e}$$

One easily verifies that $\bar{C}(\bar{a},\bar{b}) = \bar{1}$ for $\hat{a} = \pm\hat{b}$ which just reproduces the well known fact that plane rotations commute and which can already be seen from the definition of the quaternionic product (definition 2.3), since the only asymmetric term is the cross–product. In other words for arbitrary fixed $\hat{a}$ the parametrisation $\underline{F}(\cos\frac{\psi}{2}, \sin\frac{\psi}{2}\hat{a})$ defines a reducible representation of $\mathbf{SO(2)}$ on $\mathbb{R}^3$.

The similarity transform $\bar{T}_{\bar{a}}(\bar{b}) \equiv \bar{a}\bar{b}\bar{a}^{-1}$ of $\bar{b}$ for some given $\bar{a}$ is given by

$$\begin{aligned} T_{\bar{a},0}(\bar{b}) &= b_0 \\ \vec{T}_{\bar{a}}(\bar{b}) &= (a_0^2 - \|\vec{a}\|^2)\,\vec{b} + 2\vec{a}\cdot\vec{b}\,\vec{a} + 2a_0\,\vec{a}\times\vec{b} \\ &= \cos\alpha\,\sin\frac{\beta}{2}\,\hat{b} + 2\sin^2\frac{\alpha}{2}\sin\frac{\beta}{2}\cos\Phi\,\hat{a} + \sin\alpha\,\sin\frac{\beta}{2}\,\hat{a}\times\hat{b} \quad . \end{aligned} \tag{2.52}$$

Of course since the plane rotations commute, we expect $\bar{T}_{\bar{a}}(\bar{b}) = \bar{b}$ for $\hat{a} = \pm\hat{b}$ which immediately follows from equation (2.52) by setting $\hat{a}\cos\Phi \equiv \hat{b}$ and using the identity $\cos\alpha = \cos^2\frac{\alpha}{2} - \sin^2\frac{\alpha}{2}$.

Another representation of spins, inherited from quantum mechanics is the description by spinors $\check{s} \in \mathcal{S}_{\mathbb{C}} \equiv \{\check{x} \in \mathbb{C}^2 \,:\, |x_1|^2 + |x_2|^2 = 1\}$. The action of a rotation on a spinor is a transformation by a $\mathbf{SU(2)}$ matrix. The *special unitary group of complex* 2×2 *matrices*, $\mathbf{SU(2)}$ is the set of regular matrices $\underline{r} \in \mathbb{C}^{2\times 2}$ which fulfil $\underline{r}^\dagger\,\underline{r} = \underline{r}\,\underline{r}^\dagger = \underline{1}$ and $\det(\underline{r}) = +1$, where † signifies the hermitian conjugate. These matrices can be parametrised as

$$\underline{r} \equiv \begin{pmatrix} g & h \\ -h^* & g^* \end{pmatrix} \quad , \tag{2.53}$$

with $g, h \in \mathbb{C}$ and $|g|^2 + |h|^2 = 1$. The corresponding Lie algebra [HN91, WH90] is the algebra of anti–hermitian traceless matrices $\mathbf{su(2)} \equiv \{\,\underline{m} \in \mathbb{C}^2\,;\ \underline{m}^\dagger = -\,\underline{m},\ \mathrm{trace}\,(\,\underline{m}) = 0\}$. If we set

$$\underline{m} \equiv \begin{pmatrix} a & b \\ c & d \end{pmatrix} \in \mathbf{su(2)} \quad , \tag{2.54}$$

it is clear that $\Re a = \Re d = 0$, $\Im a = -\Im d$, $\Re b = -\Re c$ and $\Im b = \Im c$. Therefore we can write $\mathbf{su(2)} = i\mathbb{R}\underline{\sigma}_x + i\mathbb{R}\underline{\sigma}_y + i\mathbb{R}\underline{\sigma}_z = i\mathbb{R}\mathcal{S}_2(\mathbb{R})\cdot\vec{\underline{\sigma}}$, with the Pauli matrices and the "3–vector" of the Pauli matrices

$$\underline{\sigma}_x \equiv \begin{pmatrix} 0 & -i \\ +i & 0 \end{pmatrix} \,,\ \underline{\sigma}_y \equiv \begin{pmatrix} +1 & 0 \\ 0 & -1 \end{pmatrix} \,,\ \underline{\sigma}_z \equiv \begin{pmatrix} 0 & 1 \\ 1 & 0 \end{pmatrix} \,,\ \vec{\underline{\sigma}} \equiv (\underline{\sigma}_x, \underline{\sigma}_y, \underline{\sigma}_z) \quad . \tag{2.55}$$

In other words a matrix representation of any element $\underline{m}$ of $\mathbf{su(2)}$ can be written as $\underline{m} = -i\phi/2\,\hat{m}\cdot\vec{\underline{\sigma}}$ with $\phi \in \mathbb{R}$ and $\hat{m} \in \mathcal{S}_2(\mathbb{R})$. Here we have chosen an indexing of the Pauli matrices for convenience that differs from the usual one by a cyclic permutation $((x,y,z) \to (y,z,x))$. The Pauli matrices have the following properties

$$\underline{\sigma}_i^\dagger = \underline{\sigma}_i\,, \quad \forall i \in \{x,y,z\} \quad \text{(hermiticity)} \tag{2.56a}$$

$$\mathrm{trace}\,(\,\underline{\sigma}_i) = 0\,, \quad \forall i \in \{x,y,z\} \quad \text{(they are traceless)} \tag{2.56b}$$

$$\underline{\sigma}_i^2 = \underline{1}\,, \quad \forall i \in \{x,y,z\} \quad \text{(they are unipotent)} \tag{2.56c}$$

$$\{\,\underline{\sigma}_i,\,\underline{\sigma}_j\} = 0\,, \quad \forall i,j \in \{x,y,z\}, i \neq j \quad \text{(anti–commutativity)} \tag{2.56d}$$

$$
\begin{aligned}
[\underline{\sigma}_i, \underline{\sigma}_j] &= 2i\epsilon_{ijk}\,\underline{\sigma}_k \quad \text{(commutation relations)} && (2.56e)\\
\Rightarrow \underline{\sigma}_x\underline{\sigma}_y = -\underline{\sigma}_y\underline{\sigma}_x = i\underline{\sigma}_z \quad &, \quad \underline{\sigma}_y\underline{\sigma}_z = -\underline{\sigma}_z\underline{\sigma}_y = i\underline{\sigma}_x \;,\; \underline{\sigma}_z\underline{\sigma}_x = -\underline{\sigma}_x\underline{\sigma}_z = i\underline{\sigma}_y &&\\
(\vec{\underline{\sigma}}\cdot\vec{a})(\vec{\underline{\sigma}}\cdot\vec{b}) &= \underline{1}(\vec{a}\cdot\vec{b}) + i\vec{\underline{\sigma}}\cdot(\vec{a}\times\vec{b}) \;. && (2.56f)\\
\text{With}\quad \underline{\sigma}_+ \equiv \underline{\sigma}_z + i\underline{\sigma}_x \quad &, \quad \underline{\sigma}_- \equiv \underline{\sigma}_z - i\underline{\sigma}_x \;,\; \underline{P}_\pm \equiv \underline{\sigma}_\pm\,\underline{\sigma}_\mp &&\\
\text{and}\quad \check{u} = (1,0)^{\mathrm{T}} \quad &, \quad \check{d} = (0,1)^{\mathrm{T}} &&\\
\text{we have}\quad \underline{\sigma}_+\check{u} = \underline{\sigma}_-\check{d} = 0 \quad &, \quad \underline{\sigma}_+\check{d} = \check{u} \;,\; \underline{\sigma}_-\check{u} = \check{d} \;, && (2.56g)\\
\text{and}\quad \underline{P}_+\check{d} = \underline{P}_-\check{u} = 0 \quad &, \quad \underline{P}_+\check{u} = \check{u} \;,\; \underline{P}_-\check{d} = \check{d} \;. && (2.56h)
\end{aligned}
$$

Note already here that the property $(i\,\underline{\sigma_i})^2 = -\underline{1}$ relates the Pauli matrices to the base quaternions $(0,1,0,0)$, $(0,0,1,0)$ and $(0,0,0,1)$.

From the theory of Lie groups it is known that the matrix exponential restricted to a Lie algebra yields the corresponding group and that this mapping is surjective

$$
\begin{aligned}
\underline{m} \in \mathbf{su(2)} \quad &\Rightarrow \quad \exp\underline{m} \equiv \exp\left(-\frac{i}{2}\phi\vec{\underline{\sigma}}\cdot\hat{m}\right) \in \mathbf{SU(2)} && (2.57a)\\
\underline{r} \in \mathbf{SU(2)} \quad &\Rightarrow \quad \exists\,\underline{m} \in \mathbf{su(2)} \;:\; \exp(\underline{m}) = \underline{r} \quad . && (2.57b)
\end{aligned}
$$

Using equation (2.56f) with $\vec{a} = \vec{b} = \hat{m}$ leads to

$$
\begin{aligned}
\exp\left(-\frac{i}{2}\phi\vec{\underline{\sigma}}\cdot\hat{m}\right) &= \underline{1}\sum_{k=0}^{\infty}(-1)^k\frac{(\phi/2)^{2k}}{(2k)!} - i\vec{\underline{\sigma}}\cdot\hat{m}\sum_{k=0}^{\infty}(-1)^k\frac{(\phi/2)^{2k+1}}{(2k+1)!}\\
&= \underline{1}\cos\frac{\phi}{2} - i\vec{\underline{\sigma}}\cdot\hat{m}\sin\frac{\phi}{2} \equiv \underline{1}m_0 - i\vec{\underline{\sigma}}\cdot\vec{m} \quad . \qquad (2.58)
\end{aligned}
$$

Since $\left\|(\cos\frac{\phi}{2}, \sin\frac{\phi}{2}\hat{m})\right\| = 1$ we conclude that $\bar{m} \equiv (m_0, \vec{m})$ is a unit–quaternion. Therefore

Definition 2.5 *For all $\bar{r} \in \mathbf{S}_{\mathbb{H}}$ we define $\underline{f}: \mathbf{S}_{\mathbb{H}} \to \mathbf{SU(2)}$, $\bar{r} \mapsto \underline{f}(\bar{r})$ so that for $\underline{r} \equiv \underline{f}(\bar{r})$ we have*

$$
\underline{r} = \underline{1}r_0 - i\vec{\underline{\sigma}}\cdot\vec{r} = \begin{pmatrix} (r_0 - ir_2) & -(r_1 + ir_3) \\ (r_1 + ir_3)^* & (r_0 - ir_2)^* \end{pmatrix} \quad , \qquad (2.59)
$$

where the condition $|(r_0 - ir_2)|^2 + |(r_1 + ir_3)|^2 = 1$ directly follows from $\|\bar{r}\| = 1$.

By comparing equation (2.59) with equation (2.53) it becomes clear that $\underline{f}$ is one–to–one with

$$
\bar{f}^{-1}(\underline{r}) = (\Re a, -\Re b, -\Im a, -\Im b) \quad . \qquad (2.60)
$$

Applying again equation (2.56f) we obtain with $\bar{a} \equiv (\cos\frac{\alpha}{2}, \sin\frac{\alpha}{2}\hat{a})$ and $\bar{b} \equiv (\cos\frac{\beta}{2}, \sin\frac{\beta}{2}\hat{b})$

$$
\begin{aligned}
\underline{f}(\bar{a})\,\underline{f}(\bar{b}) &= \underline{1}\left(\cos\frac{\alpha}{2}\cos\frac{\beta}{2} - \sin\frac{\alpha}{2}\sin\frac{\beta}{2}\hat{a}\cdot\hat{b}\right) - i\vec{\underline{\sigma}}\cdot\left(\cos\frac{\alpha}{2}\hat{b} + \hat{a}\cos\frac{\beta}{2} + \sin\frac{\alpha}{2}\sin\frac{\beta}{2}\hat{a}\times\hat{b}\right)\\
&= \underline{f}(\bar{a}\bar{b}) \quad . \qquad (2.61)
\end{aligned}
$$

Therefore we have proved

Theorem 2.7 *The function $\underline{f}$ defined above is a group–isomorphism between* $\mathbf{SU(2)}$ *and* $\mathbf{S}_{\mathbb{H}}$.

Although $\mathbf{S}_{\mathbb{H}}$ and $\mathbf{SU(2)}$ are group–isomorphous they are *not* "identical". $\mathbf{SU(2)}$ is a classical matrix group, i.e. its elements are naturally related to linear maps on vector spaces. The unit–quaternions on their own do not imply any kind of linear maps. Nevertheless with the help of the functions $\underline{F}$ or $\underline{f}$ respectively, linear maps can be assigned to each unit–quaternion in a group homomorphous way.

A spinor $\check{s}$ can be written as $(\cos\rho\, e^{i\kappa}, \sin\rho\, e^{i\delta})$ where ρ, κ, δ are 3 arbitrary real numbers. A spin vector $\widehat{S} \equiv (\sin\alpha\cos\beta, \cos\alpha, \sin\alpha\sin\beta)$ on the other hand only has 2 degrees of freedom. The additional degree of freedom expresses the possibility of interference in quantum mechanics but is almost redundant in the classical description of spin motion. However in section 4.3 phase factors which are periodic functions of the orbital angles and which appear while propagating certain spinor *fields*, will play a role in the computation of the amplitude dependent spin tune . In the following we will occasionally use the notation $\check{s} \equiv (u, d) \equiv (u_R + iu_I, d_R + id_I)$ with $|u|^2 + |d|^2 = 1$

Definition 2.6 *For each spinor* $\check{s} \in \mathcal{S}_{\mathbb{C}}$ *we define* $\hat{G} : \mathcal{S}_{\mathbb{C}} \to \mathcal{S}_{\mathbb{R}}$, $\check{s} \mapsto \hat{G}(\check{s})$ *so that for* $\widehat{S} \equiv \hat{G}(\check{s})$ *we have*

$$\begin{aligned} \widehat{S} &= \check{s}^\dagger\, \underline{\vec{\sigma}}\, \check{s} \\ &\equiv \big(2\cos\rho\sin\rho\sin(\kappa-\delta),\ \cos^2\rho - \sin^2\rho,\ 2\cos\rho\sin\rho\cos(\kappa-\delta)\big) \\ &\equiv \big(2(u_R d_I - u_I d_R),\ |u|^2 - |d|^2,\ 2(u_R d_R + u_I d_I)\big) \quad . \end{aligned} \tag{2.62}$$

The norm of $\hat{G}(\check{x})$ is unity for $\|\check{x}\| = 1$ and $\hat{G}$ is a real quadratic form in the spinor components. Thus $\check{s}$ and $\check{s}e^{i\lambda}$ yield the same spin vector. We exercise the freedom to choose $u_R \equiv u \in [0, 1]$ and $u_I = 0$. Then $\widehat{S} = (2u\sqrt{1-u^2}\sin\delta, 2u^2 - 1, 2u\sqrt{1-u^2}\cos\delta)$ so that $u = \sqrt{(S_y + 1)/2}$ and $\delta = \arctan(S_x/S_z)$. Hence for each $\widehat{S} \in \mathcal{S}_{\mathbb{R}}$ we find a spinor $\check{s} = (u, \sqrt{1-u^2}e^{i\delta})$. Therefore we obtain

Lemma 2.1 $\hat{G}$ *is surjective.*

Moreover the function $\hat{G}$ is compatible with spin transport by $\mathbf{SO(3)}$ and spinor transport by $\mathbf{SU(2)}$ maps.

Theorem 2.8 *Let* $\bar{r}$ *be a unit quaternion, and* $\check{s}$ *be a spinor, then*

$$\underline{F}(\bar{r})\hat{G}(\check{s}) = \hat{G}(\,\underline{f}(\bar{r})\check{s}) \quad . \tag{2.63}$$

The proof is straightforward. We define $\underline{R} \equiv \underline{F}(\bar{r})$, $\underline{r} \equiv \underline{f}(\bar{r})$, $\widehat{S} \equiv (S_x, S_y, S_z) \equiv \hat{G}((u, d))$, $(S'_x, S'_y, S'_z) \equiv \underline{R}(S_x, S_y, S_z)$ and $\check{s}' \equiv (u', d') \equiv \underline{r}(u, d)$. Using equation (2.59) we find

$$\begin{aligned} u'_R &= u_R r_0 - d_R r_1 + u_I r_2 + d_I r_3 \quad , \quad u'_I = u_I r_0 - d_I r_1 - u_R r_2 - d_R r_3 \\ d'_R &= d_R r_0 + u_R r_1 - d_I r_2 + u_I r_3 \quad , \quad d'_I = d_I r_0 + u_I r_1 - d_R r_2 - u_R r_3 \quad . \end{aligned} \tag{2.64}$$

Then by applying the explicit $\mathbf{SO(3)}$–matrix from equation (2.27) to $(2(u_R d_I - u_I d_R), |u|^2 - |d|^2, 2(u_R d_R + u_I d_I))$ one can evaluate

$$\underline{R}\widehat{S} - \hat{G}(\check{s}') = (1 - \|\bar{r}\|^2)\widehat{S} = 0 \ . \tag{2.65}$$

□

Obviously the normalisation of $\check{s}$ and $\widehat{S}$ does not enter the proof. Hence the theorem can be extended to complex 2-vectors and real 3–vectors of arbitrary length. Note also that the isomorphy between $\mathbf{S}_{\mathbb{H}}$ and $\mathbf{SU(2)}$ together with the relation $\underline{R} \leftrightarrow \pm\bar{r}$ for all $\underline{R} \in \mathbf{SO(3)}$ and $\bar{r} \in \mathbf{S}_{\mathbb{H}}$ is a, perhaps unconventional, confirmation of the fact that the $\mathbf{SU(2)}$ covers the $\mathbf{SO(3)}$ twice.

We can make use of the isomorphism f that connects $\mathbf{S}_{\mathbb{H}}$ and $\mathbf{SU(2)}$ to derive the EOM for an $\mathbf{SU(2)}$ transport map. Writing

$$\underline{r} \equiv \begin{pmatrix} r_{11} & r_{12} \\ r_{21} & r_{22} \end{pmatrix} = \begin{pmatrix} q_0 - iq_2 & -q_1 - iq_3 \\ q_1 - iq_3 & q_0 + iq_2 \end{pmatrix} = \underline{f}(\bar{q}) \tag{2.66}$$

and

$$\bar{q} = \frac{1}{2}\left(r_{11} + r_{22} \ , \ r_{21} - r_{12} \ , \ i(r_{11} - r_{22}) \ , \ i(r_{12} + r_{21})\right) = \bar{f}^{-1}(\underline{r}) \quad , \tag{2.67}$$

we obtain

$$\mathrm{D}_\theta \, \underline{r} \;=\; \underline{f}(\underline{\Omega}_{4\times 4}\bar{f}^{-1}(\underline{r})) = \underline{\Omega}_{2\times 2}\,\underline{r} \tag{2.68a}$$

$$\text{with} \;\; \underline{\Omega}_{2\times 2} \;\equiv\; \frac{1}{2}\begin{pmatrix} -i\Omega_2 & -\Omega_1 - i\Omega_3 \\ \Omega_1 - i\Omega_3 & i\Omega_2 \end{pmatrix} = -\frac{i}{2}\,\underline{\vec{\sigma}}\cdot\vec{\Omega} \quad . \tag{2.68b}$$

In this section we have not only seen that from the classical point of view spin vectors and spinors as well as $\mathbf{SO(3)}$-,$\mathbf{SU(2)}$- and unit–quaternion maps are equivalent descriptions, but we have explicitly derived all the basic relations for describing spin motion in terms of these concepts. Furthermore we have derived the tools for switching from one representation of classical spin dynamics to the other whenever we like. In the following this will very often turn out to be beneficial since one or the other representation allows a more elegant access to the solution of particular problems. As we will see in the next section, unit–quaternions offer an especially simple opportunity for truncated power expansions w.r.t. arbitrary parameters and immediate regularisation, i.e. conservation of orthogonality.

Finally, a word about tracking codes for maps: The composition of two $\mathbf{SO(3)}$ maps consists of 9 scalar products of `REAL`[2] 3–vectors and therefore needs 18 `REAL+` and 27 `REAL*`. For the composition of two $\mathbf{SU(2)}$ maps 4 scalar products of `COMPLEX` 2–vectors are performed. One should not be misguided by the number of "only" 4 `COMPLEX+` and "only" 8 `COMPLEX*` since that means 24 `REAL+` and 32 `REAL*` in the end. The composition of two $\mathbf{S}_{\mathbb{H}}$ maps needs only 12 `REAL+` and 16 `REAL*` and is therefore twice as fast as naive explicit $\mathbf{SU(2)}$ tracking! Moreover the memory needed to store the $\mathbf{SO(3)}$ and $\mathbf{SU(2)}$ matrices is 9 respectively 8 `REAL` numbers per map in contrast to 4 `REAL`s for a unit–quaternion.

2.2.2 Approximations to the T–BMT flow

In general it is not possible to solve EOM 1) of definition 2.2 analytically for all orbital initial conditions $\vec{z}_i$. Therefore it is indispensable to find adequate approximations to the exact T–BMT flow that can be computed with reasonable effort. In this section we will derive, and comment on, various approximation schemes. In the preceding section we have seen that $\mathbf{SO(3)}$, $\mathbf{SU(2)}$ and $\mathbf{S}_{\mathbb{H}}$ maps are classically equivalent descriptions of the T–BMT flow. *Therefore in the next two subsections the symbol $\underline{R}$ means either the corresponding $\mathbf{SO(3)}$–map, the $\mathbf{SU(2)}$–map $\underline{r}$ or the unit–quaternion map $\bar{r}$. For the T-BMT driving term we use $\underline{\Omega}$ to mean $\underline{\Omega}_{3\times 3}$, $\underline{\Omega}_{2\times 2}$ or $\underline{\Omega}_{4\times 4}$ respectively. In a subsequent subsection we will stress the remarkable feature of the unit–quaternions that they can easily be "re–orthogonalised".*

Iterative computation of the flow

We assume that the T–BMT driving term in equation (2.8) along an orbital trajectory $\vec{\xi}(\vec{z}_i,\theta)$ that starts at $\vec{z}_i$, as well as the T–BMT flow can be expanded into a power series w.r.t. the initial orbital phase space point $\vec{z}_i$

$$\underline{\Omega}(\vec{z}_i,\theta) \equiv \underline{\Omega}_0(\theta) + \underline{\omega}(\vec{\xi}(\vec{z}_i,\theta),\theta) \equiv \underline{\Omega}_0(\theta) + \sum_{j=1}^{\infty}\underline{\omega}^{(j)}(\vec{z}_i;\theta) \tag{2.69}$$

[2] `REAL` and `COMPLEX` here are symbols for machine representations of *any* particularly chosen precision. `REAL+`, `COMPLEX+`, `REAL*` and `COMPLEX*` mean the machine operations for a `REAL`, or `COMPLEX` addition or multiplication respectively.

and

$$\underline{R}(\theta_f,\theta_i;\vec{z}_i) = \underline{R}_0(\theta_f,\theta_i)\left(\underline{1}+\sum_{j=1}^{\infty}\underline{B}^{(j)}(\theta_f,\theta_i;\vec{z}_i)\right) \equiv \underline{R}_0(\theta_f,\theta_i)\sum_{j=0}^{\infty}\underline{B}^{(j)}(\theta_f,\theta_i;\vec{z}_i) \quad , \tag{2.70}$$

where the $\underline{\omega}^{(j)}$ and $\underline{B}^{(j)}$ are homogeneous polynomials of order j in $\vec{z}_i$ and $\underline{R}_0$ is the flow on the design orbit with

$$\mathrm{D}_\theta\, \underline{R}_0(\theta,\theta_i) = \underline{\Omega}_0(\theta)\,\underline{R}_0(\theta,\theta_i) \quad , \quad \underline{R}_0(\theta_i,\theta_i) = \underline{1} \tag{2.71}$$

for $\theta_f \geq \theta_i$ and $\theta_f \geq \theta \geq \theta_i$. Note that $\underline{R}_0$ is orthogonal (unitary) but that the $\underline{B}^{(j)}$ as well as every truncation of the series in equation (2.70) for $j > 0$ are not! In an accelerator the $\vec{\Omega}_0$ is normally piecewise constant and thus $\underline{R}_0$ can easily be computed analytically. Inserting the power series for $\underline{\Omega}$ and $\underline{R}$ into the EOM 1) of definition 2.2 with $\theta > \theta_i$ and using equation (2.71) we obtain

$$\begin{aligned}
\mathrm{D}_\theta \sum_{j=0}^{\infty}\underline{B}^{(j)}(\theta,\theta_i;\vec{z}_i) &= \underline{R}_0^{-1}(\theta,\theta_i)\sum_{j=1}^{\infty}\underline{\omega}^{(j)}(\vec{z}_i;\theta)\,\underline{R}_0(\theta,\theta_i)\sum_{j=0}^{\infty}\underline{B}^{(j)}(\theta,\theta_i;\vec{z}_i)\\
&\equiv \sum_{j=1}^{\infty}\underline{W}^{(j)}(\vec{z}_i;\theta)\sum_{j=0}^{\infty}\underline{B}^{(j)}(\theta,\theta_i;\vec{z}_i) \quad ,
\end{aligned} \tag{2.72}$$

where in the last step we have transformed the $\underline{\omega}^{(j)}$ into the rotating frame defined by the design orbit flow $\underline{R}_0$. Assuming the convergence of both series in the product we compare the terms in equation (2.72) order by order and obtain the convolution

$$\underline{B}^{(n)}(\theta_f,\theta_i;\vec{z}_i) = \sum_{j=1}^{n}\int_{\theta_i}^{\theta_f}\underline{W}^{(j)}(\vec{z}_i,\theta)\,\underline{B}^{(n-j)}(\theta,\theta_i;\vec{z}_i)\,d\theta \quad . \tag{2.73}$$

Note that for the computation of $\underline{B}^{(n)}$ only the $\underline{B}^{(k)}$ of order lower than n are needed. This is often called the absence of *feed–down*. Therefore equation (2.73) replaces the often cumbersome direct integration of the EOM 1) of definition 2.2 by the iteration of quadratures — once the solution of equation (2.71) is known. Nevertheless if the series (2.70) is truncated, the need for restoring the orthogonality (unitarity) of $\underline{R}$ arises.

The approximation to leading powers in $G\gamma$

After application of transformation (2.17) with $\widehat{S} \to \underline{R}_0^{\mathrm{T}}\widehat{S}$ and $\underline{\Omega} \to \underline{W} = \underline{R}_0^{\mathrm{T}}\,\underline{\Omega}\,\underline{R}_0 + (\mathrm{D}_\theta\,\underline{R}_0^{\mathrm{T}})\,\underline{R}_0$ and assuming that the T–BMT driving term is Lipschitz–continuous, a solution can be found by the Picard–Lindelöf iteration scheme which can be rewritten as a θ–ordered exponential [SM86a, SM86b] analogous to the von Neumann expansion in quantum mechanics.

$$\begin{aligned}
\underline{R}(\theta_f,\theta_i;\vec{z}_i) &= \mathrm{T}\exp\left(\int_{\theta_i}^{\theta_f}\underline{W}(\vec{z}_i,\vartheta)d\vartheta\right)1\\
&\equiv \Bigg(\underline{1}+\int_{\theta_i}^{\theta_f}\underline{W}(\vec{z}_i;\vartheta)\,d\vartheta+\int_{\theta_i}^{\theta_f}\underline{W}(\vec{z}_i;\vartheta)\int_{\theta_i}^{\vartheta}\underline{W}(\vec{z}_i;\vartheta')\,d\vartheta'\,d\vartheta\\
&\quad +\int_{\theta_i}^{\theta_f}\underline{W}(\vec{z}_i;\vartheta)\int_{\theta_i}^{\vartheta}\underline{W}(\vec{z}_i;\vartheta')\int_{\theta_i}^{\vartheta'}\underline{W}(\vec{z}_i;\vartheta'')\,d\vartheta''\,d\vartheta'\,d\vartheta+\ldots\Bigg)1 \quad ,
\end{aligned} \tag{2.74}$$

where the trailing "1" is redundant in the case of $\mathbf{SO(3)}$ and $\mathbf{SU(2)}$ matrices but symbolises $\bar{1}$ in the case of unit–quaternion maps. We now recall remark 4) in section 2.1, and conclude that at high but finite energy the dominating part of $\underline{\Omega}$ is proportional to $G\gamma$. It can be factored out of $\underline{W}$ to give

$$\underline{W}(\vec{z}_i;\vartheta) \equiv G\gamma\,\underline{\mathfrak{w}}(\vec{z}_i;\vartheta) \equiv G\gamma\sum_{j=1}^{\infty}\underline{\mathfrak{w}}^{(j)}(\vec{z}_i;\vartheta) \quad , \tag{2.75}$$

where again the $\underline{\mathfrak{w}}^{(j)}$ are homogeneous polynomials in $\vec{z}_i$. Then by inserting the power expansion of $\underline{\mathfrak{w}}$ into equation (2.74) and arranging the terms w.r.t. the difference in the orders of $G\gamma$ and $\vec{z}_i$ we obtain

$$\underline{R}(\theta_f, \theta_i; \vec{z}_i) \;=\; \underline{1} + \sum_{k=1}^{\infty} \underline{\mathfrak{B}}^{(j)}(\theta_f, \theta_i; \vec{z}_i) \tag{2.76a}$$

$$\begin{aligned}\underline{\mathfrak{B}}^{(1)}(\theta_f, \theta_i; \vec{z}_i) \;\equiv\;& (G\gamma) \int_{\theta_i}^{\theta_f} \underline{\mathfrak{w}}^{(1)}\, d\vartheta + (G\gamma)^2 \int_{\theta_i}^{\theta_f} \underline{\mathfrak{w}}^{(1)} \int_{\theta_i}^{\vartheta} \underline{\mathfrak{w}}^{(1)}\, d\vartheta'\, d\vartheta \\ +\;& (G\gamma)^3 \int_{\theta_i}^{\theta_f} \underline{\mathfrak{w}}^{(1)} \int_{\theta_i}^{\vartheta} \underline{\mathfrak{w}}^{(1)} \int_{\theta_i}^{\vartheta'} \underline{\mathfrak{w}}^{(1)}\, d\vartheta''\, d\vartheta'\, d\vartheta + \ldots [O(G\gamma) = O(\vec{z}_i)]\end{aligned} \tag{2.76b}$$

$$\begin{aligned}\underline{\mathfrak{B}}^{(2)}(\theta_f, \theta_i; \vec{z}_i) \;\equiv\;& (G\gamma) \int_{\theta_i}^{\theta_f} \underline{\mathfrak{w}}^{(2)}\, d\vartheta + (G\gamma)^2 \left(\int_{\theta_i}^{\theta_f} \underline{\mathfrak{w}}^{(1)} \int_{\theta_i}^{\vartheta} \underline{\mathfrak{w}}^{(2)}\, d\vartheta'\, d\vartheta + \int_{\theta_i}^{\theta_f} \underline{\mathfrak{w}}^{(2)} \int_{\theta_i}^{\vartheta} \underline{\mathfrak{w}}^{(1)}\, d\vartheta'\, d\vartheta \right) \\ +\;& (G\gamma)^3 \left(\int_{\theta_i}^{\theta_f} \underline{\mathfrak{w}}^{(1)} \int_{\theta_i}^{\vartheta} \underline{\mathfrak{w}}^{(1)} \int_{\theta_i}^{\vartheta'} \underline{\mathfrak{w}}^{(2)}\, d\vartheta''\, d\vartheta'\, d\vartheta \right. \\ &+ \int_{\theta_i}^{\theta_f} \underline{\mathfrak{w}}^{(1)} \int_{\theta_i}^{\vartheta} \underline{\mathfrak{w}}^{(2)} \int_{\theta_i}^{\vartheta'} \underline{\mathfrak{w}}^{(1)}\, d\vartheta''\, d\vartheta'\, d\vartheta \\ &\left. + \int_{\theta_i}^{\theta_f} \underline{\mathfrak{w}}^{(2)} \int_{\theta_i}^{\vartheta} \underline{\mathfrak{w}}^{(1)} \int_{\theta_i}^{\vartheta'} \underline{\mathfrak{w}}^{(1)}\, d\vartheta''\, d\vartheta'\, d\vartheta \right) + \ldots [O(G\gamma) = O(\vec{z}_i) - 1]\end{aligned} \tag{2.76c}$$

$$\underline{\mathfrak{B}}^{(j)}(\theta_f, \theta_i; \vec{z}_i) \;\equiv\; \ldots [O(G\gamma) = O(\vec{z}_i) - j + 1] \tag{2.76d}$$

A more complete description of the computation of the $\underline{\mathfrak{B}}^{(j)}$ can be found in [SM86a, SM86b]. In the following we will call non–linear effects in the spin motion **kinetic**, in the sense that they are caused by the formal structure of the T–BMT equation, if they arise from multiple integration of linear $\vec{\omega}$. On the contrary we will call non–linear effects **dynamic**, in the sense that they are caused by the particular dependence of the T–BMT driving term $\vec{\omega}$ on $\vec{z}_i$, if they arise from single integration of higher order terms in $\vec{\omega}$.

Since $\|\vec{z}_i\|$ is considered to be a small quantity but $G\gamma$ is big at high energy the contributions from $\underline{\mathfrak{B}}^{(j)}$ decrease with j. Therefore at large enough energy and in every finite domain of phase space around the design trajectory ($\vec{z} = 0$), the "leading order in $G\gamma$" $\underline{\mathfrak{B}}^{(1)}$ which only contains combinations of $\underline{\mathfrak{w}}^{(1)}$ usually dominates the spin motion. Additionally if $\underline{\mathfrak{w}}^{(j)} \equiv 0$ for $j > k$ all the $\underline{\mathfrak{B}}^{(j)}$ with $j > k$ vanish identically and hence $\underline{R}_k \equiv \underline{1} + \sum_{j=1}^{k} \underline{\mathfrak{B}}^{(j)}$ is then an exact T–BMT solution. So in principle for an *arbitrary*[3] $\underline{W}(\vec{z}, \theta)$ one could try to find a fully orthogonal (unitary) approximation by truncating the power expansion at the linear term $\underline{W}^{(1)}(\vec{z}, \theta)$ and summing up $\underline{\mathfrak{B}}^{(1)}$ only. Since $\underline{\mathfrak{B}}^{(1)}$ contains only the linear part of $\underline{W}$ its non–linear behaviour is of purely kinetic nature. This approximation would reflect the mathematical structure of the system, i.e. orthogonality of the T–BMT flow, completely and the physical structure of the system, i.e. the explicit form of the spin trajectory as defined by the electromagnetic fields, with an accuracy that increases with the reference energy of the system. Unfortunately in general not even $\underline{\mathfrak{B}}^{(1)}$ can be computed exactly, since it is an infinite power series. Therefore the practical utility of this explicit expansion is quite limited. Nevertheless we have seen that at high energy the dominant contribution to *all* orders in $\vec{z}_i$ usually comes from iteration of $\vec{\omega}^{(1)}$ and *not* from inclusion of higher order terms in $\vec{\omega}$!

We note that for $G\gamma \to \infty$ the series for $\underline{\mathfrak{B}}^{(j)}$ diverges. This is not surprising because even for a simple system like $\mathrm{D}_\theta\, \widehat{S} = (0, G\gamma, 0) \times \widehat{S}$ which describes a uniform rotation around $\hat{y}$ with revolution "frequency" $G\gamma$ the limit $G\gamma \to \infty$ does *not* exist.

[3]Lipschitz–continuous of course.

The SPRINT approximation

The entire spin–orbit simulations for this work were carried out using the computer code SPRINT [HV01]. In a multi–turn tracking code violation of orthogonality would lead to an unwanted and unphysical blow–up or shrinking of the length of the spin vector. Therefore the crucial point in finding an approximation for the T–BMT flow is *not* the inclusion of higher orders in $\vec{z}_i$ but *re–orthogonalisation* of the map. The orthogonality or unitarity conditions for $\mathbf{SO(3)}$ or $\mathbf{SU(2)}$ maps read as $\underline{R}\,\underline{R}^{\mathrm{T}} = \underline{1}$, $\det(\underline{R}) = +1$ and $\underline{r}\,\underline{r}^{\dagger} = \underline{1}$, $\det(\underline{r}) = +1$ respectively whereas the condition for a unit–quaternion is simply $\|\bar{r}\| = 1$. In this subsection (!) $\bar{v}$ symbolises a real 4–vector representing an approximation of a unit–quaternion and $\bar{r}$ the corresponding unit–quaternion obtained by re–orthogonalisation. Once we are given the *truncated* power expansion

$$\bar{v}^{\leq n}(\theta_f, \theta_i; \vec{z}_i) = \sum_{i=0}^{n} \bar{v}^{(i)}(\theta_f, \theta_i; \vec{z}_i) \quad , \tag{2.77}$$

where the $\bar{v}^{(i)}(\theta_f, \theta_i; \vec{z})$ are homogeneous polynomials in $\vec{z}$, we can re–orthogonalise it to

$$\bar{r}^{\leq n}(\theta_f, \theta_i; \vec{z}_i) = \frac{\bar{v}^{\leq n}(\theta_f, \theta_i; \vec{z}_i)}{\|\bar{v}^{\leq n}(\theta_f, \theta_i; \vec{z}_i)\|} \quad , \tag{2.78}$$

provided that $\|\bar{v}\| \neq 0$. It has to be emphasised that this re–orthogonalisation method, although looking most natural, is *not* unique. Every re–orthogonalisation method is equivalent to finding an effective $\vec{\Omega}(\vec{z}_i, \theta_i, \theta_f) \equiv \mu\hat{a}$ for a given $\vec{z}_i$ which is treated as constant in $[\theta_i, \theta_f]$ so that $\bar{q} \equiv (\cos\frac{1}{2}\mu(\theta_f - \theta_i), \sin\frac{1}{2}\mu(\theta_f - \theta_i)\hat{a})$ is *"close"* in some sense to $\bar{v}^{\leq n}(\theta_f, \theta_i; \vec{z}_i)$. This problem of the *arbitrariness of* $\vec{\Omega}$ is similar to the *arbitrariness of the Hamiltonian* in the construction of higher order symplectic maps in orbital dynamics. In SPRINT the "closeness" condition is implemented by constructing a new unit–quaternion $\bar{r}'$ by choosing the rotation axis $\hat{r}'$ as $\hat{v} \equiv \vec{v}/\|\vec{v}\|$ and defining

$$\bar{r}' \equiv (c, s\hat{v}) \quad \text{with} \quad c \equiv \operatorname{sgn}(v_0)\,\cos\arctan\frac{\|\vec{v}\|}{v_0} \;,\; s \equiv \left|\sin\arctan\frac{\|\vec{v}\|}{v_0}\right| \quad . \tag{2.79}$$

The limits of $\hat{v}$, c and s for v_0 or $\vec{v} \to 0$ but with $\|\bar{v}\| \neq 0$ are

$$\lim_{\substack{v_0 \to \pm 0 \\ \vec{v} \neq \vec{0}}} c = 0 \;,\quad \lim_{\substack{v_0 \to \pm 0 \\ \vec{v} \neq \vec{0}}} s\hat{v} = \hat{v} \;,\quad \lim_{\substack{\vec{v} \to \vec{0} \\ v_0 \neq 0}} c = \operatorname{sgn}(v_0) = \pm 1 \;,\quad \lim_{\substack{\vec{v} \to \vec{0} \\ v_0 \neq 0}} s\hat{v} = \vec{0} \quad , \tag{2.80}$$

so that $\bar{r}'$ is well defined for $\|\bar{v}\| \neq 0$. This choice of re–orthogonalisation seems complicated but is actually equivalent to equation (2.78) since with $\alpha^2 \equiv \|\vec{v}\|^2/v_0^2$ we find

$$\frac{v_0}{\|\bar{v}\|} = \frac{\operatorname{sgn}(v_0)}{\sqrt{1+\alpha^2}} \quad = \quad \operatorname{sgn}(v_0)\,\cos\arctan\alpha \tag{2.81a}$$

$$\frac{\vec{v}}{\|\bar{v}\|} = \frac{|\alpha|}{\sqrt{1+\alpha^2}}\vec{v} \quad = \quad |\sin\arctan\alpha|\,\vec{v} \tag{2.81b}$$

even in the limits v_0, $\vec{v} \to 0$ but $\|\bar{v}\| \neq 0$. We define the deviation $\delta \equiv \|\bar{r} - \bar{v}\| = \|\bar{r} - \|\bar{v}\|\bar{r}\| = |1 - \|\bar{v}\|\,|$. In the case of $\bar{v}(\vec{z}_i) = \bar{r}_0 + \bar{\epsilon}(\vec{z}_i)$ with an exact unit–quaternion on the design orbit $\bar{r}_0$ and a given *small* 4–vector $\bar{\epsilon}$, δ is minimal if the scalar product of $\bar{\epsilon}$ and $\bar{r}_0$, seen as 4–vectors vanishes, i.e.

$$\delta = |1 - \|\bar{r}_0 + \bar{\epsilon}\|\,| = |\bar{r}_0 \cdot \bar{\epsilon}| + O(\|\bar{\epsilon}\|^2) \quad . \tag{2.82}$$

The method of re–orthogonalisation can be applied to quaternionic spin maps of any kind, i.e. one–turn maps (OTMs), transfer maps for single beam line elements, slices of beam line elements or lumped beam line elements. Given a partitioning of the interval $[0, 2\pi]$: $\{\theta_k | \theta_0 = 0, \theta_k < \theta_{k+1},$

$\theta_N = 2\pi, 0 \leq k \leq N\}$ where the θ_k are the effective boundaries of elements or slices of elements in the sharp cut–off (SCOFF) approximation and given the corresponding transfer maps

$$\bar{r}_k(\vec{z}_i) \equiv \bar{r}(\theta_k, \theta_{k-1}; \vec{z}_i) \quad , \quad \vec{T}_k(\vec{z}_i) \equiv \vec{T}(\theta_k, \theta_{k-1}, \vec{z}_i) \tag{2.83}$$

for spin and orbit (see definition A.2) respectively, slice–by–slice forward tracking means

$$\vec{T}(\theta_k, \theta_j, \vec{z}_i)|_{k>j} = \left(\bigodot_{l=j+1}^{k} \vec{T}_l \right)(\vec{z}_i) \quad , \quad \vec{T}(\theta_j, \theta_j, \vec{z}_i) \equiv \vec{z}_i \tag{2.84a}$$

$$\bar{r}(\theta_k, \theta_j; \vec{z}_i)|_{k>j} = \bigodot_{l=j+1}^{k} \bar{r}_l(\vec{T}(\theta_{l-1}, \theta_j, \vec{z}_i)) \quad , \quad \bar{r}(\theta_j, \theta_j; \vec{z}_i) \equiv \bar{1} \quad , \tag{2.84b}$$

where $\bigodot$ denotes map composition in the case of orbital maps and quaternionic (non–commutative) multiplication in the case of spin maps. The transformation of the orbital coordinates and the unit–quaternion from slice $k-1$ to the end of slice k is simply

$$\begin{pmatrix} \vec{z}_f \\ \bar{r}_f \end{pmatrix} = \begin{pmatrix} \vec{T}_k(\vec{z}_i) \\ \bar{r}_k(\vec{z}_i)\bar{r}_i \end{pmatrix} \quad . \tag{2.85}$$

The one–turn maps are

$$\vec{T}(\theta_k, \vec{z}_i) = \vec{T}(\theta_k, \theta_0, \vec{T}(\theta_N, \theta_k, \vec{z}_i)) \tag{2.86a}$$

$$\bar{r}(\theta_k; \vec{z}_i) = \bar{r}(\theta_k, \theta_0; \vec{T}(\theta_N, \theta_k, \vec{z}_i))\, \bar{r}(\theta_N, \theta_k; \vec{z}_i) \quad . \tag{2.86b}$$

In SPRINT slice–by–slice tracking is implemented to first order in $\vec{z}_i$ for $\bar{v}$ and $\vec{z}$.

$$\bar{v}_k(\vec{z}_i) = \bar{\Gamma}_k^{(0)} + \underline{\Gamma}_k^{(1)} \vec{z}_i \quad , \quad \bar{r}_k(\vec{z}_i) = \left.\frac{\bar{v}_k(\vec{z}_i)}{\|\bar{v}_k(\vec{z}_i)\|}\right|_{\|\bar{v}\| \neq 0} \quad , \quad \vec{T}_k(\vec{z}_i) = \underline{T}_k \vec{z}_i \quad . \tag{2.87}$$

The SPRINT method is actually *similar* to a discrete version of the leading power $G\gamma$ approximation of equation (2.76b). If we transformed into the system rotating with $\underline{R}_0$, which is *not* done in SPRINT, then $\bar{\Gamma}_l^{(0)} + \underline{\Gamma}_l^{(1)} \vec{z}(\theta_l)$ would be replaced by $\bar{1} + \bar{\mathfrak{b}}_l^{(1,1)}$ where $\bar{\mathfrak{b}}_l^{(1,1)} \equiv \int_{\theta_l}^{\theta_{l+1}} G\gamma \underline{\mathfrak{w}}_{4\times 4}^{(1)}(\theta; \vec{z}(\theta_l))\, d\theta\, \bar{1}$. Here $\underline{\mathfrak{w}}_{4\times 4}^{(1)}(\theta; \vec{z}(\theta_l))$ is the contribution of the transformed $\underline{W}_{4\times 4}$ that depends linearly on $\vec{z}(\theta)$ in the interval $[\theta_{l+1}, \theta_l]$, $\vec{z}(\theta)$ is the linear orbit and $\bar{\mathfrak{b}}^{(1,1)}$ corresponds to the first term in equation (2.76b) which is linear in $G\gamma$. See [CW98] for explicit formulae. Then we would replace the integrals in equation (2.76b) by sums over intermediate θ_l. The resulting not yet re–orthogonalised quaternion in the rotating frame would be

$$\begin{aligned}
\bar{v}^{(1,\leq k-j)}(\theta_k, \theta_j) &= \bar{1} + \sum_{l=j}^{k-1} \bar{\mathfrak{b}}_l^{(1,1)} + \sum_{l=j}^{k-1} \bar{\mathfrak{b}}_l^{(1,1)} \sum_{l'=j}^{l-1} \bar{\mathfrak{b}}_{l'}^{(1,1)} + \sum_{l=j}^{k-1} \bar{\mathfrak{b}}_l^{(1,1)} \sum_{l'=j}^{l-1} \bar{\mathfrak{b}}_{l'}^{(1,1)} \sum_{l''=j}^{l'-1} \bar{\mathfrak{b}}_{l''}^{(1,1)} + \cdots \\
&= \left(\bar{1} + \bar{\mathfrak{b}}_{k-1}^{(1,1)}\right) \left(\bar{1} + \sum_{l=j}^{k-2} \bar{\mathfrak{b}}_l^{(1,1)} + \sum_{l=j}^{k-2} \bar{\mathfrak{b}}_l^{(1,1)} \sum_{l'=j}^{l-1} \bar{\mathfrak{b}}_{l'}^{(1,1)} + \sum_{l=j}^{k-2} \bar{\mathfrak{b}}_l^{(1,1)} \sum_{l'=j}^{l-1} \bar{\mathfrak{b}}_{l'}^{(1,1)} \sum_{l''=j}^{l'-1} \bar{\mathfrak{b}}_{l''}^{(1,1)} + \cdots \right) \\
&\cdots \\
&= \bigodot_{l=j}^{k-1} \left(\bar{1} + \bar{\mathfrak{b}}_l^{(1,1)}\right) \quad ,
\end{aligned} \tag{2.88}$$

where we omitted the initial phase space points $\vec{z}_l$ for brevity. In SPRINT the above algorithm is changed so that the on–orbit rotation is explicitly contained in the transfer maps, i.e. $\bar{1} + \bar{\mathfrak{b}}_l^{(1,1)} \to \bar{r}_l^{(0)}(\bar{1} +$

$\bar{\mathfrak{b}}_l^{(1,1)}$), and so that $\bar{r}_l^{(0)}(\bar{1} + \bar{\mathfrak{b}}_l^{(1,1)})$ is re–orthogonalised after each step instead of re–orthogonalising $\bar{v}^{(1,\leq k-j)}(\theta_k, \theta_j)$ at the end. Slice–by–slice tracking enables us to minimise the deviation δ by refining the slicing without changing the order of the per–slice approximation. In practice it turned out that generally for a ring like HERA–p one slice per element gives a reasonable accuracy. Note that the computing time used for tracking simulations is proportional to the number of slices in the chosen representation of the lattice. In an accelerator like HERA–p there are typically 2000 beam line elements in the lattice that contribute to $\vec{\omega}^{(1)}$, so that even without any slicing of elements the one–turn map $\bar{r}^{(1,\leq\approx 2000)}(\theta; \vec{z})$ as computed with `SPRINT` contains kinetic non–linearities up to about 2000-th order!

2.3 Spin perturbations

So far, approximate solutions to the T–BMT equation have been presented in general and somewhat abstract terms as, for example, in (2.76a). Now we will analyse spin motion along synchro–betatron orbits in more concrete terms and obtain formulae which are more explicit and suitable for physical interpretation and which thereby motivate further approximations.

The main purpose of the analysis of spin dynamics in accelerators is to find ways to achieve a steady state spin distribution on phase space with high polarisation. If accelerators only had vertical magnetic guide fields, i.e. from the horizontal main dipoles, then spins would precess around the vertical direction $\hat{y}$ independently of the beam energy and the position in phase space. Therefore the vertical spin component S_y would be conserved and the perpendicular component $\widehat{S}_\perp$ would be rotated $G\gamma$ times per revolution around $\hat{y}$. Real accelerators consist of various types of beam line elements — not only horizontal bends. In particular the vertical guide field is complemented by the radial magnetic field components from quadrupoles. With these additional fields the vertical component of a spin on an orbital trajectory with non–zero vertical amplitude is no longer strictly conserved. Moreover as we see from remarks 1 and 2 in section 2.1, with the high fields needed at high energy the conservation of S_y can be strongly violated.

Since they will be important in the following, we will now define two concepts of accelerator physics that classify the magnetic fields experienced on synchro–betatron trajectories in circular accelerators (rings).

Definition 2.7 (Flat ring) *A ring is called flat (planar), if the only magnetic fields experienced on the design orbit ($\vec{z} = \vec{0}$) are vertical. Thus in a flat ring tilted bends and solenoids are explicitly excluded.*

In a flat ring the reference trajectory has no torsion. Therefore the machine coordinates w.r.t. the comoving basis vectors [HR87, MB90, BH94a, GH94, GH99b, CW98] $\hat{x}$, $\hat{y}$ and $\hat{z}$ defined before equation (2.6) are identical to the normal, conormal and tangent vectors of the Frenet–Serret system [VW97]. Once vertical orbit perturbations are introduced a ring is *not* flat any more.

Definition 2.8 (Mid–plane symmetric ring) *A flat ring is called mid–plane symmetric, if in the SCOFF approximation, i.e. as long as fringe fields can be neglected, the magnetic fields in the curvilinear coordinate system [HR87, MB90, BH94a, GH94, GH99b, CW98] defined before equation (2.6) fulfil*

$$B_x(x, -y, \tau) = -B_x(x, y, \tau) \ , \quad B_y(x, -y, \tau) = +B_y(x, y, \tau) \ , \quad B_z(x, y, \tau) = 0 \ , \tag{2.89}$$

where (x, y, τ) are the spatial components of $\vec{z}$ defined in equation (2.6). Thus in a mid–plane symmetric ring, in addition to solenoids, all tilted elements, e.g. tilted bends, tilted quadrupoles, tilted sextupoles, tilted octupoles, etc., are excluded.

We note that Maxwell's equations require a longitudinal field component in the fringe fields of all beam line elements that contain transverse fields. Thus a ring can at most in the SCOFF approximation be mid–plane symmetric. Even if the ring were designed to be mid–plane symmetric, tilts of the quadrupoles, etc., would introduce skew components to the fields and destroy the mid–plane symmetry. In the following we will *always* neglect fringe fields and the effects of misalignments. In a mid–plane symmetric ring one can show [KB82] that if $\vec{z}(\theta) = (x, a, y, b, \tau, \delta)$ is a solution of the orbital EOM, then $\tilde{z}(\theta)$ with $\tilde{x} = x$, $\tilde{a} = a$, $\tilde{\tau} = \tau$ and $\tilde{\delta} = \delta$ but $\tilde{y} = -y$ and $\tilde{b} = -b$ is also a solution of the orbital EOM. The property of a ring, to be mid–plane symmetric or not, will turn out to be essential in understanding the spectrum of the spin–orbit resonances to be defined later. Note that the absence of flatness implies the absence of mid–plane symmetry. In general, rings are not necessarily flat[4] so that even on the design orbit $\widehat{S}_y$ is not conserved.

2.3.1 The $\hat{n}_0$–axis

In an unperturbed machine the design orbit ($\vec{z} \equiv \vec{0}$) is closed and thus the unit eigenvector $\hat{n}_0$ with eigenvalue 1 of the one–turn spin map (OTM) on the design orbit.

$$\underline{R}(\theta; \vec{0})\hat{n}_0(\theta) = \hat{n}_0(\theta) \quad , \tag{2.90}$$

which is sometimes called the *spin closed orbit*, is a periodic T–BMT solution so that

$$\underline{R}(\theta + n2\pi, \theta; \vec{0})\hat{n}_0(\theta) = \hat{n}_0(\theta) \quad , \quad \forall n \in \mathbb{Z} \quad . \tag{2.91}$$

The $\hat{n}_0$–axis depends on the azimuth, the reference energy E_0 and the geometry of the design orbit only. The $\hat{n}_0$–axis is unique modulo a factor ± 1 unless the spin OTM on the design orbit degenerates to $\underline{R} = \underline{1}$.

In the case of a flat ring we find $\hat{n}_0|_{\text{flat}} = \pm\hat{y}$ and by convention the sign is fixed to $\hat{n}_0|_{\text{flat}} = +\hat{y}$. The concept of the $\hat{n}_0$–axis can easily be generalised to rings with misaligned quadrupoles and a resulting distorted *closed orbit*. In this thesis we will in general neglect the effects of magnet misalignments and the resulting closed orbit distortion so that synchro–betatron motion will take place w.r.t. the (undistorted) design orbit unless explicit mention to the contrary is made. On the design orbit the projection $I_0 \equiv \widehat{S} \cdot \hat{n}_0$ is an invariant which approaches S_y in the limit of a flat ring. At an arbitrary point θ_0 in the ring we choose a right–handed coordinate system of column vectors $(\hat{l}_0(\theta_0), \hat{n}_0(\theta_0), \hat{m}_0(\theta_0))$ and by defining

$$\left(\hat{l}_0(\theta), \hat{n}_0(\theta), \hat{m}_0(\theta)\right) \equiv \underline{R}(\theta, \theta_0, \vec{0})\left(\hat{l}_0(\theta_0), \hat{n}_0(\theta_0), \hat{m}_0(\theta_0)\right) \tag{2.92}$$

we obtain a coordinate system built from T–BMT solutions. The coordinate vectors $\hat{l}_0$ and $\hat{m}_0$ are transformed by the OTM into

$$\underline{R}(\theta_0, \vec{0}) \left(\hat{l}_0(\theta_0), \hat{m}_0(\theta_0)\right) = \left(\hat{l}_0(\theta_0), \hat{m}_0(\theta_0)\right) \begin{pmatrix} \cos 2\pi\nu_0 & +\sin 2\pi\nu_0 \\ -\sin 2\pi\nu_0 & \cos 2\pi\nu_0 \end{pmatrix} \quad , \tag{2.93}$$

where ν_0 is computed from the eigenvalues $(e^{+i2\pi\nu_0}, e^{-i2\pi\nu_0}, 1)$ of $\underline{R}(\theta; \vec{0})$ so that a rotation by $+2\pi\nu_0$ means a mathematically positive rotation around $\hat{n}_0$. In this coordinate system a spin on the design orbit does not precess since the scalar products $(\hat{l}_0 \cdot \widehat{S}, \hat{n}_0 \cdot \widehat{S}, \hat{m}_0 \cdot \widehat{S})$ are invariants of motion. If $[\nu_0] \neq 0$, the coordinate system $(\hat{l}_0, \hat{n}_0, \hat{m}_0)$ is not 2π–periodic.

[4] e.g. HERA–p.

But we can now define a new *periodic* coordinate system $(\hat{l}(\theta), \hat{n}_0(\theta), \hat{m}(\theta)) = (\hat{l}(\theta+2\pi), \hat{n}_0(\theta+2\pi), \hat{m}(\theta+2\pi))$ by uniformly winding back the rotation around $\hat{n}_0$:

$$\begin{aligned} \underline{A}(\theta) &\equiv \begin{pmatrix} \cos\theta\nu_0 & 0 & -\sin\theta\nu_0 \\ 0 & 1 & 0 \\ \sin\theta\nu_0 & 0 & \cos\theta\nu_0 \end{pmatrix} \\ \left(\hat{l}(\theta), \hat{n}_0(\theta), \hat{m}(\theta)\right) &\equiv \underline{R}(\theta, \theta_0, \vec{0})\left(\hat{l}_0(\theta_0), \hat{n}_0(\theta_0), \hat{m}_0(\theta_0)\right)\underline{A}(\theta-\theta_0) \quad , \end{aligned} \tag{2.94}$$

where $\underline{R}$ acts on the column vectors of $(\hat{l}_0, \hat{n}_0, \hat{m}_0)$ and $\underline{A}^{\mathrm{T}}$ acts on the row vectors of $(\hat{l}_0, \hat{n}_0, \hat{m}_0)$. In this coordinate system a spin on the design orbit precesses uniformly with the *on–orbit spin tune* ν_0. Note that in order to preserve the periodicity of the coordinate frame we have the freedom to change ν_0 by an arbitrary integer. Thus only the fractional part $[\nu_0]$ is uniquely defined by the eigenvalues of $\underline{R}$ for fixed sign of $\hat{n}_0$. A rotation by $2\pi\nu_0$ around $\hat{n}_0$ is equivalent to a rotation by $-2\pi\nu_0$ around $-\hat{n}_0$. If we replace $\hat{n}_0$ with $-\hat{n}_0$ we have to replace $[\nu_0]$ with $1-[\nu_0]$. So with arbitrary sign of $\hat{n}_0$ we have ν_0 equivalent to ν_0+k and to $k-\nu_0$, $k \in \mathbb{Z}$. We already know that in a flat ring the spins on the design orbit precess $G\gamma$ times around $\hat{y}$ per revolution so that it is convenient to call $G\gamma$ the on–orbit spin tune of such a machine too. But we should always keep in mind that one can find a periodic frame in which $\nu_0 = [G\gamma]+k$ for an arbitrary $k \in \mathbb{Z}$. We will call the orthogonal matrix $\underline{N}_0(\theta) \equiv (\hat{l}(\theta), \hat{n}_0(\theta), \hat{m}(\theta))^{\mathrm{T}}$ the *on–orbit spin normal form transformation* since

$$\underline{R}(\theta_f, \theta_i, \vec{0}) = \underline{N}_0(\theta_f)^{\mathrm{T}}\underline{\tilde{R}}(\theta_f-\theta_i)\,\underline{N}_0(\theta_i) \tag{2.95}$$

expresses $\underline{R}$ in a particularly transparent form. Introducing the on–orbit spin action $I_0 \equiv \hat{n}_0(\theta_i)\cdot\widehat{S}_i$, the on–orbit initial spin phase $\Phi_0 \equiv \arctan\frac{\hat{m}(\theta_i)\cdot\widehat{S}_i}{\hat{l}(\theta_i)\cdot\widehat{S}_i}$ and $\Delta \equiv \theta_f - \theta_i$, we can write any T–BMT solution on the design orbit as

$$\widehat{S}(\theta;\theta_i,\widehat{S}_i,\vec{z}_i=\vec{0}) = \hat{n}_0(\theta)I_0 + \sqrt{1-I_0^2}\left(\hat{m}(\theta)\cos(\Delta\nu_0-\Phi_0) - \hat{l}(\theta)\sin(\Delta\nu_0-\Phi_0)\right) \ . \tag{2.96}$$

Some care has to be taken whenever the $I_0 = \pm 1$ since the relation $\widehat{S} \leftrightarrow (I_0, \Phi_0)$ becomes singular! In terms of $\hat{n}_0$ and ν_0, the unit quaternion for the on–orbit OTM is $\bar{r}_0 = (\cos 2\pi\nu_0, \hat{n}_0 \sin 2\pi\nu_0)$

2.3.2 The $\underline{G}$–matrix and resonance strengths

We will now allow particles to be off–orbit, i.e. have a non–vanishing orbital amplitude. This will lead to a perturbative ansatz for solving the T–BMT equation in a small domain around $\vec{z}=0$. Calculating in the spin coordinate systems $(\hat{l}_0, \hat{n}_0, \hat{m}_0)$ and $(\hat{l}, \hat{n}_0, \hat{m})$ for motion on a synchro–betatron trajectory we write

$$\widehat{S} = \tilde{\beta}\hat{l}_0 + S_n\hat{n}_0 + \tilde{\alpha}\hat{m}_0 \quad\Rightarrow\quad \mathrm{D}_\theta\,(\tilde{\beta}, S_n, \tilde{\alpha}) = \left(\vec{\Omega}-\vec{\Omega}_0\right)\times(\tilde{\beta}, S_n, \tilde{\alpha}) \tag{2.97a}$$

$$\widehat{S} = \beta\hat{l} + S_n\hat{n}_0 + \alpha\hat{m} \quad\Rightarrow\quad \mathrm{D}_\theta\,(\beta, S_n, \alpha) = \left(\vec{\Omega}-\vec{\Omega}_0+\nu_0\hat{n}_0\right)\times(\beta, S_n, \alpha) \ . \tag{2.97b}$$

Equation 2.97b can be rewritten using (2.17) with $\underline{A} = (\hat{l}, \hat{n}_0, \hat{m})^{\mathrm{T}} = \underline{N}_0$. We recall that $\vec{\Omega}-\vec{\Omega}_0 = \vec{\omega}$ and by introducing $\omega_l \equiv \hat{l}\cdot\vec{\omega}$, $\omega_n \equiv \hat{n}_0\cdot\vec{\omega}$ and $\omega_m \equiv \hat{m}\cdot\vec{\omega}$, the EOMs for the components are then

$$\begin{aligned} \mathrm{D}_\theta\,\alpha &= \hat{m}\cdot(\vec{\omega}+\nu_0\hat{n}_0)\times\widehat{S} \\ &= (-\beta\hat{n}_0 + S_n\hat{l})\cdot(\vec{\omega}+\nu_0\hat{n}_0) = -\beta(\omega_n+\nu_0) + S_n\omega_l & \text{(2.98a)} \\ \mathrm{D}_\theta\,\beta &= \hat{l}\cdot(\vec{\omega}+\nu_0\hat{n}_0)\times\widehat{S} \\ &= (\alpha\hat{n}_0 - S_n\hat{m})\cdot(\vec{\omega}+\nu_0\hat{n}_0) = +\alpha(\omega_n+\nu_0) - S_n\omega_m & \text{(2.98b)} \\ \mathrm{D}_\theta\,S_n &= \hat{n}_0\cdot(\vec{\omega}+\nu_0\hat{n}_0)\times\widehat{S} \\ &= (\beta\hat{m} - \alpha\hat{l})\cdot(\vec{\omega}+\nu_0\hat{n}_0) \quad = \quad \beta\omega_m - \alpha\omega_l \quad . & \text{(2.98c)} \end{aligned}$$

We note that the kind of canonical coordinates introduced in equation (2.10), called α' and β' here for clarity, when defined w.r.t. the $(\hat{l}, \hat{n}_0, \hat{m})$–system are to first order identical to α and β. For $\alpha^2+\beta^2 \ll 1$ we obtain

$$\alpha' = \alpha\sqrt{\frac{4}{4-\alpha^2-\beta^2}} =_1 \alpha \quad , \quad \beta' = \beta\sqrt{\frac{4}{4-\alpha^2-\beta^2}} =_1 \beta \quad . \tag{2.99}$$

In order to decouple the equations for α and β we change to complex notation $S_\pm \equiv \frac{1}{2}(\alpha \pm i\beta)$ and $\zeta \equiv \omega_m - i\omega_l$

$$\mathrm{D}_\theta\, S_+ = i(\omega_n+\nu_0)S_+ - \frac{i}{2}\zeta^* S_n \quad , \quad \mathrm{D}_\theta\, S_- = -i(\omega_n+\nu_0)S_- + \frac{i}{2}\zeta S_n \tag{2.100a}$$

$$\mathrm{D}_\theta\, S_n \;=\; -i\left(S_+\zeta - S_-\zeta^*\right) \tag{2.100b}$$

We now calculate the deviation of $\widehat{S}(\theta;0,\hat{n}_0)$ from $\hat{n}_0$ up to first order in $\vec{\omega}$ [CR80]. At 0-th order in $\vec{\omega}$, i.e. $\omega_n = 0$, $\zeta = 0$, the equations (2.100a) and (2.100b) simply reduce to $\mathrm{D}_\theta\, S_+^{(0)} = i\nu_0 S_+^{(0)}$, $\mathrm{D}_\theta\, S_-^{(0)} = -i\nu_0 S_-^{(0)}$ and $\mathrm{D}_\theta\, S_n^{(0)} = 0$ and the solution is, using $S_n(0) \equiv I_0$ and $S_\pm(0) \equiv \frac{1}{2}(\alpha_0 \pm i\beta_0) \equiv \frac{1}{2}\sqrt{1-I_0^2}\, e^{\pm i\Phi_0}$

$$S_\pm^{(0)}(\theta) = \frac{1}{2}\sqrt{1-I_0^2}\; e^{\pm i(\Phi_0+\nu_0\theta)} \quad , \quad S_n^{(0)}(\theta) = I_0 \tag{2.101a}$$

$$\alpha^{(0)}(\theta) = \sqrt{1-I_0^2}\;\cos(\Phi_0+\nu_0\theta) \quad , \quad \beta^{(0)}(\theta) = \sqrt{1-I_0^2}\;\sin(\Phi_0+\nu_0\theta) \quad . \tag{2.101b}$$

At first order in $\vec{\omega}$ we find

$$\begin{aligned}
\mathrm{D}_\theta\, S_n^{(1)} &= -i\left(S_+^{(0)}\zeta - S_-^{(0)}\zeta^*\right) \\
\Rightarrow S_n^{(1)}(\theta) &= I_0 - \frac{i}{2}\sqrt{1-I_0^2}\left(e^{+i\Phi_0}\int_0^\theta \zeta e^{+i\nu_0\vartheta}\, d\vartheta - e^{-i\Phi_0}\int_0^\theta \zeta^* e^{-i\nu_0\vartheta}\, d\vartheta\right) \\
&= I_0 + \sqrt{1-I_0^2}\;\Im\left(e^{+i\Phi_0}\int_0^\theta \zeta e^{+i\nu_0\vartheta}\, d\vartheta\right) && (2.102a) \\
\mathrm{D}_\theta\, S_\pm^{(1)} &= \pm i\nu_0 S_\pm^{(1)} \pm i\omega_n S_\pm^{(0)} \mp \frac{i}{2}(\omega_m \pm i\omega_l)S_n^{(0)} \\
\Rightarrow S_\pm^{(1)}(\theta) &= \frac{1}{2}\sqrt{1-I_0^2}e^{\pm i(\Phi_0+\nu_0\theta)}\left(1 \pm i\int_0^\theta \omega_n\, d\vartheta\right) \\
&\quad \mp i\frac{I_0}{2}e^{\pm i\nu_0\theta}\int_0^\theta (\omega_m \pm i\omega_l)e^{\mp i\nu_0\vartheta}\, d\vartheta && (2.102b) \\
\Rightarrow \alpha^{(1)}(\theta) &= \sqrt{1-I_0^2}\left(\cos(\Phi_0+\nu_0\theta) - \sin(\Phi_0+\nu_0\theta)\int_0^\theta \omega_n\, d\vartheta\right) \\
&\quad -I_0\Im\left\{e^{-i\nu_0\theta}\int_0^\theta \zeta e^{+i\nu_0\vartheta}\, d\vartheta\right\} && (2.102c) \\
\beta^{(1)}(\theta) &= \sqrt{1-I_0^2}\left(\sin(\Phi_0+\nu_0\theta) + \cos(\Phi_0+\nu_0\theta)\int_0^\theta \omega_n\, d\vartheta\right) \\
&\quad -I_0\Re\left\{e^{-i\nu_0\theta}\int_0^\theta \zeta e^{+i\nu_0\vartheta}\, d\vartheta\right\} \quad . && (2.102d)
\end{aligned}$$

We will return to equation (2.102a) later and now perform one more linearisation with equations (2.102c) and (2.102d). If the spin perturbations are small then for $\alpha_0 = \beta_0 = 0 \Rightarrow I_0 = 1$ the variables $\alpha(\theta)$ and $\beta(\theta)$ will remain small in some interval $[0, \tilde{\theta}]$. Therefore to first order in $\|(\alpha,\beta)\|$ we have $S_n(\theta) = \sqrt{1-\alpha^2-\beta^2} =_1 1$ and we introduce the 8–dimensional spin–orbit vector

$$\vec{Z} \equiv (\vec{z}^{\mathrm{T}}, \alpha, \beta)^{\mathrm{T}} \quad . \tag{2.103}$$

At first order in $\vec{Z}$ equations (2.102c) and (2.102d) become

$$\begin{aligned}\alpha^{(1,1)}(\theta) &= \alpha_0\cos\nu_0\theta - \beta_0\sin\nu_0\theta - \Im\left\{e^{-i\nu_0\theta}\int_0^\theta \zeta^{(1)}(\vec{z}_0,\vartheta)e^{+i\nu_0\vartheta}\,d\vartheta\right\} \\ &\equiv \alpha_0\cos\nu_0\theta - \beta_0\sin\nu_0\theta + \vec{G}_\alpha(\theta,0)\cdot\vec{z}_0 \qquad (2.104a)\\ \beta^{(1,1)}(\theta) &= \alpha_0\sin\nu_0\theta + \beta_0\cos\nu_0\theta - \Re\left\{e^{-i\nu_0\theta}\int_0^\theta \zeta^{(1)}(\vec{z}_0,\vartheta)e^{+i\nu_0\vartheta}\,d\vartheta\right\} \\ &\equiv \alpha_0\cos\nu_0\theta - \beta_0\sin\nu_0\theta + \vec{G}_\beta(\theta,0)\cdot\vec{z}_0 \quad , \qquad (2.104b)\end{aligned}$$

or with $\Delta \equiv \theta_f - \theta_i$ and $\underline{G} \equiv (\vec{G}_\alpha, \vec{G}_\beta)^{\mathrm{T}}$

$$\begin{pmatrix}\alpha\\ \beta\end{pmatrix}^{(1,1)}_f = \underline{G}(\theta_f,\theta_i)\vec{z}_i + \underline{D}(\theta_f,\theta_i)\begin{pmatrix}\alpha\\ \beta\end{pmatrix}_i \quad , \quad \underline{D}(\theta_f,\theta_i) \equiv \begin{pmatrix}\cos\nu_0\Delta & -\sin\nu_0\Delta\\ \sin\nu_0\Delta & \cos\nu_0\Delta\end{pmatrix} \in \mathbf{SO(2)} \quad . \qquad (2.105)$$

Of course, equations (2.104a) to (2.105) are equivalent to the sum of the identity in (2.76a) and the first term of $\mathfrak{B}^{(1)}$ which is proportional to $G\gamma$ in equation (2.76b). We can now present the totally linearised flow $\underline{M}$ [AC79, AC80, BH94a, BH94b] for the spin–orbit vector $\vec{Z}$

$$\vec{Z}_f = \underline{M}(\theta_f,\theta_i)\vec{Z}_i \quad , \quad \underline{M}_{8\times 8} \equiv \begin{pmatrix}\underline{T}_{6\times 6}(\theta_f,\theta_i) & \underline{0}_{6\times 2}(\theta_f,\theta_i)\\ \underline{G}_{2\times 6}(\theta_f,\theta_i) & \underline{D}_{2\times 2}(\theta_f,\theta_i)\end{pmatrix} \quad , \qquad (2.106)$$

where we have omitted the superscript $(1,1)$ for brevity. The matrix $\underline{T}$ is the usual linear orbital flow, i.e. $\vec{z}_f^{(1)} = \underline{T}\vec{z}_i$, the matrix $\underline{0}$ reflects the fact that we ignore Stern–Gerlach forces [BH94a, BH94b] and the matrices $\underline{D}$ and $\underline{G}$ describe the spin motion induced by the fields on the design orbit and the spin–orbit coupling in the $(\hat{l}, \hat{n}_0, \hat{m})$–frame respectively. The orbital part of $\underline{M}$ is symplectic if $\underline{T}$ is symplectic, but the spin part is orthogonal only if $\vec{z}_i = 0$. In the case of one–turn maps we will often write

$$\underline{D} \equiv \underline{D}(2\pi, 0) \quad \text{and} \quad \underline{G}(\theta) \equiv \underline{G}(\theta + 2\pi, \theta) \qquad (2.107)$$

the $\underline{D}$- and the $\underline{G}$–matrix of the system viewed at θ.

Equations (2.102a) to (2.102d) contain the Fourier integral $\int_0^\theta (\omega_m(\vartheta;\vec{z}_i) - i\omega_l(\vartheta;\vec{z}_i))\, e^{i\nu_0\vartheta}\, d\vartheta$ where $\omega_{m/l}$ are the off–orbit contributions of the driving term of the T–BMT equation perpendicular to $\hat{n}_0$ in the $(\hat{l}, \hat{n}_0, \hat{m})$–frame evaluated along an orbital trajectory $\vec{\xi}(\theta;\vec{z}_i)$ with initial conditions $\vec{\xi}(0;\vec{z}_i) = \vec{z}_i$. This integral does not depend on the particular choice of the integer part of ν_0 since that is compensated in the rotation of $\hat{l}$ and $\hat{m}$ around $\hat{n}_0$ by $-2\pi\nu_0$ per turn. In fact a change in the choice of the integer part of ν_0, just implies a change in the $(\hat{l}, \hat{n}_0, \hat{m})$ coordinates used for describing the spin motion but of course entails *no* change in the underlying physics.

In the equations (2.104a) and (2.104b) we have assumed $\vec{\omega}$ to be a linear function of the initial orbital phase space vector $\vec{z}_i$. Referring back to equations (2.102a) to (2.102d) it is clear that at first order in $\vec{\omega}$ the EOM for $S_n^{(1)}$, $\alpha^{(1)}$ and $\beta^{(1)}$ could be solved in principle for an ω containing arbitrary orders of $\vec{z}_i$. We note that the non–linearities included by this procedure would be purely dynamical as explained in section 2.2.2 and therefore would *not* be the dominant non–linear contribution to spin motion at high energy. Nevertheless it is possible to describe these dynamical non–linearities in terms of the generalised Fourier spectrum of ζ. Therefore, and since it will help to prevent confusion about the origin of higher order resonances it is useful to discuss the spectrum of ζ here. We assume that the orbital motion is integrable, i.e. that there are action–angle variables $\vec{J}$ and $\vec{\Psi}$ with $\mathrm{D}_\theta \vec{J} = 0$, $\mathrm{D}_\theta \vec{\Psi} = \vec{Q}(\vec{J})$ so that $\vec{z} = \vec{N}(\vec{J}, \vec{\Psi}, \theta)$ is 2π–periodic in $\vec{\Psi}|_{\theta=\text{const.}}$ and $\theta|_{\vec{\Psi}=\text{const.}}$. Then $\zeta(\theta;\vec{z}_i) = \omega_m(\vartheta;\vec{z}_i) - i\omega_l(\vartheta;\vec{z}_i)$ is a *pseudo–periodic* function over the tunes $\vec{Q}$ since $\vec{\omega}(\theta,\vec{z})|_{\vec{z}=\text{const.}}$, $\hat{l}$ and $\hat{m}$ are periodic in θ (see appendix A). Therefore we can write ζ at each *fixed* reference energy as a generalised Fourier series

$$\zeta(\theta;\vec{J},\vec{\Psi}_0,E_0) = \sum_{k_0\in\mathbb{Z}}\ \sum_{\vec{k}\in\mathbb{Z}^3-\{\vec{0}\}} \epsilon_{k_0,\vec{k}}(\vec{J},\vec{\Psi}_0,E_0)e^{-i(k_0+\vec{Q}\cdot\vec{k})\theta} \quad . \qquad (2.108)$$

We then define for arbitrary real κ

$$\epsilon_\kappa(\vec{J},\vec{\Psi}_0,E_0) = \lim_{\vartheta\to\infty}\frac{1}{\vartheta}\int_0^\vartheta \zeta(\theta;\vec{J},\vec{\Psi}_0,E_0)e^{+i\kappa\theta}\,d\theta = \begin{cases} \epsilon_{k_0,\vec{k}} & : \kappa = k_0+\vec{k}\cdot\vec{Q} \\ 0 & : \text{otherwise} \end{cases} \quad . \tag{2.109}$$

The pseudo–periodicity of ζ implies that ϵ_κ vanishes identically for any κ that is not of the form $\kappa = k_0 + \vec{k}\cdot\vec{Q}$, whereas the *finite* integrals in equations (2.102a) to (2.102d) in general are non–zero for arbitrary $\nu_0(E_0)$. Note that the choice of $\vec{\Psi}_0$ in the action–angle transformation as well as the phase of $\hat{l}(0)$ in the plane perpendicular to $\hat{n}_0(0)$ are totally arbitrary so that the *absolute* phase of ϵ is meaningless.

Putting the series (2.108) back into equations (2.102a) to (2.102d) we see that at $\nu_0 = \kappa$ for some $\kappa = k_0 + \vec{k}\cdot\vec{Q}$ the corresponding term in the integral does not oscillate but instead builds up linearly and indefinitely as θ increases at the rate $\epsilon_{k_0,\vec{k}} = \epsilon_\kappa$. This is a typical manifestation of the phenomenon of *spin–orbit resonance*, namely that the change of the projection of $\widehat{S}$ on $\hat{n}_0$ from turn to turn is maximal if the spin motion is coherent with the orbital motion or, more precisely, with a harmonic of the T–BMT driving term ζ perpendicular to $\hat{n}_0$. In the perturbative regime, i.e. $|\zeta| \ll 1$ this change is maximal if the on–orbit spin motion is coherent with the orbital motion

$$\nu_0(E_0) = k_0 + \vec{k}\cdot\vec{Q} \ \text{, for some } k\in\mathbb{Z}, \vec{k}\in\mathbb{Z}^3 - \{\vec{0}\} \quad . \tag{2.110}$$

In the non–perturbative regime the change is again maximal if there is coherence between the spin motion and the orbital motion but then the design orbit spin tune ν_0 in equation (2.110) is replaced by the amplitude dependent spin tune to be defined in chapter 4.

We will assume for clarity in the following that even in the presence of orbital inter–plane coupling, the orbital eigenplanes $1, 2, 3$ can be ordered so that plane 1 has the largest projection on the (x, a)–plane, plane 2 has the largest projection on the (y, b)–plane and plane 3 has maximum projection on the (longitudinal) (τ, δ)–plane. Therefore we exercise the freedom to refer to these planes as the x, y, z planes which they would approach in the limit of vanishing inter–plane coupling. When equation (2.110) is fulfilled we speak of *intrinsic spin–orbit resonances*. The integer $|\vec{k}| \equiv \sum_i |k_i|$ is called the *order* of the resonance. The first order resonances $\nu_0 = k_0 + \vec{k}\cdot\vec{Q}$ with $|\vec{k}| = 1$, i.e.

$$\nu_0(E_0) = k_0 \pm Q_x \ , \ \nu_0 = k_0 \pm Q_y \ , \ \nu_0 = k_0 \pm Q_z \tag{2.111}$$

are called *linear intrinsic resonances*. They arise from the term proportional to $G\gamma$ of $\underline{\mathfrak{B}}^{(1)}$ in equation (2.76b). In particular if ζ is a linear function of the orbital coordinates and the orbital motion is linear as in (2.104a) and (2.104b), then because of equation (A.52c) ζ contains *only* harmonics with $|\vec{k}| = 1$. Then equation (2.109) only yields non–vanishing Fourier coefficients ϵ_κ for $|\vec{k}| = 1$. The Fourier coefficients ϵ_κ with $\kappa = k_0 + \vec{k}\cdot\vec{Q}$ and $|\vec{k}| = 1$ are called the *linear intrinsic resonance strengths* [CR80]. This definition of the resonance strength is more general than the definition in [CR80]. There a flat ring was explicitly assumed so that $\hat{n}_0 = \hat{y}$ whereas equations (2.108) and (2.109) allow application to arbitrary circular accelerators. Another equivalent way to obtain the resonance strengths is given in [BG96]. Note that a shift in the choice of the integer part of ν_0 causes an identical shift in k_0 so that the resonant energies E_0 in (2.110) are invariant under changes of the integer part.

For $|\vec{k}| = 2$ in equation (2.110) there are two main sources of coherent degradation of S_n. First there is the term in equation (2.76b) which is proportional to $(G\gamma)^2$. This term is the strongest contribution to 2-nd order spin–orbit coupling at high energy but it is a *kinetic* higher order term that contains a *double* integral over $\underline{\mathfrak{w}}^{(1)}$ and is therefore *not* included in the Fourier analysis embodied by equations (2.108) and (2.109). The second contribution is the term in equation (2.76c) which is proportional to $G\gamma$. It is a *dynamical* contribution which *is* included in equation (2.109). But at high energies these dynamical effects are weak compared to the kinetic effects. Analogously, comparing equation (2.76d) and (2.109), one easily sees that $\epsilon_{\kappa^>}$ with $|\vec{k}^>| > 2$ as defined in equation (2.109) only contains dynamical contributions to the $|\vec{k}|$–order spin–orbit resonance $\nu_0 = \kappa^>$ — and then only if ζ contains $|\vec{k}|$-th order terms in the coordinates. Therefore the ϵ_κ of higher order than $|\vec{k}| = 1$, computed with equation (2.109) are called the *dynamical resonance strengths*. We conclude that equation (2.109) which is based on a first order perturbative expansion in $\vec{\omega}$ can only treat *dynamical* higher order resonances. In later chapters using the concept of the invariant spin field and the amplitude dependent spin tune we will see how to identify and classify *kinetic* higher order resonances which have a much stronger impact on spin motion in the high energy regime. We will therefore not put any emphasis on non–linear dynamical resonance strengths here. However they might become significant in the case where no linear intrinsic or higher order kinetic resonances are excited. Note that in the case of *linear* intrinsic resonances the distinction between dynamical and kinetic contributions makes no sense.

In a ring with *exact* mid–plane symmetry there is no vertical dispersion, no linear transverse coupling and $\hat{n}_0$ is vertical everywhere. Thus, among the *linear* intrinsic resonances only those including the vertical tune Q_y have non–vanishing strengths because only excitation of vertical motion leads a spin to see radial fields along a trajectory and produce a non–zero ζ. If the vertical amplitude is zero, horizontal and longitudinal oscillations can only lead to phase space dependent modulations of the magnetic field strength $B_\perp \approx B_y$ (e.g. in the quadrupoles) and the "weight" $G\gamma$ in the T–BMT $\vec{\Omega}$. They would therefore not introduce any tilt away from $\hat{n}_0$ but rather a phase space dependent change of the number of spin precessions around $\hat{n}_0$ per particle revolution. Moreover, if we only consider the solutions (2.102a), (2.104a) and (2.104b) a non–zero vertical amplitude modifies the spin motion but does not modify the effects on the spin motion of horizontal and longitudinal orbital motion. The reason for this is that the terms proportional to $G\gamma$ in equation (2.76b) only contain a *single* integral over $\underline{\mathfrak{w}}^{(1)}$ so that for example in (2.102a) the spin components develop independently. However, whenever *kinetic* higher order effects are included, e.g. according to the terms proportional to $(G\gamma)^2$ in equations (2.76b) or alternatively in (2.88), the effect of non–commutation of rotations around *different* axes causes vertical motion to modify the effects on spin of horizontal and longitudinal amplitudes, even in mid–plane symmetric rings and when $\vec{\omega}$ depends linearly on $\vec{z}_i$. Thus in general the combined effects on spin motion of all three modes of orbital oscillations can be very complicated.

If the ring has an *exact* superperiodicity of $P \in \mathbb{N}*$, i.e. $\vec{\Omega}(\theta+2\pi/P, \vec{z}) = \vec{\Omega}(\theta, \vec{z})$ and $\underline{T}(\theta+2\pi/P) = \underline{T}(\theta)$ for all θ then $\vec{\Omega}(\theta, \vec{\xi}(\theta; \vec{z}_0))$ is pseudo–periodic with the normalised orbital phase advance per superperiod $\vec{Q}_P \equiv [\vec{Q}_P] + \vec{N}_Q \Rightarrow \vec{Q} = P\vec{N}_Q + P[\vec{Q}_P]$. Therefore $\vec{\Omega}$ only contains Fourier harmonics at $\kappa = P(l_0 + \vec{l}\cdot\vec{Q}_P)$. We define the *on–orbit spin tune for one superperiod*

$$\nu_{0,P}(E_0) \equiv [\nu_{0,P}(E_0)] + N_\nu(E_0) \quad \Rightarrow \quad \nu_0(E_0) = PN_\nu + P\,[\nu_{0,P}(E_0)] \quad , \tag{2.112}$$

with some arbitrary integer N_ν. Then $(\hat{l}(\theta), \hat{n}_0(\theta), \vec{m}(\theta))$ as defined by equation (2.94) is $2\pi/P$–periodic. The resonance strengths are non–zero only at

$$[\nu_{0,P}(E_0)] = \left[\vec{k}\cdot\vec{Q}_P\right] \equiv \tilde{k}_0(\vec{k},\vec{Q}\,) + \vec{k}\cdot\left[\vec{Q}_P\right] \quad . \tag{2.113}$$

The resonance condition for the full tunes is then

$$\nu_0 = P\,(\tilde{k}_0 + N_\nu - \vec{k}\cdot\vec{N}_Q) + \vec{k}\cdot\vec{Q} \quad . \tag{2.114}$$

Since N_ν was arbitrary we can rewrite the condition as $\nu_0 = Pk_0 + \vec{k}\cdot\vec{Q}$. In the case of even weak violation of the symmetry, e.g. by gradient errors in the quadrupoles or in the case of machines like HERA–p where even in the unperturbed machine the "obvious" 4–fold symmetry is just approximate, all types of intrinsic resonances are allowed although the additional ones are generally weaker than the resonances that fulfil equation (2.113).

In a mid–plane symmetric ring in which the main dipole fields are all the same, then $\hat{n}_0 = \text{const.} = \hat{y}$ and the spins on the design orbit precess either at a constant rate $G\gamma$ in the dipoles or not at all, outside the dipoles. One may then choose a N_ν so that $\nu_{0,P} = {}^{G\gamma}/_{P}$. Then with an exact superperiodicity P and to first order, only the resonances

$$G\gamma = Pk_0' \pm Q_y \tag{2.115}$$

with the full tunes $G\gamma$ and Q_y appear. These resonances are called *strong linear intrinsic resonances* [SL97]. See also equation (2.146).

Accelerators generally consist of arcs built from highly periodic, e.g. FODO, structures and straight sections with various layouts. It can be shown [SL97] (see equation (2.148)) that resonances are particularly enhanced if the spin motion is additionally coherent with the orbital motion in the periodic arcs. Let M be the number of periodic cells in each of the P identical arcs of a mid–plane symmetric ring and let $Q_{y,C}$ be the normalised vertical phase advance per cell. Then so–called *super–strong* linear intrinsic resonances occur at

$$\nu_0(E_0) = Pk_0' \pm Q_y \approx PM\,(k_0'' \pm Q_{y,C}) \quad . \tag{2.116}$$

According to definition 2.8, the magnetic field components (apart from the fringe fields) in mid–plane symmetric rings fulfil

$$B_x(x,-y,\tau) = -B_x(x,y,\tau) \ \ , \ \ B_y(x,-y,\tau) = +B_y(x,y,\tau) \ \ , \ \ B_z(x,y,\tau) = 0 \quad . \tag{2.117}$$

Then it is well known [KB82] that whenever the trajectory $\vec{z}(\theta) \equiv (x,a,y,b,\tau,\delta)(\theta)$ is a solution of the orbital EOM, the trajectory $\tilde{z} \equiv (x,a,-y,-b,\tau,\delta)(\theta)$ is also a solution. Note that $\tilde{z} = \underline{Y}^-\vec{z}$, where $\underline{Y}^- \equiv \underline{\mathrm{diag}}(1,1,-1,-1,1,1) \in \mathbf{Sp}(6)$. For an arbitrary real 3–vector or 3–vector field $\vec{x}$ we define

$$\tilde{x} \equiv \underline{Y}_\pi\vec{x} \ \ , \ \ \underline{Y}_\pi \equiv \underline{\mathrm{diag}}(-1,1,-1) \in \mathbf{SO(3)} \quad , \tag{2.118}$$

and note that for a mid–plane symmetric ring equation (2.117) implies $\vec{B}(\tilde{z}) = \widetilde{B}(\vec{z})$. The vector field $\vec{\Omega}(\vec{z})$ as in the T–BMT equation equation (2.8) has four terms: the magnetic field components of the T–BMT equation equation (2.8) $\vec{B}_{||} \equiv \vec{v}\,(\vec{B}\cdot\vec{v})/v^2$ and $\vec{B}_\perp \equiv \vec{v}\times(\vec{B}\times\vec{v})/v^2$, the curvature term from the design orbit $\vec{\Omega}_\rho \equiv \vec{\kappa}\times\hat{z}$ which is purely vertical and phase space independent in an accelerator with perfect mid–plane symmetry and the term due to the electric field $\vec{E}_v \equiv E(\tau)\hat{z}\times\vec{v}$. We assume, as usual in accelerator physics, that the electric field is non–zero only in the RF–cavities and that it is longitudinal and independent of x and y. The velocity $\vec{v}$ used here is: $\vec{v} \equiv (v_x = {}^{ap_0}/_{m\gamma}, v_y = {}^{bp_0}/_{m\gamma}, v_z = {}^{p_0(1+\delta_p)}/_{m\gamma})$ and $\delta_p \equiv {}^{p-p_0}/_{p_0} \approx \delta \equiv {}^{K-K_0}/_{K_0}$. By direct calculation one easily shows that with (2.117) the four terms fulfil $\vec{B}_{||}(\tilde{z}) = \widetilde{B}_{||}(\vec{z})$, $\vec{B}_\perp(\tilde{z}) = \widetilde{B}_\perp(\vec{z})$, $\vec{\Omega}_\rho(\tilde{z}) = \widetilde{\Omega}_\rho(\vec{z})$ and $\vec{E}_v(\tilde{z}) = \widetilde{E}_v(\vec{z})$. Therefore we get

$$\vec{\Omega}(\tilde{z}) = \widetilde{\Omega}(\vec{z}) \quad . \tag{2.119}$$

This immediately implies that the horizontal components of $\vec{\Omega}$ contain only *odd* Fourier harmonics in the vertical phase Ψ_y whereas the vertical components only contain *even* harmonics in Ψ_y. Since by definition mid–plane symmetry implies flatness we know that $\vec{\Omega}_0(\theta) = a(\theta)\hat{y}$ and therefore that $\hat{n}_0$ is vertical. Note that $\vec{\Omega}(\vec{0}) = \vec{\Omega}(\tilde{0}) = \widetilde{\Omega}(\vec{0})$ requires $\vec{\Omega}_0 \sim \hat{y}$. In a ring with vertical $\hat{n}_0$ only the *horizontal* components of $\vec{\omega}$ enter the resonance strength (2.109). Thus we have just proved the following theorem:

Theorem 2.9 *In an accelerator with perfect mid–plane symmetry all dynamical resonances are of odd order in* Q_y*, i.e.* $\kappa = k_xQ_x + (2l - \mathrm{sgn}(l)\,)Q_y + k_zQ_z$ *with* $k_x, k_z \in \mathbb{Z}$ *and* $l \in \mathbb{Z}^*$*.*

For the spin and orbital trajectories we have

Theorem 2.10 *If in an accelerator with perfect mid–plane symmetry* $(\vec{z}(\theta), \widehat{S}(\theta))$ *is a solution of the combined spin–orbit EOM for the initial conditions* $\widehat{S}(0) = \widehat{S}_0$ *and* $\vec{z}(0) = \vec{z}_0$*, then* $(\ \underline{Y}_\pi\widehat{S}(\theta)\ ,\ \underline{Y}^-\vec{z}(\theta)\ )$ *is a solution for the initial conditions* $\underline{Y}_\pi\widehat{S}(0) = \widetilde{S}_0$ *and* $\underline{Y}^-\vec{z}(0) = \tilde{z}_0$*.*

Since the symmetry of the orbital trajectories is well established in mid–plane symmetric rings, we only have to prove the T–BMT part. To do that we note that $\vec{z}(\theta)$ and $\tilde{z}(\theta) \equiv \underline{Y}^{-}\vec{z}(\theta)$ are solutions of the corresponding orbital initial value problems. At $\theta = 0$ the statement of the theorem is true by construction of the initial conditions. For $\theta > 0$ we find from $\widetilde{\Omega}(\vec{z}) = \vec{\Omega}(\tilde{z})$

$$\begin{aligned} \mathrm{D}_\theta\, \widehat{S}(\theta) &= \vec{\Omega}(\vec{z}) \times \widehat{S}(\theta) \Leftrightarrow \\ \mathrm{D}_\theta\, \underline{Y}_\pi \widehat{S}(\theta) &= \underline{Y}_\pi\, (\vec{\Omega}(\vec{z}) \times \widehat{S}(\theta)) \Leftrightarrow \\ \mathrm{D}_\theta\, \widetilde{S}(\theta) &= \widetilde{\Omega}(\vec{z}) \times (\underline{Y}_\pi \widehat{S}(\theta)) \;=\; \vec{\Omega}(\tilde{z}) \times \widetilde{S}(\theta) \quad , \end{aligned} \tag{2.120}$$

where we have used the abbreviation $\widetilde{S}(\theta) \equiv \underline{Y}_\pi \widehat{S}(\theta)$. □

Corollary 1: In a perfectly mid–plane symmetric ring $\underline{Y}_\pi$ commutes with the T–BMT flow in the sense that $\underline{Y}_\pi\, \underline{R}(\theta_f, \theta_i; \vec{z}_i) = \underline{R}(\theta_f, \theta_i; \tilde{z}_i)\, \underline{Y}_\pi$.

Corollary 2: In a perfectly mid–plane symmetric ring the quaternionic OTM $\bar{r}(\theta; \vec{z}_i) \equiv (e_0, o_1, e_2, o_3)$ is such that e_0 and e_2 only contain *even* harmonics in Ψ_y whereas o_1 and o_3 contain only *odd* harmonics. Equivalently the $\mathbf{SU(2)}$ OTM $\underline{r} = \underline{f}(\bar{r})$ is given by $\left(\begin{smallmatrix} e_{11} & o_{12} \\ -o_{12}^* & e_{11}^* \end{smallmatrix}\right)$, where e_{11} contains only even and o_{12} contains only odd harmonics of Ψ_y.

We return to corollary 2 in section 4.8 where we use it for a more general discussion about which resonances are allowed in mid–plane symmetric rings.

The transformation $\vec{z} \to \tilde{z}$ is symplectic and $\underline{Y}_\pi$ is orthogonal with unit determinant. Therefore both transformations are topologically connected to the identity. If the orbital motion is integrable then $\vec{z}$ and $\tilde{z}$ are on the same torus $\vec{J} =$ const. and if $\vec{z}$ belongs to Ψ_y, then $\tilde{z}$ belongs to $\Psi_y + \pi$. Therefore the parametrisation $\vec{z}(\Psi_y)$ with $\Psi_x, \Psi_z =$ const. is a circle on the torus and $\vec{z}(\Psi_y + \pi) = \tilde{z}(\Psi_y)$. We assume the orbital OTM to be continuous w.r.t. the angles Ψ_i so that it transforms any closed curve in the phase space into another closed curve. Then this circle is transported by the orbital OTM to the circle $\vec{z}(\Psi'_y \equiv \Psi_y + 2\pi Q_y)$ with $\Psi_x + 2\pi Q_x, \Psi_z + 2\pi Q_z =$ const. which again fulfils $\vec{z}(\Psi'_y + \pi) = \tilde{z}(\Psi'_y)$. We can now define infinitely many parametrisations of closed curves $\widehat{S}(\Psi_y)$ on the unit sphere so that $\widehat{S}(\Psi_y + \pi) = \widetilde{S}(\Psi_y)$. If the spin OTM is continuous w.r.t. the Ψ_i, these curves are transported by the spin OTM to the closed curves $\widehat{S}'(\Psi'_y) \equiv \underline{R}(\vec{\Psi})\widehat{S}(\Psi_y)$ which again fulfil $\widehat{S}'(\Psi'_y + \pi) = \widetilde{S}'(\Psi'_y)$. In general the shape of these curves will change from turn to turn but in chapter 4 we will introduce for the case $J_x = J_z = 0$ special curves $\hat{n}(\Psi_y)$ whose shape is invariant under the spin OTM and which in a mid–plane symmetric ring fulfil $\hat{n}(\Psi_y + \pi) = \tilde{n}(\Psi_y)$. The T–BMT equation is linear in $\widehat{S}$. Therefore also $-\underline{Y}_\pi$ commutes with the T–BMT flow in the sense of corollary 1 but it has determinant -1 and is therefore *not* topologically connected with the identity. Hence one cannot construct *closed* curves with $\widehat{S}(\Psi_y + \pi) = -\underline{Y}_\pi \widehat{S}(\Psi_y)$.

We now briefly mention another type of resonance with $\vec{k} = \vec{0}$ called *imperfection resonances.* In every "real" accelerator the closed orbit is perturbed due to quasi–random dipole errors and misaligned quadrupoles. In this paragraph we will distinguish between quantities measured w.r.t. the unperturbed design orbit indicated by the label 00 and w.r.t. the perturbed closed orbit indicated by the label 0. If the design orbit spin tune ν_{00} is an integer then the one–turn spin map evaluated on the design orbit $\underline{R}_{00}$ is just the identity and $\hat{n}_{00}$ is arbitrary. Then the perturbed orbit spin OTM $\underline{R}_0$ and the spin closed orbit $\hat{n}_0$ measured w.r.t. the "real", perturbed closed orbit is dominated by the perturbations even if they can be considered small. Nevertheless for any *given, fixed* lattice, no matter whether it is perturbed or not, the on–orbit spin OTM $\underline{R}_0$, the spin closed orbit $\hat{n}_0$ and the perturbed on–orbit spin tune ν_0 can be computed at least numerically. However, the closed orbit perturbations are in general *not* known beforehand, simply because "misalignment" and "errors" are statistical properties of the manufacturing and commissioning process. — If they were predictable and controllable in a deterministic way one could just as well set them up to be zero. The imperfection resonance strength

ϵ_{k_0} is defined as the Fourier harmonic corresponding to $\nu_{00} = k_0$ of

$$\zeta_0(\theta) \equiv (\vec{\Omega}_0(\theta) - \vec{\Omega}_{00}(\theta)) \cdot (\hat{m}(\theta) - i\hat{l}(\theta)) \quad , \tag{2.121}$$

where $\hat{m}$ and $\hat{l}$ are defined by equation (2.94) and w.r.t. the design orbit. The imperfection resonance strengths can be computed numerically for various random seeds of "misalignment" and field errors and can to some extent be corrected by means of harmonic orbit bumps [BR99a]. Large imperfection resonance strengths ϵ_{k_0} imply strong dependence of $\hat{n}_0$ on orbit distortions and potentially strong deviation of $\hat{n}_0$ from $\hat{n}_{00}$ at $\nu_{00}(E_0) = k_0$. As we will see in section 2.4 the perturbed on–orbit spin tune does *not* cross any imperfection resonance with non–vanishing strength but jumps from $\nu_0^- \equiv k_0 - \epsilon_{k_0}$ to $\nu_0^+ \equiv k_0 + \epsilon_{k_0}$ at $\nu_{00} = k_0$. Therefore for non–integral resonance strength the perturbed $\hat{n}_0$ is always uniquely defined.

The imperfection resonance strengths do not appear in the generalised Fourier expansion (2.108) of ζ since it is to be performed w.r.t. an *arbitrary* but *known* spin closed orbit $\hat{n}_0$ or $\hat{n}_{00}$.

It is worth mentioning that once a lattice produces *vertical* closed orbit perturbations, the condition in (2.119) is *not* fulfilled so that Theorem 2.9 does not rigorously apply to any "real" accelerator. But if the vertical closed orbit perturbations are small and ν_{00} is *not* close to an integer, the strengths of dynamical resonances including even multiples of Q_y are significantly weaker than those including odd multiples of Q_y. On the other hand, if ν_{00} is close to a strong imperfection resonance, the effect of the orbit perturbations on spin motion is particularly strong, i.e. $\hat{n}_0$ is strongly tilted from the vertical, and then there is generally no reason why resonances including even orders in Q_y should be significantly weaker than odd ones.

Following a derivation by Hoffstaetter [GH99a] (see also [BR99a]) the first order resonance strengths can be computed from the 8×8 linearised OTM of combined spin–orbit motion $\underline{M}$. We first rewrite the $\underline{G}$–matrix

$$\begin{aligned}
-\underline{G}(\theta)\vec{z}_i &= \begin{pmatrix} \Im\left\{e^{-i\nu_0\theta}\int_\theta^{\theta+2\pi}\zeta^{(1)}(\vec{z}_i,\vartheta)e^{+i\nu_0\vartheta}\,d\vartheta\right\} \\ \Re\left\{e^{-i\nu_0\theta}\int_\theta^{\theta+2\pi}\zeta^{(1)}(\vec{z}_i,\vartheta)e^{+i\nu_0\vartheta}\,d\vartheta\right\}\end{pmatrix} \\
&= \begin{pmatrix} \Im\left\{e^{-i\nu_0\theta}\int_\theta^{\theta+2\pi}(\hat{m}(\vartheta)-i\hat{l}(\vartheta))^{\mathrm{T}}\,\underline{W}(\vartheta)e^{+i\nu_0\vartheta}\,d\vartheta\right\} \\ \Re\left\{e^{-i\nu_0\theta}\int_\theta^{\theta+2\pi}(\hat{m}(\vartheta)-i\hat{l}(\vartheta))^{\mathrm{T}}\,\underline{W}(\vartheta)e^{+i\nu_0\vartheta}\,d\vartheta\right\}\end{pmatrix}\vec{z}_i \\
&= \underline{D}\int_\theta^{\theta+2\pi}\underline{D}^{-1}(\vartheta,\theta)\begin{pmatrix}-\hat{l}^{\mathrm{T}}(\vartheta)\\ \hat{m}^{\mathrm{T}}(\vartheta)\end{pmatrix}\underline{W}(\vartheta)\,d\vartheta\,\vec{z}_i = \underline{D}\int_\theta^{\theta+2\pi}\begin{pmatrix}-\hat{l}_0^{\mathrm{T}}(\vartheta)\\ \hat{m}_0^{\mathrm{T}}(\vartheta)\end{pmatrix}\underline{W}(\vartheta)\,d\vartheta\,\vec{z}_i \\
&= \underline{D}\,\underline{G}_0(\theta)\vec{z}_i \quad .
\end{aligned} \tag{2.122}$$

in terms of the 3×6-matrix $\underline{W}$, so that $\vec{\omega}^{(1)}(\vec{z}_i,\theta) = \underline{W}(\theta)\vec{z}_i$, and the $\underline{G}_0$–matrix

$$\underline{G}_0(\theta) \equiv \int_\theta^{\theta+2\pi}(-\hat{l}_0(\vartheta),\hat{m}_0(\vartheta))^{\mathrm{T}}\,\underline{W}(\vartheta)\,d\vartheta \quad . \tag{2.123}$$

Here we have used the relations

$$(\hat{l},\hat{m}) = (\hat{l}_0,\hat{m}_0)\,\underline{D}^{-1}(\theta-\theta_0) \quad , \quad (\hat{l},\hat{m})^{\mathrm{T}} = \underline{D}(\theta-\theta_0)(\hat{l}_0,\hat{m}_0)^{\mathrm{T}} \quad . \tag{2.124}$$

In the following we also need

$$(\hat{m}-i\hat{l}) = e^{-i(\theta-\theta_0)\nu_0}(\hat{m}_0-i\hat{l}_0) \quad , \quad \underline{R}_0(\theta)(\hat{m}_0-i\hat{l}_0) = e^{+i2\pi\nu_0}(\hat{m}_0-i\hat{l}_0) \quad . \tag{2.125a}$$

Then for $\nu_0 = k_0 + \vec{k}\cdot\vec{Q}$ and $|\vec{k}| = 1$ we obtain

$$\epsilon_{\nu_0} = \lim_{N\to\infty}\frac{1}{2\pi N}\int_0^{2\pi N}\zeta^{(1)}(\theta,\vec{J},\vec{0})e^{+i\nu_0\theta}\,d\theta$$

$$
\begin{aligned}
&= \lim_{N\to\infty} \frac{1}{2\pi N} \int_0^{2\pi N} (\hat{m} - i\hat{l})^{\mathrm{T}}\, \underline{W} e^{+i\nu_0\theta}\, d\theta\, \vec{z}_0 \\
&= \lim_{N\to\infty} \frac{1}{2\pi N} \int_0^{2\pi N} (\hat{m}_0 - i\hat{l}_0)^{\mathrm{T}}\, \underline{W}\, d\theta\, \vec{z}_0 \qquad (2.126a)\\
&= \lim_{N\to\infty} \frac{1}{2\pi N} \sum_{j=0}^{N-1} \int_0^{2\pi} (\hat{m}_0 - i\hat{l}_0)^{\mathrm{T}}\, \underline{R}^{j\mathrm{T}}\, \underline{W}\, d\theta\, \underline{T}^j\, \vec{z}_0 \\
&= \lim_{N\to\infty} \frac{1}{2\pi N} \sum_{j=0}^{N-1} \int_0^{2\pi} e^{ij2\pi\nu_0} (\hat{m}_0 - i\hat{l}_0)^{\mathrm{T}}\, \underline{W}\, d\theta\, \underline{T}^j\, \vec{z}_0 \\
&= \lim_{N\to\infty} \frac{1}{2\pi N} \sum_{j=0}^{N-1} e^{i2\pi j\nu_0} (i,1)\, \underline{G}_0\, \underline{T}^j\, \vec{z}_0 \qquad (2.126b)
\end{aligned}
$$

where we have abbreviated $\vec{z}_0 \equiv \vec{z}(\vec{J}, \vec{\Psi} = \vec{0})$. Equation (2.126b) can be further simplified [GH99a] in the case of the linear orbital motion being stable by performing a normal form transformation (see appendix A) so that

$$\underline{T} = \underline{C}^{-1}\, \underline{\mathrm{diag}}(e^{i2\pi q_1}, \cdots, e^{i2\pi q_6})\, \underline{C} \;\text{ with }\; q_{2i-1} = [Q_i],\; q_{2i} = -[Q_i] \quad . \qquad (2.127)$$

Then if there is an n so that $[\nu_0] + q_n = 0$ we can use the relation $\lim_{N\to\infty} \frac{1}{N} \sum_{j=0}^{N-1} e^{ij2\pi\kappa} = \delta_{0,[\kappa]}$ and find

$$
\begin{aligned}
\epsilon_{\nu_0} &= \frac{(i,1)}{2\pi}\, \underline{G}_0\, \underline{C}^{-1} \left(\lim_{N\to\infty} \frac{1}{N} \sum_{j=0}^{N-1} \underline{\mathrm{diag}}(e^{ij2\pi(\nu_0+q_1)}, \cdots, e^{ij2\pi(\nu_0+q_6)}) \right) \underline{C}\vec{z}_0 \\
&= \frac{(i,1)}{2\pi}\, \underline{G}_0\, \underline{C}^{-1}\, \underline{\mathrm{diag}}(\cdots, 0_{(n-1)}, 1_{(n)}, 0_{(n+1)}, \cdots)\, \underline{C}\vec{z}_0 \\
&= \frac{(i,1)}{2\pi}\, \underline{G}_0 \vec{c}_n \sqrt{2J_n} e^{i\Psi_{0,n}} \quad , \qquad (2.128)
\end{aligned}
$$

where we have used the normalised complex eigenvectors $\vec{c}_i$ of $\underline{T}$. In the case that there is no $\vec{k}$ with $|\vec{k}| = 1$ so that $\nu_0 = k_0 + \vec{k} \cdot \vec{Q}$, the resonance strength ϵ_{ν_0} is identically zero. Note that the modulus $|\epsilon_{\nu_0}|$ is independent of the initial phase.

Another way [GH99a] to proceed with equation (2.126b) again uses (2.124) and (2.125) and also the product

$$\begin{pmatrix} \underline{T} & \underline{0} \\ \underline{G} & \underline{D} \end{pmatrix}^N = \begin{pmatrix} \underline{T}^N & \underline{0} \\ \sum_{j=1}^N \underline{D}^{N-j}\, \underline{G}\, \underline{T}^{j-1} & \underline{D}^N \end{pmatrix} \quad . \qquad (2.129)$$

Therefore we find

$$
\begin{aligned}
\epsilon_{\nu_0} &= \lim_{N\to\infty} \frac{1}{2\pi N} \sum_{j=1}^{N} e^{i2\pi(j-1)\nu_0} (i,1)\, \underline{G}_0\, \underline{T}^{j-1}\, \vec{z}_0 \\
&= \lim_{N\to\infty} \frac{e^{i2\pi N\nu_0}}{2\pi N} \sum_{j=1}^{N} e^{-i2\pi(N-j)\nu_0} (i,1)\, \underline{G}\, \underline{T}^{j-1}\, \vec{z}_0 \\
&= \lim_{N\to\infty} \frac{e^{i2\pi N\nu_0}}{2\pi N} \sum_{j=1}^{N} (-i,-1)\, \underline{D}^{N-j}\, \underline{G}\, \underline{T}^{j-1}\, \vec{z}_0 \\
&= \lim_{N\to\infty} \frac{e^{i2\pi N\nu_0}}{2\pi N} (\vec{0}^{\mathrm{T}}, i, 1)\, \underline{M}^N \begin{pmatrix} \vec{z}_0 \\ 0 \\ 0 \end{pmatrix} \quad . \qquad (2.130)
\end{aligned}
$$

We have seen in (2.128), (2.130) that the linear intrinsic resonance strengths can be computed from the total linear flow $\underline{M}$ *without* actually performing a Fourier decomposition. A numerical Fourier decomposition as in equation (2.109) can become quite cumbersome at large $G\gamma$ since the integrand must be evaluated at a large number of points θ_j, $j = 1, \cdots, N$ which will normally *not* be equidistant and therefore *not* suitable for FFT–techniques. In fact matrix methods have other advantages over the use of spin–orbit integrals [BR99a]. In [GH99b] a method for obtaining the $\underline{G}$–matrix from the linearised one–turn quaternion is discussed.

2.3.3 Spin–orbit coupling integrals

We will now motivate a method for analysing the first order dependence of spin motion on the orbital motion that will turn out to give a remarkably simple and intuitive approach to decoupling spin motion from the orbital motion in the case of flat or flattened (see definition 3.2) rings. The apparent simplicity of treating symmetries in the framework of linear spin–orbit coupling integrals will in particular enable us in chapter 3 to explain the first order effect of Siberian Snakes on spin motion in accelerators. It should be noted here that this approach is well suited to performing analytic estimates in simple models of rings or for highly periodic parts of rings but that, as explained in the previous section, matrix methods are more efficient for numerical first order analysis.

The on–orbit spin action $I_0 \equiv \hat{n}_0 \cdot \widehat{S}$ as introduced in equation (2.96) is conserved only on the design orbit. For any finite orbital amplitude we obtain

$$\mathrm{D}_\theta\, I_0 = (\vec{\Omega}_0 + \vec{\omega}) \times \widehat{S} \cdot \hat{n}_0 + \widehat{S} \cdot \vec{\Omega}_0 \times \hat{n}_0 = \vec{\omega} \times \widehat{S} \cdot \hat{n}_0 = \vec{S}_\perp \times \hat{n}_0 \cdot \vec{\omega} \quad , \tag{2.131}$$

where $\vec{S}_\perp = \widehat{S} - \hat{n}_0\, \hat{n}_0 \cdot \widehat{S}$ is the component of $\widehat{S}$ perpendicular to $\hat{n}_0$. In the same manner as in the last section we can perform perturbation theory in $\vec{\omega}$ and obtain in 0–th order $I_0 = \text{const.} = I_{00}$ and that $\vec{S}_\perp$ precesses around $\hat{n}_0$. We recall that in the $(\hat{l}_0, \hat{n}_0, \hat{m}_0)$ frame of T–BMT solutions (2.92) a spin on the design orbit does not precess and rewrite $\vec{S}_\perp^{(0)}$ in terms of $\vec{k}_0(\theta) \equiv \hat{l}_0(\theta) + i\hat{m}_0(\theta)$, $\vec{k}_0 \in \mathbb{C}^3$, $||\vec{k}_0|| = \sqrt{2}$ as

$$\vec{S}_\perp^{(0)}(\theta) = \sqrt{1 - I_{00}^2}\, \Re\Big(\vec{k}_0(\theta) e^{i\Phi_0}\Big) \quad . \tag{2.132}$$

Inserting $\vec{S}_\perp^{(0)}$ into equation (2.131) we find

$$\mathrm{D}_\theta\, I_0^{(1)} = \sqrt{1 - I_{00}^2}\, \Re\Big(e^{i\Phi_0} \vec{k}_0 \times \hat{n}_0 \cdot \vec{\omega}\Big) = \sqrt{1 - I_{00}^2}\, \Im\Big(e^{i\Phi_0} \vec{k}_0 \cdot \vec{\omega}\Big) \quad . \tag{2.133}$$

Note that equation (2.133) has two unphysical unstable fixed points at $I_0 = \pm 1$ introduced by the polar decomposition of $\widehat{S}$. These fixed points reflect the fact that the derivative of I_0, which is the cosine of the angle between $\hat{n}_0$ and $\widehat{S}$, w.r.t. this angle vanishes for vanishing angle. Also note that this first order approximation of I_0 violates orthogonality since $I_0(\theta)$ is not necessarily bounded for arbitrary $\vec{\omega}$. We can modify it to preserve orthogonality by substituting the constant $\sqrt{1 - I_{00}^2}$ in the r.h.s of equation (2.133) with the variable $\sqrt{1 - (I_0^{(1)})^2}$. The resulting ODE is still solvable and with

$$F(\theta; \Phi_0, \vec{z}_0) \equiv \Im\left(e^{i\Phi_0} \int_0^\theta \vec{k}_0(\theta') \cdot \vec{\omega}(\theta'; \vec{z}_0)\, d\theta'\right) \tag{2.134}$$

and $-1 < I_{00} < +1$ we obtain by separation of variables

$$\begin{aligned} \arcsin \tilde{I}_0(\theta) - \arcsin I_{00} &= F(\theta; \Phi_0, \vec{z}_0) \\ \Rightarrow \tilde{I}_0(\theta) &= I_{00} \cos F(\theta; \Phi_0, \vec{z}_0) + \sqrt{1 - I_{00}^2} \sin F(\theta; \Phi_0, \vec{z}_0) \end{aligned} \tag{2.135}$$

which satisfies $\tilde{I}_0(\theta) \in [-1,1]$ and stays well defined also in the limit $I_{00} \to \pm 1$! In fact this approximation just represents the rotation of $\widehat{S}$ from its initial direction by the angle F. More precisely, the angle between $\hat{n}_0$ and $\widehat{S}$, $\tilde{\alpha} \equiv \arccos I_0$ is given by

$$|\tilde{\alpha}(\theta) - \tilde{\alpha}_{00}| = |F(\theta; \Phi_0, \vec{z}_0)| \bmod \pi \quad . \tag{2.136}$$

Therefore if we start with $\widehat{S}(0) \parallel \hat{n}_0(0)$ and if $|F(\theta; \Phi_0, \vec{z}_0)| \le \tilde{\epsilon} < \pi$ for all θ the motion of $\tilde{\alpha}(\theta) - \tilde{\alpha}_{00}$ is bounded in the interval $[-\tilde{\epsilon}, +\tilde{\epsilon}]$ — in the above approximation. In the higher order approximations mentioned in section 2.2.2 the deviation of the actual spin precession rate from ν_0 (e.g. by the terms $-\beta\omega_n$ and $\alpha\omega_n$ in equations (2.98a) and (2.98b)) and the coupling between I_0 and $\vec{S}_\perp$ are successively included.

We note that following the definition in equation (2.123) we have

$$\underline{G}_0(0)\vec{z}_0 = \begin{pmatrix} -F^{(1)}(2\pi; \frac{\pi}{2}, \vec{z}_0) \\ +F^{(1)}(2\pi; 0, \vec{z}_0) \end{pmatrix} \quad , \tag{2.137}$$

where $F^{(1)}$ indicates that $\vec{\omega} = \vec{\omega}^{(1)}$ is used. Also from equation (2.126a) for any linear intrinsic resonance $\nu_0(E_0) = k_0 + \vec{k} \cdot \vec{Q}$, $|\vec{k}| = 1$ we obtain

$$-i\epsilon_{\nu_0}(\vec{J}, \vec{\Psi}_0, E_0) = \lim_{\theta \to \infty} \left. \frac{F^{(1)}(\theta; 0, \vec{z}_0)}{\theta} \right|_{\vec{z}_0(\vec{J}, \vec{\Psi}_0), E_0} \quad . \tag{2.138}$$

We now assume that the orbital motion is linear, that the transverse phase space planes are decoupled and that $\vec{\omega} = \vec{\omega}^{(1)}$ depends only linearly on the orbital coordinates. Under these assumptions $\vec{\omega}^{(1)}$ can be decomposed into the contributions due to radial (x), vertical (y) and longitudinal (z) orbital motion.

$$\vec{\omega}^{(1)}(\theta; \vec{J}, \vec{\Psi}_0) \equiv \vec{\omega}_x(\theta; J_x, \Psi_{x,0}) + \vec{\omega}_y(\theta; J_y, \Psi_{y,0}) + \vec{\omega}_z(\theta; J_z, \Psi_{z,0}) \quad . \tag{2.139}$$

If the effects of $\vec{B}_{||}$ and $\vec{E}$ in $\vec{\Omega}$ can be neglected, these contributions can be written in terms of β–functions $\beta_{x,y}$, periodic dispersions $\vec{x}_D$, $\vec{y}_D$, the focusing function K and orbital phase advances $\psi_{x,y}$ [CY81, SM93, BR99a]

$$\vec{\omega}_j(\theta; J_j, \Psi_{i,0}) \equiv \frac{1}{2}\sqrt{2J_j}\left(\vec{\omega}_j^+(\theta)e^{+i\Psi_{j,0}} + \vec{\omega}_j^-(\theta)e^{-i\Psi_{j,0}}\right), \quad j = x, y, z \tag{2.140a}$$

$$\vec{\omega}_x^\pm(\theta) = (G\gamma + 1)\,K(\theta)\,\sqrt{\beta_x(\theta)}\,e^{\pm i\psi_x(\theta)}\,\hat{y} \tag{2.140b}$$

$$\vec{\omega}_y^\pm(\theta) = -(G\gamma + 1)\,K(\theta)\,\sqrt{\beta_y(\theta)}\,e^{\pm i\psi_y(\theta)}\,\hat{x} \tag{2.140c}$$

$$\vec{\omega}_z^\pm(\theta) = (G\gamma + 1)\,K(\theta)\,(x_D(\theta)\hat{y} - y_D(\theta)\hat{x})\,e^{\pm i\psi_z(\theta)} \quad . \tag{2.140d}$$

We now define the 6 *linear spin–orbit coupling integrals*[5] as the one–turn integrals

$$I_j^\pm(\theta) = \int_\theta^{\theta+2\pi} \vec{\omega}_j^\pm(\theta') \cdot \vec{k}_0(\theta')\,d\theta' \quad , \quad j = x, y, z \quad . \tag{2.141}$$

An accelerator is said to be *linearly spin matched* [BR99a] at an azimuth θ_0 if all the $I_j^\pm(\theta_0)$ vanish. Then in *first order perturbation theory* in $\vec{\omega}^{(1)}$ a spin starting on an arbitrary synchro–betatron trajectory $\vec{\xi}(\theta; \vec{z}_0, \theta_0)$ with initial conditions $\widehat{S}(\theta_0; \vec{z}_0, \theta_0) \equiv \hat{n}_0(\theta_0)$ will return after one revolution, $\widehat{S}(\theta_0 + 2\pi; \vec{z}_0, \theta_0) = \hat{n}_0(\theta_0)$. This linear approximation is of course only valid in a finite and normally rather small vicinity of $\vec{z}_0 = \vec{0}$ and it does *not* mean that $\widehat{S}(\theta; \vec{z}_0, \theta_0) = \hat{n}_0(\theta)$ for all $\theta \in [\theta_0, \theta_0 + 2\pi]$.

[5] Don't confuse the on–orbit spin action I_0 with the linear spin–orbit coupling integrals $I_j^\pm$!

In an unperturbed ring with mid–plane symmetry, i.e. when $\vec{k}_0$ is in the horizontal plane and $y_D \equiv 0$, all contributions to the $I_j^\pm$ which are proportional to $\hat{y}$ or y_D vanish identically. Therefore only the vertical spin–orbit coupling integrals $I_y^\pm$ survive and

$$I_x^{\pm,\mathrm{mps}}(\theta) \equiv I_z^{\pm,\mathrm{mps}}(\theta) \equiv 0 \quad . \tag{2.142}$$

Additionally we can set $\hat{l}_0(0) \equiv \hat{x}$ and $\hat{m}_0(0) \equiv \hat{z}$ at some reference azimuth $\theta_0 = 0$ and hence express $\vec{k}_0(\theta)$ in terms of $\hat{x} + i\hat{z}$ and the on–orbit spin phase advance $\phi(\theta)$ in the Frenet–Serret comoving coordinate system with

$$\phi(0) \equiv 0 \ \ , \ \ \phi(\theta + 2\pi) - \phi(\theta) = 2\pi\nu_0 \quad . \tag{2.143}$$

We find $\vec{k}_0(\theta) = (\hat{x} + i\hat{z})e^{i\phi(\theta)}$ and therefore

$$I_y^{\pm,\mathrm{mps}}(\theta) = -(G\gamma + 1) \int_\theta^{\theta+2\pi} K(\theta') \sqrt{\beta_y(\theta')}\, e^{i(\phi(\theta') \pm \psi_y(\theta'))}\, d\theta' \quad . \tag{2.144}$$

If the ring has a superperiodicity $P \in \mathbb{N}^*$, then with $h(\theta) \equiv -(G\gamma+1)K(\theta)\sqrt{\beta(\theta)}$ and $T \equiv 2\pi/P$ the condition $h(\theta + T) = h(\theta)$ holds. As a consequence of Floquet's theorem (see appendix A) we have

$$\phi(\theta + 2\pi) - \phi(\theta) = 2\pi\nu_0 \quad , \quad \phi(\theta + T) - \phi(\theta) = T\nu_0 \equiv 2\pi\nu_{0,P} \tag{2.145a}$$
$$\psi_y(\theta + 2\pi) - \psi_y(\theta) = 2\pi Q_y \quad , \quad \psi_y(\theta + T) - \psi_y(\theta) = TQ_y \equiv 2\pi Q_{y,P} \tag{2.145b}$$

and hence [KS88b, VA98, GH99c, SL97]

$$\begin{aligned} I_y^{\pm,\mathrm{mps}}(\theta) &= \sum_{j=0}^{P-1} e^{i2\pi j(\nu_{0,P} \pm Q_{y,P})} \int_\theta^{\theta+T} h(\theta')\, e^{i(\phi(\theta') \pm \psi_y(\theta'))}\, d\theta' \\ &= \frac{1 - e^{i2\pi P(\nu_{0,P} \pm Q_{y,P})}}{1 - e^{i2\pi(\nu_{0,P} \pm Q_{y,P})}} \int_\theta^{\theta+T} h(\theta')\, e^{i(\phi(\theta') \pm \psi_y(\theta'))}\, d\theta' \\ &\equiv \xi_P(2\pi(\nu_{0,P} \pm Q_{y,P})))\ I_{y,P}^{\pm,\mathrm{mps}}(\theta) \quad , \end{aligned} \tag{2.146}$$

where we have defined the complex amplification function

$$\xi_P(x) \equiv \frac{1 - e^{iPx}}{1 - e^{ix}} \quad \text{with} \tag{2.147a}$$
$$|\xi_P(x)| = \left| \frac{\sin \frac{Px}{2}}{\sin \frac{x}{2}} \right| \quad , \quad \Re\xi_P(x) = \frac{1}{2}\left(1 + \frac{\cos((P-1)x) - \cos Px}{1 - \cos x}\right) \tag{2.147b}$$
$$\xi_P(x)\Big|_{x=0 \bmod 2\pi} = P \quad , \quad \xi_P(x)\Big|_{x=l\frac{2\pi}{P} \bmod 2\pi, 1\le l\le P-1} = 0 \tag{2.147c}$$

and the spin–orbit coupling integral for one period $I_{y,P}^{\pm,\mathrm{mps}}(\theta)$. It is easy to show that $|\xi_P(x)|$ is 2π–periodic and that in the interval $[0, 2\pi)$ it has one global maximum at $x = 0$ and $P - 2$ additional local maxima. These additional local maxima strongly decay for sufficiently large P and for odd P we have $\xi_P(\pi)/\xi_P(0) = 1/P$. Therefore we conclude

1. at the resonance $\nu_{0,P} \pm Q_{y,P} = 0 \bmod 1$ the spin–orbit coupling is particularly enhanced (see (2.113)).

2. There are *magic* energies $E_P^\pm$ with $\nu_{0,P}(E_P^\pm) \pm Q_{y,P} = \frac{l}{P}$, $1 \le l < P$ where *one* of the $I_y^{\pm,\mathrm{mps}}(\theta)$ identically vanishes. Assuming that $Q_{y,P} \neq 1/2$ we can never make both integrals vanish simultaneously.

We now assume that each superperiod consists of a $^1/_2$ *leading* straight section from $\theta = 0 \bmod T$ to $\theta_l \bmod T$, an arc made of M identical cells (e.g. FODO cells) from $\theta = \theta_l \bmod T$ to $\theta_t \bmod T$ and a $^1/_2$ *trailing* straight section from $\theta = \theta_t \bmod T$ to $T \bmod T$. Then using $T_C = (\theta_t - \theta_l)/M$ we obtain

$$
\begin{aligned}
I^{\pm,\mathrm{mps}}_{y,P}(0 \bmod T) &= \int_0^{\theta_l} h\, e^{i(\phi \pm \psi_y)}\, d\theta + \int_{\theta_l}^{\theta_t} h\, e^{i(\phi \pm \psi_y)}\, d\theta + \int_{\theta_t}^{T} h\, e^{i(\phi \pm \psi_y)}\, d\theta \\
&\equiv I_l^{\pm} + \xi_M(2\pi(\nu_{0,C} \pm Q_{y,C}))\, I_C^{\pm,\mathrm{mps}} + I_t^{\pm} \quad , \qquad (2.148)
\end{aligned}
$$

where we have introduced the integral over one arc–cell $I_C^{\pm,\mathrm{mps}} \equiv \int_{\theta_l}^{\theta_l + T_C} h\, e^{i(\phi \pm \psi)}\, d\theta$ and the spin and orbital phase advance per cell $2\pi\nu_{0,C} = \phi(\theta_l + T_C) - \phi(\theta_l)$ and $2\pi Q_{y,C} = \psi_y(\theta_l + T_C) - \psi_y(\theta_l)$ respectively. Obviously $\nu_{0,C} \pm Q_{y,C}$ do *not* produce magic energies since they don't affect the contribution from the straight sections, but whenever $\nu_{0,C} \pm Q_{y,C} = 0 \bmod 1$ the contribution from the highly periodic arcs is strongly enhanced (see (2.116)).

The six linear spin–orbit coupling integrals $I_j^{\pm}$, $j = x, y, z$ can each be expressed in terms of integrals over *single* complex orbital eigenmodes $\vec{V}_j^{\pm}(\theta) e^{\pm i Q_j \theta}$ (see appendix A for the definition of the orbital eigenvectors). This procedure can easily be generalised to coupled orbital motion in rings without mid–plane symmetry [SM86b]. Each integrand is therefore an *elementarily pseudo–periodic* function over one *single* tune $\pm Q_{j,P}$ and its generalised Fourier coefficients can be generated by one–turn integrals. Using equations (2.138) to (2.141) we can construct the linear intrinsic resonance strength $\epsilon_{k_0 \pm Q_j}$ if $\nu_{0,P} = k_0 \pm Q_{j,P}$ and obtain

$$
\begin{aligned}
i\epsilon_{k_0 \pm Q_j}(J, \Psi_0, E_0) &= \sqrt{2J_j} e^{\mp i \Psi_{0,j}} \lim_{N \to \infty} \frac{1}{2\pi N} \xi_N(2\pi(\nu_0 - k_0 \mp Q_{j,P})) \frac{1}{2} I_j^{\mp}(0) \Big|_{\nu_{0,P}(E_0) = k_0 \pm Q_{j,P}} \\
&= \frac{\sqrt{2J_j}\, e^{\mp i \Psi_{0,j}}}{4\pi} I_j^{\mp}(0) \Big|_{\nu_{0,P}(E_0) = k_0 \pm Q_{j,P}} \quad . \qquad (2.149)
\end{aligned}
$$

Resonance strengths are in general *not* the same as spin–orbit coupling integrals — not even in the case of a ring with perfect mid–plane symmetry. In particular $\epsilon_{k_0, \vec{k}}$ is the generalised Fourier component of a function ζ which is pseudo–periodic over the tunes $\vec{Q}_P$ and therefore vanishes identically for all $\nu_{0,P}(E_0) \neq k_0 + \vec{k} \cdot \vec{Q}_P$. In contrast to the resonance strengths, the spin–orbit coupling integrals which are one–turn integrals *never* identically vanish except for some magic energies. Nevertheless, if the spin–orbit coupling can be decomposed into contributions from different *elementarily* pseudo–periodic orbital modes and the $I_j^{\pm}$ are evaluated at the resonant spin tune they provide a tool for obtaining the generalised Fourier coefficients of the T–BMT driving term perpendicular to $\hat{n}_0$ in terms of one–turn integrals. This is a second viewpoint on how equations (2.146) and (2.148) explain the significance of the strong and super–strong resonances as defined in equations (2.113) and (2.116).

2.4 The single resonance model

So far we have treated spin–orbit coupling using the full $\vec{\omega}$ and the approximations of (2.102a) to (2.102d) and (2.133). However, if a particular resonance dominates the spin motion, then by noting that the contribution to $\vec{\omega}$ from this harmonic represents a vector rotating in the plane perpendicular to $\hat{n}_0$, an exactly solvable model containing just a *single* resonance can be employed [CR80, SM88, SM92, HH96, SL97]. Although this *single resonance model* (SRM) was originally motivated by the calculation of first order resonance effects [CR80], it has wider applicability so that in the following a general form will be presented. Since the model includes only one resonance the coupling between spin and all but one phase space plane is neglected. The orbital motion is assumed to be integrable so that one can either eliminate the dependence of $\vec{\Omega}$ on the orbital phases [CR80, SL97] or on the azimuth [SM88, HH96]. We will keep the phase as well as the azimuthal dependence and define the

SRM as

$$\begin{aligned}
&\mathrm{D}_\theta J = 0 \quad , \quad \Psi(\theta) = \Psi_0 + Q\theta \ , \ \mathrm{D}_\theta \widehat{S} = (\vec{\Omega}_0 + \vec{\omega}) \times \widehat{S} \\
&\vec{\Omega}_0 = \text{const.} = \hat{y}\,\nu_0 \quad , \quad \vec{\omega}(\Psi,\theta) = \epsilon\ (\hat{x}\ \sin(k_0\theta + k\Psi + \psi_\epsilon) \ + \ \hat{z}\ \cos(k_0\theta + k\Psi + \psi_\epsilon)) \quad , \qquad (2.150)
\end{aligned}$$

where $k \neq 0$ and k_0 are integers, Q and ν_0 may contain an integer part and where in principle $\epsilon \in \mathbb{R}^+$ and $\nu_0 \in \mathbb{R}$ can be arbitrary functions of E_0 and J. ψ_ϵ is some real phase factor. We discuss a physical interpretation of the model below but note here that if equation (2.150) is meant to represent spin motion on a vertical betatron trajectory in a mid–plane symmetric ring, then k must be odd. We will not perform any perturbation expansions within this model — since we can solve the EOM analytically — but normally one assumes ϵ to be continuous w.r.t. J in some vicinity of $J = 0$ and $\epsilon|_{J=0} = 0$. Also ν_0 is normally assumed to be independent of J so that it can be identified with the on–orbit spin tune. The only constraints on $(\hat{x}, \hat{y}, \hat{z})$ are that they form a right–handed basis and that they are periodic in θ and Ψ. The most simple choices are the *lab–system* or the *Frenet–Serret–system* which are trivially periodic. Then $\vec{\Omega}$ is assumed to model the precession as described by the original T–BMT equations in the lab- or Frenet–Serret–system respectively. Nevertheless the model is rather general and we will occasionally use a more complicated periodic frame and drop the assumptions on ϵ and ν_0 in later chapters (e.g. 4.8). Note that $\vec{\Omega} = \vec{\Omega}_0 + \vec{\omega}$ is 2π–periodic w.r.t. θ and Ψ so that $\vec{\Omega}(\Psi(\theta), \theta)$ is pseudo–periodic over Q or, to be more precise, elementarily pseudo–periodic over kQ (see appendix A.1.3). Since $\vec{\Omega}_0 = \nu_0\hat{y} = $ const. we find $\hat{n}_0(\theta) = \pm\hat{y}$ and without loss of generality choose the sign to be $+$. In the limit $\epsilon \to 0$ a spin is transported in the $(\hat{x}, \hat{y}, \hat{z})$ frame by

$$\underline{R}_0(\theta_f, \theta_i) = \begin{pmatrix} \cos\nu_0\Delta & 0 & -\sin\nu_0\Delta \\ 0 & 1 & 0 \\ \sin\nu_0\Delta & 0 & \cos\nu_0\Delta \end{pmatrix} \quad , \qquad (2.151)$$

with $\Delta \equiv \theta_f - \theta_i$. At $\theta_0 = 0$ we choose our right–handed coordinate systems $(\hat{l}(0), \hat{n}_0(0), \hat{m}(0)) \equiv (\hat{l}_0(0), \hat{n}_0(0), \hat{m}_0(0)) \equiv (\hat{x}, \hat{y}, \hat{z})$. At any other $\theta \in \mathbb{R}$ we obtain

$$\begin{aligned}
(\hat{l}_0(\theta), \hat{m}_0(\theta)) &= \underline{R}_0(\theta, 0)(\hat{l}_0(0), \hat{m}_0(0)) = (\hat{x}, \hat{z}) \begin{pmatrix} \cos\nu_0\theta & \sin\nu_0\theta \\ -\sin\nu_0\theta & \cos\nu_0\theta \end{pmatrix} &(2.152a)\\
\Rightarrow \vec{k}_0(\theta) &= (\hat{x} + i\hat{z})e^{i\nu_0\theta} &(2.152b)\\
(\hat{l}(\theta), \hat{m}(\theta)) &= \underline{R}_0(\theta_f, \theta_i)(\hat{l}_0(0), \hat{m}_0(0)) \begin{pmatrix} \cos\nu_0\Delta & -\sin\nu_0\Delta \\ \sin\nu_0\Delta & \cos\nu_0\Delta \end{pmatrix} = (\hat{x}, \hat{z}) &(2.152c)\\
\Rightarrow \zeta(\theta) &= \omega_z - i\omega_x = \epsilon\, e^{-i(k\Psi_0 + \psi_\epsilon + k_0\theta + kQ\theta)} \quad . &(2.152d)
\end{aligned}$$

Therefore we find

$$\epsilon_\kappa = \epsilon\, e^{-i(k\Psi_0 + \psi_\epsilon)} \lim_{N\to\infty} \frac{1}{2\pi N} \int_0^{2\pi N} e^{-i(k_0 + kQ)\theta} e^{i\kappa\theta}\, d\theta = \epsilon\, e^{-i(k\Psi_0 + \psi_\epsilon)}\, \delta_{\kappa, k_0 + kQ} \quad , \qquad (2.153)$$

proving that our single resonance model has indeed only one single resonance with the modulus of the strength being ϵ.

The SRM can be interpreted in terms of dynamical k–th order spin–orbit coupling integrals and. Since $\vec{\omega}$ is pseudo–periodic over Q and elementarily pseudo–periodic over kQ it has only one generalised Fourier coefficient which is proportional to the orbital amplitude to the k–th power. We introduce the normal form orbital coordinates $q = \sqrt{2J}\cos\Psi$ and $p = -\sqrt{2J}\sin\Psi$ and the two complex conjugate eigenmodes $\xi = q - ip = \sqrt{2J}e^{i\Psi}$ and $\xi^* = q + ip = \sqrt{2J}e^{-i\Psi}$. A homogeneous complex k–th order form in the complex eigenmodes then has the general form $h^+(\theta)\xi^k(\theta) + h^-(\theta)\xi^{*k}(\theta)$ where h^+ and h^- are two independent functions. We assume $h^\pm$ to contain only the k_0–th harmonic of the revolution frequency, i.e. $h^{\pm} \equiv \epsilon_0 e^{\pm i k_0 \theta}$ and construct the contributions to $\vec{\omega}$ from the two complex eigenmodes as in equation (2.140a)

$$\vec{\omega} = \frac{1}{2}(2J)^{\frac{k}{2}} \left(\vec{\omega}^{(k)+} e^{+ik\Psi_0} + \vec{\omega}^{(k)-} e^{-ik\Psi_0} \right) \quad , \quad \vec{\omega}^{(k)\pm} = \epsilon_0 \, (\hat{z} \mp i\hat{x}) e^{\pm i(\psi_\epsilon + (k_0+kQ)\theta)} \quad . \tag{2.154}$$

In this interpretation we obtain a model of the J–dependence of ϵ as in equation (2.150) for a *dynamical* k–th order resonance

$$\epsilon = \epsilon_0 \, (2J)^{\frac{k}{2}} \, e^{-i(k\Psi_0 + \psi_\epsilon)} \quad , \quad \epsilon_0 = \text{const.} \quad . \tag{2.155}$$

Now we define the two dynamical k–th order spin–orbit coupling integrals

$$\begin{aligned} I^{(k)\pm}(\theta) &= \int_\theta^{\theta+2\pi} \vec{\omega}^{(k)\pm}(\theta') \cdot \vec{k}_0(\theta') \, d\theta' \\ &= \epsilon_0 e^{\pm i\psi_\epsilon} \int_\theta^{\theta+2\pi} (\hat{z} \mp i\hat{x}) \cdot (\hat{x} + i\hat{z}) e^{i(\nu_0 \pm (k_0+kQ))\theta'} \, d\theta' \\ &= 2i\delta_-^{\pm} \, \epsilon_0 e^{-i\psi_\epsilon} \int_\theta^{\theta+2\pi} e^{i(\nu_0 - (k_0+kQ))\theta'} \, d\theta' \\ &= 2i\delta_-^{\pm} \, \epsilon_0 e^{i(\nu_0-(k_0+kQ))\theta - i\psi_\epsilon} \, \frac{e^{i2\pi(\nu_0-(k_0+kQ))} - 1}{i(\nu_0 - (k_0+kQ))} \quad , \end{aligned} \tag{2.156}$$

where we have used $(\hat{z} - i\hat{x}) \cdot (\hat{x} + i\hat{z}) = 0$, $(\hat{z} + i\hat{x}) \cdot (\hat{x} + i\hat{z}) = 2i$ and rather symbolically introduced $\delta_-^{\pm} = 0$ for $I^{(k)+}$ and $\delta_-^{\pm} = 1$ for $I^{(k)-}$. At $\nu_0 = k_0 + kQ$ we find $I^{(k)-} = 4\pi\epsilon_0 e^{-i\psi_\epsilon}$ and use of equations (2.149) and (2.153) yields

$$i \, \epsilon_{k_0+kQ}(J, \Psi_0, E_0) = \frac{e^{-ik\Psi_0}(2J)^{\frac{k}{2}}}{4\pi} \, I^{(k)-}\Big|_{\nu_0(E_0)=k_0+kQ} \quad . \tag{2.157}$$

Two remarks are needed here.

1. The $\vec{\omega}$ in equation (2.150) describes a rotating field. For $k = 1$ we could think of a ring made of one long combined function magnet with constant horizontal curvature and constant focusing strength K to obtain $\vec{\omega} \sim \sin(k_0 + Q)\theta$ along the radial direction. If we drop either $\hat{x}$ or $i\hat{z}$ in equation (2.154) we obtain $\vec{\omega}(\Psi, \theta) \sim \hat{z}\cos(\psi_\epsilon + k_0\theta + \Psi)$ or $\vec{\omega}(\Psi, \theta) \sim \hat{x}\sin(\psi_\epsilon + k_0\theta + \Psi)$ respectively. As one can easily see from equation (2.156), in such a system I^- and I^+ in general are both non–zero and we would end up with 2 resonances at k_0+Q and k_0-Q with strength $\epsilon/2$ each. Indeed equation (2.154) represents the sum of two counter rotating fields. One produces a resonance at $\nu_0 = k_0 + Q$ the other at $\nu_0 = k_0 - Q$. Whenever the resonances are "sufficiently separated" (see section 4.7) and the system is close to one resonance we might be able to neglect the other resonance [CR80].

2. The key assumption of the SRM is that $\vec{\omega}$ has only one generalised Fourier harmonic. We could extend the model to full 6–dimensional orbital motion with $\xi_j \equiv \sqrt{2J_j}e^{i\Psi_j}$, $\vec{\omega}^{(\vec{k})\pm} = \epsilon_0(\hat{z} \mp i\hat{x})e^{\pm i(\psi_\epsilon + (k_0 + \vec{k}\cdot\vec{Q})\theta)}$ and would obtain a single resonance with strength proportional to the $|\vec{k}|$–th order monomial $(2\vec{J})^{\vec{k}/2} = \prod(2J_j)^{|k_j|/2}$ in the orbital amplitudes at position $\nu_0 = k_0 + \vec{k}\cdot\vec{Q}$. These additional degrees of freedom would *not* introduce any new dynamics but only shift the resonance position. The SRM is defined to contain one single harmonic of $\vec{\omega}$. This property is embodied in the dependence of $\vec{\omega}$ on θ and Ψ. The vector $\vec{\omega}$, evaluated along an orbital trajectory, rotates in the plane perpendicular to $\hat{n}_0$ with the *constant* rate $\kappa = k_0 + k\Psi$ and is *periodic* w.r.t. θ and Ψ. The extension simply implies $\vec{\omega}/\epsilon = \hat{x}\sin(k_0\theta + \vec{k}\cdot\vec{\Psi} + \psi_\epsilon) + \hat{z}\cos(k_0\theta + \vec{k}\cdot\vec{\Psi} + \psi_\epsilon)$ so that $\vec{\omega}$ rotates with the constant rate $\kappa = k_0 + \vec{k}\cdot\vec{Q}$ and is periodic w.r.t. θ and the Ψ_i.

We will now solve the EOM (2.150) explicitly for constant ν_0 and ϵ. For this purpose we introduce the following abbreviations:

$$\text{the resonance position} \quad \kappa \equiv k_0 + kQ \quad , \tag{2.158a}$$
$$\text{the resonance phase} \quad \phi(\theta,\Psi) \equiv \psi_\epsilon + k_0\theta + k\Psi \quad , \tag{2.158b}$$
$$\text{with} \quad \mathrm{D}_\theta\,\phi \equiv (\partial_\theta + Q\partial_\Psi)\phi = \kappa \tag{2.158c}$$
$$\text{the proximity parameter} \quad \delta \equiv \nu_0 - \kappa \tag{2.158d}$$
$$\text{and} \quad \lambda \equiv \sqrt{\delta^2+\epsilon^2} \quad , \tag{2.158e}$$

so that $\vec{\omega} = \epsilon(\hat{x}\sin\phi + \hat{z}\cos\phi)$. We note that ϕ mod 2π is 2π–periodic in θ as well as in Ψ so that *every* 2π–periodic function of only ϕ is also 2π–periodic in θ and Ψ. This function, if evaluated along a trajectory, would then be elementarily pseudo–periodic. Equation (2.150) can now be solved using equation (2.17) where $\underline{A}$ is a rotation around $\hat{y}$ by $-\phi(\theta,\Psi)$:

$$\underline{A}(\theta,\Psi) \equiv \begin{pmatrix} \cos\phi & 0 & -\sin\phi \\ 0 & 1 & 0 \\ \sin\phi & 0 & \cos\phi \end{pmatrix} \quad \Leftrightarrow \quad \bar{a}(\theta,\Psi) \equiv \left(\cos\frac{\phi}{2}, 0, \sin\frac{-\phi}{2}, 0\right) \tag{2.159}$$

and

$$(\mathrm{D}_\theta\,\underline{A})\,\underline{A}^{\mathrm{T}} = \begin{pmatrix} 0 & 0 & -\kappa \\ 0 & 0 & 0 \\ \kappa & 0 & 0 \end{pmatrix} \quad \text{and} \quad \underline{A}\,\underline{\Omega}\,\underline{A}^{\mathrm{T}} = \begin{pmatrix} 0 & -\epsilon & \nu_0 \\ \epsilon & 0 & 0 \\ -\nu_0 & 0 & 0 \end{pmatrix} \quad , \tag{2.160}$$

so that in the *resonance precession frame* we find

$$\vec{\Omega}_a = (0,\delta,\epsilon) \quad , \quad \partial_\theta\,\vec{\Omega}_a = \partial_\Psi\,\vec{\Omega}_a = \vec{0} \quad . \tag{2.161}$$

In this frame the solution is just a rotation around $\hat{n}_a = \text{const.} = \vec{\Omega}_a/\lambda$ by the angle $\lambda\,(\theta_f-\theta_i)$ so that the flow in the resonance precession frame is independent of Ψ and reads in quaternion notation as

$$\bar{r}_a(\theta_f,\theta_i) = \left(\cos\frac{\lambda}{2}(\theta_f-\theta_i),\ 0,\ \frac{\delta}{\lambda}\sin\frac{\lambda}{2}(\theta_f-\theta_i),\ \frac{\epsilon}{\lambda}\sin\frac{\lambda}{2}(\theta_f-\theta_i)\right) \quad . \tag{2.162}$$

Therefore the flow in the $(\hat{x},\hat{y},\hat{z})$ frame is

$$\bar{r}(\theta_f,\theta_i;\Psi_i) = \bar{a}^{-1}(\theta_f,\Psi_i+Q(\theta_f-\theta_i))\ \bar{r}_a(\theta_f,\theta_i)\ \bar{a}(\theta_i,\Psi_i) \tag{2.163}$$

or explicitly with $\Delta \equiv \theta_f - \theta_i$ and $\phi_\epsilon(\theta_f,\theta_i) \equiv \psi_\epsilon + k_0\theta_i + \frac{\kappa\Delta}{2}$

$$r_0(\theta_f,\theta_i;\Psi_i) = \cos\frac{\lambda\Delta}{2}\cos\frac{\kappa\Delta}{2} - \frac{\delta}{\lambda}\sin\frac{\lambda\Delta}{2}\sin\frac{\kappa\Delta}{2} \tag{2.164a}$$
$$= \sqrt{1-\frac{\epsilon^2}{\lambda^2}\sin^2\frac{\lambda\Delta}{2}}\ \cos\left(\frac{\kappa\Delta}{2} + \arctan(\frac{\delta}{\lambda}\tan\frac{\lambda\Delta}{2})\right) \tag{2.164b}$$
$$r_1(\theta_f,\theta_i;\Psi_i) = \frac{\epsilon}{\lambda}\sin\frac{\lambda\Delta}{2}\sin(\phi_\epsilon(\theta_f,\theta_i)+k\Psi_i) \tag{2.164c}$$
$$r_2(\theta_f,\theta_i;\Psi_i) = \cos\frac{\lambda\Delta}{2}\sin\frac{\kappa\Delta}{2} + \frac{\delta}{\lambda}\sin\frac{\lambda\Delta}{2}\cos\frac{\kappa\Delta}{2} \tag{2.164d}$$
$$= \sqrt{1-\frac{\epsilon^2}{\lambda^2}\sin^2\frac{\lambda\Delta}{2}}\ \sin\left(\frac{\kappa\Delta}{2} + \arctan(\frac{\delta}{\lambda}\tan\frac{\lambda\Delta}{2})\right) \tag{2.164e}$$
$$r_3(\theta_f,\theta_i;\Psi_i) = \frac{\epsilon}{\lambda}\sin\frac{\lambda\Delta}{2}\cos(\phi_\epsilon(\theta_f,\theta_i)+k\Psi_i) \quad . \tag{2.164f}$$

Sometimes [SL97] the formulae (2.164b) and (2.164e) for $\bar{r}_0$ and $\bar{r}_2$ are considered more convenient than (2.164a) and (2.164d). Both (2.164b) and (2.164e) are derived by using the $(1,1)$–component

$r_{11} = r_0 - ir_2 = (\cos\frac{\kappa\Delta}{2} - i\sin\frac{\kappa\Delta}{2})(\cos\frac{\lambda\Delta}{2} - i\frac{\delta}{\lambda}\sin\frac{\lambda\Delta}{2})$ of the corresponding $\mathbf{SU(2)}$–matrix $\underline{r} = \underline{f}(\bar{r})$. Note that r_0 and r_2 are independent of Ψ_i and depend only on the difference of θ_f and θ_i. For a first order dynamical resonance we can recall the normal form coordinates $q = \sqrt{2J}\cos\Psi$ and $p = -\sqrt{2J}\sin\Psi$ and the J–dependence of $\epsilon = \epsilon_0\sqrt{2J}$ to find

$$r_1^{(1),\mathrm{dyn}}(\theta_f, \theta_i; q_i, p_i) = \frac{\epsilon_0}{\lambda}\sin\frac{\lambda\Delta}{2}\,(\sin\phi_\epsilon\; q_i - \cos\phi_\epsilon\; p_i) \tag{2.165a}$$

$$r_3^{(1),\mathrm{dyn}}(\theta_f, \theta_i; q_i, p_i) = \frac{\epsilon_0}{\lambda}\sin\frac{\lambda\Delta}{2}\,(\cos\phi_\epsilon\; q_i + \sin\phi_\epsilon\; p_i) \quad . \tag{2.165b}$$

Thus on each *fixed* torus $J =$ const. the exact flow $\bar{r}^{(1),\mathrm{dyn}}$ can be rewritten as an affine–linear function of the normal form coordinates q and p. Nevertheless, due to the non–linear dependence on J which is embedded in ϵ and λ, the flow is in general not linear in the orbital coordinates.

From equations (2.164a) to (2.164f) one immediately computes the one–turn map $\bar{r}(\theta, \Psi) \equiv \bar{r}(\theta + 2\pi, \theta, \Psi) \equiv (\cos\pi\mu_r, \hat{r}\sin\pi\mu_r)$ as:

$$r_0(\theta, \Psi) = \cos\pi\lambda\cos\pi\kappa - \frac{\delta}{\lambda}\sin\pi\lambda\sin\pi\kappa \tag{2.166a}$$

$$r_1(\theta, \Psi) = \frac{\epsilon}{\lambda}\sin\pi\lambda\sin(\psi_\epsilon + \pi\kappa + k_0\theta + k\Psi) \tag{2.166b}$$

$$r_2(\theta, \Psi) = \cos\pi\lambda\sin\pi\kappa + \frac{\delta}{\lambda}\sin\pi\lambda\cos\pi\kappa \tag{2.166c}$$

$$r_3(\theta, \Psi) = \frac{\epsilon}{\lambda}\sin\pi\lambda\cos(\psi_\epsilon + \pi\kappa + k_0\theta + k\Psi) \quad , \tag{2.166d}$$

which describes a rotation by the angle $2\pi\mu_r(\theta, \Psi)$ around the unit eigenvector $\hat{r}(\theta, \Psi)$ with eigenvalue 1 of $\underline{R}(\theta, \Psi)$. Strikingly r_0 and r_2 depend neither on θ nor on Ψ. Moreover from equations (2.166b) to (2.166d) we see that $\hat{r}(\theta, \Psi)$ is on a cone with half polar opening angle ϑ_r around $+\hat{y}$ where

$$\tan\vartheta_r \equiv \frac{\sqrt{r_1^2 + r_3^2}}{r_2} = \frac{\epsilon|\sin\pi\lambda|}{\lambda\cos\pi\lambda\sin\pi\kappa + \delta\sin\pi\lambda\cos\pi\kappa} \quad . \tag{2.167}$$

Here $0 \le \vartheta_r \le \pi$ is defined so that $\vartheta_r > {}^{\pi}/_{2}$ describes a cone with half polar opening angle $\pi - \vartheta_r$ around $-\hat{y}$. Note that $(\cos\frac{\phi}{2}, \sin\frac{\phi}{2}\hat{q})$ and $(\cos\frac{-\phi}{2}, -\sin\frac{-\phi}{2}\hat{q})$ are identical. In anticipation of chapter 4 we note that the periodic unit vector field $\hat{r}(\theta, \Psi)$ is transformed by the OTM $\underline{R}(\theta, \Psi)$ into $\hat{r}(\theta, \Psi)$ but for non–integral kQ it is *not* mapped into $\hat{r}(\theta, \Psi + 2\pi Q)$ and hence it is *not* an invariant of the spin OTM! In other words $\hat{r}(\theta, \Psi)$ is *not* the $\hat{n}$–axis of chapter 4. Moreover we will see in chapter 4 that the spin tune can in general not be computed from r_0.

Following the notation introduced in definition 2.6 and equation (2.66) the spinor representation of a vertical spin ($S_y = 1$) is $\check{y} \equiv e^{i\xi}(1, 0)$ with some arbitrary phase $\xi \in \mathbb{R}$. It is transported by the spinor OTM to $\check{y}' = \underline{r}\check{y} = e^{i\xi}(r_{11}, r_{21})$. Since $|r_{11}|^2 + |r_{21}|^2 = 1$ and $|r_{21}|^2 = r_1^2 + r_3^2$ we find $S_y' = 1 - 2|r_{21}|^2 = 1 - 2(r_1^2 + r_3^2)$. We define the "vertical response function" V_ϵ for the SRM with strength ϵ or in general the "$\hat{n}_0$–response function" $V_{\vec{J}}$ on some given invariant torus to be

$$V_{\vec{J}}(\vec{\Psi}, \theta) = 1 - 2\|\vec{r}_{\vec{J}}(\theta; \vec{\Psi}) \times \hat{n}_0(\theta)\|^2 \;\; , \;\; -1 \le V_{\vec{J}}(\vec{\Psi}, \theta) \le +1 \quad , \tag{2.168}$$

where $\vec{r}_{\vec{J}}(\theta; \vec{\Psi})$ is the vector part of the spin one–turn quaternion on the torus $\vec{J} =$ const. with initial condition $\vec{\Psi}$. For the SRM with $\hat{n}_0 \equiv \hat{y}$ one immediately finds

$$V_\epsilon = \mathrm{const.} = 1 - 2\frac{\epsilon^2}{\lambda^2}\sin^2\pi\lambda \quad . \tag{2.169}$$

This function has so–called nodal points [SL97] $V_\epsilon = 1$, $\partial_\Psi V_\epsilon = 0$ whenever λ is an integer. At these nodal points (and in general *only* at these) an initially vertical spin returns back to the vertical after one–turn independently of the orbital phase. At pathological resonance strengths $\epsilon \in \mathbb{N}$, even exactly on resonance, i.e. $\delta = 0$, a nodal point appears.

It is interesting to look at some special and/or limiting cases. For an imperfection resonance ($k = 0 \Rightarrow [\kappa] = 0$) we find substituting ν_{00} for ν_0 and $\hat{n}_{00}$ for $\hat{y}$ in (2.150)

$$\begin{aligned} \bar{r}(\theta, \Psi)\Big|_{k=0} &= \Big(\pm \cos \pi\lambda,\ \pm\frac{\epsilon}{\lambda} \sin \pi\lambda \sin(\psi_\epsilon + k_0\theta), \\ &\qquad \pm\frac{\delta}{\lambda} \sin \pi\lambda, \pm\frac{\epsilon}{\lambda} \sin \pi\lambda \cos(\psi_\epsilon + k_0\theta)\Big) \qquad (2.170a) \\ |\tan \vartheta_r| &= \frac{\epsilon}{|\delta|} \quad , \qquad (2.170b) \end{aligned}$$

where the sign "+/−' is valid for even/odd $\kappa = k_0$. Therefore $\hat{n}_0 = \frac{\mathrm{sgn}(\delta)}{\lambda}\ (\epsilon \sin(\psi_\epsilon + k_0\theta), \delta, \epsilon \cos(\psi_\epsilon + k_0\theta))$ and $\nu_0 = \mathrm{sgn}(\delta)\ \lambda$ with $\delta \equiv \nu_{00} - k_0$ are the perturbed spin closed orbit and the perturbed spin tune in the limiting case of a single imperfection resonance. The factor $\mathrm{sgn}(\delta)$ has been inserted so that $\hat{n}_0 \to +\hat{n}_{00} \equiv (0, 1, 0)$ and $\nu_0 \to +\nu_{00}$ independently of the sign of δ in the limit $\epsilon \to 0$.

If $[\kappa] = {}^1/_2$ we obtain

$$\begin{aligned} \bar{r}(\theta, \Psi)\Big|_{[\kappa]={}^1/_2} &= \Big(\mp \frac{\delta}{\lambda} \sin \pi\lambda, \frac{\epsilon}{\lambda} \sin \pi\lambda \cos(\psi_\epsilon + k_0\theta + k\Psi), \\ &\qquad \pm \cos \pi\lambda,\ \ \frac{\epsilon}{\lambda} \sin \pi\lambda \sin(\psi_\epsilon + k_0\theta + k\Psi)\Big) \qquad (2.171a) \\ |\tan \vartheta_r| &= \frac{\epsilon}{\lambda} |\tan \pi\lambda| \quad , \qquad (2.171b) \end{aligned}$$

where the sign "+/−' is valid for even/odd $\kappa - {}^1/_2$.

If ${}^1/_2 \neq \kappa \neq 0$ in equation (2.167), then ϑ_r is $\pi/2$ whenever λ fulfils the transcendental equation $\frac{\delta}{\lambda} \tan \pi\lambda + \tan \pi\kappa = 0$ with the additional constraint that $\lambda \notin \mathbb{N}$. Therefore for any intrinsic resonance, and for any order, the eigenvector of the spin OTM in the *single* resonance model tilts over into the horizontal plane infinitely many times as δ is varied from $-\infty$ to $+\infty$! Nevertheless the widths (in δ) of these peaks in $\tan \vartheta_r$ go to zero for $\delta \to \pm\infty$.

Exactly *on* resonance we have $\delta = 0 \Rightarrow \lambda = \epsilon$, $\delta/\lambda = 0$ and $\epsilon/\lambda = 1$ and hence

$$\begin{aligned} \bar{r}(\theta, \Psi)\Big|_{\delta=0} &= \Big(\cos \pi\epsilon \cos \pi\kappa,\ \sin \pi\epsilon \sin(\psi_\epsilon + \pi\kappa + k_0\theta + k\Psi), \\ &\qquad \cos \pi\epsilon \sin \pi\kappa,\ \sin \pi\epsilon \cos(\psi_\epsilon + \pi\kappa + k_0\theta + k\Psi)\Big) \qquad (2.172a) \\ \tan \vartheta_r\Big|_{\delta=0} &= \frac{|\sin \pi\epsilon|}{\cos \pi\epsilon \sin \pi\kappa} \quad . \qquad (2.172b) \end{aligned}$$

Note that in general, i.e. when neither $[\epsilon] = {}^1/_2$ nor $[\kappa] = 0$, the rotation vector $\hat{r}$ is *not* in the horizontal plane when the system on resonance, i.e. $\delta = 0$. For $\epsilon/\delta \to 0$ we find $\lambda \to |\delta|$, $\delta/\lambda \to \mathrm{sgn}(\delta)$, $\epsilon/\lambda \to 0$ and get

$$\lim_{\epsilon/\delta \to 0} \bar{r}(\theta, \Psi) = (\cos \pi\nu_0, 0, \sin \pi\nu_0, 0) \quad , \quad \lim_{\epsilon/\delta \to 0} \tan \vartheta_r = 0 \quad . \qquad (2.173)$$

Obviously when ν_0 is "sufficiently" far away from κ compared to ϵ, then the spin motion is approximately described by $\vec{\Omega}_0$ and the OTM is just a rotation around $\hat{y}$ by the angle $2\pi\nu_0$. In section 4.7 we will give a more precise definition for the effective width of a single resonance. Nevertheless, suppose that we are given a system with *many* resonances $\{\kappa_i\}_{1 \le i \le n}$, pairwise "sufficiently" separated, i.e. $\kappa_i - \kappa_j \gg \max(\epsilon_i, \epsilon_j)$, $\forall 1 \le i, j \le n$, then we could hope to have a fairly good approximation of the spin dynamics in that system by describing it piecewise with the SRM in some interval around κ_i with the appropriate resonance strength ϵ_i. Under the assumption of well separated resonances we will call the description of a spin–orbit system by piecewise application of a SRM with suitably chosen parameters an *isolated resonance model*. This is one reason why the SRM is potentially so useful. In section 4.8 we will motivate a heuristic model that generalises the SRM to systems in which the sources of spin perturbations are not well isolated. — This is another reason why the SRM is important.

The n–turn map $\bar{r}_n(\theta,\Psi) \equiv \bar{r}(\theta+n2\pi,\theta,\Psi) = \bigodot_{j=0}^{n-1}\bar{r}(\theta,\Psi+j2\pi Q)$ is obtained from equations (2.166a) to (2.166d) by simply replacing π with $n\pi$. The unit eigenvector $\hat{r}_n$ of the n–turn map seen as a function of the orbital phase Ψ is on a cone around $+\hat{y}$ with the n–dependent opening angle

$$\tan\vartheta_r(n) = \frac{\epsilon|\sin n\pi\lambda|}{\lambda\cos n\pi\lambda\sin n\pi\kappa+\delta\sin n\pi\lambda\cos n\pi\kappa} \quad . \tag{2.174}$$

Note that as long as $[Q]\neq 0$ and $k\neq 0$, $\hat{r}_n$ is *not* the image of the rotation vector of the OTM $\hat{r}=\hat{r}_1$ under n iterations of the OTM. Note also that in general, i.e. when both κ and λ are irrational, the opening angle $\vartheta_r(n)$ at fixed Ψ, κ, δ and ϵ and for $1\leq n\leq\infty$ will cover almost the whole interval $[0,\pi]$ even far off–resonance. The significance of this property will become clear in section 3.2.3.

In the special case of an orbital resonance where $nQ=m$ with $n,m\in\mathbb{N}$ all trajectories on the torus close after n turns. Therefore the $2n$–turn spin map is just the square of the n–turn spin map and the field of unit eigenvectors $\hat{r}_n(\theta,\Psi)$ of the n–turn map is an invariant of motion. Since $n\kappa\equiv nk_0+nkQ=nk_0+km\in\mathbb{Z}$ we find for the n–turn map

$$\begin{aligned}
\bar{r}_n(\theta,\Psi)\Big|_{nQ=m} &= \pm\Big(\cos n\pi\lambda,\frac{\epsilon}{\lambda}\sin n\pi\lambda\sin(\psi_\epsilon+k_0\theta+k\Psi),\\
&\qquad \frac{\delta}{\lambda}\sin n\pi\lambda,\frac{\epsilon}{\lambda}\cos n\pi\lambda\cos(\psi_\epsilon+k_0\theta+k\Psi)\Big) && (2.175a)\\
\text{and hence}\quad \hat{r}_n(\theta,\Psi)\Big|_{nQ=m} &= \frac{\pm 1}{\lambda}\Big(\epsilon\sin(\psi_\epsilon+k_0\theta+k\Psi),\delta,\epsilon\cos(\psi_\epsilon+k_0\theta+k\Psi)\Big) \quad . && (2.175b)
\end{aligned}$$

The global sign $+/-$ in (2.175a) refers to m even/odd. But of course it does not enter the $\mathbf{SO(3)}$ representation of the map. Additionally the sign of the eigenvector is of course totally arbitrary and can be changed to $\mathrm{sgn}(\delta)$ so that $\lim_{\epsilon\to 0}\hat{r}_n(\theta,\Psi)|_{nQ=m}=\hat{n}_0\equiv+\hat{y}$.

Now that the basic mathematical methods have been established we are in a position to move on and begin the discussion of spin motion in general rings.

Chapter 3

Siberian Snakes

As we have seen in section 2.3 and 2.4, in any real ring, i.e. in any ring containing not only horizontal bends, radial and longitudinal field components experienced on synchro–betatron trajectories potentially tilt an initially vertical spin away from the vertical. Even if these additional field components are *small* compared to the vertical holding fields, the disturbance of spin motion can be large whenever there is coherence between the spin precession and the perturbing field evaluated along a trajectory, i.e. at some spin–orbit resonance $\nu_0 = k_0 + \vec{k} \cdot \vec{Q}$. Moreover since ν_0 depends on the reference energy E_0, it is impossible to avoid resonances during acceleration unless special measures are taken. But this problem could be immediately circumvented for the first order intrinsic and imperfection resonances ($\nu_0 = k_0 + \vec{k} \cdot \vec{Q}$ with $|\vec{k}| = 1$ or k_0 respectively) if ν_0 could be fixed independently of energy at a value far enough away from all integers and all the $[Q_i]$. ν_0 can be made energy independent with sets of magnetic devices called Siberian Snakes [DK75, DK78, DK79, DK89]. They are usually set up so that $\nu_0 = 1/2$. Then with orbital tunes suitable for stable operation, i.e. incommensurable with 1 and somewhat away from the strong *low* order resonances, the low order spin–orbit resonances are avoided as required. Snakes are also essential for running at fixed high energy.

However, it will become clear that although snakes are essential for attaining high polarisations, at high energy the spin perturbations from the quadrupoles are so strong that resonances still have a large influence. It is then not guaranteed that polarisation can be preserved even with snakes. Nevertheless, it *is* found that some snake layouts are more effective than others.

In this chapter we will define the characteristics of Siberian Snakes and give a first notion of how to use these characteristics to achieve the required impact on spin motion. We will explicitly derive the quaternion maps for spin transport on the closed orbit through sections of accelerators that contain Siberian Snakes and discuss to what extent local spin perturbations are cancelled due to the snakes. Furthermore we will discuss the effect of snakes on spin–orbit coupling integrals and the modifications that snakes impose on the spin one turn map of the single resonance model. One key result will be the derivation of symmetry properties of the spin OTM in mid–plane symmetric rings in the presence of certain combinations of Siberian Snakes.

An *ideal Siberian Snake* ($\equiv$ point–like or synthetic Siberian Snake) is a magnetic field configuration that rotates a spin by π around some axis $\hat{a}$, called the *snake axis*. This rotation is *independent* of the *reference energy* and the orbital *phase space* vector $\vec{z}$. The ideal Siberian Snake does *not* affect the orbital motion, i.e. it can be treated as a drift, or a unit transformation in the case of a point–like snake. In reality these *ideal* devices do not exist but can be manufactured in some rather good approximation. A real Siberian Snake rotates the spin by an angle which is *approximately* π around an axis which is approximately $\hat{a}$ and both are *almost* independent of energy and $\vec{z}$. It always introduces some coupling and/or extra horizontal and vertical dispersion and/or higher order multipoles that affect the orbital transfer map. At low energy and for a longitudinal $\hat{a}$ solenoids can be used according to equation (2.3). The coupling created by the solenoid has in general to be compensated by means of skew quadrupoles. But at high energy it is difficult to obtain the high field integrals required for a solenoidal snake since $\vec{\Omega}_{\rm sol}$ is proportional to $(1+G)/\gamma$. Thus transverse (dipole) fields must be used. But as pointed out in section 2.1, a spin rotation by π in a transverse field still requires a field integral of about 5.48 Tm so that naive insertion of such a field would cause significant orbit distortion. The (partial) solution to this dilemma is to use a local set of nested horizontal and vertical closed bumps created by interleaving horizontal and vertical bends. Then, although the orbit closes, the non–commutation of large spin rotations (see remarks 1 and 2 in section 2.1) around the radial and vertical axes can be used to devise a system with the required rotation axis and spin rotation (π) but with minimal distortion of the orbit *outside of the snake*. The ultimate and most compact form of interleaving can be found in the helical dipole snakes to be used at RHIC [BS99].

Since the transverse component $\vec{\Omega}_{\rm trv}$ of $\vec{\Omega}$ as computed with equation (2.8) is essentially independent of energy, constant magnetic fields must be used. But the maximum closed orbit deviation *inside* such a dipole snake of course does depend on energy via $B_\perp\rho = p/e$ where ρ is the radius of orbital curvature, p is the (kinetic) momentum and e is the elementary charge. Hence dipole snakes are impractical at low energy where ρ would be very small. Actually, with existing technology the region between 5–10 GeV is sometimes called the "snake gap", since neither solenoidal snakes nor dipole snakes are practical. Dipole snakes of any kind create additional dispersion in *both* transverse planes which then drives, for example, the longitudinal spin–orbit coupling integrals $I_z^\pm$ and has also to be matched to the rest of the ring to avoid a dispersion beat. We conclude that the simple presence of a *real* snake, whether it is solenoidal or dipole–like, violates mid–plane symmetry and hence the premises of theorem 2.9. Concepts for building real snakes, the required field symmetries and effects on orbital motion can be found for example in [SL97, KS88a, LR94, AL95, AL96, TR94, EC94, EC96, FP95, MS96a, MS96b, VP94, WF96, BS99, VA99].

Definition 3.1 (Point–like spin rotator maps) *A linear spin–orbit transfer map $(\underline{R}_s(\vec{z}, E_0),\ \underline{T}(E_0))$ is called a (point–like, ideal, synthetic) spin rotator map with snake axis $\hat{r}_s$, if $\underline{T} = \underline{1}$ for all energies and $\underline{R}_s$ does not depend on energy and $\vec{z}$. It is called a snake map (Siberian Snake map, full snake map or just snake map), if the spin rotation angle is $\Psi_s = \pi$, i.e. the corresponding unit–quaternion has the form*

$$\bar{r}_s = (0, \hat{r}_s) \tag{3.1}$$

The snake map is called "horizontal" if the snake axis is in the horizontal plane, i.e. $\hat{r}_s = (\cos\phi_s, 0, -\sin\phi_s)$ with the so–called snake angle ϕ_s. It is called "radial" if $\phi_s = 0$ and "longitudinal" if $\phi_s = {}^{\pi}/_{2}$. The snake map is called "vertical" (sometimes also "Type III") if $\hat{r}_s = (0, 1, 0)$.

Spin rotators with $0 < \Psi_s \ll {}^{\pi}/_{2}$ are sometimes called *partial* snakes and spin rotators with $\Psi_s = {}^{\pi}/_{2}$ are called 90°–rotators. The $\mathbf{SO(3)}$ and $\mathbf{SU(2)}$ representations $\underline{R}_s$ and $\underline{r}_s$ of an ideal snake map fulfil $\mathrm{trace}\,(\underline{R}_s) = -1$ and $\mathrm{trace}\,(\underline{r}_s) = 0$ respectively.

3.1 The effect of Siberian Snakes on spin motion on the design orbit

We will now derive some simple but quite useful properties of snakes.

Lemma 3.1 *Let $\hat{r}\perp\hat{s}$ be mutually perpendicular unit 3–vectors, $\bar{s} \equiv (0, \hat{s})$ the unit–quaternion for a point–like snake and $\bar{r} \equiv (\xi, \eta\hat{r})$ with $\xi^2 + \eta^2 = 1$ an arbitrary spin rotation around $\hat{r}$, then*

$$\bar{r}\bar{s} = \bar{s}\bar{r}^{-1} \quad . \tag{3.2}$$

Proof: $\bar{r}\bar{s} = (0, \xi\hat{s} + \eta\hat{r}\times\hat{s}) = (0, \xi\hat{s} + \eta\hat{s}\times(-\hat{r})) = \bar{s}\bar{r}^{-1}$.□

Lemma 3.2 (Steffen's Lemma) *[KS88a] An arbitrary horizontal Siberian Snake map with snake angle ϕ_s can be decomposed into a radial Siberian Snake and a vertical spin rotator map with rotation angle $2\phi_s$*

$$(0, \cos\phi_s, 0, -\sin\phi_s) = (\cos\phi_s, 0, \sin\phi_s, 0)\ (0,1,0,0) = (0,1,0,0)\ (\cos\phi_s, 0, -\sin\phi_s, 0) \quad . \tag{3.3}$$

Note that $(0, \cos\phi_s, 0, -\sin\phi_s)$ describes a rotation by π around the unit vector $(\cos\phi_s, 0, -\sin\phi_s)$ but that $(\cos\phi_s, 0, \pm\sin\phi_s, 0)$ describes a rotation by $\pm 2\phi_s$ around $\hat{y}$. The proof follows immediately from the definition of quaternion multiplication (definition 2.3).□

In the following we will often meet products of the form $\bar{a}_2\bar{h}\bar{a}_1$, where $\bar{a}_1$, $\bar{a}_2$ are some rotations by $\phi_{1,2}$ around the vertical and $\bar{h}$ is a rotation around some horizontal axis $\hat{h} \equiv (\cos\phi, 0, -\sin\phi)$ by an arbitrary angle η. In principle the composition of these 3 rotations, seen as a $\mathbf{SO(3)}$–matrix $\underline{R}$, is a representation $\underline{R}(\phi_2, \eta, \phi_1)$ of $\underline{R}$ by Euler angle like parameters (ϕ_2, η, ϕ_1) since $\hat{y}$ and $\hat{h}$ are orthogonal by definition. Therefore $(\phi_2, \eta, \phi_1) \in [0, 2\pi) \times [0, \pi] \times [0, 2\pi)$ generates the whole $\mathbf{SO(3)}$. In an accelerator $\bar{a}_{1,2}$ could be on–orbit spin maps for flat portions of the arcs and $\bar{h}$ could be the spin map of a horizontal snake or a horizontal perturbation. For later convenience we now will give an explicit result

$$\begin{aligned}
\bar{a}_2\bar{h}\bar{a}_1 &= \left(\cos\frac{\phi_2}{2}, 0, \sin\frac{\phi_2}{2}, 0\right)\left(\cos\frac{\eta}{2}, \sin\frac{\eta}{2}\cos\phi, 0, -\sin\frac{\eta}{2}\sin\phi\right)\left(\cos\frac{\phi_1}{2}, 0, \sin\frac{\phi_1}{2}, 0\right)\\
&= \left(\cos\frac{\eta}{2}\cos\frac{\phi_2+\phi_1}{2}, \sin\frac{\eta}{2}\cos(\phi+\frac{\phi_2-\phi_1}{2}), \cos\frac{\eta}{2}\sin\frac{\phi_2+\phi_1}{2}, -\sin\frac{\eta}{2}\sin(\phi+\frac{\phi_2-\phi_1}{2})\right) \ .
\end{aligned}\tag{3.4}$$

We note that the only term in equation (3.4) that is anti–symmetric w.r.t. permutation of $\bar{a}_1$ and $\bar{a}_2$ is $\phi_2 - \phi_1$.

3.1.1 One horizontal Siberian Snake

Consider a flat ring with one Siberian Snake with snake axis in the horizontal plane at $\theta = 0$. Then the spin OTM on the design orbit with respect to the symmetry point $(\bar{r}_0(\theta = \pi))$ is $\bar{a}\bar{s}\bar{a}$ with the spin map of one symmetric half ring $\bar{a} = (\cos\frac{\pi G\gamma}{2}, 0, \sin\frac{\pi G\gamma}{2}, 0)$ and the spin map of the horizontal snake $\bar{s} = (0, \cos\phi_s, 0, -\sin\phi_s)$. Using either lemma 3.1 or equation (3.4) with $\eta = \pi$ and $\phi_1 = \phi_2$ yields

$$\bar{r}_0(\pi) = (0, \cos\phi, 0, -\sin\phi_s) = \bar{s} \quad . \tag{3.5}$$

Therefore we find that $\cos\pi\nu_0 = 0 \Rightarrow [\nu_0] = {}^1\!/_2$ and that $\hat{n}_0(\pi) = \hat{s}$ *independently of the energy.* For arbitrary θ we obtain with $\phi_1 = \theta G\gamma$ and $\phi_2 = (2\pi - \theta)G\gamma$

$$\begin{aligned}
\bar{r}_0(\theta) &= \left(0, \cos(\phi + \frac{\phi_2-\phi_1}{2}), 0, -\sin(\phi+\frac{\phi_2-\phi_1}{2})\right) &(3.6a)\\
&= (0, \cos(\phi + G\gamma(\pi-\theta)), 0, -\sin(\phi+G\gamma(\pi-\theta))) \quad , &(3.6b)
\end{aligned}$$

showing that $\hat{n}_0(\theta) = (\cos(\phi + G\gamma(\pi-\theta), 0, -\sin(\phi + G\gamma(\pi-\theta))$ in general depends on azimuth as well as energy.

We will now analyse the effect of a small localised horizontal perturbation and define for an arbitrary given point in a flat ring with one horizontal Siberian Snake

$$\begin{aligned}
\bar{r}_0 &\equiv \bar{a}_3\ \bar{s}\ \bar{a}_2\ \bar{p}\ \bar{a}_1 \\
\bar{a}_j &\equiv \left(\cos\tfrac{\Theta_j G\gamma}{2}, 0, \sin\tfrac{\Theta_j G\gamma}{2}, 0\right)\ ,\ j=1,2,3\ ,\ \Theta_1+\Theta_2+\Theta_3 = 2\pi \quad &\text{(arcs)}\\
\bar{s} &\equiv (0, \cos\phi, 0, -\sin\phi) &\text{(snake)}\\
\bar{p} &\equiv \left(\cos\tfrac{\epsilon}{2}, \sin\tfrac{\epsilon}{2}\cos\varphi, 0, -\sin\tfrac{\epsilon}{2}\sin\varphi\right) &\text{(perturbation)} \quad ,
\end{aligned}\tag{3.7}$$

where the Θ_j are the horizontal bend angles of each arc section. In the case of no perturbation ($\epsilon = 0$) and no snake ($\bar{s} = \bar{1}$) the OTM is $\bar{a}_3\bar{a}_2\bar{a}_1 = (\cos\pi G\gamma, 0, \sin\pi G\gamma, 0)$ and we find for non–integral $G\gamma$ that the $\hat{n}_0$–axis is uniquely defined (up to its sign) by $\hat{n}_0(\theta) = \hat{y}$. For $G\gamma \in \mathbb{N}^*$ the OTM is the identity so that the eigenproblem is maximally degenerate. Therefore every unit vector $\hat{n}_0' \in \mathcal{S}_{\mathbb{R}}$ is invariant under $\bar{r}_0|_{G\gamma\in\mathbb{N}}$ and hence $\hat{n}_0$ is not *uniquely* defined.

In the case of a finite perturbation ($\epsilon > 0$) but still without a snake we can use equation (3.4) with $\phi_2 \to \phi_2 + \phi_3$ and obtain with $\Delta' \equiv (\Theta_3 + \Theta_2 - \Theta_1)G\gamma/2 = (\pi - \Theta_1)G\gamma$

$$\begin{aligned} \bar{a}_3\,\bar{a}_2\,\bar{p}\,\bar{a}_1 &= \Big(\cos\frac{\epsilon}{2}\cos\pi G\gamma, \sin\frac{\epsilon}{2}\cos(\varphi+\Delta'), \cos\frac{\epsilon}{2}\sin\pi G\gamma, -\sin\frac{\epsilon}{2}\sin(\varphi+\Delta')\Big) &(3.8a)\\ &=_1 \Big(\cos\pi G\gamma, \frac{\epsilon}{2}\cos(\varphi+\Delta'), \sin\pi G\gamma, -\frac{\epsilon}{2}\sin(\varphi+\Delta')\Big)\quad , &(3.8b)\end{aligned}$$

where we have introduced the notation "$X =_n Y$" meaning that $X - Y = O(\epsilon^{n+1})$. The norm of the linearised quaternion in equation (3.8b) is $1 + O(\epsilon^2)$ so that (3.8b) is a "unit–quaternion up to $O(\epsilon)$". From equations (3.8a) and (3.8b) we see that as long as $G\gamma \notin \mathbb{N}$, the $\hat{n}_0$–axis is $\hat{y}+O(\epsilon)$ or in other words the angle α between $\hat{n}_0$ and $\hat{y}$ is $O(\epsilon)$. If on the contrary $G\gamma \in \mathbb{N}$, then the $\hat{n}_0$–axis of the perturbed system without a snake is $(\cos(\varphi+\Delta'), 0, -\sin(\varphi+\Delta'))$ and hence completely in the horizontal plane independently of ϵ. Finally with the snake and the perturbation we use lemma 3.1 and equation (3.4) and find with $\Sigma \equiv (-\Theta_3+\Theta_2+\Theta_1)G\gamma/2 = (\pi-\Theta_3)G\gamma$ and $\Delta \equiv (-\Theta_3+\Theta_2-\Theta_1)G\gamma/2 = (\Theta_2-\pi)G\gamma$

$$\begin{aligned} \bar{r}_0 &= \bar{s}\,\bar{a}_3^{-1}\,\bar{a}_2\,\bar{p}\,\bar{a}_1 \\ &= \bar{s}\,\Big(\cos\frac{\epsilon}{2}\cos\Sigma, \sin\frac{\epsilon}{2}\cos(\varphi+\Delta), \cos\frac{\epsilon}{2}\sin\Sigma, -\sin\frac{\epsilon}{2}\sin(\varphi+\Delta)\Big) \\ &= \Big(-\sin\frac{\epsilon}{2}\cos(\phi-\varphi-\Delta), \cos\frac{\epsilon}{2}\cos(\phi-\Sigma), -\sin\frac{\epsilon}{2}\sin(\phi-\varphi-\Delta), -\cos\frac{\epsilon}{2}\sin(\phi-\Sigma)\Big) &(3.9a)\\ &=_1 \Big(-\frac{\epsilon}{2}\cos(\phi-\varphi-\Delta), \cos(\phi-\Sigma), -\frac{\epsilon}{2}\sin(\phi-\varphi-\Delta), -\sin(\phi-\Sigma)\Big)\quad . &(3.9b)\end{aligned}$$

We conclude: (1.) $\cos\pi\nu_0 = -\sin\frac{\epsilon}{2}\cos(\phi-\varphi-(\Theta_2-\pi)G\gamma)$ does *not* depend on the position of the viewpoint in the ring but only on the "distance" Θ_2 between the snake and the perturbation. (2.) The deviation of $\cos\pi\nu_0$ from $\cos{}^{\pi}/_{2}$ is $O(\epsilon)$. (3.) The $\hat{n}_0$–axis is $(\cos(\phi-\Sigma), 0, -\sin(\phi-\Sigma)) + O(\epsilon)$. (4.) In the special case of both the perturbation and the viewpoint being exactly π apart from the snake ($\Theta_1 = 0$, $\Theta_2 = \Theta_3 = \pi$) we find $\Delta = \Sigma = 0$ and hence that $\bar{r}_0$ is energy independent. (5.) The snake does not cancel the spin perturbation completely but ensures that the perturbation $\bar{p}$ of $O(\epsilon)$ has an impact on $\bar{r}_0$ which is not more than $O(\epsilon)$ independent of the energy.

Since with *one* horizontal snake even in a perfectly mid–plane symmetric ring $\hat{n}_0$ is in the horizontal plane the radial and longitudinal spin–orbit coupling integrals $I^{\pm}_{x,z}$ (2.141) do no longer identically vanish. We will see in section 3.2.1 that an even number of of horizontal snakes is needed to preserve mid–plane symmetry. Moreover, due to the vertical fields of the main horizontal bends in the arcs, a $\hat{n}_0$ in the horizontal plane is strongly depending on energy. In section 4.10 it will become clear that such an energy dependence can lead to depolarisation during acceleration. We will see in the next section that certain snake configurations fulfil both the conditions $\nu_0 = {}^{1}/_{2}$ and $\hat{n}_0 = \hat{y}$ in all the flat sections of the ring. In section 3.2.2 we will see that we have additional freedom to choose the snake angles such that certain spin–orbit coupling integrals are minimised.

3.1.2 An even number of horizontal snakes

We now consider a flat unperturbed ring with an even number of $2N$ snakes with snake axes in the horizontal plane. We define the $\bar{a}_j$ to be rotations around the vertical by $\Theta_j G\gamma$ and the $\bar{s}_j$ represent horizontal snakes with snake angle ϕ_j analogously to equation (3.7). Without loss of generality we define the on–orbit spin OTM seen at a viewpoint somewhere in the $2N$-th arc between the $2N$-th and the first snake as

$$\bar{r}_0 \equiv \bar{a}'_{2N}\bar{s}_{2N} \bigodot_{j=1}^{2N-1} (\bar{a}_j\bar{s}_j)\,\bar{a}'_0 \quad , \tag{3.10}$$

where $\bar{a}'_{2N}\bar{a}'_0 \equiv \bar{a}_{2N}$ represents the arc between the $2N$-th and the first snake.

Theorem 3.1 (Steffen's theorem) *[KS88a] In a flat unperturbed ring with an even number of horizontal point–like Siberian Snakes as in equation (3.10)*

1. *the fractional part of the spin tune on the design orbit is given by*

$$[\nu_0] = \left[\frac{\pm 1}{2\pi}\sum_{j=1}^{2N}(-1)^j(2\phi_j + G\gamma\Theta_j)\right] \quad , \tag{3.11}$$

where ϕ_j and Θ_j are defined analogously to equation (3.7) and $[\pm x]$ indicates that the fractional part is $[x]$ for $x \geq 0$ or $1 - [|x|]$ for $x < 0$,

2. *if the design orbit spin tune is not an integer, then $\hat{n}_0 = \pm\hat{y}$ is uniquely defined up to its sign all along the ring and the sign flips at each of the snakes and*

3. *the* $\mathbf{SO(3)}$ *spin OTM associated with $\bar{r}_0$ does not depend on the position of the viewpoint.*

We first show that $\bar{r}_0$ does not depend on the position of the viewpoint inside an arc section. Due to lemma 3.1 and since $2N$ is even we find $\bar{r}_0 = \bar{a}'_{2N}\bar{s}_{2N}\bar{a}'^{-1}_0 \bigodot_{j=1}^{2N-1}(\bar{a}_j\bar{s}_j) = \bar{a}_{2N}\bar{s}_{2N}\bigodot_{j=1}^{2N-1}(\bar{a}_j\bar{s}_j) = \bigodot_{j=1}^{2N}(\bar{a}_j\bar{s}_j)$, so that the OTM does not depend on the position inside an arc section. Therefore it suffices to prove the theorem for $\bar{a}'_0 \equiv \bar{1}$, i.e. at an initial viewpoint directly before the first snake. With lemma 3.2 we rewrite each of the $2N$ arc/snake pairs as

$$\bar{a}_j\bar{s}_j = \left(\cos\frac{G\gamma\Theta_j + 2\phi_j}{2}, 0, \sin\frac{G\gamma\Theta_j + 2\phi_j}{2}, 0\right)(0,1,0,0) \equiv \bar{c}_j\bar{s}_x \quad , \tag{3.12}$$

with $\bar{s}_x \equiv (0,1,0,0)$ and $\bar{c}_j$ being a rotation by $2\phi_j + G\gamma\Theta_j$ around the vertical. Thus we obtain

$$\begin{aligned}\bar{r}_0 &= \bigodot_{j=1}^{N}(\bar{c}_{2j}\bar{s}_x\bar{c}_{2j-1}\bar{s}_x) = \bigodot_{j=1}^{N}\left(-\bar{c}_{2j}\bar{c}_{2j-1}^{-1}\right)\\ &= (-1)^N(\cos\pi\nu'_0, 0, \sin\pi\nu'_0, 0) \quad , \quad \nu'_0 = \frac{1}{2\pi}\sum_{j=1}^{2N}(-1)^j(2\phi_j + G\gamma\Theta_j) \quad .\end{aligned} \tag{3.13}$$

Therefore the fractional part of the on–orbit spin tune is $[\nu_0] = [\pm\nu'_0]$, which proves part 1 of the theorem. If $[\nu_0] = 0$, then $\bar{r}_0$ is the identity so that $\hat{n}_0$ is not uniquely defined and the $\mathbf{SO(3)}$ OTM is the identity for all viewpoints. If $[\nu_0]$ is non–zero, then $\bar{r}_0$ is a rotation around the vertical so that $\hat{n}_0 = \pm\hat{y}$ in the whole ring. We define $\hat{n}_0 \equiv +\hat{y}$ in the arc section $j = 2N$, which then according to equation (3.13) fixes the fractional part of the on–orbit spin tune to $[\nu] \equiv [+\nu'_0]$. Moving the viewpoint to the next or preceding arc leads to $\nu_{0,\pm} \equiv \frac{1}{2\pi}\sum_{j=1}^{2N}(-1)^{j\pm 1}(2\phi_j + G\gamma\Theta_j) = -\nu_0$ which leaves $\cos\pi\nu_{0,\pm} = \cos\pi\nu_0$ invariant but converts $\sin\pi\nu_{0,\pm}$ to $-\sin\pi\nu_0$. This shows that $\hat{n}_0$ flips its sign at each snake, proving part 2. We recall that a rotation by ϕ around $\hat{r}$ is always equivalent to a rotation by $-\phi$ around $-\hat{r}$. Therefore the $\mathbf{SO(3)}$ OTM is totally independent of the viewpoint, which proves part 3 of theorem 3.1. □

Corollary: If $\sum_{j=1}^{2N}(-1)^j\Theta_j = 0$, then the on–orbit spin tune is independent of energy and if furthermore $\sum_{j=1}^{2N}(-1)^j\phi_j = {}^{\pi}\!/_2 \bmod \pi$, then $[\nu_0] = {}^1\!/_2$.

We thus have a layout which delivers the desired vertical $\hat{n}_0$ and $\nu_0 = {}^1/_2$ mentioned at the end of the last section.

As becomes clear from the derivation of theorem 3.1 the total spin phase advance on the design orbit $\Delta\Phi_0$ over two adjacent sections j and $j \pm 1$ is energy independent if the horizontal bend angles are equal, $\Theta_j = \Theta_{j\pm1}$. In a flat ring where at least the geometry, i.e. the distribution of horizontal bends has an even superperiodicity $P_B = 2N_B$ and with a number of snakes $2N$, where N fulfils $2Nk = 2N_B$ with $k \in \mathbb{N}^*$, and snake placements that reflect this superperiodicity we have $\Theta_i = \Theta_j$ $\forall 1 \leq i, j \leq 2N$. Therefore the total on–orbit spin phase advance over each two adjacent sections is energy independent. This is surely desirable since on–orbit perturbations which are periodic with $2\pi/P_B$ will add up coherently if $[\Delta\Phi_0/(2\pi)] = 0$ — which will happen at certain energies if $\Delta\Phi_0$ is energy dependent. If additionally N can be chosen to be odd, then the choice $|\phi_{2j} - \phi_{2j-1}| = {}^\pi/_2$ which leads to $[\Delta\Phi_0/(2\pi)] = {}^1/_2$ is compatible with $[\nu_0] = {}^1/_2$. In that case $2\pi/P_B$–periodic perturbations accumulated in one double section will partially cancel in the next double section. Note that for even N the condition $[\Delta\Phi_0/(2\pi)] = {}^1/_2$ implies $[\nu_0] = 0$, which is *not* a suitable choice for polarised beam operation.

In order to illustrate this cancellation we will now calculate the on–orbit spin map for a ring with $2N$ *identical* arcs $\bar{a}$ with horizontal bend angle Θ_0, $2N$ horizontal snakes $\bar{s}_j$ with snake angles ϕ_j so that the unperturbed on–orbit spin tune is ${}^1/_2$ and with a local horizontal perturbation $\bar{p}$ in *one* arbitrary arc section. The unit–quaternions of type $\bar{a}$, $\bar{s}$ and $\bar{p}$ are defined as in equation (3.7). Without loss of generality we index the snakes so that the first snake is downstream of the viewpoint. We divide the ring into N "sections" $\bar{y}_j$ with $\bar{y}_j \equiv \bar{a}\bar{s}_{2j}\bar{a}\bar{s}_{2j-1} = -(\cos(\phi_{2j} - \phi_{2j-1}), 0, \sin(\phi_{2j} - \phi_{2j-1}), 0)$ for all sections without the perturbation and locate the perturbation somewhere in section k represented as $\bar{q}_k$. We have to distinguish two cases: (1) $\bar{q}_k^{(o)} = \bar{a}\bar{s}_{2k}\bar{a}_3\bar{p}\bar{a}_2\bar{s}_{2k-1}$, with $\Theta_3 + \Theta_2 = \Theta_0$. This implies an odd number of snakes between the viewpoint and the perturbation. (2) $\bar{q}_k^{(e)} = \bar{a}_3\bar{p}\bar{a}_2\bar{s}_{2k}\bar{a}\bar{s}_{2k-1}$, which implies an even number of snakes between the viewpoint and the perturbation. The on–orbit spin OTM for an arbitrary viewpoint between snake $2N$ and 1 is

$$\bar{r}_0^{(o,e)} = \bar{a}_4\ \bar{s}_{2N}\ \bar{a}\ \bar{s}_{2N-1} \bigodot_{j=k+1}^{N-1} \bar{y}_j\ \ \bar{q}_k^{(o,e)} \bigodot_{j=1}^{k-1} \bar{y}_j\ \ \bar{a}_1 \quad , \tag{3.14}$$

with $\Theta_4 + \Theta_1 = \Theta_0$. Introducing

$$\bar{y}_> \equiv \bigodot_{j=k+1}^{N} \bar{y}_j \equiv (-1)^{N-k}(\cos\phi_>, 0, \sin\phi_>, 0) \quad , \quad \bar{y}_< \equiv \bigodot_{j=1}^{k-1} \bar{y}_j \equiv (-1)^{k-1}(\cos\phi_<, 0, \sin\phi_<, 0) \quad ,$$
$$\bar{y}_\leq \equiv \bigodot_{j=1}^{k} \bar{y}_j \equiv (-1)^{k}(\cos\phi_\leq, 0, \sin\phi_\leq, 0) \quad , \quad \bar{a}_{i-j} \equiv \bar{a}_i\,\bar{a}_j^{-1} \quad , \quad \bar{a}_{i+j} \equiv \bar{a}_i\,\bar{a}_j \tag{3.15}$$

with $\phi_> + \phi_\leq = \phi_> + \phi_{2k} - \phi_{2k-1} + \phi_< = {}^\pi/_2$ and neglecting the global signs, since they do not enter the $\mathbf{SO(3)}$ representation of the map, we obtain with equation (3.4)

$$\begin{aligned}
\bar{r}_0^{(o)} &= \bar{a}_1^{-1}\ \bar{y}_>\ \bar{a}\ \bar{s}_{2k}\ \bar{a}_3\ \bar{p}\ \bar{a}_2\ \bar{s}_{2k-1}\ \bar{y}_<\ \bar{a}_1 = \bar{s}_{2k}\ \bar{y}_>^{-1}\ \bar{a}_{3+1-0}\ \bar{p}\ \bar{a}_{2-1}\ \bar{y}_<^{-1}\ \bar{s}_{2k-1} \\
&= \pm\Big(0 \ ,\ \ \sin\frac{\epsilon}{2}\cos(\varphi + \phi_< - \phi_> - \phi_{2k} - \phi_{2k-1} + G\gamma(\Theta_1 - \Theta_2)), \\
&\qquad \cos\frac{\epsilon}{2},\ -\sin\frac{\epsilon}{2}\sin(\varphi + \phi_< - \phi_> - \phi_{2k} - \phi_{2k-1} + G\gamma(\Theta_1 - \Theta_2))\Big)
\end{aligned} \tag{3.16a}$$

$$\begin{aligned}
\bar{r}_0^{(e)} &= \bar{a}_1^{-1}\ \bar{y}_>\ \bar{a}_3\ \bar{p}\ \bar{a}_2\ \bar{s}_{2k}\ \bar{a}\ \bar{s}_{2k-1}\ \bar{y}_<\ \bar{a}_1 = \bar{y}_>\ \bar{a}_{3-1}\ \bar{p}\ \bar{a}_{2+1-0}\ \bar{y}_\leq \\
&= \pm\Big(0 \ ,\ \ \sin\frac{\epsilon}{2}\cos(\varphi + \phi_> - \phi_\leq + G\gamma(\Theta_0 - \Theta_2 - \Theta_1)), \\
&\qquad \cos\frac{\epsilon}{2},\ -\sin\frac{\epsilon}{2}\sin(\varphi + \phi_> - \phi_\leq + G\gamma(\Theta_0 - \Theta_2 - \Theta_1))\Big) \quad .
\end{aligned} \tag{3.16b}$$

In both cases the spin OTM is an exact π–rotation around some axis $\hat{y}+O(\epsilon)$. Therefore the two–turn map is just $-\bar{1}$ and the local perturbation is cancelled every two turns. The case with only two snakes is included by setting $\phi_> = \phi_< = 0$. If there is more than one local perturbation and they are in different "$\bar{s}\bar{a}\bar{s}\bar{a}$"–sections, then the situation becomes more complicated. If N is odd, one can constrain the snake angles to fulfil $\phi_{2k}-\phi_{2k-1} = {}^{\pi}/_{2}$. Then each spin transfer map through a perturbed section is of the form (3.16a) or (3.16b). Nevertheless if the local perturbation *axes* are considered uncorrelated, then in general the 0-th component of the one–turn quaternion for more than one local perturbation does *not* exactly vanish but is $O(\epsilon^2)$. We will treat only the case of 2 perturbed sections (k_1 and k_2), N odd and $\phi_{2k}-\phi_{2k-1} = {}^{\pi}/_{2}$. Then the composition of the unperturbed "$\bar{s}\bar{a}\bar{s}\bar{a}$"–sections before, in between and after the perturbed sections depends on whether the number of the included sections is odd or even. We find

$$\bar{y}_{\rm odd} = \pm(0,0,1,0) \equiv \pm\bar{s}_y \quad , \quad \bar{y}_{\rm even} = \pm\bar{1} \quad . \tag{3.17}$$

For simplicity the small rotation angles of the two perturbations are set equal ($\epsilon_1 = \epsilon_2 \equiv \epsilon$) but the rotation axes are in the horizontal plane with independent angles φ_1 and φ_2. Moreover we set the viewpoint directly before the first section. According to (3.16a) or (3.16b) the two perturbed sections $\bar{q}_1$ and $\bar{q}_2$ are described by

$$\bar{q}_j = (0, \xi c_j, \eta, -\xi s_j) \quad , \quad j = 1,2 \quad , \tag{3.18}$$

with $\xi \equiv \sin\frac{\epsilon}{2}$, $\eta \equiv \cos\frac{\epsilon}{2}$, $c_j \equiv \cos\alpha_j$ and $s_j \equiv \sin\alpha_j$, where the α_j depend on φ_j, ϕ_{2k}, ϕ_{2k-1} and $G\gamma$. There are 4 cases to distinguish

$$\begin{aligned}
\pm\bar{r}_0 = \bar{s}_y\;\bar{q}_2\;\bar{q}_1 &= \Big(\xi^2 S_{2-1},\; -2\eta\xi S_- S_+,\; -\eta^2-\xi^2 S_{2-1},\; 2\eta\xi S_- C_+\Big)\\
\pm\bar{r}_0 = \bar{q}_2\;\bar{s}_y\;\bar{q}_1 &= \Big(\xi^2 S_{2-1},\; 2\eta\xi C_- C_+,\; \eta^2-\xi^2 S_{2-1},\; -2\eta\xi C_- S_+\Big)\\
\pm\bar{r}_0 = \bar{q}_2\;\bar{q}_1\;\bar{s}_y &= \Big(\xi^2 S_{2-1},\; 2\eta\xi S_- S_+,\; -\eta^2-\xi^2 S_{2-1},\; -2\eta\xi S_- C_+\Big)\\
\pm\bar{r}_0 = \bar{s}_y\;\bar{q}_2\;\bar{s}_y\;\bar{q}_1\;\bar{s}_y &= \Big(\xi^2 S_{2-1},\; -2\eta\xi C_- C_+,\; -\eta^2-\xi^2 S_{2-1},\; 2\eta\xi C_- S_+\Big)
\end{aligned} \tag{3.19}$$

with $C_{2-1}, S_{2-1} \equiv \cos,\sin(\alpha_2-\alpha_1)$ and $C_\pm, S_\pm \equiv \cos,\sin\frac{\alpha_2\pm\alpha_1}{2}$. We see that in all 4 cases the deviation of $\cos\pi\nu_0$ from 0 is $O(\epsilon^2)$ and that the deviation of $\hat{n}_0$ from $\hat{y}$ is order $O(\epsilon)$.

If the two rotation axes of the perturbations are the same ($\varphi_1 = \varphi_2$) but the small rotation angles are different ($\epsilon_1 \neq \epsilon_2$), we parametrise the quaternion maps of the perturbed sections by

$$\bar{q}_j = (0, \xi_j c, \eta_j, -\xi_j s) \quad , \quad j = 1,2 \quad , \tag{3.20}$$

with $\xi_j = \sin\frac{\epsilon_j}{2}$, $\eta_j = \cos\frac{\epsilon_j}{2}$, $c \equiv \cos\alpha$ and $s \equiv \sin\alpha$, and find for all four cases

$$\begin{aligned}
\pm\bar{r}_0 = \bar{s}_y\;\bar{q}_2\;\bar{q}_1 &= \Big(0,\; c\xi_{2-1},\; -\eta_{2-1},\; -s\xi_{2-1}\Big)\\
\pm\bar{r}_0 = \bar{q}_2\;\bar{s}_y\;\bar{q}_1 &= \Big(0,\; -c\xi_{2-1},\; -\eta_{2-1},\; s\xi_{2-1}\Big)\\
\pm\bar{r}_0 = \bar{q}_2\;\bar{q}_1\;\bar{s}_y &= \Big(0,\; -c\xi_{2+1},\; -\eta_{2+1},\; s\xi_{2+1}\Big)\\
\pm\bar{r}_0 = \bar{s}_y\;\bar{q}_2\;\bar{s}_y\;\bar{q}_1\;\bar{s}_y &= \Big(0,\; -c\xi_{2+1},\; \eta_{2+1},\; s\xi_{2+1}\Big) \quad ,
\end{aligned} \tag{3.21}$$

where we introduced $\eta_{2\pm1} \equiv \cos\frac{\epsilon_2\pm\epsilon_1}{2}$ and $\xi_{2\pm1} \equiv \sin\frac{\epsilon_2\pm\epsilon_1}{2}$. We now note that a π–rotation around *whatever* axis, if applied twice, produces a unit operation! Therefore in the case of 2 different *strengths* of perturbation (3.21) the cancellation in every $2n$–turn map is exact whereas in the case of 2 different *axes* of perturbation (3.19) the cancellation is not complete but $\bar{r}_0$ has a 0-th component of order $O(\epsilon^2)$.

To summarize the last two sections, one might say that Siberian Snakes, particularly an even number of horizontal snakes and especially in rings with a superperiodicity of $P = 2N$ with odd N make it possible to reduce the effect of small local spin perturbations. But of course for large ϵ even snakes cannot sufficiently control $\hat{n}_0$ and ν_0.

3.1.3 Siberian Snakes in rings with vertical bends

In the derivation of theorem 3.1 we explicitly required the accelerator to be flat, i.e. we required that the only magnetic fields acting on the design orbit besides the fields inside the snakes were the vertical holding fields from the horizontal bends. In this context flatness means less than mid–plane symmetry, since it only constrains spin motion on the closed orbit. However, the proton ring of HERA (called HERA–p) is built on top of the $e^{\pm}$–ring in the arcs and in order to make $e^{\pm}$–p collisions possible the protons are bent to the level of the $e^{\pm}$–ring in 3 of the 4 straight sections. Therefore in a ring like HERA–p which includes vertical bends, Steffen's theorem cannot directly be applied. To be more precise, in the proof of theorem 3.1 we made use of lemma 3.1 and the fact that in a flat perfectly aligned ring the on–orbit spin rotation axes are either vertical in the horizontal bends or are in the horizontal plane in the horizontal snakes. Steffen's theorem can be trivially extended to rings that contain certain sections whose on–orbit spin transfer maps are either an arbitrary rotation around the vertical, an energy independent rotation around some horizontal axis by π (= effective horizontal snake) or a unit transformation ("spin drift"). The vertical bends in HERA–p do not themselves cause problems. Indeed, since the protons in HERA-p have to be first bent down *to* and up *into* the level of the $e^{\pm}$ ring upstream of the interaction point (IP) and then up *to* and down *into* the level of the p–ring in the arcs downstream of the IP, the effective vertical bend angles would cancel on each side of each IP, if the vertical bends were not interleaved with horizontal bends. In HERA–p the down and up bends *are* interleaved with horizontal bends on each side of the IPs. Then owing to the non–commutation of rotations around different axes the spin rotations caused by the vertical bends do *not* cancel. Using equation (2.52) the transfer map through such a *vertical bend section* with two embedded horizontal bending sections of equal bend angle is

$$\begin{aligned}
\bar{q} \;&\equiv\; \Big(\cos\frac{G\gamma\Theta_v}{2}, \sin\frac{G\gamma\Theta_v}{2}, 0, 0\Big)\Big(\cos\frac{G\gamma\Theta_h}{2}, 0, \sin\frac{G\gamma\Theta_h}{2}, 0\Big)\\
&\quad\Big(\cos\frac{G\gamma\Theta_h}{2}, 0, \sin\frac{G\gamma\Theta_h}{2}, 0\Big)\Big(\cos\frac{G\gamma\Theta_v}{2}, -\sin\frac{G\gamma\Theta_v}{2}, 0, 0\Big) \;\equiv\; \bar{v}_+\,\bar{h}\,\bar{h}\,\bar{v}_-\\
&= \Big(\cos\frac{G\gamma\Theta_v}{2}, \sin\frac{G\gamma\Theta_v}{2}, 0, 0\Big)\Big(\cos G\gamma\Theta_h, 0, \sin G\gamma\Theta_h, 0\Big)\Big(\cos\frac{G\gamma\Theta_v}{2}, -\sin\frac{G\gamma\Theta_v}{2}, 0, 0\Big)\\
&= \Big(\cos G\gamma\Theta_h, 0, \sin G\gamma\Theta_h\cos G\gamma\Theta_v, \sin G\gamma\Theta_h\sin G\gamma\Theta_v\Big) \quad . \qquad (3.22)
\end{aligned}$$

The rotation angle $2G\gamma\Theta_h$ is just the same as without vertical bends, but the rotation *axis* which would be vertical in the absence of vertical bends is now strongly energy dependent. Since in the planar arcs the spins rotate around the vertical and rotations around different axes do *not* commute, even one vertical bend section in the ring would produce a non–linear dependence of $\hat{n}_0$ and ν_0 on the energy. Of course for each section of the type $\bar{v}_+\bar{h}\bar{h}\bar{v}_-$ there must be a section of type $\bar{v}_-\bar{h}\bar{h}\bar{v}_+$ in order to make the ring close.

Luckily the vertical bend sections in HERA–p have a symmetry point in between the 2 horizontal bends. Therefore the effect of each vertical bend section can be compensated by placing a *radial* Siberian Snake ($\bar{s}_x \equiv (0,1,0,0)$) at the symmetry point [KS88a, AP97]. Using lemma 3.1 it becomes clear that on the design orbit

$$\bar{v}_{\pm}\,\bar{h}\,\bar{s}_x\bar{h}\,\bar{v}_{\mp} = \bar{s}_x \quad . \qquad (3.23)$$

Note that the compensation *only* works with radial snakes. Therefore each compensated vertical bend section yields one horizontal snake which is fixed in position and snake angle. In the case of HERA–p both vertical bend sections of each IP are directly adjacent to the straight sections — where here "straight section" means that the *total* bend angle of the straight is zero, as long as the effect of misalignments is neglected. Hence the combined spin transfer map on the design orbit of each of the 3 straights with its 2 *compensated* vertical bend sections is a unit transform. Therefore in the case of HERA–p the two radial snakes around the IPs do *not* impose any constraints on the choice of snake angles for the main snakes. From now on we will distinguish between Siberian Snakes used to compensate the effect of vertical bends sections which we will call **flattening snakes** and Siberian Snakes that, by means of Steffen's theorem, fix $\hat{n}_0 = \pm\hat{y}$ and $\partial_\gamma \nu_0 = 0$, which we will call **main snakes**.

In a ring with vertical bend sections compensated in the above way and with pairwise cancellation of all flattening snakes and without main snakes, the $\hat{n}_0$–axis is vertical outside the vertical bend sections but the on–orbit spin tune is *not* $G\gamma$. Assume that by means of flattening snakes we have cancelled away the total amount $G\gamma\Theta_{\text{comp}}$ of spin precession due to the horizontal bends inside compensated vertical bend sections, then the fractional part of the spin tune on the design orbit is

$$[\nu_0]\Big|_{\text{flattened}} = \left[G\gamma\frac{2\pi - \Theta_{\text{comp}}}{2\pi}\right] = \left[G\gamma\left(1 - \frac{\Theta_{\text{comp}}}{2\pi}\right)\right] \quad . \tag{3.24}$$

Definition 3.2 (Flattened ring) *An accelerator in which — with the exception of N_v sections whose accumulated horizontal bend angle is Θ_{comp} — the $\hat{n}_0$–axis is vertical and $[\nu_0] = \left[G\gamma\left(1 - \frac{\Theta_{\text{comp}}}{2\pi}\right)\right]$ is called a flattened ring.*

Following the proof of Steffen's theorem, it becomes clear that in the presence of compensated vertical bend sections theorem 3.1 must be slightly modified.

1. The fractional part of the spin tune on the design orbit is given by

$$[\nu_0] = \left[\frac{\pm 1}{2\pi}\sum_{j=1}^{2N}(-1)^j(2\phi_j + G\gamma(\Theta_j - \Theta_{\text{comp},j}))\right] \quad , \tag{3.25}$$

   where $\Theta_{\text{comp},j}$ is the compensated horizontal bend angle of the j–th section.

2. If the design orbit spin tune is not an integer, then $\hat{n}_0 = \pm\hat{y}$ is uniquely defined up to its sign all along the ring *outside* the compensated vertical bend sections.

3. The $\mathbf{SO(3)}$ spin OTM associated with $\bar{r}_0$ *only* depends on the position of the viewpoint *inside* the compensated vertical bend sections.

Therefore in order to obtain an energy independent spin tune on the design orbit in a flattened ring, the constraint $\sum_{j=1}^{2N}(-1)^j(\Theta_j - \Theta_{\text{comp},j}) = 0$ must be fulfilled, so that the positions of the main snakes in a flattened ring have to be shifted w.r.t. the case of a naturally flat ring.

In a ring with uncompensated vertical bends the spin tune is a complicated function of energy and no simple rules exist that predict the energies at which the resonance condition 2.110 is fulfilled. In a flattened ring the resonance positions are shifted in energy w.r.t. an exactly flat ring. If the flattened ring has an exact superperiodicity P then the fractional part of the spin tune for one superperiod is

$$[\nu_{0,P}^{(\text{fl})}(E_0)] = \left[\frac{G\gamma}{P}\left(1 - \frac{\Theta_{\text{comp}}}{2\pi}\right)\right] \tag{3.26}$$

where we note that if the ring with uncompensated vertical bends was superperiodic then the completely flattened ring is also superperiodic and that the missing bend angle per superperiod is the same for all superperiods. Since the off–orbit T–BMT driving term $\vec{\omega}$ has only Fourier harmonics at $\kappa_P = P(k_0 + \vec{k}\cdot\vec{Q}_P)$ as in equation (2.113), resonances are located at energies where $\nu_{0,P}^{(\text{fl})}(E_0) = k_0 + \vec{k}\cdot\vec{Q}_P$. If the superperiodicity is only approximate then the resonances that fulfil $\nu_{0,P}^{(\text{fl})}(E_0) = k_0 + \vec{k}\cdot\vec{Q}_P$ are still enhanced (strong resonances). Nevertheless, if in a flattened ring the majority M' of the M periodic arc cells are still exactly flat, the spin tune per flat arc cell is still defined by $[\nu_{0,C}] = [G\gamma\Theta_C/(2\pi)]$ so that the condition for a super–strong intrinsic resonances in the presence of M flat cells per arc is $\nu_{0,P}^{(\mathrm{fl})}(E_0) = k_0 \pm Q_{y,P}$ and $\nu_{0,C} \approx k_0' \pm Q_{y,C}$. The resonance spectrum in a flattened ring is hence not only simply shifted but also the relative positions of weak, strong and super–strong resonances might be different from those in an exactly flat model of the ring, i.e. with the vertical bends simply "switched off".

In a distorted ring the closed orbit is normally never flat. Unfortunately the shape of the perturbed closed orbit is in general neither fully predictable nor exactly reproducible from run to run. If the *typical* rms closed orbit deviation is sufficiently small, then the spin perturbations due to radial fields experienced on the perturbed closed orbit contribute significantly only at the *imperfection* resonances $\nu_0 \in \mathbb{Z}$. Thus for snake schemes which in the absence of distortion fulfil $\nu_0 = {}^1\!/_2$ no serious spin disturbance is then expected. This is no longer true for large imperfection resonance strength. Then with $[\nu_{00}] = {}^1\!/_2$ one is still not far enough away from the "snake–less" imperfection resonance $\nu_{00} \in \mathbb{N}$. Equivalently, for sufficiently large rms closed orbit distortion and/or large asymmetries between the perturbed horizontal bend angles of different arc sections between snakes, the premises of Steffen's theorem become invalid and the resulting on–orbit spin tune becomes energy dependent. Snake schemes for practical applications must therefore be tested to see how well they can handle misalignments and closed orbit distortions.

3.2 The effect of Siberian Snakes on spin motion with finite orbital amplitudes

In the last section we have discussed the effect of small perturbing rotations in the presence of snakes for particles restricted to the design orbit. Now we will allow non–zero orbital amplitudes which are small enough to allow us to assume that coherence between spin precession and orbital motion is still described by equation (2.110), i.e. that the characteristic spin precession tune is still approximately ν_0.

3.2.1 Siberian Snakes in rings with perfect mid–plane symmetry

As we have seen in section 2.3.2, in a perfectly mid–plane symmetric ring we have $\vec{\Omega}(\theta, \underline{Y}^- \vec{z}) = \underline{Y}_\pi \vec{\Omega}(\theta, \vec{z})$, with $\underline{Y}^- \equiv \underline{\mathrm{diag}}(1, 1, -1-1, 1, 1) \in \mathbf{SP(6)}$ and $\underline{Y}_\pi \equiv \underline{\mathrm{diag}}(-1, 1, -1) \in \mathbf{SO(3)}$. Then we found that $\hat{n}_0(\theta) = \pm\hat{y}$, that $\underline{Y}_\pi\, \underline{R}(\theta; \vec{z}) = \underline{R}(\theta; \underline{Y}^- \vec{z})\, \underline{Y}_\pi$ and that dynamical resonances which include even multiples of Q_y are excluded. Now we must check whether point–like spin rotators, which we represent by maps rather than by differential equations, destroy these properties or if the effects of mid-plane symmetry can be preserved. Spin maps for point–like spin rotators are independent of the position in phase space. A *necessary* condition for the preservation of the consequences of mid–plane symmetry is then that the relation $\underline{Y}_\pi\, \underline{R} = \underline{R}\, \underline{Y}_\pi$ is preserved. This in turn requires that the $\mathbf{SO(3)}$ group commutator $\underline{Y}_\pi\, \underline{S}\, \underline{Y}_\pi\, \underline{S}^{\mathrm{T}}$ between the snake map $\underline{S}$ and $\underline{Y}_\pi$ is the identity. Translated to quaternion maps of point like spin rotators $\bar{s}$ this condition implies that the $\mathbf{S}_{\mathbb{H}}$ group commutator (2.50) has to fulfil

$$\bar{C}(\bar{y}_\pi, \bar{s}) \equiv \bar{y}_\pi \bar{s} \bar{y}_\pi^{-1} \bar{s}^{-1} = \pm\bar{1} \quad , \tag{3.27}$$

with $\bar{y}_\pi = (0, 0, 1, 0)$. Note again that any two quaternions $\bar{q}$ and $-\bar{q}$ lead to the same $\mathbf{SO(3)}$ map. Taking into account the explicit form of $\bar{C}(\bar{y}_\pi, \bar{s})$ given in equations (2.51b) and (2.51e), and that $\bar{y}_\pi$ itself describes a vertical full snake it is easy to see that only those spin rotators commute with $\bar{y}_\pi$ which either represent arbitrary rotations around the vertical direction $\bar{y}_\psi \equiv (\cos{}^\psi\!/_2, 0, \sin{}^\psi\!/_2, 0)$ or horizontal full snakes $\bar{h}_\phi \equiv (0, \cos\phi, 0, -\sin\phi)$. Explicitly we obtain $\bar{C}(\bar{y}_\pi, \bar{y}_\psi) = +\bar{1}$ and $\bar{C}(\bar{y}_\pi, \bar{h}_\phi) = -\bar{1}$. Moreover introducing $\widetilde{S} \equiv \underline{Y}_\pi \widehat{S}$ we indeed find for $\underline{H}_\phi \equiv \underline{F}(\bar{h}_\phi) = \underline{F}(\bar{y}_{2\phi})\, \underline{F}(\bar{s}_x) \equiv \underline{Y}_{2\phi}\, \underline{X}_\pi$

where $\underline{F}$ is from definition 2.4,

$$\widehat{S}_1 \equiv \begin{pmatrix} S_x \\ S_y \\ S_z \end{pmatrix} \xrightarrow{\underline{X}_\pi} \begin{pmatrix} S_x \\ -S_y \\ -S_z \end{pmatrix} \equiv \widehat{S}_2 \xrightarrow{\underline{Y}_{2\phi}} \begin{pmatrix} \cos(2\phi)S_x - \sin(2\phi)S_z \\ -S_y \\ -\sin(2\phi)S_x - \cos(2\phi)S_z \end{pmatrix} \equiv \widehat{S}_3 \tag{3.28a}$$

$$\widetilde{S}_1 = \begin{pmatrix} -S_x \\ S_y \\ -S_z \end{pmatrix} \xrightarrow{\underline{X}_\pi} \begin{pmatrix} -S_x \\ -S_y \\ S_z \end{pmatrix} = \widetilde{S}_2 \xrightarrow{\underline{Y}_{2\phi}} \begin{pmatrix} -\cos(2\phi)S_x + \sin(2\phi)S_z \\ -S_y \\ +\sin(2\phi)S_x + \cos(2\phi)S_z \end{pmatrix} = \widetilde{S}_3 \quad . \tag{3.28b}$$

We denote the subset of $\mathbf{S}_{\mathbb{H}}$ of rotations which commute up to a factor -1 with $\bar{y}_\pi$ by $\mathbf{Y} \equiv \{\bar{s} \in \mathbf{S}_{\mathbb{H}} : \bar{C}(\bar{y}_\pi, \bar{s}) = \pm\bar{1}\}$ and find using $\bar{s}_x \equiv (0,1,0,0)$ and Steffen's lemma 3.2

1. quaternionic multiplication is an inner operation on $\mathbf{Y}$ since $\bar{y}_{\psi_1}\bar{y}_{\psi_2} = \bar{y}_{\psi_1+\psi_2}$, $\bar{h}_{\phi_1}\bar{h}_{\phi_2} = \bar{y}_{2\phi_1}\bar{s}_x\bar{s}_x\bar{y}_{-2\phi_2} = -\bar{y}_{2(\phi_1-\phi_2)}$, $\bar{y}_\psi\bar{h}_\phi = \bar{y}_\psi\bar{y}_{2\phi}\bar{s}_x = \bar{h}_{\phi+\psi/2}$ and $\bar{h}_\phi\bar{y}_\psi = \bar{s}_x\bar{y}_{-2\phi}\bar{y}_\psi = \bar{h}_{\phi-\psi/2}$,
2. $\bar{1} = \bar{y}_0 \in \mathbf{Y}$ and
3. for $\bar{s} \in \mathbf{Y}$ also $\bar{s}^{-1} \in \mathbf{Y}$ since $\bar{y}_\psi^{-1} = \bar{y}_{-\psi}$ and $\bar{h}_\phi^{-1} = -\bar{h}_\phi$.

Therefore we find

Lemma 3.3 $\mathbf{Y}$ *is a subgroup of* $\mathbf{S}_{\mathbb{H}}$.

Unfortunately $\mathbf{Y}$ consists of two distinct domains which are each connected, i.e. it has a connected subgroup $\mathbf{Y}^+ \equiv \{\bar{s} : \exists\psi \in \mathbb{R}, \bar{s} = \bar{y}_\psi\}$ but for its complement w.r.t. $\mathbf{Y}$, $\mathcal{Y}^- \equiv \mathbf{Y}\backslash\mathbf{Y}^+ = \{\bar{s} : \exists\phi \in \mathbb{R}, \bar{s} = \bar{h}_\phi\}$ the quaternionic product is not even an inner operation in $\mathcal{Y}^-$. For example in a mid–plane symmetric (flat) ring with *one* horizontal snake, $\hat{n}_0$ is in the horizontal plane although the on–orbit spin OTM (3.6a) which is of the form $\bar{r}_0 = \bar{h}_\phi$ is an element of $\mathbf{Y}$. This shows that condition (3.27) is *not* sufficient to guarantee that the spin OTM is compatible with mid–plane symmetry, i.e. that the one–turn quaternion $\bar{r}$ is given by (e_0, o_1, e_2, o_3) where the e_i contain only even harmonics in the vertical orbital phase Ψ_y and the o_i contain only odd harmonics in Ψ_y as in corollary 2 to theorem 2.10. This property will turn out in section 4.8 to be the key to understanding the occurrence or absence of even order kinetic resonances in certain rings with certain snake arrangements. Assume that we are given a map $\bar{q} = (e_0, o_1, e_2, o_3)$, then $\bar{h}_\phi\bar{q} = (-\cos\phi o_1 + \sin\phi o_3, \cos\phi e_0 + \sin\phi e_2, -\sin\phi o_1 - \cos\phi o_3, -\sin\phi e_0 + \cos\phi e_2)$ is of the form $\bar{h}_\phi\bar{q} = (o'_0, e'_1, o'_2, e'_3)$ and is therefore not compatible with mid–plane symmetry. It is plain to see that $\bar{q}\bar{h}_\phi$ has the same form. Nevertheless the composition of (o'_0, e'_1, o'_2, e'_3) and $(o''_0, e''_1, o''_2, e''_3)$ yields a map of the form $(e'''_0, o'''_1, e'''_2, o'''_3)$ — and so does of course the composition of (e'_0, o'_1, e'_2, o'_3) and $(e''_0, o''_1, e''_2, o''_3)$. We finally obtain

Theorem 3.2 *If* $2N_h$ *point–like horizontal full snakes and/or* N_v *point–like vertical spin rotators are inserted into a perfectly mid–plane symmetric ring, then*

1. $\hat{n}_0 = \pm\hat{y}$.
2. *The spin OTM fulfils* $\underline{R}(\theta; \underline{Y}^-\vec{z})\,\underline{Y}_\pi = \underline{Y}_\pi\,\underline{R}(\theta;\vec{z})$.
3. *The one–turn quaternion map* $\bar{r}(\theta;\vec{z})$ *is of the form* $\bar{r} = (e_0, o_1, e_2, o_3)$ *where the* e_i *contain only even harmonics of* Ψ_y *and the* o_i *contain only odd harmonics. Equivalently the* $\mathbf{SU(2)}$ *OTM* $\underline{r} = \underline{f}(\bar{r})$ *is given by* $\left(\begin{smallmatrix} e_{11} & o_{12} \\ -o_{12}^* & e_{11}^* \end{smallmatrix}\right)$, *where* e_{11} *contains only even and* o_{12} *contains only odd harmonics of* Ψ_y.

In other words the insertion of $2N_h$ *point–like horizontal full snakes and/or* N_v *point–like vertical spin rotators does* not *destroy the mid–plane symmetry of the ring.*

3.2.2 Spin–orbit coupling integrals with $2N$ snakes

We now investigate the effect of snakes on spin–orbit coupling integrals. We start with an unperturbed mid–plane symmetric ring with an even number $2N$ of horizontal snakes placed and oriented such that $\nu_0 = \text{const.} = {}^1\!/_2$ as explained in the corollary to theorem 3.1. Then for orbital tunes incommensurable with 1 the resonance condition (2.110) cannot be fulfilled. One might even assume that for practical orbital tunes the system is reasonably far away from any low order spin–orbit resonance. Since the ring is assumed to be flat $I_x^\pm$ and $I_z^\pm$ vanish identically if we have point–like snakes. We note that with realistic snakes which incorporate interleaved vertical and horizontal bends, helical dipoles or solenoids the ring *inside* the snakes by definition is no longer flat [CY81] ! In any case the spin–orbit coupling integrals $I_y^\pm$ will generally *not* vanish for all energies and at all azimuths in the ring.

We divide the ring into $2N+1$ not necessarily identical sections so that the view point is at $\theta_0 \equiv \theta_{2N+1}$ and the horizontal snakes are located at the θ_j, $1 \le j \le 2N$. We introduce the spin phase advance $\phi_j(\theta) \equiv \phi(\theta) - \phi(\theta_j)$ and the orbital betatron phase advance $\psi_j(\theta) \equiv \psi(\theta) - \psi(\theta_j)$ beyond θ_j and the phase advances $\widetilde{\phi}_j(\theta) \equiv \phi(\theta_{j+1}) - \phi(\theta_j)$, $\widetilde{\psi}_j(\theta) \equiv \psi(\theta_{j+1}) - \psi(\theta_j)$ between θ_j and θ_{j+1}. Then the vertical linear spin–orbit coupling integrals at θ_0 *without* snakes are according to equation (2.144)

$$I_{y,0}^\pm(\theta_0) = \sum_{j=0}^{2N} e^{i\sum_{k=0}^{j-1}\widetilde{\phi}_k \pm \widetilde{\psi}_k} \int_{\theta_j}^{\theta_j+1} h(\theta) e^{i\left(\phi_j(\theta) \pm \psi_j(\theta)\right)}\, d\theta \quad , \tag{3.29}$$

where we have used $h(\theta) \equiv -(G\gamma+1)K(\theta)\sqrt{\beta_y(\theta)}$. According to Steffen's Lemma the spins are rotated around the radial axis by π and around the *positive* vertical axis by the angle $2\varphi_j$ at the azimuth θ_j of the j–th snake $\bar{s}_j \equiv (0, \cos\varphi_j, 0, -\sin\varphi_j)$. Therefore we obtain [GH99b] for the spin–orbit coupling integral *with* snakes

$$I_y^\pm(\theta_0) = \sum_{j=0}^{2N} e^{i(\sum_{k=0}^{j-1}(-1)^k(\widetilde{\phi}_k + 2\varphi_k) \pm \widetilde{\psi}_k)} \int_{\theta_j}^{\theta_j+1} h(\theta) e^{i\left((-1)^j(\phi_j(\theta)+2\varphi_j) \pm \psi_j(\theta)\right)}\, d\theta \quad , \tag{3.30}$$

where we have introduced $\varphi_0 = \widetilde{\phi}_0 \equiv 0$ for convenience. Specialising to rings whose superperiodicity was $P = 2N$ before the snakes were introduced, shifting the view point to the position just before the first snake $\theta_0 \to \theta_1$ and distributing the θ_j uniformly ($\theta_j = 2\pi j/P$) we obtain with $\widetilde{\phi} \equiv \widetilde{\phi}_k$, $\widetilde{\psi} \equiv \widetilde{\psi}_k$ for all k and $h(\theta) = h(\theta + \pi/N)$

$$\begin{aligned}
I_y^\pm(\theta_1) \;&=\; \sum_{j=1,\text{odd}}^{2N-1} e^{i\left(\pm(j-1)\widetilde{\psi} + 2\sum_{k=1}^{j-1}(-1)^k\varphi_k\right)} \int_{\theta_1}^{\theta_2} h(\theta) e^{i\left(-(\phi_1(\theta)+2\varphi_j) \pm \psi_1(\theta)\right)}\, d\theta \\
&\quad + \sum_{j=2,\text{even}}^{2N} e^{i\left(-\widetilde{\phi} \pm (j-1)\widetilde{\psi} + 2\sum_{k=1}^{j-1}(-1)^k\varphi_k\right)} \int_{\theta_1}^{\theta_2} h(\theta) e^{i\left(\phi_1(\theta) + 2\varphi_j \pm \psi_1(\theta)\right)}\, d\theta \\
&=\; (I_{y,P}^\mp)^* \sum_{j=1,\text{odd}}^{2N-1} e^{i\left(\pm(j-1)\widetilde{\psi} + 2\sum_{k=1}^{j}(-1)^k\varphi_k\right)} \\
&\quad + I_{y,P}^\pm \sum_{j=2,\text{even}}^{2N} e^{i\left(-\widetilde{\phi} \pm (j-1)\widetilde{\psi} + 2\sum_{k=1}^{j}(-1)^k\varphi_k\right)}
\end{aligned} \tag{3.31a}$$

$$I_{y,P}^\pm \;\equiv\; \int_{\theta_1}^{\theta_2} h(\theta) e^{i(\phi_1(\theta) \pm \psi_1(\theta))}\, d\theta \quad . \tag{3.31b}$$

We note that in the superperiodic case $2N\widetilde{\psi} = 2\pi Q_y$ and $\sum_{k=1}^{2N}(-1)^k\varphi_k = \pi\nu_0$. Then we find by (3.30) or, in the superperiodic case by (3.31a), that the spin–orbit system is on a first order resonance with strength proportional to $I_y^\pm$ and given by equation (2.149) whenever $\nu = k_0 \pm Q_y$. In the resonant case the spin–orbit coupling integral $I_y^\pm$ is independent of θ except for a trivial phase factor.

As discussed in section 2.3.3, vanishing $I_y^\pm(\theta)$ means that to *first order* a spin parallel to $\hat{n}_0(\theta)$ returns to be parallel to $\hat{n}_0(\theta)$ after each turn. The technique of choosing snake angles φ_j and orbital phase advances $\widetilde{\psi}_j$ so that I_y^+ and I_y^- vanish identically for all energies at one azimuth is called a *strong spin match* [KS88a] or a *snake match* [GH99b, GH99c]. In [GH99b] it has been shown that 8 snakes are needed to obtain an energy independent snake match for arbitrary orbital tune in a fourfold superperiodic ring. The 4 additional snakes have to be placed at $\theta_j + \Delta$ so that the spin phase advance from the beginning of each superperiod θ_j to $\theta_j + \Delta$ is the same as the spin phase advance from $\theta_j + \Delta$ to the beginning of the next superperiod θ_{j+1}. It was also shown in [GH99b] that in a ring with four identical regular arcs but different straight sections (e.g. HERA–p) it is possible to exploit the global asymmetry and obtain a partial snake match in which the strong contributions from the regular arcs are cancelled independently of energy with only four snakes. Let $\widetilde{\psi}_{ij}$ be the orbital phase advance from the beginning of the i-th arc to the beginning of the j-th arc and note that the $\widetilde{\psi}_{ij}$ contain $|i-j|$ identical contributions from the regular arcs and $|i-j|$ different contributions from the straight sections. It can be shown [GH99b] that energy independent cancellation of the contributions of the regular arcs to the spin–orbit coupling integrals requires e.g. $\widetilde{\psi}_{13} = \widetilde{\psi}_{24} = \pi$. The vertical tune is given by $2\pi Q_y = \widetilde{\psi}_{13} + \widetilde{\psi}_{24} - \widetilde{\psi}_{23} + \widetilde{\psi}_{41}$ and therefore small changes in the phase advances of the 4 straight sections allow cancellation of the regular arcs *without* changing the vertical tune. [KS88a] considers the case of N identical pairs of snakes (snake–periods) and is therefore in principle more suited for rings with a large number of snakes.

3.2.3 The single resonance model with 2 snakes

In section 2.4 we have introduced the single resonance model (SRM) and derived an explicit formula for the flow (equations (2.164a) to (2.164f)) and the spin OTM ((2.166a) to (2.166d)). In this section we will modify the SRM by placing 2 horizontal snakes with snake angles ϕ_1 and $\phi_2 = {}^{\pi}\!/_2 + \phi_1$ at $\theta_1 = 0$ and $\theta_2 = \pi$ so that $\nu_0 = \text{const.} = {}^1\!/_2$. The spin OTM at $\theta = 0$ is then

$$\bar{r}(0,\Psi) = \bar{r}_{\text{srm}}(2\pi,\pi;\Psi+\pi Q)\ (0,-\sin\phi,0,-\cos\phi)\ \bar{r}_{\text{srm}}(\pi,0;\Psi)\ (0,\cos\phi,0,-\sin\phi)\quad , \tag{3.32}$$

where $\bar{r}_{\text{srm}}$ is defined in equations (2.164a) – (2.164f). In the following we want to compute the n–turn map and therefore write down explicitly the *one* turn map at $\theta = 0$ and $\Psi + 2j\pi Q$, $0 \le j \le n-1$

$$\bar{r}(0,\Psi+2j\pi Q) = (2\xi^2 S_j C_j,\ 2\xi\eta c C_j,\ 2\xi^2 C_j^2 - 1,\ -2\xi\eta s C_j) \tag{3.33}$$

with

$$\xi \equiv \frac{\epsilon}{\lambda}\sin\frac{\pi\lambda}{2} \quad , \quad \eta \equiv \sqrt{1-\xi^2} \tag{3.34a}$$

$$(\ -1 \le \xi,\eta \le +1 \quad , \quad -{}^1\!/_2 \le \xi\eta \le +{}^1\!/_2\ )$$

$$C_j \equiv \cos(\phi - \psi_\epsilon - \kappa\pi - k\Psi - 2kj\pi Q) \quad , \quad S_j \equiv \sin(\phi - \psi_\epsilon - \kappa\pi - k\Psi - 2kj\pi Q) \tag{3.34b}$$

$$c \equiv \cos\left(\phi + \kappa\pi + \arctan(\frac{\delta}{\lambda}\tan(\frac{\lambda\pi}{2}))\right) \quad , \quad s \equiv \sin\left(\phi + \kappa\pi + \arctan(\frac{\delta}{\lambda}\tan(\frac{\lambda\pi}{2}))\right)\ . \tag{3.34c}$$

Note that $\epsilon \in \mathbb{R}^+$ here is *not* considered to be a small quantity but the modulus of the resonance strength as defined in equation (2.150). Obviously the spin OTM is in general not a π rotation so that we cannot expect the perturbation due to the resonance to cancel at every even number of turns. In passing we note that in analogy to the pure SRM the field of unit eigenvectors $\hat{r}(0,\Psi)$ of the OTM (3.33) is *not* an invariant of the spin OTM unless $kQ \in \mathbb{Z}$ and that the net rotation angle μ_r around $\hat{r}(0,\Psi)$ divided by 2π in one revolution defined by $\cos\pi\mu_r = 2\xi^2 S_j C_j$ depends on the orbital phase

Ψ. Therefore $\mu_r(\Psi)$ does not describe long term coherence and cannot be interpreted as the off–orbit spin tune of the system. The vertical response function V_ϵ of equation (2.168) at $\theta = 0$ can be found from (3.33) by setting $j = 0$,

$$V_\epsilon(\Psi, 0) = 1 - 4\xi^2\eta^2\Big(\cos(2[\phi - \psi_\epsilon - \kappa\pi - k\Psi]) + 1\Big) \quad . \tag{3.35}$$

It has nodal points, $V_\epsilon(\Psi, 0) = 1$, at every *even* integer λ since $\xi \sim \sin\frac{\pi\lambda}{2}$ and an additional pathological nodal point at $\delta = 0$ in the case of integer ϵ since $\eta = \sqrt{1-\xi^2}$ and $\xi(\delta = 0) = 0$ for even ϵ and $\xi(\delta = 0) = 1$ for odd ϵ.

For arbitrary given $n \geq 1$, the n–turn map $\bar{r}_n \equiv \bar{r}(2n\pi, 0; \Psi)$ can now be computed recursively by

$$\bar{r}(2n\pi, 0; \Psi) = \bar{r}(0, \Psi + 2(n-1)\pi Q)\ \bar{r}(2(n-1)\pi, 0; \Psi) \quad . \tag{3.36}$$

Following the prescription in [LT86, SL88, SL97], we define for the computation of the n–turn quaternion the "leading order" in ξ by $\bar{r}_n =_{\text{l.o.}} (a_0, b_1, a_2, b_3)$ where the a_i contain ξ in 2-nd order and the b_i contain $\eta\xi$ in first order. We have to note that (1.) an exact expression can in principle always be obtained for finite n and (2.) that ξ is generally *not* a small quantity but can become $O(1)$ if $\epsilon \approx 2l + 1$ with $l \in \mathbb{N}$. Nevertheless for $\epsilon < 1$ we have $\max_{\delta\in\mathbb{R}} |\xi| = \sin{}^{\pi\epsilon}/_2$ at $\delta = 0$ which justifies a truncated power series expansion in ξ^2 and $\xi\eta$ for the n–turn map. Then by induction one can show in a straightforward manner that to "leading order" the n–turn map ($n \leq 1$) is given by

$$\bar{r}_n =_{\text{l.o.}} \begin{cases} (\ 2\xi^2\Gamma_n\ ,\ 2\xi\eta c\Sigma_n\ , 2\xi^2\Xi_n - 1\ , -2\xi\eta s\Sigma_n\ ) & \text{if } n \bmod 4 = 1 \\ (\ 2\xi^2\Xi_n - 1\ ,\ 2\xi\eta s\Sigma_n\ ,\ -2\xi^2\Gamma_n\ ,\ 2\xi\eta c\Sigma_n\ ) & \text{if } n \bmod 4 = 2 \\ (\ -2\xi^2\Gamma_n\ , -2\xi\eta c\Sigma_n\ , 1 - 2\xi^2\Xi_n\ ,\ 2\xi\eta s\Sigma_n\ ) & \text{if } n \bmod 4 = 3 \\ (\ 1 - 2\xi^2\Xi_n\ , -2\xi\eta s\Sigma_n\ ,\ 2\xi^2\Gamma_n\ , -2\xi\eta c\Sigma_n\ ) & \text{if } n \bmod 4 = 0 \end{cases} \tag{3.37}$$

with

$$\Gamma_n \equiv \sum_{j=0}^{n-1} S_j C_j \ \ , \ \ \Xi_n \equiv \sum_{j=0}^{n-1} C_j^2 \ \ , \ \ \Sigma_n \equiv \sum_{j=0}^{n-1} (-1)^j C_j \quad . \tag{3.38}$$

The "leading order" n–turn quaternion as in equation (3.37) is not properly normalised, but a unit quaternion can easily be obtained by the method described in equation (2.78). This re–unitarisation procedure does not affect the *direction* of the eigenvector $\vec{r}$. In the limit $\xi \to 0$ equation (3.37) reduces to an alternation of arcs and snakes as in equation (3.10). If $0 < \xi \ll 1$ then the corrections to equation (3.10) imposed by (3.37) are $O(\xi^2)$ for the zeroth and vertical component of $\bar{r}_n$, and $O(\xi)$ for the horizontal components. For increasing n the horizontal contribution which is proportional to Σ_n can build up, in this level of perturbation theory, if an orbital phase advance of π cancels the alternating sign in equation (3.38). In fact one can show that

$$|\Sigma_n| = \begin{cases} |\cos(\phi - \psi_\epsilon - \kappa\pi - k\Psi - k\pi Q)\, \xi_n(2\pi(\frac{1}{2} - kQ))|\ ,\ n \bmod 2 = 1 \\ |\sin(\phi - \psi_\epsilon - \kappa\pi - k\Psi + k\pi Q)\, \xi_n(2\pi(\frac{1}{2} + kQ))|\ ,\ n \bmod 2 = 0 \end{cases} \quad . \tag{3.39}$$

Here $|\xi_n(x)| = |\sin(nx/2)/\sin(x/2)|$ is the modulus of the complex amplification function defined in equation (2.147a). Therefore to "leading order" the horizontal components of $\bar{r}_n$ are enhanced by a factor n if $1/2 \pm kQ \in \mathbb{Z}$. It has been shown [LT86, SL88] that for $|k| = 1$ and for higher orders in ξ one obtains enhanced build up of the horizontal components of $\bar{r}_n$ whenever

$$\nu_0 \equiv \frac{1}{2} = l_0 \pm (2l + 1)Q \ \ , \ \ l \in \mathbb{N}\ ,\ l_0 \in \mathbb{Z} \quad . \tag{3.40}$$

This phenomenon has been named $(2l + 1)$–th order *snake resonance* [LT86, ST86, SL97] and it has been claimed that even order snake resonances should not exist at all. We note that since the order k of the Fourier harmonic put into equation (3.39) via (3.32) was arbitrary so that *non*–mid–plane symmetric rings are included (according to theorem 2.9), then already with $l = 0$ and $k \in \mathbb{Z}$ all kinds of coherence conditions of type $^1/_2 = l_0' + l'Q$ with $l_0', l' \in \mathbb{Z}$ are obtained from (3.39).

This resonance analysis has two problematic points. First, for $k \neq 0$ and irrational orbital tune Q the sequence of the eigenvectors $\hat{r}_n$ of the n–turn maps $\bar{r}_n$ does *not* describe the evolution of a spin. Even if, for example, a spin at Ψ is set initially parallel to $\hat{r}_2(\Psi)$, it will be transformed by the *two* turn map to $\hat{r}_2(\Psi)$, but the *one* turn map at Ψ will in general *not* transform it to either $\hat{r}_1(\Psi)$ or to $\hat{r}_1(\Psi + 2\pi Q)$. Moreover $\hat{r}_2(\Psi)$ is *not* $\hat{r}_2(\Psi + 4\pi Q)$ and therefore a second application of the two turn map starting at $\Psi + 4\pi Q$ will in general rotate $\hat{r}_2(\Psi)$ around $\hat{r}_2(\Psi + 4\pi Q)$ by the rotation angle $2\pi\mu_r(\Psi + 4\pi Q)$. In chapter 4 we will find the appropriate tools to treat spin–orbit resonances in the presence of snakes. Second, we have shown in equation (2.153) that the SRM contains only one dynamical resonance at $\delta = 0$. Moreover, in section 4.7 we will see that the SRM contains only one resonance at all. We have seen in equation (2.174) that for irrational ϵ and κ the angle $\vartheta_r(n)$ that the unit eigenvector of the n–turn map of the SRM *without snakes* makes with the vertical covers almost the whole interval $[0, \pi]$ as n approaches ∞. Thus the eigenvector tilts over into the horizontal plane even at large distance δ. Therefore the sole fact that the eigenvector $\hat{r}_n$ of the SRM *with* snakes tilts over into the horizontal plane does *not* on its own indicate the existence of a new type of resonance.

Nevertheless, a key aim of the introduction of Siberian Snakes is to circumvent spin–orbit resonances by fixing the on–orbit spin tune to a value where low order spin–orbit resonances are rather unlikely because the orbital tunes required for stable machine operation would not fulfil equation (2.110). Therefore setting the orbital tunes to a snake resonant value, i.e. $[Q_{\text{s.r.}}] = {}^{2m-1}/_{2n}$ with $n, m \in \mathbb{N}^*$ and $1 \leq m \leq n$, and particularly to a low order snake resonant value, trivially removes the advantage of fixing $\nu_0 = {}^1/_2$ — apart from probably seriously destabilising the orbital motion. But it is clear even without analysing n–turn spin maps, that every snake resonant tune fulfils an equation like (3.40). Therefore there is coherence between spin motion on or close to the design orbit and orbital motion on a dense subset (although of zero measure) of the real tunes. Hence instead of concentrating on the eigenvectors of n–turn spin maps one should rather ask how snakes influence the frequency spectrum of spin motion on synchro–betatron trajectories, i.e. at which amplitudes can a resonance condition be met, which orders of spin–orbit resonances still contribute to a significant extent to spin motion and how big has the distance to such resonances to be in order to minimise spin disturbance. These questions will be answered at least partially in chapter 4.

While studying polarisation losses during acceleration, S. Tepikian has found [ST86] that if one accelerates through an energy which would correspond to the resonance condition $\nu_0 = k_0 \pm Q_y$ in the absence of snakes, then the spin transfer matrix for accelerating through the same energy region in the presence of $2N$ horizontal Siberian Snakes exhibits potential depolarisation whenever Q_y fulfils an *odd* order snake resonance condition. Potential depolarisation here means that a spin started vertical at $\delta = -\infty$ and that can be tilted into the horizontal plane while being close to the resonance at $\nu_0(\delta = 0) = \kappa$ will possibly *not* recover to the vertical at $\delta = +\infty$. Acceleration of spins will be treated in the framework of adiabatic invariance in chapter 4.

In exact agreement with theorem 3.2 the one–turn quaternion from equation (3.33) with odd k fulfils the conditions of mid–plane symmetry, i.e. we find r_0 and r_2 contain only even harmonics in Ψ whereas r_1 and r_3 contain only odd harmonics. This can be seen using the relations $2\cos x \sin x = \sin 2x$ and $2\cos^2 x - 1 = \cos 2x$. Note that, according to theorem 2.9, in mid–plane symmetric rings only odd order dynamical resonance harmonics w.r.t. the vertical tune are allowed. If the model is supposed to describe a ring without mid–plane symmetry, also even k are allowed and r_1 and r_3 may become even.

For the one–turn quaternion $\bar{t}$ for the SRM with *one* horizontal snake π apart from the viewpoint we find on the contrary

$$\begin{aligned}\bar{t}(0, \Psi) &= \bar{r}_{\text{srm}}(2\pi, \pi; \Psi + \pi Q)\ (0, \cos\phi, 0, -\sin\phi)\ \bar{r}_{\text{srm}}(\pi, 0; \Psi) \\ &= \Big(2\xi\eta c' \sin(\phi - \psi_\epsilon - \kappa\pi - k\Psi),\ \eta^2\cos\phi + \xi^2\cos(\phi - 2\psi_\epsilon - 2\kappa\pi - 2k\Psi),\end{aligned}$$

$$2\xi\eta s'\sin(\phi-\psi_\epsilon-\kappa\pi-k\Psi),\ -\eta^2\sin\phi+\xi^2\sin(\phi-2\psi_\epsilon-2\kappa\pi-2k\Psi)\Big) \quad (3.41)$$

with $c', s' = \cos, \sin\left(\kappa\pi + \arctan(\frac{\delta}{\lambda}\tan(\frac{\lambda\pi}{2}))\right)$ and ξ, η as in (3.34a). In contrast to (3.33) it is clearly visible that for k odd t_0 and t_2 are odd whereas t_1 and t_3 are even, but one might argue that since $\hat{n}_0(0)$ is parallel to the snake axis and hence in the horizontal plane we have just observed an example of a "rotated mid–plane symmetry like" behaviour. By transforming $\bar{t}$ into the $(\hat{l}(0), \hat{n}_0(0), \hat{m}(0))$–frame, we find

$$\begin{aligned}
\bar{t}'(0,\Psi) &\equiv \bar{q}(\hat{n}_0(0),\hat{y})\,\bar{t}(0,\Psi)\,\bar{q}(\hat{y},\hat{n}_0(0)) \\
&= \Big(2\xi\eta c'\sin(\phi-\psi_\epsilon-\kappa\pi-k\Psi)\ ,2\xi\eta s'\sin(\phi-\psi_\epsilon-\kappa\pi-k\Psi), \\
&\quad -\eta^2-\xi^2\cos(2[\phi-\psi_\epsilon-\kappa\pi-k\Psi])\ ,\xi^2\sin(2[\phi-\psi_\epsilon-\kappa\pi-k\Psi])\Big) \qquad (3.42)
\end{aligned}$$

where $\bar{q}(\hat{y}, \hat{n}_0(0))$ is the quaternion that rotates $\hat{n}_0(0)$ into $\hat{y}$ as defined in equation (2.49) and $\bar{q}(\hat{n}_0(0), \hat{y})$ is its inverse. For odd k the components t'_0 and t'_1 are odd and the components of t'_2 and t'_3 are even. Therefore we see that the one–turn quaternion $\bar{t}'$ in the tilted frame mixes odd and even harmonics in the components belonging to the diagonal and off-diagonal part of the $\mathbf{SU(2)}$ map $\underline{t}'$. This means that the rotations that cause a tilt away from $\hat{n}_0$ contain both odd and even harmonics in Ψ and that the system does *not* behave like a "rotated mid–plane symmetric" system. The $\hat{n}_0$–response function at $\theta = 0$ for the case of one horizontal snake is

$$\begin{aligned}
V_\epsilon(\Psi,0) &= 1-2((t'_1)^2+(t'_3)^2) \\
&= 1-2\xi^2\Big(4\eta^2 s'^2\sin^2(\phi-\psi_\epsilon-\kappa\pi-k\Psi)+\xi^2\sin^2(2[\phi-\psi_\epsilon-\kappa\pi-k\Psi])\Big)\quad , \quad (3.43)
\end{aligned}$$

and has nodal points at least at every δ for which λ is an *even* integer.

Chapter 4

The invariant spin field and the amplitude dependent spin tune

In this chapter we will introduce the concept of the invariant spin field ($\hat{n}$–axis, Derbenev–Kondratenko vector) and the amplitude dependent spin tune. The concept of the $\hat{n}$–axis $\hat{n}(\vec{z},\theta)$, which is a field constructed from a family of special solution of the TBMT–equation, was originally introduced in 1972 by Derbenev and Kondratenko [DK72, DK73] in a quasi–classical description of the constructive and destructive effects of the synchrotron radiation field on electron polarisation. In the presence of the Sokolov–Ternov effect [ST64] and the counteracting spin diffusion the local polarisation $\vec{P}_{\rm loc}$ at a phase space point settles basically along $\hat{n}(\vec{z},\theta)$. The equilibrium value $|\vec{P}_{\rm equ}|$ and the characteristic polarisation/depolarisation time scales can be computed once the invariant spin field and its derivative w.r.t. the relative energy offset δ of the particle are known all around the ring and all across phase space [SM86a, SM86b, DK72, DK73]. But even at high energies up to some TeV the synchrotron radiation for protons is usually so weak that Sokolov–Ternov build up as well as radiative depolarisation can be neglected.

In low energy rings the proton spin dynamics is sufficiently well described by the SRM [FS60, CR80, SM88, HH96]. In the single resonance approximation one can solve the EOM for the spin directly and constraints on the working energy and acceleration procedures can be obtained in a straightforward manner (see sections 2.4 and 4.10). But at high energies where the spin–orbit coupling integrals are large the spin motion becomes so complicated that a better tool is needed. For example with increasing energy the Fourier coefficients ε_κ of $\vec{\omega}$ increase. At a certain stage the 'width' of some stronger resonances, i.e. the energy range in which these resonances have a non negligible effect on spin motion, start to overlap. Beyond this energy the assumptions made in the single resonance model become invalid. The flow of the T–BMT equation of course can still be computed numerically and one way to proceed is to do straightforward tracking with many particles for many turns to study spin motion at high energy. Normally one starts with a vertically aligned ensemble of spins in a given initial region in phase space. Even under static conditions, i.e. when all parameters of the T–BMT equation remain constant, one will usually observe a strongly oscillating component of $\vec{P}_{\rm ens} \equiv \langle \widehat{S} \rangle_{\rm ens}$ viewed at subsequent revolutions around the ring. This indicates that for an initially vertical spin ensemble, $\vec{P}_{\rm ens}$ is *not* invariant under the one–turn spin map (OTM). In other words such an ensemble does *not* describe an equilibrium spin distribution. But we cannot understand variation of polarisation without first understanding the equilibrium. For that we need the $\hat{n}$–axis. In the field of proton polarisation the $\hat{n}$–axis was introduced by Yokoya [KY88] during the SSC project and then extensively used here at DESY for the "Polarised Protons at HERA" project [DB95a, DB95b, BH96a, BH96b, BH96c, BH96d, BH98a, BH98b, BV98, HV99, VB98, BH99a, BH99b].

In the following sections we will define the invariant spin field as a phase space and azimuth dependent unit vector field that is invariant under the T–BMT one–turn map. We will then introduce the amplitude dependent spin tune. Knowledge of both the $\hat{n}$–axis and the amplitude dependent spin tune allow an action–angle representation of spin motion, a description of the stationary spin distribution and a formulation of adiabatic invariance under variation of the lattice parameters and/or the reference momentum.

For the rest of this chapter we will assume the orbital motion to be integrable, so that for every azimuth θ there is a symplectic transformation from the coordinates $\vec{z}$ to action–angle coordinates $\vec{J}$, $\vec{\Psi}$ where the inverse transformation is periodic w.r.t. θ and the Ψ_i. See also definition A.10. Sometimes we will *silently* assume the initial azimuth to be $\theta_i = 0$. We will often associate the orbital flow on the invariant torus $\mathcal{T}_{\vec{J}}$, $\vec{\Psi}(\theta;\vec{\Psi}_0) = \vec{\Psi}_0 + \vec{Q}(\vec{J})\theta$ with the vector of tunes $\vec{Q}(\vec{J})$. Then every function of the azimuth and the coordinates is, when evaluated along a trajectory, pseudo–periodic (see definition A.13) with the tunes $\vec{Q}$. We will assume the eigenplanes of linearised orbital motion to have a unique maximum projection on one of the (x,a)-, (y,b)- and (τ,δ)–planes so that we may conveniently label the eigenplane and the corresponding tune as the x-, y- or z–plane and as Q_x, Q_y or Q_z respectively. The domain $\mathcal{A} \subset \mathcal{P}$ in which the motion is bounded at least for a large number of revolutions and in which at least approximations of action–angle variables can be found, is called the *dynamic aperture* of a lattice. If the dynamic aperture of a lattice is too small, the accelerator cannot be operated in storage mode or even in slow acceleration mode. Thus the constraint of integrable orbital motion does not imply any practical restriction for the applicability of the results derived in this chapter.

4.1 Basic properties of the invariant spin field and the amplitude dependent spin tune

Dynamical variables, apart from trivial examples, are implicitly time dependent via the EOM. In accelerator coordinates we replace the time variable by the generalised azimuth $\theta \equiv 2\pi l/L$, $\theta \in \mathbb{R}$. A solution, e.g. of the orbital EOM $\vec{z}(\theta)$ is generally *not* periodic in θ.

Definition 4.1 (Lattice field) *We will call a field* $\vec{f}_{\vec{J}} : \mathbb{R}^3 \times \mathbb{R} \to \mathbb{R}^d$, $(\vec{\Psi},\theta) \mapsto \vec{f}_{\vec{J}}(\vec{\Psi},\theta)$ *on the torus* $\vec{J} = \text{const.}$ *a lattice field if it is* 2π*–periodic in* θ *as well as in the* Ψ_i. *We will call it a lattice function if it does not depend on the* Ψ_i.

The periodicity w.r.t. $\vec{\Psi}$ implies that $\vec{f}_{\vec{J}}$ is a *function* of the phase space. We will sometimes symbolise such a function by defining the domain to be $\mathcal{T}_{\vec{J}} \times \mathbb{R}$ where $\mathcal{T}_{\vec{J}}$ is the torus $\vec{J}$ =const. The periodicity w.r.t. θ implies that $\vec{f}_{\vec{J}}$ is a function of the *position* in the lattice. Examples for lattice functions are the Courant–Snyder functions $\beta(\theta)$, $\alpha(\theta)$, $\gamma(\theta)$ $(d=1)$ or the matrix of the orbital eigenvectors of the linear orbital OTM $(d=36)$. Examples for lattice fields are the Lorentz force $\vec{F}(\vec{J},\vec{\Psi},\theta)$ and the T–BMT precession vector $\vec{\Omega}(\vec{J},\vec{\Psi},\theta)$ $(d=3)$.

The spin field is the natural generalisation of a dynamical spin variable, which obeys the T–BMT equation, to a field on the extended phase space $\mathcal{P}^\star \equiv \mathcal{P} \times \mathbb{R}$. We will only discuss spin fields on the torus $\mathcal{T}_{\vec{J}}$

Definition 4.2 (Spin field) *A* $\mathcal{C}^1$ *field* $\hat{f}_{\vec{J}} : \mathcal{T}_{\vec{J}} \times \mathbb{R} \to \mathcal{S}_{\mathbb{R}}$, $(\vec{\Psi},\theta) \mapsto \hat{f}_{\vec{J}}(\vec{\Psi},\theta)$ *on the torus* $\mathcal{T}_{\vec{J}}$ *is called a spin field of some lattice field* $\vec{\Omega}_{\vec{J}}$ *and some orbital flow* $\vec{\Psi}(\theta;\vec{\Psi}_0) = \vec{\Psi}_0 + \vec{Q}(\vec{J})\theta$ *if it is a solution of:*

$$\mathrm{D}_\theta \hat{f}_{\vec{J}} \;\equiv\; \partial_\theta \hat{f}_{\vec{J}} + \vec{Q}^{\mathrm{T}} \partial_{\vec{\Psi}} \hat{f}_{\vec{J}} \;=\; \vec{\Omega}_{\vec{J}}(\vec{\Psi},\theta) \times \hat{f}_{\vec{J}} \quad . \tag{4.1}$$

Normally we will presume that lattice fields and spin fields can be defined for $\vec{J} \in \mathcal{A} \subset \mathbb{R}^3$ where $\mathcal{A}$ is connected and includes $\vec{0}$. When it is clear which torus or which set of tori is meant, we will often drop the subscript $\vec{J}$.

Lemma 4.1

1. *Let $\hat{f}$ be a spin field for given $\vec{\Omega}$ and $\vec{Q}$, then $\widehat{S}_{\hat{f}}(\theta;\vec{\Psi}_0) \equiv \hat{f}(\vec{\Psi}(\theta;\Psi_0),\theta)$ solves the initial value problem $\mathrm{D}_\theta\,\widehat{S} = \vec{\Omega}\times\widehat{S}$, $\widehat{S}(0) = \hat{f}(\vec{\Psi}_0,0)$ on the orbital trajectory $\vec{\Psi}(\theta) = \vec{\Psi}_0 + \vec{Q}\theta$.*
2. *Conversely if $\hat{\xi}_{\vec{\Psi}_0}(\theta)$, $\vec{\Psi}_0 \in \mathcal{T}$ is a $\mathcal{C}^1$ family of spin trajectories on the torus which obey the initial value problem $\mathrm{D}_\theta\,\hat{\xi}_{\vec{\Psi}_0} = \vec{\Omega}\times\hat{\xi}_{\vec{\Psi}_0}$, $\hat{\xi}_{\vec{\Psi}_0}(0) = \hat{\xi}^{(0)}_{\vec{\Psi}_0}$, then $\hat{g}(\vec{\Psi},\theta) \equiv \hat{\xi}_{\vec{\Psi}-\vec{Q}\theta}(\theta)$ is a spin field for $\vec{\Omega}$ and $\vec{Q}$.*

The proof of 1 is obvious:

$$\mathrm{D}_\theta\,\widehat{S}_{\hat{f}}(\theta;\vec{\Psi}_0) = \partial_\theta\,\hat{f} + \vec{Q}^{\mathrm{T}}\partial_{\vec{\Psi}}\,\hat{f} = \vec{\Omega}(\vec{\Psi}(\theta;\vec{\Psi}_0),\theta)\times\widehat{S}_{\hat{f}}(\theta;\vec{\Psi}_0) \quad . \tag{4.2}$$

Since $\vec{\Psi}_0 = \vec{\Psi}(\theta,\vec{\Psi}_0) - \vec{Q}\theta \quad \forall\,\vec{\Psi}_0,\theta$, there is one initial condition $\hat{g}(\vec{\Psi}_0,0) = \widehat{S}_{\vec{\Psi}_0}(0) = \widehat{S}^{(0)}_{\vec{\Psi}_0}$ for every $(\vec{\Psi},\theta)$. Moreover we find at $(\vec{\Psi}',\theta')$

$$\left(\partial_\theta + \vec{Q}^{\mathrm{T}}\partial_{\vec{\Psi}}\right)\hat{g}|_{\vec{\Psi}',\theta'} = \mathrm{D}_\theta\,\widehat{S}_{\vec{\Psi}_0}(\theta)|_{\vec{\Psi}_0=\vec{\Psi}'-\vec{Q}\theta',\theta'} = \vec{\Omega}(\vec{\Psi}',\theta')\times\widehat{S}_{\vec{\Psi}'-\vec{Q}\theta'}(\theta') = \vec{\Omega}(\vec{\Psi}',\theta')\times\hat{g}|_{\vec{\Psi}',\theta'} \tag{4.3}$$

which proves 2. □

Corollary: A spin field $\hat{f}$ evolves on the torus by means of the T–BMT flow

$$\hat{f}(\vec{\Psi}+\vec{Q}\Delta,\theta+\Delta) = \underline{R}(\theta+\Delta,\theta;\vec{\Psi})\hat{f}(\vec{\Psi},\theta) \quad . \tag{4.4}$$

A spin field is therefore equivalent to a continuously partially differentiable family of spin trajectories. Now we can define the invariant spin field

Definition 4.3 (Invariant spin field) *A spin field $\hat{n}_{\mathcal{J}}$ is called an invariant spin field (also $\hat{n}$–axis or Derbenev–Kondratenko vector) if it is a lattice field, i.e. if:*

$$\hat{n}_{\mathcal{J}}(\vec{\Psi},\theta+2\pi) = \hat{n}_{\mathcal{J}}(\vec{\Psi},\theta) = \hat{n}_{\mathcal{J}}(\vec{\Psi}+2\pi\vec{k},\theta) \;\; \text{with}\; \vec{k}\in\mathbb{Z}^3 \quad . \tag{4.5}$$

Since it is a spin field it obeys $\underline{R}_{\mathcal{J}}(\theta_f,\theta_i;\vec{\Psi}_i)\;\hat{n}_{\mathcal{J}}(\vec{\Psi}_i,\theta_i) = \hat{n}_{\mathcal{J}}(\vec{\Psi}_f,\theta_f)$. Definition 4.3 is equivalent to the requirement that the $\hat{n}$–axis is invariant under the spin OTM in the sense that

$$\underline{R}(\theta;\vec{\Psi})\hat{n}(\vec{\Psi},\theta) = \hat{n}(\vec{\Psi}+2\pi\vec{Q},\theta) \quad . \tag{4.6}$$

This means that the image $\hat{n}(\mathcal{T},\theta) \equiv \{\hat{n}(\vec{\Psi},\theta)\,:\,\vec{\Psi}\in\mathcal{T}\}$ of $\mathcal{T}$ on $\mathcal{S}_{\mathbb{R}}$ is an invariant of the spin OTM. Since for any two T–BMT solutions $\widehat{S}_1$ and $\widehat{S}_2$ the scalar product $\widehat{S}_1\cdot\widehat{S}_2$ is an invariant of motion, for any spin field $\hat{f}$

$$P^{(\hat{f})}_{\mathrm{dyn}} \equiv \frac{1}{(2\pi)^3}\int_{\mathcal{T}} d\vec{\Psi}^3\;\hat{f}(\vec{\Psi},\theta)\cdot\hat{n}(\vec{\Psi},\theta) \equiv \langle\hat{f}\cdot\hat{n}\rangle_{\vec{\Psi}} \tag{4.7}$$

is an invariant of motion. Furthermore

$$P_{\mathrm{lim}}(\theta) \equiv \left\|\frac{1}{(2\pi)^3}\int_{\mathcal{T}} d\vec{\Psi}^3\;\hat{n}(\vec{\Psi},\theta)\right\| \equiv \|\langle\hat{n}\rangle_{\vec{\Psi}}\| \tag{4.8}$$

is an invariant of the OTM. In other words if infinitely many spins are aligned parallel to the invariant spin field at some azimuth θ and uniformly distributed in $\vec{\Psi}$, then after one revolution around the ring they are redistributed on the torus according to the orbital phase advance $2\pi\vec{Q}$ but $P_{\mathrm{dyn}} = 1$ and $P_{\mathrm{lim}}(\theta)$ remain unchanged. Therefore with an ensemble of spins aligned along their local $\hat{n}$–axis the polarisation on the torus does not depend on time — this is the stationary polarisation state. Because of the periodicity constraint resonances show up in $\hat{n}$ and P_{lim}. We will discuss P_{lim} and P_{dyn} later in section 4.4.

The evaluation $\widehat{S}_{\hat{n}}(\theta) \equiv \hat{n}(\vec{\Psi}(\theta), \theta)$ of $\hat{n}$ along an orbital trajectory $\vec{\Psi}(\theta)$ is sometimes identified with the $\hat{n}$–axis itself. Then the invariant spin field is often called the "periodic T–BMT solution", although for any trajectory $\vec{\Psi}(\theta)$ $\widehat{S}_{\hat{n}}(\theta)$ is only pseudo–periodic with the orbital tunes $\vec{Q}$.

Since the orbital OTM $\underline{T}$ is origin preserving and both the orbit and spin maps do not depend on $\vec{\Psi}$ for $\vec{J} = \vec{0}$, the $\hat{n}$–axis contains the $\hat{n}_0$–axis as a trivial case

$$\hat{n}_0(\theta) = \hat{n}_{\vec{0}}(\vec{\Psi}, \theta) \quad , \quad \hat{n}_0(\theta + 2\pi) = \underline{R}_0(\theta)\hat{n}_0(\theta) \quad . \tag{4.9}$$

Historically the above property of the $\hat{n}_0$–axis caused a lot of confusion: by analogy many have taken the $\hat{n}$–axis to be the unit rotation vector of the spin OTM even for $\vec{J} \neq \vec{0}$. Here we should stress the point that the $\hat{n}$–axis is, except for trivial examples, *not* the unit rotation vector $\hat{r}$ of the spin OTM $\underline{R}$. The orbital OTM $\underline{T}_{\vec{J}}(\theta; \vec{\Psi}_i)$ and the spin one–turn matrix $\underline{R}_{\vec{J}}(\theta; \vec{\Psi})$ are lattice fields. Hence the rotation vector $\hat{r}_{\vec{J}}(\vec{\Psi}, \theta)$ is a lattice field, but propagating it with the spin OTM with $\vec{J} \neq \vec{0}$ yields

$$\underline{R}_{\vec{J}}(\theta; \vec{\Psi}_i)\hat{r}_{\vec{J}}(\vec{\Psi}_i, \theta) = \hat{r}_{\vec{J}}(\vec{\Psi}_i, \theta) \tag{4.10}$$

and generally *not* $\underline{R}_{\vec{J}}(\theta; \vec{\Psi}_i)\hat{r}_{\vec{J}}(\vec{\Psi}_i, \theta) = \hat{r}_{\vec{J}}(\vec{\Psi}_i + 2\pi\vec{Q}, \theta)$. Therefore according to the corollary to lemma 4.1 $\hat{r}_{\vec{J}}(\vec{\Psi}, \theta)$ is *not* a spin field and hence *not* an $\hat{n}$–axis. Moreover it was already clear in chapter 2 and 3 that an evaluation $\hat{r}_{\vec{J}}(\vec{\Psi}(\theta), \theta)$ of $\hat{r}_{\vec{J}}$ does in general *not* obey the TBMT–equation. $\hat{r}_{\vec{J}}$ is of course an $\hat{n}$–axis if the tunes are integral $[Q_i] = 1$, $i = x, y, z$, i.e. if the orbit system is on an integer resonance in all planes. But if the tunes are incommensurable with 1 then $\hat{r}_{\vec{J}}$ can in general not be an $\hat{n}$–axis for non–vanishing orbital amplitudes. This can also be seen be combining equations (4.10) and (4.6) to $\hat{r}_{\vec{J}}(\vec{\Psi}, \theta) = \hat{r}_{\vec{J}}(\vec{\Psi} + 2\pi\vec{Q}, \theta)$ for all $\vec{\Psi}$. Iteration yields the constraint $\hat{r}_{\vec{J}}(\vec{\Psi}, \theta) = \hat{r}_{\vec{J}}(\vec{\Psi} + 2N\pi\vec{Q}, \theta)$, $N \in \mathbb{N}$. Since $\{\vec{\Psi} + 2N\pi\vec{Q} \,:\, N \in \mathbb{N}\}$ is a dense subset of $\mathcal{T}$ for incommensurable tunes, we see that $\hat{r}_{\vec{J}}(\vec{\Psi}, \theta)$ could not depend on $\vec{\Psi}$. Therefore $\hat{r}_{\vec{J}}$ can only be an $\hat{n}$–axis in a spin–orbit system with incommensurable tunes, if the $\hat{n}$–axis does *not* depend on the orbital phases. In principle these examples are trivial and have no significance for real accelerators. The presence of quadrupoles implies spin–orbit coupling and therefore a phase dependent $\hat{r}_{\vec{J}}$. Moreover the orbital motion, in fact already the closed orbit, is unstable under small perturbations for integral tunes. Figure 4.1 (left) shows $\hat{r}(\Psi_y)$ on the unit sphere in HERA–p at 805 GeV for purely vertical motion on an invariant ellipse enclosing a normalised emittance of 40 π mm mrad. The lattice is the 1996 luminosity optics of HERA–p with 6 flattening snakes around the East- (O), South- (S) and North- (N) interaction points (IP) and four horizontal snakes close to the O-, S-, W- and N–IP with snake angles measured from the radial direction $\pi/2$, 0, 0 and 0. The viewpoint θ_0 is at the O–IP and the vertical tune used for the simulation was close to 32.2725.[1] Most figures on spin motion in HERA–p in *this* chapter will actually use this particular lattice and snake scheme, which we will call "3111". The HERA optics and the snake scheme are described in much more detail in chapter 5 and a table for the coding of snake schemes used in this thesis is given in appendix C. Figure 4.1 (right) shows in "dark" the corresponding locus of the invariant spin field, i.e. the result of successive application of the spin OTM on a spin initially parallel to $\hat{n}(\Psi_{y,i})$, and in "light" the locus of $\hat{r}$. The $\hat{n}$–axis was computed (see section 4.5) at one point $\Psi_{y,i}$ and then $\widehat{S}_n \equiv \hat{n}(\Psi_{y,i}, \theta_i)$ tracked for 1000 turns leading to a closed curve on the unit sphere, in other words for those M, N for which the distance $[(M - N)Q_y]$ on the invariant ellipse is sufficiently small, the difference of $\hat{n}(\Psi_{y,i} + 2\pi M Q_y)$ and $\hat{n}(\Psi_{y,i} + 2\pi N Q_y)$ is small (see lemma 4.2). The tracking of the $\widehat{S}_r \equiv \hat{r}(\Psi_{y,i}, \theta_i)$ obviously leads to a cloud of points around the $\hat{n}$–axis instead of a closed curve. In Summary for systems with incommensurable orbital tunes, if $\hat{r}$ is viewed as a lattice field $\hat{r}(\vec{\Psi}, \theta) = \hat{r}(\vec{\Psi}, \theta + 2\pi)$ as in figure 4.1 (left), it is *not* a spin field and on the other hand if $\hat{r}'$ is viewed as a spin field for the initial conditions $\hat{r}'(\vec{\Psi}, \theta_i) = \underline{R}(\vec{\Psi}, \theta_i)\hat{r}'(\vec{\Psi}, \theta_i)$ at θ_i as in 4.1 (right), it is *not* periodic in θ and hence *not* a lattice field.

[1]But as "irrational" as possible in a floating point representation.

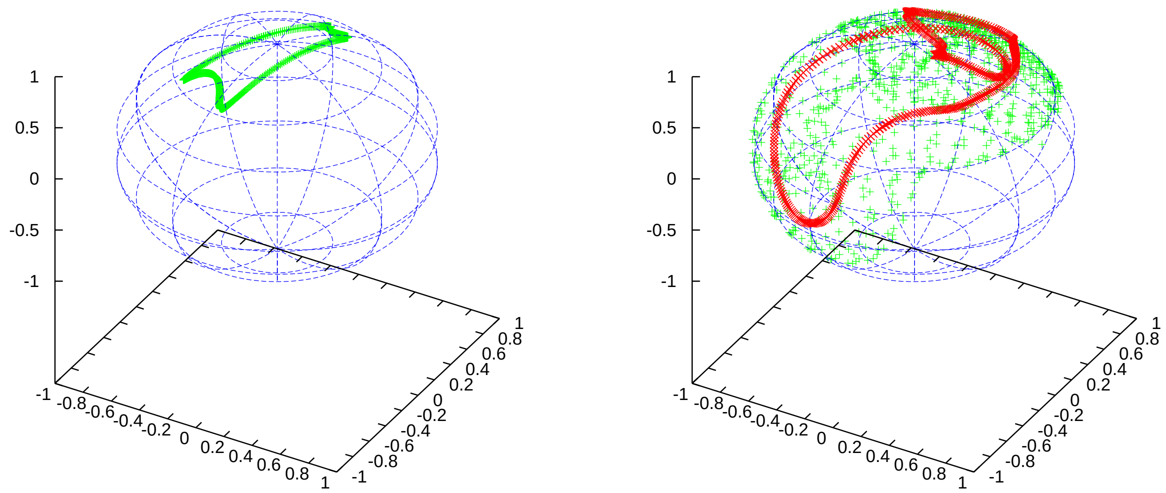

Figure 4.1: Left: The rotation vector $\hat{r}(\Psi_y)$ in HERA–p at 805 GeV with enclosed vertical emittance of 40 π mm mrad on the unit sphere. Right: Scatter–plot of successive iterations of the spin OTM on a spin initially parallel to $\hat{r}(\Psi_{y,i})$ (light) in comparison with the invariant spin field (dark).

Nevertheless for orbit resonances of sufficiently high order the orbital motion might be sufficiently stable to allow operation. Therefore it is worthwhile to look at the general case of $\vec{k}\cdot\vec{Q}=k_0$, $\vec{k}\in\mathbb{N}^3$, $k_0\in\mathbb{N}$ with $|\vec{k}|\gg 1$ or equivalently $N\vec{Q}=\vec{0}$ mod 1 where N is the smallest common multiple of the k_i.

Theorem 4.1 (The $\hat{n}$–axis on an orbital resonance) *If in a combined spin-orbit system* $N\vec{Q}=(0,0,0)$ mod 1 *for some* $N\in\mathbb{N}$ *then an $\hat{n}$–axis exists. It is given by*

$$\hat{n}_{\rm res}(\vec{\Psi},\theta)=\hat{r}^{(N)}(\vec{\Psi},\theta)\quad , \tag{4.11}$$

where $\pm\hat{r}^{(N)}(\vec{\Psi},\theta)$ *is the unit eigenvector with eigenvalue 1 (unit rotation vector) of the N–turn spin map* $\underline{R}^{(N)}(\theta;\vec{\Psi})$ *and the sign has been chosen to make* $\hat{n}_{\rm res}$ *continuous.*

If in addition $\underline{R}^{(N)}(\theta;\vec{\Psi})=\underline{1}\ \forall\vec{\Psi}$*, an (almost) arbitrary spin field generated by propagating a continuous family of spins* $\widehat{S}^{(0)}_{\vec{\Psi}}$ *at some* θ_0 *which fulfils* $\underline{R}^{(l)}(\theta_0,\vec{\Psi})\widehat{S}^{(0)}_{\vec{\Psi}}=\widehat{S}^{(0)}_{\vec{\Psi}+2l\pi\vec{Q}}$, $1\le l\le N$ *is an $\hat{n}$–axis and therefore the $\hat{n}$–axis is not unique, otherwise the $\hat{n}$–axis is unique up to a global sign.*

The proof requires some care in order to guarantee continuity of $\hat{n}$ and can be found in [GH99b].

A general proof for the existence of an invariant spin field for non–resonant tori has not yet been found. In the SRM the $\hat{n}$–axis can be computed analytically (see section 4.7). Furthermore, in many cases of realistic lattices numerical approximations (see sections 4.3 and 4.5) of the $\hat{n}$–axis can be found. If an $\hat{n}$–axis exists on a non–resonant torus and a particle starting at $(\vec{\Psi},\theta)$ with a spin $\widehat{S}_{\hat{n}}$ parallel to $\hat{n}(\vec{\Psi},\theta)$ is tracked by the combined spin–orbit OTM for $m=1,2,\ldots$ times, then due to the incommensurability of the tunes the set $\mathcal{Z}\equiv\{\vec{\Psi}+2m\pi\vec{Q}\bmod 2\pi|m\in\mathbb{N}\}$ is dense on $\mathcal{T}$ at θ and $\mathcal{S}\equiv\{\underline{R}^{(m)}(\theta;\vec{\Psi})\widehat{S}_{\hat{n}}|m\in\mathbb{N}\}$ is dense on $\mathcal{L}\equiv\hat{n}(\mathcal{T},\theta)$. Since $\hat{n}$ is assumed $\mathcal{C}^1$, knowledge of $\hat{n}$ on a dense subset of $\mathcal{T}$ suffices to determine $\hat{n}$ completely. In order to obtain $\hat{n}$ at θ' from $\widehat{S}_{\hat{n}}$ one first computes $\widehat{S}'_{\hat{n}}\equiv\underline{R}(\theta',\theta;\vec{\Psi})\widehat{S}_{\hat{n}}$ at $\vec{\Psi}'=\vec{\Psi}+(\theta'-\theta)\vec{Q}$ and then constructs the sets $\mathcal{Z}'\equiv\{\vec{\Psi}'+2m\pi\vec{Q}\bmod 2\pi|m\in\mathbb{N}\}$ and $\mathcal{S}'\equiv\{\underline{R}^{(m)}(\theta;\vec{\Psi}')\widehat{S}'_{\hat{n}}|m\in\mathbb{N}\}$. We have just proved

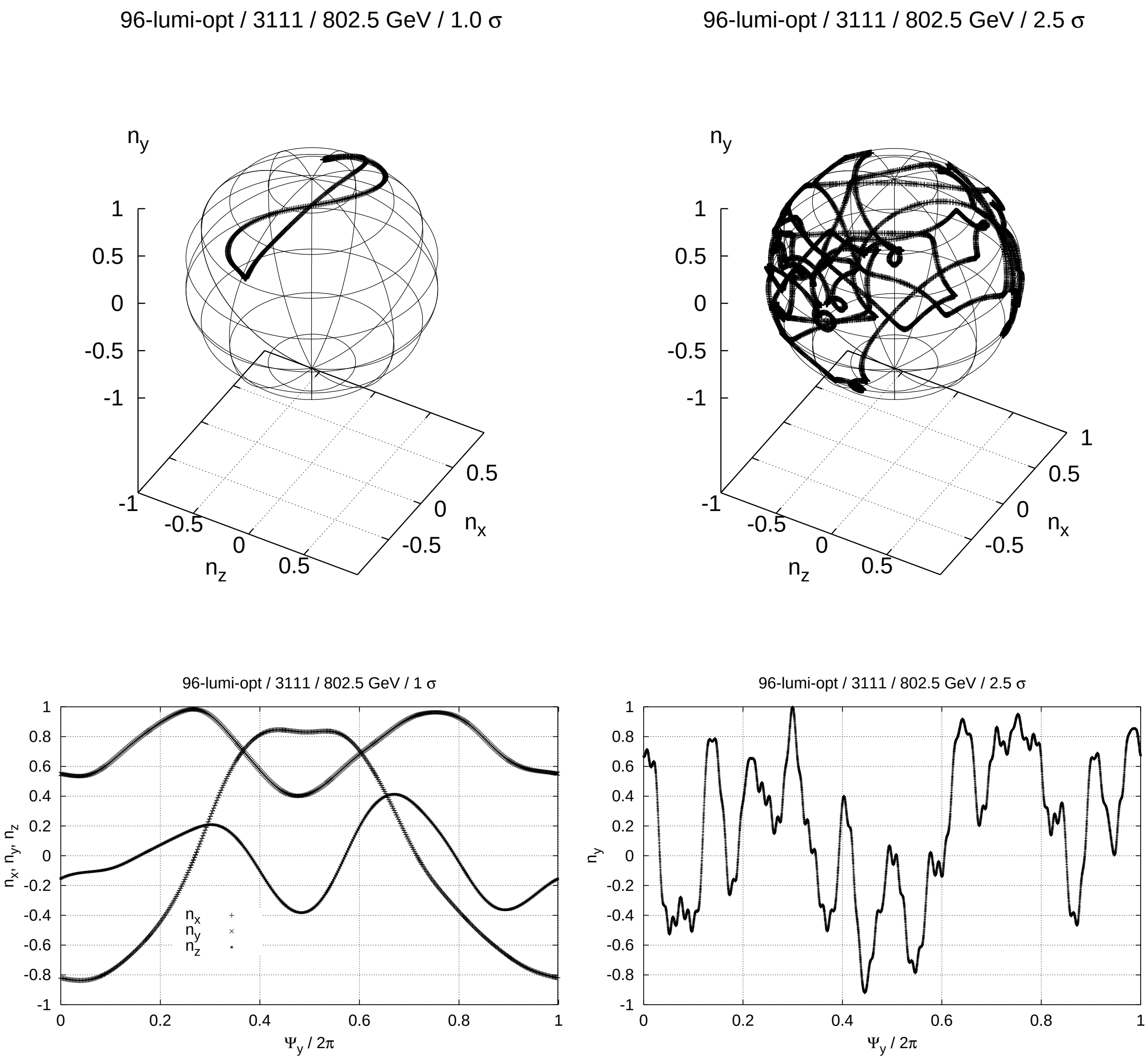

Figure 4.2: The locus of the $\hat{n}$–axis for the HERA–p 1996–luminosity optics with 6 flattening snakes around the O-, S-, and N–IP and 4 snakes, from O to N: long., rad., rad., rad. (3111) at a reference momentum of 802.5 GeV and for purely vertical motion. Top left: on the 1 σ invariant ellipse and top right: for 2.5 σ. Bottom left: $\hat{n}(\Psi_y)$ for 1 σ and bottom right: $n_y(\Psi_y)$ for 2.5 σ.

Theorem 4.2 *If on some torus an invariant spin field exists for a spin–orbit system with orbital tunes incommensurable with 1, then the invariant spin field on this torus is completely determined by one spin $\widehat{S}_{\hat{n}} \equiv \hat{n}(\vec{\Psi}_0, \theta_0)$ at one arbitrary $(\vec{\Psi}_0, \theta_0)$.*

Therefore one may say that $(\widehat{S}_{\hat{n}}, \vec{\Psi}_0, \theta_0)$ is a *seed* of the invariant spin field. We now want to find a method of quantifying the accuracy of a numerical approximation of the invariant spin field. Let $d_1(\hat{a}, \hat{b}) \equiv \arccos \hat{a} \cdot \hat{b}$. Then one easily shows for all $\hat{b}, \hat{a}, \hat{c} \in \mathcal{S}_{\mathbb{R}}$

$$d_1(\hat{a},\hat{b}) = d_1(\hat{b},\hat{a}) \quad , \quad d_1(\hat{a},\hat{b}) \geq 0 \quad , \quad d_1(\hat{a},\hat{b}) = 0 \Rightarrow \hat{a} = \hat{b} \quad , \quad d_1(\hat{a},\hat{c}) \leq d_1(\hat{a},\hat{b}) + d_1(\hat{b},\hat{c}) \tag{4.12}$$

so that $0 \leq d_1 \leq \pi$ is a metric on $\mathcal{S}_{\mathbb{R}}$. Alternatively we can choose the metric $d_2(\hat{a}, \hat{b}) \equiv \|\hat{a} - \hat{b}\| = 2\sin(^1/_2 d_1(\hat{a}, \hat{b}))$ with $0 \leq d_2 \leq 2$ to define a distance on $\mathcal{S}_{\mathbb{R}}$.

Definition 4.4 (Pseudo–seed of the invariant spin field) *We will call a triple $(\widehat{S}, \vec{\Psi}_0, \theta_0)^{(\epsilon,M)}$ at the Poincaré section at θ_0 a pseudo–seed for an invariant spin field or a seed for a pseudo–$\hat{n}$–axis for at least M turns to accuracy $\epsilon > 0$ when a $\mathcal{C}^1$ function $\hat{f} : \mathcal{T} \to \mathcal{S}_{\mathbb{R}}$, $\vec{\Psi} \mapsto \hat{f}(\vec{\Psi}) = \hat{f}(\vec{\Psi} + 2\pi\vec{k})$, $\vec{k} \in \mathbb{Z}^3$ exists and for $0 \leq m \leq M$*

$$d\left(\underline{R}^{(m)}(\theta_0; \vec{\Psi}_0)\widehat{S},\ \hat{f}(\vec{\Psi}_0 + 2m\pi\vec{Q} \bmod 2\pi)\right) < \epsilon \quad , \tag{4.13}$$

where d is either d_1 or d_2.

In other words the spin $\widehat{S}$, when tracked from $(\vec{\Psi}_0, \theta_0)$ for less than M turns, stays inside a band of width 2ϵ around some continuously partially differentiable function $\hat{f}$ on the torus $\mathcal{T}$. It is clear that if an $\hat{n}$–axis exists and $(\widehat{S}, \vec{\Psi}, \theta)$ is a seed of that $\hat{n}$–axis, then for arbitrarily small $\epsilon > 0$ $(\widehat{S}, \vec{\Psi}, \theta)$ is a pseudo–seed $(\widehat{S}, \vec{\Psi}, \theta)^{(\epsilon,\infty)}$. Also if an $\hat{n}$–axis exists and $\widehat{S}$ is an approximation of $\hat{n}$ at $(\vec{\Psi}, \theta)$ with $d(\widehat{S}, \hat{n}(\vec{\Psi}, \theta)) < \epsilon$ then $(\widehat{S}, \vec{\Psi}, \theta)$ is a pseudo–seed $(\widehat{S}, \vec{\Psi}, \theta)^{(\epsilon,\infty)}$. Even if no $\hat{n}$–axis strictly exists we might find some seed of a pseudo–$\hat{n}$–axis $(\widehat{S}, \vec{\Psi}, \theta)^{(\epsilon,M)}$. If ϵ can be chosen sufficiently small and M can be chosen sufficiently large, then we might not be able to decide whether or not an exact $\hat{n}$–axis exists. The advantage of this definition is that ϵ can easily be estimated visually by tracking a pseudo–seed for M turns and plotting the results on the Poincare section $\theta = \theta_0$. We note that if only one orbital amplitude is non–zero, the torus degenerates to a circle $\mathcal{T}_1$, i.e. a closed curve in $\mathbb{R}^6$. Since the image of a closed curve under a continuous map is a closed curve we obtain

Lemma 4.2 *If the orbital motion is restricted to one eigenplane, i.e. $\vec{J} \to J$ and $\mathcal{T} \to \mathcal{T}_1$, then the locus of the $\hat{n}$–axis $\mathcal{L} \equiv \hat{n}(\mathcal{T}_1, \theta_0)$ is a closed curve on the unit sphere $\mathcal{S}_{\mathbb{R}}$.*

Figure 4.2 (top) shows loci of the $\hat{n}$–axis, $\hat{n}(\mathcal{T}_1, \theta_0)$ for the 1996 luminosity optics of HERA–p with the same snakes as in figure 4.1. Both plots are for purely vertical orbit motion, i.e. $J_x = J_z = 0$. The viewpoint is the O–IP. Figure 4.2 (bottom) shows the components of $\hat{n}(\vec{\Psi})$. The left plots (top and bottom) were created by tracking a particle on the invariant ellipse that corresponds to the typical rms beam size σ. This means a typical enclosed normalised emittance of 4 π mm mrad. We recall (appendix A) that a normalised emittance of 4 π mm mrad means a Courant–Snyder invariant $\varepsilon = 4$ mm mrad/$\beta\gamma$ or an orbital action $J_y = 2$ mm mrad/$\beta\gamma$. The right plots (top and bottom) are for 2.5 σ. The pseudo–$\hat{n}$–axis was computed using stroboscopic averaging (see section 4.5) at one point in phase space and then tracked for 10^3 (left) and 10^4 (right) turns to fill the curve with sufficiently many points. The curve in figure 4.2 (top left) is rather simple and the components n_x, n_y and n_z shown bottom left are clearly 2π–periodic functions of Ψ_y within the resolution of the plot $0 < \epsilon < 10^{-3}$. If we had tracked a spin with some noticeable angle η w.r.t. the $\hat{n}$–axis evaluated at the starting point we would have seen points scattered inside a band of width 2η around $\mathcal{L}$. Note that tests have been made with up to 10^6 turns which yield the same results on the accuracy of $\hat{n}$ but lead to data files of hardly printable size! Since HERA–p is *not* mid–plane symmetric, the locus of the $\hat{n}$–axis does not fulfil the

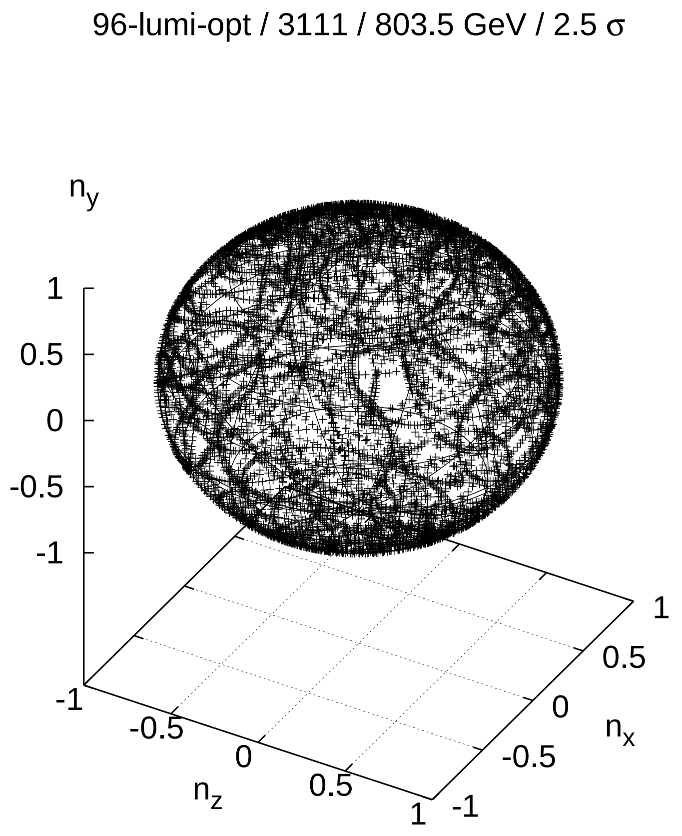

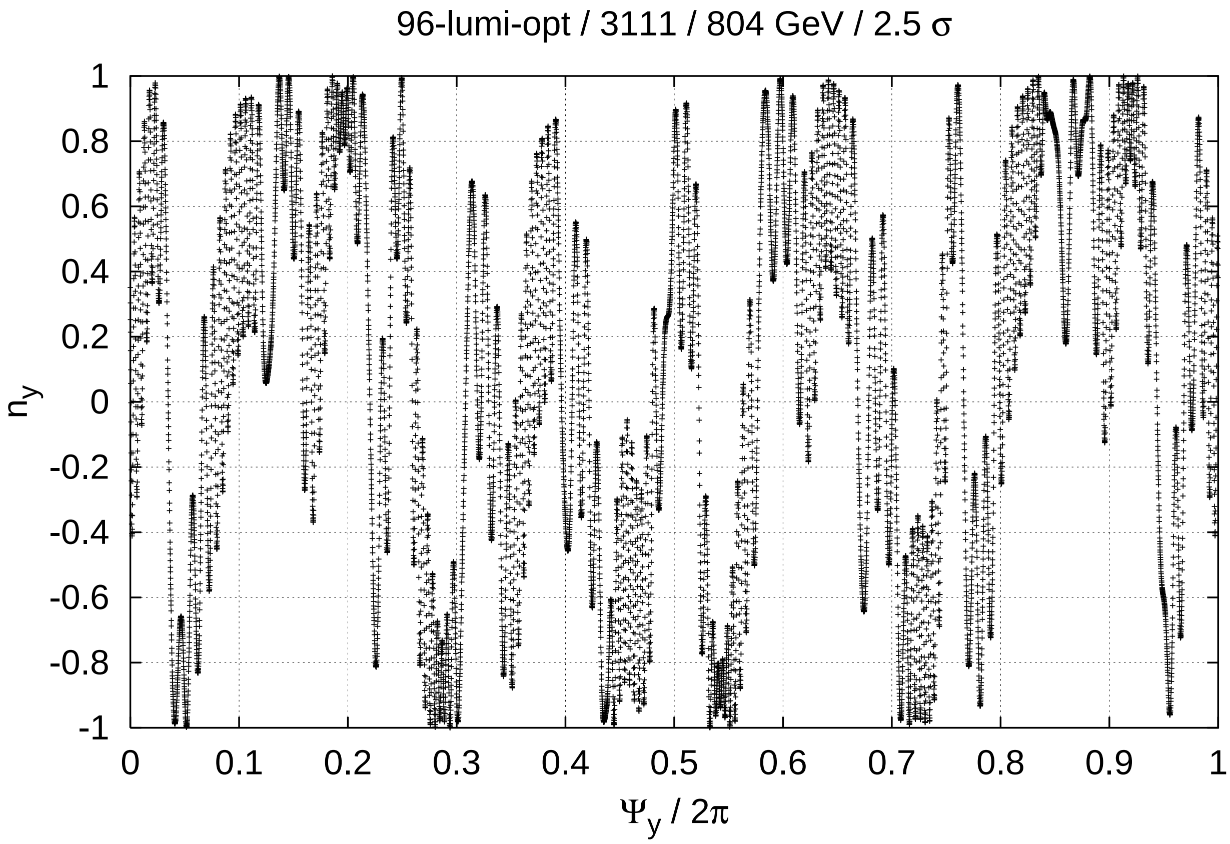

Figure 4.3: The $\hat{n}$–axis for HERA–p as in figure 4.2 tracked for 10^4 turns but at 803.5 GeV and on the invariant 2.5 σ ellipse. Top: locus on unit sphere. Bottom: $n_y(\Psi_y)$ showing that $\hat{n}$ is indeed at least a useful pseudo–$\hat{n}$–axis.

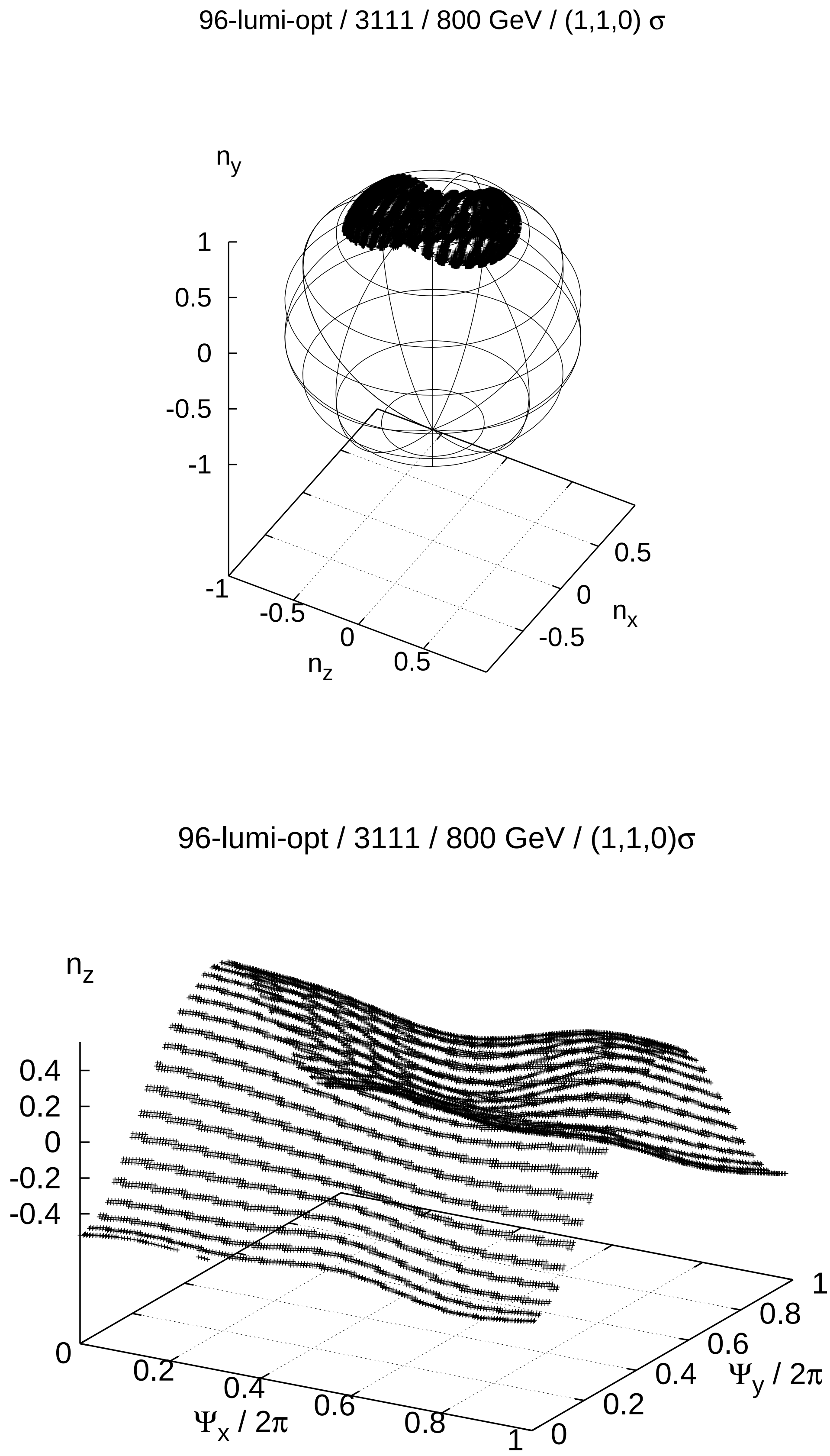

Figure 4.4: The $\hat{n}$–axis for HERA–p as in figure 4.2 and 4.3 but at 800 GeV and with horizontal and vertical orbit motion (both 1 σ) excited. Top: locus on unit sphere. Bottom: $n_z(\Psi_x, \Psi_y)$.

constraint $\hat{n}(\Psi_y+\pi) = \underline{Y}_\pi \hat{n}(\Psi_y)$ (see the paragraph after corollary 2 to theorem 2.10). Figures 4.2 and 4.3 show clearly that the mid–plane symmetry is broken by the vertical bends, even if flattening snakes are applied to compensate the vertical bends on the design orbit. Thus approximations of HERA–p incorporating mid–plane symmetry are certainly inadequate. In figure 4.2 (right) the curve $\mathcal{L}$ (top right) is much more complicated then for 1 σ but it is still a closed curve up to the graphical resolution. The plot of $n_y(\vec{\Psi}_y)$ (bottom right) is also clearly 2π–periodic although it is a much wilder function than at bottom left. We conclude that the two numerically computed pseudo–$\hat{n}$–axes shown in figure 4.2 are accurate to a precision of less than 10^{-3} for more than 10^4 turns.

Figure 4.3 shows a much more exotic example of a pseudo–$\hat{n}$–axis. The lattice, the snake scheme and the viewpoint are the same but the reference momentum has been increased slightly to 803.5 GeV and the vertical rms beam size is again 2.5 σ. The curve (top) is so chaotic that one might not dare to call it a closed curve. Nevertheless $n_y(\Psi_y)$ (bottom) can be identified as a violently oscillating but 2π–periodic continuous function. Therefore figure 4.3 shows a further example of a pseudo–$\hat{n}$-axis that is accurate to the level of 10^{-3} for at least 10^4 turns. Figure 4.4 again shows the pseudo–$\hat{n}$–axis for the same set up but for vertical *and* horizontal motion excited at the same time. Both orbital amplitudes correspond to an rms beam size of 1 σ. The longitudinal motion is *not* excited and the reference momentum is 800 GeV. Since the invariant torus $\mathcal{T}_2$ now is a 2–dimensional manifold we cannot expect the locus of the $\hat{n}$–axis to be a closed curve. Indeed we see (figure 4.4 top) that the tracked pseudo–seed covers an area on $\mathcal{S}_{\mathbb{R}}$ rather than a curve. Figure 4.4 (bottom) shows $n_z(\Psi_x,\Psi_y)$ obtained by tracking the pseudo–seed, which turns out to be a function which is 2π–periodic in Ψ_x as well as Ψ_y and obviously smooth. It is worth mentioning that in any non–linear treatment of spin motion on synchro–betatron trajectories the horizontal amplitudes, *do* have an impact on the invariant spin field because of the non–commutation of the rotations inside quadrupoles around $\hat{x}$ due to vertical displacements and around $\hat{y}$ due to horizontal displacements. We conclude from figures 4.2 to 4.4 that even in an asymmetric ring, with about 2000 beam line elements, at high energy, with more than one non–zero orbital amplitude and close to a very strong intrinsic resonance ($\approx$ 803.5 GeV) *useful* seeds for pseudo–$\hat{n}$–axes can in principle be found — no matter whether or not the existence of the invariant spin field in such a case can be rigorously proved. From now on we will not distinguish any more between $\hat{n}$–axes and pseudo–$\hat{n}$–axes.

Since the invariant spin field is a lattice field, the spin trajectory $\widehat{S}_{\hat{n}}(\theta) \equiv \hat{n}(\vec{\Psi}_0+\theta\vec{Q},\theta)$ is pseudo–periodic with the tunes $\vec{Q}$, i.e. it contains only integer combinations of the orbital frequencies. An arbitrary spin trajectory $\widehat{S}(\theta)$ starting at the same point on the torus can be decomposed into $\widehat{S} = \vec{S}_{\|} + \vec{S}_{\perp}$ where $\vec{S}_{\|} \equiv (\widehat{S}\cdot\hat{n})\hat{n}$ and $\vec{S}_{\perp} \equiv \widehat{S} - \vec{S}_{\|}$. Obviously $\|\vec{S}_{\|}\| \equiv I \equiv \widehat{S}\cdot\hat{n}$ and $\|\vec{S}_{\perp}\| \equiv \sqrt{1-I^2}$ are invariants of motion and $\vec{S}_{\perp}$ precesses in the plane locally perpendicular to $\hat{n}$. Since $I = \text{const.}$, $\vec{S}_{\|}$ is also pseudo–periodic with the tunes $\vec{Q}$, but $\vec{S}_{\perp}$ contains in addition the frequency spectrum of the precession around $\hat{n}$. We now transform into a phase space and azimuth dependent orthonormal right–handed coordinate system $(\tilde{u}_1(\vec{\Psi},\theta), \hat{n}(\vec{\Psi},\theta), \tilde{u}_2(\vec{\Psi},\theta))$ which is 2π–periodic in θ as well as in the Ψ_i and with

$$\widehat{S}' \equiv \begin{pmatrix} s_1 \\ I \\ s_2 \end{pmatrix} \equiv (\tilde{u}_1, \hat{n}, \tilde{u}_2)^{\mathrm{T}}\, \widehat{S} \tag{4.14}$$

we find for the spin OTM in the new coordinates

$$\widehat{S}'_f = \underline{R}'(\theta;\vec{\Psi}_i)\widehat{S}'_i \quad , \quad \underline{R}'(\theta;\vec{\Psi}_i) \equiv \begin{pmatrix} \cos(2\pi\tilde{\nu}(\vec{\Psi}_i,\theta)) & 0 & \sin(2\pi\tilde{\nu}(\vec{\Psi}_i,\theta)) \\ 0 & 1 & 0 \\ -\sin(2\pi\tilde{\nu}(\vec{\Psi}_i,\theta)) & 0 & \cos(2\pi\tilde{\nu}(\vec{\Psi}_i,\theta)) \end{pmatrix} \quad . \tag{4.15}$$

The amplitude-, angle-, and azimuth dependent quantity $\tilde{\nu}$ is called the pseudo spin tune. Since $\underline{R}'$ is a lattice function $\tilde{\nu}$ is 2π–periodic in θ and $\vec{\Psi}_i$. The ordering of the base vectors has been chosen so that in the limit $\hat{n}\to\hat{y}$ one can choose $(\tilde{u}_1,\hat{n},\tilde{u}_2)\to(\hat{x},\hat{y},\hat{z})$. We note that $\underline{R}'$ is a 3–dimensional representation of the *Abelian* group $\mathbf{SO(2)}$ (see section 2.2.1). Therefore we can write

$$\vec{S}_\perp(\theta+2\pi) = \sqrt{1-I^2}\,\Im\left((\tilde{u}_1 + i\tilde{u}_2)\Big|_{(\vec{\Psi}+2\pi\vec{Q},\theta)} e^{i(\phi(\vec{\Psi},\theta)+\Phi_0)}\right) \quad , \tag{4.16}$$

with $s_1(\theta) = \sqrt{1-I^2}\sin\Phi_0$, $s_2(\theta) = \sqrt{1-I^2}\cos\Phi_0$ and $\phi(\vec{\Psi},\theta) = 2\pi\tilde{\nu}(\vec{\Psi},\theta)$ being the spin phase advance from θ to $\theta+2\pi$ when starting at $\vec{\Psi}$. Let $\vec{\Omega}' = (0,\zeta(\vec{\Psi},\theta),0)$ be the precession vector of the T–BMT equation transformed to the $(\tilde{u}_1,\hat{n},\tilde{u}_2)$ system, then

$$\phi(\vec{\Psi},\theta) = \int_\theta^{\theta+2\pi} \zeta(\vec{\Psi}+\vartheta\vec{Q},\vartheta)\,d\vartheta \equiv \int_\theta^{\theta+2\pi} \xi(\vartheta)\,d\vartheta \quad . \tag{4.17}$$

Since $\vec{\Omega}$ and $(\tilde{u}_1,\hat{n},\tilde{u}_2)$ are periodic in $\vec{\Psi}$ and θ, ζ is also periodic. Therefore ξ is pseudo–periodic with $\vec{Q}$. We split ξ into two parts

$$\begin{aligned}\xi(\theta) = \xi^{(0)}(\theta) + \xi^{>}(\theta) \quad &= \quad \sum_{k_0\in\mathbb{Z}}\sum_{\vec{k}\in\mathbb{Z}^3} \xi_{k_0,\vec{k}}\, e^{i(k_0+\vec{k}\cdot\vec{Q})\theta} \\ &= \quad \sum_{k_0\in\mathbb{Z}} \xi^{(0)}_{k_0}\, e^{ik_0\theta} + \sum_{k_0\in\mathbb{Z}}\sum_{\substack{\vec{k}\in\mathbb{Z}^3\\|\vec{k}|\neq 0}} \xi^{>}_{k_0,\vec{k}}\, e^{i(k_0+\vec{k}\cdot\vec{Q})\theta}\end{aligned} \tag{4.18}$$

and find that in the case that $\vec{Q}$ is *strongly incommensurable with 1* (see definition A.6) and ξ has an analytic extension, the integral of $\xi^{(>)}$ converges [ems3, LM88]. The integral over 2π of $\xi^{(0)}$ just contributes with $2\pi\xi^{(0)}_0$. Owing to the strong incommensurability of the tunes the integral does not contain any terms with $\vec{k}\cdot\vec{Q}\in\mathbb{Z}$. Therefore $\phi(\vec{\Psi},\theta)$ can be written

$$\phi(\vec{\Psi},\theta) = \phi_{0,\vec{0}} + \sum_{k_0\in\mathbb{Z}}\sum_{\substack{\vec{k}\in\mathbb{Z}^3\\|\vec{k}|\neq 0}} \phi_{k_0,\vec{k}}\, e^{i(k_0\theta+\vec{k}\cdot\vec{\Psi})} \quad . \tag{4.19}$$

Since the only constraints on $\tilde{u}_1$ and $\tilde{u}_2$ were periodicity and local orthogonality to $\hat{n}$ we can transform (4.16) into another periodic orthonormal system $(\hat{u}_2,\hat{n},\hat{u}_1)$ by rotating around $\hat{n}$ with $(\hat{u}_1+i\hat{u}_2) = e^{i\chi(\vec{\Psi},\theta)}(\tilde{u}_1+i\tilde{u}_2)$ so that

$$\vec{S}_\perp(\theta+2\pi) = \sqrt{1-I^2}\,\Im\left((\hat{u}_2 + i\hat{u}_1)\Big|_{(\vec{\Psi}+2\pi\vec{Q},\theta)} e^{i(\phi(\vec{\Psi},\theta)-\chi(\vec{\Psi},\theta)+\chi(\vec{\Psi}+2\pi\vec{Q},\theta+2\pi)+\Phi_0)}\right) \quad . \tag{4.20}$$

The factor $e^{i\chi}$ has to be periodic in the Ψ_i and θ and therefore it has to be of the form

$$\chi(\vec{\Psi},\theta) \equiv \chi^{\mathrm{per}}(\vec{\Psi},\theta) + \vec{l}\cdot\vec{\Psi} + l_0\theta \;\; , \;\; \vec{l}\in\mathbb{Z}^3\, , \; l_0\in\mathbb{Z} \tag{4.21}$$

where $\chi^{\mathrm{per}}(\vec{\Psi},\theta)$ is 2π–periodic w.r.t. θ and $\vec{\Psi}$. Fourier transforming (see A.55) $\kappa(\vec{\Psi},\theta) \equiv \phi(\vec{\Psi},\theta) - \chi^{\mathrm{per}}(\vec{\Psi},\theta) + \chi^{\mathrm{per}}(\vec{\Psi}+2\pi\vec{Q},\theta+2\pi)$ yields

$$\kappa(\vec{\Psi},\theta) = \phi_{0,\vec{0}} + \sum_{k_0\in\mathbb{Z}}\sum_{\substack{\vec{k}\in\mathbb{Z}^3\\|\vec{k}|\neq 0}} \left(\phi_{k_0,\vec{k}} - \chi^{\mathrm{per}}_{k_0,\vec{k}}(1-e^{i2\pi\vec{k}\cdot\vec{Q}})\right) e^{i(k_0\theta+\vec{k}\cdot\vec{\Psi})} \quad , \tag{4.22}$$

since the terms $\chi^{\mathrm{per}}_{k_0,\vec{0}}$ do not contribute. When the orbital tunes are *strongly incommensurable with 1* and $\phi(\vec{\Psi},\theta)$ has an analytic extension then one can eliminate all terms except $\phi_{0,\vec{0}}$ by choosing

$$\chi^{\mathrm{per}}_{k_0,\vec{k}} = \frac{\phi_{k_0,\vec{k}}}{1-e^{i2\pi\vec{k}\cdot\vec{Q}}} \tag{4.23}$$

and the generalised Fourier series still converges [ems3, LM88]. We now define the *amplitude dependent spin tune* $\nu \equiv \phi_{0,\vec{0}}/2\pi$ which only depends on the $\vec{J} = \text{const.}$ of the torus. After having eliminated all the phase and azimuth dependent parts by properly choosing $\hat{u}_1$ and $\hat{u}_2$ we obtain

$$\vec{S}_\perp(\theta) = \sqrt{1-I^2}\,\Im\left((\hat{u}_1 + i\hat{u}_2)\Big|_{(\Psi(\theta),\theta)} e^{i((\nu+\vec{l}\cdot\vec{Q}+l_0)\theta+\Phi_0)}\right) \quad . \tag{4.24}$$

In this equation it becomes clear that we can apply an additional uniform rotation around $\hat{n}$ by $\theta(m_0 + \vec{m}\cdot\vec{Q})$ and obtain a flow of the same form with $\nu' \equiv \nu + m_0 + \vec{m}\cdot\vec{Q}$. Additionally we can perform a global rotation of the coordinate system around e.g. $\hat{u}_1$ by π and get $\nu'' = -\nu$. Therefore ν is only unique up to a change of sign and an integer combination of the Q_i and 1. The coordinate vector $\widehat{S}'' \equiv (S_1, I, S_2)^{\mathrm{T}}$ w.r.t. the $(\hat{u}_1, \hat{n}, \hat{u}_2)$–system is transported by

$$\widehat{S}''(\theta_f) = \underline{R}''_{\vec{J}}(\theta_f,\theta_i)\widehat{S}''(\theta_i) \quad , \quad \underline{R}''_{\vec{J}}(\theta_i,\theta_f) \equiv \begin{pmatrix} \cos((\theta_f-\theta_i)\nu(\vec{J})) & 0 & \sin((\theta_f-\theta_i)\nu(\vec{J})) \\ 0 & 1 & 0 \\ -\sin((\theta_f-\theta_i)\nu(\vec{J})) & 0 & \cos((\theta_f-\theta_i)\nu(\vec{J})) \end{pmatrix} \tag{4.25}$$

or with I and $\Phi \equiv \arctan\frac{S_1}{S_2}$ the flow can be written

$$I = \text{const.} \quad , \quad \Phi(\theta) = \Phi_0 + \theta\,\nu \quad . \tag{4.26}$$

Therefore we have proved:

Theorem 4.3 *If for a given spin–orbit system an invariant spin field exists on a torus $\vec{J} = \text{const.}$, if the $Q_i(\vec{J})$ are strongly incommensurable with 1 and if the spin precession frequency $\xi(\theta)$ in an arbitrary periodic basis $(\tilde{u}_1, \hat{n}, \tilde{u}_2)$ has an analytic extension for all starting values $\vec{\Psi}_i$, then*

1. *a periodic basis $(\hat{u}_1, \hat{n}, \hat{u}_2)$ exists in which the spin precesses uniformly with the amplitude dependent spin tune $\nu(\vec{J})$,*
2. *for all $l_0 \in \mathbb{Z}$ and $\vec{l} \in \mathbb{Z}^3$, $\nu'(\vec{J}) \equiv \pm\nu(\vec{J}) + l_0 + \vec{l}\cdot\vec{Q}$ is also an amplitude dependent spin tune and*
3. *the transformation $\widehat{S} \mapsto (I,\Phi) \equiv (\widehat{S}\cdot\hat{n}, \arctan\frac{\hat{u}_1\cdot\widehat{S}}{\hat{u}_2\cdot\widehat{S}})$ defines action–angle variables for the spin–orbit system. Since the inverse transform is 2π–periodic in Φ, the spin–orbit system is integrable.*

Equivalent definitions of the amplitude dependent spin tune can be found in [BH92, KY86] and a similar theorem based only on one–turn maps is in [GH99b]. The amplitude dependent spin tune defines another independent basic frequency of the spin–orbit system. The spin component $\widehat{S}_\perp(\theta)$ perpendicular to the $\hat{n}$–axis is a pseudo–periodic function with the tunes $(\vec{Q}(\vec{J}), \nu(\vec{J}))$ only. It contains not only the orbital frequencies but also ν. In order to describe long term coherence of spin motion with the orbital degrees of freedom on a torus, not only $\vec{Q}$ but also ν is essential. The long term coherence condition is then

$$\nu(\vec{J}) = k_0 + \vec{k}\cdot\vec{Q}(\vec{J}) \tag{4.27}$$

and it must be stressed that (4.27) contains $\nu(\vec{J})$ and *not* ν_0, $G\gamma$ or even worse the normalised angle computed from the complex eigenvalues of the off–orbit OTM as often stated incorrectly in the literature. Equation (4.27) is the modification to equation (2.110) needed to go beyond perturbation theory announced in section 2.3.2.

It can be shown [KY86] that there is a canonical transformation from the coordinates (K,φ) in (2.13) to the coordinates (I,Φ) introduced in theorem 4.3. Both sets of coordinates define a chart of $\mathcal{S}_{\mathbb{R}}$ which is singular at $K, I = \pm 1$, i.e. the North- and South pole of the unit–sphere. Therefore it is sometimes more convenient to use the coordinate pair (S_1, S_2) which is transported according to equation (4.25) and which we will call the *spin normal form coordinates*. Introducing the complex scalar $S \equiv (S_1 + iS_2)$ the notation is most compact

$$S(\theta_f) = e^{i(\theta_f - \theta_i)\nu(\vec{J})}\, S(\theta_i) \quad . \tag{4.28}$$

Assuming that $\nu(\vec{J})$ and $\hat{n}_{\vec{J}}(\vec{\Psi}, \theta)$ are continuous functions of $\vec{J}$ in some vicinity of the closed orbit $\vec{J} = \vec{0}$ and that ν_0 is not in resonance with the orbital tunes, one can choose the integers l_0 and $\vec{l}$ defined in theorem 4.3 and the sign of ν so that $\lim_{\vec{J}\to\vec{0}} \nu(\vec{J}) = \nu_0$ and $\lim_{\vec{J}\to\vec{0}} \hat{n}_{\vec{J}}(\vec{\Psi}, \theta) = \hat{n}_0(\theta)$. Finally we can decide whether the invariant spin field is unique:

Theorem 4.4 (Uniqueness of the invariant spin field) *If an $\hat{n}$–axis and two lattice fields $\hat{u}_1$, $\hat{u}_2$ exist on a torus $\vec{J} =$ const. so that $\nu(\vec{J})$ can be defined according to theorem 4.3 and $\nu \neq k_0 + \vec{k} \cdot \vec{Q}$ for all $k \in \mathbb{Z}$ and $\vec{k} \in \mathbb{Z}^3$, then the $\hat{n}$–axis is unique up to a global sign.*

We assume that another invariant spin field $\hat{n}'$ exists which differs from $\hat{n}$ in some neighbourhood of $\vec{\Psi}_0, \theta_0$. We write $\hat{n}'(\vec{\Psi}, \theta)$ in spin normal form coordinates w.r.t. the basis $(\hat{u}_1, \hat{n}, \hat{u}_2)$, i.e. $\hat{n}'(\vec{\Psi}, \theta) = \left(S_1'\hat{u}_1 + \sqrt{1 - (S_1')^2 + (S_2')^2}\hat{n} + S_2'\hat{u}_2\right)\Big|_{(\vec{\Psi},\theta)}$. The complex scalar S' does not vanish in some vicinity of $\vec{\Psi}_0, \theta_0$ by construction. Since it represents an invariant spin field, it has to be periodic and owing to the conservation of the angle between two T–BMT solutions it has to have constant modulus. With $S' \equiv \sqrt{1 - (I')^2}\, e^{i\rho}$, $I' = \hat{n}' \cdot \hat{n} =$ const. and $\rho(\vec{\Psi}, \theta) \equiv \rho^{\mathrm{per}}(\vec{\Psi}, \theta) + \vec{l} \cdot \vec{\Psi} + l_0\theta$ where ρ^{per} is periodic, the invariance constraint (4.6) reads as

$$\begin{aligned} S'(\vec{\Psi} + 2\pi\vec{Q}, \theta + 2\pi) &= e^{i2\pi\nu}\, S'(\vec{\Psi}, \theta) \\ \Rightarrow 1 &= e^{i\left(2\pi(\nu - \vec{l}\cdot\vec{Q}) + \rho^{\mathrm{per}}(\vec{\Psi},\theta) - \rho^{\mathrm{per}}(\vec{\Psi} + 2\pi\vec{Q},\theta)\right)} \end{aligned} \tag{4.29}$$

for all $\vec{\Psi}$, θ. We conclude that since $\vec{Q}$ is incommensurable with 1, the periodic part of ρ does not depend on $\vec{\Psi}$. Therefore $\rho = \rho_0^{\mathrm{per}}(\theta) + \vec{l} \cdot \vec{\Psi} + l_0\theta$. Then we see that $\nu - \vec{l} \cdot \vec{Q}$ has to be an integer in contradiction with the premises of theorem 4.4. □
A similar proof can be found in [GH99b].

We note that in contrast to the *orbital* tunes $\vec{Q}(\vec{J})$ that can depend on the *orbital* actions, the *spin* tune does *not* depend on the *spin* action but only on the *orbital* actions, i.e. $\nu(\vec{J})$. This has two reasons: First, we only treated the “triangular system” as pointed out in [BG98a], i.e. without any Stern–Gerlach back reaction of the spin onto the orbit. Therefore $\partial_I \vec{Q} = \vec{0}$. Second, the T–BMT equation is linear in the spin and hence $\partial_I \nu = 0$. If we were to include the Stern–Gerlach force, we would expect new tunes (Q_1, Q_2, Q_3, Q_4) depending on all of the four actions (J_1, J_2, J_3, J_4) since in the fully spin–orbit/orbit–spin coupled system the spin and orbit normal forms could in general not be separated.

In the next sections we will discuss several methods to numerically compute the invariant spin field and the amplitude dependent spin tune that have been proved useful during this project.

4.2 The linear approximation of $\hat{n}$

In this *and the following* sections all quantities refer to the Poincarè section at one fixed θ_0. We will therefore omit the parameter θ_0 wherever possible for brevity.

In section 2.3 we have found a completely linearised description of spin–orbit motion.(2.106). In equations (2.103) and (2.106) we have defined the column 8–vector $\vec{Z} \equiv (\vec{z}^{\mathrm{T}}, \alpha, \beta)^{\mathrm{T}}$, where $\alpha = \widehat{S} \cdot \vec{m}$ and $\beta = \widehat{S} \cdot \vec{l}$ are the spin components perpendicular to $\hat{n}_0$ measured in the $\hat{l}, \hat{n}_0, \hat{m}$ system defined in equation (2.94). The OTM for $\vec{Z}$ at some given θ is to first order in the initial coordinates represented by the 8×8 matrix

$$\underline{M}_{8\times8} \equiv \begin{pmatrix} \underline{T}_{6\times6} & \underline{0}_{6\times2} \\ \underline{G}_{2\times6} & \underline{D}_{2\times2} \end{pmatrix} \quad , \tag{4.30}$$

where $\underline{T}_{6\times6}$ is the linear orbital OTM, $\underline{0}_{6\times2}$ reflects the absence of a Stern–Gerlach force in this particular model $\underline{D}_{2\times2}\in\mathbf{SO(2)}$ is a rotation by $2\pi\nu_0$ around $\hat{n}_0$ and the "$\underline{G}$–matrix" $\underline{G}_{2\times6}$ contains the spin–orbit coupling to first oder in $\vec{Z}$. We define an arbitrary spin field $\hat{f}(\vec{z})$ in linear order as $\vec{F}\equiv(\vec{z}^{\mathrm{T}},\alpha_f^{(1)}(\vec{z}),\beta_f^{(1)}(\vec{z}))^{\mathrm{T}}$ with $\binom{\alpha_f^{(1)}(\vec{z})}{\beta_f^{(1)}(\vec{z})}=\underline{L}^{(f)}_{2\times6}\vec{z}$. Then the invariance condition (4.6) of the $\hat{n}$–axis under the OTM applied to its first order approximation $\vec{N}$ is

$$\vec{N}(\underline{T}_{6\times6}\vec{z}) \equiv \begin{pmatrix} \underline{T}_{6\times6}\vec{z} \\ \underline{L}^{(n)}_{2\times6}\underline{T}_{6\times6}\vec{z} \end{pmatrix} = \underline{M}_{8\times8}\begin{pmatrix} \vec{z} \\ \underline{L}^{(n)}_{2\times6}\vec{z} \end{pmatrix} \equiv \underline{M}_{8\times8}\vec{N}(\vec{z}) \Leftrightarrow \begin{pmatrix} \underline{1}_{6\times6} \\ \underline{L}^{(n)}_{2\times6} \end{pmatrix}\underline{T}_{6\times6} = \underline{M}_{8\times8}\begin{pmatrix} \underline{1}_{6\times6} \\ \underline{L}^{(n)}_{2\times6} \end{pmatrix} \quad . \tag{4.31}$$

Again we assume the linear orbital motion to be integrable and stable. Let now

$$\underline{A}_{6\times6} \equiv (\vec{v}_x^{\,+},\vec{v}_x^{\,-},\vec{v}_y^{\,+},\vec{v}_y^{\,-},\vec{v}_z^{\,+},\vec{v}_z^{\,-}) \text{ with } \underline{T}_{6\times6}\vec{v}_l^{\,\pm} = e^{\pm i2\pi Q_l}\vec{v}_l^{\,\pm}\ ,\ l=x,y,z \tag{4.32}$$

be the column matrix of the 6–dimensional eigenvectors of $\underline{T}_{6\times6}$, normalised so that $\underline{A}_{6\times6}$ is symplectic, i.e. $(\vec{v}_l^{\,+})^{\mathrm{T}}\underline{J}\vec{v}_l^{\,-}=1$ and $(\vec{v}_l^{\,+})^{\mathrm{T}}\underline{J}\vec{v}_{l'}^{\,-}=0$ for $l\neq l'$. Furthermore let

$$\underline{C}_{8\times6} \equiv (\vec{w}_x^{\,+},\vec{w}_x^{\,-},\vec{w}_y^{\,+},\vec{w}_y^{\,-},\vec{w}_z^{\,+},\vec{w}_z^{\,-}) = \begin{pmatrix} \underline{A}_{6\times6} \\ \underline{B}_{2\times6} \end{pmatrix} \text{ with } \underline{M}_{8\times8}\vec{w}_l^{\,\pm} = e^{\pm i2\pi Q_l}\vec{w}_l^{\,\pm}\ ,\ l=x,y,z \tag{4.33}$$

be the column matrix of the six 8–component eigenvectors of $\underline{M}_{8\times8}$ which are associated with the orbital tunes Q_l. First we find with $\underline{\Lambda}_{6\times6}=\underline{A}^{-1}_{6\times6}\underline{T}\,\underline{A}_{6\times6}=\underline{\mathrm{diag}}(e^{+i2\pi Q_x},\ldots,e^{-i2\pi Q_z},)$ that $\underline{C}_{8\times6}\underline{\Lambda}_{6\times6}=\underline{M}_{8\times8}\underline{C}_{8\times6}$. Then multiplying (4.31) from the right with $\underline{A}_{6\times6}$ yields

$$\begin{pmatrix} \underline{A}_{6\times6} \\ \underline{L}^{(n)}_{2\times6}\underline{A}_{6\times6} \end{pmatrix}\underline{\Lambda}_{6\times6} = \underline{M}_{8\times8}\begin{pmatrix} \underline{A}_{6\times6} \\ \underline{L}^{(n)}_{2\times6}\underline{A}_{6\times6} \end{pmatrix} \tag{4.34}$$

showing that the columns of $\binom{\underline{A}_{6\times6}}{\underline{L}^{(n)}_{2\times6}\underline{A}_{6\times6}}$ are eigenvectors of $\underline{M}_{8\times8}$. Since the upper 6 rows are identical to those of $\underline{C}_{8\times6}$, the lower 2 rows also have to be identical to those of $\underline{C}_{8\times6}$:

$$\vec{N}(\vec{z}) = \underline{C}_{8\times6}\underline{A}^{-1}_{6\times6}\vec{z} = \begin{pmatrix} \vec{z} \\ \underline{B}_{2\times6}\underline{A}^{-1}_{6\times6}\vec{z} \end{pmatrix} \quad . \tag{4.35}$$

Thus the form for $\underline{L}^{(n)}_{2\times6}$ which delivers $\binom{\alpha_n^{(1)}}{\beta_n^{(1)}}$ with the required periodicity to first order is fixed and $\underline{L}^{(n)}_{2\times6}=\underline{B}_{2\times6}\underline{A}^{-1}_{6\times6}$.

With the eigenvectors $\vec{w}_l^{\,\pm}\equiv((\vec{v}_l^{\,\pm})^{\mathrm{T}},(\vec{b}_l^{\,\pm})^{\mathrm{T}})^{\mathrm{T}}$ of $\underline{M}_{8\times8}$, the $\vec{b}_l^{\,\pm}$ have to fulfil the constraint

$$\underline{G}_{2\times6}\vec{v}_l^{\,\pm} + \underline{D}_{2\times2}\vec{b}_l^{\,\pm} = e^{\pm i2\pi Q_l}\vec{b}_l^{\,\pm} \Rightarrow \vec{b}_l^{\,\pm} = (e^{\pm i2\pi Q_l}-\underline{D}_{2\times2})^{-1}\underline{G}_{2\times6}\vec{v}_l^{\,\pm} \quad . \tag{4.36}$$

The above solution only exists if $(e^{\pm i2\pi Q_l}-\underline{D}_{2\times2})$ is regular, namely *not* at the first order intrinsic resonances

$$\nu_0 = k_0 + \vec{k}\cdot\vec{Q}\ ,\ |\vec{k}|=1 \quad . \tag{4.37}$$

Moreover, whenever ν_0 is sufficiently *close* to an intrinsic first order resonance condition, the corresponding $\vec{b}_k^{\,\pm}$ gets large and the linearisation condition $(\alpha_n^{(1)})^2+(\beta_n^{(1)})^2\ll 1$ is violated. Therefore the range of validity is strictly speaking reduced to the cases where $\|\hat{n}(\vec{\Psi},\theta)-\hat{n}_0(\theta)\|\ll 1$ for all $\vec{\Psi}$ and

θ. Moreover $||\hat{n} - \hat{n}_0||$ increases as the components of $\underline{G}_{2\times 6}$ increase, or equivalently, as the spin–orbit coupling integrals of chapters 2 and 3.

It can be shown [GH99b, BH92] that the "amplitude dependent spin tune" at first order does *not* depend on the orbital amplitude and is equal to

$$\nu =_1 \nu_0 \quad . \tag{4.38}$$

The linear approximation of the invariant spin field also SLIM–$\hat{n}$–axis has been included in the computer code SLIM which computes the equilibrium polarisation for $e^{\pm}$–rings in this linear approximation. An explicit description of the SLIM algorithm and of extensions to higher order can be found in [AC80, SM86a, BH92, BH94a, BH94b]. The SLIM algorithm is very fast because of its linearity and is implemented in the code SPRINT for *fast* energy scans of the average opening angle of the linear approximation of the invariant spin field on a torus.

4.3 Fourier expansion in the orbital angles

Every spin field $\hat{f}$ on a torus $\vec{J} =$ const. evaluated at some given θ is a function of the phase space and is hence periodic in $\vec{\Psi}$. Therefore it can be Fourier expanded w.r.t. $\vec{\Psi}$. The same argument applies to the corresponding spinor fields $\check{f}$ related to $\hat{f} = \hat{G}(\check{f})$ with the function $\hat{G}$ from definition 2.6. Recall that $\check{f}$ and $e^{i\kappa}\check{f}$ with $\kappa \in \mathbb{R}$ lead to the same $\hat{f}$. If $\underline{r} \in \mathbf{SU(2)}$ is the spinor OTM at θ, then for every $\vec{\Psi}$ the spinor field propagated once around the ring, $\check{f}|_{\theta+2\pi} = \underline{r}\check{f}|_{\theta}$ is again periodic in $\vec{\Psi}$. Therefore if $\check{f}|_{\theta+2\pi}$ is written as $e^{i\kappa}\check{g}|_{\theta}$, not only $\check{g}$ but also κ has to be a periodic function of $\vec{\Psi}$. Let now $\check{n}'$ be an *invariant spinor field* so that $\hat{n} = \hat{G}(\check{n}')$. Then

$$\underline{r}(\vec{\Psi})\check{n}'(\vec{\Psi}) = e^{-i\pi\tilde{\nu}(\vec{\Psi})}\check{n}'(\vec{\Psi} + 2\pi\vec{Q}) \tag{4.39}$$

with a 2π–periodic function $\tilde{\nu}$. We assume that the orbital tunes are strongly incommensurable with 1. Then in analogy with (4.20) to (4.23) for $\chi^{\rm per}$ there is a 2π–periodic function $\phi(\vec{\Psi})$ with

$$2\pi\tilde{\nu}(\vec{\Psi}) - \phi(\vec{\Psi}) + \phi(\vec{\Psi} + 2\pi\vec{Q}) = 2\pi\nu(\vec{J}) = \text{const.} \tag{4.40}$$

so that $\check{n}(\vec{\Psi}) \equiv e^{i/2\phi(\vec{\Psi})}\check{n}'(\vec{\Psi})$ fulfils the constraint

$$\underline{r}(\vec{\Psi})\check{n}(\vec{\Psi}) = e^{-i\pi\nu}\check{n}(\vec{\Psi} + 2\pi\vec{Q}) \tag{4.41}$$

and ν is the spin tune. Equation (4.41) only contains 2π–periodic functions of $\vec{\Psi}$. Fourier expansion yields with $\underline{r}(\vec{\Psi}) = \sum_{\vec{k}\in\mathbb{Z}^3}\underline{r}_{\vec{k}}e^{i\vec{k}\cdot\vec{\Psi}}$ and $\check{n}(\vec{\Psi}) = \sum_{\vec{k}\in\mathbb{Z}^3}\check{n}_{\vec{k}}e^{i\vec{k}\cdot\vec{\Psi}}$ the invariance constraint

$$e^{-i2\pi\vec{k}\cdot\vec{Q}}\sum_{\vec{m}\in\mathbb{Z}^3}\underline{r}_{\vec{k}-\vec{m}}\check{n}_{\vec{m}} = e^{-i\pi\nu}\check{n}_{\vec{k}} \quad . \tag{4.42}$$

This can formally be interpreted as an infinite–dimensional eigenproblem for the eigenvector $\check{n} \equiv (\check{n}_{\vec{k}})_{\vec{k}\in\mathbb{Z}^3}$ of the eigenvalue $\lambda = e^{-i\pi\nu}$. So far it is not clear for which classes of "matrices" $(\mathfrak{R}^\infty)_{\vec{k}\vec{m}} \equiv e^{-i2\pi\vec{k}\cdot\vec{Q}}\,\underline{r}_{\vec{k}-\vec{m}}$ the eigenproblem (4.42) is solvable, but numerical approximations with finite cut–off M so that $\max_{\vec{k}}|k_i| \le M$ and $\max_{\vec{m}}|m_i| \le M$ have been shown to generate pseudo–$\hat{n}$–axes of high accuracy for sufficiently high M. This numerical algorithm was invented by Yokoya [KY99] and will be called the SODOM-2 algorithm since it is based on the method implemented in the code SODOM [KY92] which computes the equilibrium polarisation in $e^{\pm}$–rings. The modern revised version is implemented in the code SPRINT. The original version from 1992 used a parametrisation of $\check{n}$ that explicitly guaranteed unitarity independently of the accuracy of the solution. This parametrisation led to a non–linear fixed point equation. Solving this fixed point equation in general required $||\hat{G}(\check{n}) -$

$\hat{n}_0\| \ll 1$ and therefore failed for exotic invariant spin fields such as that presented in figure 4.3. The modern revised version does *not* explicitly guarantee unitarity but checks whether the moduli of the coefficients on the edge of $(\mathfrak{R}^M)$, i.e. with $\max_{\vec{k}}|k_i| \le M$, $\max_{\vec{m}}|m_i| \le M$ and $|k_i| \approx M$ or $|m_i| \approx M$, are small enough compared to those at the centre with $\vec{k} = \vec{m} = \vec{0}$. Then the accuracy of the pseudo–$\hat{n}$–axis is sufficiently high and unitarity is almost preserved.

We know already from theorem 4.3 that the spin tune ν is not unique and therefore expect an infinite spectrum of eigenvalues of the form $\lambda_j = e^{-i\pi((-1)^{s_j}\nu + l_j + \vec{l}_j\cdot\vec{Q})}$ with eigenvectors $\tilde{n}_j$ which belong to spinors representing $(-1)^{s_j}\hat{n}$. In particular the spinor $\check{m} \equiv i\underline{\sigma}_x\check{n}$ which represents $-\hat{n}$ corresponds to $-\nu$. This spectrum is discussed in great detail in [KY99]. In practice, to ensure $\lim_{\vec{J}\to\vec{0}}\nu \to \nu_0$, it turns out to be a good strategy [KY99] to use the eigenvalue λ_j which belongs to the eigenvector $\check{n}_j$ with largest $\|\check{n}_{\vec{0}}^{(j)}\|$. The family of spinor fields [KY92] $\check{u}_\varphi = {}^1/_{\sqrt{2}}(e^{-i\varphi/2}\check{n} - e^{+i\varphi/2}\check{m})$ are, like $\check{n}$, functions of phase space (i.e. periodic in $\vec{\Psi}$) and the represent unit vector fields $\hat{G}(\check{u}_\varphi)$ perpendicular to $\hat{n}$ for all φ. They also fulfil the constraint

$$\underline{r}(\vec{\Psi})\check{u}_\varphi(\vec{\Psi}) = \check{u}_{\varphi+2\pi\nu}(\vec{\Psi} + 2\pi\vec{Q}) \tag{4.43}$$

so that $\widehat{S}_\perp$ precesses at rate ν w.r.t. the $\hat{G}(\check{u}_\varphi)$ for all $\vec{\Psi}$. Each two such vector fields $\hat{G}(\check{u}_\varphi)$ and $\hat{G}(\check{u}_{\varphi'})$ have a constant included angle $|\varphi - \varphi'|$. Thus by setting $\hat{u}_1(\vec{\Psi}) = \hat{G}(\check{u}_0(\vec{\Psi}))$, $\hat{u}_2(\vec{\Psi}) = \hat{G}(\check{u}_{\pi/2}(\vec{\Psi}))$ we have immediately computed the complete $(\hat{u}_1, \hat{n}, \hat{u}_2)$ coordinate system. The Fourier–expansion

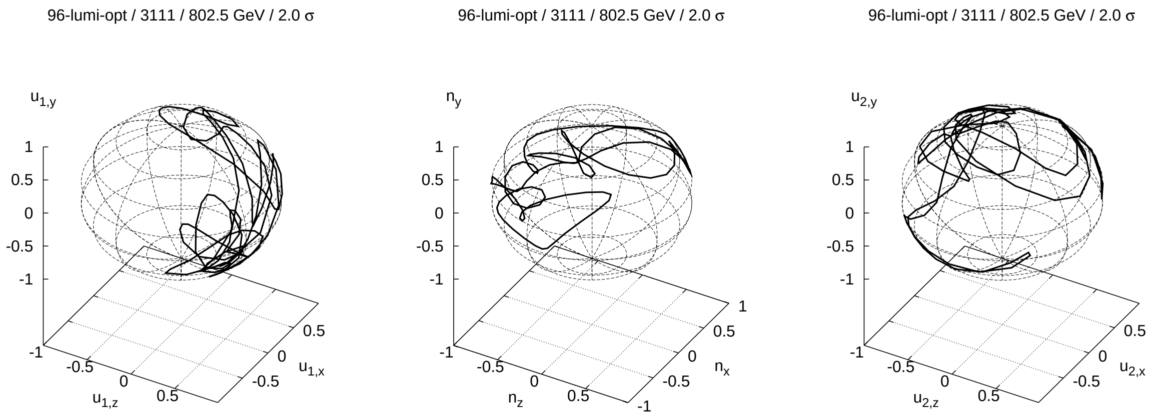

Figure 4.5: The locus of (left to right) $\hat{u}_1$, $\hat{n}$ and $\hat{u}_2$ for the HERA–p 1996–luminosity optics with 6 flattening snakes around the O-, S-, and N–IP and 4 snakes, from O to N: long., rad., rad., rad. (3111) at a reference momentum of 802.5 GeV and for 2 σ purely vertical motion computed with the `SODOM-2` algorithm

is performed in both the old and the revised version by a discrete Fourier transform (DFT) using the unit quaternions rather then explicit $\mathbf{SU(2)}$ matrices. In order to perform the DFT, the one–turn quaternion is evaluated at orbital phases uniformly distributed on the direct product of the 1–dimensional tori $\mathcal{T}_1$.

$$\begin{array}{ccc} \Psi_{x,k_x} = k_x\frac{2\pi}{M_x} \ , & \Psi_{y,k_y} = k_y\frac{2\pi}{M_y} \ , & \Psi_{z,k_z} = k_z\frac{2\pi}{M_z} \\ 0 \le k_x \le M_x - 1 \ , & 0 \le k_y \le M_y - 1 \ , & 0 \le k_z \le M_z - 1 \\ & M = M_x M_y M_z \ \ . & \end{array} \tag{4.44}$$

Therefore the inverse DFT of an arbitrary solution $\tilde{n}$ of equation (4.42) simultaneously yields the $(\hat{u}_1, \hat{n}, \hat{u}_2)$–system at M different points, uniformly distributed on the torus in sense just defined.

Figure 4.5 shows the loci of the $\hat{u}_1$, $\hat{n}$, $\hat{u}_2$ fields for the HERA–p 1996–luminosity optics with the same snake setup as in figures 4.2 to 4.4 at 802.5 GeV and on a vertical invariant ellipse with size 2

σ. The fields were computed using the `SODOM-2` implementation in `SPRINT` and $M = M_y = 127$. A comparison with stroboscopic averaging (see section 4.5) in figure 4.6 shows that both methods agree to a high precision. $M = 127$ is about the number of harmonics needed for this case. On the contrary, when the vertical amplitude is increased to 2.5 σ, $M = 127$ does *not* suffice any more.

The `SODOM-2` algorithm is only practical when only *one* orbital mode is excited. A nice feature of the `SODOM-2` algorithm is that the invariant spin field and the amplitude dependent spin tune are computed simultaneously. When d modes are excited the dimensionality of the truncated eigenproblem (4.42) is $\prod_i^d M_i$. Thus $d > 1$ either implies small M_i or an enormous computational effort to solve the eigenproblem. All results of simulations with the `SODOM-2` algorithm presented in this thesis were computed with $d = 1$.

4.4 The static polarisation limit

As we have seen in the previous section the $\hat{n}$–axis, given that it exists, is an invariant of the OTM. The physics of this is that a sufficiently large spin ensemble initially aligned parallel to $\hat{n}$ and uniformly distributed in $\vec{\Psi}$ will return to itself after each revolution around the ring apart from a redistribution of the particles in phase space. Therefore this spin ensemble defines a *stationary* polarisation state and that is why we introduced $\hat{n}$. In general and in the continuous limit the average polarisation of a beam with spins aligned parallel to $\hat{n}$ is $\vec{P}_{\text{aligned}} = \int_{\mathcal{P}} \rho(\vec{J},\vec{\Psi})\hat{n}_{\vec{J}}(\vec{\Psi})\, d\vec{\Psi}^3 d\vec{J}^3$, with the normalised phase space density ρ. We assume that the orbital motion is purely Hamiltonian and integrable and that the phase space density is stationary so that $\partial_{\vec{\Psi}}\,\rho = \vec{0}$. Then the beam average of an aligned spin ensemble is

$$\vec{P}_{\text{aligned}} = \int_{\mathbb{R}^{+3}} \rho(\vec{J}) P_{\text{lim}}(\vec{J}) \hat{u}_{\langle n\rangle}(\vec{J})\, d\vec{J}^3 \tag{4.45a}$$

$$\text{with } P_{\text{lim}}(\vec{J}) \equiv \frac{1}{(2\pi)^3}\left\| \int_{\mathcal{T}} \hat{n}_{\vec{J}}(\vec{\Psi})\, d\vec{\Psi}^3 \right\| \tag{4.45b}$$

$$\text{and } \hat{u}_{\langle n\rangle}(\vec{J}) \equiv \frac{1}{(2\pi)^3 P_{\text{lim}}(\vec{J})} \int_{\mathcal{T}} \hat{n}_{\vec{J}}(\vec{\Psi})\, d\vec{\Psi}^3 \text{ if } P_{\text{lim}} \neq 0 \quad . \tag{4.45c}$$

P_{lim} is called the *static polarisation limit* since it is the upper limit to the average *stationary* polarisation on the torus and $\hat{u}_{\langle n\rangle}$ is the average polarisation direction on the torus. In mid–plane symmetric rings (see the paragraph after corollary 2 to theorem 2.10) the invariant spin field fulfils the constraint $\hat{n}_{\vec{J}}(\Psi_x, \Psi_y + \pi, \Psi_z) = \underline{Y}_\pi \hat{n}_{\vec{J}}(\Psi_x, \Psi_y + \pi, \Psi_z)$. Thus in a mid–plane symmetric ring and with purely vertical motion, the average polarisation direction is constant up to a sign

$$\hat{u}^{\text{sym}}_{\langle n\rangle}(J_y) = \pm\hat{n}_0 = \pm\hat{y},\ \forall J_y \quad . \tag{4.46}$$

An arbitrary spin ensemble, or an arbitrary spin field, in general does *not* describe a stationary state. If the spin OTM is not the identity, the polarisation will fluctuate from turn to turn. Writing the j–turn spin map as $\underline{R}^{(j)}$, the *local turn–by–turn averaged polarisation* of an arbitrary spin field $\hat{f}$ is

$$\left\langle \hat{f}(\vec{\Psi}) \right\rangle = \lim_{N\to\infty} \frac{1}{N+1} \sum_{j=0}^{N} \underline{R}^{(j)}(\vec{\Psi} - 2\pi j\vec{Q}) \hat{f}(\vec{\Psi} - 2\pi j\vec{Q}) \quad , \tag{4.47}$$

i.e. the average over all trajectories that pass through $\vec{\Psi}$. We will now show that P_{lim} is actually the maximum possible time averaged polarisation on the torus. For this purpose we need

Definition 4.5 (Strongly non–spin–orbit resonant) *[GH99b] We call the spin–orbit system strongly non–spin–orbit–resonant if there are positive real numbers c, ρ so that for all $\vec{k} \in \mathbb{Z}^3$, $\vec{k} \neq \vec{0}$ and $\chi_{\vec{k}} \equiv [\vec{k}\cdot\vec{Q} - \nu]$ the inequality* $\min(\chi_{\vec{k}}, 1 - \chi_{\vec{k}}) > c|\vec{k}|^{-\rho}$ *holds.*

Note that definition 4.5 is weaker than strong incommensurabilty (definition A.6) of $(\nu, \vec{Q})$ with 1 since ν is not multiplied with an integer.

Theorem 4.5 *[GH99b] If an $\hat{n}$–axis and two lattice fields $\hat{u}_1$, $\hat{u}_2$ exist so that $\nu(\vec{J})$ can be defined according to theorem 4.3 and the spin–orbit system is strongly non–spin–orbit–resonant on a torus $\vec{J} = \text{const.}$, then any spin field defined by the initial condition $\hat{f}(\vec{\Psi}, \theta_0) = \hat{g}(\vec{\Psi})$ which has an analytic extension in $\vec{\Psi}$, has at each $\vec{\Psi}$ a local turn–by–turn averaged polarisation $\left\langle \hat{f}(\vec{\Psi}) \right\rangle$ parallel to $\hat{n}(\vec{\Psi})$ and the maximum $\left|\left\langle \hat{f}(\vec{\Psi}) \right\rangle\right| = 1$ for all $\vec{\Psi}$ is obtained only for $\hat{g} = \hat{n}$.*

The lengthy proof can be found in [GH99b] and will only be sketched here. Since the periodic basis $(\hat{u}_1, \hat{n}, \hat{u}_2)$ is explicitly assumed to exist we can write $\hat{f}(\vec{\Psi}) = (f^{(1)}\hat{u}_1 + I^{(f)}\hat{n} + f^{(2)}\hat{u}_2)\Big|_{\vec{\Psi}}$ and find for $\left\langle \hat{f} \right\rangle \equiv \hat{u}_1 \left\langle f^{(1)} \right\rangle + \hat{n}\left\langle I_f \right\rangle + \hat{u}_2 \left\langle f^{(2)} \right\rangle$ and the complex scalar $f \equiv f^{(1)} + i f^{(2)}$ that the j–th contribution to the sum in (4.47) is

$$
\begin{aligned}
I_j^{(f)}(\vec{\Psi}) &= I_0^{(f)}(\vec{\Psi} - 2\pi j \vec{Q}\,) = \sum_{\vec{k}} I_{0;\vec{k}}^{(f)} e^{i(-2\pi j \vec{k}\cdot\vec{Q} + \vec{k}\cdot\vec{\Psi})} && \text{(4.48a)}\\
f_j(\vec{\Psi}) &= e^{i2\pi\nu} f_{j-1}(\vec{\Psi} - 2\pi\vec{Q}\,) = \sum_{\vec{k}} f_{0;\vec{k}} e^{i(2\pi j(\nu - \vec{k}\cdot\vec{Q}\,) + \vec{k}\cdot\vec{\Psi}\,)} && \text{(4.48b)}
\end{aligned}
$$

where $I_0^{(f)}(\vec{\Psi}) = \hat{n}(\vec{\Psi}) \cdot \hat{f}(\vec{\Psi})$ and $f_0(\vec{\Psi}) = \hat{f}(\vec{\Psi}) \cdot (\hat{u}_1(\vec{\Psi}) + i\hat{u}_2(\vec{\Psi}))$, as phase space functions periodic in $\vec{\Psi}$. Finally the turn–by–turn averages yield

$$
\begin{aligned}
\left\langle I^{(f)} \right\rangle &= I_{0;\vec{0}}^{(f)} + \lim_{N\to\infty} \frac{1}{N+1} \sum_{\vec{k}\neq\vec{0}} \frac{1 - e^{-i2\pi(N+1)\vec{k}\cdot\vec{Q}}}{1 - e^{-i2\pi\vec{k}\cdot\vec{Q}}} I_{0;\vec{k}}^{(f)} e^{i\vec{k}\cdot\vec{\Psi}} && \text{(4.49a)}\\
|\langle f \rangle| &\leq \lim_{N\to\infty} \frac{1}{N+1} \sum_{\vec{k}} \frac{2|f_{0;\vec{k}}|}{\left|1 - e^{i2\pi(\nu - \vec{k}\cdot\vec{Q})}\right|} \quad . && \text{(4.49b)}
\end{aligned}
$$

The Fourier series in (4.49a) converges to a finite value due to the implicitly assumed strong incommensurability of the orbital tunes with one and $\hat{f}$ being explicitly assumed to have an analytic extension. The Fourier series in (4.49b) converges to a finite value because the spin–orbit system is explicitly assumed to be strongly non–spin–orbit resonant. Therefore $\left\langle \hat{f}(\vec{\Psi}) \right\rangle = \hat{n}(\vec{\Psi}) I_{0;\vec{0}}^{(f)} = \hat{n}(\vec{\Psi})\hat{n}(\vec{\Psi}) \cdot \hat{f}(\vec{\Psi}, \theta_0)$ which has a norm less or equal to 1 and equal to 1 if and only if $\hat{f}(\vec{\Psi}) = \hat{n}(\vec{\Psi})$. □

We note that the *instantaneous average polarisation* on the torus $\vec{P}_{\hat{f}}(\theta_0) = \int_{\mathcal{T}} \hat{f}(\vec{\Psi})\, d\vec{\Psi}^3$ can be bigger than P_{lim}. Nevertheless operating an experiment at θ_0 requires a large polarisation averaged over the beam as well over a large number of bunch crossings. Therefore the usable polarisation of the beam is always smaller then or equal to $\|\vec{P}_{\text{aligned}}\|$.

If we restrict ourselves to spin fields where the initial condition $\hat{f}(\vec{\Psi}, \theta_0) = \hat{g}(\vec{\Psi})$ fulfils $\partial_{\vec{\Psi}} I^{(f)} = \partial_{\vec{\Psi}} (\hat{g} \cdot \hat{n}) = \vec{0}$, then P_{dyn} of equation (4.7) is simply $I^{(f)}$. Since P_{dyn} is an invariant of the spin OTM we obtain

$$
\left\langle \vec{P} \right\rangle = \int_{\mathbb{R}^{+3}} \rho\, P_{\text{lim}}\, \hat{u}_{\langle n \rangle}\, P_{\text{dyn}}\, d\vec{J}^3 \quad . \tag{4.50}
$$

Now we will prove that a similar equation is true for arbitrary finite spin ensembles. Let $\{\widehat{S}_k\}_{1\leq k\leq N}$ be an ensemble of spins at $\vec{\Psi}_k$ on the torus $\vec{J} = \text{const.}$ with $I_k = \widehat{S}_k \cdot \hat{n}_{\vec{J}}(\vec{\Psi}_k, \theta_0)$. The T–turn average over each spin trajectory $\widehat{S}_k(\theta)$ yields

$$
\left\langle \widehat{S}_k \right\rangle_T \equiv \frac{1}{T} \sum_{j=0}^{T-1} \widehat{S}_k(\theta_0 + 2\pi j)
$$

$$
\begin{aligned}
&= \frac{1}{T}\sum_{j=0}^{T-1}\Big(I_k\hat{n}_{\vec{J}}(\vec{\Psi}_k+2\pi j\vec{Q}) \\
&\quad +\sqrt{1-I_k^2}\,\Big(\hat{u}_{1,\vec{J}}(\vec{\Psi}_k+2\pi j\vec{Q})\cos(\Phi_k+2\pi j\nu)-\hat{u}_{2,\vec{J}}(\vec{\Psi}_k+2\pi j\vec{Q})\sin(\Phi_k+2\pi j\nu)\Big)\Big) \\
&= \frac{1}{T}\sum_{j=0}^{T-1} I_k\hat{n}_{\vec{J}}(\vec{\Psi}_k+2\pi j\vec{Q})+\sqrt{1-I_k^2}\,\Re\left\{\vec{U}_{\vec{J}}(\vec{\Psi}_k+2\pi j\vec{Q})e^{i(\Phi_k+2\pi j\nu)}\right\} \\
&\equiv I_k\vec{A}_k^{(T)}+\sqrt{1-I_k^2}\,\Re\left\{\vec{B}_k^{(T)}\right\} \quad , \qquad (4.51)
\end{aligned}
$$

with $\vec{U}_{\vec{J}}\equiv\hat{u}_{1,\vec{J}}+i\hat{u}_{2,\vec{J}}$. Using the periodicity of $\hat{n}_{\vec{J}}$ and $\vec{U}_{\vec{J}}$, i.e.

$$
\hat{n}_{\vec{J}}(\vec{\Psi})=\sum_{\vec{l}}\vec{n}_{\vec{l}}e^{i\vec{l}\cdot\vec{\Psi}} \quad , \quad \vec{U}_{\vec{J}}(\vec{\Psi})=\sum_{\vec{l}}\vec{U}_{\vec{l}}e^{i\vec{l}\cdot\vec{\Psi}} \quad , \qquad (4.52)
$$

and absorbing the dependence on the initial phases $\vec{\Psi}_k$ into $\tilde{n}_{k,\vec{l}}\equiv\vec{n}_{\vec{l}}e^{i\vec{l}\cdot\vec{\Psi}_k}$ and $\widetilde{U}_{k,\vec{l}}\equiv\vec{U}_{\vec{l}}e^{i\vec{l}\cdot\vec{\Psi}_k}$ we find

$$
\vec{A}_k^{(T)}=\tilde{n}_{0,\vec{0}}+\frac{1}{T}\sum_{\vec{l}\neq\vec{0}}\tilde{n}_{k,\vec{l}}\,\frac{1-e^{iT2\pi\vec{l}\cdot\vec{Q}}}{1-e^{i2\pi\vec{l}\cdot\vec{Q}}} \quad \text{and} \quad \vec{B}_k^{(T)}=\frac{e^{i\Phi_k}}{T}\sum_{\vec{l}}\widetilde{U}_{k,\vec{l}}\,\frac{1-e^{iT2\pi(\vec{l}\cdot\vec{Q}+\nu)}}{1-e^{i2\pi(\vec{l}\cdot\vec{Q}+\nu)}} \qquad (4.53)
$$

where $\tilde{n}_{0,\vec{0}}$ is the average $\langle\hat{n}\rangle_{\vec{\Psi}}\equiv P_{\rm lim}\hat{u}_{\langle n\rangle}$. If $\hat{n}_{\vec{J}}$ has an analytic extension w.r.t. $\vec{\Psi}$, i.e. the Fourier coefficients $\vec{n}_{\vec{l}}$ decay exponentially with $|\vec{l}|$, and the orbital tunes are strongly incommensurable with 1, then in complete analogy to the proof of theorem 4.5 in section 2.2.8 of [GH99b], the i-th component $(i=x,y,z)$ of $\vec{A}_k^{(T)}-\tilde{n}_{0,\vec{0}}$ fulfils

$$
\left|\left(\vec{A}_k^{(T)}-\tilde{n}_{0,\vec{0}}\right)_i\right|\leq\frac{1}{T}\sum_{\vec{l}\neq\vec{0}}\tilde{n}_{k,\vec{l}}\,\frac{2}{|1-e^{i2\pi\vec{l}\cdot\vec{Q}}|}\leq\frac{1}{T}\sum_{\vec{l}\neq\vec{0}}\tilde{n}_{k,\vec{l}}\,2c_0|\vec{l}|^{-\rho_0}\leq\frac{A_0}{T} \qquad (4.54)
$$

with some positive constants c_0, ρ_0 and A_0. Therefore $\vec{A}_k^{(T)}$ converges linearly with $1/T$ to $\tilde{n}_{0,\vec{0}}=(2\pi)^{-3}\int_{\mathcal{T}_3}\hat{n}_{\vec{J}}(\vec{\Psi})d\vec{\Psi}^3\equiv P_{\rm lim}\hat{u}_{\langle n\rangle}$. If furthermore $\vec{U}_{\vec{J}}$ has an analytic extension w.r.t. $\vec{\Psi}$ and the spin–orbit system is strongly non–spin–orbit–resonant according to definition 4.5, then

$$
\left|\left(\vec{B}_k^{(T)}\right)_i\right|\leq\frac{1}{T}\sum_{\vec{l}}\widetilde{U}_{k,\vec{l}}\,2c|\vec{l}|^{-\rho}\leq\frac{A}{T} \qquad (4.55)
$$

with some positive constants c, ρ and A. Therefore $\vec{B}_k^{(T)}$ converges linearly with $1/T$ to $\vec{0}$. We note [LM88], that instead of demanding analyticity of $\hat{n}_{\vec{J}}$ and $\vec{U}_{\vec{J}}$ it suffices to demand that $\hat{n}_{\vec{J}}$ and $\vec{U}_{\vec{J}}$ are $\mathcal{C}^{r_n}$ or $\mathcal{C}^{r_U}$ functions respectively with $r_n>\rho_0+1$ and $r_U>\rho+1$. Thus we have proved

Lemma 4.3 *If the periodic vector fields $\hat{u}_1$, $\hat{n}$ and $\hat{u}_2$ exist on a torus $\vec{J}=$ const., if they are analytic or sufficiently smooth [LM88], if the orbital tunes are strongly incommensurable with 1 and if the spin–orbit system is strongly non–spin–orbit–resonant, then the T–turn average of an arbitrary spin trajectory $\widehat{S}(\theta)$ with the spin action $I=\widehat{S}\cdot\hat{n}$ yields*

$$
\lim_{T\to\infty}\left\langle\widehat{S}\right\rangle_T=P_{\rm lim}\hat{u}_{\langle n\rangle}I \quad . \qquad (4.56)
$$

Returning to our spin ensemble $\{\widehat{S}_k\}_{1\leq k\leq N}$ we find

$$
\left\langle\{\widehat{S}_k\}_{1\leq k\leq N}\right\rangle\equiv\lim_{T\to\infty}\left\langle\{\widehat{S}_k\}_{1\leq k\leq N}\right\rangle_T=P_{\rm lim}(\vec{J})\hat{u}_{\langle n\rangle}(\vec{J})\,\frac{1}{N}\sum_{k=1}^{N}I_k \quad . \qquad (4.57)
$$

We note that $P^{(N)}_{\rm dyn} \equiv 1/N\sum_{k=1}^{N} I_k$ is an invariant of the spin OTM. The results of the last paragraphs can be merged into

Theorem 4.6 (Factorisation theorem) *Under the premises of lemma 4.3, for an arbitrary spin ensemble $\{\widehat{S}_k\}_{1\le k\le N}$ on a given torus $\vec{J}=$ const. the turn–by–turn averaged ensemble polarisation can be factorised into two parts. One part, $P_{\rm lim}(\vec{J})\hat{u}_{\langle n\rangle}(\vec{J}) = 1/(2\pi)^3\int_{\mathcal{T}_3}\hat{n}_{\vec{J}}(\vec{\Psi})d\vec{\Psi}^3$ is a* static *property of the spin-orbit system. It does* not *depend on the history of the spin ensemble. The other part $P^{(N)}_{\rm dyn}\equiv 1/N\sum_{k=1}^{N} I_k$ is defined by the history of the spin ensemble. Only the N invariants of motion I_k of the $2N$constants that determine the initial conditions $\widehat{S}_k(\theta_0) = I_k\hat{n} + \Re\{\vec{U}e^{i\Phi_k}\})$, contribute to the turn–by–turn averaged ensemble polarisation. This polarisation is given by*

$$\left\langle \{\widehat{S}_k\}_{1\le k\le N}\right\rangle = P_{\rm lim}(\vec{J})\hat{u}_{\langle n\rangle}(\vec{J})P^{(N)}_{\rm dyn} \quad . \tag{4.58}$$

If the $\vec{\Psi}_k$ are uniformly distributed on the torus $\vec{J}=$ const. and the $\widehat{S}_k(\theta_0)$ are given by $\widehat{S}_k(\theta_0) = \hat{g}(\vec{\Psi}_k,\theta_0)$ with some $\mathcal{C}^1$ spin field $\hat{g}$ at θ_0, then $P^{(N)}_{\rm dyn}\to P^{(g)}_{\rm dyn}$ in the limit $N\to\infty$. We will therefore in the following, whenever it is clear whether a spin field or a discrete ensemble is described,*not* distinguish between $P_{\rm dyn}$ and $P^{(N)}_{\rm dyn}$.

Sometimes it is more convenient to use the average half polar opening angle of the $\hat{n}$–axis on a torus

$$\vartheta_n(\vec{J}) \equiv \frac{1}{(2\pi)^3}\int_{\mathcal{T}}\arccos\left(\hat{n}_{\vec{J}}(\vec{\Psi})\cdot\hat{u}_{\langle n\rangle}(\vec{J})\right)\,d\vec{\Psi}^3 \tag{4.59}$$

instead of the static polarisation limit $P_{\rm lim}$. The opening angle describes the average spread of $\hat{n}_{\vec{J}}$. We note that $0\le\vartheta_n\le{}^{\pi}/_2$ in contrast to $\vartheta_{n0}\equiv 1/(2\pi)^3\int_{\mathcal{T}}\arccos(\hat{n}_{\vec{J}}(\vec{\Psi})\cdot\hat{n}_0)\,d\vec{\Psi}^3$ which fulfils $0\le\vartheta_n\le\pi$. In the case of $\hat{n}_{\vec{J}}\cdot\hat{u}_{\langle n\rangle}(\vec{J})$ being independent of $\vec{\Psi}$ we get $P_{\rm lim}=\cos\vartheta_n$. When the spread of $\hat{n}_{\vec{J}}\cdot\hat{u}_{\langle n\rangle}(\vec{J})$ w.r.t. $\vec{\Psi}$ is small then an average opening angle $\vartheta_n\approx 60^\circ$ corresponds to $P_{\rm lim}\approx 0.5$.

Since the `SODOM-2` algorithm, according to equation (4.44), generates the $\hat{n}$–axis at M uniformly distributed points on the torus simultaneously, $P_{\rm lim}$ can be approximated without *further* tracking by

$$P^{\tt SODOM-2}_{\rm lim} = \frac{1}{M}\left\|\sum_{i=1}^{M}\hat{n}_i\right\| \tag{4.60}$$

whenever M is sufficiently big to obtain an approximation of the $\hat{n}$–axis with reasonable accuracy.

4.4.1 The linear static polarisation limit and filtering of Siberian Snakes

In the range of applicability of the linear `SLIM`–approximation, according to equation (4.35) the $\hat{n}$–axis is given by $\binom{\alpha_n^{(1)}(\vec{z})}{\beta_n^{(1)}(\vec{z})} = \underline{B}\,\underline{A}^{-1}\vec{z} = \underline{B}\vec{\xi}$. Here

$$\vec{\xi}\equiv(\sqrt{J_x}e^{+i\Psi_x},\sqrt{J_x}e^{-i\Psi_x},\sqrt{J_y}e^{+i\Psi_y},\sqrt{J_y}e^{-i\Psi_y},\sqrt{J_z}e^{+i\Psi_z},\sqrt{J_z}e^{-i\Psi_z}) \tag{4.61}$$

is the complex vector of the orbital normal form coordinates and $\underline{B}\equiv(\vec{b}_x^+,\vec{b}_x^-,\ldots)$ is defined by equation (4.33). One easily obtains for the rms deviation of the linear $\hat{n}$–axis from the $\hat{n}_0$–axis

$$\Delta_n^{(1)}(\vec{J}) = \sqrt{\langle(\alpha_n^{(1)}(\vec{J},\vec{\Psi}))^2+(\beta_n^{(1)}(\vec{J},\vec{\Psi}))^2\rangle_{\vec{\Psi}}} = \sqrt{2\sum_{l=x,y,z}(\vec{b}_l^+\cdot\vec{b}_l^-)J_l} \quad . \tag{4.62}$$

In the approximation that $\langle\arctan x\rangle\approx\arctan\langle x\rangle$ and $\langle 1/(1+x)\rangle\approx 1/(1+\langle x\rangle)$, i.e. in the limit $\langle(\|\hat{n}-\hat{n}_0\|-\Delta_n^{(1)})^2\rangle_{\vec{\Psi}}\to 0$, the linear opening angle $\vartheta_n^{(1)}$ and the linear static polarisation limit $P^{(1)}_{\rm lim}$ are

$$\vartheta_n^{(1)}(\vec{J})\approx\arctan\Delta_n^{(1)}(\vec{J}) \quad , \quad P^{(1)}_{\rm lim}(\vec{J})\approx\frac{1}{1+\left(\Delta_n^{(1)}(\vec{J})\right)^2} \quad . \tag{4.63}$$

Close to first order intrinsic resonances $\alpha_n^{(1)}$ and $\beta_n^{(1)}$ diverge. On the contrary, the normalised first order quantities $0 \leq \vartheta_n^{(1)} \leq {}^{\pi}/_{2}$ and $0 \leq P_{\rm lim}^{(1)} \leq 1$ stay finite. Although the condition $(\alpha_n^{(1)})^2 + (\beta_n^{(1)})^2 \ll 1$ is needed for the applicability of the linear theory, the fact that $\vartheta_n^{(1)}$ becomes large can serve as an indicator that higher order effects have become important. The `SLIM` algorithm is very fast. Therefore it is the ideal tool for a first guess at the qualitative nature of spin motion for a given lattice and energy range.

Linear automatic filtering of snake schemes

Equation (4.58) implies that in order to obtain a large beam average of the polarisation $P_{\rm lim}$ should be maximised. Moreover as we will see now, in accelerators with Siberian Snakes the snake angles can be chosen to optimise $P_{\rm lim}$. No generally applicable strategies to maximise $P_{\rm lim}$ beyond the linear level are yet known but several first order methods can be applied in order to maximise $P_{\rm lim}^{(1)}$.

In section 3.2.2 we have discussed snake matching [GH99b, GH99c] which defines constraints on the snake angles which cause the spin–orbit coupling integrals to vanish or at least decrease under certain symmetry requirements for the ring. Moreover the so–called strong spin match [KS88a] and, restricted to the maximisation of $P_{\rm lim}$ at constant energy, the harmonic spin match [CY81, BR99a] provide means to minimise the spin–orbit coupling integrals or equivalently the $\underline{G}$–matrix. In these methods one exploits the fact that whenever the spin–orbit coupling integrals are small and the system is sufficiently far from any linear intrinsic spin–orbit resonance then at least $P_{\rm lim}^{(1)}$ is high [GH99b, BH92, BH94a, BH94b] since $\|\hat{n} - \hat{n}_0\|$ is small (see (4.36) and (4.62)).

Another, more direct way to maximise $P_{\rm lim}^{(1)}$ is by so–called linear filtering [GH99a, GH99b]. Here the computational speed of the `SLIM` approximation is exploited to evaluate a large set of snake schemes over a given momentum range. The automatic linear filtering algorithm which is implemented in the `SPRINT` code is based on complete enumeration of snake schemes on a uniform discrete subset (grid) of the continuous set of vectors of snake angles $(\phi_1, \ldots, \phi_{2N}) \in [0, \pi)^{2N}$ for $2N$ snakes. The procedure is the following

1. The lattice is assumed to be flat or flattened in the sense of definition 3.2 but not necessarily exactly mid–plane symmetric. The fixed snake positions θ_i are assumed to fulfil the minimal condition $\sum_{i=1}^{2N}(-1)^i \Theta_i = 0$ according to theorem 3.1 for energy independent design orbit spin tune, where the Θ_i are the accumulated horizontal bend angles between snakes. A uniform partitioning $\tilde{\phi}_k = k\pi/n$, $k = 0, \ldots, n-1$ of the interval $[0, \pi)$ for the snake angles ϕ_i and a reference torus are specified. A snake scheme with $2N$ snakes is characterised by the $2N$–tuple $(k_1, \ldots, k_{2N})$. Then the i-th snake is either a horizontal snake with snake angle $\phi_i = \tilde{\phi}_{k_i}$ for $k_i = 0, \ldots, n-1$ or a vertical snake for $k = n$.

2. Eliminate all schemes that do *not* fulfil $\nu_0 = {}^1/_2$ and $\hat{n}_0(\theta_0) = \hat{y}$.

3. Compute the average of the linear opening angle $\vartheta_n^{(1)}$ on the reference torus in a specified energy interval for all schemes that survive step 2.

4. Then sort the schemes by increasing average $\vartheta_n^{(1)}$.

The reason for applying the linear `SLIM` algorithm is that it is the fastest. If we neglect the vertical snakes for the moment, then a scheme with $2N$ horizontal snakes has $2N-1$ free snake angles that are not constrained by step 2. With n snake angles from 0 to $(n-1)\pi/n$ this gives n^{2N-1} schemes to be evaluated in step 3! The `SODOM-2` algorithm which is relatively fast for 2–dimensional orbital motion would also be a candidate for filtering. It contains higher order effects and additionally would allow to filter for minimal spin tune shift $\nu(J_{\rm reference}) - \nu_0$, but filtering with the `SODOM-2` algorithm is currently still too slow by far for *automatic* filtering. Also note that in principle it is possible to filter for minimal change of $\vartheta_n^{(1)}$ (linear or non–linear) per energy step but this has not yet been implemented.

After the automatic filtering has been done one should check the "best" schemes with higher order algorithms manually, i.e. perform various simulations with explicitly given snake schemes. Finally, tracking under realistic ramp conditions is necessary to verify that the filtered schemes offer a maximum of surviving $P_{\rm dyn}$. The results of filtering and ramp–simulations for HERA–p will be discussed in chapter 5.

4.5 Stroboscopic Averaging

We have shown in theorem 4.5 that for strongly non–spin–orbit resonant systems in which the $\hat{n}$–axis and the amplitude dependent spin tune exist, the turn–by turn average of an arbitrary sufficiently smooth spin field at a given point on the torus settles along the $\hat{n}$–axis at that point. This result can actually be used to compute the $\hat{n}$–axis. We choose a special spin field with $\hat{f}(\vec{\Psi} - 2\pi j\vec{Q}) = \hat{f}_0$ for all $j \in \mathbb{N}$. One particular choice for $\hat{f}_0$ is $\hat{n}_0$ so that for the local turn–by–turn average polarisation $P_{\rm loc}^{(\hat{n}_0)}(\vec{\Psi})$ of a spin field initially parallel to $\hat{n}_0$ we obtain

$$\begin{aligned} P_{\rm loc}^{(\hat{n}_0)}(\vec{\Psi})\,\hat{n}(\vec{\Psi}) &= \lim_{N\to\infty}\frac{1}{N+1}\sum_{j=0}^{N}\underline{R}^{(j)}(\vec{\Psi}-2\pi j\vec{Q})\hat{n}_0 \\ &= \lim_{N\to\infty}\frac{1}{N+1}\sum_{j=0}^{N}\bigodot_{k=0}^{j-1}\underline{R}(\vec{\Psi}-2\pi(j-k)\vec{Q})\hat{n}_0 \\ &\equiv \lim_{N\to\infty}\underline{A}_N^-(\vec{\Psi})\hat{n}_0 \quad . \end{aligned} \tag{4.64}$$

This is one form of the *stroboscopic averaging* algorithm of K. Heinemann and G. H. Hoffstaetter [HH96, GH99b]. $P_{\rm loc}^{(\hat{n}_0)}(\vec{\Psi})$ is called the *stroboscopic average* of $\hat{n}_0$ at $\vec{\Psi}$. In theorem 4.5 we have explicitly assumed a unique invariant spin field to exist and then the only pitfall in the above construction of the $\hat{n}$–axis might be that $P_{\rm loc}^{(\hat{n}_0)}(\vec{\Psi}) = \vec{0}$, which means that $\underline{A}_N^-(\vec{\Psi})\hat{n}_0 \to 0$ for $N \to \infty$ or in other words $\hat{n}_0 \in \mathrm{kern}(\underline{A}_\infty^-(\vec{\Psi}))$. Nevertheless in all practical examples studied so far — even those with $P_{\rm lim} \approx 0$ and $\|\hat{u}_{\langle n\rangle} - \hat{n}_0\| \approx 1$ — the choice of $\hat{f} = \hat{n}_0$ seemed to be at least not worse than any other.

In practice one does *not* know beforehand whether the invariant spin field exists but vanishing of the stroboscopic average of some spin field $\hat{f}$ implies that a beam described by this spin field has vanishing local turn–by–turn averaged polarisation at $\vec{\Psi}$.

It can be shown [HH96, GH99b] that whenever a positive $\xi < {}^{\pi}/_{2}$ exists so that for $1 \le j \le N+1$ the inequality $\angle\left(\underline{R}^{(j)}(\vec{\Psi} - 2\pi j\vec{Q})\hat{n}_0 - \hat{n}_0\right) \le \xi$ is fulfilled and the pseudo–$\hat{n}$–axis defined by

$$\hat{n}_N(\vec{\Psi}) \equiv \frac{\underline{A}_N^-(\vec{\Psi})\hat{n}_0}{\left\|\underline{A}_N^-(\vec{\Psi})\hat{n}_0\right\|} \tag{4.65}$$

exists, then the invariance condition (4.6) is fulfilled up to

$$\Delta_N \equiv \|\,\underline{R}(\vec{\Psi})\hat{n}_N(\vec{\Psi}) - \hat{n}_N(\vec{\Psi}+2\pi\vec{Q})\| \le \frac{4\sin{}^{\xi}/_{2}}{(N+1)\cos\xi} \quad . \tag{4.66}$$

Moreover the accuracy $\|\hat{n}_N - \hat{n}\|$, given an $\hat{n}$–axis exists, is proportional to ${}^{1}/_{N}$. The premise that the spin motion is bound to a subset of $\mathcal{S}_{\mathbb{R}}$ with opening angle $\xi < {}^{\pi}/_{2}$ turns out to be too strong in practice. Invariant spin fields have been computed numerically to a reasonable accuracy (see figure

4.3) which covered almost the whole unit sphere. Indeed equation (4.66) does not define an asymptotic relation but a strict bound on Δ_N for all $N > 1$.

Now we note that the $\hat{n}$–axis for the time–reversed motion $\hat{n}_-(\vec{\Psi})$ fulfils the invariance constraint

$$\underline{R}^{-1}(\vec{\Psi} - 2\pi\vec{Q})\hat{n}_-(\vec{\Psi}) = \hat{n}_-(\vec{\Psi} - 2\pi\vec{Q}) \quad . \tag{4.67}$$

Substituting $\vec{\Psi}' = \vec{\Psi} + 2\pi\vec{Q}$ and multiplying with $\underline{R}(\vec{\Psi}')$ one finds that this condition is equivalent to the standard condition (4.6). So if $\hat{n}_-$ exists it is also an $\hat{n}$–axis of the forward system. Then we can rewrite equation (4.64) to find the form of stroboscopic averaging implemented in SPRINT,

$$P_{\mathrm{loc};N}(\vec{\Psi}_0)\hat{n}_N(\vec{\Psi}_0) = \frac{1}{N+1}\sum_{j=0}^{N}\bigodot_{k=0}^{j-1}\underline{R}^{\mathrm{T}}(\vec{\Psi}_0 + 2\pi k\vec{Q})\hat{n}_0 = \underline{A}_N^{+}(\vec{\Psi}_0)\hat{n}_0 \quad , \tag{4.68}$$

for some given point $\vec{\Psi}_0$ on the torus. Here $P_{\mathrm{loc};N}$ is the N-turn approximation of $P_{\mathrm{loc}}^{(\hat{n}_0)}$. If it does not vanish, then $\hat{n}_N(\vec{\Psi}_0)$ is an approximation of the $\hat{n}$–axis — given it exists. The spin $\widehat{S}_N \equiv \hat{n}_N(\vec{\Psi}_0)$ at $\vec{\Psi}_0, \theta_0$ is then the seed of a pseudo–$\hat{n}$–axis. An approximation of the static polarisation limit can then be computed as the average over successive applications of the spin OTM on this seed

$$P_{\mathrm{lim}}^{\mathtt{SPRINT}} = \frac{1}{N'+1}\left\|\sum_{i=0}^{N'}\underline{R}^{(i)}(\vec{\Psi})\widehat{S}_N\right\| \quad . \tag{4.69}$$

The implementation of stroboscopic averaging described in equation (4.68) needs only *forward* tracking which can in principle be performed without the explicit use of the orbital action–angle variables. It can therefore easily applied even to non–linear orbit systems where the inverse orbit map and the transformation to action–angle variables would be cumbersome to compute. In the current version of SPRINT forward stroboscopic averaging is implemented in an *adaptive* way, i.e. the number of tracking turns N is doubled until the numerical error $\delta_N \equiv \angle(\hat{n}_N, \hat{n}_{N/2})$ has decreased below a user defined limit. The method of stroboscopic averaging has been shown [BH96a, BH96b, BH96c, BH96d, VB98, BH98a, BH98b, BV98, BH98c, BH99a, BH99b, HV99] to be the most flexible and most efficient method of computing $\hat{n}$ in cases where invariant spin fields vary strongly over the phase space like that presented in figure 4.3. The linear convergence with N and the simple structure of the algorithm, namely forward tracking and the adding up of tracked spins obtained at consecutive turns means that the algorithm converges linearly with the actual CPU–time consumption per simulation run. In contrast to this, the SODOM-2 algorithm which is much faster than stroboscopic averaging for *moderately* complicated invariant spin fields and when restricted to one degree of orbital motion, i.e. where the Fourier coefficients of the OTM decay fast enough, solves an eigenproblem of order $2M$ when M harmonics in total are included. The typical CPU–time consumption of eigenproblem routines is $\sim M^3$ for M dimensional matrices. Therefore for sufficiently complicated invariant spin fields the SODOM-2 method with a fixed maximal number of harmonics M just fails but going to arbitrary numbers of harmonics increases the CPU–time consumption $\sim M^3$. But for stroboscopic averaging the number of tracking turns needed *in principle*, i.e. apart from quasi–resonant orbital motion, does *not* depend on the dimensionality of the orbital phase space motion. A drawback of stroboscopic averaging of course is that we do not get the amplitude dependent spin tune *for free* as we do with SODOM-2. Of course in their range of convergence SODOM-2 and stroboscopic averaging yield the same result. Figure 4.6 shows $n_y(\Psi_y)$ on an invariant vertical ellipse that corresponds to a beam width of 2 σ for the 1996–luminosity optics of HERA–p with 6 flattening snakes and a longitudinal and 3 radial snakes as used in figure 4.5. The function plotted with lines was obtained by the SODOM-2 algorithm as implemented in SPRINT with $M = M_y = 127$ harmonics included. The crosses are results of computing the $\hat{n}$–axis at some point on the ellipse with stroboscopic averaging with $N = 8000$ turns and then tracking the $\hat{n}$–axis seed obtained for another 1000 turns to fill the curve. The resulting stroboscopic

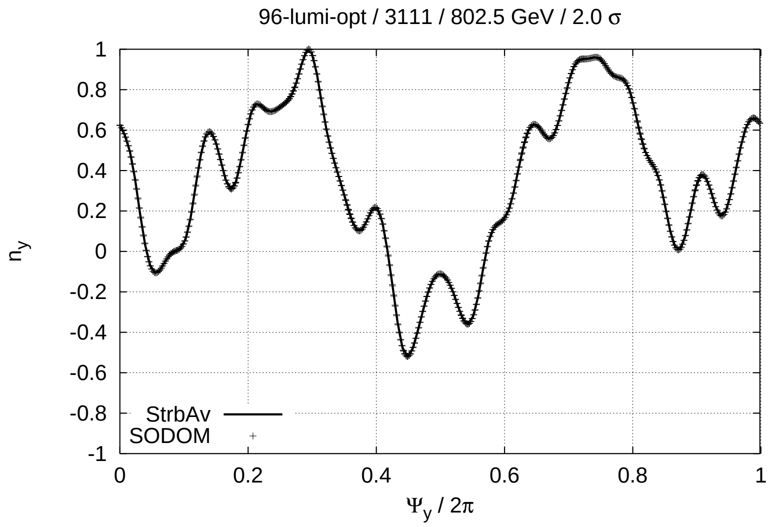

Figure 4.6: Comparison of $n_y(\Psi_y)$ for HERA–p as in figure 4.5 computed with the `SODOM-2` algorithm (lines) and stroboscopic average (crosses).

average $P_{\rm loc}$ at that point was 0.3474 and the numerical accuracy was $\vartheta_{8000} = 0.5664$ mrad. Among the 8000 turns, 2808 yielded a tracked spin which had an angle with $\hat{n}_0 = \hat{y}$ of more then $^{\pi}/_{2}$. As one easily sees, the two $\hat{n}$–axes are identical up to the graphical resolution. It must be stressed that two absolutely independent algorithms have obtained the same result within a few per–mille for such a complicated system. The `SODOM-2` run took about a third of the time of the stroboscopic average run. The long range energy scans with `SODOM-2` in this study included only vertical motion and only needed a moderate number of harmonics for $\hat{n}$, namely $65 \le M_y \le 85$, *most of the time.* Under these conditions the gain in computational speed is about a factor 10. The invariant spin field as described in the right half of figure 4.2 could not be reproduced with `SODOM-2` and only 127 harmonics. In fact it needs more than 250 harmonics and then `SODOM-2` is slower then stroboscopic averaging.

A comment should be made about phase space sampling close to resonances. The `SODOM-2` algorithm, by definition, does *not* work exactly on orbital resonances. In fact, cases have been observed where *very* close to low order orbital resonances the accuracy of the algorithm was poor. Stroboscopic averaging does not explicitly forbid orbital resonances, *but* the number of turns needed to get a realistic estimate of the turn–by turn average defined in equation (4.64) diverges close to low order orbital resonances. This can be seen in the following way: We know from section 4.3 that it is necessary to sample the periodic structure of the spin OTM with sufficient accuracy. When the tunes fulfil $[\vec{k}\cdot\vec{Q}] \ll 1$ with sufficiently low order $|\vec{k}|$ and the least common multiple of the k_i is m, then successive applications of the orbital OTM will stay inside m well separated domains on the torus for a long time and the complement of the union of these domains will be badly sampled. Therefore low order orbital resonances lower the computational accuracy of both algorithms, `SODOM-2` and stroboscopic averaging. When using the adaptive version of stroboscopic averaging one can of course beat the problem by increasing the initial number of averaging turns. Note that the same argument applies to the computation of $P_{\rm lim}^{\tt SPRINT}$ by single particle tracking.

4.6 An averaging method for the spin tune

Although the amplitude dependent spin tune can be obtained with the `SODOM-2` algorithm, the first algorithm for spin tune in this project was based on averaging of spin phase advances. We have seen in the proof of theorem 4.3 that when the orbital tunes are strongly incommensurable with 1 and for sufficiently smooth spin precession an amplitude dependent spin tune can be found which is basically the constant term in the generalised Fourier expansion of the precession frequency measured in some periodic orthonormal coordinate system consisting of $\hat{n}$ and two other vectors $\tilde{u}_1$, $\tilde{u}_2$. We have also seen that after transforming to the $(\tilde{u}_1, \hat{n}, \tilde{u}_2)$–system the flow $\underline{\widetilde{R}}(\theta_f, \theta_i, \vec{\Psi}_i)$ can be written in a 3–dimensional representation

$$\mathbf{SO(2)} \to \mathbf{GL}(\mathbb{R}^3) \ , \ \begin{pmatrix} \cos(x) & -\sin(x) \\ \sin(x) & \cos(x) \end{pmatrix} \mapsto \begin{pmatrix} \cos(x) & 0 & \sin(x) \\ 0 & 1 & 0 \\ -\sin(x) & 0 & \cos(x) \end{pmatrix} \tag{4.70}$$

of the Abelian group $\mathbf{SO(2)}$ so that two arbitrary spin transport maps in this coordinates commute. In `SPRINT` $\tilde{u}_1$ is chosen to be the unit vector perpendicular to $\hat{n}$ which lies in the $(\hat{n}, \hat{x})$–plane with positive x (radial) component. The vectors $\hat{u}_1$, $\hat{u}_2$ which also have to be perpendicular to $\hat{n}$ and therefore are in the same plane as $\tilde{u}_1$ and $\tilde{u}_2$ are obtained by rotating $\tilde{u}_1$ and $\tilde{u}_2$ around $\hat{n}$ by $\Delta(\Psi, \theta)$. This rotation is described in the $(\tilde{u}_1, \hat{n}, \tilde{u}_2)$–system by the periodic transformation matrix

$$\underline{A}(\vec{\Psi}, \theta) = \begin{pmatrix} \cos\Delta & 0 & \sin\Delta \\ 0 & 1 & 0 \\ -\sin\Delta & 0 & \cos\Delta \end{pmatrix} \tag{4.71}$$

with a periodic transformation $\underline{A}$ that belongs to the same 3–dimensional representation of $\mathbf{SO(2)}$. Therefore the spin flow in the $(\tilde{u}_1, \hat{n}, \tilde{u}_2)$–system is

$$\underline{\widetilde{R}}(\theta_f, \theta_i)(\vec{\Psi}) = \underline{A}(\vec{\Psi} + \vec{Q}\delta, \theta_f)\, \underline{D}(\delta)\, \underline{A}^{\mathrm{T}}(\vec{\Psi}, \theta_i) \tag{4.72a}$$

$$\underline{D}(\delta) = \begin{pmatrix} \cos(\delta\nu(\vec{J})) & 0 & \sin(\delta\nu(\vec{J})) \\ 0 & 1 & 0 \\ -\sin(\delta\nu(\vec{J})) & 0 & \cos(\delta\nu(\vec{J})) \end{pmatrix} \ , \ \delta = \theta_f - \theta_i \quad . \tag{4.72b}$$

We will now compute the spin N–turn maps at some given θ_0. The spin N–turn map in the $(\tilde{u}_1, \hat{n}, \tilde{u}_2)$–system starting at $\vec{\Psi}$ is given by

$$\begin{aligned} \underline{\widetilde{R}}^{(N)}(\vec{\Psi}) &= \prod_{k=0}^{N-1} \underline{\widetilde{R}}(\vec{\Psi} + 2k\pi\vec{Q}) \\ &= \prod_{k=0}^{N-1} \underline{A}(\vec{\Psi} + 2(k+1)\pi\vec{Q})\, \underline{D}(2\pi)\, \underline{A}^{\mathrm{T}}(\vec{\Psi} + 2k\pi\vec{Q}) \\ &= \underline{A}\left(\vec{\Psi} + 2(N+1)\pi\vec{Q}\right)\ \underline{D}(2N\pi)\ \underline{A}^{\mathrm{T}}\left(\vec{\Psi}\right) \end{aligned} \tag{4.73}$$

and describes a rotation around the $\hat{n}$–axis . The rotation angle is

$$\phi^{(N)}(\vec{\Psi}) = 2\pi \sum_{k=0}^{N-1} \tilde{\nu}(\vec{\Psi} + k2\pi\vec{Q}) = 2\pi N\nu(\vec{J}) + \Delta\left(\vec{\Psi} + 2(N+1)\pi\vec{Q}\right) - \Delta\left(\vec{\Psi}\right) \quad , \tag{4.74}$$

where $0 \le \Delta(\vec{\Psi}) \le 2\pi$ is the rotation angle of $\underline{A}(\vec{\Psi})$ measured in the $(\tilde{u}_1, \hat{n}, \tilde{u}_2)$–system. Therefore we find, given that the $(\hat{u}_1, \hat{n}, \hat{u}_2)$–system exists according to theorem 4.3, $\nu(\vec{J}) = \lim_{N\to\infty} \frac{1}{N}\sum_{k=0}^{N-1} \tilde{\nu}(\vec{\Psi} + k2\pi\vec{Q})$ and that with

$$\nu_N(\vec{J}) \equiv \frac{1}{N} \sum_{k=0}^{N-1} \tilde{\nu}(\vec{\Psi} + k2\pi\vec{Q}) \tag{4.75}$$

the error $|\nu_N(\vec{J}) - \nu(\vec{J})|$ decays like $^1/_N$.

The spin tune ν is only unique up to an arbitrary integer plus an integer combination of the orbital tunes. Thus changing to another starting coordinate system $(\tilde{u}'_1, \hat{n}, \tilde{u}'_2)$ might lead to another spin tune $\nu' = \nu + l_0 + \vec{l} \cdot \vec{Q}$. Moreover there is no reason why the vector $\tilde{u}_1$ constructed in the same way for all system parameters, namely reference momentum, orbital amplitudes and lattice parameters should reproduce the same branch of the amplitude dependent spin tune for all values of the parameters. For one value of the system parameters, parametrised by λ, the algorithm finds $\nu|_{\lambda_0}$ and for some close–by by parameter $\lambda_0 + \delta\lambda$ the averaging method, using $\tilde{u}_1$, $\tilde{u}_2$ constructed in the same way as at λ_0, may yield $\nu|_{\lambda_0+\delta\lambda} + l_0 + \vec{l} \cdot \vec{Q}$ with some integers l_0 and $\vec{l}$. This will then produce a *branch jump* of $[\nu]$ around λ_0 . Figure 4.7 shows a spin tune scan with SPRINT for HERA–p with the 1996

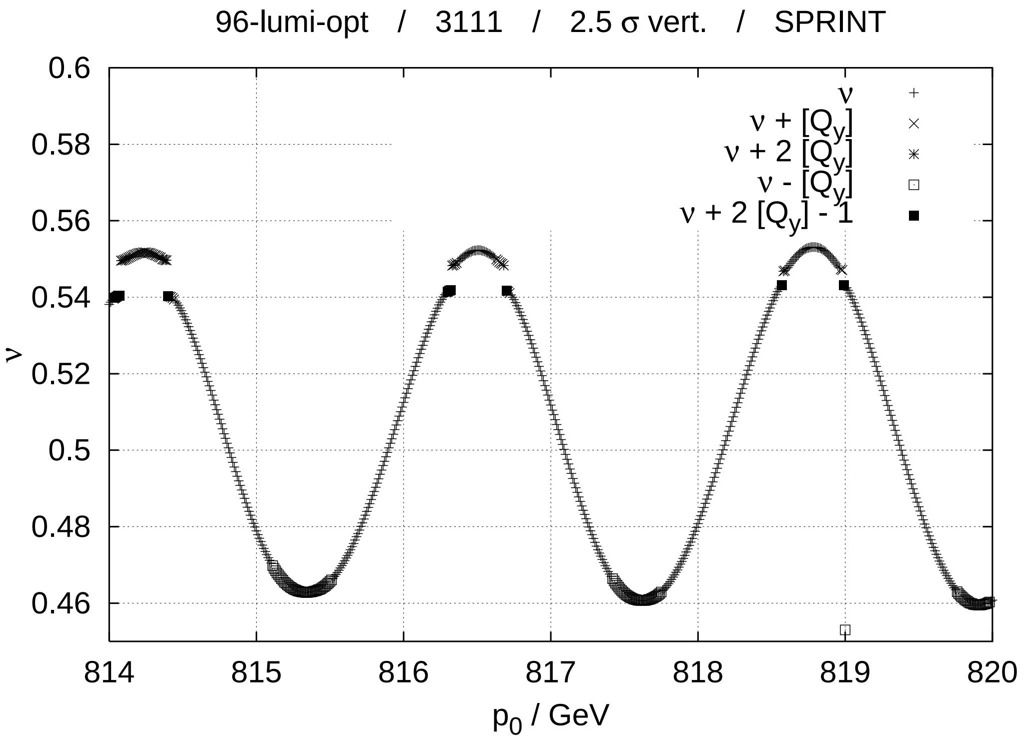

Figure 4.7: Scan of ν w.r.t. the reference momentum p_0 with SPRINT for the HERA–p 1996 luminosity optics with 6 flattening snakes and the snake scheme 3111 and $[Q_y] \approx 0.2725$. Almost all of the spin tune jumps have been corrected manually by plotting various branches of ν. The symmetric discontinuities around the resonance condition $\nu = 2[Q_y]$ cannot be resolved without violating $\lim_{J_y \to 0} \hat{n} \to +\hat{n}_0$.

luminosity optics and the 3111 snake scheme. The branch jumps have been manually compensated by plotting the 5 branches ν, $\nu + [Q_y]$, $\nu - [Q_y]$, $\nu + 2[Q_y]$ and $\nu + 2[Q_y] - 1$. The corrected spin tune appears to be a piecewise continuous curve with symmetric discontinuities around the resonance condition $\nu = 2[Q_y]$. In sections 4.7 and 4.8 we will find an explanation for this behaviour. We note that any such discontinuity $\nu_- = \kappa - \epsilon \to \nu_+ = \kappa + \epsilon$ with $\kappa = k_0 + \vec{k} \cdot \vec{Q}$ can in principle be resolved by choosing $\nu'_+ = -\nu_+ + 2\kappa$ but that a sign change in ν in general requires $\lim_{J_y \to 0} \hat{n} \to -\hat{n}_0$.

Only the fractional part $[\tilde{\nu}]$ can be computed by means of the OTM. We assume that with properly chosen $\tilde{u}_1$, $\tilde{u}_2$ the pseudo spin tune $\tilde{\nu}(\vec{\Psi})$ is a periodic and continuous function of $\vec{\Psi}$. But the fractional part $[\tilde{\nu}]$ can have discontinuities. In some range of parameters, the integer part of $\tilde{\nu}$ might be constant on the torus, leading to a continuous $[\tilde{\nu}]$, but outside this range the integer part might fluctuate. When averaging over $\tilde{\nu}(\vec{\Psi})$, such discontinuities of $[\tilde{\nu}]$ produce wrong results that might be misinterpreted as branch jumps. Therefore the integer part of $\tilde{\nu}(\vec{\Psi})$ should be automatically corrected. For orbital motion in one phase plane, this can be done by sorting the $\tilde{\nu}_k \equiv \tilde{\nu}(\Psi + 2k\pi Q)$ by increasing orbital phase

$\Psi_k \equiv \Psi + 2k\pi Q$ and then mutually adding or subtracting 1 whenever $|[\tilde{\nu}_k] - [\tilde{\nu}_{k+1}] \pm 1| < |[\tilde{\nu}_k] - [\tilde{\nu}_{k+1}]|$. This method of pseudo spin tune averaging is implemented in `SPRINT`. The averaging method is algorithmically similar to stroboscopic averaging since it employs multi–turn tracking starting from one initial phase Ψ on the invariant ellipse. Computing the $\hat{n}$–axis by stroboscopic averaging and/or computing the amplitude dependent spin tune by pseudo spin tune averaging will in the following be called the `SPRINT` algorithm. Figure 4.8 shows 2 pseudo spin tune functions $[\tilde{\nu}(\Psi_y)]$ for the HERA–p

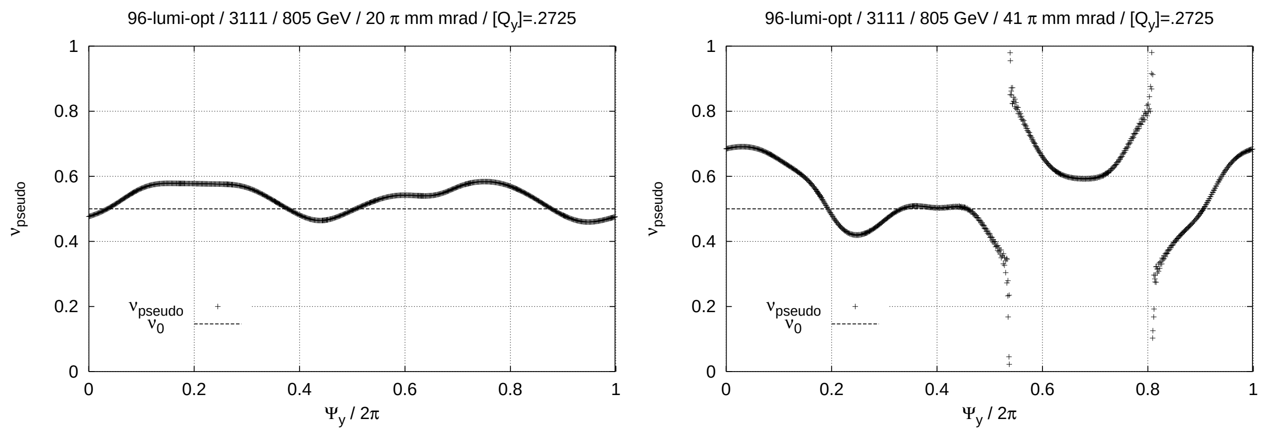

Figure 4.8: The pseudo spin tune function $[\tilde{\nu}(\Psi_y)]$ for the HERA–p 1996 luminosity optics in the same set up as in figure 4.2 at a reference momentum of 805 GeV and for purely vertical motion. Left: On an invariant ellipse enclosing a normalised emittance of 20 π mm mrad. Right: On an invariant ellipse enclosing a normalised emittance of 41 π mm mrad.

1996 luminosity optics with 6 flattening snakes and 4 Siberian Snakes with snake angles as in all figures shown so far. See figure 4.2 for the snake angles. A reference momentum of 805 GeV was chosen. In both plots the design orbit spin tune $\nu = {}^1\!/_2$ is shown to guide the eye. Both plots are for purely vertical orbital motion which is the only case for which the `SPRINT` algorithm can compute the spin tune so far. The left plot is on an invariant ellipse which encloses a normalised emittance of 20 π mm mrad corresponding to approximately 2.24 σ. The spread of $[\tilde{\nu}(\Psi_y)]$ is small so that no integers have to be corrected. Note that $\tilde{\nu}$ is almost symmetric around ν_0 so that averaging over the orbital phase phase yields only a small spin tune shift of $|\nu - \nu_0| \approx 0.03$. On the right the normalised emittance is 43 π mm mrad corresponding to approximately 3.28 σ. Obviously here the integer part of the pseudo spin tune decreases by 1 at ${}^{\Psi_y}\!/_{2\pi} \approx 0.54$ and returns to its former value at ${}^{\Psi_y}\!/_{2\pi} \approx 0.81$. The amplitude dependent spin tune computed by averaging $\tilde{\nu}$ after subtracting 1 when ${}^{\Psi_y}\!/_{2\pi}$ is inside $[0.54, 0.81]$ is $\nu \approx 0.435$ whereas the spin tune obtained from the uncorrected $\tilde{\nu}$ is much closer to ν_0. The amplitude dependent spin tune computed with the `SODOM-2` method, which tends to have less branch jumps is shown later in figure 4.16. It should be noted that the integer correction algorithm in its current form can easily be confused in the case of violent oscillations of $\tilde{\nu}$ and that therefore not all branch jumps can be eliminated.

Having obtained an approximation of the spin tune ν_N on a torus where $\vec{Q}$ is strongly incommensurable with 1 and with the instantaneous spin precession frequency $\zeta(\vec{\Psi}, \theta)$ being sufficiently smooth, one can in principle construct the corresponding choice of $\hat{u}_1^{(N)}(\vec{\Psi}, \theta)$ by starting with $\hat{u}_1^{(N)}(\vec{\Psi}_0, \theta_0) = \tilde{u}_1(\vec{\Psi}_0, \theta_0)$ and subsequently rotating the vector $\tilde{u}_1(\vec{\Psi}(\theta), \theta)$ around $\hat{n}(\vec{\Psi}(\theta), \theta)$ by the angle $\phi(\theta, \theta_0) = \int_{\theta_0}^{\theta} \zeta(\vec{\Psi}(\vartheta), \theta)\, d\vartheta - (\theta - \theta_0)\nu_N$. If ν_N were exactly ν, then this procedure would yield in the limit $\theta \to \infty$ the periodic vector $\hat{u}_1(\vec{\Psi}, \theta)$ on a dense subset of the torus. To obtain the approximation $\hat{u}_1^{(N)}(\vec{\Psi}, \theta_0)$ on the Poincaré section at θ_0 it suffices to construct $\hat{u}_1^{(N)}(\vec{\Psi} + 2k\pi\vec{Q}, \theta_0)$ by rotating $\tilde{u}_1^{(N)}(\vec{\Psi} + 2k\pi\vec{Q}, \theta_0)$ by the angle $2\pi \left(\sum_{i=1}^{k} \tilde{\nu}(\vec{\Psi} + 2k\pi\vec{Q}) - k\nu_N \right)$. If we write $\nu = l + [\nu]$ and $\nu_N = l' + [\nu] + \epsilon$ with

$\epsilon \sim {}^1/_N \ll 1$, we find that the absolute error of the rotation angle after k turns divided by 2π is

$$\Big|[k\nu_N] - [k\nu]\Big| = \Big|\Big[[k[\nu]] + [k\epsilon]\Big] - \Big[k[\nu]\Big]\Big| \tag{4.76}$$

which can take arbitrary values between 0 and 1 for sufficiently large k even when ϵ is reasonably small. Therefore this procedure for computing the vectors $\hat{u}_1$ and $\hat{u}_2$ is numerically unstable and is hence *not* recommended if ν is not known to high accuracy.

4.7 The $\hat{n}$–axis in the single resonance model

So far the only non–trivial spin–orbit system for which an exact analytical formula for the invariant spin field has been found is the SRM as described in section 2.4 *without* snakes.

When deriving the spin transfer quaternion (2.164a)–(2.164f) we found that the precession vector $\vec{\Omega}_a$ (see (2.161)) in the resonance precession frame (RPF) neither depends on Ψ nor on θ. The coordinate transformation $\underline{A}$ (see (2.159)) to this frame is 2π–periodic in Ψ and θ. Therefore a periodic spin field in the RPF is also periodic in any other frame which is obtained from the RPF by a periodic coordinate transformation. In the RPF the invariant spin field is simply

$$\hat{n}_a \equiv \pm\frac{(0,\delta,\epsilon)^{\mathrm{T}}}{\lambda} = \text{const.} \tag{4.77}$$

Transforming back to the original $(\hat{x},\hat{y},\hat{z})$ system we find

$$\hat{n}(\Psi,\theta) = \underline{A}^{\mathrm{T}}(\theta,\Psi)\hat{n}_a = \frac{\operatorname{sgn}(\delta)}{\lambda}\left(\hat{x}\epsilon\sin(\psi_\epsilon + k_0\theta + k\Psi) + \hat{y}\delta + \hat{z}\epsilon\cos(\psi_\epsilon + k_0\theta + k\Psi)\right) \quad , \tag{4.78}$$

where the sign has been chosen so that $\hat{n}\Big|_{\epsilon=0} = \hat{n}_0 \equiv +\hat{y}$ is independently of δ. This result was already obtained by Mane [SM88] for $k_0 = 0$ and $k = 1$. Following a derivation by Heinemann and Hoffstaetter [HH96, GH99b] one can choose

$$\begin{aligned} \hat{u}_1'(\Psi,\theta) &= \operatorname{sgn}(\delta)\,\left(-\hat{x}\cos\phi(\Psi,\theta) + \hat{z}\sin\phi(\Psi,\theta)\right) &\quad (4.79\text{a})\\ \hat{u}_2'(\Psi,\theta) &= \frac{1}{\lambda}\left(-\hat{x}\delta\sin\phi(\Psi,\theta) + \hat{y}\epsilon - \hat{z}\delta\cos\phi(\Psi,\theta)\right) &\quad (4.79\text{b}) \end{aligned}$$

with $\phi(\Psi,\theta) \equiv \psi_\epsilon + k_0\theta + k\Psi$, so that $(\hat{u}_1', \hat{n}, \hat{u}_2')$ is an orthonormal right–handed periodic basis with the amplitude dependent spin tune $\nu'(\epsilon) = \operatorname{sgn}(\delta)\,\lambda$. Since the spin tune is not unique, one may rotate the $(\hat{u}_1', \hat{n}, \hat{u}_2')$–system around $\hat{n}$ by $-\phi(\Psi,\theta)$ to obtain

$$\begin{aligned} \hat{u}_1(\Psi,\theta) &= \hat{u}_1'(\Psi,\theta)\cos\phi(\Psi,\theta) - \hat{u}_2'(\Psi,\theta)\sin\phi(\Psi,\theta) &\quad (4.80\text{a})\\ \hat{u}_2(\Psi,\theta) &= +\hat{u}_1'(\Psi,\theta)\sin\phi(\Psi,\theta) + \hat{u}_2'(\Psi,\theta)\cos\phi(\Psi,\theta) &\quad (4.80\text{b})\\ \nu(\epsilon) &= \operatorname{sgn}(\delta)\,\lambda + \kappa = \operatorname{sgn}(\nu_0 - k_0 - kQ)\,\sqrt{\epsilon^2 + (\nu_0 - k_0 - kQ)^2} + k_0 + kQ \quad . &\quad (4.80\text{c}) \end{aligned}$$

The amplitude dependent spin tune $\nu(\epsilon)$ defined in the $(\hat{u}_1, \hat{n}, \hat{u}_2)$–system gives $\nu(0) = +\nu_0$ independently of δ. With this sign convention and for finite ϵ the spin tune jumps from $\kappa - \epsilon$ to $\kappa + \epsilon$ and $\hat{n}$ changes sign from $\epsilon(\hat{x}\epsilon\sin\phi + \hat{z}\epsilon\cos\phi)$ to $-\epsilon(\hat{x}\epsilon\sin\phi + \hat{z}\epsilon\cos\phi)$ when δ crosses 0. Of course one can choose the sign differently so that ν as well as $\hat{n}$ are continuous at $\delta = 0$ for $\epsilon > 0$, but then one has the counterintuitive situation in which $\hat{n}$ flips from $\hat{n}_0$ to $-\hat{n}_0$ at the resonance position $\nu_0 = \kappa$ when the resonance is *not* excited, i.e. $\epsilon = 0$. Therefore the sign convention used above seems to be reasonable.

The locus of the $\hat{n}$–axis is on a cone around $\hat{u}_{\langle n\rangle} = \hat{n}_0$ with opening angle

$$\vartheta_n(\epsilon,\delta) = \arccos\hat{n}\cdot\hat{n}_0 = \arccos\frac{|\delta|}{\lambda} \tag{4.81}$$

which for $\epsilon > 0$ has one unique maximum $\vartheta_n = {}^{\pi}/_{2}$ at the resonance position $\delta = 0$. Note that spin motion as described by the invariant spin fields shown in figure 4.2, 4.3 and 4.5 is *by far* beyond the applicability of the single resonance model! We also note that in contrast to $\hat{n}$ the unit rotation vector $\hat{r}$ lives on a cone whose opening angle ϑ_r (see equation (2.167)) can have local maxima even far off–resonance. In particular ϑ_r does not always have a local maximum at $\delta = 0$.

The static polarisation limit can easily be written in terms of the distance from the resonance of the on–orbit spin tune $\delta = \nu_0 - \kappa$ as well as the distance of the amplitude dependent spin tune from the resonance $\Delta(\epsilon) = \nu(\epsilon) - \kappa$

$$P_{\mathrm{lim}} = \frac{|\delta|}{\lambda} = \sqrt{1 - \left(\frac{\epsilon}{\Delta(\epsilon)}\right)^2}. \tag{4.82}$$

In the literature and so far, for convenience, in this thesis the spin–orbit resonance condition for the SRM has been taken to be $\delta = 0$. However, the correct expression of resonance is given by (4.27) and although ν_0 can cross the condition $\delta = 0$, the minimum of $\Delta(\epsilon)$ is ϵ so that the resonance is never strictly reached in this way. Nevertheless a minimum is reached at $\delta = 0$ and P_{lim} has a unique minimum $P_{\mathrm{lim}} = 0$ at $\nu_0 = k_0 + kQ$ or in other words when ν is closest to $k_0 + kQ$. Additionally we see that $\lim_{\delta \to \pm\infty} P_{\mathrm{lim}} = 1$, that $P_{\mathrm{lim}}(\delta)$ is monotonic on both sides of $\delta = 0$ and that $P_{\mathrm{lim}}(\delta = \pm\epsilon) = {}^{1}/_{\sqrt{2}}$. Therefore we may say that the characteristic width of the resonance is $O(\epsilon)$ in the sense that for $|\delta| \gg \epsilon$ the influence of the resonance on spin motion becomes weak. Models of accelerators where more than one resonance is excited but in which all positions of the resonances with non–vanishing strengths are well separated compared to their strengths are called *isolated* resonance models (see section 2.4).

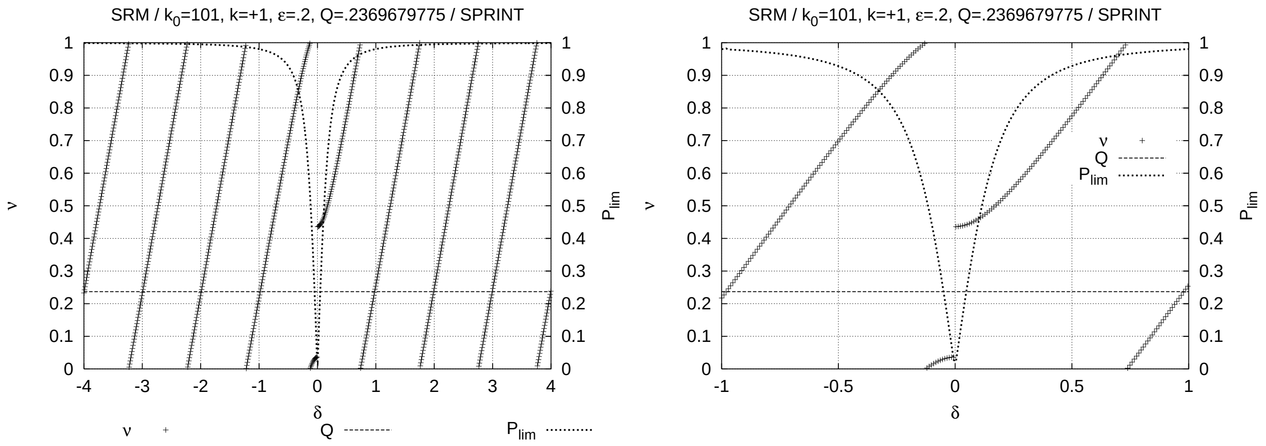

Figure 4.9: The functional dependence of $[\nu]$ and P_{lim} on the distance parameter $\delta \equiv \nu_0 - \kappa$ for the SRM. Left: global view to show the local character of the resonance. Right: zoomed view to explain the behaviour of $[\nu]$ and P_{lim} close to $\delta = 0$.

Figure 4.9 shows $[\nu]$ (left ordinate) and P_{lim} (right ordinate) for the plain SRM computed with the `SPRINT` method. The parameters are $k_0 = 101$, $k = +1$, $\epsilon = 0.2$, $\psi_\epsilon = 0$, and $Q = \sqrt{5} - 2 \approx 0.2360679775$. The left plot with $-4 \le \delta \le +4$ shows that the resonance is local, i.e. that there are no further minima of P_{lim} apart from $\delta = 0$. The right plot is a zoomed version that shows the behaviour of ν and P_{lim} close to the resonance $\kappa = k_0 + kQ$. The amplitude dependent spin tune approaches the resonance with $\nu \approx \nu_0$, then in a vicinity of $\nu = \kappa$, with characteristic half width ϵ, it starts levelling off to jump from $\kappa - \epsilon$ to $\kappa + \epsilon$ at $\nu_0 = \kappa$. In this region P_{lim} has a pronounced minimum $P_{\mathrm{lim}}(\delta = 0) = 0$ and for $|\delta| \to \infty$ it *monotonically* approaches 1. This rather simple figure is meant to train the eye since in the following we will often meet combined scans of ν and P_{lim} as functions of *some* system parameter.

The vertical response function $V_\epsilon = 1 - 2(\sin^2 \pi\lambda)\, {}^{\epsilon^2}/_{\lambda^2}$ defined in equation (2.169) has nodal points $V_\epsilon = 1$ whenever λ is an integer. At the nodal points $\hat{n}'(\vec{\Psi}, \theta) \equiv \hat{n}_0(\theta)$ is another possible $\hat{n}$–axis. This is in agreement with theorem 4.4 since at the nodal points the amplitude dependent spin tune is on resonance $\nu(\epsilon) = m_0 + kQ$ and the $\hat{n}$–axis is therefore *not* unique at these δ. Nevertheless, in the SRM these additional "resonances" have zero strength and therefore do not affect the polarisation. Integer resonance strengths can be considered pathological since then a nodal point exists even at $\delta = 0$. Note that $\nu(\epsilon)$ is not given by the μ_r from (2.166a).

4.8 The amplitude dependent spin tune and the static polarisation limit in mid–plane symmetric rings

We will now analyse the differential algebra (DA) approximation of the $(\hat{u}_1, \hat{n}, \hat{u}_2)$–system on the fixed Poincaré section at some θ_0 for mid–plane symmetric rings and with linear orbital motion. We assume that the reader is familiar with the basic concepts of DA [MB92, BG92, BG93, GH94, BG98a, HV99] and with the restrictions on the radius of convergence for DA normal form transformations. It is convenient to formulate this normal form transformation in a $\mathbf{SU(2)}$ representation. In particular we will show that in the case of a mid–plane symmetric ring a DA normal form transformation to the $(\hat{u}_1, \hat{n}, \hat{u}_2)$–system up to an arbitrary finite order m can be found even if the spin–orbit system is on a "resonance", in the perturbative sense of chapter 2, of the form $\nu_0 = k_x Q_x + 2k_y Q_y + k_z Q_z$ with $|k_x| + 2|k_y| + |k_z| \le m$.

We define for this paragraph $\vec{q} \equiv (Q_x, -Q_x, Q_y, -Q_y, Q_z, -Q_z)$, and the linear complex orbital normal form coordinates $\vec{\xi_i} \equiv (\xi_x^+, \xi_x^-, \xi_y^+, \xi_y^-, \xi_x^z, \xi_z^-)$, $\xi_l^+ = \sqrt{J_l}e^{i\Psi_l}$, $\xi_l^- = \sqrt{J_l}e^{-i\Psi_l}$, $J_l = \xi_l^+\xi_l^-$ which when transported once around the ring become $\vec{\xi_f} = (\xi_x^+ e^{i2\pi Q_x}, \xi_x^- e^{-i2\pi Q_x}, \ldots)$. Then the monomial $\vec{\xi}^{\vec{k}} \equiv \prod_{j=1}^6 \xi_j^{k_j}$, $\vec{k} \in \mathbb{N}^6$ fulfils the constraint $\vec{\xi}_f^{\vec{k}} = \vec{\xi}_i^{\vec{k}} e^{i2\pi\vec{k}\cdot\vec{q}}$. The $(J_l)_{l=x,y,z} = \xi_l^+\xi_l^-$ are the orbital actions. We note that $\vec{k}\cdot\vec{q} = (k_1 - k_2)Q_x + (k_3 - k_4)Q_y + (k_5 - k_6)Q_z$. Introducing $\tilde{k} \equiv (k_2, k_1, k_4, k_3, k_6, k_5)$ for every $\vec{k} \in \mathbb{N}^6$ we find that $(a_{\vec{k}}\vec{\xi}^{\vec{k}})^* = a^*_{\tilde{k}}\vec{\xi}^{\tilde{k}}$ and $\sum_{\vec{k}} a^*_{\tilde{k}}\vec{\xi}^{\vec{k}} = \sum_{\vec{k}} a^*_{\tilde{k}}\vec{\xi}^{\tilde{k}}$. In the next few paragraphs we will use the convention that x_l is a polynomial *up to* order l, that $x^{(l)}$ is a *homogeneous* polynomial of order l only and that the character e represents "even" functions in the sense that their Taylor coefficients vanish for odd $k_3 - k_4$ whereas o represents "odd" functions in the sense that their Taylor coefficients vanish for even $k_3 - k_4$. For a mid–plane symmetric ring theorem 2.10 and its corollaries and theorem 3.2 guarantee that the spin OTM in the $(\hat{l}, \hat{n}_0, \hat{m})$–system, given to m–th order in the initial phase space coordinates, has the following properties:

$$\underline{r}_m \equiv \begin{pmatrix} e_m & o_m \\ -o_m^* & e_m^* \end{pmatrix} =_0 \underline{r}_0 \equiv \begin{pmatrix} e^{-i\pi\nu_0} & 0 \\ 0 & e^{+i\pi\nu_0} \end{pmatrix} \tag{4.83a}$$

$$e_m \equiv \sum_{\substack{\vec{k}\in\mathbb{N}^6 \\ 0\le|\vec{k}|\le m}} e_{\vec{k}}\,\vec{\xi}^{\vec{k}} \quad , \quad e_{\vec{k}} = 0 \text{ if } k_3 - k_4 \text{ odd} \tag{4.83b}$$

$$o_m \equiv \sum_{\substack{\vec{k}\in\mathbb{N}^6 \\ 1\le|\vec{k}|\le m}} o_{\vec{k}}\,\vec{\xi}^{\vec{k}} \quad , \quad o_{\vec{k}} = 0 \text{ if } k_3 - k_4 \text{ even} \quad , \tag{4.83c}$$

where the real constant ν_0 is the closed orbit spin tune. We will call such a matrix an *even/odd* matrix up to order m. Note that since $q_1 = -q_2$, $q_3 = -q_4$ and $q_5 = -q_6$, there are contributions with $k_1 = k_2$, $k_3 = k_4$, $k_5 = k_6$ which do *not* contain any orbital phases. The even/odd matrices form an algebra in the sense that they build a $\mathbb{C}$–vector space which is closed under matrix multiplication. The vector space property is trivial and for the matrix product we find

$$\begin{pmatrix} e_{11} & o_{12} \\ o_{21} & e_{22} \end{pmatrix}\begin{pmatrix} e'_{11} & o'_{12} \\ o'_{21} & e'_{22} \end{pmatrix} = \begin{pmatrix} e_{11}e'_{11} + o_{12}o'_{21} & e_{11}o'_{12} + o_{12}e'_{22} \\ o_{21}e'_{11} + e_{22}o'_{21} & o_{21}o'_{12} + e_{22}e'_{22} \end{pmatrix} = \begin{pmatrix} e''_{11} & o''_{12} \\ o''_{21} & e''_{22} \end{pmatrix} \quad . \tag{4.84}$$

Our aim is to find a unitary transformation $\underline{c}$ so that

$$\underline{r}_{m;m} \equiv \underline{c}(\vec{\xi}_f)\,\underline{r}_m\,\underline{c}^\dagger(\vec{\xi}_i) =_m \begin{pmatrix} e^{-i\pi\nu_m} & 0 \\ 0 & e^{+i\pi\nu_m} \end{pmatrix} \quad , \quad \underline{c} = \bigodot_{j=1}^{m} \exp(\,\underline{t}^{(j)}) \quad , \tag{4.85}$$

where ν_m is the m–th order approximation of the amplitude dependent spin tune or at least of the pseudo spin tune $\tilde{\nu}$. The $\underline{t}^{(j)}$ are traceless anti–hermitian matrices so that the matrices $\exp(\,\underline{t}^{(j)})$ are unitary.

$$\underline{t}^{(j)} \equiv \begin{pmatrix} ig^{(j)} & iu^{(j)} \\ iu^{(j)*} & -ig^{(j)} \end{pmatrix} \quad , \quad \exp(\,\underline{t}^{(j)}) =_j (\,\underline{1} + \underline{t}^{(j)}) \tag{4.86}$$

where $g^{(j)}$ is a *real* homogeneous polynomial of order j and $u^{(j)}$ is a *complex* homogeneous polynomial of order j in $\vec{\xi}$. We will show later that the in a mid–plane symmetric ring the $g^{(j)}$ can be chosen even and the $u^{(j)}$ can be chosen odd so that $\underline{t}^{(j)}$ is even/odd and $\exp(\,\underline{t}^{(j)})$ is even/odd up to order m. Note that each $\underline{t}^{(j)}$ contributes potentially to all orders beyond j too since its exponential is involved. This is called *feed–up*. Also note that only orders up to m have to be considered since $\underline{r}_m$ is a spin map only up to order m. With this $\underline{c}$ the spinor representing the $\hat{n}$–axis is $\check{n}(\vec{\xi}) = \underline{c}^\dagger(\vec{\xi})\,\binom{1}{0}$ because

$$\underline{r}_m\,\check{n}(\vec{\xi}_i) = \underline{r}_m\,\underline{c}^\dagger(\vec{\xi}_i)\begin{pmatrix}1\\0\end{pmatrix} = \underline{c}^\dagger(\vec{\xi}_f)\,\underline{r}_{m;m}\begin{pmatrix}1\\0\end{pmatrix} = e^{-i\pi\nu_m}\,\check{n}(\vec{\xi}_f) \tag{4.87}$$

analogously to (4.39). Suppose now that the transformation has been done to $(j-1)$–th order. Then the spinor OTM in the new coordinates is

$$\underline{r}_{m;j-1} = \exp(+\underline{t}^{(j-1)})\cdots\exp(+\underline{t}^{(1)})\,\underline{r}_m\exp(-\,\underline{t}^{(1)})\cdots\exp(-\,\underline{t}^{(j-1)}) =_{j-1} \begin{pmatrix} e^{-i\pi\nu_{j-1}} & 0 \\ 0 & e^{+i\pi\nu_{j-1}} \end{pmatrix} \quad . \tag{4.88}$$

To j–th order $\underline{r}_{m;j}$ is given by

$$\underline{r}_{m;j}(\vec{\xi}_i) =_j \underline{r}_{m;j-1}(\vec{\xi}_i) + \underline{t}^{(j)}(\vec{\xi}_f)\,\underline{r}_0 - \underline{r}_0\,\underline{t}^{(j)}(\vec{\xi}_i) \quad . \tag{4.89}$$

We now have to find a $\underline{t}^{(j)}$ that eliminates as many j–th order coefficients as possible. That means

$$\begin{pmatrix} e^{-i\pi\nu_j} & 0 \\ 0 & e^{+i\pi\nu_j} \end{pmatrix} =_j$$

$$\begin{pmatrix} e'_j + ie^{-i\pi\nu_0}\left(g^{(j)}(\vec{\xi}_f) - g^{(j)}(\vec{\xi}_i)\right) & o'_j + ie^{i\pi\nu_0}\,u^{(j)}(\vec{\xi}_f) - ie^{-i\pi\nu_0}\,u^{(j)}(\vec{\xi}_i) \\ -o'^* + ie^{-i\pi\nu_0}\,u^{(j)*}(\vec{\xi}_f) - ie^{i\pi\nu_0}\,u^{(j)*}(\vec{\xi}_i) & e'^*_j - ie^{i\pi\nu_0}\left(g^{(j)}(\vec{\xi}_f) - g^{(j)}(\vec{\xi}_i)\right) \end{pmatrix} \tag{4.90}$$

where the e'_j and o'_j are the j-th order terms of $\underline{r}_{m;j}$ and include the accumulated feed–up of previous steps. Therefore the e'_j and o'_j are in general *not* identical to $e_j =_j e_m$ and $o_j =_j o_m$. If the spin–orbit system is not on a spin–orbit resonance $\nu_0 = \vec{k}\cdot\vec{q} + k_0$ then we can eliminate all the o'_j, leading to a diagonal matrix $\underline{r}_{m;j}$ up to order j. If, in addition, the orbital system is not on an orbital resonance $\vec{k}\cdot\vec{q} = k_0$ up to order j, then all phase dependent coefficients in e'_j can be eliminated leading to a ν_j that depends only on the orbital actions up to order j. This is done by choosing for all $|\vec{k}| = j$ the Taylor coefficients

$$g_{\vec{k}} = \frac{ie^{i\pi\nu_0}\,e'_{\vec{k}}}{1 - e^{i2\pi\vec{k}\cdot\vec{q}}} \quad , \quad u_{\vec{k}} = \frac{ie^{i\pi\nu_0}\,o'_{\vec{k}}}{1 - e^{i2\pi(\vec{k}\cdot\vec{q}+\nu_0)}} \quad . \tag{4.91}$$

Note that the additional ν_0 in the exponent of the denominator of the $u_{\vec{k}}$ allows to eliminate the off–diagonal terms with $k_1 = k_2$, $k_3 = k_4$ and $k_5 = k_6$. On a j–th order orbit or spin–orbit resonance certain $g_{\vec{k}}$ or $u_{\vec{k}}$ cannot be chosen in this way but can be set to zero, thereby preserving a dependence of $\underline{r}_{m;j}$ on the orbital phases.

So far we did *not* use the even/odd character of e_m/o_m. If e'_j and o'_j are even and odd respectively, i.e. their coefficients $e'_{\vec{k}}$ with $k_3 - k_4$ odd and $o'_{\vec{k}}$ with $k_3 - k_4$ even vanish identically, then on a spin–orbit resonance with $\nu_0 = k_x Q_x + 2k_y Q_y + 2k_z Q_z$ and therefore even order in Q_y the potentially dangerous off–diagonal terms $o'_{\vec{k}}$ would be zero already. Therefore setting the corresponding $u_{\vec{k}} = 0$ would *not* leave any off–diagonal parts in $\underline{r}_{m;j}$. The corresponding diagonal terms $e'_{\vec{k}}$ would in general be non–zero on these resonances but they can be eliminated if we assume that the *orbital* system is not on a resonance of order j. Thus the homogeneous polynomials $g^{(j)}$ and $u^{(j)}$ can hence be chosen to be even and odd in the same manner as e_m and o_m. Then $\underline{t}^{(j)}$, $\exp(\underline{t}^{(j)})$ and $\underline{r}_{m;j}$ are even/odd matrices up to order m since the even/odd matrices are an algebra. This means that the feed–up process does not destroy the even/odd character of the higher orders terms of $\underline{r}_{m;j}$, and thus that for all orders up to m a vanishing denominator problem at resonances of type $\nu_0 = k_x Q_x + 2k_y Q_y + k_z Q_z$ does not arise.

It is well known [BG92, BG93], and in particular independent of any even/odd assumptions on $\underline{r}_m$, that if the system is neither on an orbital nor on a spin resonance of order up to m, a DA normal form transformation into the $(\hat{u}_1, \hat{n}, \hat{u}_2)_m$ system can be performed. Nevertheless, it might be interesting to sketch the proof of Balandin and Golubeva [BG92, BG93] that the $g^{(j)}$ can be chosen real as demanded by the unitarity of $\exp(\underline{t}^{(j)})$ and at the same time eliminating the dependence of $\underline{r}_{m;j}$ on the orbital phases up to order j. By definition $\underline{r}_m$ is unitary up to order m. Assume now that

$$\underline{r}_{m;j-1} = \begin{pmatrix} e^{-i\pi\nu_{j-1}} & 0 \\ 0 & e^{+i\pi\nu_{j-1}} \end{pmatrix} + \begin{pmatrix} \sum_{i=j}^{m} e'^{(i)} & \sum_{i=j}^{m} o'^{(i)} \\ -\sum_{i=j}^{m} o'^{(i)*} & \sum_{i=j}^{m} e'^{(i)*} \end{pmatrix} \tag{4.92}$$

has been constructed to be unitary up to order m. Then the $e'^{(j)}$ fulfil the constraint

$$1 =_m \det(\underline{r}_{m;j-1}) =_j 1 + e^{-i\pi\nu_0} e'^{(j)*} + e^{+i\pi\nu_0} e'^{(j)} \tag{4.93}$$

where the $e^{\pm i\pi\nu_0}$ are the zeroth order terms in $e^{\pm i\pi\nu_{j-1}}$. Let $\vec{k}$ have $|\vec{k}| = j$, then expanding $e'^{(j)}$ and selecting the terms containing $\xi^{\vec{k}}$ and its complex conjugate we find

$$0 = e^{+i\pi\nu_0} e'_{\vec{k}} \xi^{\vec{k}} + e^{-i\pi\nu_0} (e'_{\vec{k}} \xi^{\vec{k}})^* = e^{+i\pi\nu_0} e'_{\vec{k}} \xi^{\vec{k}} + e^{-i\pi\nu_0} e'^*_{\vec{k}} \xi^{\vec{k}} \Rightarrow e^{+i\pi\nu_0} e'_{\vec{k}} + e^{-i\pi\nu_0} e'^*_{\vec{k}} = 0 \ . \tag{4.94}$$

Therefore the $g_{\vec{k}}$ from equation (4.91) can be ordered in pairs

$$\begin{aligned} g_{\vec{k}} \xi^{\vec{k}} + g_{\bar{k}} (\xi^{\vec{k}})^* &= \frac{i e^{i\pi\nu_0} e'_{\vec{k}}}{e^{i2\pi\vec{k}\cdot\vec{q}} - 1} \xi^{\vec{k}} + \frac{i e^{i\pi\nu_0} e'_{\bar{k}}}{e^{-i2\pi\vec{k}\cdot\vec{q}} - 1} (\xi^{\vec{k}})^* \\ &= i \left(\frac{e^{i\pi\nu_0} e'_{\vec{k}}}{e^{i2\pi\vec{k}\cdot\vec{q}} - 1} \xi^{\vec{k}} - \left(\frac{e^{i\pi\nu_0} e'_{\vec{k}}}{e^{i2\pi\vec{k}\cdot\vec{q}} - 1} \xi^{\vec{k}} \right)^* \right) \in \mathbb{R} \ . \end{aligned} \tag{4.95}$$

Thus the unitary of $\underline{r}_{m;j-1}$ implies that the $g^{(j)} = \sum_{|\vec{k}|=j} g_{\vec{k}} \xi^{\vec{k}}$, chosen according to (4.91), are indeed real, and hence that $\underline{t}^{(j)}$ is anti–hermitian and finally that $\underline{r}_{m;j}$ is unitary.

We summarize the results of the last paragraphs in

Theorem 4.7 *In a perfectly mid–plane symmetric ring, with possibly N_v vertical ideal spin rotators and possibly $2N_h$ ideal horizontal full snakes, the DA normal form transformation does not contain resonance denominators at $\nu_0 = k_x Q_x + 2k_y Q_y + k_z Q_z$, i.e. at spin–orbit resonances that involve an even order in Q_y.*

In chapter 2 we saw that mid–plane symmetry caused the resonance strengths ϵ_κ of even order dynamical resonances to vanish. In corollary 2 to theorem 2.10 we also saw that mid–plane symmetry led to certain evenness/oddness properties for the elements of the $\mathbf{SU(2)}$ OTM $\underline{r}$. But corollary 2 refers to general solutions of the T–BMT equation so that theorem 4.7 refers to resonances from all sources and not only dynamical resonances. Close to resonances, when the denominators become small the DA normal form transformation and therefore the $\hat{n}$–axis given by $\hat{G}(\underline{C}^{\dagger}(1,0)^{\rm T})$ become strongly varying functions of phase space. This in general implies low $P_{\rm lim}$ close to resonances. If, as in the case of an even order resonance in mid–plane symmetric rings, the resonant parts of the DA normal form transformation can simply be set to zero, then the resonance does not contribute to the phase space dependence of the $\hat{n}$–axis and does not lower $P_{\rm lim}$. But it has to be stressed that for rings *without* mid–plane symmetry, e.g. HERA–p, all orders in Q_y contribute to resonance denominators and hence affect spin motion. We have of course just found a perturbative argument why in mid–plane symmetric rings even order resonances in Q_y should not occur. A problem of this type of perturbation theory is not only its restricted radius of convergence but even worse that the resonance conditions on a torus with $\vec{J} \neq \vec{0}$ are given in terms of the on–orbit spin tune ν_0 rather than in terms of the amplitude dependent spin tune ν. In any case the perturbation theory collapses when the resonance denominators in (4.91) vanish.

We have just seen that the $\hat{n}$–axis computed with DA becomes a strongly varying function of phase space whenever ν_0 is in resonance with the orbital tunes $\nu_0 = k_0 + \vec{k}\cdot\vec{Q}$ with $\vec{k} \in \mathbb{Z}^3$, if we assume mid–plane symmetry to be broken. But heuristically we expect that when using more sophisticated approximations to the $\hat{n}$–axis, the static polarisation limit is potentially reduced rather when the coherence condition 4.27 with the amplitude dependent spin tune is fulfilled, or almost fulfilled, with sufficiently low order $\vec{k}$. Moreover there should be no vanishing resonance denominators in such an approach. For example if the resonant terms appearing in a perturbative treatment of the SRM are formally summed, one arrives at (4.78) [SM92]. Indeed we will see shortly in numerical examples that $P_{\rm lim}$ tends to have pronounced minima, in regions of the parameter space where

$$\nu(\vec{J}) \approx k_0 + \vec{k}\cdot\vec{Q} \quad , \quad \text{moderate}\,|\vec{k}| \quad , \tag{4.96}$$

and where $\vec{k}$ has to fulfil the condition $k_y = 2l+1$ in mid–plane symmetric rings. This behaviour of $P_{\rm lim}$ close to resonances can be motivated as follows: Assume that a special quasi–normal form transformation for the spin

$$\underline{\widetilde{N}}(\vec{\Psi},\theta) \equiv \left.\begin{pmatrix} \tilde{u}_{1,x} & \tilde{u}_{1,y} & \tilde{u}_{1,z} \\ \tilde{n}_x & \tilde{n}_y & \tilde{n}_z \\ \tilde{u}_{2,x} & \tilde{u}_{2,y} & \tilde{u}_{2,z} \end{pmatrix}\right|_{(\vec{\Psi},\theta)} \tag{4.97}$$

has been found which eliminates all but the closest by harmonic $\vec{k}$ in the sense that the transformed spin $\widetilde{S} \equiv \underline{\widetilde{N}}\widehat{S}$ fulfils an EOM of the type (2.150) with $\hat{x} \to \tilde{u}_1$, $\hat{y} \to \tilde{n}$, $\hat{z} \to \tilde{u}_2$ and $\nu_0 \to \tilde{\nu} \approx$ const.

$$\mathrm{D}_\theta\,\widetilde{S} = \Big(\,\tilde{\nu}\tilde{n} + \epsilon_\kappa\,\Big(\tilde{u}_1 \sin\phi_\kappa(\vec{\Psi},\theta) + \tilde{u}_2\cos\phi_\kappa(\vec{\Psi},\theta)\Big)\,\Big) \times \widetilde{S} \tag{4.98}$$

Equation (4.98) describes a SRM in the $(\tilde{u}_1,\tilde{n},\tilde{u}_2)$ system. We assume that $\tilde{\nu}$ is close to $\kappa = k_0 + \vec{k}\cdot\vec{Q}$. Furthermore we assume $\tilde{\nu}$ is sufficiently far from any resonance condition $\tilde{\nu} = k_0' + \vec{k}'\cdot\vec{Q}$ with the harmonics with $\vec{k}' \neq \vec{k}$ that have been absorbed in the quasi–normal form transformation (4.97). Therefore these harmonics do not contribute strongly to the inverse transform $\underline{N}^{\rm T}$ so that in the limit $\epsilon_\kappa \to 0$ $P_{\rm lim}$ in the $(\hat{x},\hat{y},\hat{z})$–system is a moderately varying function of the quasi spin tune $\tilde{\nu}$. In the periodic $(\tilde{u}_1,\tilde{n},\tilde{u}_2)$ system we can at least for $\partial_{\vec{\Psi}}\,\tilde{\nu} = \vec{0}$ compute the $\hat{n}$–axis , the "ϵ–dependent spin tune" and $\widetilde{P}_{\rm lim}$ measured in the $(\tilde{u}_1,\tilde{n},\tilde{u}_2)$ system

$$\nu(\epsilon_\kappa) \;=\; \mathrm{sgn}(\tilde{\nu}-\kappa)\,\sqrt{\epsilon_\kappa^2 + (\tilde{\nu}-\kappa)^2} + \kappa \tag{4.99a}$$

$$\widetilde{P}_{\rm lim} \;=\; \sqrt{1 - \left(\frac{\epsilon_\kappa}{(\nu(\epsilon_\kappa)-\kappa)}\right)^2} \quad . \tag{4.99b}$$

We see that ν jumps from $\kappa - \epsilon_\kappa$ to $\kappa + \epsilon_\kappa$ whenever we let $\tilde{\nu}$ cross κ and that $\widetilde{P}_{\rm lim}$ has a minimum $\widetilde{P}_{\rm lim} \to 0$ of characteristic width ϵ at $\tilde{\nu} = \kappa$. Therefore when transforming back to the $(\hat{x},\hat{y},\hat{z})$–system we expect to see a more or les pronounced minimum at $\tilde{\nu} = \kappa$. It is clear that when the non–resonant contribution to $\hat{n}$ has already diminished $P_{\rm lim}$ to a great extent, the dip due to the resonance cannot be very deep, in other words $P_{\rm lim}$ cannot be *less* than zero. This is of course not a strict proof since we do not know whether the transformation $\underline{\tilde{N}}$ exists but it serves as a heuristic argument for why one should expect a pronounced dip in $P_{\rm lim}$ whenever the spin–orbit system is close to a resonance in the sense of equation (4.96).

The rotation vector $\hat{r}$ of the spin OTM in the single resonance model with snakes has been analysed in great detail in [LT86, SL88, SL97] but the invariant spin field has not yet been calculated analytically to higher order for such models. Ptitsin and Shatunov [PS96] have given an expression for the $\hat{n}$–axis in linear approximation. Of course the `SPRINT` and the `SODOM-2` methods can be used to numerically compute the invariant spin field and the amplitude dependent spin tune for any model where the spin OTM can be computed in some approximation. In section 3.2.3 we have computed the one–turn quaternion for the SRM with 2 snakes. Analogously we can compute the one–turn quaternion $\bar{r}$ for any number N of point–like Siberian Snakes located at arbitrary positions $\{\theta_i \in [0, 2\pi] | i = 0, \dots N-1\}$

$$\bar{r}(\theta_0, \Psi) = \bigodot_{i=0}^{N-1} \bar{r}_{\rm srm}(\theta_{i+1}, \theta_i; \Psi + (\theta_i - \theta_0) Q_y)\ \bar{s}_i \tag{4.100}$$

where $\bar{r}_{\rm srm}$ is the spin transport quaternion of the SRM defined in equations (2.164a) to (2.164f) and $\bar{s}_i$ is an arbitrary point like spin rotator map as in definition 3.1.

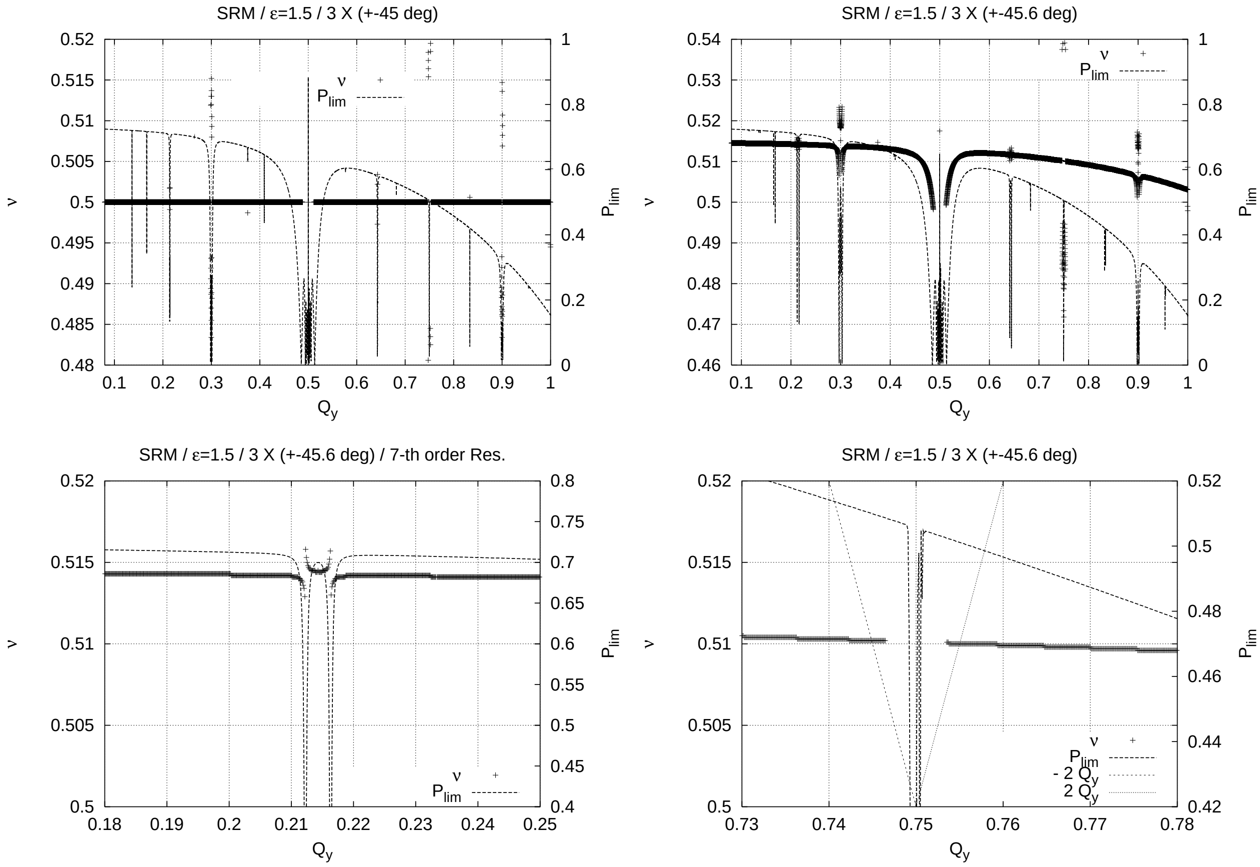

Figure 4.10: The dependence of $P_{\rm lim}$ and ν on the orbital tune Q_y in the SRM with 3 identical snake periods of 2 horizontal snakes.

We will now specialise to systems with either one or an even number $2N$ of horizontal snakes distributed uniformly over the "ring", i.e. with $\theta_{i+1} - \theta_i = {}^{\pi}/_{N}$. Moreover we will only treat the case of a highly superperiodic model with $P = 120$ which we then divide into 10, 8, 6, 4 or 2 identical periodic sections. The model system without snakes is specified to have exactly one first order intrinsic "parent" resonance at $\kappa = 120 + Q_y$. Figures 4.10 and 4.11 show various scans of the amplitude dependent spin tune (left ordinate) and static polarisation limit (right ordinate) performed with the `SODOM-2` method using `SPRINT`'s rampable optics system (`ROS`) to keep the distance $\delta \equiv \nu_0 - \kappa$ from the resonance constant while varying the tune Q_y. This is done by actually scanning the reference momentum while linearly interpolating the tune parameter between its minimum $Q_y(p_{\min}, \delta = \text{const.})$ and maximum $Q_y(p_{\max}, \delta = \text{const.})$ value. We say that a resonance is excited whenever the amplitude dependent spin tune crosses or visibly levels off and jumps over, a resonance condition defined by the line $\kappa = [kQ_y]$ and at the same time $P_{\lim}$ has a pronounced minimum. If the order of the parent resonance is odd as in our case, then the SRM can be regarded as a model of a mid–plane symmetric accelerator. If we introduce an even number of horizontal snakes this quality is *not* changed according to theorem 3.2. We therefore do *not* expect any even order resonances to show up in the tune scan. For figure 4.10 the scan was performed for the SRM with 6 snakes arranged in 3 identical snake–periods of 2 snakes and with a resonance strength of $\epsilon = 1.5$. In each snake period the snake angle ϕ was chosen to be $\pm 45°$ in the top right plot and $\pm 45.6°$ in the three other plots. The first striking result is that with $3 \times \pm 45°$ the amplitude dependent spin tune seems not to depend on Q_y at all — apart from small regions around the resonance conditions ${}^1\!/_2 = [(2l+1)Q_y]$, which happen to be low order resonance orbital resonance conditions. Moreover the spin tune in similar simulations but with different resonance strengths ϵ did not show any dependence on ϵ. We recall that close to low order orbital resonance conditions the `SODOM-2` and `SPRINT` method can become inaccurate. The vanishing of any spin tune shift

$$\Delta\nu \equiv \nu - \nu_0 = \nu - \frac{1}{2} \tag{4.101}$$

on the torus as in figure 4.10 (top left) was already proposed by Yokoya [KY88] for superperiodic rings which allow an odd number of snake periods so that in each snake period the on–orbit spin phase advance is π. As a test we can increase the snake angles to $\pm 45.6°$. Then the design orbit spin tune is 0.52 and assuming $\nu \approx \nu_0$ we expect the spin resonances $\nu = [kQ_y]$ to be separated from the orbital resonances. Figure 4.10 (top right) shows a combined scan of ν and $P_{\lim}$ for this modification. Obviously not only $\nu \neq \nu_0$ but moreover the amplitude dependent spin tune has become dependent on the system parameters, i.e. the orbital tune Q_y. We conclude that an on orbit spin phase advance of $(2l+1)\pi$ per snake period seems necessary to prevent spin tune shift even in this simple highly symmetric model. The resonances evidenced by dips in $P_{\lim}$ can be identified from left to right as 3-rd, 7-th, 5-th, and 1-st order at $Q_y = {}^1\!/_2$, then 7-th, 11-th, 9-th, 5-th and 11-th order at $Q_y \approx 0.95$. The 7-th order resonance close to $Q_y = 0.2$ and the suspicious looking drop of $P_{\lim}$ at $Q_y = 0.75$ are zoomed in figure 4.10 (bottom left and right) respectively. On the left we clearly see that due to the spin tune shift the 7-th order resonance has been split into a doublet almost symmetrically around $Q_y = {}^3\!/_{14} \approx 0.2143$. The amplitude dependent spin tune levels of at the resonance lines $\kappa = 2 - 7Q_y$ jumps across it close to $Q_y = 0.212$, levels off again at the line $\nu = 7Q_y - 1$, jumps across it approximately at $Q_y = 0.217$ and after leaving the resonant region varies only mildly with Q_y. The resonance lines $\kappa = 7Q_y - 1$ and $\kappa = 2 - 7Q_y$ are *not* drawn in order not to diminish the visibility of the functional dependence of $P_{\lim}$ and ν on Q_y. Exactly at positions of the jumps there are sharp minima of $P_{\lim}$, thus showing the behaviour close to resonances which is predicted by the heuristic model described below. Note that the spin tune behaves like a step function due to the restricted number of digits of the carried in output file. On the right side of the bottom of figure 4.10 the region around $Q_y = 0.75$ is zoomed. Obviously the amplitude dependent spin tune crosses the resonance lines $\kappa = 2 - 2Q_y$ and $\kappa = 2Q_y - 1$ without any actual signs of discontinuities or breakdown of $P_{\lim}$. Rather the numerical algorithm becomes unstable in the vicinity of $Q_y = {}^3\!/_4$. The real spin–orbit resonances did already appear in figure 4.10 (top left) but in order to distinguish them from the failures of the numerical algorithm close to orbital resonances the introduction of a small disturbance of the snake angles was needed. We conclude that the example studied shows various kinds of odd but no even order resonances. Note that these higher order resonances are *not* caused by any higher order terms in $\vec{\omega}$ since the parent resonance according to equation (2.150) was first order. We will call such higher order spin–orbit resonances **kinetic resonances** because they arise from kinetic higher order effects as explained in section 2.2.2 to distinguish them from higher order resonances already included in $\vec{\omega}$ which we will call **dynamical resonances**. Furthermore we will call the half of the symmetric spin tune jump $\epsilon_\kappa = \lim_{\tilde{\nu}\to\kappa} |\nu - \kappa|$ with $\tilde{\nu}$ from (4.98) the **kinetic resonance strength**. Additionally it should be noted here that adjusting the snake angles and thereby shifting the design orbit spin tune from 0.5 to 0.52 did *not* change the global behaviour of $P_{\rm lim}$ as a function of Q_y with the exception that the spin–orbit resonances were split into doublets.

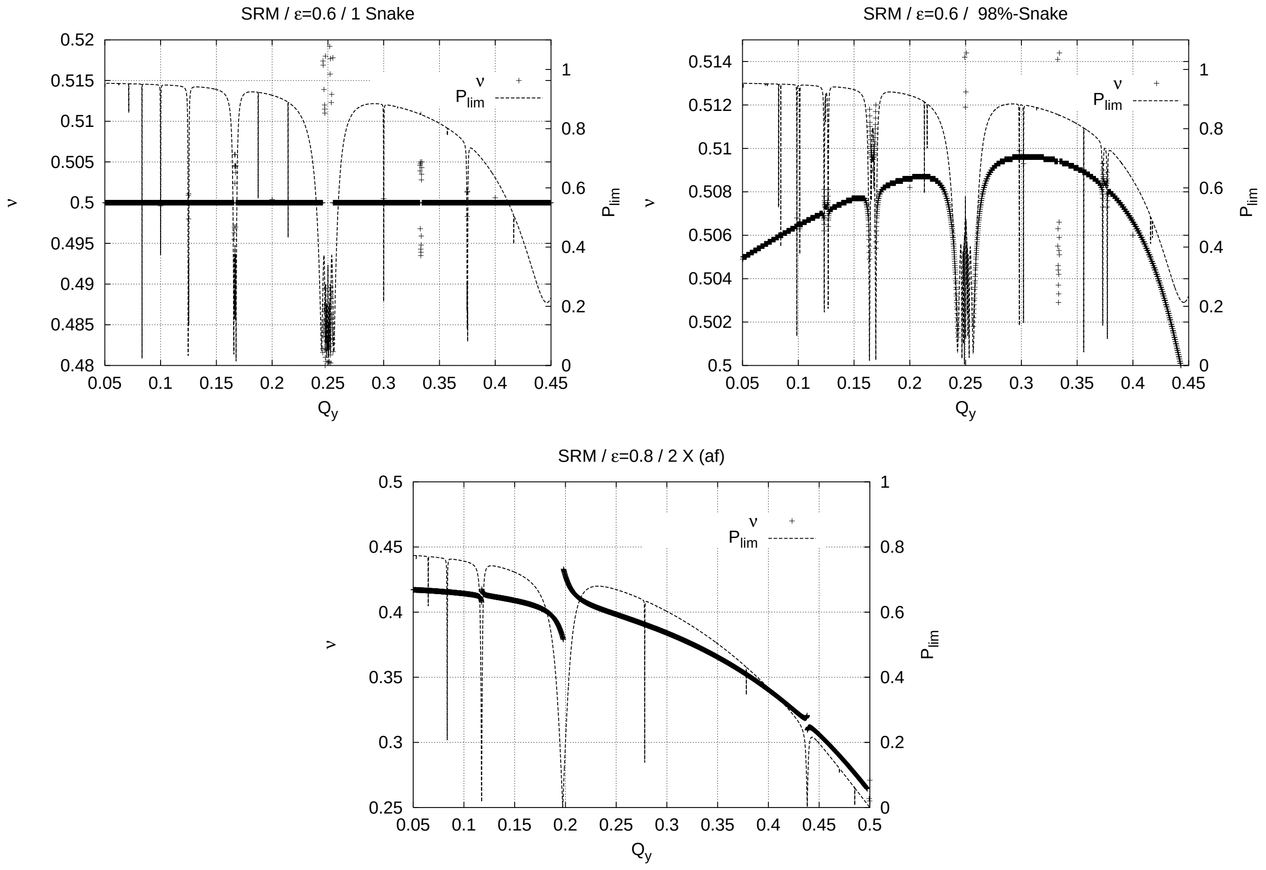

Figure 4.11: The dependence of $P_{\rm lim}$ and ν on the orbital tune Q_y in the SRM with 1 and with 4 horizontal snakes.

The plots in figure 4.11 show tune scans of ν and $P_{\rm lim}$ for the SRM with one and with 4 snakes. The top left of figure 4.11 has been computed with $\epsilon = 0.6$ and with one longitudinal *full* snake at the viewpoint whereas for the top right figure the snake rotation angle was reduced to 176°, i.e. a 98% snake was used. We note that with one Siberian Snake $\hat{n}_0$ is in the horizontal plane. With the single full snake there is obviously no spin tune shift. We therefore change the full snake to a 176° spin rotator. With this change and using equation (3.4) we find that with a spin rotator with rotation angle ψ around an arbitrary axis in the horizontal plane the on–orbit spin tune depends on ψ and on the on–orbit spin tune without snake $\delta + \kappa$ via

$$\cos\pi\nu_0 = \cos\frac{\psi}{2}\cos\pi(\delta+\kappa) \quad \Rightarrow \quad 0.49 \le \nu_0(\delta)\Big|_{\psi=176°} \le 0.51 \quad . \tag{4.102}$$

With the 98% partial snake the amplitude dependent spin tune immediately develops a slight dependence on the system parameters (here Q_y) and is in particular moved away from $^1/_2$.

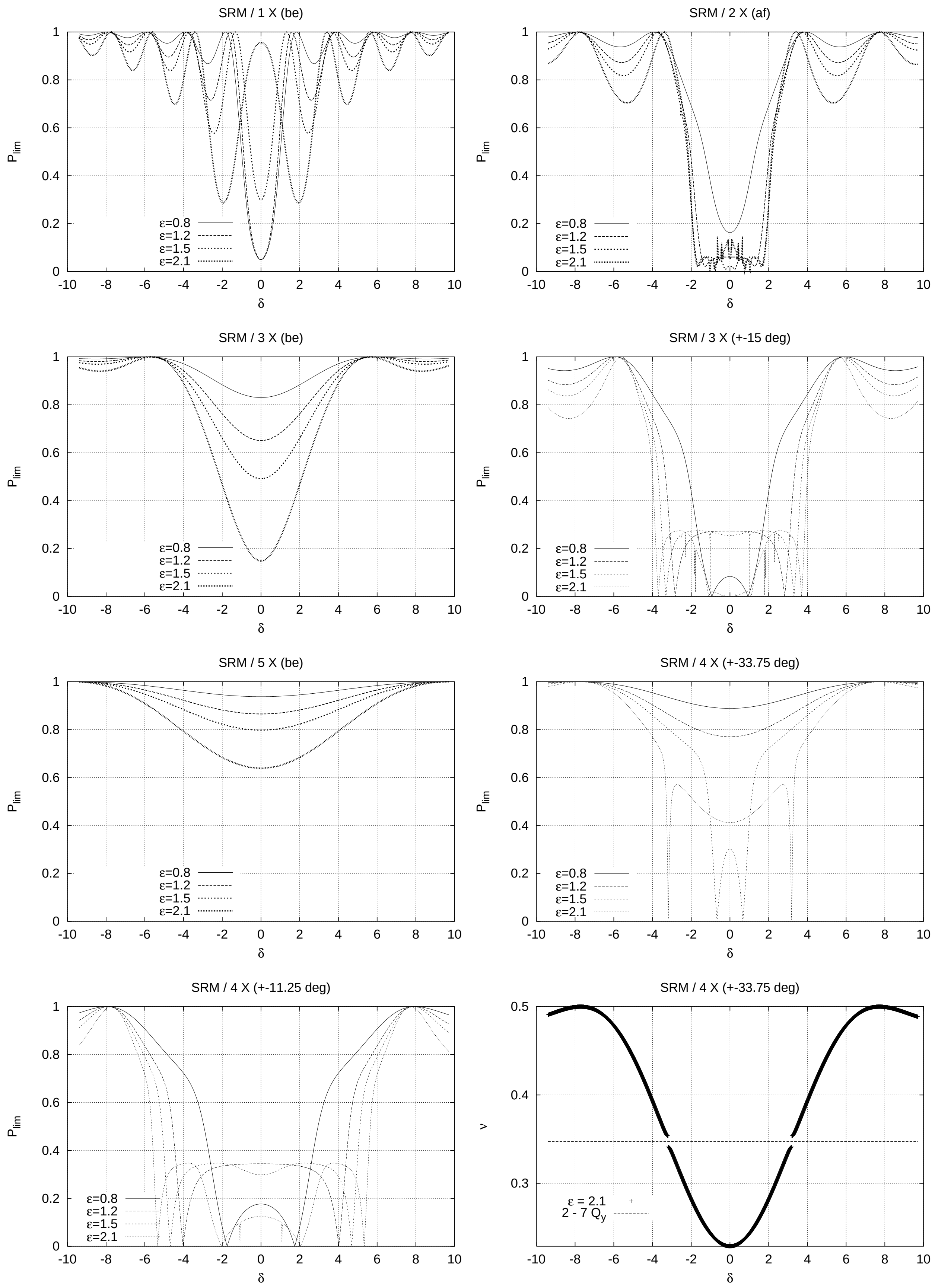

Figure 4.12: Comparison of $P_{\mathrm{lim}}(\epsilon, \delta)$ for various snake schemes in the SRM

Thus we are able to clearly identify the resonances in figure 4.11 (top right). Starting from the first resonance just below $Q_y = 0.1$ we find 6-th, 5-th, 4-th, 3-rd, 7-th order resonance doublets up to the strong 2-nd order doublet around $Q_y = 0.25$. Then from $Q_y = 0.3$ to 0.45 we find a 5-th order doublet, a numerical instability at $Q_y = 1/3$ (which cannot be a spin–orbit resonance with this spin tune) and 7-th, 4-th and 6-th order resonances. The fact that even and odd resonances appear in a model based on a mid–plane symmetric SRM and *one* horizontal snake numerically confirms that $2N_h$ horizontal snakes are necessary in order to avoid even order spin–orbit resonances in mid–plane symmetric rings. We note again that apart from the resonances of figure 4.11 (top left) being split into doublets in figure 4.11 (top right) the global functional dependence of P_{lim} on Q_y has not changed under the switch from a full to a 98% snake. Figure 4.11 (bottom) finally shows the SRM with 4 full Siberian Snakes arranged in 2 snake periods of 2 snakes with a $+22.5°$ and a $-22.5°$ snake. This arrangement has $\nu_0 = \frac{1}{2}$ but no snake scheme with an even number of snake pairs can have a spin phase advance per snake period which is equal to π, since then the on–orbit spin tune would be integral. Therefore the condition given in [KY88] for the vanishing of the second order spin tune cannot be satisfied. Correspondingly, we actually see an enormous spin tune shift varying from -0.08 at $Q_y = 0.05$ to almost 0.25 at $Q_y = 0.45$. The resonances can be identified from left to right as 9-th, 5-th or 7-th sitting on top of each other (around $Q_y = 0.12$), 5-th, 3-rd at $Q_y \approx 0.02$, 5-th, 7-th and 3-rd order just below $Q_y = 0.45$. We note that due to the enormous spin tune shift the doublets have been separated so far that they get interleaved with resonances from other doublets. Again, since the model was mid–plane symmetric with an even number of horizontal snakes, no even order resonances show up.

We will now briefly compare the dependence of P_{lim} on δ and on ϵ for the SRM with various snake schemes. In particular we will investigate the behaviour of snake schemes with an odd number of snake periods with 2 snakes each, so that we have the freedom to choose the spin phase advance per snake period to be π and simultaneously $\nu_0 = 1/2$. These schemes are called Lee–Courant schemes [LT86, SL88, SL97, EC94, EC96]. Furthermore we will investigate snake schemes in which we have either explicitly changed the spin phase advance per snake period *or* in which the number of snake periods is even so that $\nu_0 = 1/2$ disallows choosing the spin phase advance per snake period to be π. The schemes with a snake number of 4 and 8 are of particular interest for HERA–p since HERA has 4 straight sections and 4 arcs and therefore suggests a distribution of the snake positions that is compatible with this "arc–periodicity". Note that HERA is *not* superperiodic with $P = 4$ — only the distribution of the *horizontal* bends is fourfold periodic. In all of the following simulations the parameters of the parent resonance are $k_0 = 120$, $k = +1$, $Q_y = \sqrt{5} - 2 \approx 0.2360679775$ leading to $\kappa = 120.2360679775$ and resonance strengths of $\epsilon = 0.8$, 1.2, 1.5 and 2.1. Figure 4.12 shows P_{lim} for 7 such schemes (and in one case also ν), all of them fulfilling $[\nu_0] = 1/2$ and $\hat{n}_0 = \hat{y}$:

1. A scheme with 2 Siberian Snakes and snake angles of $\pm 45°$, called "1 X (be)". This is a Lee–Courant scheme and does *not* produce any spin tune shift. P_{lim} is shown in the top–most (1-st) row left.

2. A scheme with 3 snake periods of two snakes, each with snake angles of $\pm 45°$, called "3 X (be)". This is also a Lee–Courant scheme and does *not* produce any spin tune shift. P_{lim} is shown in the 2-nd row left.

3. A scheme with 5 snake periods of two snakes, each with snake angles of $\pm 45°$, called "5 X (be)". Again this is a Lee–Courant scheme and does *not* produce any spin tune shift. P_{lim} is shown in the 3-rd row left.

4. A 4–snake scheme with 2 snake periods of two snakes with snake angles of $\pm 22.5°$, called "2 X (af)", which is *not* a Lee–Courant scheme but has been suggested for HERA because it was proposed to be similarly effective. The spin phase advance per snake period is $\frac{1}{2}\pi$. P_{lim} is shown in the 1-st row right

5. A snake scheme with 3 snake periods of 2 snakes but with snake angles of $\pm 15°$, called "3 X ($\pm$15 deg)", so that the spin phase advance per snake period is $\frac{2}{3}\pi$. $P_{\rm lim}$ is shown in the 2-nd row right.

6. An 8–snake scheme with 4 snake periods and snake angles of $\pm 33.75°$, called "4 X ($\pm$33.75 deg)". The spin phase advance per snake period is $\frac{3}{4}\pi$. $P_{\rm lim}(\delta)$ shown in the 3-rd row right and additionally $\nu(\delta)$ is shown just below in the 4-th row right.

7. Another eight snake scheme with 4 snake periods and snake angles of $\pm 11.25°$, called "4 X ($\pm$11.25 deg)". The spin phase advance per snake period is $\frac{1}{4}\pi$. $P_{\rm lim}$ is shown in the 4-th row left.

Looking at the Lee–Courant schemes to the left of the first 3 rows of figure 4.12, it becomes clear that for these type of schemes a larger odd number (1,3,5) of snake periods leads to smoother dependence of $P_{\rm lim}$ on δ even for large ϵ. Since they do *not* produce any spin tune shift and the orbital tune Q_y is chosen *not* to fulfil $\frac{1}{2} = [(2l+1)Q_y]$ for any l of reasonable magnitude, the dependence of $P_{\rm lim}$ on δ is purely non–resonant. The other schemes which produce fairly big spin tune variation show resonant behaviour, i.e. sudden drops of $P_{\rm lim}$ to values close to 0 when the amplitude dependent spin tune crosses or jumps over an odd order resonance condition. As an example the spin tune is plotted for the "4 X ($\pm$33.75 deg)" scheme and for $\epsilon = 2.1$ in the 4-th row to the right. When the spin tune approaches the resonance it starts levelling off and then has a symmetric discontinuity around $\kappa = 2 - 7Q_y$ at $\delta \approx \pm 3.3$ and $P_{\rm lim}$ drops to 0 at these points. All the non–Lee–Courant type schemes show resonant effects at certain resonance strengths. It is interesting to note that with the exception of the "4 X ($\pm$33.75 deg)" scheme which can avoid resonance crossing up to $\epsilon = 1.2$, increasing the number of snakes in the non–Lee–Courant schemes hardly improves the situation — in this simple model.

In order to demonstrate that the fundamental results of theorems 2.9, 3.2 and 4.7 are not restricted to simple models like the SRM we will now discuss the amplitude dependent spin tune and $P_{\rm lim}$ in a flat model of HERA–p obtained by simply switching off the vertical bends. Figure 4.13 shows Q_y–scans of ν (left ordinate) and $P_{\rm lim}$ (right ordinate) without snakes (top left), with one snake (bottom left) and with 4 snakes. In all simulations the *unperturbed* 1996 luminosity optics without the vertical bends and therefore without flattening snakes has been used. The lattice does *not* contain any solenoids or skew elements, i.e. skew quadrupoles and vertical bends and is therefore mid–plane symmetric. All simulations have been performed with purely vertical orbit motion on an invariant ellipse that corresponds to a beam width of 2 σ. The top left scan of figure 4.13 was performed without snakes. The resonances are from left to right: a 5-th order doublet, a 3-rd order doublet and a 5-th order doublet. Then there is the big 1-st order resonance at approximately $Q_y = 0.425$ and a 3-rd order resonance at $Q_y \approx 0.475$. Figure 4.13 top right was produced with 4 snakes added. The snake scheme is the 3111 type described earlier. Again we see only odd order resonances, namely from left to right 5-th, 3-rd, 7-th (weak), 5-th and the strong 1-st order resonance at about $Q_y = 0.45$. Note that the resonances are not visibly split into doublets due to the weak spin tune shift at this particular reference momentum of 815 GeV. The region around $Q_y = 0.25$ has been zoomed in the bottom right figure, showing that the tiny dip in $P_{\rm lim}$ is not the result of a spin–orbit resonance but of the `SODOM-2` method becoming unstable close to the low order orbital resonance $Q_y = {}^1\!/_4$. The resonance lines $\kappa = 2[Q_y]$ and $\kappa = 1 - 2[Q_y]$ are crossed slightly before and after the dip which occurs exactly at $Q_y = {}^1\!/_4$. No even order resonances show up even in such a complicated lattice as the flat HERA without snakes or with an even number of horizontal snakes. Conversely, by inserting *one* horizontal snake the mid–plane symmetry is immediately destroyed. Figure 4.13 bottom left presents a scan for this case. The resonances are from left to right: 6-th, 5-th, 4-th, 3-rd, 8-th, 7-th, the strong 2-nd order resonance at $[Q_y] = 0.25$. Then 5-th, 4-th, 6-th and 8-th order resonances follow. Additionally there are numerical instabilities at $[Q_y] = {}^2\!/_5$ and ${}^1\!/_3$ neither of which fulfils the resonance condition

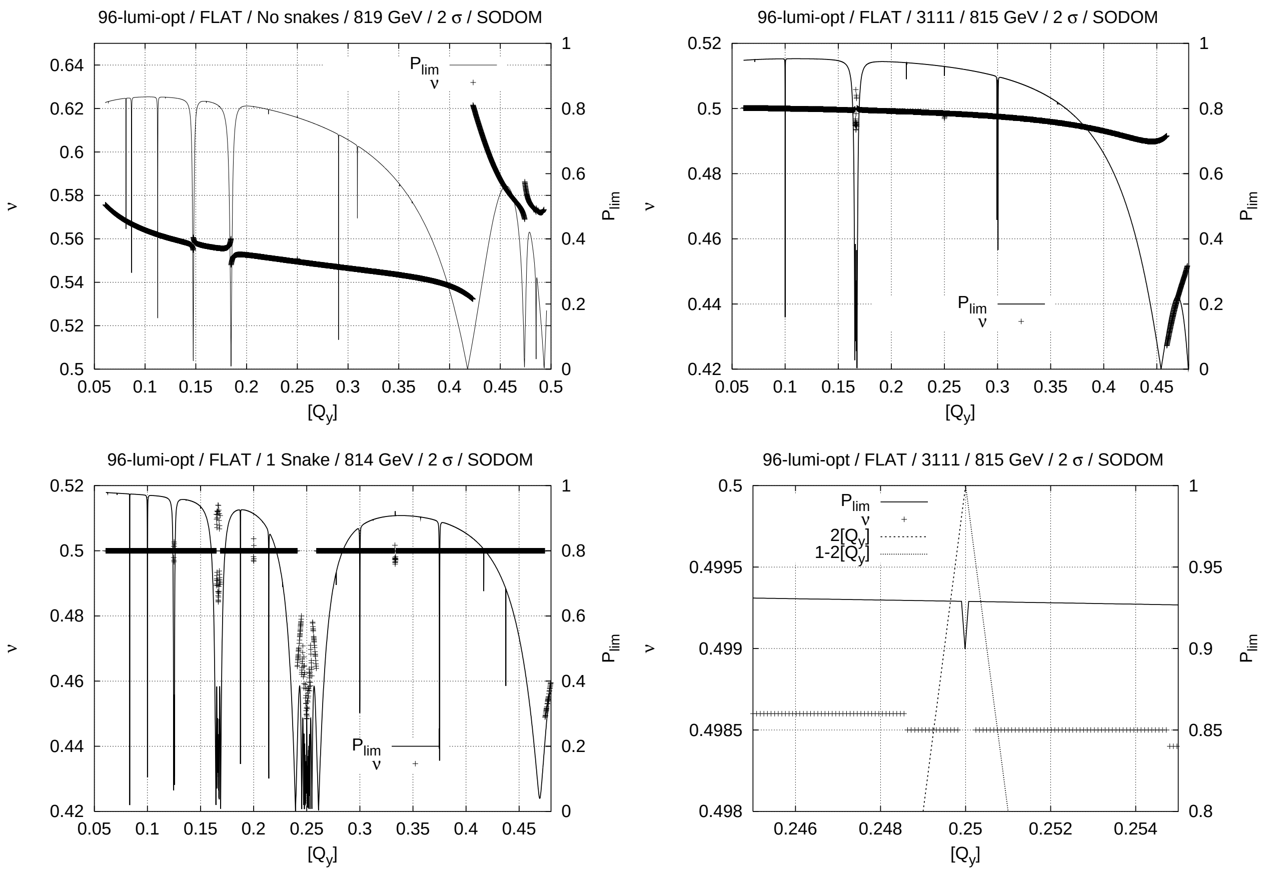

Figure 4.13: The dependence of P_{lim} and ν on the orbital tune Q_y for a *flat* model of HERA–p. Top left: No snakes. Top right and bottom right: 4 horizontal snakes. Bottom left: 1 horizontal snake.

$\nu = {}^1\!/_2 = [kQ_y]$. We note that even in this flat model of HERA no spin tune shift occurs in the case where only one snake is introduced.

We conclude that the consequences for spin motion of the perturbative argument of theorem 4.7 based on theorem 3.2, can be extended to kinetic resonances which involve the amplitude dependent spin tune in mid–plane symmetric rings. Moreover the exceptional behaviour of the OTM discussed under the heading of "snake resonances" at (3.40) can now be appreciated in a wider context.

4.9 Examples of the amplitude dependent spin tune and the static polarisation limit in HERA

The real lattice of HERA–p is not mid–plane symmetric. The interleaved vertical and horizontal bends used to bring the proton beam into the central plane of the electron machine at the beginning and the end of the East (O), South (S) and North (N) straight sections break the mid–plane symmetry. Moreover the non–periodic distribution of these beam line elements — the West (W) straight is flat — reduce the possible superperiodicity of HERA–p to $P = 1$. Note that also the Courant–Snyder functions in the straight sections are different. Inserting flattening snakes at the symmetry points of the vertical bend sections as described in section 3.1.3 cancels the spin rotation of the vertical bends only as far as spin motion on the design orbit is considered. Furthermore it does *not* restore the 4–fold "arc–periodicity" since the arc octants with a flattened vertical bend section (NL, NR, OL, OR, SL, SR) contribute less to the spin phase advance on the design orbit than those without (WL, WR). Spin motion on synchro–betatron trajectories can therefore lead to kinetic and dynamic spin–orbit resonances of all orders.

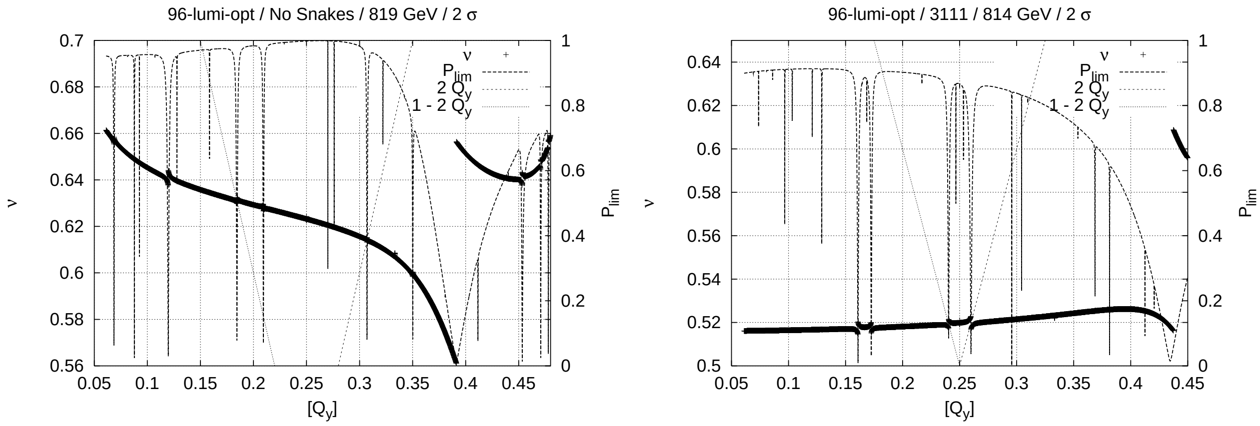

Figure 4.14: Q_y–scans of the 1996 luminosity optics. Left: without snakes. Right : with the 3111 snake scheme described in figure 4.1.

In figures 4.10, 4.11 4.13 we have seen Q_y–scans for basically mid–plane symmetric models. Figure 4.14 shows ν and $P_{\rm lim}$ as functions of $[Q_y]$ for the original 1996 HERA–p luminosity lattice. Both plots are with purely vertical motion on the 2 σ invariant ellipse. The left plot is without snakes at 819 GeV, the right plot is with 6 flattening snakes and the 3111 snake scheme. In both plots the resonance lines $\kappa_+ = 2[Q_y]$ and $\kappa_- = 1 - 2[Q_y]$ have been drawn in order to show that $P_{\rm lim}$ has isolated minima wherever ν jumps across these lines. In the left plot (without snakes) the resonances are from left to right: 5-th, 4-th, 7-th, 3-rd, a narrow 5-th order close to the 3-rd order, 4-th, the 2-nd order at the line κ_-, 3-rd, then a long range without resonances that are visible on this scale around $[Q_y] = 0.25$, followed by 6-th, 5-th, 2-nd at the line κ_+, 5-th, 4-th and the strong 1-st order resonance at $[Q_y] \approx 0.38$. After crossing the 1-st order resonance there are a 3-rd, a 5-th and a 7-th order resonance almost on the edge of the plot. We note that at all odd order resonance conditions $\kappa = [(2l+1)Q_y]$ merge at $[Q_y] = {}^1/_2$. The resonance doublets, which can be nicely identified because $\nu \approx {}^1/_2$, in the right plot (with the flattened 3111 scheme) are from left to right: 7-th and 6-th, both of them with one resonance of the doublet either very weak or almost in the middle of two tune steps, the 5-th order doublet around $[Q_y] = 0.1$, 4-th, 3-rd with a 9-th order inside, a very weak single 7-th order, the strong 2-nd order doublet with a 6-th order doublet inside around $[Q_y] = 0.25$, then a 5-th followed by a weak single 7-th, a 4-th and a 6-th directly before the strong 1-st order resonance at $[Q_y] \approx 0.43$. We conclude that in HERA–p with or without snakes odd *and* even order resonances appear and that in general even and odd resonances with similar absolute order have similar strength.

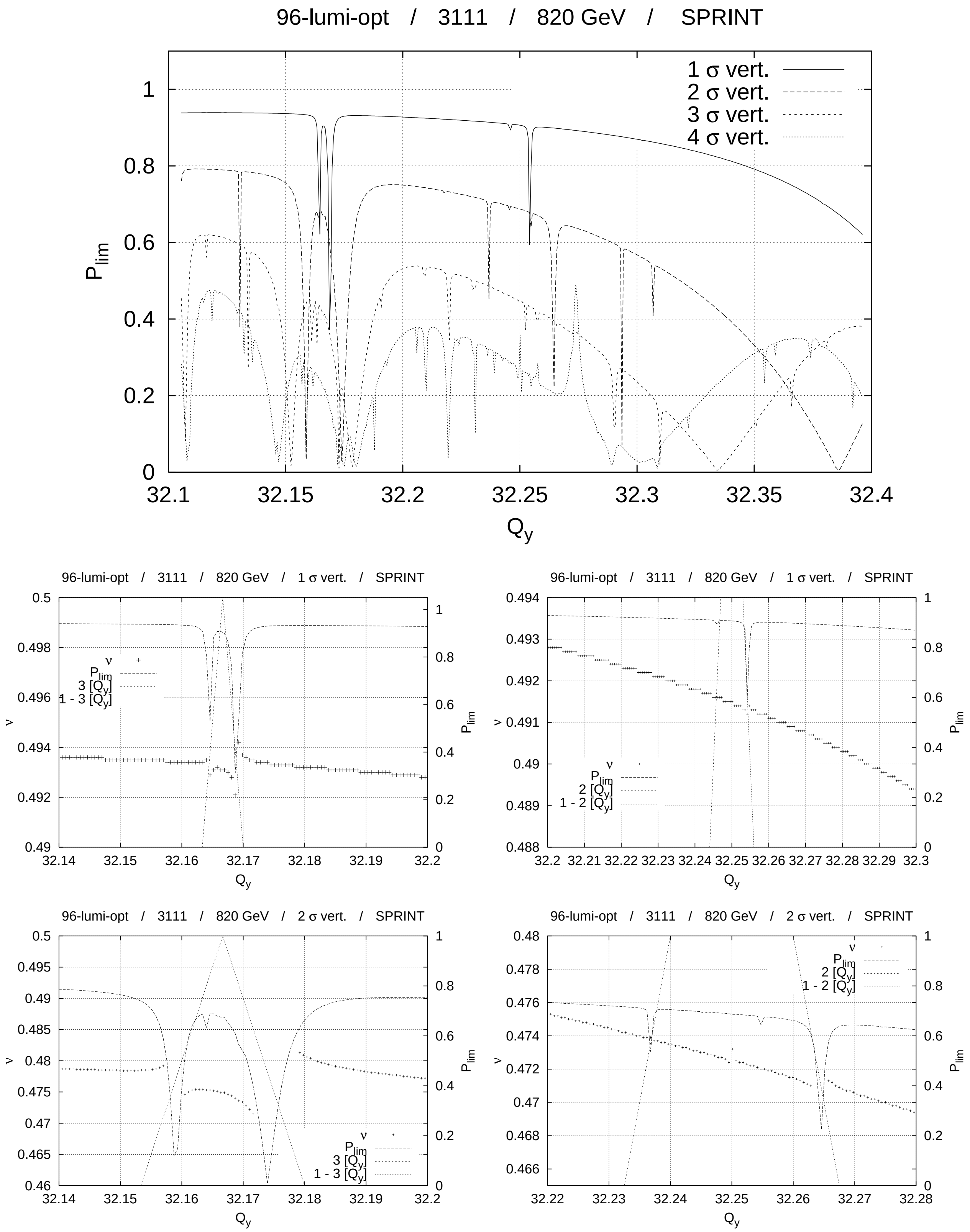

Figure 4.15: Tune scans of ν and P_{lim}. Top: P_{lim} for various invariant ellipses. Below the regions around $[Q_y] = {}^1/_6$ (left) and $[Q_y] = {}^1/_4$ (right) for the 1 (upper row) and 2 σ (lower row).

Figure 4.15 shows a tune scan with the 1996 luminosity optics, 6 flattening snakes and the 3111 scheme at a reference momentum of 820 GeV for various invariant vertical ellipses. The big plot on top shows $P_{\rm lim}(Q_y)$ for the vertical 1, 2, 3 and 4 σ ellipses. It is clearly to be seen that going outwards in phase space strongly reduces the average $P_{\rm lim}$ even off-resonance. The four small plots below show zoomed scans of ν and $P_{\rm lim}$ in the range around $[Q_y] = {}^1/_6$ (left) and $[Q_y] = {}^1/_4$ (right) for the 1 σ (upper row) and 2 σ (lower row) ellipse. In order to show the resonant behaviour of ν and $P_{\rm lim}$ the resonance lines $\kappa = 3[Q_y]$, $\kappa = 1 - 3[Q_y]$ and $\kappa = 2[Q_y]$, $\kappa = 1 - 2[Q_y]$ are drawn. At this particular energy the 2-nd order resonance is obviously weaker, i.e. less wide, than the 3-rd order resonance. Comparing the separation of the 3-rd order doublet for different ellipses demonstrates that the tune shift $\Delta\nu = \nu - \nu_0$ increases with increasing emittance.

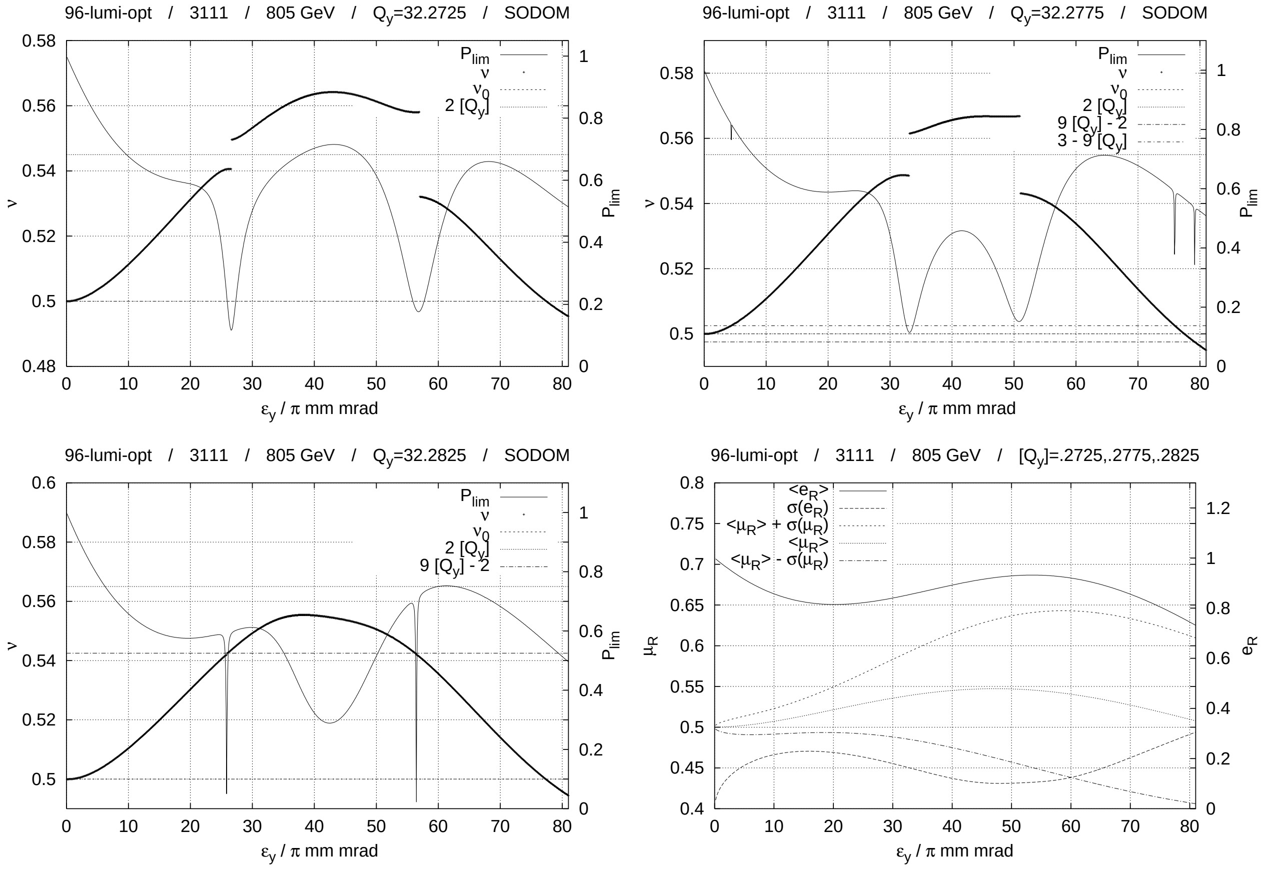

Figure 4.16: Amplitude scans of ν and $P_{\rm lim}$ at 805 GeV with $[Q_y] \approx 0.2725$ (top left), 0.2775 (top right) and 0.2825 (bottom left). For comparison the bottom right plot shows the averaged rotation vector and normalised rotation angle and their spreads.

Figure 4.16 shows ν and $P_{\rm lim}$ as functions of the orbital action J_y indicated by the normalised emittance enclosed in the invariant ellipse. Note that 81 π mm mrad correspond to approximately 4.5 σ. The reference momentum was taken to be 805 GeV and the fractional vertical tune $[Q_y]$ was chosen to be approximately 0.2725 (top left), 0.2775 (top right) and 0.2825 (bottom left). In all three plots we find on the design orbit $P_{\rm lim}(J_y = 0) = \|\frac{1}{2\pi}\int \hat{n}_0 \, d\Psi_y\| = 1$ and $\nu(J_y = 0) = \nu_0 = {}^1/_2$. Note (again) that ν is taken from the left and $P_{\rm lim}$ from the right ordinate. For comparison also the phase averages and the spreads of the rotation vector of the spin OTM $\hat{r} \equiv \hat{e}_R$ and the normalised rotation angle μ_R are shown in 4.16 (bottom right). This plot is identical for all three $[Q_y]$: 0.2725, 0.2775 and 0.2825. When increasing the enclosed normalised emittance the amplitude dependent spin tune deviates more and more from ν_0 while $P_{\rm lim}$ smoothly decreases until ν approaches the first resonance condition for the chosen orbital tune. For $[Q_y] \approx 0.2725$ (top left) the first resonance is

$\kappa_2 = 2[Q_y]$ and the spin tune starts levelling off from the resonance line until it has a discontinuity $\nu^- = \kappa_2 - \epsilon \to \nu + = \kappa_2 + \epsilon$ symmetric w.r.t. κ at about 27 π mm mrad. At the same time P_{lim} has an isolated minimum. Increasing J_y even further produces a maximum spin tune shift at about 43 π mm mrad from which ν begins returning to ν_0 for increasing ε_y. At about 58 π mm mrad ν performs another symmetric jump around κ_2 while P_{lim} has an isolated minimum. The close–by resonance $\kappa_- = 3 - 9[Q_y]$ is obviously not excited for these lattice parameters. For $[Q_y] \approx 0.2775$ (top right) the first resonance line to be crossed is κ_- which causes a narrow dip in P_{lim} at about 4 π mm mrad. Note that now κ_- is not only visibly excited but of course changed its position compared to the plot with $[Q_y] \approx 0.2725$. Due to the increased tune the first crossing of κ_2 occurs at a larger amplitude, namely 32 π mm mrad and the second, downwards, crossing occurs already earlier at 51 π mm mrad. Finally beyond 75 π mm mrad the doublet κ_- and $\kappa_+ = 9[Q_y] - 2$ is crossed. Increasing the tune even more to $Q_y \approx 0.2825$ (bottom left) not only moves the 2-nd order resonance κ_2 out of the range of the spin tune shift but shifts the crossing of κ_+ to orbital amplitudes where the resonance is stronger excited. Hence the minima of P_{lim} when ν crosses κ_+ are slightly broader. In the region between 30 and 50 π mm mrad P_{lim} has a smooth minimum as ν gets relatively close to κ_2.

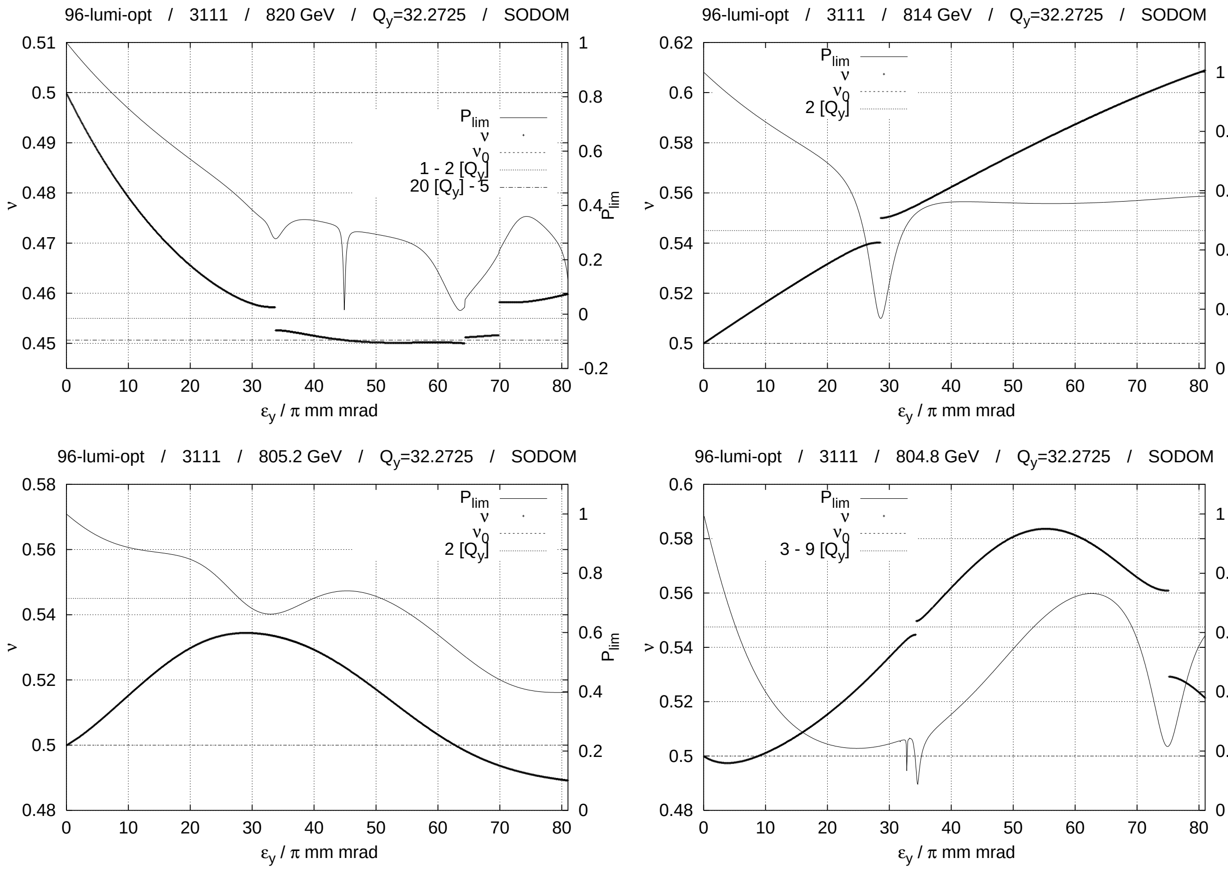

Figure 4.17: Emittance scans at various reference momenta. Top left: 820 GeV, top right: 814 GeV, bottom left: 805.2 GeV, bottom right: 804.8 GeV.

Let $\langle x \rangle = {}^1\!/_{2\pi} \int_{\mathcal{T}_1} x(\Psi_y)\, d\Psi_y$ denote the phase average of x on $\mathcal{T}_1$ defined by $J_x = J_z = 0$, $J_y =$ const. and $\hat{r}(\Psi_y)$ and $\mu_R(\Psi_y)$ be the rotation vector and the normalised rotation angle of the spin one–turn quaternion $\bar{r}(\theta_0; \vec{\Psi}) \equiv (\cos \pi\mu_R, \sin \pi\mu_R \hat{r})$. Figure 4.16 (bottom right) contains the following quantities for comparison with P_{lim} and ν:

$$\langle \hat{e}_R \rangle \equiv \|\langle \hat{r} \rangle\| \quad , \quad \sigma(\hat{e}_R) \equiv \sqrt{\langle \arccos^2(\hat{r} \cdot \langle \hat{r} \rangle) \rangle} \tag{4.103a}$$

$$\langle \mu_R \rangle \quad , \quad \sigma(\mu_R) \equiv \sqrt{\langle (\mu_R - \langle \mu_R \rangle)^2 \rangle} \quad . \tag{4.103b}$$

If $\hat{r}$ and μ_R were appropriate measures for analysing higher order resonances, then $\hat{r}$ and μ_R would show a behaviour similar to $\hat{n}$ and ν. First of all, within the resolution of 4.16 (bottom right) $\langle\hat{e}_R\rangle$, $\langle\mu_R\rangle$ and their spread parameters do not show any dependence on the chosen $[Q_y]$. Second, $\langle\hat{e}_R\rangle$ appears to be a mild function of J_y and neither $\langle\hat{e}_R\rangle$ nor $\langle\mu_R\rangle$ show any kind of resonant behaviour although $\langle\mu_R\rangle$ crosses $\kappa_\pm$ and at least for $[Q_y] \approx 0.2725$ also crosses κ_2. Note that of course in the limit $J_y \to 0$ we obtain $\hat{r} \to \hat{n} \to \hat{n}_0$ and $\langle\mu_R\rangle \to \nu \to \nu_0$ and that in the limit $Q_y \to {}^n/_m$ $\hat{n}$ approaches $\pm\hat{r}^{(m)}$ and $[m\nu]$ approaches $[\langle\mu_R^{(m)}\rangle]$ where $\hat{r}^{(m)}$ and $\mu_R^{(m)}$ are the rotation vector and the normalised rotation angle of the m–turn spin map. In addition the spreads $\sigma(\hat{e}_R)$ and $\sigma(\mu_R)$ do not show any singular behaviour at $\langle\mu_R\rangle = \kappa_{\pm,2}$. It is remarkable anyway that at least in this example the relation $\langle\mu_R\rangle - \sigma(\mu_R) < \nu < \langle\mu_R\rangle + \sigma(\mu_R)$ holds. It must be noted on the contrary that the 1 σ–interval around $\langle\mu_R\rangle$ appears to be an over–estimation of the variation of ν. We may conclude that except for trivial examples and despite the general opinion in the community, the rotation vector $\hat{r}$ and the normalised rotation angle μ_R are more or less useless quantities at *finite* orbital amplitudes and with irrational orbital tunes.

Figure 4.17 demonstrates that the functional dependence of ν and P_{lim} on J_y is not the same for different energies. The orbit tune in all plots is $[Q_y] \approx 0.2725$. Figure 4.17 (top left) which was obtained at 820 GeV shows in addition to the 2-nd order resonance a 20-th (!) order resonance which has non–negligible strength. We note that resonances κ do not necessarily have to be noticeably excited, i.e. ϵ_κ can be so small that with the chosen step size for scanning, the spin tune jump as well as the drop of P_{lim} are hidden in between two adjacent steps. We also note that although asymptotically the resonance strengths have to decay with increasing order TO allow the existence of an $\hat{n}$–axis and an amplitude dependent spin tune , there is no reason why already for finite order the should decay monotonically. To the right, at 814 GeV, P_{lim} stays almost constant after crossing the 2-nd order resonance. The two plots at the bottom of figure 4.17 demonstrate in comparison with figure 4.16 (top left) the potentially strong dependence of ν and P_{lim} on the reference momentum. All three simulations are just separated by 200 MeV in reference momentum, namely the were performed at 805.2 (4.17 bottom left), 805.0 (4.16 top left) and 804.8 GeV (4.17 bottom right). In spite of this closeness in energy ν and P_{lim} show totally different behaviour. Also, among the close–by resonance lines κ_2 and κ_- always at most one is visibly excited.

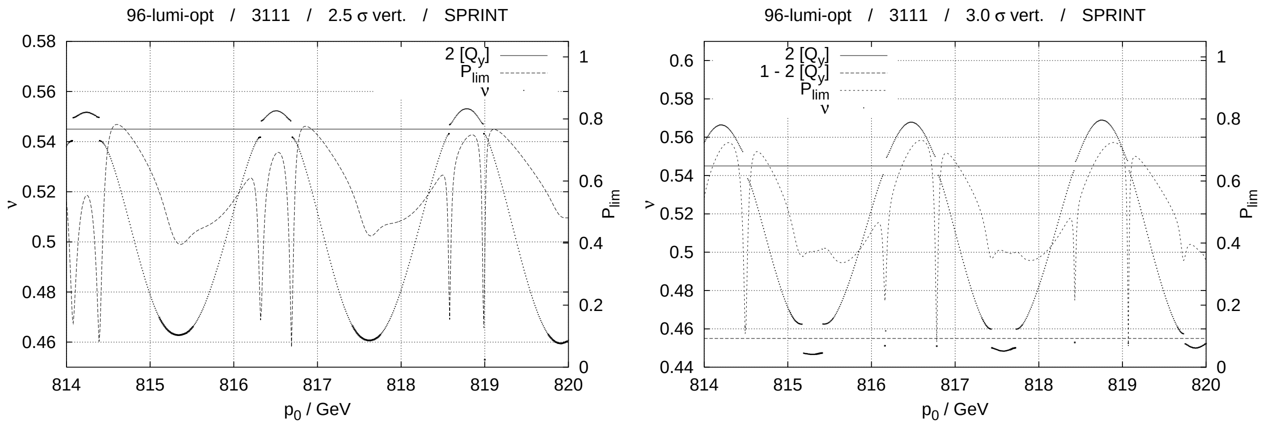

Figure 4.18: Momentum scans of ν and P_{lim} for the 1996 luminosity optics with 6 flattening snakes and the 3111 scheme on invariant ellipses corresponding to 2.5 (left) and 3.0 σ (right) vertical beam width. The vertical tune is approximately 32.2725.

Figure 4.18 shows scans of ν and P_{lim} w.r.t. the reference momentum p_0 between 814 and 820 GeV for 2.5 (left) and 3 σ (right) vertical motion. The vertical tune was chosen to be $Q_y \approx 32.2725$. In this limited momentum region ($\Delta p_0 = 6$ GeV) ν as well as P_{lim} appear to be almost periodic in p_0 with a period of about 2.2 GeV. This approximate periodicity can be explained in the following way: The spin tune on the design orbit for the *flattened* lattice *without* main snakes is not equal to $\nu_0^{\rm flat} = G\gamma$ but, according to the modifications to theorem 3.1 induced by flattening as explained in definition 3.2, $\nu_0^{\rm flttd} \equiv G\gamma(1 - {}^{\Theta_{\rm comp}}/_{2\pi})$. In HERA the proposed 6 flattening snakes would compensate about 362.496 mrad of the total horizontal bend angle of 2π per revolution. Therefore the on–orbit spin tune is increased by an integer every 555 MeV instead of the 523 MeV of a flat ring. When we now add the 4 main snakes the spin tune on the design orbit becomes $^1/_2$ but the spin phase advance in between snakes is, neglecting the asymmetry of HERA with flattening snakes, approximately $^\pi/_2\nu_0^{\rm flttd}$, increasing by an integer every 2.22 GeV. We assume the dominant contribution to $P_{\rm lim}$ and ν to be induced by the almost periodically repeating structure "arc, straight section, snake". Therefore in regions where no extraordinary strong linear intrinsic resonances perturb the spin motion rather locally we may expect ν and $P_{\rm lim}$ to be almost periodic in $E_0 \approx p_0$ with period about 2.2 GeV. In figure 4.18 (left) on the 2.5 σ invariant ellipse the spin tune crosses the resonance line $\kappa_{+2} \equiv 2[Q_y]$ at 6 different momenta. In each case $P_{\rm lim}$ has a sharp isolated minimum. Because of the approximately sinusoidal dependence on p_0 and because the distance $\kappa_{+2} - \nu_0$ is of the order of the spin tune variation, the resonance crossings appear in close–by pairs in which both resonances have a similar strength. We note that when kinetic resonances are crossed along a variation of the momentum they are normally crossed in close–by pairs which are probably related in strength — provided the resonances are sufficiently far away from ν_0 compared to the average of $|\Delta\nu|$ w.r.t. p_0. The variation of the spin tune with energy is obviously *not* symmetric w.r.t. ν_0 and therefore the resonance line $\kappa_{-2} \equiv 1 - 2[Q_y]$ is *not* crossed although it has exactly the same distance to $\nu_0 = {}^1/_2$. Nevertheless $P_{\rm lim}$ goes through a smooth minimum when ν gets close to κ_{-2}. In figure 4.18 (right) the vertical amplitude has been increased to 3 σ and the spin tune

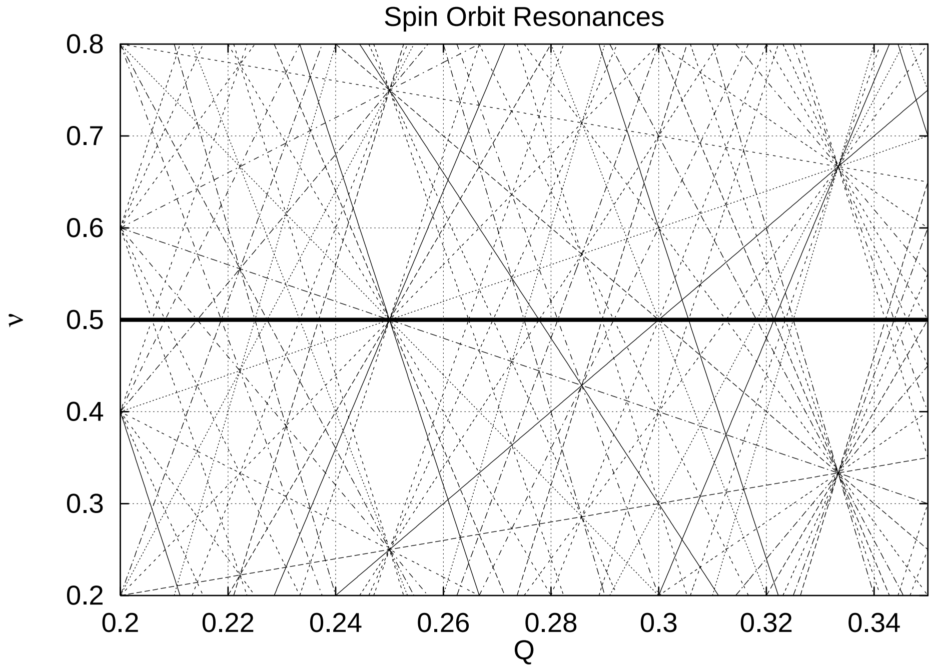

Figure 4.19: The possible spin–orbit resonance lines up to 20-th order.

shift at some momenta has sufficiently increased to let ν cross the resonance line κ_{-2} also. Moreover the pairs of adjacent crossings of κ_{+2} are separated by a larger momentum range. We note that the minima of $P_{\rm lim}$ at resonance crossing are more pronounced when the non–resonant contribution to the diminution of $P_{\rm lim}$ is small, i.e. at the crossings of κ_{+2}, than when the non–resonant contribution to the diminution of $P_{\rm lim}$ is already high, i.e. at the crossings of κ_{-2}. When arguing for the existence of kinetic resonances in section 4.8 we expected that when the minima of $\widetilde{P}_{\rm lim}$ as defined in equation

Order n	$Q_m^{(n)} \equiv {}^{2m+1}/_{2n}$ with $Q_m^{(n)} \leq {}^1/_2$										$Q_1^{(n)}$ (8 dig.)
1	$^1/_2$										.5
2	$^1/_4$										.25
3	$^1/_6$	$(^1/_2)$									.16666667
4	$^1/_8$	$^3/_8$									.125
5	$^1/_{10}$	$^3/_{10}$	$(^1/_2)$								.1
6	$^1/_{12}$	$(^1/_4)$	$^5/_{12}$								.08333333
7	$^1/_{14}$	$^3/_{14}$	$^5/_{14}$	$(^1/_2)$							.07142857
8	$^1/_{16}$	$^3/_{16}$	$^5/_{16}$	$^7/_{16}$							.0625
9	$^1/_{18}$	$(^1/_6)$	$^5/_{18}$	$^7/_{18}$	$(^1/_2)$						.05555556
10	$^1/_{20}$	$^3/_{20}$	$(^1/_4)$	$^7/_{20}$	$^9/_{20}$						.05
11	$^1/_{22}$	$^3/_{22}$	$^5/_{22}$	$^7/_{22}$	$^9/_{22}$	$(^1/_2)$					.04545455
12	$^1/_{24}$	$(^1/_8)$	$^5/_{24}$	$^7/_{24}$	$(^3/_8)$	$^{11}/_{24}$					.04166667
13	$^1/_{26}$	$^3/_{26}$	$^5/_{26}$	$^7/_{26}$	$^9/_{26}$	$^{11}/_{26}$	$(^1/_2)$				.03846153
14	$^1/_{28}$	$^3/_{28}$	$^5/_{28}$	$(^1/_4)$	$^9/_{28}$	$^{11}/_{28}$	$^{13}/_{28}$				.03571428
15	$^1/_{30}$	$(^1/_{10})$	$(^1/_6)$	$^7/_{30}$	$(^3/_{10})$	$^{11}/_{30}$	$^{13}/_{30}$	$(^1/_2)$			.03333333
16	$^1/_{32}$	$^3/_{32}$	$^5/_{32}$	$^7/_{32}$	$^9/_{32}$	$^{11}/_{32}$	$^{13}/_{32}$	$^{15}/_{32}$			.03125
17	$^1/_{34}$	$^3/_{34}$	$^5/_{34}$	$^7/_{34}$	$^9/_{34}$	$^{11}/_{34}$	$^{13}/_{34}$	$^{15}/_{34}$	$(^1/_2)$		.02941177
18	$^1/_{36}$	$(^1/_{12})$	$^5/_{36}$	$^7/_{36}$	$(^1/_4)$	$^{11}/_{36}$	$^{13}/_{36}$	$(^5/_{12})$	$^{17}/_{36}$		.02777778
19	$^1/_{38}$	$^3/_{38}$	$^5/_{38}$	$^7/_{38}$	$^9/_{38}$	$^{11}/_{38}$	$^{13}/_{38}$	$^{15}/_{38}$	$^{17}/_{38}$	$(^1/_2)$	.02631579
20	$^1/_{40}$	$^3/_{40}$	$(^1/_8)$	$^7/_{40}$	$^9/_{40}$	$^{11}/_{40}$	$^{13}/_{40}$	$(^3/_8)$	$^{17}/_{40}$	$^{19}/_{40}$	.025
m :	0	1	2	3	4	5	6	7	8	9	

Table 4.1: The classical odd and even order snake resonances $n\,Q_m^{(n)} = {}^1/_2 + m,\ m, n \in \mathbb{Z}^+,\ n \neq 0$ up to 20-th order (n) and with $Q_m^{(n)} \leq {}^1/_2$, i.e. $0 \leq 2m+1 \leq n$. Those resonant tunes which are identical to *lower* order resonant tunes are in parenthesis.

(4.99b) are transformed back to the lab–frame they might get partially washed out whenever the non–resonant contribution to the invariant spin field already has a large spread.

Figure 4.19 shows all spin–orbit resonance conditions with a single orbit tune Q and up to 20-th order in the rectangle defined by $0.2 \leq Q \leq 0.35$ and $0.2 \leq \nu \leq 0.8$. When the spin tune on the design orbit is $^1/_2$, e.g. with properly placed and chosen snakes, then all resonance lines are symmetrically distributed w.r.t. ν_0. Whenever a resonance line crosses $^1/_2$, the orbit tune is said to be on a *classical snake resonance* or simply to be *snake–resonant*. We recall that in mid–plane symmetric rings with an even number of horizontal snakes only odd order snake resonances in Q_y have to be taken into account. Even if the spin tune shift on some tori is large, as long as no coherent orbital modes are excited the majority of particles is concentrated around the closed orbit. We have seen in figures 4.16 and 4.17 that the spin tune ν approaches ν_0 smoothly when J approaches 0 and when there are no spin–orbit resonances to be crossed on its way. When there is a resonance of finite strength close to $J = 0$ then P_{lim} will be significantly reduced in some small neighbourhood of the closed orbit. Therefore if the closed orbit spin tune is in resonance or close to being in resonance with the orbital tunes, a large fraction of the particles of the beam contributes essentially nothing to the beam polarisation and hence the beam average of the polarisation is low. Moderate order snake–resonant orbit tunes are therefore *not* recommended for acceleration and storage. Table 4.1 shows the classical odd and even order snake resonant tunes up to 20-th order. Those tunes which happen to be identical with a *lower* order snake resonance are in parenthesis. Note that *all* odd orders contain $Q_l^{(2l+1)} = {}^1/_2$.

4.10 The acceleration process

So far we have only treated spin motion with *constant* parameters in the T–BMT equation such as the Lorentz–γ of the synchronous particle γ_0, the orbital actions $\vec{J}$ and various parameters of the accelerator lattice, e.g. the tunes $\vec{Q}$. We have found that when the parameters are kept constant and the invariant spin field exists, the spin action $I \equiv \widehat{S} \cdot \hat{n}$ is an invariant of motion. Furthermore we have seen that under certain circumstances the periodic $(\vec{\Psi}, \vec{J})$ dependent coordinate system $(\hat{u}_1, \hat{n}, \hat{u}_2)$ exists so that one an define an action–angle pair (I, Φ) for spin motion. But if we assume that the parameters are changed continuously (e.g. with time) on a curve in the parameter space so that for each point on this curve the vectors $\hat{u}_1$, $\hat{n}$ and $\hat{u}_2$ stay defined, it can in general not be guaranteed that the spin action I is preserved. The reason for this is that for constant parameters the precession vector $\vec{\Omega}$ of the T–BMT equation is periodic with θ whereas for explicitly time dependent parameters it is in general not. The spin obeys the T–BMT equation whether the latter is periodic or not, but the $(\hat{u}_1, \hat{n}, \hat{u}_2)$–system is only defined for periodic $\vec{\Omega}$.

The acceleration process is of particular interest since a spin ensemble prepared to be (almost) completely aligned to the invariant spin field at injection at low energy has to be accelerated (ramped) to the working energy. We will often use the word ramp instead of acceleration to indicate that together with the reference γ_0 other lattice parameters can be changed also.

4.10.1 The Froissart–Stora formula

If in the SRM described in section 2.4 and 4.7 the design orbit spin tune ν_0 is set to $G\gamma_0$ and γ_0 is varied with time, then an acceleration process can be simulated. In this model the rate of change of ν_0 is usually chosen to be constant, with $\nu_0(\theta) = \kappa + \alpha\theta$ so that a single resonance at κ with strength ϵ_κ is crossed at $\theta = 0$. Then the ratio $\frac{\langle \widehat{S}(\theta_f = +\infty) \cdot \hat{n}_0 \rangle_\Psi}{\langle \widehat{S}(\theta_i = -\infty) \cdot \hat{n}_0 \rangle_\Psi}$ has been calculated by Froissart and Stora [FS60, CR80, SL97] to be

$$\frac{\langle \widehat{S}(\theta_f = +\infty) \cdot \hat{n}_0 \rangle_\Psi}{\langle \widehat{S}(\theta_i = -\infty) \cdot \hat{n}_0 \rangle_\Psi} = 2e^{-(\frac{\pi}{2}\epsilon^2/\alpha)} - 1 \ . \tag{4.104}$$

We note that for $\delta \equiv \nu_0 - \kappa \to \pm\infty$ the $\hat{n}$–axis coincides with $\hat{n}_0$ and hence $\langle \widehat{S} \cdot \hat{n}_0(\theta_i = +\infty) \rangle_\Psi$ can be interpreted as $P_{\rm dyn}$ on the torus whose actions correspond to the resonance strength ϵ. For $\epsilon^2 \ll \alpha$ and $\epsilon^2 \gg \alpha$ the ratio in (4.104) is ≈ 1 and ≈ -1 respectively. In the first case the $\hat{n}$–axis tilts away from $\hat{n}_0$ into the horizontal plane *and back* so quickly compared to the rate of precession of the spin that the spin hardly sees any change of the $\hat{n}$–axis in one precession. In the second case the $\hat{n}$–axis moves so slowly that at any intermediate time the spin will precess around it many times before the tilt of the $\hat{n}$–axis has significantly changed. Hence the small changes in $\vec{S}_\perp$ will almost average away and the projection $\widehat{S} \cdot \hat{n}$ will hardly change. Some care has to be taken about the discontinuous change of $\hat{n}$ at $\delta = 0$ which was introduced in equation (4.78) in order to ensure $\lim_{\epsilon \to 0} \hat{n} \cdot \hat{n}_0 = +1$ independently of δ. If the acceleration is slow enough spins will follow the continuous function $\text{sgn}(\delta)\,\hat{n}$ and hence slowly tilt over to $-\hat{n}_0$ at $\theta_f = +\infty$. We will treat adiabatic acceleration in more detail later. In *all* other cases polarisation will be lost to some extent. This behaviour has been observed in many *low energy* accelerators and therefore the model is quite popular and well understood. Unfortunately at high energy, resonance strengths are increased due to the higher fields needed to focus the beam, and as ϵ becomes larger the region in δ over which the resonance strongly influences the spin motion becomes larger too. The single resonance model is based on the assumptions that the resonances are isolated. At high energy this is no longer true.

4.10.2 An equation for the spin action

In this section we will derive a formula for the spin motion in the $(\hat{u}_1, \hat{n}, \hat{u}_2)$–system introduced in section 4.1. Let

$$\mathrm{D}_\theta \widehat{S} = \underline{\Omega}\widehat{S} \ , \quad \underline{\Omega}^{\mathrm{T}} = -\underline{\Omega} \ , \quad \underline{\Omega} = \underline{\Omega}(\vec{\Psi}, \theta, \lambda) \tag{4.105}$$

be a T–BMT equation and $\underline{\Omega}$ be a lattice field for constant $\lambda \in \mathcal{A}$. The symbol λ represents some one–dimensional parametrisation $\lambda(t)$ of the free parameters of the T–BMT equation so that $\lambda(\mathbb{R})$ is a continuous curve in the parameter space $\mathcal{A}$. We will later see explicit numerical examples in which λ is the reference γ_0, the vertical orbital action J_y or the focusing strength of a certain group of quadrupoles in the lattice.

We assume that as in (2.17) for all constant $\lambda_0 \in \lambda(\mathbb{R})$ the spin normal form transformation

$$\underline{N}(\vec{\Psi}, \theta, \lambda) \equiv \left.\begin{pmatrix} u_{1,x} & u_{1,y} & u_{1,z} \\ n_x & n_y & n_z \\ u_{2,x} & u_{2,y} & u_{2,z} \end{pmatrix}\right|_{(\vec{\Psi},\theta,\lambda)} \tag{4.106}$$

exists, so that the EOM for the coordinate vector $\widehat{S}' \equiv \underline{N}\widehat{S} = (\hat{u}_1 \cdot \widehat{S}, \hat{n} \cdot \widehat{S}, \hat{u}_2 \cdot \widehat{S})^{\mathrm{T}}$ at constant λ is

$$\begin{aligned} \mathrm{D}_\theta \widehat{S}' &= \left((\partial_\theta \underline{N} + \sum_{i=x,y,z} Q_i \partial_{\Psi_i} \underline{N}) \underline{N}^{\mathrm{T}} + \underline{N}\,\underline{\Omega}\,\underline{N}^{\mathrm{T}} \right) \widehat{S}' \\ &= \begin{pmatrix} 0 & 0 & \nu(\lambda) \\ 0 & 0 & 0 \\ -\nu(\lambda) & 0 & 0 \end{pmatrix} \widehat{S}' \equiv \underline{\widetilde{\Omega}}\,\widehat{S}' \quad . \end{aligned} \tag{4.107}$$

Then the solution of the equations of motion in the $(\hat{u}_1, \hat{n}, \hat{u}_2)$–system for constant λ parametrised via the action–angle coordinates I and $\Phi(\theta) = \Phi_0 + \nu\theta$ is $\widehat{S}'(\theta; I, \Phi_0) = (\sqrt{1-I^2}\cos\Phi, I, -\sqrt{1-I^2}\sin\Phi)^{\mathrm{T}}$. We note again that these action–angle coordinates define a chart of $\mathcal{S}_{\mathbb{R}}$ which is singular at $I = \pm 1$.

Now we furthermore assume that $\underline{N}$ is continuously partially differentiable w.r.t. λ and that we are given a continuously differentiable parametrisation $\lambda(\theta)$ with $\mathrm{D}_\theta \lambda = \alpha(\theta)$. Then the equations of motion become

$$\begin{aligned} \mathrm{D}_\theta \widehat{S}' &= \left((\partial_\theta \underline{N} + \sum_{i=x,y,z} Q_i \partial_{\Psi_i} \underline{N} + \alpha \partial_\lambda \underline{N}) \underline{N}^{\mathrm{T}} + \underline{N}\,\underline{\Omega}\,\underline{N}^{\mathrm{T}} \right) \widehat{S}' \\ &\equiv (\underline{\widetilde{\Omega}} + \underline{\eta})\,\widehat{S}' \quad , \end{aligned} \tag{4.108}$$

with the anti–symmetric matrix

$$\underline{\eta}(\vec{\Psi}, \theta, \lambda) \equiv \alpha(\theta) \left.\begin{pmatrix} 0 & -\hat{u}_1 \cdot \partial_\lambda \hat{n} & \hat{u}_2 \cdot \partial_\lambda \hat{u}_1 \\ \hat{u}_1 \cdot \partial_\lambda \hat{n} & 0 & -\hat{n} \cdot \partial_\lambda \hat{u}_2 \\ -\hat{u}_2 \cdot \partial_\lambda \hat{u}_1 & \hat{n} \cdot \partial_\lambda \hat{u}_2 & 0 \end{pmatrix}\right|_{(\vec{\Psi},\theta,\lambda(\theta))} \tag{4.109}$$

Note that since $(\hat{u}_1, \hat{n}, \hat{u}_2)$ is an orthonormal basis it may only be changed by a rotation of the base vectors around the same rotation vector, namely $\vec{\eta} \equiv (\hat{n} \cdot \partial_\lambda \hat{u}_2, \hat{u}_2 \cdot \partial_\lambda \hat{u}_1, \hat{u}_1 \cdot \partial_\lambda \hat{n})$. The vector $\vec{\eta}$ can be given in coordinate independent form [GH99b]

$$\vec{\eta} = \frac{1}{2}(\hat{u}_1 \times \partial_\lambda \hat{u}_1 + \hat{n} \times \partial_\lambda \hat{n} + \hat{u}_2 \times \partial_\lambda \hat{u}_2) \quad . \tag{4.110}$$

By direct substitution one finds

$$\mathrm{D}_\theta I = \alpha\sqrt{1-I^2}(\eta_2\cos\Phi - \eta_1\sin\Phi) \equiv \alpha f_I(\vec{J}, I, \lambda; \vec{\Psi}, \Phi, \tilde{\theta}) \tag{4.111a}$$

$$\mathrm{D}_\theta \Phi = \nu + \alpha\left(\eta_2 + \frac{I}{\sqrt{1-I^2}}(\eta_2\sin\Phi + \eta_1\cos\Phi)\right) \equiv \nu + \alpha g_\Phi(\vec{J}, I, \lambda; \vec{\Psi}, \Phi, \tilde{\theta}) \quad . \tag{4.111b}$$

This coupled set of equations is obviously singular at $I = \pm 1$ so we must restrict the motion to the subset of $\mathcal{S}_{\mathbb{R}}$ with $1 - I^2 > \delta$, $\delta > 0$. A similar set of equations was derived by Yokoya [KY88] by perturbation theory and an asymptotic solution is given in the limit of slowly varying I. Hoffstaetter has shown [GH99b] that in the system

$$\mathrm{D}_\theta \begin{pmatrix} \vec{J} \\ I \\ \lambda \\ \vec{\Psi} \\ \Phi \\ \tilde{\theta} \end{pmatrix} = \begin{pmatrix} 0 \\ 0 \\ 0 \\ \vec{Q}(\vec{J},\lambda) \\ \nu(\vec{J},\lambda) \\ 1 \end{pmatrix} + \alpha \begin{pmatrix} \vec{f}_{\vec{J}}(\vec{J},\lambda;\vec{\Psi},\tilde{\theta}) \\ f_I(\vec{J},I,\lambda;\vec{\Psi},\Phi,\tilde{\theta}) \\ 1 \\ \vec{g}_{\vec{\Psi}}(\vec{J},\lambda;\vec{\Psi},\tilde{\theta}) \\ g_\Phi(\vec{J},I,\lambda;\vec{\Psi},\Phi,\tilde{\theta}) \\ 0 \end{pmatrix} \tag{4.112}$$

with $\vec{f}_{\vec{J}}$ and $\vec{g}_{\vec{\Psi}}$ being the perturbations in $\vec{J}$ and $\vec{\Psi}$ due to the slow variation of λ and $\tilde{\theta}(\theta) = \theta$, the actions $(\vec{J}, I)$ are almost adiabatic invariants (see definition A.15) if the Jacobian of the map $(\vec{J},\lambda) \mapsto (\vec{Q}(\vec{J},\lambda), \nu(\vec{J},\lambda))$ has rank 4. This condition prevents each of the actions from staying long enough in a region where the tunes are resonant and thereby destroy the adiabaticity. We now define the averaged system (see equation (A.65))

$$\mathrm{D}_\theta \begin{pmatrix} \vec{K} \\ \tilde{I} \end{pmatrix} = \alpha \begin{pmatrix} \vec{f}_{\vec{K}}(\vec{K},\lambda) \\ 0 \end{pmatrix} \ , \ \vec{f}_{\vec{K}}(\vec{K},\lambda) \equiv \frac{1}{(2\pi)^4} \int_{\mathcal{T}_4} \vec{f}_{\vec{K}}(\vec{K},\lambda;\vec{\Psi},\tilde{\theta})\, d\vec{\Psi}^3 d\tilde{\theta} \ , \ \begin{pmatrix} \vec{K}(0) \\ \tilde{I}(0) \end{pmatrix} = \begin{pmatrix} \vec{J}(0) \\ I(0) \end{pmatrix} . \tag{4.113}$$

We note that the phase average of f_I vanishes due to the form of its dependence on Φ.

Theorem 4.8 (Adiabatic invariance of I) *[GH99b] If in the spin–orbit system (4.112) the functions $\vec{f}_{\vec{J}}$, f_I, $\vec{g}_{\vec{J}}$ and g_Φ are $\mathcal{C}^1$, 2π–periodic in $\vec{\Psi}$, Φ and $\tilde{\theta}$ and if these functions have analytic extensions for $\vec{\Psi}$, Φ and $\tilde{\theta}$ inside a finite band around the real axis in $\mathbb{C}$, and the determinant of the Jacobian of $(\vec{J},\lambda) \mapsto (\vec{Q}(\vec{J},\lambda), \nu(\vec{J},\lambda))$ does not vanish, then for every continuous function $\rho(\alpha)$ with $a\sqrt{\alpha} \le \rho(\alpha) \le b$, $a, b \in \mathbb{R}^+$ the phase space $\mathcal{P} = \mathbb{R}^3 \times (-\sqrt{1-\delta}, \sqrt{1-\delta}) \times \mathcal{T}_4$ is partitioned $\mathcal{P} = \mathcal{G}(\alpha,\rho(\alpha)) \bigcup \mathcal{B}(\alpha,\rho(\alpha))$ for sufficiently small α so that*

$$\sup_{0 \le \theta \le 1/\alpha} \left\| (\vec{J}(\theta), I(\theta)) - (\vec{K}(\theta), I(0)) \right\| \le \rho(\alpha) \tag{4.114}$$

for initial conditions in $\mathcal{G}$ and $(\vec{J}'(\theta), I(0))$ being the solutions of the averaged system (4.113). Moreover the Lebesgue measure of $\mathcal{B}$ is less then $c\sqrt{\alpha}/\rho(\alpha)$, $c \in \mathbb{R}^+$ and for arbitrary small α we can chose δ arbitrarily small.

The proof which is based on averaging in multi–frequency systems [ems3, LM88] can be found in [GH99b]. Due to theorem 4.8 the spin action I is an almost adiabatic invariant in systems described by equation (4.112). We note that the orbital actions might change even in the averaged system. This is in good agreement with the fact that for example under acceleration $\vec{J}\beta_0\gamma_0$ is an adiabatic invariant rather then $\vec{J}$.

Practically, “almost adiabatic invariance” means that, provided the parameters of the spin–orbit system are changed sufficiently slowly, then the fraction of the beam in which the projection $\widehat{S} \cdot \hat{n}$ changes by more than some maximum acceptable number ρ can be made sufficiently small. Following the argument that led to equation (4.99b) we assume that if the amplitude dependent spin tune is close to a resonance the spread of $\hat{n}$ over phase space is large and depends strongly on λ. Therefore we expect those regions in parameter space where

$$\nu(\lambda) \approx k_0 + \vec{k} \cdot \vec{Q} \ , \ \text{moderate}\, |\vec{k}| \tag{4.115}$$

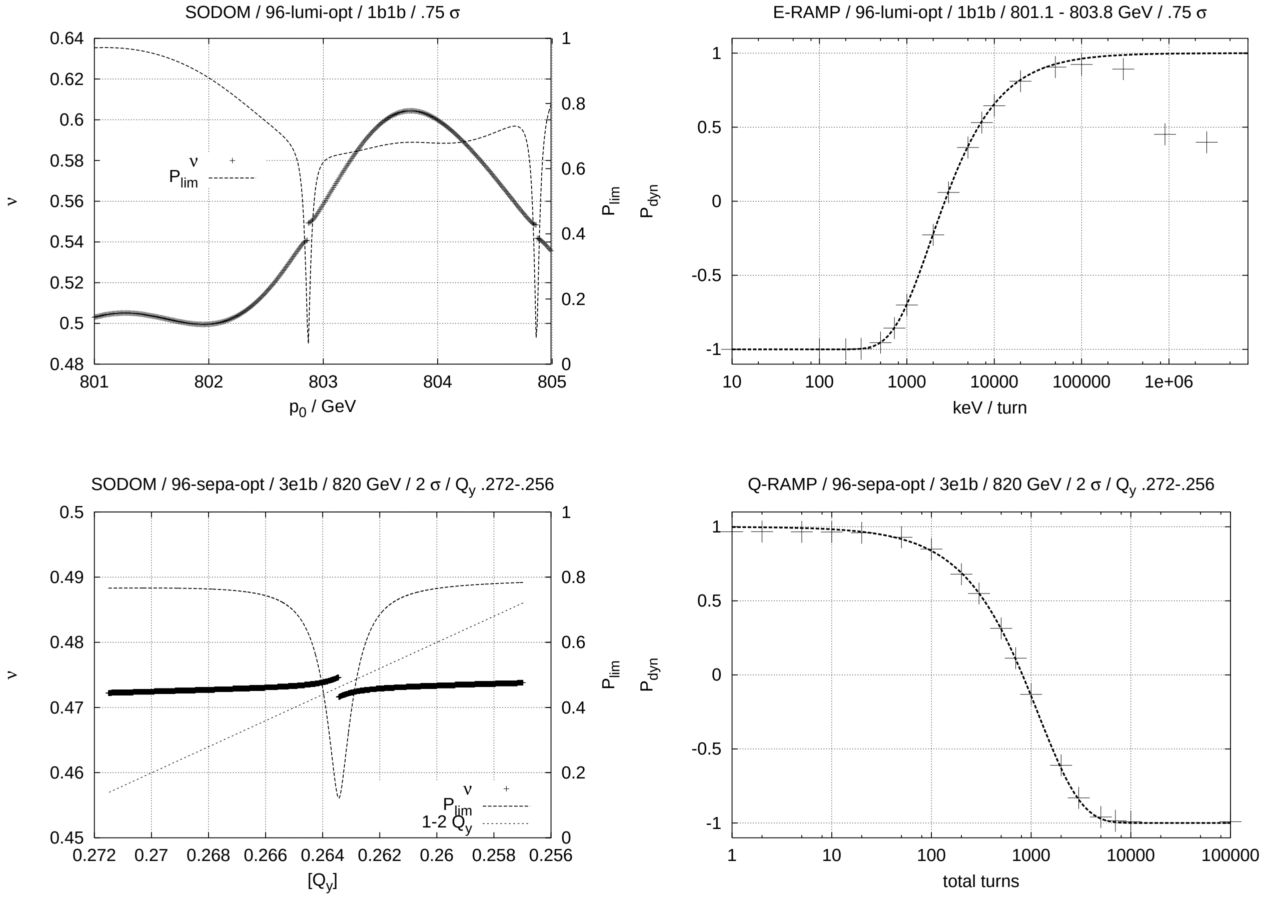

Figure 4.20: Top left: Energy scan of P_{lim} and ν for HERA–p with flatteners and a 4 snake scheme (rad., 45°, rad., 45°) with purely vertical motion at 0.75 σ. Top right: The dependence on the energy gain per turn of the final P_{dyn} after ramping through the resonance at approximately 802.7 GeV. Bottom left: Tune scan of P_{lim} and ν for HERA–p with flatteners and a 4 snake scheme (long., −45°, rad., 45°) with purely vertical motion at 2 σ. Bottom right: The dependence on the total number of turns of the final P_{dyn} after ramping through the resonance at $[Q_y] \approx 0.2635$.

to require particularly small α. This means that possibly no reasonable α, for example a ramp–speed that is operationally feasible, can be found so that the polarisation losses are acceptable !

In section 4.9 we have seen many examples of more ore less isolated kinetic resonances in the parameter space. Thus one feels tempted to use the heuristic model of equation (4.98) once more and try whether the Froissart–Stora formula (4.104) can be modified to explain and describe the outcome of moving a spin–orbit system through one of these isolated resonances. Froissart and Stora, who published their famous paper 12 years before the $\hat{n}$–axis was invented by Derbenev and Kondratenko, employed the SRM in a way which is equivalent to removing the sign change of $\hat{n}$ at $\delta = 0$. By directly solving the T–BMT equation they found an asymptotic formula (4.104) for $P_{\mathrm{dyn}}(\delta = +\infty)/P_{\mathrm{dyn}}(\delta = -\infty)$ which shows that the absolute value of the spin action $|I|$ of all particles on the torus described by ϵ is preserved in the limit of infinitely low *and* high ramp speed α. For the *ramp* simulations of figures 4.20 and 4.21 we have adopted *their* sign convention. Within the SRM the relation $\lim_{\delta\to\pm\infty} P_{\mathrm{lim}} = 1$ and with the sign convention which is equivalent to the approach of Froissart and Stora in particular $\lim_{\delta\to\pm\infty} \hat{n} = \pm\hat{n}_0$ is fulfilled. However, for infinitely fast variation of the parameters I will in general not be preserved anymore if we start from and end up at a point in parameter space where the invariant spin field already has a finite spread on the torus. Therefore one should *not* expect equation (4.104) to be a good approximation outside the quasi adiabatic region. Figure 4.20 shows two different ramp simulations. The top left plot is a combined momentum scan of ν an P_{lim}. The simulation was performed using the 1996 luminosity optics of HERA–p with 6 flattening snakes and 4 main snakes close to the IPs, namely radial snakes at the O- and W–IP and +45° at the N- and S–IP. The vertical amplitude was chosen to be 0.75 σ, the momentum range was chosen to cover the position of the strongest intrinsic resonance (without snakes) at about 803.5 GeV. The two tune jumps are crossings of the 2-nd order kinetic resonance $\kappa = [2Q_y]$. The half jump height is $\epsilon \approx (4.2 \pm 0.1)\ 10^{-3}$ We note that $P_{\rm lim}$ at 801 GeV is about 0.9716 whereas at 803.8 GeV $P_{\rm lim}$ is only about 0.6811 and that the slope of ν in the region from 802.5 GeV to 803.4 GeV is almost constant except at the resonance itself at 802.8 GeV. We would now like to linearly vary the quasi spin tune $\tilde{\nu}$ of equation (4.99a)

$$\tilde{\nu} = \kappa + \theta\alpha \ , \quad \alpha \approx \mathrm{D}_{p_0}\,\tilde{\nu}|_{\theta=0}\,\mathrm{D}_\theta\,E_0 \approx (.0135 \pm 0.0020)\,10^{-6}\,\mathrm{keV}^{-1}\,(\Delta E_0)_{\rm turn} \quad , \tag{4.116}$$

where $\beta_0 = p_0/E_0 \approx 1$ has been used and $(\Delta E_0)_{\rm turn}$ is the energy gain in keV per turn. The slope $\mathrm{D}_{p_0}\,\tilde{\nu}|_{\theta=0}$ is estimated from a linear fit to ν in some momentum range around the resonance position. At the start of the ramp 9 spins were uniformly distributed on the 0.75σ vertical ellipse and set parallel to their respective $\hat{n}$–axis to give $P_{\rm dyn} = 1$. Figure 4.20 (top right) shows the final average of I for the 9 particles, which serves as an approximation of $P_{\rm dyn}$, as a function of the energy gain per turn (crosses) and the prediction using equation (4.104) with $\alpha = 0.0148 \cdot 10^{-6}\mathrm{keV}^{-1}\,(\Delta E_0)_{\rm turn}$ and $\epsilon = 4.2 \cdot 10^{-3}$ (line). Note that α and ϵ are not orthogonal parameters in equation (4.104) which contains ϵ^2/α only. The agreement between the simulation and the heuristic extension of the Froissart–Stora result to kinetic resonances is qualitatively excellent in the quasi–adiabatic region $(\Delta E_0)_{\rm turn} \leq 1 \cdot 10^5$ keV per turn and the quantitative agreement is consistent with the accuracy of the input quantities. We note in particular that the estimate for the slope of $\tilde{\nu}$ has some ambiguity since the slope of ν is asymptotically *not* constant. Figure 4.20 (bottom left) shows a combined ν and $P_{\rm lim}$ scan w.r.t. the vertical tune with 2 σ purely vertical orbit motion at 820 GeV. The 1996 separation optics with 6 flattening snakes and the 3e1b snake scheme obtained by filtering and described in figure 4.19 was used. Here $P_{\rm lim}$ is about 0.78 at $[Q_y] = 0.272$ and about 0.79 at $[Q_y] = 0.256$. $P_{\rm lim}$ and ν are almost constant except for the crossing of the resonance $\kappa(Q_y) = 1 - 2[Q_y]$ where we find the half jump height $\epsilon \approx (1.47 \pm 0.04)\,10^{-3}$. Note that the ramp was performed *downwards* from $[Q_y] = 0.272$ to 0.256 and that the rate of change of the distance between $\tilde{\nu}$ and κ is mainly given by the rate of change of $\kappa(Q_y)$. Let ξ be a parametrisation of Q_y with $[Q_y(0)] = 0.272$ and $[Q_y(1)] = 0.265$, $\mathrm{D}_\xi\,Q_y = $ const. Then we obtain

$$\alpha \approx \frac{2([Q_y(1)] - [Q_y(0)]) - \tilde{\nu}(1) + \tilde{\nu}(0)}{2\pi N} \approx \frac{(3.9 \pm 0.1)\,10^{-3}}{N} \quad , \tag{4.117}$$

where N is the total number of turns required for the tune ramp while linearly interpolating between $[Q_y(0)]$ and $[Q_y(1)]$ using again the rampable optics facility of `SPRINT` . At the start of the downwards tune ramp 9 spins were uniformly distributed on the 2σ invariant ellipse with the spins set parallel to their respective $\hat{n}$–axis, giving $P_{\rm dyn} = 1$. Figure 4.20 (bottom right) shows the approximation of $P_{\rm dyn}$ for the ensemble average over the 9 particles as a function of N (crosses) and the prediction of the Froissart–Stora formula with $\epsilon = 1.45 \cdot 10^{-3}$ and $\alpha = 3.9 \cdot 10^{-3}/N$. Again the qualitative agreement is excellent, in particular in particular in the quasi–adiabatic region $N > 20$, and the qualitative agreement is consistent with the errors of α and ϵ. We may conclude that the heuristic model introduced in section 4.8 not only helps to understand the functional dependence of ν and $P_{\rm lim}$ on the parameters of the spin–orbit system but also enables us to identify those areas in the parameter space which are potentially harmful when the system is steered from one stable state to another. It furthermore enables us to quantify the degree of violation of adiabaticity when passing such a critical area with a given speed.

The idea of generalising the Froissart–Stora formula to kinetic resonances was to a great extent inspired by a comment by Andreas Lehrach which he made during a talk by the author.

4.10.3 Anti–damping

The adiabatic invariance of the spin action $I = \widehat{S} \cdot \hat{n}$ actually suggests another method to compute the invariant spin field at finite orbital amplitudes. The spin $\widehat{S}$ of a particle on the design orbit $\vec{J} = \vec{0}$ and which is aligned parallel to $\hat{n}_0$ is tracked and over subsequent revolutions around the ring the amplitudes $a_i = \sqrt{J_i}$, $i = x, y, z$ are slowly increased. As long as the process stays adiabatic the spin will stay aligned along the invariant spin field on all tori that are crossed during this *anti–damping* procedure. It will therefore generate a one parameter family $\widehat{S}_{\hat{n}}(\vec{J}(\theta), \vec{\Psi}(\theta), \theta)$ of seeds of

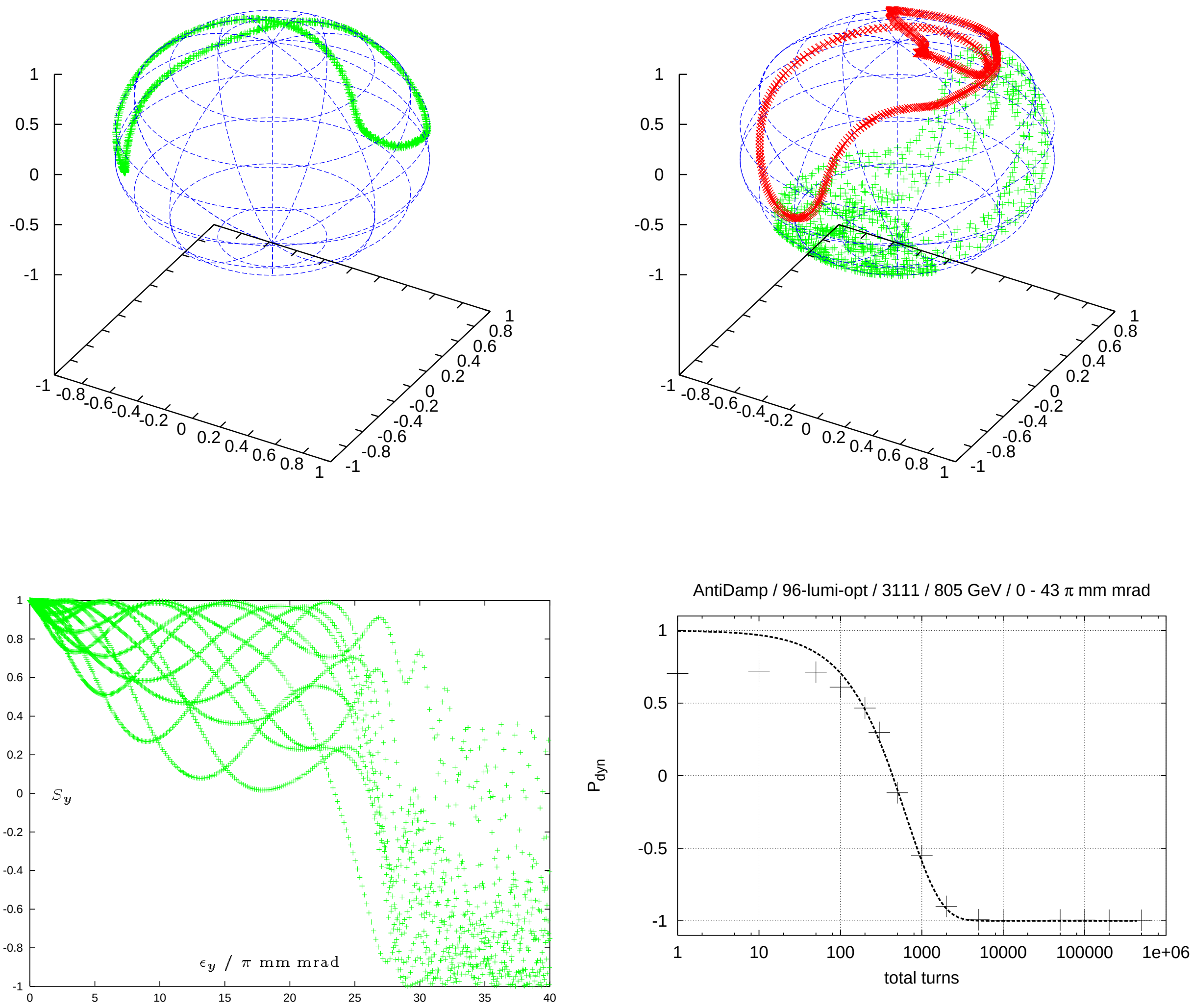

Figure 4.21: Top left: The locus of the $\hat{n}$–axis for purely vertical motion as computed with stroboscopic averaging *or* anti–damping at 16 π mm mrad. Top right: The locus of the $\hat{n}$–axis computed with stroboscopic averaging and the locus of the anti–damped spin at 43 π mm mrad. Bottom left: The vertical component of $\widehat{S}$ as it evolves under anti–damping through the resonance $\nu = 2Q_y$ at 805 GeV. Bottom right: The dependence of the final P_{dyn} on the total number of turns required for anti–damping

pseudo–$\hat{n}$–axes which will give the better approximations to the invariant spin field the slower the anti–damping is performed. We note that equations (4.35) and (4.63) together with figures 4.16 and 4.17 suggest applying a *linear* variation of the amplitude rather than of the action close to $\vec{J} = \vec{0}$.

At $\vec{J} = \vec{0}$, $\partial_{\vec{J}}\, \underline{B}_{2\times 6}\, \underline{A}^{-1}_{6\times 6} \vec{z}(\vec{J})$ has a singularity of type $1/\sqrt{\|\vec{J}\|}$ but the gradient w.r.t. $\vec{z}$ which is proportional to the amplitudes is finite. A similar method which is based on the RF–dipole technique used in [E880, MB99] was subsequently developed at BNL [AL99] to compute an approximation to the invariant spin field.

Figure 4.21 (top) shows the locus of the pseudo–$\hat{n}$–axis computed by anti–damping with 2000 turns in the 1996 luminosity optics at 805 GeV and with $[Q_y] \approx 0.2725$ on an invariant ellipse which encloses 16 π mm mrad (left) and 43 π mm mrad (right). The amplitude dependent spin tune and $P_{\lim}$ are depicted in figure 4.16 (top left). The anti–damped invariant spin field on the 16 π mm mrad invariant ellipse agrees to the level of less then 1 mrad with those computed with the `SPRINT` or `SODOM-2` method. Figure 4.21 (top right) shows the locus of the pseudo–$\hat{n}$–axis obtained by anti–damping to the 43 π mm mrad invariant ellipse (light crosses) and the locus of the invariant spin field obtained by the `SPRINT` method (dark "X–es"). Obviously the anti–damped spin has performed a partial spin flip while crossing the resonance at about 27 π mm mrad. Therefore when tracked at fixed amplitude it generates a band around $-\hat{n}$. Figure 4.21 (bottom left) shows the evolution of the anti–damped S_y as a function of the enclosed emittance. Here we we note that the vertical orbit tune is relatively close to the *orbital* resonance $[Q_y] = {}^3\!/_{11} = 0.\overline{27}$. Therefore each 11-th turn leads to a similar orbital phase and as long as the spin motion is adiabatic S_y appears to lie on 11 distinct quasi–continuous curves. While approaching the enclosed emittance that corresponds to the first resonance crossing in figure 4.16, namely about 27 π mm mrad, the 11 curves not only start tilting over to the lower hemisphere but also begin to decay. This demonstrates the partial spin flip of $\widehat{S}$ for too rapid anti–damping through the resonance. In figure 4.16 the resonance strength is $\epsilon \approx (4.5 \pm 0.1)\, 10^{-3}$ and for the *amplitude* linearly increasing from zero, α is

$$\alpha \approx \mathrm{D}_\theta\, \tilde{\nu}|_{\varepsilon_\kappa} = \mathrm{D}_\varepsilon\, \tilde{\nu}|_{\varepsilon_\kappa} \mathrm{D}_\theta\, \varepsilon|_{\varepsilon_\kappa} \frac{\mathrm{D}_\varepsilon\, \tilde{\nu}|_{\varepsilon_\kappa}}{\pi N} \sqrt{\varepsilon_\kappa \varepsilon_N} \approx \frac{.021 \pm 0.001}{N} \quad , \tag{4.118}$$

where ε_κ and ε_N are the enclosed emittances of the resonant ellipse and the final ellipse and N is the total number of turns used for anti–damping from 0 to ε_N. Figure 4.21 (bottom right) shows the approximation of P_{dyn} by an ensemble average over 9 particles uniformly distributed over the invariant ellipse as a function of N (crosses) and the prediction of equation (4.104) with $\epsilon = 4.5 \cdot 10^{-3}$ and $\alpha = 0.02/N$. Again the agreement of tracking simulation and the prediction of the extension of the Froissart–Stora formula to kinetic higher order resonances is rather impressive in the quasi adiabatic region $N > 200$.

Anti–damping is an effective way to compute the $\hat{n}$–axis on a whole family of tori. The drawback is of course are that once $\widehat{S} \cdot \hat{n}$ is reduced it is generally lost for all subsequent tori and that there is no a–priori control mechanism for the accuracy of the $\hat{n}$–axis in contrast to the `SODOM-2` and `SPRINT` methods. The spin $\widehat{S}$ is always correctly anti–damped to every torus — no matter what its final spin action is. Therefore one has to check the quality of the resulting pseudo–$\hat{n}$–axis manually. The principle of anti–damping was already employed in [SM86a, SM86b, BH92] where it was used to derive an analytical perturbative formalism to compute the invariant spin field with the required azimuthal periodicity.

Finally the ramp simulations in section 4.10 show that the spin tune jumps observed in *static* scans using stroboscopic averaging or Fourier analysis and the kinetic resonances strengths associated with these jumps have a significant physical meaning. Moreover they show that the impact of higher order (kinetic) resonances in the presence of Siberian snakes on the acceleration process can be explained in the framework of the invariant spin field and the amplitude dependent spin tune. The concepts traditionally used in the literature, in addition to being based on false assumptions, fail to give quantitative predictions on the dependence of the polarisation on the ramp speed through "snake resonances".

Chapter 5

Polarisation in HERA–p

In the previous chapters we have derived a consistent formalism for describing spin motion in high energy proton accelerators and storage rings. In order to estimate the "Bounds on the Maximum Attainable Equilibrium Spin Polarisation at High Energy in HERA" and push the limit as far as possible, two major questions must now be answered.

1. Can modifications to the HERA–p lattice, beam parameters, and the collision energy be conceived, which are consistent with the requirement of beam stability and high luminosity, and which allow the invariant spin field at the interaction points (IPs) to be bundled, i.e. so that P_{lim} is large on all reasonably populated tori?
2. Are these modifications also capable of supplying a high beam average of $I = \widehat{S} \cdot \hat{n}$ after ramping a fully polarised beam from the injection energy of 40 GeV to the collision energy and the required optics with reasonable ramp speed?

This chapter addresses both questions on the basis of Hamiltonian, linear and unperturbed orbit motion. Neither the effect of orbital misalignment nor of non–linear orbital motion and stochastic effects like intra–beam scattering (IBS) or any other source of noise will be discussed. It is only sensible to study such further complications after a way has been found to maintain polarisation at the level of linear unperturbed orbital motion at high energy in HERA–p. HERA–p currently runs at a reference momentum of 920 GeV. It will turn out in the following, that obtaining polarisation around 820 GeV is already a challenge. We will therefore *not* study spin dynamics at higher energies in great detail. To maintain internal consistency of the simulation data only the 1996 set of optics (hp96in40, hp96zw300, hp96se820 and hp96lu820) was used. Simulations using the "lumi–upgrade" optics to be commissioned in 2001, can be found in [GH99b]. The results are in any case similar.

5.1 The pre–accelerator chain

Since the only promising way to obtain polarised protons at HERA energy is by acceleration of polarised protons from the source, it is necessary to address the second question stated above, i.e. the question of whether polarisation is lost during acceleration and transfer, for the whole pre–accelerator chain of HERA–p. Since this is not the topic of this thesis and preliminary results have already been published in [SPC96, SPC99], the HERA–p pre–accelerator chain will be only briefly described here.

The pre–accelerator chain consists of the following stages: At the source H^- ions are produced at low energy and then transported via the low energy beam transport channel (LEBT) to the RF–quadrupole (RFQ). In the RFQ the ions are accelerated to a kinetic energy of 750 keV. Then the particles are transfered through the medium energy beam transport channel (MEBT) to the Alvarez–type linear accelerator LINAC-III in which the kinetic energy is increased to 50 MeV. The high energy beam transport channel (HEBT) then transfers the ions to the synchrotron DESY–III. At injection into DESY–III the ions are stripped to protons and adiabatically captured in the 11 RF–buckets. During acceleration to the momentum of 7.5 GeV the frequency of the RF system is swept from about 3 MHz to about 10 MHz. At flat top 10 bunches are ejected into the transport line (P–Weg) from DESY–III to PETRA–p. The eleventh bunch is destroyed during the rise time of the ejection kicker. After 6×10 bunches have been filled into PETRA–p they are accelerated to a momentum of 40 GeV. The acceleration procedure in PETRA–p takes some minutes. At 40 GeV all the 60 bunches can be ejected at once into the transfer line (PR–Weg) to HERA–p. After 3×60 proton bunches have been injected into HERA–p the complete filling is accelerated to 820 GeV, or even 920 GeV, in 25 to 30 minutes.

There is little point in having polarised protons unless the same or more luminosity can be achieved at the same time. For Gaussian beams and matched beam sizes at the interaction points the luminosity is given by

$$L = \frac{1}{4\pi e^2 f_0 N_b}\,\frac{I_p I_e}{\sigma_x \sigma_y}\ , \tag{5.1}$$

where e is the elementary charge, f_0 is the revolution frequency, N_b is the number of colliding bunches, I_p, I_e are proton and electron currents averaged around the ring and σ_x and σ_y are the horizontal and vertical beam sizes of *both* beams. Thus high luminosity requires high currents, small β–functions at the interaction points and small emittances. The proton current under luminosity conditions in HERA–p is determined by the current from the source and the losses during the various acceleration stages. The emittances of a proton beam are determined by the initial emittances from the source and the potential subsequent increase produced by space charge forces, external noise, intra–beam scattering and mismatches between the optical functions at ejection from one accelerator and injection into the next accelerator. Strong quadrupoles with high β–functions close to the interaction points (low–beta insertions) are required to squeeze the β–functions at the interaction points to the lowest values. Moreover the beam lifetime must be high enough to maximise the integrated luminosity $\int L\,dt$. It clear that all modifications to be done on the pre–accelerator chain as well as on HERA–p in order to achieve high polarisation must conform with the requirement for high luminosity.

5.1.1 The H^- source

In order to maximise the bunch current in HERA–p, multi–turn charge exchange injection into DESY–III is applied. Therefore an H^- source is needed. Currently DESY only has an unpolarised magnetron source that is able to produce about 60 mA of H^-–ions. A volume source is also being commissioned. A pulsed optically pumped polarised ion source (OPPIS) is under construction at TRIUMF and BNL [ZL96, ZL99]. In order to attain the current luminosity and high polarisation, the goals for the operational parameters for HERA should be

H^- current	$\geq$ 20 mA
polarisation	$\geq$ 80 %
emittance (transv.)	$\leq$ 2π mm mrad
pulse duration	100 μs
repetition rate	0.25 Hz

With this or a similar source and an optimised match to the RFQ and LINAC–III the injection current into DESY–III, which is roughly 10—20 mA in 10 bunches at the present, could almost be preserved. Since the beginning of the 1998 run period the DESY H^- injection has had a switchable MEBT connecting two low LEBTs and their respective RFQs with LINAC–III. So the change from polarised to unpolarised operation could be made without long down–times. The polarisation direction produced by the OPPIS is longitudinal, so that it would be best to mount the polarised source on the straight arm of the switch–yard.

5.1.2 RFQ, LINAC–III and transfer lines

Polarisation transport in the straight parts of the pre–accelerator chain is considered to be relatively straightforward for the following reasons:

1. The spin enhancement factor $G\gamma$ is small due to the low energy.
2. At these energies the directional distribution of the invariant spin field at the entrance/exit of the following/preceding circular accelerator will be tightly bundled, i.e. $P_{\text{lim}} \approx 1$ since the transfer energy can be chosen to be off–resonance.
3. The strongest spin perturbations in circular accelerators arise from the periodic lattice where small perturbations can coherently add up turn by turn. This is excluded for linear (single–pass) structures by definition.
4. The transfer lines, the LEBTs and the MEBT do not change the reference energy of the beam. Thus the spin action I is an invariant of motion.

Nevertheless there are still some topics to care about:

1. The spin enhancement factor $G\gamma$ for the PR–Weg is about 76. The impact of this should be analysed separately.
2. In order to preserve luminosity the transfer efficiency has to be optimised.
3. The HEBT, the P–Weg, and the PR–Weg include horizontal, vertical, and otherwise tilted bends. Hence they will apply an energy dependent rotation to the polarisation. Note also that the polarisation from the OPPIS source would be longitudinal, but in the circular machines it is preferably vertical. Thus spin direction tuners are needed to tune the polarisation axis and compensate the effect of interleaved horizontal and vertical bends. Spin direction tuners are simply spin rotators designed for the chosen beam line and operated at a single energy.
4. Since the spin action I is constant for constant energy, the spin transfer function must be matched from the preceding to the following accelerator to maintain polarisation.

This implies for the following different stages of the pre–accelerator chain:

- LEBT, RFQ, MEBT and LINAC–III: It is not clear yet whether $\hat{n}_0$ has to be tuned at all. Improving on transfer efficiency would help to maintain luminosity.
- HEBT: Probably the best place to rotate the polarisation vector $\hat{n}_0$ into vertical direction for acceleration in DESY–III and PETRA–p.
- P–Weg and PR–Weg: The polarisation axis must be tuned to overcome the rotation from the tilted and vertical bends.

5.1.3 DESY-III

DESY–III is a strong focusing flat synchrotron with a superperiodicity of 8. Each period consists of 3 cells comprised of 2 focusing and defocusing combined function magnets (BD, BF). In addition each period has 4 independent quadrupoles (QD1, QF1, QD2, QF2). Multi–turn injection is done through a stripping foil. Since the injection is at 50 MeV kinetic energy and the ejection momentum is 7.5 GeV, there are 14 imperfection resonances in the DESY–III energy range. DESY–III has 4 weak intrinsic resonances with strength 0.002 to 0.01 corresponding to an invariant vertical emittance of 4π

mm mrad [HV99]. The resonances are well separated so that the isolated resonance model is probably applicable. The imperfection resonances can probably be overcome with a partial snake [AK96a]. The intrinsic resonances can be overcome by applying tune jumps [AK96a], or resonance excitation with a vertical RF-dipole [E880, MB99] can be used to ensure full spin flip at resonance crossing. To decide which of these methods seems more promising, a more detailed analysis is necessary. The large tune spread at injection caused by space charge forces as well as the observed emittance blow–up on the ramp have to be taken into account, both for spin as well as for orbital stability.

5.1.4 PETRA–p

The situation for PETRA–p is more difficult. PETRA–p consists of 8 identical arcs, each with 13 FODO cells. There are 4 long straight sections (N, O, S, W) and 4 short straight sections (NO, SO, SW, NW). However, the protons have to be bypassed around the RF–cavities used for $e^{\pm}$ acceleration in the South straight section, so that the superperiodicity of PETRA–p is just 1 in the end, although there is mirror symmetry with respect to the North–South axis. Thus there are many intrinsic resonances in PETRA and they are up to 5 times stronger than in DESY–III. Therefore in the high energy part of the ramp they are close to overlapping [HV99]. In that region only Siberian Snakes are expected to preserve polarisation and at least two would be needed [AK96b]. Warm snakes would be about 13 m long [AK96b]. This has to be compared to the typical length of a drift space between quadrupoles of 7.5m. For superconducting snakes a liquid helium supply line from HERA would be needed. So further evaluations would be needed before a choice could be made. Snakes would be the best solution at low energy too. But at 7.5 GeV the field integrals of solenoidal snakes would be impractically large and dipole snakes would produce large orbit distortions. For further comments see [AK96b].

5.1.5 Polarimeters

Experiments using the polarised proton beam need accurate knowledge of the polarisation and for that a polarimeter suitable for 820 GeV is required. But polarimeters are also needed at almost all stages of the pre–accelerator chain for diagnostics. Even if the LEBT–RFQ–LINAC section can be considered to be spin transparent, polarimeters are needed at the following places and energies:

- Source polarisation: the polarisation must be surveyed either directly after the source or somewhere before the HEBT. This implies an operating energy for the polarimeter somewhere in the region of a few keV to 50 MeV.

- The polarisation must be measured after the HEBT or directly after injection into DESY–III in order to adjust the matching of the polarisation direction. The required working energy is 50 MeV

- The polarisation at DESY–III must be measured at ejection to optimise orbit corrections, partial snake and tune–jump or RF–dipole settings. At a momentum of 7.5 GeV polarisation measurements (e.g. with elastic p–p scattering) already take a significant time. In order to optimise the compensation of the intrinsic resonances step by step, a procedure to eject the beam at momenta other than 7.5 GeV is necessary.

- A polarimeter is needed at the end of the P–Weg or at injection into PETRA.

- It must be possible to measure polarisation at various energies on the PETRA ramp from 7.5 to 40 GeV. If the P–Weg polarimeter were to be placed inside PETRA, it could possibly handle the low energy end of this range. Note that PETRA cannot be cycled as quickly as DESY so that the time for a polarisation measurement should be not much more than the beam lifetime in PETRA at the required energy.

- Since the time for polarisation measurements increases with energy, it makes no sense to have a polarimeter in the PR–Weg. Thus the spin transfer through the PR–Weg can only be checked with the HERA "low energy" polarimeter.
- The spin perturbations are expected to be worst in HERA. Therefore it must be possible to measure the polarisation at any stage of the ramp. It is not clear yet how many polarimeters are needed to cover the whole energy range from 40 to 820 GeV. In any case no tested technique is known for 820 GeV but ideas are being investigated. For example Coulomb nuclear interference (CNI) and inclusive pion production [GB99] are being considered.

A more detailed analysis on the pre–accelerator chain can be found in [SPC96, SPC99], but it should be mentioned that a complete analysis, including spin tracking with snakes in PETRA, has not yet been carried out.

5.2 HERA–p

The HERA proton ring consists of 4 arcs and 4 straight sections. In the arcs the p–ring is located *above* the $e^{\pm}$-ring. The p- and $e^{\pm}$–beams are only brought to collision in the South (**S**) and North (**N**) straight sections. Therefore these straights include mini–beta regions and magnets for horizontal beam separation. The East (**O**) straight contains the HERMES internal target experiment which only uses the $e^{\pm}$–beam. The β–functions for the p–ring are rather relaxed in the East. Nevertheless, the East straight was originally designed for potentially colliding beam experiments and hence both beams are separated only horizontally. Finally, in the West (**W**) straight the p–beam is used in the HERA–B internal target experiment and has rather high β–functions and negative horizontal dispersion at the IP. Figure 5.1 shows a sketch of the general layout of the HERA proton ring. The straight sections are indicated as O, S, W and N. Actual collision points (S and N) are indicated by face–to–face double arrows. The proton beam goes counter clockwise around the ring. The vertical bend sections around the straight sections O, S and N are indicated by the filled rectangles. For later use, flattened vertical bend sections are introduced as filled rectangles crossed by a perpendicular line. The full and dashed lines at O and W indicate that these straight sections have different layouts. In order to have both beams in one horizontal plane in the O-, S- and N–straights, there are sections made from interleaved horizontal and vertical bends (and quadrupoles) at the ends of the arc octants OL, OR, SL, SR, NL and NR, where L/R means left/right of the interaction point (IP) when looking in the outwards radial direction. The vertical bends are located inside of the combined matching and dispersion suppressor sections. When entering a vertical bend section from the arc, the beam is bent downwards by a superconducting magnet (BV) by about 5.74 mrad. Then the beam encounters two dispersion suppressor cell which are of the missing magnet FODO type. Each cell has two horizontal bends (made from 2×BP3 and 2×BPA)[1] which each produce a horizontal deflection of about 15.104 mrad and quadrupoles, i.e. QY/QV, QX/QW and QQ magnets (OQ in the East). Finally the beam is bent back into the horizontal plane by three normal conducting vertical bends (BU00). We note that at 820 GeV a 5.7 (15.1) mrad orbital deflection corresponds to approximately 1.4 (3.8) complete spin precessions. Thus in order to make $\hat{n}_0$ vertical in the arcs the concept of *flattening* snakes [KS88a, AP97] was introduced whereby 6 radial Siberian Snakes are placed at the symmetry points of the 6 vertical bend sections, transforming their on–orbit spin transport maps into the maps of radial snakes themselves. This flattening effect was explained in detail in section 3.1.3. These 6 *distributed snakes* [BS99] then cancel themselves pair–wise since they are separated by straight sections only.

The HERA arcs *outside* the vertical bend sections consist of 24 FODO cells of which the inner 18 (with QP42/QP40 magnets) are strictly periodic and the outer 2×3 already belong to the matching sections.

[1] These are the names used in the HERA–p optics files and are familiar to people running the machine.

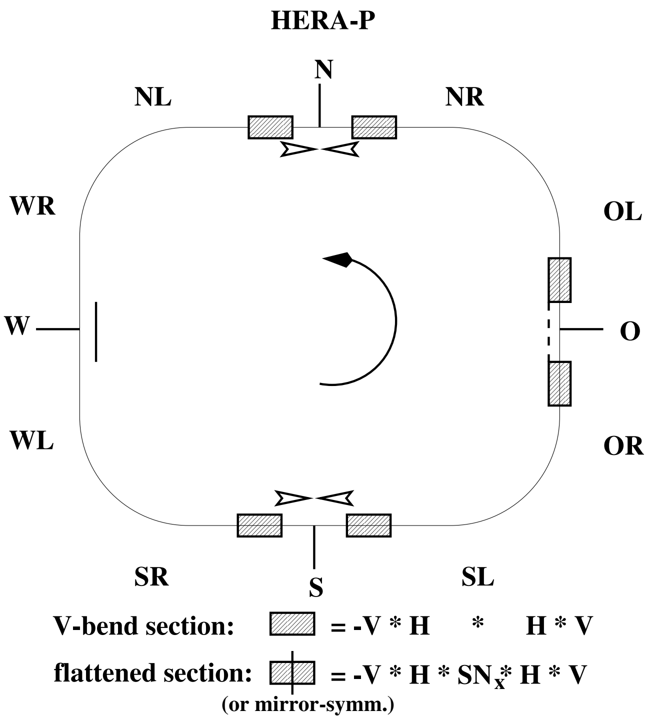

Figure 5.1: HERA–p with arc–octants OR, SL, SR,... and the straight sections O, S, W, N with vertical bend sections around O, S and N.

We conclude that HERA–p is *not* a flat ring so that the on–orbit spin tune $\nu_0 \neq G\gamma$ and $\hat{n}_0$ is strongly energy dependent in the unmodified machine! Only 3 out of 4 straight sections are surrounded with vertical bend sections, which immediately implies a superperiodicity $P = 1$. Even if the vertical bend sections are flattened then even on the design orbit the superperiodicity is 1 since in the quadrants WR–NL and SR–WL the spin phase advance is larger than in NR–OL and OR–SL owing to the effective cancellation of the horizontal bends inside the flattened vertical bend sections. At high energy the intrinsic resonances are potentially strong and because of the lack of symmetry they populate the HERA–p energy range densely. Since during acceleration there are about 3000[2] linear intrinsic (Q_y) resonances to be crossed, we do *not* expect that acceleration of a polarised proton beam is feasible without Siberian Snakes. In the vertical bend sections and just outside of them there is generally enough space (10–14m) to place Siberian Snakes, whereas putting snakes at the centres of the arcs would require additional hardware modifications. This implies that as far as the technical effort is concerned, the natural number of snakes is: 4 main snakes plus 6 flattening snakes. Neglecting the fact that the Courant–Snyder functions are left/right asymmetric close to the W–straight one finds an approximate mirror symmetry w.r.t. the O–W–axis. So an optimal scheme for placing the main snakes should reflect this level of symmetry.

HERA–p is not only a high energy proton storage ring but it is also capable of increasing the reference momentum of the protons by a factor of more than 20. The protons are injected at a reference momentum of 40 GeV into the injection optics and then accelerated up to 820 or even 920 GeV. The optic is not changed until 150 GeV. During acceleration from 150 to 300 GeV the injection optics is changed to an intermediate optics at 300 GeV and from 300 to 670 GeV to the so–called separation optics which then remains unchanged up to the final energy. The standard ramp procedure contains various steps and takes about 20—30 minutes. Then, after acceleration of the $e^\pm$ beam the beams are brought into collision and the optics are changed to their so–called luminosity settings. All

[2]since (820−40) GeV / 523 MeV $\times 2 \approx 3000$.

optics changes are accomplished by linear interpolation of the magnet currents with respect to the reference momentum. We call the overall procedure of accelerating the beam, changing the optics and bringing the proton beam to collision with the $e^{\pm}$ beam, the *ramp procedure* or simply the *ramp*. When simulating spin motion in HERA–p one therefore has to deal with a whole set of optics. In order to optimise the working point for high $P_{\rm lim}$ only the luminosity optics is needed whereas discussion of the ramp process includes the whole sequence of different optics called the *ramp sequence*.

Of course all lattices in the ramp sequence share the same beam line elements and element positions. The various optics are achieved by varying the focusing strengths of the quadrupoles. In order to be able to place the main snakes at positions where there is enough space, i.e. directly adjacent to the vertical bend sections, *and* fulfil the condition of the corollary to theorem 3.1 for energy independent spin tune it is necessary to ensure that each of the 4 straight sections is "globally straight" in the sense that $\sum_{\rm hor.\,bends}^{\rm straight}\Theta_i = 0$. Thus for this study the small bend angles of less than 1 μrad of the QB28 and OL11 magnets were set to zero and the bend angles of the QS10 and OS10 were changed from 0.4028 to 0.4976 mrad and from 0.3964 to 0.4290 mrad respectively. After these manipulations the accumulated horizontal bend angle of each of the 4 straight sections was less than 1 μrad. Moreover in order to allow simulations of spin motion at high energy for the unperturbed machine, i.e. with the design orbit as reference trajectory, with sufficient accuracy, the bend angles of QP and BP3 magnets had to be slightly adjusted. In addition the vertical bump for the fast beam dump system was set to zero. By these manipulations the ring was closed, i.e. $\sum_{\rm hor.\,bends}\Theta_i = 2\pi + \delta_x$ and $\sum_{\rm ver.\,bends}\Theta_i = \delta_y$, to a level of $\delta_x, \delta_y < 10^{-3}$ μrad. Moreover with these modifications the 4 IPs are ${}^{\pi}/_{2} \pm 10^{-2}$ μrad apart. These modifications enable the calculations with snakes to be interpreted in an unambiguous way. Naturally, at a later stage of this project the small bend angles must be reinstalled. Their effects must be handled along with the effects of misalignments.

For convenience and to conform with the "HERA–slang" we introduce the following names for the linear unperturbed optics with the geometric modifications mentioned above:

- hp96inj40 : the injection optics at 40 GeV.
- hp96zw300 : the intermediate optics at 300 GeV. The lattices hp96inj40 and hp96zw300 will first be used at a later stage with modified tunes.
- hp96se820 : the "separation" optics at 820 GeV. The tunes computed with the lattice file are $Q_x = 31.301693835$, $Q_y = 32.308127270$ and $Q_z = 0.625108440 \cdot 10^{-3}$.
- hp96lu820 : the luminosity optics at 820 GeV. The tunes computed with the lattice file are $Q_x = 31.278984723$, $Q_y = 32.272532721$ and $Q_z = 0.625108440 \cdot 10^{-3}$.

It should be noted that the above tunes and the tunes produced by the unmodified lattices are the same up to an absolute difference of 10^{-5}. Moreover it should be noted that HERA is currently normally operated at $Q_x \approx 31.292$ and $Q_y \approx 32.297$ during the ramp and sometimes with interchanged fractional tunes, i.e. $Q_x \approx 31.297$ and $Q_y \approx 32.292$ in storage and collision mode. But $Q_y \approx 32.297$, at least, is not very likely to be suitable for operation with polarised protons since the 5-th order resonance conditions $\kappa = 5[Q_y] - 1$ and $\kappa = 2 - 5[Q_y]$ are just separated by 0.015 from the design orbit spin tune $\nu_0 = {}^{1}/_{2}$ with snakes. That only allows the amplitude dependent spin tune to deviate by less than 0.015 from ν_0.

Figure 5.2 shows the horizontal and vertical envelopes $\sqrt{\beta_x}$, $\sqrt{\beta_y}$ and the horizontal and vertical periodic dispersions x_D and y_D for the hp96lu820 and hp96se820 optics as functions of the generalised azimuth θ for one turn around HERA. The Courant–Snyder functions have been generated using the `SPRINT` code. The IPs are at $\theta = 0$ ($\theta = 2\pi$): O, $\theta = {}^{\pi}/_{2}$: S, $\theta = \pi$: W and $\theta = {}^{3}/_{2}\pi$: N. Note that the official HERA lattice files run clockwise whereas the beam runs anti–clockwise[3]. The upper

[3] This is just the way it is and the question of why it is as it is might forever go unanswered. . .

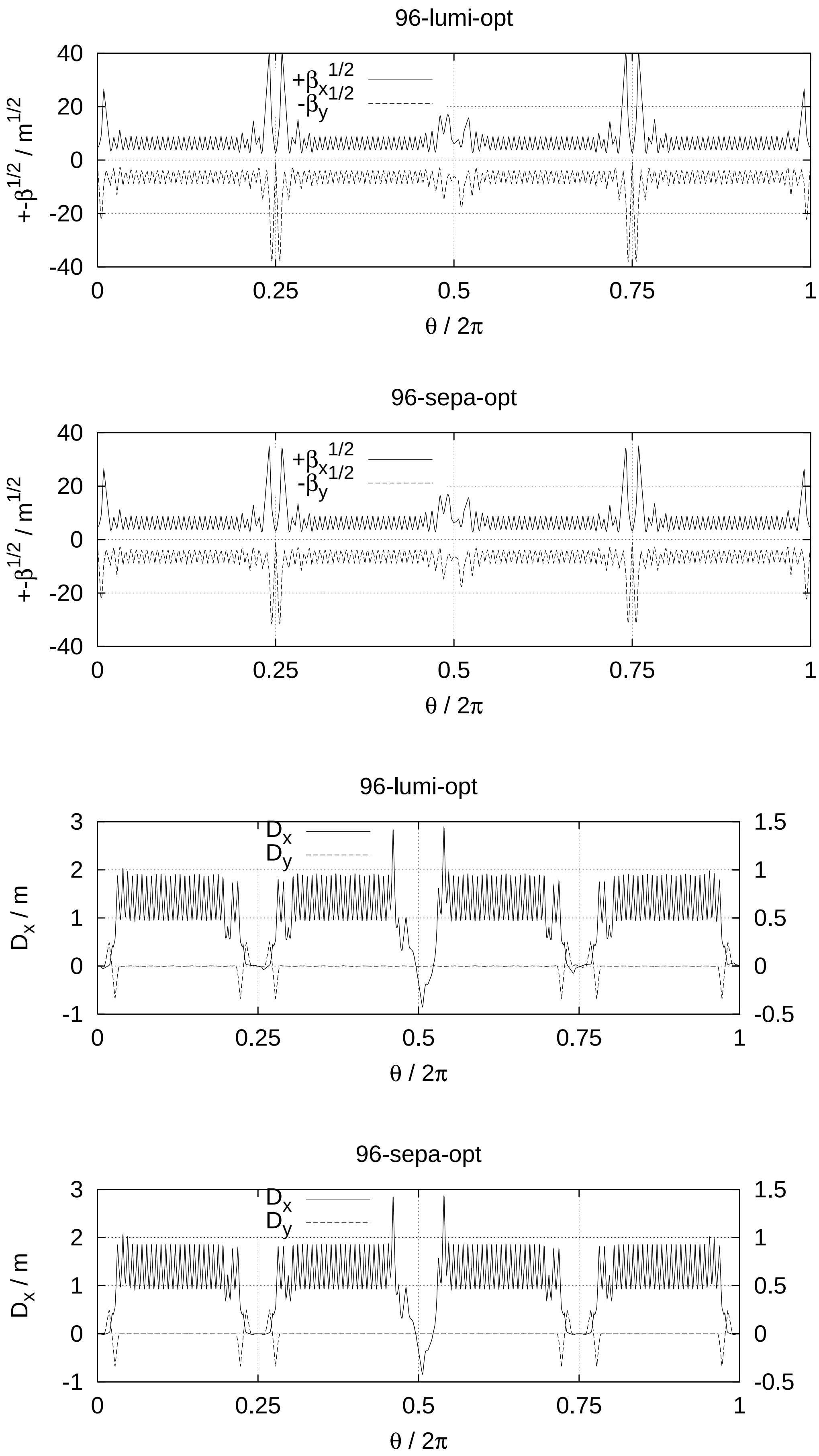

Figure 5.2: The vertical and horizontal envelopes $\sqrt{\beta_x}$, $\sqrt{\beta_y}$ (upper two) and periodic dispersions x_D, y_D (lower two) for the 1996 luminosity optics hp96lu820 (1-st and 3-rd) and the 1996 separation optics hp96se820 (2-nd and 4-th).

two plots show the envelope functions $\sqrt{\beta}$. A side–effect of plotting $\sqrt{\beta}$ instead of β is the relative compression of *large* values of β in the low–beta insertions w.r.t. the *small* values of β in the periodic arcs. The vertical envelopes have been plotted with a negative sign in order not to hide them under the horizontal envelopes. The β functions at the S- and N–IP are $\beta_x = 7$ m and $\beta_y = 0.7$ m for the luminosity optics and $\beta_x = 10$ m and $\beta_y = 1$ m for the separation optics. Therefore the β–functions in the low–beta–insertions are relaxed from 1600 m and 1400 m under luminosity conditions to 1200 m and 1000 m with the separation optics. With the exception of the West straight itself the β–functions are mirror symmetric w.r.t. the East–West axis. The apparent vertical β–beat is an artifact of the dotted line style and disappears when zooming the picture to a larger scale. The lower two plots show the horizontal and vertical dispersion for the luminosity and separation optics. Note that the vertical dispersion is non–zero only directly around the vertical bend regions surrounding the O-, S-, N–IPs. Again, except for the W–IP, the dispersion is mirror symmetric w.r.t. the East–West axis.

Figure 5.3 shows strengths of the vertical linear intrinsic spin–orbit resonances for p_0 from 500 to 1000 GeV for the luminosity optics on an invariant ellipse which encloses an invariant emittance of 16 π mm mrad. They were computed with `SPRINT` by using the eigenvector method (2.128). The topmost plot is for HERA–p as it is, i.e. with the full effect of the vertical bend sections. The middle plot was made with a flat version of HERA with the BU00 and BV magnets simply switched off in the lattice file. The bottom plot was generated with the vertical bend sections compensated by inserting 6 point–like flattening snakes at the symmetry point of each section. The resonance spectrum is described and explained in great detail in [GH99b]. Here it will only be discussed briefly. For the non–flat HERA (top) the resonance spectrum shows little regular structure. That is because of the energy dependent tilt of $\hat{n}_0$. In the flat and flattened HERA (middle and bottom) the resonance spectra show more periodicity w.r.t. p_0. We note that since the superperiodicity of HERA is 1, no resonance condition $\nu_0 = k_0 \pm [Q_y]$ is forbidden. The groups of 4 very strong resonances are the super–strong resonances generated by the almost coherent interference of *all* periodic FODO cells in the arcs as shown in equation (2.148). The strength of the strongest resonance in the group scales approximately with $\sqrt{\gamma}$ and the relative distribution of strengths inside the group repeats itself approximately from group to group. The groups of super–strong resonances are at resonance conditions $\kappa_i = k_0 \pm [Q_y]$, $i = 1, 2, 3, 4$ such that

$$G\gamma_{1,3}\frac{\Theta_B}{\pi} \approx 2l - 1 \pm Q_B \quad , \quad G\gamma_{2,4}\frac{\Theta_B}{\pi} \approx 2l \pm Q_B \quad , \tag{5.2}$$

is most closely fulfilled. Here $\Theta_B \approx 30.21$ mrad is the horizontal deflection angle caused by the bends in one *half* FODO cell in the periodic arcs, i.e. by 4 QP and 4 BPA magnets, and $Q_B \approx 0.243$ is the vertical phase advance per cell divided by 2π. We assume, for the moment, that the FODO cell has a symmetry point so that the spin phase advance ϕ as well as the vertical orbital phase advance ψ are the same from the beginning of the cell to the symmetry point as from the symmetry point to the end. Then for even i the phase advance $\phi \pm \psi$ in the exponent of the spin–orbit coupling integrals between a vertically focusing (2×QP42, QY, 2×QP42) and a defocusing (2×QP40, QX, 2×QP40) cluster of quadrupoles is $2\pi l$. Thus the alternating sign of the focusing strength causes the second half cell to cancel partly the contribution from the first half cell. Since β_y is bigger in a defocusing quadrupole than in a focusing quadrupole this cancellation can never be complete. If i is odd, then this phase advance is $2\pi(l + {}^1\!/_2)$ and the two half cells interfere constructively. Therefore the resonances at γ_2 and γ_4, although they are super–strong according to equation (2.116), are not so strongly enhanced as the resonances at γ_1 and γ_3. Table 5.1 lists the index i, the reference momentum, $G\gamma_i$, the integer $G\gamma^{\Theta_B}/_{\pi} \pm Q_B$ and the modulus of the resonance strengths $|\epsilon_i|$, for the group of 4 super–strong resonances with $l = 8$ in the flat version of HERA–p. The resonance at 803.19 GeV is the strongest resonance below 820 GeV. In a fourfold superperiodic model of HERA–p studied in [GH99b] the resonance strengths $|\epsilon_1|$, $|\epsilon_3|$ and $|\epsilon_2|$, $|\epsilon_4|$ are pair–wise approximately equal. In this model with superperiodicity 1 the spin orbit coupling integrals I^+ and I^- have different absolute values so that we find $|\epsilon_1| > |\epsilon_3| > |\epsilon_2| > |\epsilon_4|$ in the end. Since (5.2) is only a condition for enhancement of nearby resonances there are usually clusters of relatively strong resonances around the super–strong

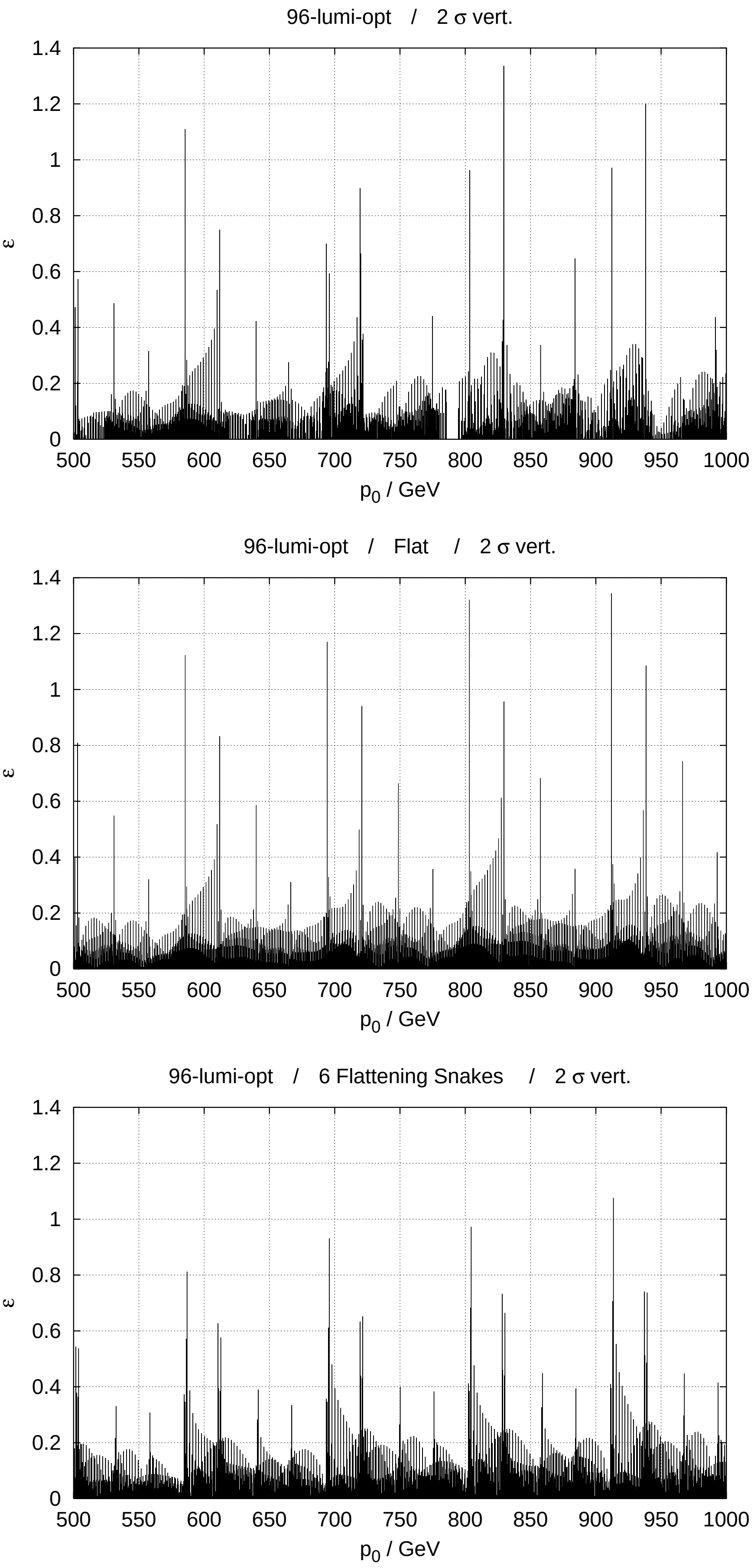

Figure 5.3: 1996 luminosity optics : linear intrinsic resonance strengths for the original lattice with vertical bends and without snakes (top), a flat model (BU00s and BVs switched off) (middle) and the original lattice with additional Flattening Snakes at the centres of the vertical bend sections around the East, North and South IPs (bottom).

i	p_0 / GeV	$G\gamma_i$	$^{\Theta_B}/_{\pi}G\gamma + Q_B$	$^{\Theta_B}/_{\pi}G\gamma - Q_B$	$\lvert\epsilon_i\rvert$
1	803.19	1534.73	15		1.32
3	829.64	1585.27		15	0.96
2	857.62	1638.73	16		0.68
4	884.07	1689.27		16	0.36

Table 5.1: The positions of the 4 super–strong resonances belonging to $l = 8$ for the flat version of HERA–p.

resonances. In the case of the flattened HERA–p the missing bend angle in the octants NL, NR, OL, OR, SL and SR causes the symmetry to be broken so strongly that the super–strong resonance at 803.19 GeV decays into 5 resonances at 802.37, 802.93, 803.48, 804.04 and 804.6 GeV with strengths of 0.41, 0.38, 0.22, 0.68 and 0.97. These resonances are interleaved with weak resonances with strengths of about 0.1. They represent an enhanced concentration of strong resonances around 803.5 GeV. We will call such clusters of strongly enhanced resonances that occur in the flattened HERA–p ring at momenta where the exact super–strong resonances are located in the flat ring super–strong resonances also. The momentum range around 803.5 GeV will be discussed in more detail in section 5.3

The approximate envelope of the spectrum, $\epsilon_\kappa < \epsilon_0\sqrt{\gamma}$ is due to the adiabatic shrinking of the phase space volume described in section A.2.3 and the proportionality of $\vec{\omega}$ to $(G\gamma + 1)$ in the main quadrupoles: $\epsilon \sim (G\gamma + 1)\sqrt{J_y} \sim (G\gamma + 1)/(\sqrt{\beta\gamma}) \sim \sqrt{\gamma}$ in the limit $\gamma \to \infty$.

For the non–flat as well as for the flattened version of HERA–p, first order resonances involving the horizontal and longitudinal tunes also exist. Their spectrum is explained in [GH99b]. In particular they are much weaker, namely with $\epsilon_x < 0.03$ and $\epsilon_z < 0.008$.

The large number of super–strong and close–by strong vertical intrinsic resonances requires the installation of Siberian Snakes in the ring. We note that in all three plots of figure 5.3 the "background" resonances are particularly strong around 820 GeV!

5.2.1 Snake schemes

In the following we will discuss various snake schemes. The snakes are always modelled by point–like spin rotator maps. Owing to the number of tested schemes and the number of parameters needed to unambiguously characterize each of them, a convention to abbreviate the parameters was introduced. The key to this coding is explicitly given in appendix C. All simulations except those for the ramps in section 5.4.2 were done using the 1996 luminosity optics hp96lu820 or the 1996 separation optics hp96se820 with the modifications explained above in section 5.2. All snake schemes include 6 radial flattening snakes to compensate the vertical bend sections at the beginning of the arc octants OL, OR, SL, SR, NL and NR. Note that since the straight sections are globally straight the flattening snakes cancel each other pairwise and hence their only contribution to the spin tune apart from cancelling the effects of the vertical bends is that each of them takes $G\gamma$ times 60.416 mrad spin precession angle out of the total spin precession balance in theorem 3.1. The design orbit spin tune in HERA–p with 6 flattening snakes is

$$\nu_0^{\mathrm{HERA,6fs}} \approx G\gamma\left(1 - \frac{6 \times 60.416\,\mathrm{mrad}}{2\pi}\right) \approx \frac{E_0}{555\,\mathrm{MeV}} \quad . \tag{5.3}$$

We will in general call a scheme with 6 flattening and $2N$ main snakes a "$2N$ snake scheme". Schemes with 4 and 8 (main) snakes have been tested. All schemes have 4 main Siberian Snakes. Three of them are placed at the beginning of the octants NL, OR, SR directly after the superconducting vertical BV magnet as seen from the IP and the fourth is inside the straight section around the West IP. These snake positions will be named after the closest IP, i.e. O, S, W and N. With these snake positions and properly chosen snake angles, the design orbit spin tune is typically $\nu_0 = 0.499955 \pm 0.000003$ in the energy range from 40 to 820 GeV. These snake positions are at places where drift spaces of about 10 m can be created without too much effort. The 4 additional snakes of the 8 snake schemes are placed at the centres of the arcs, i.e. "on top of" the cryogenic supplies. We will call these positions SO, SW, NW and NO. Because of the technical difficulties mentioned above, the 8–snake schemes are mainly of theoretical interest but there are proposals for "bending snakes" that could replace dipoles in the arcs [YD97].

If the results obtained with the SRM with snakes in section 4.8 can at some level be considered as a guideline for HERA–p, then one might conclude that for *uniformly* distributed snake positions 10 snakes are "better" than 6 which are "better" than 2 but that 8 snakes are *not* necessarily "better" than 4 which are rather "worse" than 2. Here "better" means that a snake scheme provides a *larger* $P_{\rm lim}$ averaged over $\nu_0 - \kappa$ even for *larger* resonance strength ϵ, that the spin tune spread is *less* and that it generates *fewer* higher order kinetic resonances. The suggestion was made in [SPC99] to put 6 main snakes in HERA–p. But it must be noted again here that it is far from clear that the isolated resonance model is a useful approximation of spin dynamics in rings with strongly overlapping resonances as in HERA–p. Owing to the low superperiodicity of $P = 1$ all intrinsic resonances are allowed in HERA. The fractional vertical betatron tune is approximately 0.3, so that the separations $\Delta\kappa$ in units of ν_0 the vertical linear intrinsic resonances are approximately 0.6 between $k_0 - [Q_y]$ and $k_0 + [Q_y]$ and 0.4 between $k_0 + [Q_y]$ and $k_0 + 1 - [Q_y]$. Therefore in order to apply the isolated resonance model, the resonance strengths have to be $|\epsilon_\kappa| \ll 0.4$. Looking at figure 5.3 we find that in the neighbourhood of the super–strong resonances there are many resonances with strengths which are of the order of and greater than 0.4. Moreover in the high energy regime the "background" resonance strengths are all of the order of 0.1 which is still *not* small compared with 0.4, if we take into account that the opening angle ϑ_n of the $\hat{n}$–axis in the SRM from equation (4.81) at δ/ϵ =1, 2, 3, 4 and 10 is 45°, 26.6°, 18.4°, 14.0° and 5.7° respectively. Thus the opening angle created by any of the weakest resonances of approximate strength 0.1, when treated as isolated, at a distance $\delta = 0.4$ is 14.0°. If the closest by neighbour resonance is located at this distance, then the resonances must be treated as overlapping. The simulations in section 4.8 were performed with $P = k_0 = 120$ which implies very high symmetry and allows 2, 4, 6, 8, 10, 12, 20, 24, 30, 40, 60 or 120 snakes to be *uniformly* distributed w.r.t. the azimuth θ. HERA–p has 4 identical periodic arcs interleaved with 4 individual insertions which each consist of a straight section and the adjacent matching sections with or without vertical bends at the borders to the periodic arcs. If we, in a very crude approximation, neglect the differences between the insertions, then HERA–p has a superperiodicity of 4. We will call this level of symmetry the *arc–periodicity* $P_a = 4$. Now we assume a snake scheme which is *uniformly* distributed w.r.t. the uncompensated bend angle per arc $\widetilde{\Theta} \equiv \Theta_{\rm arc} - \Theta_{\rm comp,arc}$ (see section 3.1.3) as in the case of the Lee–Courant schemes discussed in section 4.8 and which contains a number $2(2l+1)$ of snakes which implies that the number of snakes is *not* a multiple of 4. Such a snake scheme is then incompatible even with the crudest approximation of symmetry in HERA–p. Therefore, and because of the technical difficulties introduced by placing snakes *in* the arcs due to lack of drift spaces, schemes with 6 snakes will *not* be discussed here.

In order to obtain longitudinal polarisation at the S- and N–IP 90° spin rotators have to be included at the entrance and the exit of the S and N straight sections. There are some advanced ideas [BS99] on *combining* flattening-, main–snakes and 90° spin rotators, in order to minimise the number of additional magnets. Nevertheless, since no decision on explicit rotator schemes was made yet, the simulations for this thesis do *not* contain any 90° spin rotators.

When equipping a flattened accelerator with $2N$ horizontal Siberian Snakes one can fix the design orbit spin tune $[\nu_0] = {}^1\!/_2$ and fix $\hat{n}_0$ to be vertical in all but the flattened vertical bend section. This requires that the positions of the main snakes be chosen so that the uncompensated horizontal bend

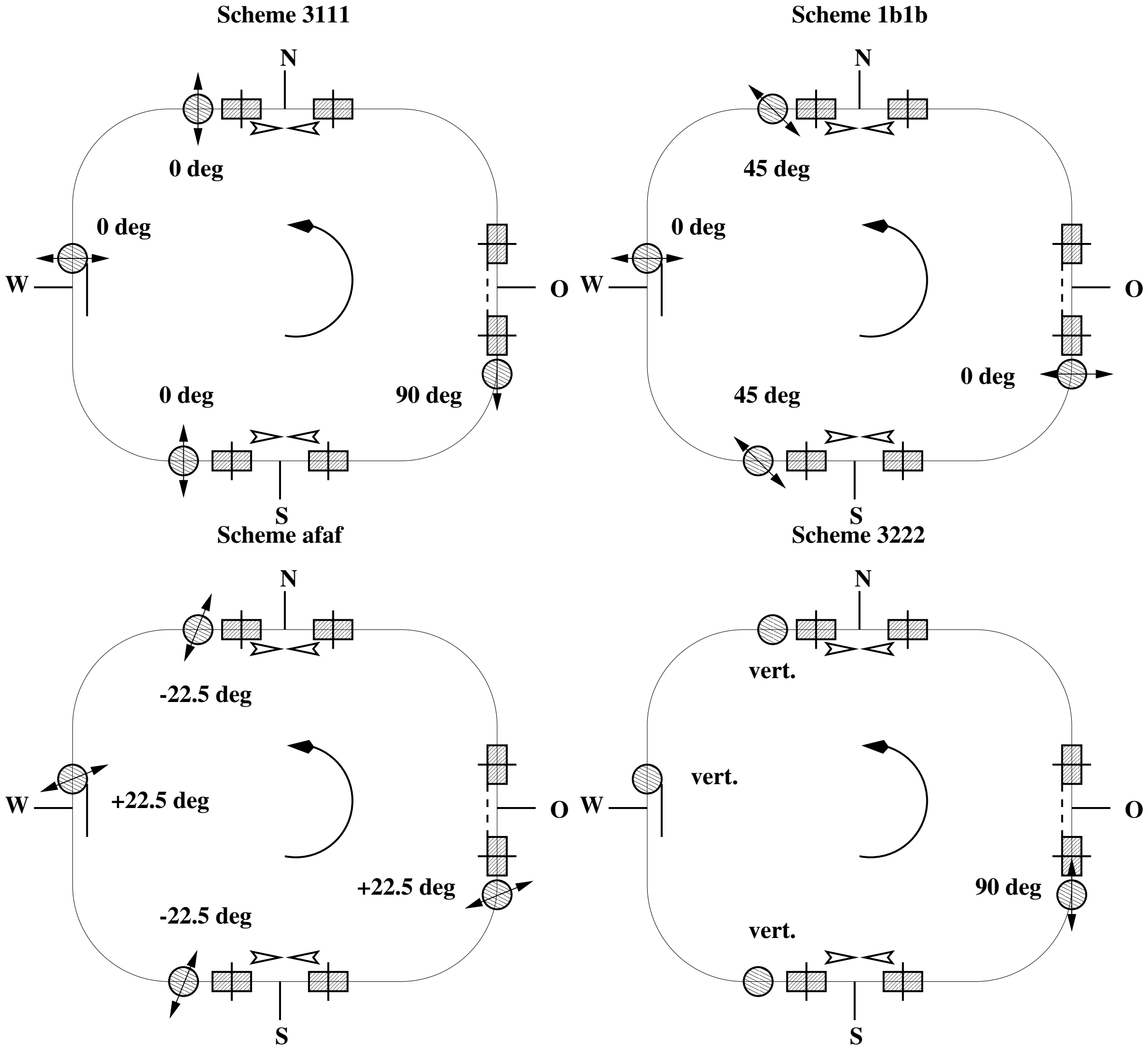

Figure 5.4: Standard 4–snake arrangements for HERA–p

angles $\widetilde{\Theta}_i \equiv \Theta_i - \Theta_{i,\mathrm{comp.}}$ between the main snakes balance to zero

$$\sum_{i=1}^{2N} (-1)^i \widetilde{\Theta}_i = 0 \tag{5.4}$$

and that the snake angles ϕ_i fulfil the condition

$$\sum_{i=1}^{2N} (-1)^i \phi_i = \frac{\pi}{2} \bmod \pi \quad . \tag{5.5}$$

Nevertheless for $2N$ horizontal snakes this leaves $2N-1$ free snake angles. How are the snake angles to be chosen? Perhaps some special combinations of snake angles can maximise P_{lim} at some given working energy *and* minimise losses of the average spin action during the ramp procedure. To investigate this we define the *snake periodicity* P_s to be the number of identical sub–sequences of snake angles in the snake scheme. We also need the *mirror parity* M w.r.t. the O–W–axis. For the snake angles ϕ_{octant}, $M = \pm 1$ signifies

$$\phi_{\mathrm{SO}} = \pm\phi_{\mathrm{NO}} \quad , \quad \phi_{\mathrm{S}} = \pm\phi_{\mathrm{N}} \quad , \quad \phi_{\mathrm{SW}} = \pm\phi_{\mathrm{NW}} \quad , \tag{5.6}$$

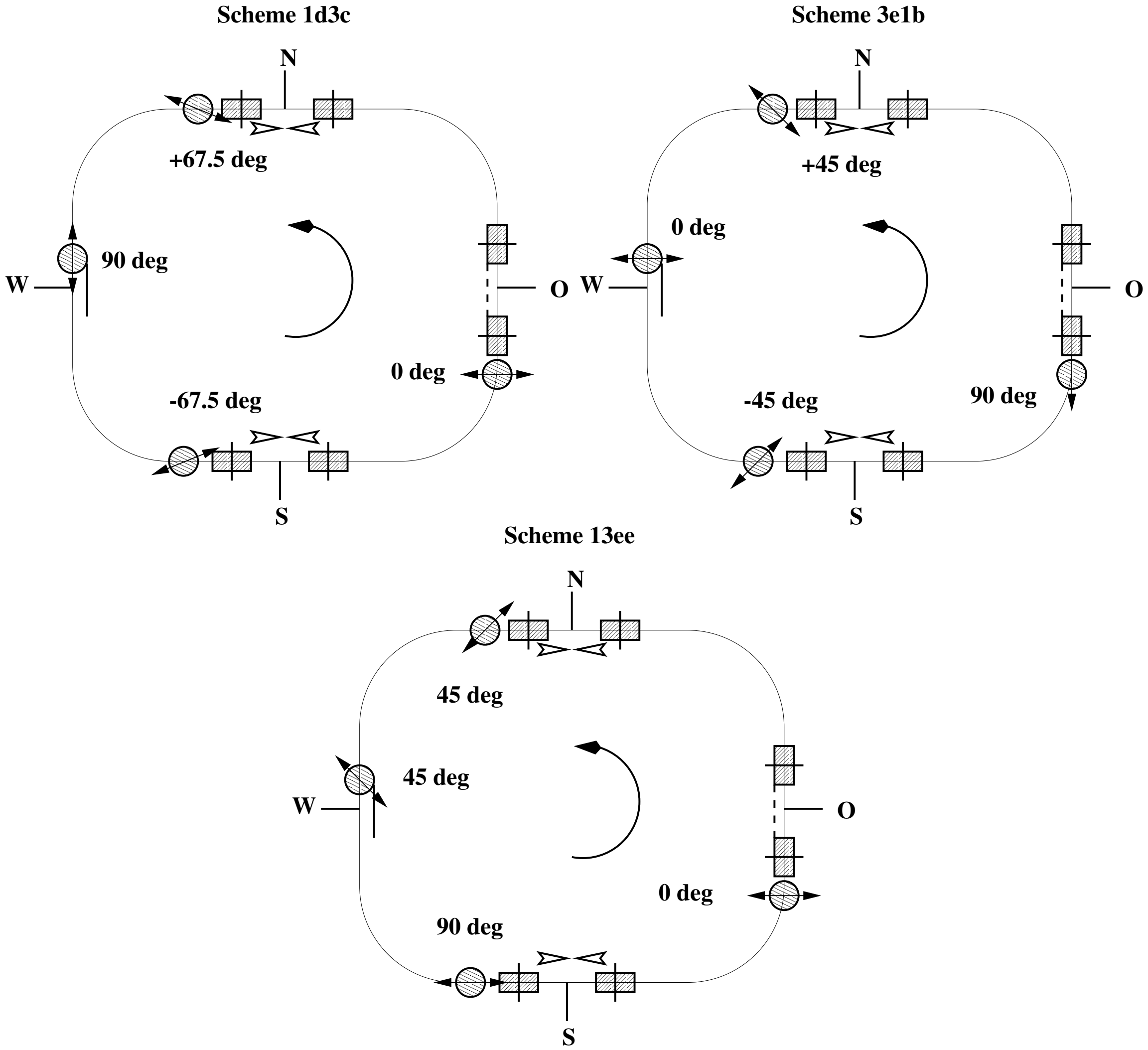

Figure 5.5: 4–snake arrangements for HERA–p found by filtering

and $M = 0$ signifies no mirror symmetry at all. The schemes are (see appendix C for the naming convention):

Schemes with four (main) Siberian Snakes

- Standard schemes which either have the maximal snake periodicity $P_s = 2$ for 4 snakes or are built from the two basic horizontal snakes types, namely longitudinal and radial.
  - **3111** : A longitudinal snake at O and radial snakes at S, W and N. This scheme has $P_s = 1$ and $M = +1$. It was first proposed in [SPC96] and a similar scheme with the snakes at O and W interchanged was suggested even earlier in [BG96]. A schematic sketch of the 3111 scheme is presented in figure 5.4 (top left).
  - **1b1b** : Radial snakes at O and W and snake angles of $+45°$ at S and N. This scheme has the maximum snake periodicity $P_s = 2$ and is O–W even: $M = +1$. This and the next scheme were motivated by the popular opinion that the snake periodicity should be as high as possible and by the popular prejudice that HERA–p is 4–fold superperiodic. The 1b1b scheme is depicted in figure 5.4 (top right).

- **afaf** : Snake angles of $+22.5°$ at O and W and $-22.5°$ at S and N. It also has $P_s = 2$ and $M = +1$. Actually afaf can be obtained from 1b1b by subtracting $22.5°$ from each snake angle and multiplying the result with -1. The afaf scheme is depicted in figure 5.4 (bottom left).

- **3222** : A longitudinal snake at O and 3 *vertical* snakes at S, W and N. This is not a standard scheme since it only contains one horizontal snake. Therefore $\hat{n}_0$ is in the horizontal plane as explained in section 3.1.1. The vertical snakes shift the spin phase advance between adjacent sections of the ring and can therefore help to minimise spin–orbit coupling integrals at certain energies. This scheme was obtained [BH96a, BH96c] in an early stage of filtering where only radial, vertical and longitudinal snakes where taken into account. The filtering range was from 815 to 820 GeV. The 3222 scheme is shown in figure 5.4 (bottom right).

- 4–snake schemes found by filtering (see section 4.4.1) with snake angles ranging from $0°$ to $157.5°$ in steps of $22.5°$.
  - **1d3c** : A radial snake at O, a longitudinal snake at W and $\pm 67.5°$–snakes at S and N [VB98]. This scheme minimised the linear opening angle with the luminosity optics hp96lu820 in the range from 39.5 GeV to 821.5 GeV. The snake periodicity is $P_s = 1$ and the O–W mirror parity is $M = -1$. 1d3c is shown in figure 5.5 (top left).
  - **3e1b** : A longitudinal snake at O, a radial snake at W and two $\pm 45°$–snakes at S and N [VB98]. This scheme minimised the linear opening angle averaged over the interval from 39.5 GeV to 821.5 GeV with the separation optics hp96se820. It has $P_s = 1$ and $M = -1$ and is shown in figure 5.5 (top right).
  - **13ee** : A radial snake at O, a longitudinal snake at S and two $-45°$ snakes at W and N. This fairly exotic and asymmetric scheme ($P_s = 1$ and $M = 0$) minimised the linear opening angle in the energy range 815 to 820 GeV with the optics hp96lu820. It is shown in figure 5.5 (bottom).

Schemes with eight (main) Siberian Snakes

- Standard schemes that were derived by generalising the 3111, 1b1b and afaf schemes to 8 snakes.
  - **31111111** : A simple generalisation of 3111, namely a longitudinal snake at O with all others (SO, S, SW, W, NW, N and NO) being radial. It has a snake periodicity of $P_s = 1$ and an O–W mirror parity $M = +1$. A sketch of 31111111 is shown in figure 5.6 (top left).
  - **4X1a** : Radial snakes at O, S, W and N and $+22.5°$ snakes at SO, SW, NW and NO. This is a generalisation of the 1b1b scheme with $P_s = 4$ and $M = +1$. It is shown in figure 5.6 (top right).
  - **4Xpm1125** : $+11.25°$ snakes at O, S, W and N and $-11.25°$ snakes at SO, SW, NW and NO. This is a generalisation of the afaf scheme to 8 snakes with $P_s = 4$ and $M = +1$. It is shown in figure 5.6 (bottom left).

- **32121212** : A longitudinal snake at O, 3 radial snakes at S, W and N, and four vertical snakes at SO, SW, NW and NO. This scheme is like 3111 with 4 additional vertical snakes at the centres of the arcs. Again the vertical snakes change the spin phase advances between adjacent sections and therefore change the dependence of the spin–orbit coupling integrals on energy. A sketch of 32121212 is shown in figure 5.6 (bottom right).

- 8–snake schemes found by filtering with snake angles ranging from $0°$ to $135°$ in steps of $45°$.

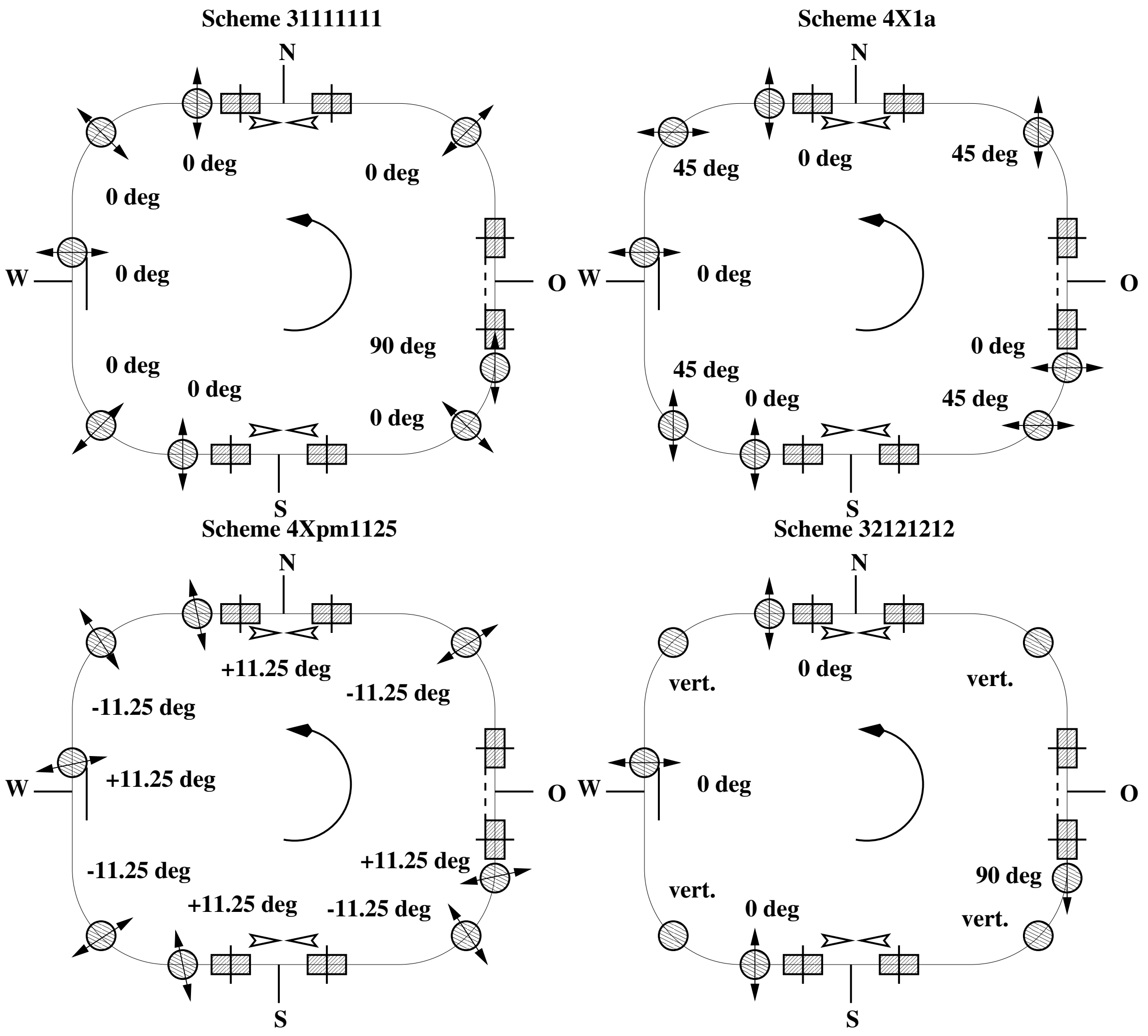

Figure 5.6: Standard 8–snake arrangements for HERA–p

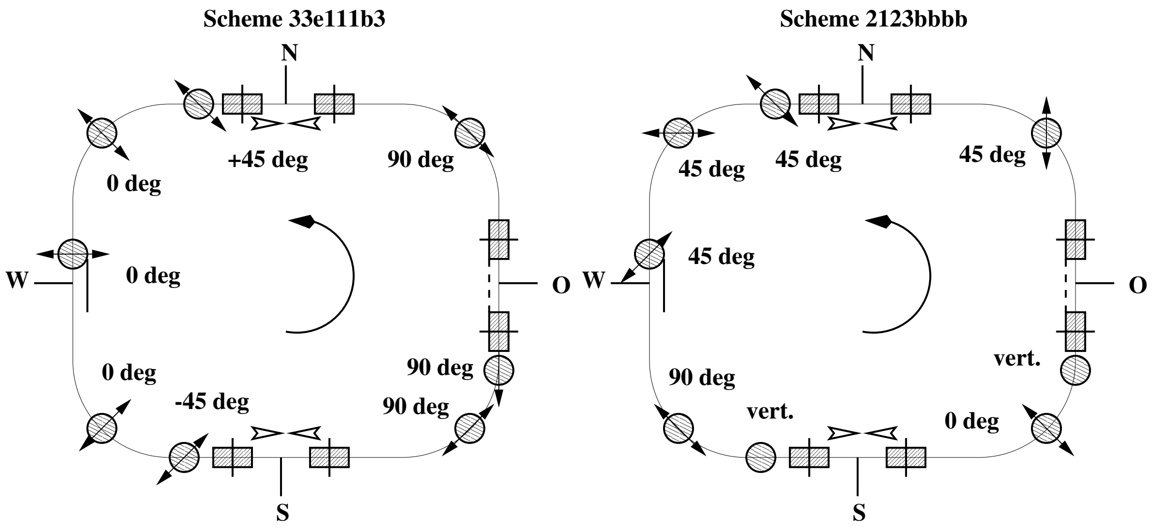

Figure 5.7: 8–snake arrangements for HERA–p found by filtering

– **33e111b3** : A longitudinal snake at O, a radial snake at W, two $\pm 45°$–snakes at S and N, two longitudinal snakes at SO and NO and two radial snakes at SW and NW. This actually means 3e1b at the positions close to the IPs plus 2 radial and 2 longitudinal snakes at the centres of the arcs. Among the 8–snake schemes it minimised the linear opening angle from 39.5 GeV to 821.5 GeV with the luminosity optics hp96lu820 and has a snake periodicity of $P_s = 1$ and an O–W mirror parity of $M = -1$. It is shown in figure 5.7 (left).

– **2123bbbb** : Clockwise from O to NO the snakes are vertical, radial, vertical, longitudinal and 4 times $+45°$. This scheme minimised the linear opening angle in the range from 815 to 820 GeV with the luminosity optics. It has $P_s = 1$ and $M = 0$ and is shown in figure 5.7 (right).

We note that for 4- as well as for 8–snake schemes long range filtering with the HERA lattices, i.e. filtering over momentum ranges in which super–strong resonances as well as regions with "only" background resonances are included, seems to give preference to schemes with odd mirror parity $M = -1$ rather than with high snake periodicity.

5.3 Simulations with the unmodified orbital tunes

At an early stage of this study scans of P_{lim} w.r.t. the reference momentum p_0 where only performed at high energy with the optics hp96lu820. The orbital tunes were taken from the official HERA–p optics files, although at a later stage it turned out that modified orbital tunes might help to increase P_{lim}. One purpose of those scans was to find a snake scheme which maximises P_{lim} on all tori with significant particle density over some sufficiently wide momentum range close to the 1996 reference momentum of 820 GeV. Another purpose was to estimate the potential for depolarisation during acceleration through the region of the strongest linear intrinsic resonance around 803.5 GeV by looking at the dependence of P_{lim} on p_0 in this momentum range.

All these scans were performed using the linear (`SLIM` , see section 4.2) and stroboscopic averaging (`SPRINT` , see section 4.5) methods to compute the invariant spin field on various invariant tori and in certain momentum ranges. The qualitative reason for possible depolarisation around 803.5 GeV, to be presented in section 5.3.1 will be confirmed by ramp simulations in section 5.3.2. At that stage neither the pseudo spin tune averaging (`SPRINT` , see section 4.6) nor the Fourier (`SODOM-2` , see section 4.3) methods for computing the amplitude dependent spin tune were implemented in the `SPRINT` code. At a later stage the `SODOM-2` method for computing $\hat{n}$ as well as ν was employed to scan larger momentum ranges with purely vertical motion. The results of these simulations will be presented in section 5.3.3.

All simulations were made taking the East interaction point (O–IP) as the viewpoint. The amplitude dependent spin tune is of course independent of θ but in general P_{lim} does depend on the viewpoint. Preliminary studies which will perhaps be published elsewhere indicate that P_{lim} is a weakly varying function of θ in the arcs, that the dependence of P_{lim} on θ is strongest at the S and N straight sections, that the variation of P_{lim} with θ increases with increasing orbital actions and that the explicit form of the θ–dependence depends on the snake scheme. Therefore in [GH99b] which contains the data of more recent simulations, the S–IP was chosen as the viewpoint. We begin by studying the static behaviour of P_{lim}.

5.3.1 Momentum scans using stroboscopic averaging

Figures 5.8 and 5.9 show P_{lim} for the 4–snake schemes 3111, 1b1b, afaf and 3222 (figure 5.8) and 1d3c and 13ee (figure 5.9) computed with the `SLIM` method from 800 to 820 GeV (top) and with the `SPRINT` method, i.e. stroboscopic averaging, from 800 to 808 GeV and from 814 to 822 GeV (below). Note that in the linear case $P_{\text{lim}}^{(1)}$ is basically $1/(1+\Delta^2)$ where Δ is the linear deviation of $\hat{n}$ from

$\hat{n}_0$ and scales with the orbital amplitudes. See (4.63). The linear approximation is very fast but is only capable of providing a first impression. The non–perturbative SPRINT method shows much more structure caused by the higher order kinetic effects that are invisible in the SLIM approximation. In both figures *only* vertical orbital motion is excited and the normalised vertical emittance enclosed by the invariant ellipse is chosen to be $\varepsilon_y^N = 20\pi$ mm mrad. The momentum range of 800 — 821

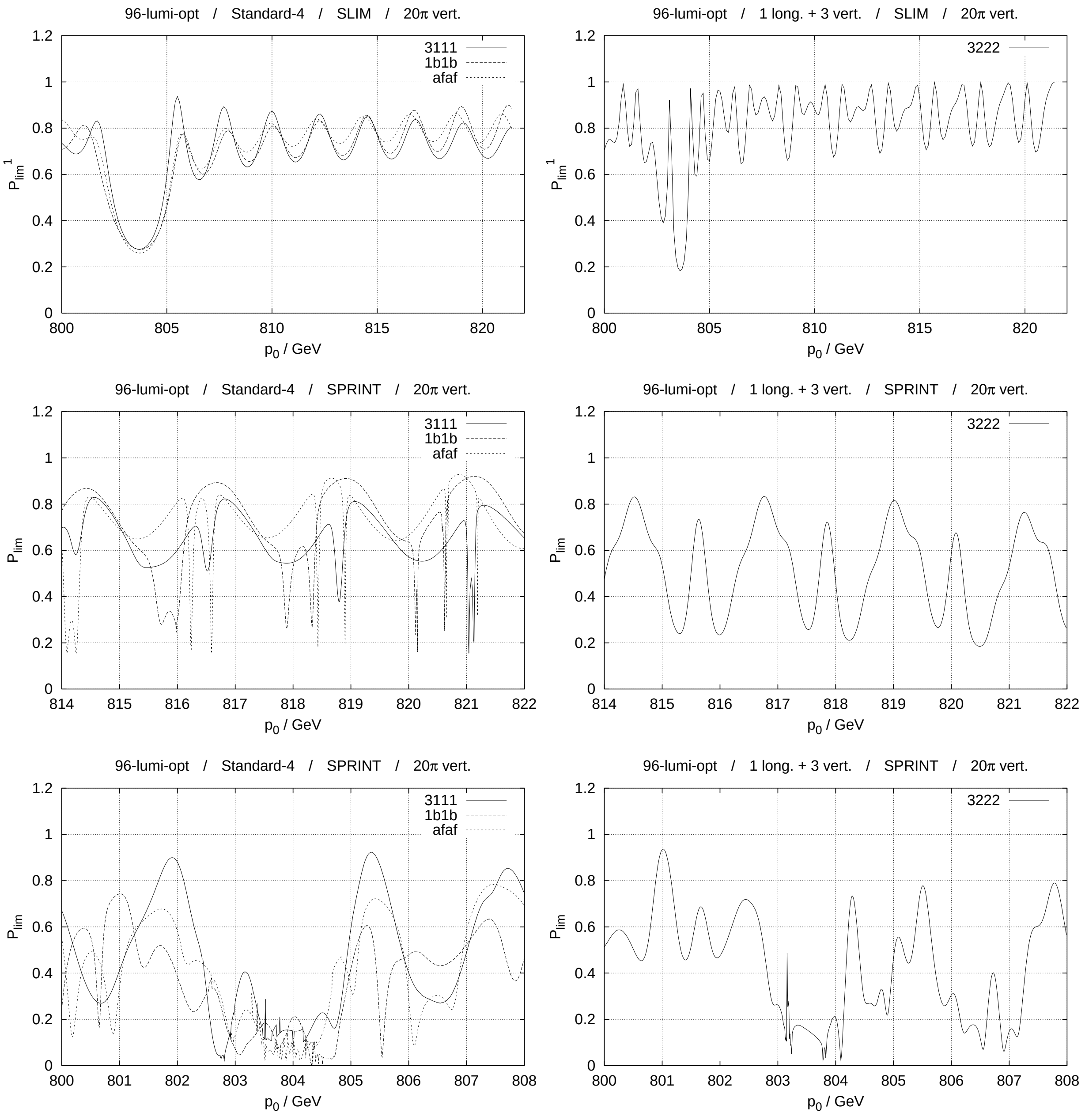

Figure 5.8: Standard 4–snake schemes: P_{lim} for an enclosed vertical emittance of 20 π mm mrad. Top: Linear (SLIM) approximation in the momentum range 800 to 821 GeV. Below: computed with the SPRINT method from 814 to 822 GeV (middle) and from 800 to 808 GeV (bottom).

GeV for the SLIM runs was chosen because it contains the 1996 HERA–p working point as well as the strongest linear intrinsic resonance of HERA–p without snakes at about 803.5 GeV (see figure 5.3). The momentum ranges for the stroboscopic averaging were chosen to be shorter, i.e. 8 GeV, because of the larger computation time. The momentum step is 10 MeV in all simulations. As we can see in figure 5.8, the linear P_{lim} (top left) looks qualitatively similar for the conventional 3111, 1b1b and afaf schemes. The momentum dependence in the region above 810 GeV is relatively smooth and the polarisation is approximately in the intervals $[0.65, 0.85]$ for 3111, $[0.65, 0.9]$ for 1b1b and $[0.7, 0.85]$ for afaf. The strong dip in the polarisation curve in the region around 803.5 GeV goes down to about 0.28. At the linear level this can be explained by the following argument: A linear intrinsic resonance with purely vertical motion occurs at the reference momentum p_0 whenever the spin tune $\nu(p_0)$, which is just $\nu_0(p_0)$ at the linear level, fulfils the condition $\nu_0(p_0) = k_0 \pm Q_y$. Siberian Snakes cause ν_0 to be independent of the momentum and in particular ensure that the condition $\nu_0(p_0) = k_0 \pm Q_y$ can never be fulfilled with a reasonable vertical tune. The spin–orbit coupling integrals are nevertheless in general non–zero even with snakes. In other words Siberian Snakes cannot be expected to cancel finite perturbations of the spin motion completely. The reason for enhancement of the super–strong resonances in superperiodic rings is coherence between the contributions to the spin–orbit coupling integrals of the regular FODO cells in the arcs *close* to an actual resonance condition $\nu_0(p_0) = k_0 \pm Q_y$ without snakes. Even if, *with* snakes and $\nu_0 = {}^1\!/_2 =$ const., no linear intrinsic resonance condition can be fulfilled, the almost coherent adding up of the contributions of the regular cells in each section *between* the snakes still occurs at approximately the same momenta as without snakes. We will therefore call a large variation of P_{lim} that arises when the spin–orbit coupling integrals are enhanced due to the approximate coherence of the regular arc cells and which are at momentum ranges that would include a super–strong resonance or a super–strong cluster of resonances if there were no main snakes, a **residual resonance structure (RRS)**. Note that the coherence condition for the strictly periodic cells of each arc alone is, for HERA–p, not affected by the flattening snakes which are located inside the matching sections. The phase relation between the spin–orbit coupling integrals of the 4 different quadrants on the other hand *is* affected by the flatteners as well as the snake angles of the main snakes. Thus we cannot expect the centre of a RRS to be *exactly* at the same momentum as its corresponding super–strong resonance or the centre of its corresponding super–strong cluster in the absence of snakes.

Obviously the linear approximation to P_{lim} reaches the edge of its applicability at these RRSs since the condition $\Delta \ll 1$ is violated. In the following, when higher order kinetic effects are taken into account, we will see that RRSs define the momentum ranges in which not only P_{lim} is strongly energy dependent and potentially low but also in which the amplitude dependent spin tune strongly deviates from ν_0 (see section 5.3.3) and in which the kinetic resonance strengths are particularly enhanced. We note that by means of a partial spin match [GH99b] the residual resonance structures can be eliminated *on the linear level*, but that in particular in these regions the kinetic non–linearities become important. Furthermore inside these RRSs and on certain invariant tori the non–perturbative `SPRINT` and `SODOM-2` algorithms exhibit momenta at which they apparently both do not converge. This might be caused by a simultaneous breakdown of the two independent algorithms but it might as well be a sign of non–integrability of the spin–orbit system at these momenta and invariant tori.

The 3222 scheme shown in figure 5.8 (top right) differs strongly from the other 3 schemes already in the linear approximation. First of all the momentum dependence of the polarisation is much less smooth and covers a larger interval, approximately $[0.65, 0.99]$. In addition the minimum around 803.5 GeV goes down to 0.2 rather than 0.28. This is not surprising since the effect of partial cancellation of spin perturbations is caused by the horizontal snakes (section 3.1.1 and 3.1.2) whereas the vertical snakes mainly redistribute the magnitudes of the spin–orbit coupling integrals w.r.t. the reference momentum. But note that $P^{(1)}_{\text{lim}}$ reaches almost 1 for the scheme 3222 whereas for the 3 standard schemes it is hardly more than 0.9 even at the local maxima.

For the non–perturbative P_{lim} computed by stroboscopic averaging the differences between the various snake schemes become clearer. Figure 5.8 (middle row) shows the momentum range from 814 to 822 GeV. The schemes 3111 (solid line), 1b1b (dashed line) and afaf (dotted line) are shown to the left and 3222 is shown to the right. The snake scheme 3111 has the weakest variation in this momentum range but 3222, although showing the largest variation, is the smoothest. In particular the minima are the least narrow. The 1b1b and afaf schemes show many sharp pronounced minima indicating possible closeness to kinetic higher order resonances. The 3111 layout has only two close–by ($\Delta p_0 \approx 0.1$ GeV) pronounced minima which suggest a resonance doublet at approximately 821 GeV. The sharp minima of $P_{\rm lim}$ with the 1b1b and afaf schemes can also be interpreted as resonance doublets of larger separation ($\Delta p_0 \approx 0.5$ GeV) indicating a larger spin tune shift. The kinetic resonances will be analysed in more detail in section 5.3.3. Figure 5.8 (bottom row) shows $P_{\rm lim}$ inside and close to the strong RRS from 800 to 808 GeV. In this region none of the schemes is able to maintain a smooth dependence of $P_{\rm lim}$ on the reference momentum. Between 803 and 805 GeV all curves show various singular dips of the static polarisation limit indicating that possibly many kinetic resonances occur there. It has to be noted that inside the RRS at points where $P_{\rm lim}$ is close to zero also the accuracy of stroboscopic averaging is potentially low. At some isolated points there was no sign of convergence of the stroboscopic average — even after 8000 turns. Thus it is possible that for certain parameters of the spin–orbit system the $\hat{n}$–axis does *not* exist. Nevertheless large errors of the numerical pseudo–$\hat{n}$–axis never occur when $P_{\rm lim}$ is sufficiently large. It is clear that the working point for polarised $e^{\pm}$–p collisions must not be inside such a RRS. Nevertheless during the ramp procedure many residual resonance structures have to be crossed. For the discussion of possible depolarisation during acceleration it is almost immaterial whether the invariant spin field exists and the parameter space is filled with kinetic depolarising resonances or whether the spin motion is not integrable at all. In both cases a large fraction of the initial polarisation is lost during acceleration through the RRS. This is the reason why the strong RRSs, indicated by sudden drops of $P_{\rm lim}$ are considered potentially dangerous during the ramp procedure. For the discussion of the RRS around 803.5 GeV in this section it was assumed that, although the ramp procedure in this energy range is performed with the separation optics, the *basic* phenomena that are potentially responsible for polarisation losses during the acceleration process can be studied also with the luminosity optics. That this seems a good starting point can be seen by comparison of the Courant–Snyder functions for hp96lu820 and hp96se820 in figure 5.2.

In figure 5.9 the schemes 1d3c and 13ee are compared. The momentum ranges and invariant ellipses are the same as for figure 5.8. The linear $P_{\rm lim}$ (top) shows the same smooth dependence on the reference momentum above 810 GeV as for the 3 conventional schemes, but with a different polarisation range: approximately $[0.65, 0.97]$ for 1d3c and $[0.7, 0.98]$ for 13ee. Both were chosen to minimise the linear opening angle in a certain energy range, which is 39 to 821 GeV in the case of 1d3c and 815 to 820 GeV in the case of 13ee. The most significant difference w.r.t. the "standard schemes" is that the dip of $P_{\rm lim}$ inside the RRS around 803.5 GeV only goes down to 0.5 (1d3c) and 0.4 (13ee). Note that 13ee which was filtered for high energy only supplies a larger $P_{\rm lim}^{(1)}$ for $p_0 > 806$ GeV but that the minimum around 803.5 GeV is deeper. The non–perturbative scans of $P_{\rm lim}$ in the momentum range from 814 to 822 GeV (bottom left) show that the average $P_{\rm lim}$ is still above the level of the "standard schemes" but that there are minima which for both schemes show the onset of resonance doublets at certain momenta. Around 804 GeV (bottom right) the RRS is clearly visible with the low average $P_{\rm lim}$ and the large number of sharp minima. Note that inside the RRS, $P_{\rm lim}$ is larger for 1d3c than for 13ee. Again, inside the RRS where $P_{\rm lim}$ approaches zero and oscillates strongly, the accuracy of the computation of $\hat{n}$ can become insufficient and at isolated momenta the stroboscopic average might not even converge. Since these isolated momenta at which the algorithm breaks down occurred with all snakes schemes, this is obviously a fundamental aspect of the lattice parameters and the momentum range.

One may draw two conclusions from figures 5.8 and 5.9. First, at high energy, even outside the strong RRS around 803.5 GeV and even with purely vertical motion, the linear approximation is not sufficient to determine a possible working point and to detect potential sources of depolarisation during acceleration. Second, with purely vertical motion the filtered schemes produce, even on the non–perturbative level, a larger average $P_{\rm lim}$ in the momentum ranges over which filtering was performed.

Figures 5.10 and 5.11 show the static polarisation limit computed with the `SPRINT` algorithm for various invariant tori. The tori are characterised by the orbital amplitudes normalised by the rms

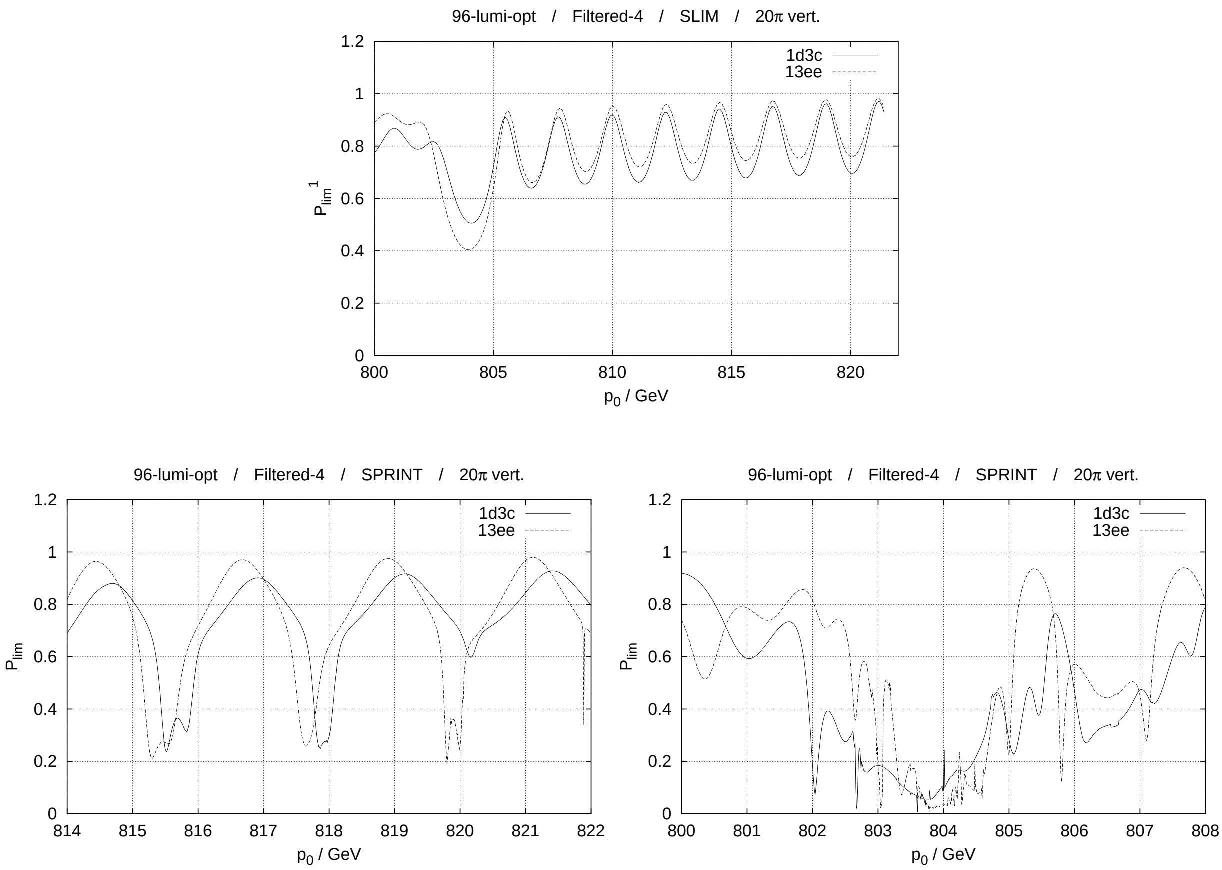

Figure 5.9: Filtered 4–snake schemes: $P_{\rm lim}$ for an enclosed vertical emittance of 20 π mm mrad. Top: Linear (`SLIM`) approximation in the momentum range 800 to 821 GeV. Below: computed with the `SPRINT` method from 814 to 822 GeV (left) and from 800 to 808 GeV (right).

beam width σ in each eigenplane. The phase space distribution was assumed to be Gaussian. In particular the symbol $(a_x, a_y.a_z)$ means that the horizontal (vertical, longitudinal) amplitude is $a_x\sigma_x$ $(a_y\sigma_y,\ a_z\sigma_z)$.

1 σ corresponds to 4 π mm mrad in the horizontal and vertical planes and to about 1.8 π 10^{-2} m rad in the longitudinal plane. The latter corresponds to a relative energy spread of about $1.2\cdot 10^{-4}$ and a bunch length of about 20 cm at 820 GeV.

Using equation (A.115) of the appendix and the relation $J_{a\sigma} = a^2 J_{1\sigma}$ we find that the fraction of the beam contained in the phase space volume enclosed by the product of the invariant ellipse of $a\sigma$ in one eigenplane and the complete integral over the two other planes is

$$F_1(a) \equiv 1 - e^{-a^2/2} \Rightarrow F_1(1) \approx 0.39 \ , \ \ F_1(2) \approx 0.86 \ , \ \ F_1(2.45) \approx 0.95 \ , \ \ F_1(3) \approx 0.99 \ . \tag{5.7}$$

If we assume for simplicity that the distributions in the three eigenplanes are independent, then we find that the fraction of particles contained *inside* the torus with $a_x\sigma_x$, $a_y\sigma_y$ and $a_z\sigma_z$, i.e. with $J_x < a_x^2 J_{x,1\sigma}$, $J_y < a_y^2 J_{y,1\sigma}$ and $J_z < a_z^2 J_{z,1\sigma}$ is

$$\begin{aligned} F_3(a_x, a_y, a_z) \quad &= \quad F_1(a_x)F_1(a_y)F_1(a_z) \Rightarrow \\ F_3(1,1,1) \approx 0.06\ ,\ F_3(1.5,1.5,1.5) \approx 0.31 \quad &, \quad F_3(2,2,2) \approx 0.65\ ,\ F_3(2.5,2.5,2.5) \approx 0.87\ . \end{aligned} \tag{5.8}$$

If one can demonstrate that all particles *inside* the $(a_x, a_y, a_z)\sigma$ torus provide $P_{\rm dyn}P_{\rm lim} \approx 1$ at some properly chosen working energy, then the beam average of the polarisation is at *least* $F_3(a_x, a_y, a_z)$. If,

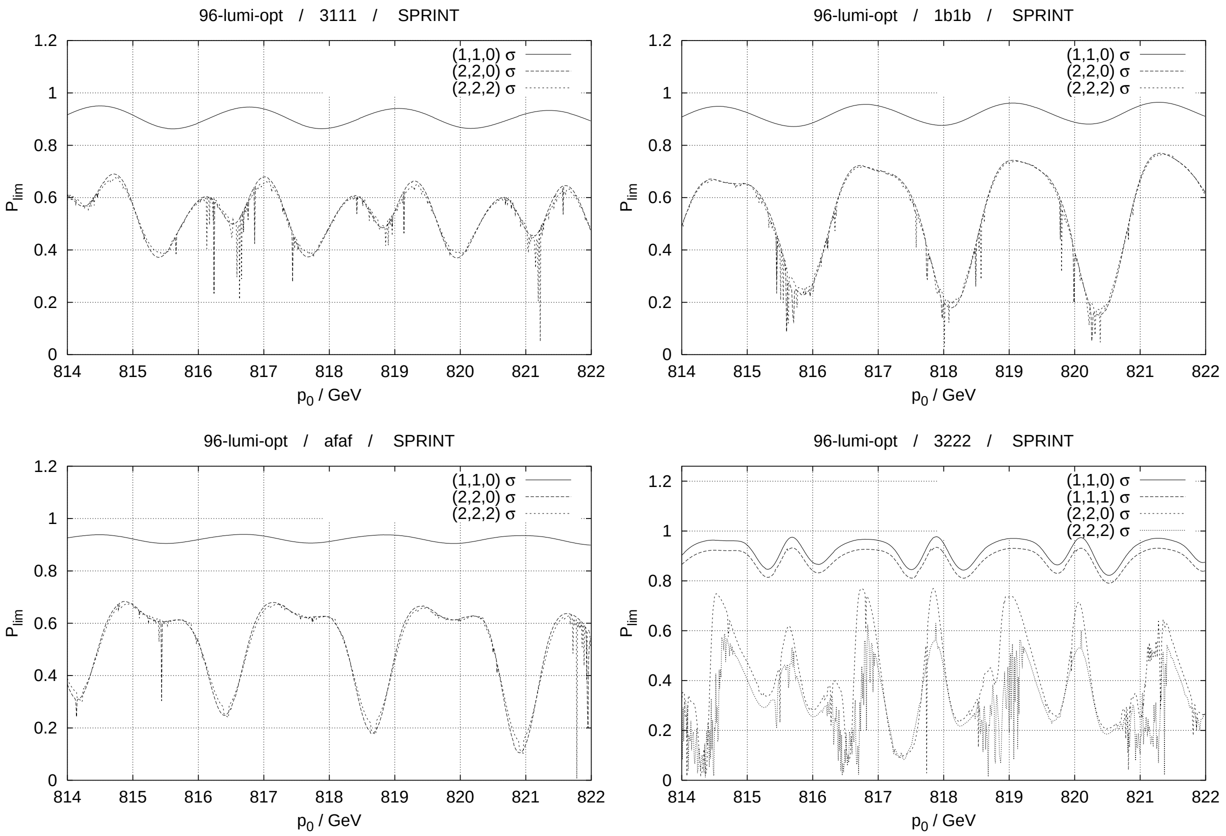

Figure 5.10: Standard 4–snake schemes: $P_{\lim}(p_0)$ computed with the SPRINT method in the momentum range from 814 to 822 GeV with invariant tori corresponding to (1,1,0), (1,1,1), (2,2,0) and (2,2,2)σ beam sizes.

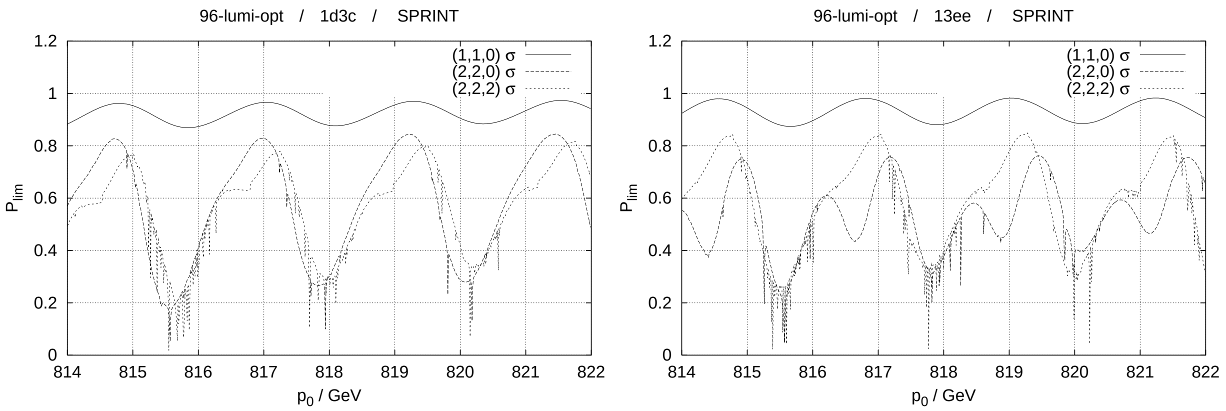

Figure 5.11: Filtered 4–snake schemes: $P_{\lim}(p_0)$ computed with the SPRINT method in the momentum range from 814 to 822 GeV with invariant tori corresponding to (1,1,0), (2,2,0) and (2,2,2)σ beam sizes.

on the contrary, one can show that all particles *outside* the $(a_x, a_y, a_z)\sigma$ torus provide $P_{\rm dyn}P_{\rm lim} \approx 0$, then the beam average of the polarisation is at *most* $F_3(a_x, a_y, a_z)$. Here "inside" means that a particle has orbital amplitudes a_i' which *all* fulfil the constraint $a_i' \leq a_i$ whereas "outside" means that *one* of the orbital amplitudes, say the k-th, has $a_k' > a_k$. A typical strategy to either verify or falsify the assumption that polarised beam operation is possible at some energy and with some set of parameters would be to create a large ensemble of particles so that the ensemble approximates a (truncated) Gaussian phase space distribution of sufficient width and with spins initially parallel to the invariant spin field and accelerate it from injection energy to the top energy. Then at the final energy and at additional intermediate steps the ensemble average of $P_{\rm dyn}P_{\rm lim}$ could be computed and the evolution of the approximate beam polarisation could be simulated. But much more can be learned from simulations of individual tori. By scanning $P_{\rm lim}(p_0)$ and $\nu(p_0)$ (e.g. in section 5.3.3) on these tori, not only potential candidates for a working energy but also regions in momentum and orbital amplitudes which contain higher order kinetic resonances and which therefore potentially diminish $P_{\rm dyn}$ during the acceleration process can be identified much more specifically. The price one has to pay for this is a significant increase of computing time. Therefore one can only sample the amplitude space with a rather small set of triples (a_x, a_y, a_z). In this study we will take the somewhat conservative view that for a high beam average of the polarisation it is necessary to ensure that $P_{\rm lim}$ as well as $P_{\rm dyn}$ are sufficiently high at least inside the (2.5,2.5,2.5)σ torus. Here I have simulated tori with (1,1,0), (1,1,1), (2,2,0) and (2,2,2)σ. In contrast to the linear case (`SLIM`), there is no simple scaling law for the dependence of the polarisation on the emittances but generally the average $P_{\rm lim}$ decreases if the reference torus goes outwards in phase space. With the exception of the 3222 scheme there is, within the numerical precision (<0.1 mrad in the opening angle ϑ_n), no difference between the polarisation on the (1,1,0)σ and the (1,1,1)σ torus in this energy range. In figure 5.10 the polarisation curves for the 3111 (top left), 1b1b (top right), afaf (bottom left) and 3222 (bottom right) schemes are shown. The maximum achievable polarisation on the (1,1,0)σ torus is quite respectable, namely 0.85 to 0.95 and for 3222 it is still high with longitudinal motion (1,1,1) taken into account. When going to 2 σ in the horizontal and vertical planes one observes that the maxima of $P_{\rm lim}$ are shifted to different momenta. Therefore to find a momentum for operating HERA with maximum polarisation, care has to be taken to optimise the average of $P_{\rm lim}$ of *all* tori weighted with their particle density. Furthermore sharp minima appear at certain energies for all the schemes, indicating possible kinetic resonances. A large number of such dips is obviously disadvantageous for operation with polarisation. There is no significant difference between the global behaviour of $P_{\rm lim}$ for the (2,2,0)σ and the (2,2,2)σ tori for 3111, 1b1b and afaf but the number of singular dips is increased as the longitudinal mode is switched on. On the one hand the increase in the number of sharp minima is biggest with 3111 and 1b1b, but on the other the variation of polarisation with energy is lowest for 3111 compared to the other two. The 3222 scheme obviously fails most when going from (2,2,0) to (2,2,2). Not only has the overall average polarisation dropped but also the number of dips has significantly increased and there are regions (e.g. around 819 GeV) where the polarisation curve appears to be almost discontinuous.

Figure 5.11 is analogous to figure 5.10 but for the filtered 1d3c and 13ee schemes. As already expected from the linear energy scans (figures 5.8, and 5.9 top) the average polarisation is slightly higher on the (1,1,0)σ and (1,1,1)σ tori than for the conventional schemes. As with the 3111, 1b1b and afaf schemes the curves on both tori are identical up to the numerical precision. The interval $[P_{\rm lim}^{(\rm min)}, P_{\rm lim}^{(\rm max)}]$ defined by the minimum and the maximum of the *smooth approximation* of $P_{\rm lim}$ in the momentum range from 814 to 822 GeV on the (2,2,0)σ torus and the (2,2,2)σ torus with the filtered schemes (both about $[0.2, 0.8]$) is similar to the interval with 1b1b ($[0.15, 0.75]$) and afaf ($[0.1, 0.65]$). Nevertheless, $P_{\rm lim}^{(\rm max)}$ is higher for both filtered schemes. The variation of the polarisation with 3111 is lower in this momentum range: $[0.35, 0.7]$. Both, 1d3c and 13ee show strong differences between (2,2,0) and (2,2,2). Not only is the number of singular minima increased when longitudinal motion is taken into account, but also the extrema of $P_{\rm lim}$ are shifted to different momenta, so that for noticeable parts of the momentum range the polarisation is higher *with* longitudinal motion than *without*. We note in particular, by comparison of figure 5.9, which was produced with purely vertical motion at 20 π mm mrad, with the curves on the (2,2,0)σ torus in figure 5.11, which correspond to 16 π mm mrad in the horizontal *and* in the vertical plane, that the average P_{lim} can even be higher with slightly *larger* vertical amplitudes as long as *no* horizontal motion is excited. Therefore, despite the popular opinion that horizontal motion only affects the spin motion in the case of strong transverse coupling, horizontal motion definitely *has* to be taken into account.

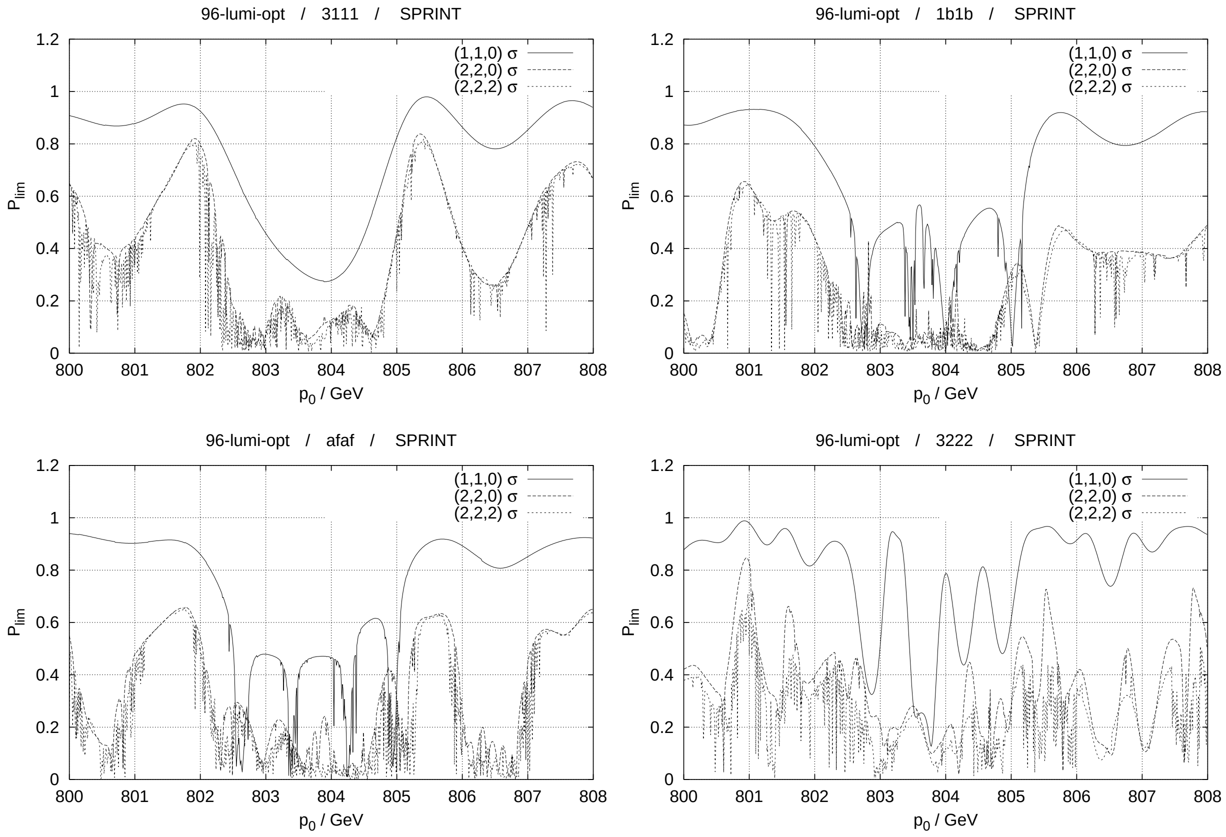

Figure 5.12: Standard 4–snake schemes: $P_{\text{lim}}(p_0)$ computed with the `SPRINT` method in the momentum range from 800 to 808 GeV. The invariant tori correspond to (1,1,0), (2,2,0) and (2,2,2)σ beam sizes.

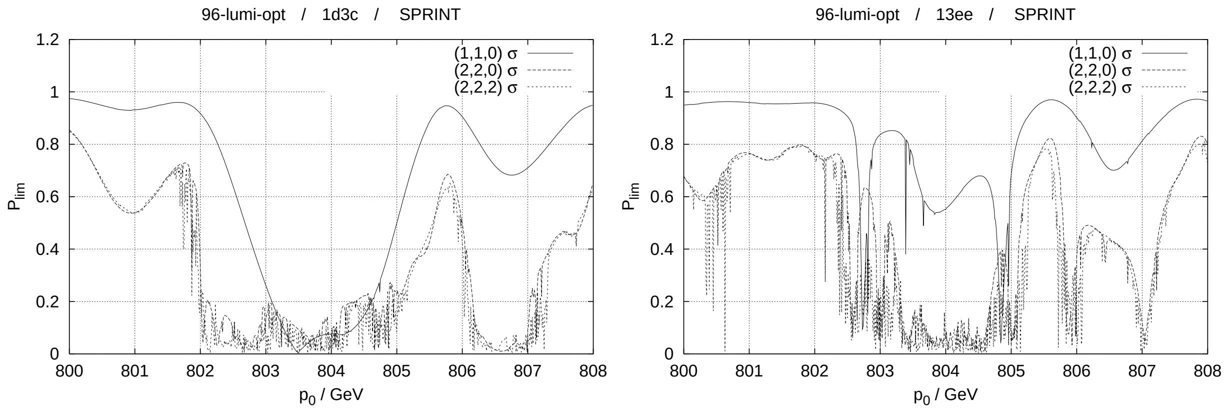

Figure 5.13: Filtered 4–snake schemes: $P_{\text{lim}}(p_0)$ computed with the `SPRINT` method in the momentum range from 800 to 808 GeV. The invariant tori correspond to (1,1,0), (2,2,0) and (2,2,2)σ beam sizes.

Figures 5.12 and 5.13 show $P_{\rm lim}(p_0)$ around the strong RRS at 803.5 GeV for the standard schemes (5.12) and the filtered schemes (5.13). This momentum range was scanned to obtain an estimate for the possible survival of polarisation during the final stage of the acceleration process. Considering the $(1,1,0)\sigma$ torus, the 3111 scheme (top left of figure 5.12) provides the smoothest $P_{\rm lim}(p_0)$ of all, including the filtered schemes. In particular the 4–fold periodic schemes 1b1b and afaf and the scheme 13ee, which was obtained by filtering in the narrow momentum range from 815 to 820 GeV, fail already for these moderate amplitudes. Using equations (5.7) and (5.8) this means that even the *innermost* $F_1(1)^2 \approx 15\%$ of the beam might loose polarisation during acceleration. The 3222 scheme (bottom right of figure 5.12) and the long range filtered scheme 1d3c also provide relatively smooth polarisation curves. The $(2,2,0)\sigma$ and $(2,2,2)\sigma$ tori show many singular minima and points of weak convergence. The density of these possible resonances or points of non–integrability of spin motion increases typically by a factor of 5 to 10 when longitudinal motion is added. Therefore we might expect that none of the tested 4–snake schemes is able to guarantee the survival of the spin action $I = \widehat{S} \cdot \hat{n}$ during acceleration through the strong RRS around 803.5 GeV with the unmodified lattice parameters.

Figures 5.14 and 5.15 show $P_{\rm lim}(p_0)$ for the 8–snake schemes described in section 5.2.1 in linear (`SLIM`) approximation (top) and using the non–perturbative `SPRINT` method for purely vertical orbital motion on an invariant ellipse enclosing an emittance of 20 π mm mrad. These two figures are analogous to 5.8 and 5.9 which were produced with 4 Siberian Snakes. The simulation data for the 3 standard schemes 31111111, 4X1b and 4Xpm1125 is displayed on the left side of the figure 5.14 and the 32121212 scheme which contains 4 horizontal and 4 vertical snakes is shown on the right side. The general impression is that the standard 8–snake schemes, at least on the linear level, smoothen the dependence of $P_{\rm lim}$ on p_0 but that they hardly increase the average $P_{\rm lim}$ in the momentum range scanned. Note that with the scheme 32121212, which can be interpreted as 3111 with 4 additional vertical snakes at the arc centres, the broad minimum at the RRS around 803.5 GeV which can be seen in figure 5.8 is split into two more narrow minima around 802 and 805 GeV (top right of figure 5.14). This effect is caused by the shift of the spin phase advance between the adjacent octants in each arc, which redistributes the strengths of spin–orbit coupling integrals w.r.t. different reference momenta. According to an argument similar to the one used for the derivation of equation (2.146), the spin–orbit coupling integral over one complete arc consisting of two identical halves is $\xi_2(2\pi\Delta^{\pm})$ times the integral over one half, where ξ_2 is the complex amplification function defined in equation (2.147a) and $\Delta^{\pm}$ is the normalised spin phase advance $\pm$ the normalised orbital phase advance over one half arc. The modulus of ξ_2 has a maximum whenever $[\Delta^{\pm}] = 0$. A vertical snake produces an energy independent extra spin phase advance of π at its position. Then the spin–orbit coupling integral over the complete arc has a maximum whenever $[\Delta^{\pm}] = {}^1\!/_2$. Moreover the spin phase advance per arc is increased by π so that the condition for constructive interference of the arcs is changed. The effect is discussed in more detail in [GH99b, VA98] but the effect was actually observed for the first time in[BH96a, BH96c].

The lower two rows in figure 5.14 show data produced with `SPRINT` momentum scans in the range from 814 to 822 GeV (middle) and from 800 to 808 GeV (bottom). The three schemes with 8 *horizontal* snakes provide a particularly smooth polarisation curve around the reference momentum of the 1996 luminosity operation (middle left), whereas the 32121212 scheme (middle right) shows clear candidates for resonance doublets around 814.3 GeV, 817.6 GeV and 818.9 GeV. Note that comparison with 3111 in figure 5.8 (middle left) shows a clear difference between 3111 and 32121212. Unfortunately the comparison also suggests that the four additional vertical snakes are rather disadvantageous in this momentum range and in this region of phase space. The 31111111 scheme, although providing smooth $P_{\rm lim}$, has the lowest average polarisation, namely about 0.4 in the range from 814 to 822 GeV of *all* 4- and 8–snake schemes. But it remains the smoothest when approaching the RRS around 803.5 GeV (bottom left). The two schemes with snake period $P_s = 4$ show more pronounced minima which could be candidates for resonance doublets around 802.4 GeV (4Xpm1125) and 805.5 (4X1a). The 32121212

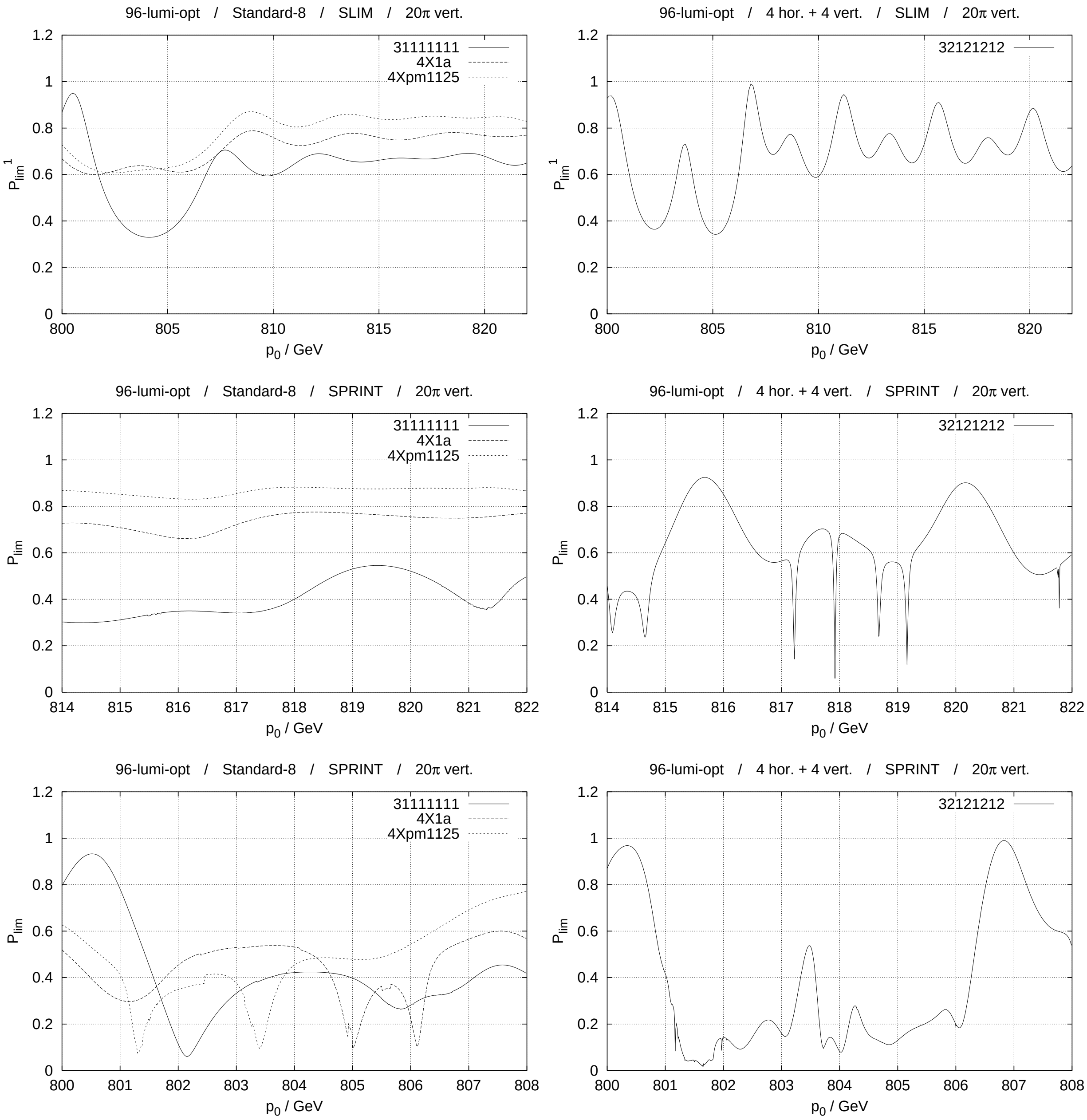

Figure 5.14: Standard 8–snake schemes: $P_{\rm lim}$ for an enclosed vertical emittance of 20 π mm mrad. Top: Linear (`SLIM`) approximation in the momentum range 800 to 821 GeV. Below: computed with the `SPRINT` method from 814 to 822 GeV (middle) and from 800 to 808 GeV (bottom).

scheme provides the least smooth polarisation curve inside the RRS. This is not surprising since it contains only four horizontal snakes.

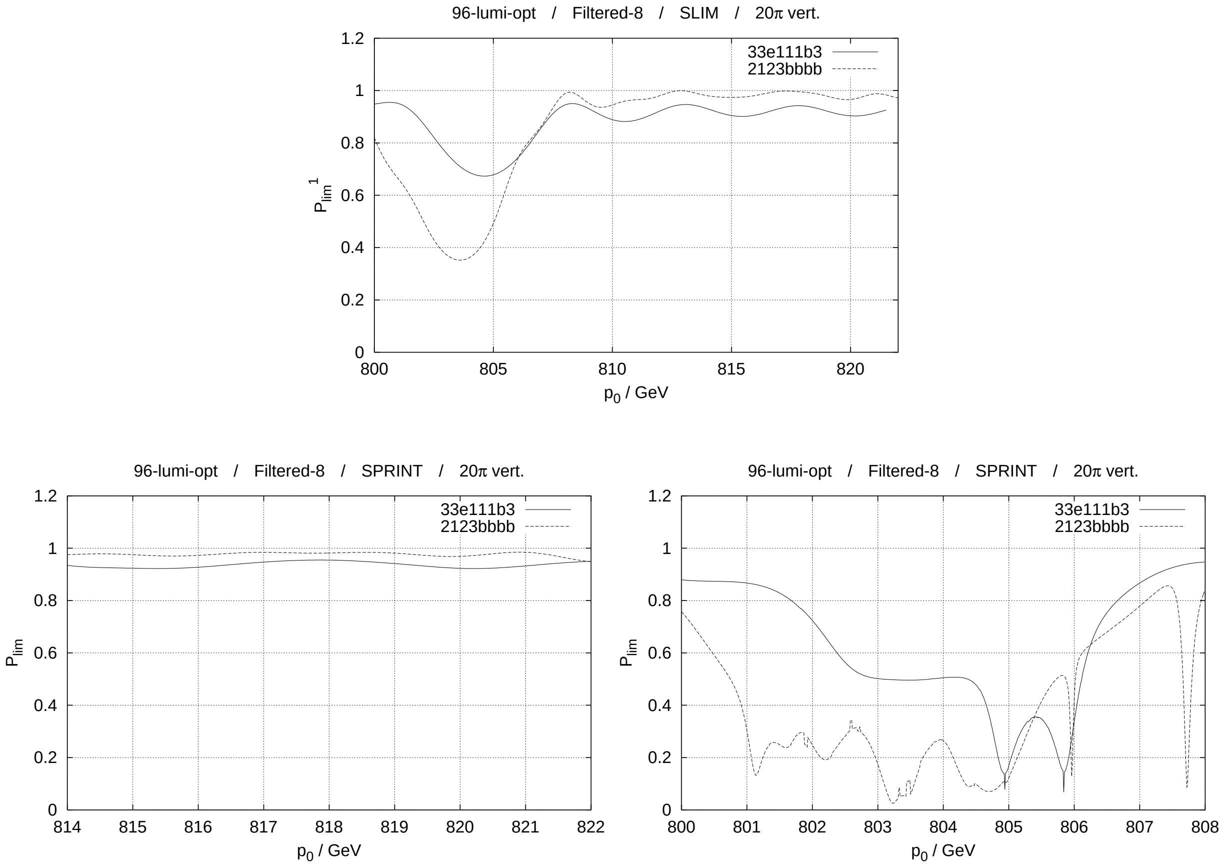

Figure 5.15: Filtered 8–snake schemes: $P_{\rm lim}$ for an enclosed vertical emittance of 20 π mm mrad. Top: Linear (`SLIM`) approximation in the momentum range 800 to 821 GeV. Below: computed with the `SPRINT` method from 814 to 822 GeV (left) and from 800 to 808 GeV (right).

Figure 5.15 contains the linear approximation of $P_{\rm lim}$ (top) and $P_{\rm lim}$ computed by the `SPRINT` algorithm (bottom) in the momentum ranges used before but for the two 8–snake schemes obtained by filtering. Note that 33e111b3 was obtained by filtering over a large momentum range (39.5 to 821.5 GeV) whereas 2123bbbb was obtained over the interval from 815 to 820 GeV. Both filtered schemes supply a high average degree of polarisation from 814 to 820 GeV (bottom left) at the `SLIM` level as well as with `SPRINT`. The average non–perturbative $P_{\rm lim}$ in this range is $\langle P_{\rm lim}\rangle_{p_0} \approx 0.94$ for 33e111b3 and even 0.97 for 2123bbbb. Unfortunately both schemes fail to provide a reasonably smooth polarisation curve from 800 to 808 GeV (bottom right). The 2123bbbb scheme which was not filtered for this region is the worst but even 33e111b3 shows a candidate for a resonance doublet around 805.4 GeV.

Figures 5.16 and 5.17 show $P_{\rm lim}(p_0)$ computed with the `SPRINT` method for the standard 8–snake schemes (5.16) and the 8–snake schemes obtained by filtering (5.17) for the (1,1,0), (2,2,0) and (2,2,2)σ tori in the momentum range from 814 to 820 GeV. In figure 5.16 all schemes with 8 *horizontal* snakes, namely 31111111, 4X1a and 4Xpm1125 (from top left to bottom left) provide a high average $P_{\rm lim}$ on the (1,1,0)σ and (1,1,1)σ tori. One finds $\langle P_{\rm lim}\rangle_{p_0} \approx 0.86$, 0.91 and 0.93 for 31111111, 4X1a and 45Xpm1125 respectively and $\langle P_{\rm lim}\rangle_{p_0} \approx 0.90$ with much stronger modulation for 32121212 (bottom right). When moving out to 2σ horizontally and vertically the average $P_{\rm lim}$ drops noticeably for all four schemes but with the exception of 32121212 the curves do not exhibit any singular minima. Among

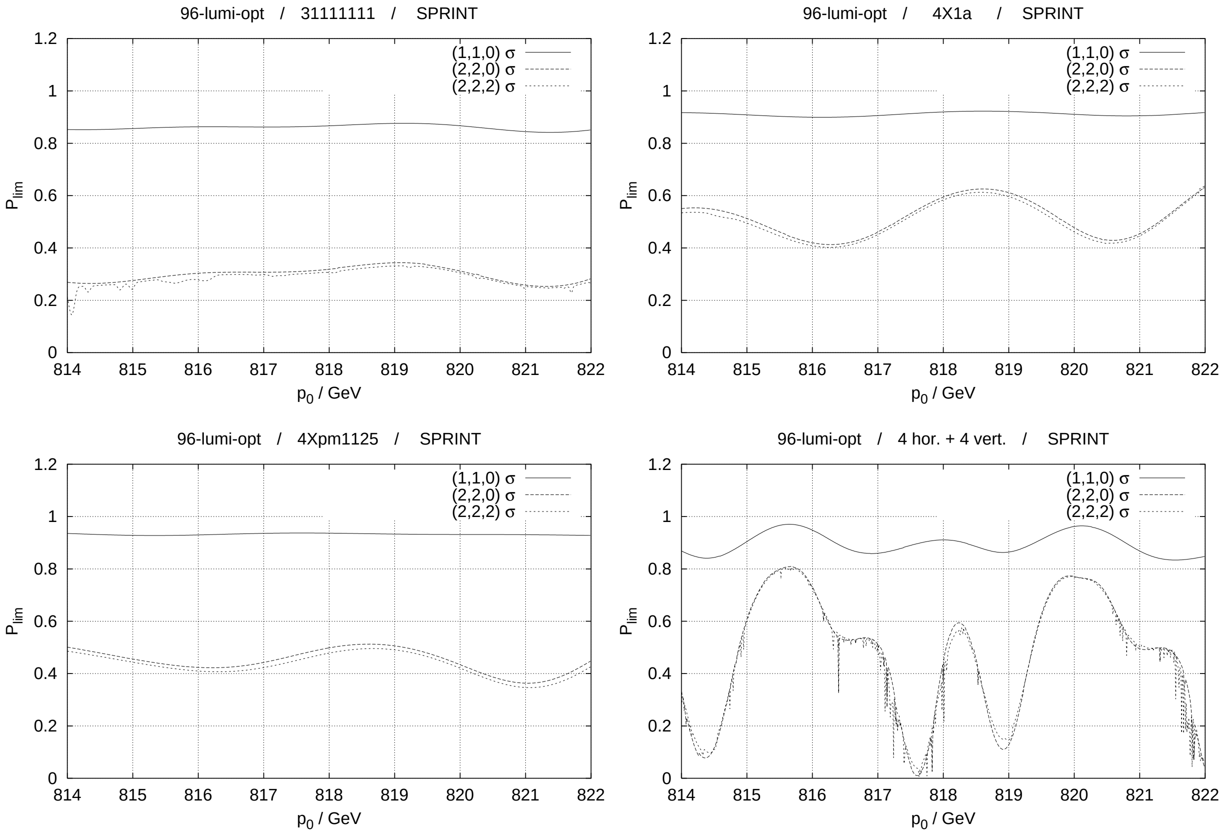

Figure 5.16: Standard 8–snake schemes: $P_{\text{lim}}(p_0)$ computed with the SPRINT method in the momentum range from 814 to 822 GeV. The invariant tori correspond to (1,1,0), (2,2,0) and (2,2,2) σ beam sizes.

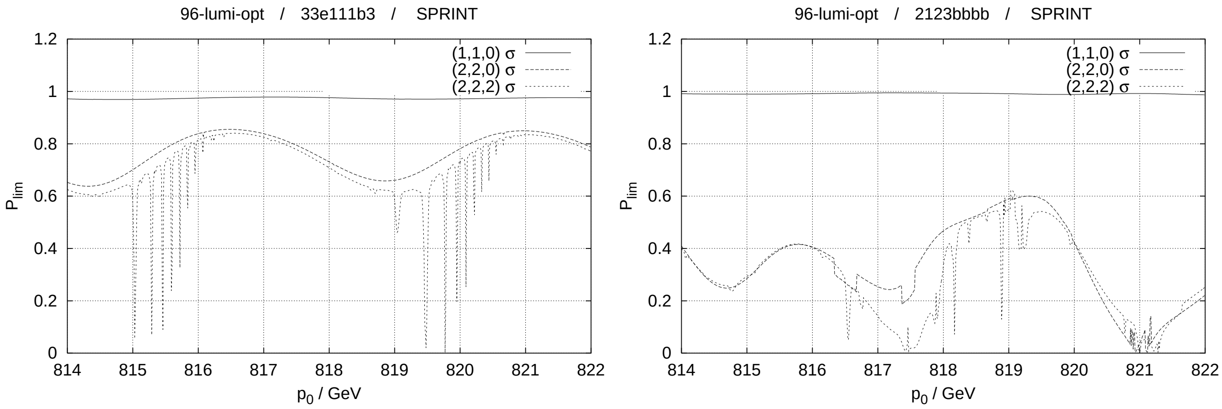

Figure 5.17: Filtered 8–snake schemes: $P_{\text{lim}}(p_0)$ computed with the SPRINT method in the momentum range from 814 to 822 GeV. The invariant tori correspond to (1,1,0), (2,2,0) and (2,2,2)σ beam sizes.

the 3 schemes with only horizontal snakes the average polarisation on the (2,2,0)σ torus is highest for 4X1a, i.e. $\langle P_{\rm lim}\rangle_{p_0} \approx 0.52$ compared to 0.44 (4Xpm1125) and 0.30 (31111111). On the (2,2,2)σ torus the two schemes with $P_s = 4$, namely 4X1a and 4Xpm1125, still provide a smooth polarisation curve, although with a few percent less polarisation. On this torus the curve for the 31111111 scheme looks similar to those for 4X1a and 4Xpm1125, but a closer look at the data reveals not only that $P_{\rm lim}$ is slightly more wiggly but also that the convergence of the stroboscopic average suffered. In certain regions the approximation of the $\hat{n}$–axis obtained from 16000 turns of stroboscopic averaging and the approximation after 8000 turns had an angle w.r.t. each other of about 300 mrad, indicating that the stroboscopic average did not converge until then. Note that whenever synchrotron motion is included the low synchrotron tune $Q_z \approx 0.6 \cdot 10^{-3}$ requires about 1700 turns to be tracked in order to sample the synchrotron period at least once. For 32121212 inclusion of the longitudinal phase space mainly increased the number of visible singular dips by a factor of approximately 5.

In figure 5.17 the two filtered schemes are compared. On the (1,1,0)σ torus the average $P_{\rm lim}$ with 33e111b3 (left) is 0.975 and with 2123bbbb (right) even 0.99. In this momentum range and with these moderate vertical and horizontal amplitudes the linear filtering, which was performed for vertical motion only, still produces snake schemes that provide higher average $P_{\rm lim}$ than any schemes based on "common wisdom". But in figure 5.17 (right) the strong overall drop of $P_{\rm lim}$ on the (2,2,0)σ torus reveals the limitations of linear filtering. The 8–snake scheme 2123bbbb, which was filtered in the narrow momentum range and which has an extremely asymmetric distribution of snake angles and of horizontal and vertical snakes, produces not only a particularly low but also strongly varying $P_{\rm lim}$ even inside the region in which it was filtered. The isolated *discontinuities* of $P_{\rm lim}$ from one smooth curve to another smooth curve are *not* caused by lack of convergence of stroboscopic averaging or possible resonances. Instead they are due to the fact that the adaptive computer routine, which averages $\hat{n}$ over many turns to compute $P_{\rm lim}$, is being confused and taking too few turns for averaging. The mirror symmetric scheme 33e111b3 provides the largest average $P_{\rm lim}$, about 0.75, on the (2,2,0)σ torus but there are two hardly visible sharp minima of $P_{\rm lim}$ at about 816.1 and 820.7 GeV at which the otherwise good accuracy of the pseudo–$\hat{n}$–axis falls below 100 mrad. When exciting the longitudinal degree of freedom the overall polarisation drops by just a few percent but two series of sharp polarisation dips appear in the ranges 815 to 816.5 GeV and 819 to 820.7 GeV. These dips might be caused by resonant modulations of the spin enhancement factor $G\gamma_0(1 + \delta(\theta))$ due to the momentum oscillations on a synchro–betatron trajectory. These sharp minima would then be related to synchrotron sidebands [LB96] of a kinetic resonance condition between ν and the transverse orbital tunes. Note that there is so far no algorithm, not even `SODOM-2` , that is able to compute the amplitude dependent spin tune on a phase space torus with more than than 1 dimension *in the close vicinity* of a spin–orbit resonance.

In figures 5.18 and 5.19 the same 8–snake schemes were scanned on the same set of tori but in the range from 800 to 808 GeV. On the (1,1,0)σ torus the average of $P_{\rm lim}$ is highest (about 0.85) and the curve is smoothest for the 4X1a scheme (top right of figure 5.18). The 31111111 scheme (top left) produces a smooth dip down to $P_{\rm lim} \approx 0.35$ at 804 GeV but is also absolutely smooth. The schemes 4Xpm1125 (bottom left) and the 32121212 (bottom right) both exhibit possible resonance doublets around 802 and 804.2 GeV and around 805.4 GeV respectively. We note that the splitting, due the vertical snakes, of the broad minimum of the RRS into two in the case of the 32121212 scheme as suggested by figure 5.8 (top right) is not just an artifact of the linearisation but survives in the non–perturbative regime even on the (2,2,2)σ torus. On the (2,2,0) and (2,2,2)σ tori *all* schemes show a large number of sharp singular minima, but with the 4X1a scheme, which appeared to be best with low orbital amplitudes, the polarisation vanishes almost completely in almost the whole momentum range. Actually, the 31111111 scheme produces the least number of sharp dips but it is clear that *one* tiny energy range, such that either a kinetic resonance is not crossed adiabatically or such that the invariant spin field does not exist inside the range, is in principle enough to severely damage the polarisation on the torus during acceleration.

The results of simulations performed with the `SLIM` and `SPRINT` methods and presented in this

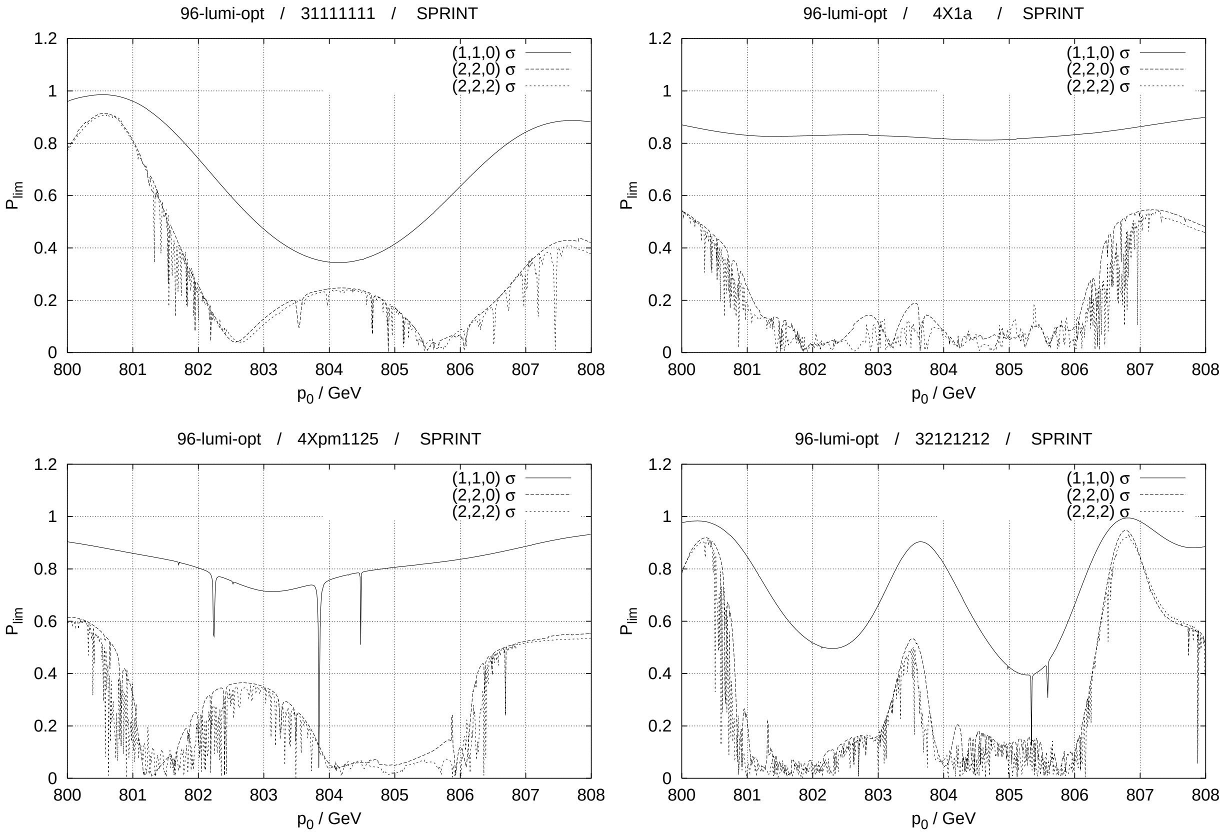

Figure 5.18: Standard 8–snake schemes: $P_{\rm lim}(p_0)$ computed with the SPRINT method in the momentum range from 800 to 808 GeV. The invariant tori correspond to (1,1,0), (1,1,1), (2,2,0) and (2,2,2)σ beam sizes.

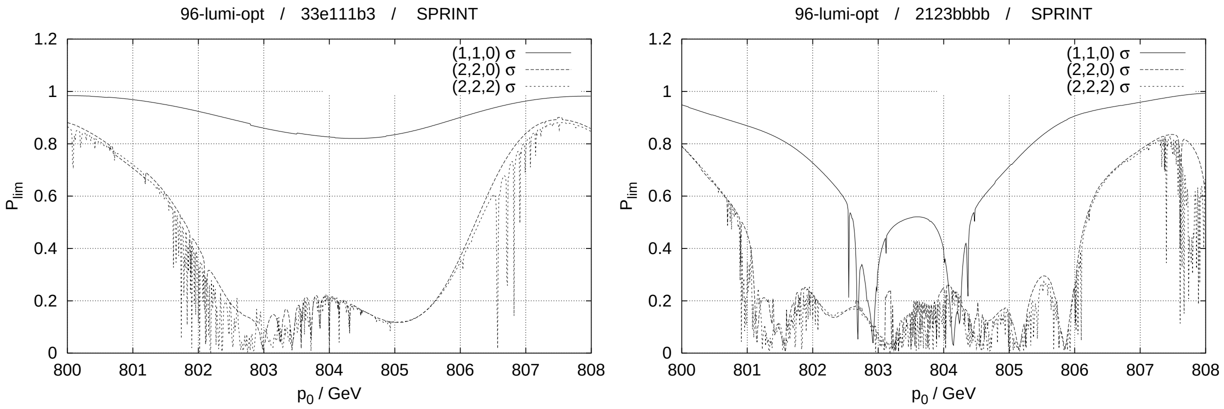

Figure 5.19: Filtered 8–snake schemes: $P_{\rm lim}(p_0)$ computed with the SPRINT method in the momentum range from 800 to 808 GeV. The invariant tori correspond to (1,1,0), (1,1,1), (2,2,0) and (2,2,2)σ beam sizes.

section allow us to draw several conclusions.

1. The smoothness of $P_{\rm lim}$ w.r.t. the reference momentum p_0 in the range from 814 to 822 GeV can be improved considerably when using 8 instead of 4 snakes.
2. In particular more *horizontal* snakes tend to improve the smoothness.
3. The average $P_{\rm lim}$ in some given momentum range strongly depends on the chosen snake angles.
4. Moreover, even with 8 snakes, e.g. 31111111, the average $P_{\rm lim}$ can be considerably *smaller* than with 4 snakes with optimised snake angles, e.g. 1d3c — at least for moderate orbital amplitudes.
5. Having a low average $P_{\rm lim}$ around 820 GeV does *not* imply particularly many singular minima inside the RRS around 803.5 GeV. An example for this is the 31111111 scheme.
6. Nevertheless, as far as the behaviour of $P_{\rm lim}$ in the strong RRS around 803.5 GeV is concerned, 8 snakes bring hardly any improvement in comparison with 4 snakes.
7. In a flattened ring like HERA–p with $P = 1$ and at high energy, maximising the snake periodicity P_s does *not* improve $P_{\rm lim}$ neither around 803.5 nor close to 820 GeV.
8. Linear filtering is able to improve $P_{\rm lim}$ in the range of validity of the linear approximation, i.e. for moderate orbital amplitudes.
9. Odd O–W parity seems to be profitable. In particular, *all* schemes obtained by long range filtering, 1d3c, 3e1b, 33e111b3 have $M = -1$. The two which were tested in this section, namely 1d3c and 33e111b3 turned out to be the most successful in providing a large average $P_{\rm lim}$.
10. But far out in phase space linear filtering in general does not select schemes with sufficient spin stability. In other words sharp dips in $P_{\rm lim}$ indicating spin–orbit resonances may occur at sufficiently large amplitudes even for the schemes obtained by filtering.

5.3.2 Ramp studies with the unmodified tunes

The static simulations, presented in section 5.3.1, suggest that the domain in the orbital phase space in which spin motion can be controlled by 4 or 8 Siberian Snakes is small. The boundary of this domain of "spin stability"cannot be determined with high accuracy on the basis of the simulations presented so far. But if we take the existence of sharp minima in $P_{\rm lim}$ as an indicator for spin–orbit resonances and thus for potential depolarisation during the ramp, then most likely for all orbital amplitudes $a_i \leq 1\sigma$ the polarisation survives acceleration through the RRS around 803.5 GeV whereas for all amplitudes $a_i \geq 2\sigma$ the polarisation is lost. Nevertheless since no computational tools exist yet to clearly identify and label kinetic spin–orbit resonances driven by 4- or 6–dimensional orbital motion, the indications of the last section have to be verified with ramp simulations. These will be described in this and other sections following. The simulations in this section were performed with the 4–snake schemes 3111, 1b1b, 1d3c and 3e1b using the separation optics hp96se820, and with the 8–snake scheme 33e111b3 using the luminosity optics hp96lu820. The scheme 3e1b has been obtained by filtering with the hp96se820 optics, whereas 1d3c and 33e111b3 were filtered out with the hp96lu820 optics.

We will now present a method to simulate the evolution of the polarisation of an ensemble of spins under variation of general system parameters. The system parameters such as field strength, the reference momentum p_0, etc. are parametrised by a common parameter λ as in section 4.10.2. In *this* section the ramp is actually a pure acceleration process. By that we mean that the focusing strengths and hence the Courant–Snyder parameters, are kept constant as p_0 is increased so that the field strengths of the magnets are proportional to p_0. Therefore we could in principle replace λ by the more intuitive Lorentz–γ of the synchronous particle γ_0. But since we want to employ this method also for the simulations to be presented in section 5.4.2 where the lattice parameters and the energy are changed simultaneously we will stick to λ in our explanation of the simulation method.

The ramp simulation is performed with an initial ensemble of N spins

$$\widehat{S}_l^0 \equiv \widehat{S}_l(\theta = 0) = \hat{n}_{\vec{J}}(\vec{\Psi}_l^0, 0, \lambda(0)) \ , \ 1 \le l \le N \quad , \tag{5.9}$$

set parallel to the invariant spin field on the torus $\vec{J} =$ const. at the initial phases $\vec{\Psi}_l^0$. Then the trajectories $\widehat{S}_l(\theta)$ evolve under

$$\mathrm{D}_\theta \, \widehat{S}_l(\theta) = \vec{\Omega}\left(\vec{J}(\theta), \vec{\Psi}_l(\theta), \theta, \lambda(\theta)\right) \times \widehat{S}_l(\theta) \tag{5.10}$$

until $\theta = \theta_k$ where $0 \le k \le k_f$ is the number of steps at which the ensemble polarisation is to be to be viewed. Note that during acceleration not $\vec{J}$ but $\vec{J}\gamma_0\beta_0$ is an adiabatic invariant (see section A.2.3). In the case of ideal acceleration $p_0(\lambda(\theta))$ is strictly monotonic w.r.t. θ, i.e. invertible to $\theta(p_0)$. At each θ_k, or equivalently $p_{0,k}$, we make a copy of the ensemble

$$\hat{\xi}_l^k(0) \equiv \widehat{S}_l(\theta_k) \ , \ 1 \le l \le N \tag{5.11}$$

and propagate it with constant $\lambda_k \equiv \lambda(\theta_k)$ and $\vec{J}_k \equiv \vec{J}(\theta_k)$

$$\mathrm{D}_\vartheta \, \hat{\xi}_l^k(\vartheta) = \vec{\Omega}\left(\vec{J}_k, \vec{\Psi}(\vartheta), \vartheta, \lambda_k\right) \times \hat{\xi}_l^k(\vartheta) \quad . \tag{5.12}$$

Since (5.12) is applied with constant λ, the spin actions

$$I_l^k \equiv \hat{\xi}_l^k(\vartheta) \cdot \hat{n}_{\vec{J}_k}(\vec{\Psi}_l(\vartheta), \vartheta, \lambda_k) \tag{5.13}$$

are invariants of motion. The *ramped turn–by–turn averaged polarisation* or just the *ramped polarisation*

$$P_{\mathrm{rmp}}(\vec{J}_k, \theta_k; N, T) \equiv \left\| \frac{1}{N} \sum_{l=1}^{N} \frac{1}{T} \sum_{j=1}^{T} \hat{\xi}_l^k(\theta_k + j2\pi) \right\| \tag{5.14}$$

can, if the system is strongly non–spin–orbit–resonant and if $\hat{n}$, $\hat{u}_1$ and $\hat{u}_2$ are sufficiently smooth, according to theorem 4.6, be written in the limit $T \to \infty$ as

$$\begin{aligned}
\lim_{T\to\infty} P_{\mathrm{rmp}}(\vec{J}_k, \theta_k; N, T) &= \lim_{T\to\infty} \left\| \frac{1}{N} \sum_{l=1}^{N} I_l^k \frac{1}{T} \sum_{j=1}^{T} \hat{n}_{\vec{J}_k}(\vec{\Psi}_l(\theta_k + j2\pi), \theta_k + j2\pi, \lambda_k) \right\| \\
&= |P_{\mathrm{dyn}}^{(N)}(p_{0,k})| \, P_{\mathrm{lim}}(\vec{J}_k, \theta_k, \lambda_k) \quad .
\end{aligned} \tag{5.15}$$

Therefore $P_{\mathrm{rmp}}(\vec{J}_k, \theta_k; N, T)$ can serve as an approximation for the product $|P_{\mathrm{dyn}}(p_{0,k})| \, P_{\mathrm{lim}}(\vec{J}_k, \theta_k, \lambda_k)$ even for finite N, T. Note that in chapter 4 we have defined $\hat{n}_{\vec{J}} \to \hat{n}_0$ in the limit $\vec{J} \to \vec{0}$ so that $\hat{n}_{\vec{J}}(p_0)$ changes its sign at each p_0 where the amplitude dependent spin tune crosses a resonance with the orbital tunes. Therefore adiabatically crossing a resonance implies a sign change of $I_l(\theta) = \widehat{S}_l(\theta) \cdot \hat{n}_{\vec{J}(\theta)}(\vec{\Psi}_l(\theta), \theta, \lambda(\theta))$. In order to apply the Froissart–Stora formula directly one has to change this definition such that $\hat{n}_{\vec{J}}$ is continuous at resonance crossing and therefore only fulfils the constraint $\lim_{\vec{J}\to\vec{0}} \hat{n}_{\vec{J}} = \pm\hat{n}_0$. But with this definition of P_{rmp} the *global* sign of the I_l^k does not enter the result so that the choice of the sign of $\hat{n}_{\vec{J}}(p_0)$ is irrelevant. In section 5.4.2 we will introduce an additional quantity $u_y^{\langle\xi\rangle}$ which allows us to determine whether the average dynamic polarisation has changed its sign or not.

For the ramp simulations presented in this section the "quickest and dirtiest" approximation has been used, namely $N = 1$. Note that the computing time is approximately proportional to the number of tracked particles so that one is tempted to keep N small. The number of turns for averaging was chosen adaptively between 400 and 3200. We call this the *single particle multi–turn polarisation*. The approximation of $P_{\rm dyn}$ for a beam of typically 10^{13} particles by just a single spin action will turn out to produce artifacts like apparently increasing polarisation after resonance crossing, but a qualitative discussion of the depolarising effects of non–adiabatic crossing of kinetic resonances is still possible and ambiguities can be dispelled by looking closely at the new tracking data to be presented in section 5.4.2. Although the approximation of a beam by just one particle is crude, it still has the advantage compared to other simulations of spin ramps in the literature, that the turn–by–turn average of the polarisation of the tracked "ensemble" is computed. Usually in the literature the polarisation of an ensemble is approximated by the instantaneous average over the spins. Thus with that method the components of $\widehat{S}_l$ which are perpendicular to $\hat{n}$ and which rapidly precess produce fluctuations of the ensemble polarisation and therefore noisy polarisation curves. In contrast, the single particle multi–turn polarisation is $|I|P_{\rm lim}$ and therefore proportional to the stationary polarisation computed by an aligned ensemble.

The ramp simulation was made for all schemes in the following way: In the momentum range from 785 to 788 GeV the $\hat{n}$–axis was scanned in order to find a good starting momentum where the accuracy for the computation of the initial $\hat{n}$–axis was high. On the torus $\vec{J} =$ const. one particle was created with $\widehat{S}$ parallel to the $\hat{n}$–axis. The particle was accelerated with an energy gain per turn of 13 keV. This is approximately 1.5 times the average energy gain per turn for the whole HERA–p ramp procedure. In fact the ramp speed at high energy is higher, about 22 keV. The energy gain is produced at each cavity crossing where the particle momenta are rescaled according to section A.2.3 and the orbit and spin maps are recomputed with the new reference momentum. `SPRINT` recomputes the orbital and spin maps each time the particles traverse an RF–cavity. Therefore, and since all cavities in HERA–p are in straight section WR interleaved only with drift lengths, the two 52 MHz systems and the four 208 MHz systems have been replaced by one single cavity at the central position between the four 208 MHz cavities. This procedure leads to the adiabatic shrinking of the phase space volume and to the relation $\vec{J}\beta_0\gamma_0 =$ const. as described in section A.2.3. Note that since the orbital maps are linearised in `SPRINT` only the *product* of cavity voltage and frequency enters the transfer matrix (A.107) and (A.116). The θ_k were chosen so that the ramped polarisation was computed in steps of 0.5 or 0.25 GeV. At the given $p_{0,k}$ the invariant spin field and $P_{\rm lim}$ were also computed with the `SPRINT` method for comparison. Note that in the meantime the ramp routines in `SPRINT` have been refined so that automatised scans of $P_{\rm rmp}$ can be provided with much smaller, and adjustable step size. These refined routines and furthermore larger ensembles were used for the simulations in section 5.4.2.

The procedure described has been used to simulate particle acceleration beginning somewhere between 785 and 788 GeV with an initial $P_{\rm dyn} \equiv 1$. In figures 5.20, 5.21, 5.22, 5.23, 5.24 and 5.25 the ramped single particle multi–turn polarisation $P_{\rm rmp}$ is plotted versus the reference momentum p_0 for the snake schemes 3111, 1b1b, 3e1b, 1d3c and 33e111b3 and various invariant phase space tori. The plots also include the static polarisation limit $P_{\rm lim}$ in order to identify polarisation losses.
Figure 5.20 shows the ramp simulation for the 3111 scheme on the $(1,1,1)\sigma$ torus (left) and the $(1.5,1.5,1.5)\sigma$ torus (right). The ramped polarisation stays close to the static polarisation limit until the RRS around 803.5 GeV is met. Then compared to $P_{\rm lim}$ the ramped polarisation drops by about 5% in the $(1,1,1)\sigma$ case and by about 40% in the case of the $(1.5,1.5,1.5)\sigma$ torus. Note that this RRS is located at the strongest intrinsic resonance but that there are at least 31 resonances with comparable strength and comparable density of neighbouring resonances to cross before reaching the 803 GeV region! In figures 5.21 we have the ramp simulation for the scheme 1b1b on the $(1,1,1)\sigma$ torus (left) and the $(1.5,1.5,1.5)\sigma$ torus (right). We see that this scheme, which has a higher snake periodicity ($P_s = 2$ instead of 1 for 3111), fails already at 1σ. The polarisation drops to 30% after crossing the

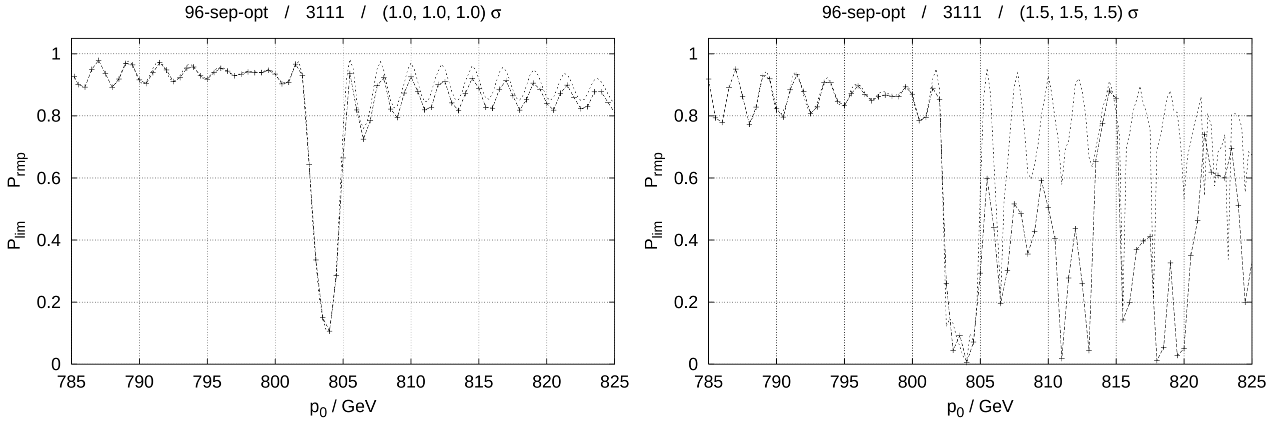

Figure 5.20: Scheme 3111: comparison between P_{rmp} and P_{lim} for 1.0 (left) and 1.5 σ (right) in all 3 planes.

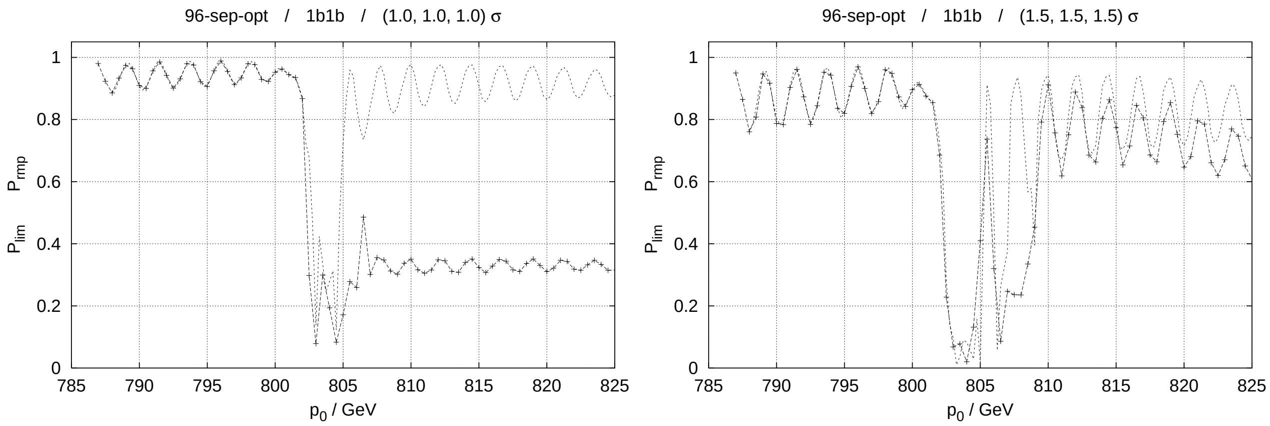

Figure 5.21: Scheme 1b1b: comparison between P_{rmp} and P_{lim} for 1.0 (left) and 1.5 σ (right) in all 3 planes.

RRS. In the (1.5,1.5,1.5)σ case one might gain the impression that the polarisation recovers, but after a closer look at the tracking data it becomes obvious that this is an artifact of the single particle simulation. Actually at (1.5,1.5,1.5)σ neighbouring resonances (up to approximately 808 GeV) are enhanced so much that the direction of $\widehat{S}$ averaged over 400 to 3200 turns at constant energy, which is close to $\pm\hat{y}$ away from the resonances, changes its sign 3 times. The lowest absolute spin action $|I_l| = 0$ after the m-th resonance crossing occurs when the l-th spin $\widehat{S}_l$ is perpendicular to $\hat{n}_{\mathcal{J}}$. If the $m+1$-st resonance crossing is non–adiabatic then $|I_l|$ can only be increased and hence the single particle polarisation recovers. Note that the actual change of the spin action during resonance crossing along each orbital trajectory is sensitive to the initial orbital phases. During the simulations that lead to figures 4.20 and4.21 the spread of the I_l has been observed to be largest in cases where the final P_{dyn} is approximately 0. So the fewer the number of particles accelerated the higher the possibility that the depolarising effects of adjacent resonances lead to a fake recovery. But if a large number N of spins is ramped non–adiabatically through a sequence of resonances the result will be a distribution of the I_l in the interval $[-1, +1]$ that is almost symmetrical w.r.t. 0. Therefore the ensemble average $P_{\mathrm{dyn}} = \langle I_l \rangle_l$ will usually vanish. Once $|P_{\mathrm{dyn}}|$ is reduced it is reduced for ever! On the contrary, if the single particle multi–turn polarisation remains close to P_{lim}, it is reliable.

Figure 5.22 shows the result of the ramp simulation for the filtered 3e1b scheme. For the (1,1,1)σ torus (top left) the polarisation is almost exactly preserved. Unfortunately when going to (1.5,1.5,1.5)σ

(top right) about 30% of the polarisation is lost. For $(2,2,2)\sigma$ (bottom left) large polarisation loss already occurs around 795 GeV. The "recovery" around 800 GeV is again an artifact of single particle tracking as in the case of the 1b1b configuration. Finally, at $(2.5,2.5,2.5)\sigma$ (bottom right) already the static polarisation limit ($P_{\rm lim}$) is low. The polarisation decays immediately after starting the ramp. Figure 5.23 shows $P_{\rm rmp}$ for the scheme 1d3c which was obtained by filtering with the luminosity optics hp96lu820. The ramp simulation was nevertheless performed with the hp96se820 optics. Although the configurations 3e1b and 1d3c look quite similar, namely the longitudinal and radial snakes at O and W are just interchanged and the $\pm 67.5°$ snakes of 1d3c at S and N are converted to $\pm 45°$–snakes, the scheme 1d3c totally fails with the separation optics. The polarisation drops to roughly 20% already in the case of $(1,1,1)\sigma$ (left). On the $(1.5,1.5,1.5)\sigma$ torus (right) the fraction $P_{\rm rmp}/P_{\rm lim}$ seems to fluctuate but again a closer look at the tracking data shows that the multi–turn average of the spin direction changes its sign at many additional resonances after crossing the major resonance at 803 GeV. Hence the fluctuating polarisation is again an artifact of single spin analysis. The results would be easier to interpret with a large spin ensemble. But that would increase the computation time significantly.

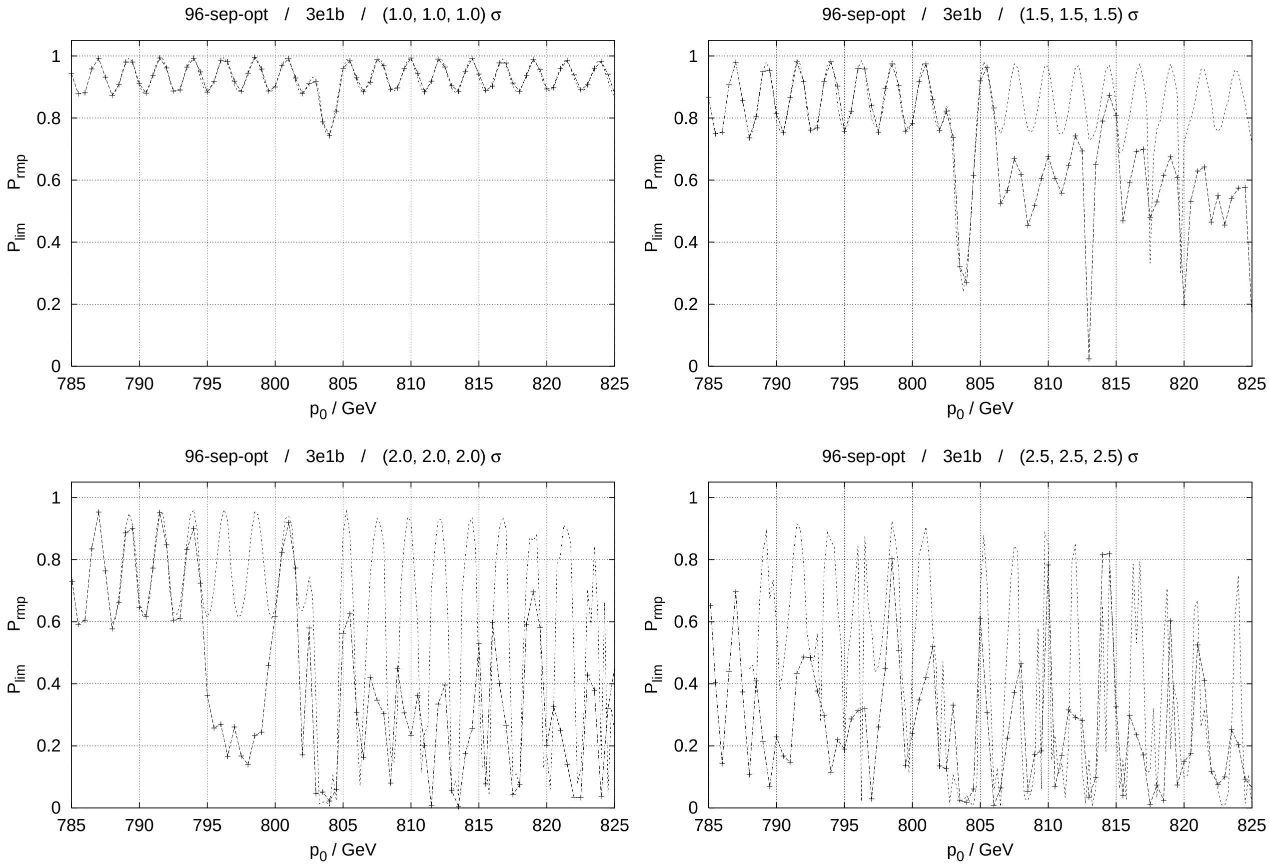

Figure 5.22: Scheme 3e1b: comparison between $P_{\rm rmp}$ and $P_{\rm lim}$ for 1.0 (top left) 1.5 (top right), 2 (bottom left) and 2.5 σ (bottom right) in all 3 planes.

Figures 5.24 and 5.25 show the ramp simulations for the 8–snake scheme 33e111b. It is obvious from figure 5.24 that in case of the $(1,1,1)\sigma$ torus (top left) the polarisation is preserved over the full momentum range of the simulation. On the $(1.5,1.5,1.5)\sigma$ torus (top right) the polarisation drops by 3%, but a few percent loss during acceleration through the RRS located at the strongest resonance in the whole range of 40 to 820 GeV seems tolerable. In the $(2,2,2)\sigma$ case (bottom) there are already four momenta *before* the RRS at which losses occur

1. a drop of about 5% occurs directly at the beginning of the ramp,

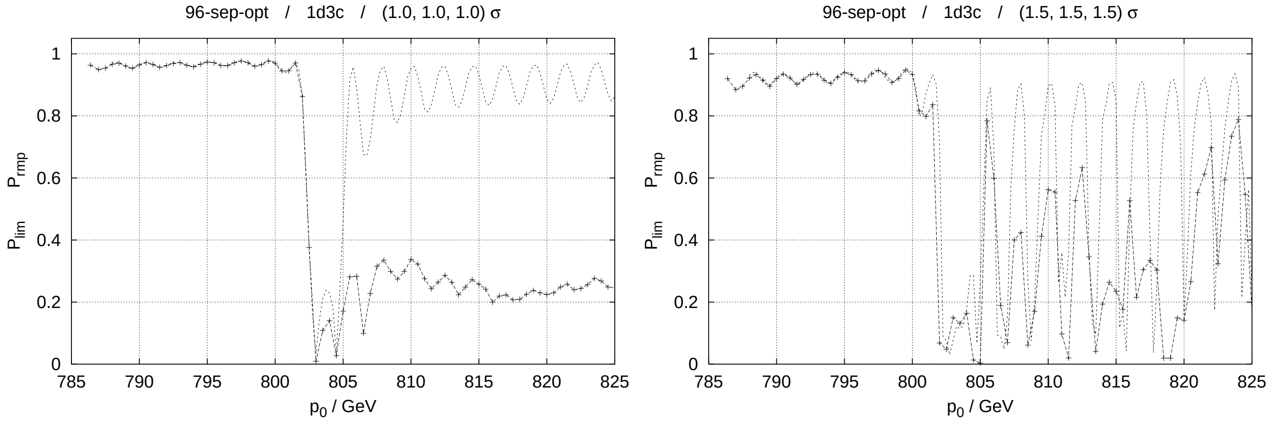

Figure 5.23: Scheme 1d3c: comparison between $P_{\rm rmp}$ and $P_{\rm lim}$ for 1.0 (left) and 1.5 σ (right) in all 3 planes.

2. around 792 GeV the polarisation drops by about 20%,
3. around 796 GeV the polarisation drops by another 40% and
4. around 800 GeV the polarisation drops to 0.

Each of these is separated by about 4.4 GeV. From equation (5.3) we know that the approximate on–orbit spin tune for the flattened HERA without main snakes is $\nu_0 = E_0/555\text{MeV}$. We have seen in section 4.9 that with 4 main snakes the on–orbit spin phase advance between the main snakes increases by 2π every 2.22 GeV and have observed a modulation with an approximate period of 2.2 GeV in $P_{\rm lim}(p_0)$. Analogously we find 4.44 GeV for 8 main snakes and can easily observe in figures 5.16 to 5.17 and 5.24 to 5.25 a modulation with an approximate period of 4.4 GeV in $P_{\rm lim}(p_0)$. If we assume that certain types of higher order kinetic resonances are enhanced in particular close to points where the on–orbit spin phase advance between adjacent snakes reaches a certain value, then it is reasonable that these resonances occur with approximately the same periodicity w.r.t. p_0. Since even the filtered 8–snake scheme only preserves polarisation during acceleration through the strong RRS around 803.5 GeV with amplitudes of less than 1.5 σ in all three eigenplanes it is worthwhile to analyse the effect of the different orbital modes in more detail. Figure 5.25 shows $P_{\rm lim}$ and $P_{\rm rmp}$ for tori where the orbital amplitudes are *not* the same in all three planes. With the exception of the right plot in the middle row all tori include 2 σ vertical motion. With purely vertical motion on the (0,2,0)σ torus (top left), the polarisation survives almost completely. Also with additional 1 σ excitation in the longitudinal plane (top right) the spin action is preserved. But with a horizontal amplitude of only 1 σ together with 2 σ vertical motion, i.e. on the (1,2,0)σ torus (middle left), the polarisation is almost completely lost already at about 803 GeV. Figure 5.25 (middle right) is for the (2,1,0)σ torus for comparison. Here the polarisation only drops slightly by approximately 4%. The bottom row is for the (1,2,1)σ torus (bottom left) and the (2,2,0)σ torus (bottom right). On both tori the polarisation decays at approximately the same momentum as on the (1,2,0)σ torus (middle left), namely at about 803 GeV. The evolution of $P_{\rm rmp}$ is nevertheless different for all three tori. In particular the additional 1 σ of longitudinal excitation produces a rich spectrum of sharp dips beyond the first depolarisation. We note that in general the momentum resolution of these first ramp simulations does *not* suffice to explicitly identify resonances by means of sharp minima of $P_{\rm lim}$. But figure 5.25 allows the conclusion that with the 33e111b3 scheme around 803.5 GeV, polarisation losses on tori with 2 σ vertical amplitude are mainly caused by additional *horizontal* excitation.

The outermost torus without polarisation losses using the 4–snake schemes 3e1d and 3111 has amplitudes of 1σ in all three planes corresponding to enclosed normalised emittances of $\varepsilon_x^n = \varepsilon_y^n =$

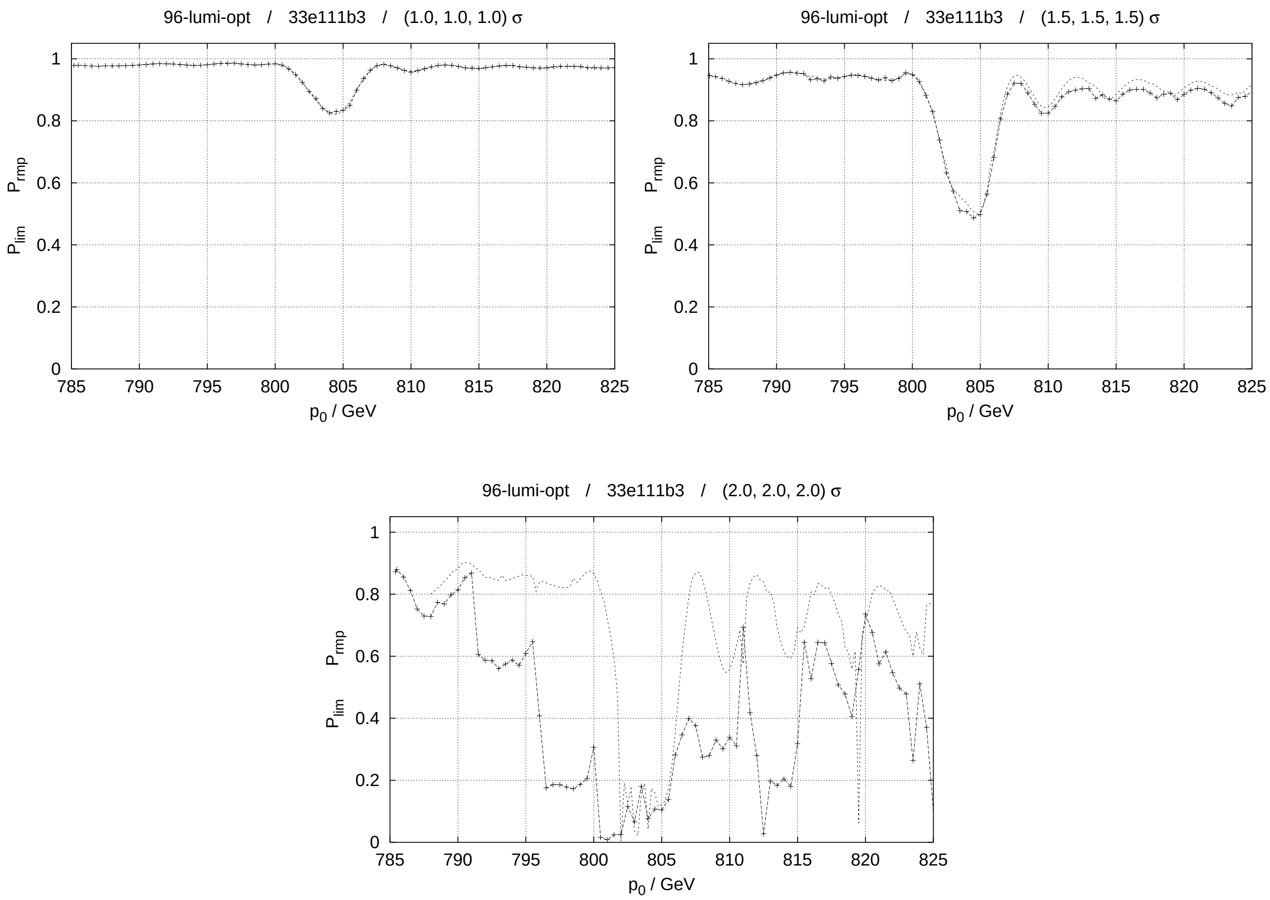

Figure 5.24: Scheme 33e111b3: comparison between P_{rmp} and P_{lim} for 1.0 (top left), 1.5 σ (top right) and 2.0 σ (bottom) in all 3 planes.

4π mm mrad and $\varepsilon_z^n = 1.78\ 10^{-2}\pi$ m rad. The outermost torus without polarisation losses using the 8–snake scheme 33e111b3 has 1.5σ in all three planes, corresponding to $\varepsilon_x^n = \varepsilon_y^n = 9\pi$ mm mrad and $\varepsilon_z^n = 4.00\ 10^{-2}\pi$ m rad.

Although we have only sampled the phase space with a rather small number of tori, we can already give a crude estimate for the achievable beam polarisation at high energy in HERA–p with the lattice parameters studied so far. If we assume that polarisation losses *vanish* whenever *one* of the orbital amplitudes is *less* than 2.0 σ, then according to equation (5.8) about 65% of the beam stays polarised. Assuming an initial polarisation from the source of about 80%, that no polarisation is lost in the pre–accelerator chain and $P_{\mathrm{lim}} \approx 0.9$ up to 2σ in all planes and for some optimal reference momentum $p_0 > 810$ GeV the average beam polarisation is about 51%. This is an optimistic scenario. If we, on the other hand, assume that polarisation losses *occur* whenever *one* of the orbital amplitudes is *greater* than 1.0 (1.5)σ, then only 6% (30%) of the beam stays polarised. Under the same assumptions as before the average beam polarisation is about 5% (24%). This scenario is surely too pessimistic. Assuming that the maximum attainable polarisation is between 5 and 51% seems discouraging but in section 5.4 modifications to the HERA–p tunes will be discussed that improve the situation to some extent.

To summarize the results of these ramp simulations for HERA–p we conclude the following:

1. Crossing of the strongest RRS at 803.5 GeV seems possible with negligible polarisation losses only for the inner part of the beam, namely up to about 1 or 1.5 σ.

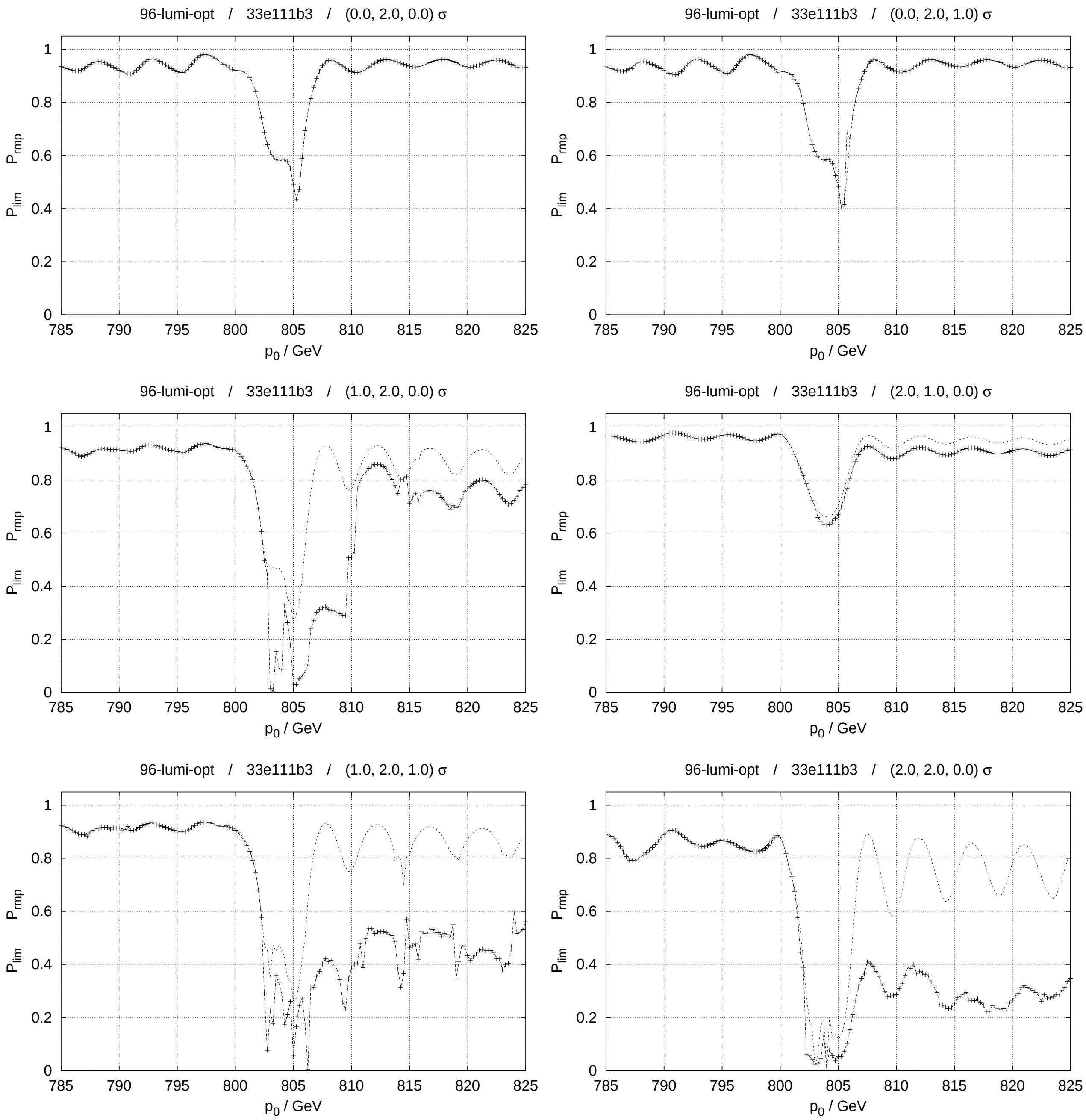

Figure 5.25: Scheme 33e111b3: comparison between $P_{\rm rmp}$ and $P_{\rm lim}$ for different invariant tori. Top left: $(0,2,0)\sigma$. Top right: $(0,2,1)\sigma$. Middle left: (1,2,0) σ. Middle right: $(2,1,0)\sigma$. Bottom left: $(1,2,1)\sigma$. Bottom right: $(2,2,0)\sigma$.

2. The outer parts up to the 95% emittances are still critical. The dynamic polarisation P_{dyn} drops to zero even with the best schemes on the (2,2,2)σ torus when crossing the RRS around 803.5 GeV.

3. 8 snakes, even with *properly chosen* snake angles, seem to relax the situation only slightly. In the following we will therefore restrict ourselves to 4–snake schemes.

5.3.3 Long range momentum scans using Fourier analysis

In section 5.3.1 we have observed that, in the limited momentum ranges for which the simulations were performed, on certain invariant tori P_{lim} shows pronounced sharp minima which are candidates for higher order kinetic resonances as described in section 4.9. Furthermore in section 4.10 we have shown evidence that a generalised Froissart–Stora formula for the change of $P_{\mathrm{dyn}} \equiv < I >$ during acceleration through a kinetic resonance may be applied. In section 5.3.2 it was demonstrated that the P_{dyn} is potentially diminished when the RRS at 803.5 GeV is crossed during the ramp. Moreover we have confirmed the weaknesses of linear filtering in momentum and amplitude ranges where $\|\hat{n} - \hat{n}_0\|$ is not small. In particular even the filtered schemes cannot provide sufficiently high P_{lim} and sufficient preservation of P_{dyn} when large amplitudes are taken into account at the assumed top energy of approximately 820 GeV and when the RRS around 803.5 GeV has to be crossed. The automatic filtering procedure described in section 4.4.1 can so far only be performed at the linear level. In order to find measures to circumvent depolarisation and to increase P_{lim}, we have to identify and label the kinetic resonances that are relevant for the depolarisation during the ramp and that affect P_{lim} at possible working energies. Thus we need approximations of the invariant spin field and the amplitude dependent spin tune that include higher order effects. We will now exploit the relatively good performance of the `SODOM-2` algorithm for simulating long range scans (500 to 1000 GeV) for certain snake schemes with the luminosity optics hp96lu820 and the separation optics hp96se820. Owing to time limitations we no longer include simulations with 8–snake schemes. The 8–snake schemes, which are encumbered with considerable technical problems, have so far *not* shown sufficient improvement to justify the effort. The `SODOM-2` method is fast enough for doing long range scans and accurate enough to describe spin motion close to higher order resonances, only if the orbital motion is restricted to *one* eigenplane. Therefore in this section we will only discuss the effects of vertical orbital amplitudes.

Figures 5.26 to 5.31 are all organised in the same way. Each figure shows P_{lim} and ν as a function of p_0 in the momentum range from 500 to 1000 GeV for a given snake scheme and a given optics (either hp96lu820 or hp96se820) with vertical amplitudes of 1, 1.5, 2 and 2.5 σ. Figures 5.26 to 5.29 were produced with the optics hp96lu820 whereas figures 5.30 and 5.31 were made with the optics hp96se820. The momentum discretisation was chosen to be 10 MeV leading to $5 \cdot 10^4$ momentum steps per `SODOM-2` run. The first row shows $P_{\mathrm{lim}}(p_0)$ with 1 σ (left) and 1.5 σ (right) vertical amplitude. Directly below the P_{lim}–scans, in the second row, the corresponding amplitude dependent spin tune is plotted versus p_0, i.e. for 1 σ to the left and for 1.5 σ to the right. The third and fourth rows are made in an analogous way but with 2 σ and 2.5 σ vertical amplitudes. The plots of ν also show the closest by resonance conditions with order $k < 10$ drawn as straight lines. In the case of the luminosity optics with the unmodified vertical tune, computed from the official lattice file, $Q_y \approx 32.27253$, there are the 4 resonance conditions $\kappa = 2[Q_y]$, $1 - 2[Q_y]$, $9[Q_y] - 2$ and $\kappa = 3 - 9[Q_y]$ close to $\nu_0 = {}^1\!/_2$. The 2-nd order resonances lie at a distance of approximately 0.0451 from $\nu_0 = {}^1\!/_2$, whereas the 9-th order resonances are 0.0472 away. In the case of the separation optics with the unmodified vertical tune from the official lattice file being $Q_y = 32.30812$, there are only 2 lines $\kappa = 5[Q_y] - 1$ and $\kappa = 2 - 5[Q_y]$ of order $k < 10$ close to ν_0, namely at a distance of 0.0406. The `SODOM-2` runs for up to 2 σ vertical amplitude were performed with 63 Fourier harmonics and the simulations with 2.5 σ included 85 Fourier harmonics. It should be be noted here that in almost all simulations with sufficiently high orbital amplitudes, depending on the snake scheme and the lattice, there were singular momenta where the number of Fourier harmonics was not enough to obtain a suitable accuracy of the invariant spin field and the amplitude dependent spin tune. Nevertheless in these long range scans these points are in the minority and do *not* invalidate the global qualitative results.

We define the averaged P_{lim} over some momentum range $\mathcal{R}' = [p_{\text{min}}, p_{\text{max}}]$, that does *not* contain any residual resonance structures

$$\langle P_{\text{lim}} \rangle_{p_0} \equiv \frac{1}{p_{\text{max}} - p_{\text{min}}} \int_{\mathcal{R}'} P_{\text{lim}}(p_0)\, dp_0. \tag{5.16}$$

When scanning the momentum for a good working point, we exclude the RRSs already from the beginning. But we assume that for stable operation not only a narrow maximum of P_{lim} close to 1 but also a certain momentum range with high $\langle P_{\text{lim}} \rangle_{p_0}$ and only moderate oscillations of P_{lim} is necessary. Moreover we define the spin tune spread $\Delta_{p_0}(\nu)$ and the *symmetrised* spin tune spread $\Delta_{p_0}^{\text{sym}}(\nu)$ over some momentum range $\mathcal{R} = [p_{\text{min}}, p_{\text{max}}]$

$$\Delta_{p_0}(\nu) \equiv \max_{\mathcal{R}} \nu - \min_{\mathcal{R}} \nu \quad , \quad \Delta_{p_0}^{\text{sym}}(\nu) \equiv \max_{\mathcal{R}} |\nu - \frac{1}{2}| \quad , \tag{5.17}$$

where the branch of ν with $\lim_{J_y \to 0} \nu = \nu_0$ has to be used. In contrast to $\mathcal{R}'$ the range $\mathcal{R}$ *may* include residual resonance structures. For every resonance condition $\kappa = [kQ_y]$ with distance $\Delta\kappa = \kappa - {}^1/_2$ from the design orbit spin tune ν_0 with properly chosen snakes, there is another resonance condition $\kappa' = 1 - [kQ_y]$ with the same order k and with $\Delta\kappa' = -\Delta\kappa$. Therefore the *symmetrised* spin tune spread $\Delta_{p_0}^{\text{sym}}(\nu)$ determines the minimal distance that κ to $\nu_0 = {}^1/_2$ may have so that neither of the conditions $\nu = \kappa$ and $\nu = \kappa'$ can be fulfilled.

The first set of figures, 5.26 to 5.29, was produced in order to find a suitable momentum range for the storage and collision mode and to analyse the differences between various snake schemes. The second set of figures, 5.30 and 5.31, gives an estimate of to which energy a polarised beam might be accelerated without polarisation losses. Another purpose of figures 5.26 to 5.31 is to demonstrate the evolution from a (hopefully) well–behaved spin–orbit system with a large average P_{lim}, small oscillation amplitudes and a low spin tune spread at *low* vertical amplitudes, to a possibly badly behaved system with low average P_{lim}, large oscillation amplitudes and a large spin tune spread with spin tune jumps at low order resonances at *high* vertical amplitudes. For example figure 5.27 below shows an astonishing "blooming" of resonance structure as the amplitude increases.

Figure 5.26 shows this evolution for the 3111 scheme with the optics hp96lu820. At 1 σ (first row left and second row left) the average static polarisation limit $\langle P_{\text{lim}} \rangle_{p_0}$ is about 95% except for 14 pronounced minima. Note that we have observed 19 super–strong resonances in figure 5.3 (bottom). The dips in figure 5.26 are very close to these super–strong resonances with every fourth resonance missing or comparable to the background oscillations of P_{lim}. We therefore identify them as residual resonance structures. The fact that some RRSs are missing can be explained as follows: According to lemma 3.2 every horizontal snake can be decomposed into a radial snake and a vertical spin rotator with a rotation angle that is twice the snake angle of the horizontal snake. Therefore schemes with mixed snake angles have different spin phase advances in different arc sections between the snakes. Even if the spin perturbations due to the periodic FODO cells of *each* arc add up coherently, the combined effects of *all* four arcs can cancel to some extent. Therefore the spin–orbit coupling integrals at the positions of the former linear intrinsic resonances can be significantly changed and a potential RRS belonging to a super–strong resonance might in principle not appear. We note that P_{lim} has maxima close to 100% even near to the RRSs. The spin tune stays close to ${}^1/_2$, namely in the interval $[0.48, 0.52]$. The symmetrised spin tune spread over the whole range from 500 to 1000 GeV in figure 5.26 (second row left) is $\Delta_{p_0}^{\text{sym}}(\nu) \approx 0.02$. When increasing the vertical amplitude to 1.5 σ (upper two rows right), the average P_{lim} outside the RRSs is slightly reduced to about 85% and $\Delta_{p_0}^{\text{sym}}(\nu)$ is increased to approximately 0.03. Moreover the drops of P_{lim} at the RRSs are more pronounced and additional strong dips directly adjacent to the main RRSs appear, e.g. around 803.5 GeV. The

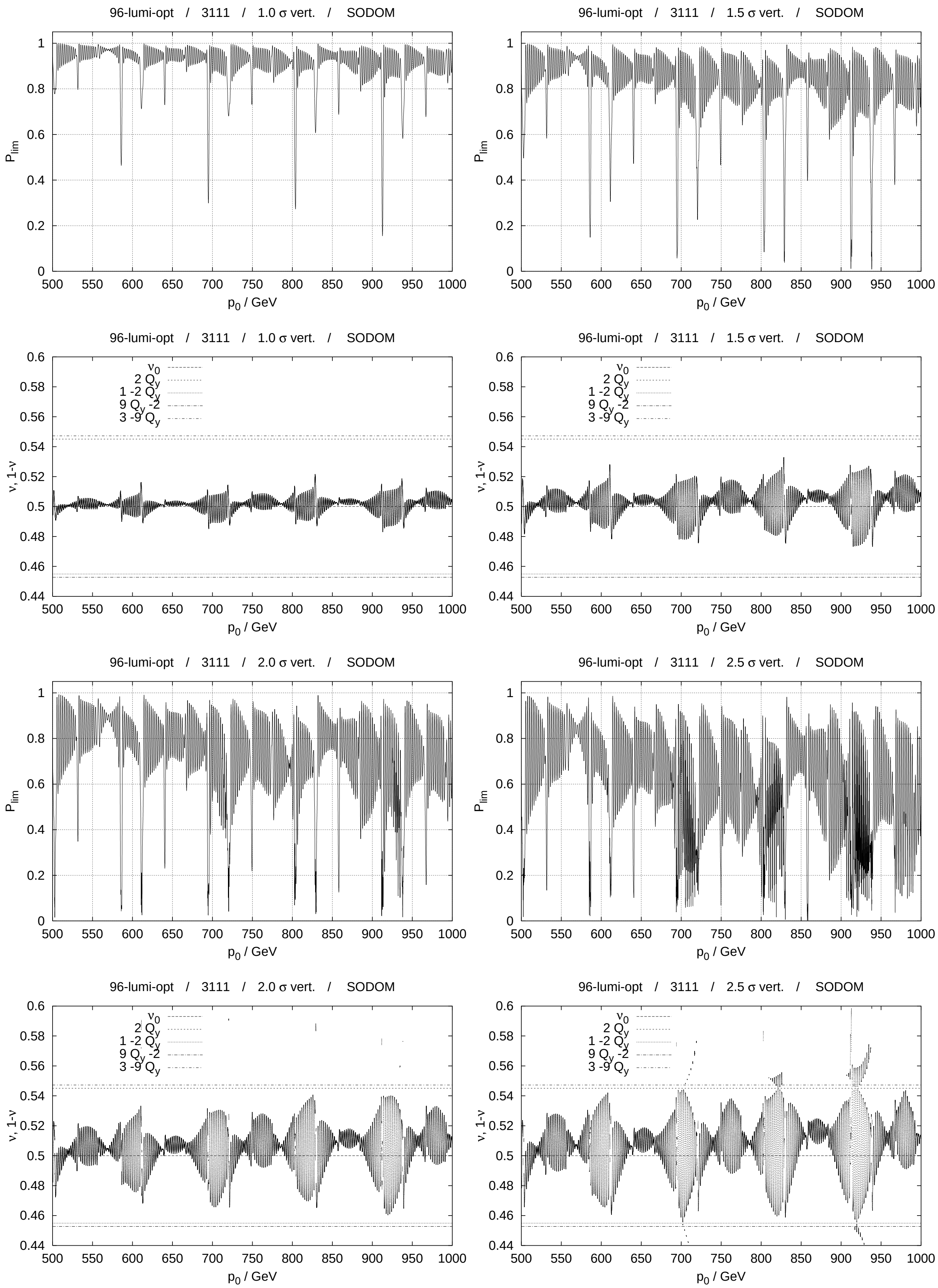

Figure 5.26: SODOM-2 scans of $P_{\mathrm{lim}}(p_0)$ and $\nu(p_0)$ for 1, 1.5, 2 and 2.5 σ vertical amplitude with the luminosity optics hp96lu820 and the snake scheme 3111.

oscillation amplitude of $P_{\rm lim}$ has increased by a factor of 2 in the region around 820 GeV. But still there are momenta, e.g. just above 830 GeV where $P_{\rm lim} \approx 100\%$. With 2 σ vertical amplitude (lower two rows left) certain RRSs, i.e. around 720, 803, 920 and 970 GeV have been joined by many neighbouring minima of comparable depth. Even in regions at some distance from the strongest RRSs $\langle P_{\rm lim}\rangle_{p_0}$ is hardly more than 80%. At momenta above 700 GeV there is only one region, from the RRS at about 830 GeV to the next RRS at about 860 GeV where $\langle P_{\rm lim}\rangle_{p_0}$ is above 80%. The amplitude dependent spin tune shows certain singular jumps, e.g. around 830 and 920 GeV, which might be due to the `SODOM-2` algorithm switching between different branches $\nu + l[Q_y]$. But since they occur at the main RRSs it is still possible that they are caused by symmetric jumps around higher order kinetic resonant tunes. The symmetrised spin tune spread of the subset of data points that belong to a continuous curve has increased to 0.04 and therefore ν is already dangerously close to the 2-nd and 9-th order resonance conditions. At 2.5 σ vertical amplitude (lower two rows right), in between the pairs of RRSs at 690 and 720 GeV, 803 and 830 GeV and the pairs from 920 to 980 GeV, a whole “forest” of sharp and deep minima of $P_{\rm lim}$ has grown. We just note that the region between 830 and 860 GeV still has high $P_{\rm lim}$ with relatively small oscillations. The spin tune shows a whole series of symmetric jumps around the 2-nd order resonance $2[Q_y]$ between 700 and 720 GeV — the spin tune jumps between the disjoint segments of curve arcing upwards above $2[Q_y]$ and the curve below $2[Q_y]$. In this region the kinetic resonance strengths, i.e. the half height of the jumps, range from approximately 10^{-3} to $3 \cdot 10^{-2}$. There are also series of symmetric jumps around 800 and 830 GeV, and between 900 and 940 GeV as evidenced by the “fish tails”. Again the kinetic resonance strength ϵ is not constant with energy but has certain minima $\epsilon \approx 0$. If we totally neglected the effect of possible polarisation losses during acceleration and the negative impact of the horizontal and longitudinal motion on $P_{\rm lim}$, then we would conclude that the region from 830 to 860 GeV supplies good conditions for operating HERA–p with polarised protons. Of course, due to the obviously many kinetic resonances between 700 and 820 GeV with 2.5 σ of purely vertical motion, it is not very likely that a reasonable fraction of the beam can be accelerated to this energy without significant loss of polarisation.

The next two figures, 5.27 and 5.28 are presented as “horrifying” examples and to demonstrate that high snake periodicity does *not* help but can even be harmful in the case of an asymmetric machine like HERA–p. Figure 5.27 contains the results of simulations with the 1b1b scheme and figure 5.28 is for the snake scheme afaf. Both schemes have the highest possible snake periodicity, $P_s = 2$, for 4 snakes and with $\nu_0 = {}^1/_2$. For 1σ vertical amplitude the average $P_{\rm lim}$ outside the residual resonance structures is above 95% and the oscillation amplitude outside the RRSs is small, approximately 5% for both schemes. But the highly periodic schemes are the only ones tested so far that provide spin tune jumps at the 2-nd order resonance conditions already for 1 σ vertical amplitude! In fact the ramp simulation in figure 4.20 (top right) was performed with the 1b1b scheme at 0.75 σ. At the low momentum end of the scans, these resonance crossings are at just two of the four RRSs, namely the pair framing 600 GeV. With increasing momentum the spin tune shift becomes large enough to meet the 2-nd order resonance condition at the third RRS of each set. At 1.5 σ almost every RRS contributes a pair of resonances. With increasing orbital amplitudes, in more and more ranges of p_0, $P_{\rm lim}$ begins to oscillate between 0 and its steadily decreasing maximal values. In particular the afaf scheme at 2.5 σ produces strong oscillations of $P_{\rm lim}$ between 0% and 90% almost everywhere beyond 630 GeV. At 2.0 and 2.5 σ with both schemes we observe regions in which almost every oscillation of the amplitude dependent spin tune crosses the 2-nd order resonance. It is in precisely these regions that the curve of $P_{\rm lim}$ oscillates strongest. Thus, the two highly periodic schemes 1b1b and afaf are definitely *not* capable of providing a large beam polarisation at high energy in HERA–p.

Figure 5.29 shows the results of the `SODOM-2` simulations with the luminosity optics and the snake scheme 1d3c, which was obtained by linear long range filtering with the optics hp96lu820. With 1σ vertical amplitude, not only is the average $P_{\rm lim}$ outside the RRSs with 97% the largest so far, but also only every 4-th RRS generates a deep minimum of $P_{\rm lim}$. Actually only three out of four RRSs are visible at all and only one is particularly pronounced with this low orbital amplitude. The symmetrised

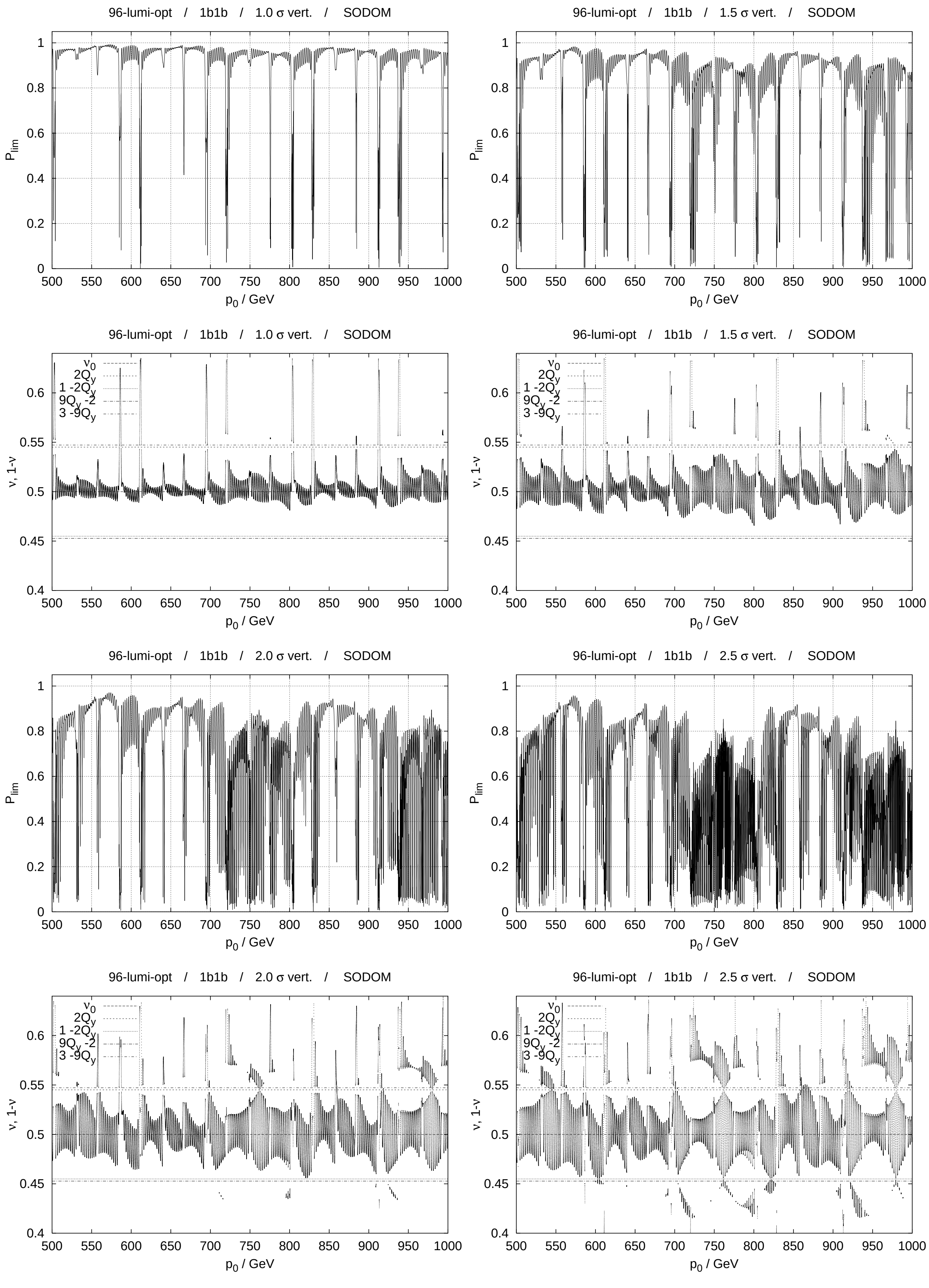

Figure 5.27: SODOM-2 scans of $P_{\rm lim}(p_0)$ and $\nu(p_0)$ for 1, 1.5, 2 and 2.5 σ vertical amplitude with the luminosity optics hp96lu820 and the snake scheme 1b1b.

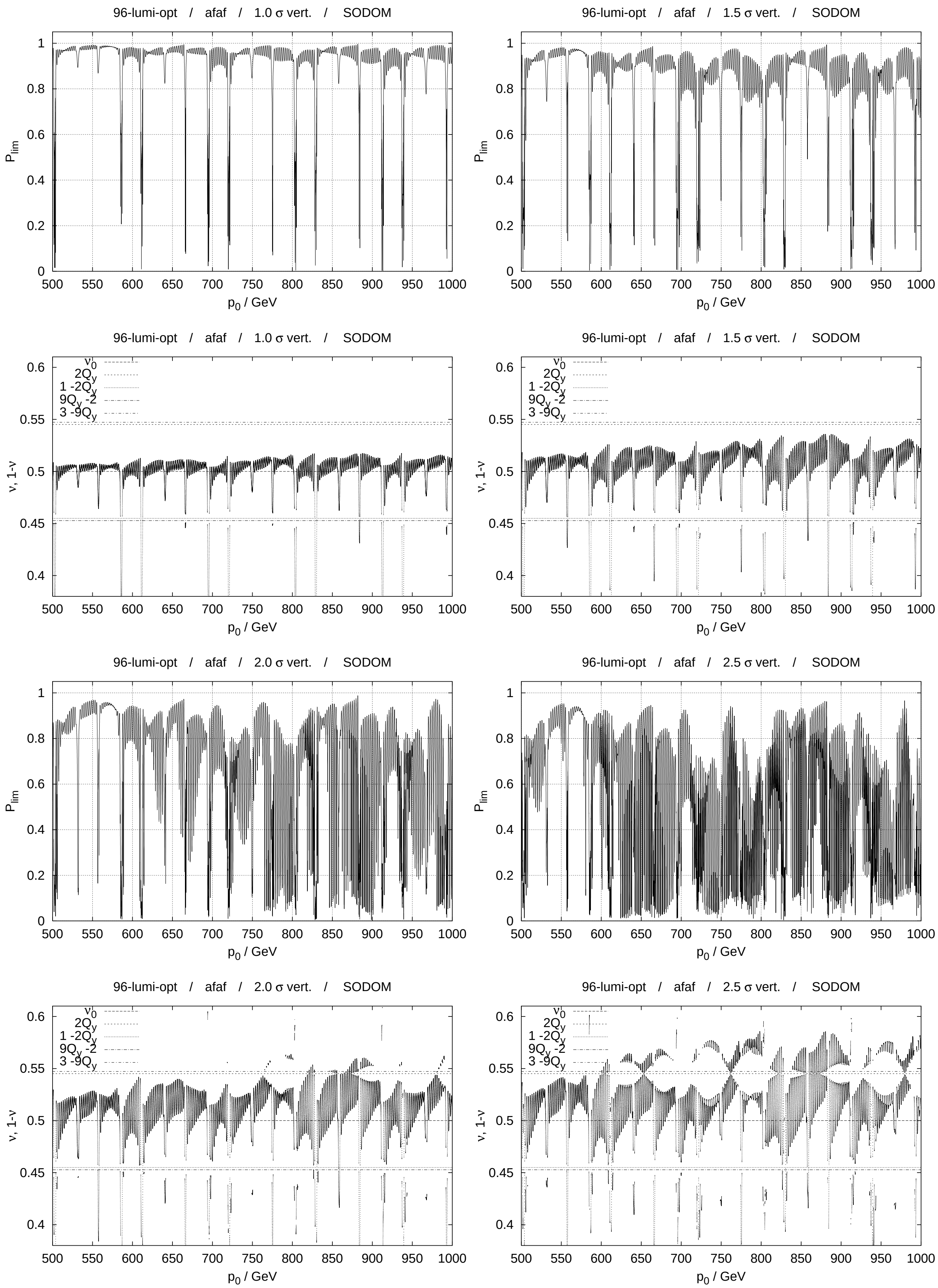

Figure 5.28: SODOM-2 scans of $P_{\mathrm{lim}}(p_0)$ and $\nu(p_0)$ for 1, 1.5, 2 and 2.5 σ vertical amplitude with the luminosity optics hp96lu820 and the snake scheme afaf.

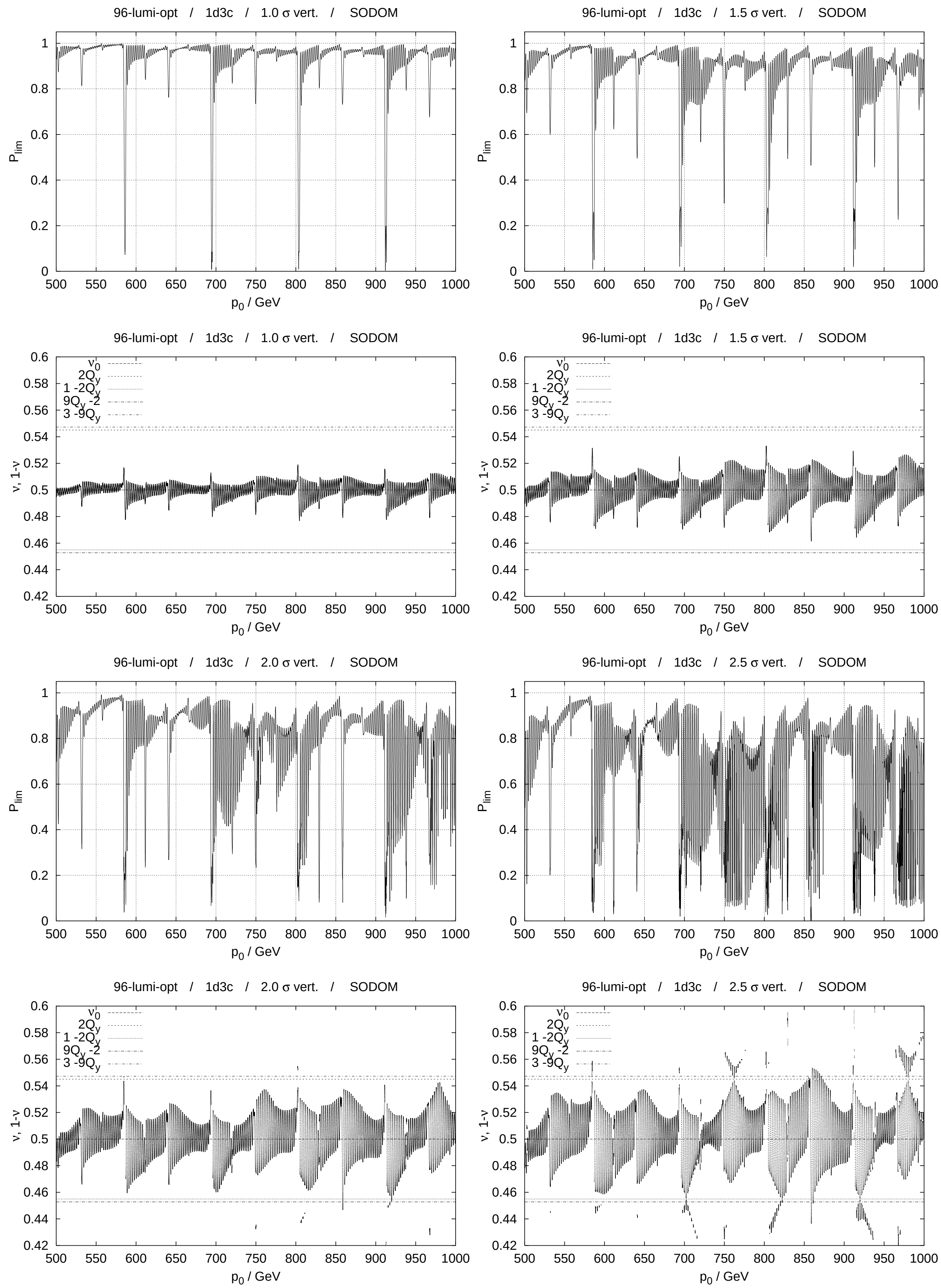

Figure 5.29: SODOM-2 scans of $P_{\lim}(p_0)$ and $\nu(p_0)$ for 1, 1.5, 2 and 2.5 σ vertical amplitude with the luminosity optics hp96lu820 and the snake scheme 1d3c.

spin tune spread is about 0.02 and therefore approximately the same as for the 3111 scheme presented in figure 5.26. We note that with the exception of the 3111 scheme *all* snake schemes produce relatively large oscillations of $P_{\rm lim}$ around a relatively low average particularly in the range from 800 to 830 GeV. On the contrary, the scheme 3111 (figure 5.26) has the lowest $\langle P_{\rm lim}\rangle_{p_0}$ with just 1 σ vertical amplitude in the whole momentum range from 500 to 1000 GeV among all tested schemes. With the scheme 1d3c and at 1.5 σ (figure 5.29) the average $P_{\rm lim}$ outside the RRSs is reduced but there are still regions around 550, 660 and 840 GeV in which $\langle P_{\rm lim}\rangle_{p_0}$ is more than 95% *and* the oscillations are small. The strongest RRSs at 580, 690, 803 and 920 GeV have acquired some close–by minima of significant depth. Moreover the background oscillations in the region between the strongest RRSs and the adjacent weak RRSs at higher momentum are particularly large. The symmetrised spin tune spread $\Delta_{p_0}^{\rm sym}(\nu)$ has grown to 0.035 but is still sufficiently small to exclude crossing of the closest by low order resonances. At 2 σ the amplitude dependent spin tune touches or crosses the resonance lines at several places, namely near 580, 750, 803 and 920 GeV. In these regions $\langle P_{\rm lim}\rangle_{p_0}$ is significantly diminished. But even at 2.5 σ the momentum regions around 570, 660 and 840 GeV provide $\langle P_{\rm lim}\rangle_{p_0} \approx 95\%$, 85% and 83% respectively and with low oscillation amplitudes. If one did not have to care about acceleration and if horizontal and longitudinal motion was neglected, one might select these momentum ranges as possible working points for polarised luminosity operation in HERA–p.

The next two figures, 5.30 and 5.31, were produced for predicting regions of potential polarisation losses during acceleration. The simulations were performed using the separation optics hp96se820. Actually in the HERA–p ramp procedure the focusing strengths are interpolated from hp96zw300 at 300 GeV to hp96se820 at 670 GeV, but the variations are small. Moreover at the stage of the development of `SPRINT` at which these simulations were performed, the `R`ampable `O`ptics `S`ystem (`ROS`) was not yet implemented. Figure 5.30 presents the results obtained with the snake scheme 3111. With 1 σ vertical amplitude the overall shape of $P_{\rm lim}(p_0)$ is approximately the same as with with hp96lu820 in figure 5.26. The average $P_{\rm lim}$ is hardly reduced but the oscillation amplitudes are about 1.2 times larger with hp96se820 than with hp96lu820. Moreover each three out of four RRSs produce deeper minima. Nevertheless, with the separation optics each 4-th RRS still almost vanishes and $\Delta_{p_0}^{\rm sym}(\nu)$ is approximately 0.02, as with the luminosity optics. Note that owing to the increased vertical tune, which is 32.27253 for hp96lu820 and 32.30812 for hp96se820, the 2-nd order resonance condition is out of the plotted spin tune range and the lowest order resonances in this range are $\kappa = 5[Q_y] - 1$ and $\kappa = 2 - 5[Q_y]$ which are both at a distance of 0.0406 from $\nu_0 = {}^1\!/_2$. The fact that the closest by low order resonances are actually closer to ν_0 than with the optics hp96lu820, i.e. about 0.041 instead of 0.045, explains why $P_{\rm lim}$ is decreased and shows stronger oscillation amplitudes even outside the strong RRSs. At 1.5 σ the static polarisation limit is still relatively calm and $\Delta_{p_0}^{\rm sym}(\nu) \approx 0.03$ does not allow any crossing of low order resonances. At 2.0 σ the only obvious jumps of the spin tune across the 5-th order resonance line are around 830 and between 920 and 930 GeV. In these regions $P_{\rm lim}$ is strongly oscillating and its average over the momentum is significantly reduced. Note that at the RRSs around 690 and 720 GeV there are spin tune points outside the displayed range that might be caused either by lack of convergence of the algorithm used, by switching between different branches of ν or by the perturbing impact of resonances of order higher then 5. At 2.5 σ the amplitude dependent spin tune crosses the 5-th order resonance repeatedly between the pairs of strong RRSs around 600, 700, 820 and 930 GeV. In each of these momentum ranges $P_{\rm lim}$ is strongly oscillating and at least in the latter three ranges $\langle P_{\rm lim}\rangle_{p_0}$ is below 50%. Therefore even with horizontal and longitudinal motion *not* taken into account, we can see that acceleration with the 3111 scheme and the fractional vertical betatron tune of approximately 0.31 is not possible beyond 580 GeV without depolarising a noticeable fraction of the beam.

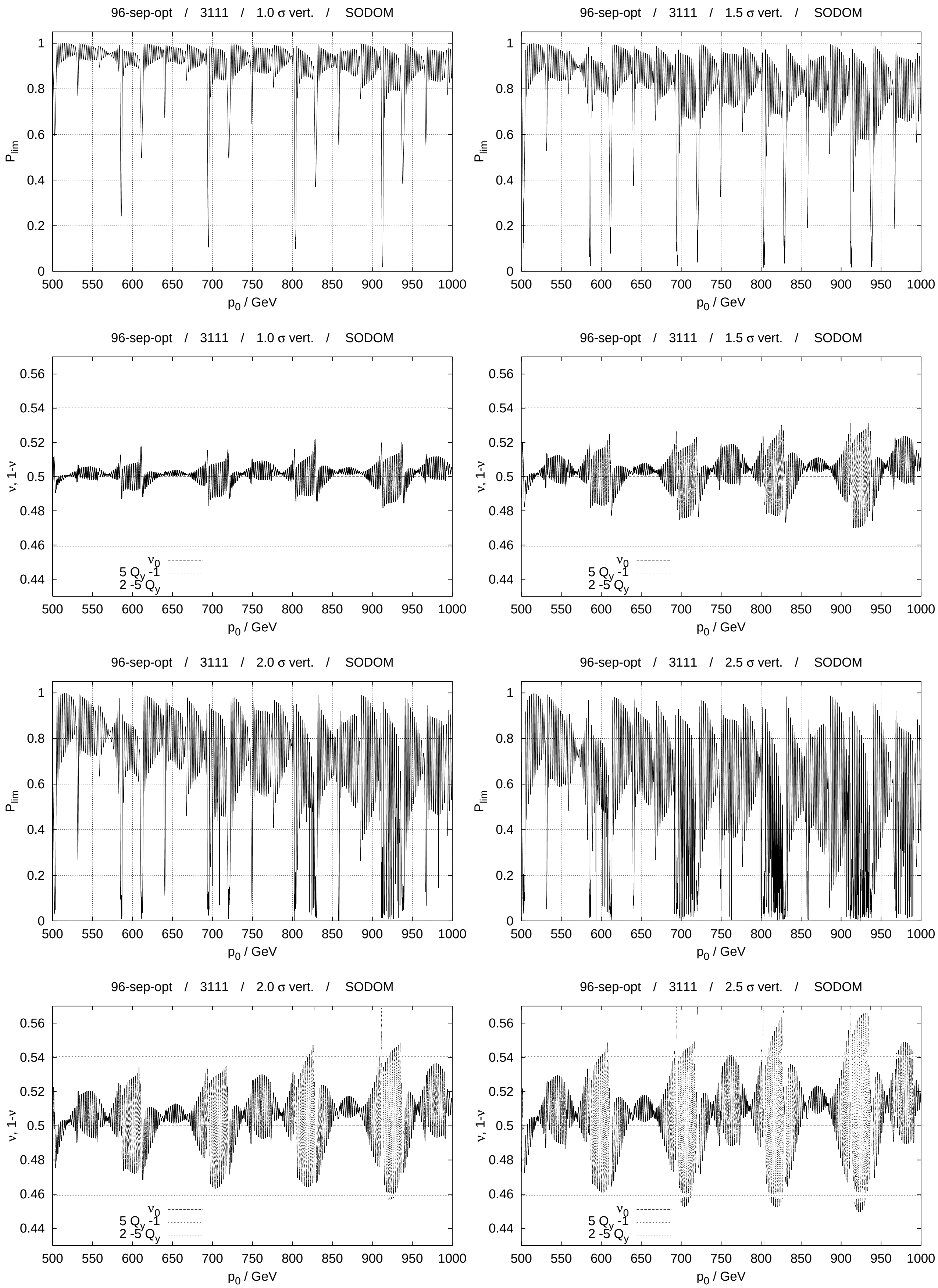

Figure 5.30: SODOM-2 scans of $P_{\lim}(p_0)$ and $\nu(p_0)$ for 1, 1.5, 2 and 2.5 σ vertical amplitude with the separation optics hp96se820 and the snake scheme 3111.

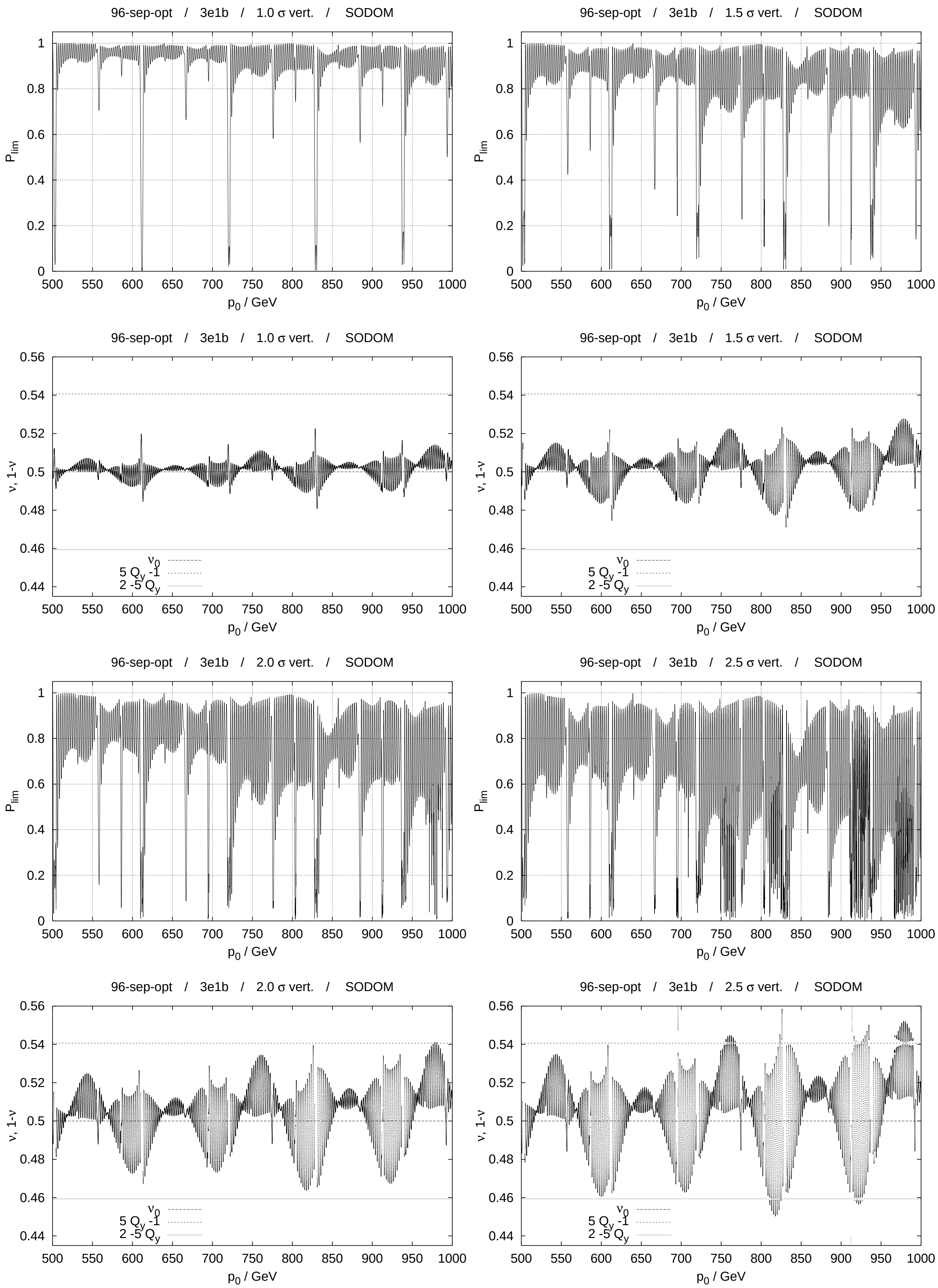

Figure 5.31: SODOM-2 scans of $P_{\lim}(p_0)$ and $\nu(p_0)$ for 1, 1.5, 2 and 2.5 σ vertical amplitude with the separation optics hp96se820 and the snake scheme 3e1b.

The simulation data for the snake schemes 1b1b and afaf with the separation optics hp96se820 are *not* displayed because of lack of time, but the results are qualitatively the same, if not worse, than the results obtained with the luminosity optics in figures 5.27 and 5.28. Both schemes generate crossings of the 5-th order resonance at three of each four RRSs already with 1 σ vertical motion. This just verifies the result from the simulation using the hp96lu820 optics, namely that both schemes are *not* capable of providing any usable polarisation at high energy in HERA–p.

Figure 5.31 shows the results of the `SODOM-2` momentum scans performed with the hp96se820 lattice and the snake scheme 3e1b. At 1 σ the average P_{lim} outside the RRSs is larger than it was with 3111. We recall that the snake scheme 3e1b was obtained by linear filtering in the range from 39.5 to 821.5 GeV with the hp96se820 lattice. In fact over a wide momentum range the maxima of P_{lim} are close to 100%. The depths of the minima at the RRSs are distributed differently, compared to snake scheme 3111 (figure 5.30). With both schemes every 4-th RRS almost vanishes but the strongest among the other three out of each four is much more enhanced compared to 3111. The symmetrised spin tune spread is approximately 0.02. At 1.5 σ the oscillations of P_{lim} are increased. The average outside the RRSs is nevertheless, with more than 90%, still higher than with snake scheme 3111 of figure 5.30. At the strongest RRSs around 500, 610, 720, 830 and 940 GeV the tendency of P_{lim} to develop deep neighbouring minima can clearly be seen. Note that the RRS at 803.5 GeV analysed in detail in section 5.3.1 is not among the strongest although the corresponding intrinsic resonance strength for the flattened HERA–p without main snakes in figure 5.3 (bottom) is the strongest up to that energy. On increasing the vertical amplitude to 2.0 σ we find that although the average P_{lim} decreases further there are still regions with maximal P_{lim} close to 99%. In particular there are such momenta just below 800 GeV. The number of neighbouring deep minima has continuously increased especially around 720, 830 and 940 GeV, but at least below 800 GeV there are no visible signs of the spin tune crossing one of the two close–by 5-th order resonances. Around 830 and 970 GeV ν comes very close to $\kappa = 5[Q_y] - 1$ and P_{lim} oscillates strongly in these regions but the amplitude dependent spin tune has no visible discontinuities, indicating that the kinetic resonance strengths are weak. Increasing the vertical amplitude further to 2.5 σ finally generates broad regions from 750 to 770 GeV, from 800 to 830 GeV, from 920 to 950 GeV and from 970 to 1000 GeV in which P_{lim} oscillates violently. In these regions and in particular at the RRS at 690 GeV the amplitude dependent spin tune crosses the 5-th order resonances. This snake scheme 3e1b is the only one among those tested so far which does *not* show any kinetic resonances with 2σ vertical amplitude up to an energy close to 800 GeV. Thus we expect it to allow acceleration of a polarised beam with purely vertical motion to about 800 GeV. Nevertheless, in section 5.3.2 we have seen in figure 5.22 that *with* horizontal and longitudinal motion polarisation is lost at the RRS at 803.5 GeV.

One way to maintain adiabaticity during the ramp and have high P_{lim} at some constant collision energy has not yet been exploited, namely the optimisation of the orbital tunes. In this section we have seen that the amplitude dependent spin tune seen as a function of the reference momentum oscillates around ν_0 with some characteristic spread $\Delta^{\text{sym}}_{p_0}(\nu)$. If the resonance conditions $[\nu] = [\vec{k} \cdot \vec{Q}]$ with moderate $|\vec{k}|$ cannot be met, then the spin motion is most likely to be adiabatic, i.e. $P_{\text{dyn}} \approx$ const. Therefore it is worthwhile to optimise the orbital tunes inside the bandwidth of orbital stability of HERA–p. Owing to the limited computing power, it is *not* yet possible to perform long range scans of $P_{\text{lim}}(p_0)$ with more than one orbital mode excited to a significant value and with reasonable accuracy close to a RRS. Moreover the amplitude dependent spin tune cannot yet be calculated with more than one orbital mode in a RRS at all. Therefore, to get an estimate for the feasibility of polarised protons in HERA at high energy, ramp simulations with snake schemes and optics, that have been optimised on the basis of qualitative experience, have to be performed. In sections 5.4.1 and 5.4.2 a hypothetical ramp table will be introduced that fixes at least the vertical tune to a value acceptable for orbital stability during the acceleration *and* which is optimal in the sense that the space for spin tune variations is maximised.

5.4 HERA–p with modified orbital tunes

In sections 4.8 and 4.9 we have seen that P_{lim} has a pronounced minimum of characteristic width ϵ_κ whenever the amplitude dependent spin tune ν crosses a resonance condition $\kappa = k_0 + \vec{k} \cdot \vec{Q}$ with a kinetic resonance strength ϵ_κ. Moreover we have seen that P_{lim} can be seriously diminished whenever ν is sufficiently close to some κ with sufficiently large kinetic resonance strength. In section 4.10 we have seen that whenever some parameter λ of the spin–orbit system is continuously changed so that ν crosses the resonance condition κ, then the average spin action changes in the adiabatic limit according to a generalised Froissart–Stora formula (4.104) with $\epsilon = \epsilon_\kappa$ and the ramp speed $\alpha \approx (\mathrm{D}_\lambda \tilde{\nu}) \mathrm{D}_\theta \lambda \Big|_{\tilde{\nu}=\kappa}$. In sections 4.9, 5.3.1, 5.3.2 and 5.3.3 we have seen that the closeness to or crossing of higher order kinetic resonances in HERA-p with 6 flattening snakes and 4 or 8 main snakes has a strong impact on the maximum attainable polarisation at high energy in HERA–p. Therefore it seems quite natural to try to find a set of orbital tunes such that the allowable symmetrised spin tune spread $\Delta_{p0}^{\text{sym}}(\nu)$ on all reasonably populated tori is maximal — under the constraint that this set of orbital tunes is still acceptable for acceleration and storage. The limitations on the tunes due to the dynamic aperture in storage mode are quite strong. In principle the transverse tunes should be kept very close to the actual luminosity tunes $[Q_x] = 0.292$ and $[Q_y] = 0.297$ or to the interchanged tunes $[Q_x] = 0.297$ and $[Q_y] = 0.292$. Thus shifting at least the vertical tune as far as possible *below* the classical snake resonant tune ${}^3\!/_{10}$ is a potential source of improvement. This puts preference on $[Q_x] \approx 0.297$ and $[Q_y] \approx 0.292$ with a tendency to seek even lower possible values of $[Q_y]$ and $[Q_x]$.

In this and the following sections we will restrict ourselves to a sequence of optics (ramp scheme) with tunes optimised for ramping, since it became clear in section 5.3.3 that even with the old tunes one can find a suitable working point at high energy although *not* in particular at 820 GeV. From figure 4.19 we conclude that the allowable $\Delta_{p0}^{\text{sym}}(\nu)$ has local maxima at *odd* order orbital resonances. In HERA–p, getting too close to the 4-th and 3-rd order resonances $[Q_{x,y}] = {}^1\!/_4, {}^1\!/_3$ decreases the beam life time significantly and accidental crossing of one of these two resonances leads to a complete loss of the beam. Therefore the lowest odd order orbital resonance close to the standard tunes mentioned above is $[Q_y] = {}^2\!/_7 = 0.\overline{285714}$. A preliminary experiment [HPlb] after the $e^\pm$ beam was dumped showed that the vertical tune can be set very close to ${}^2\!/_7$ and even cross it without significant increase of the beam loss rates at 920 GeV if no beam–beam effect from the $e^\pm$ beam is present. Thus the order of the orbital resonance (7) is already high enough to allow beam operation at least during the ramp procedure. Nevertheless, the order of the resonance is still low enough to potentially cause problems with the evaluation of the turn–by–turn average of the ramped polarisation P_{rmp} due to a too crude sampling of the orbital phase space (analogous to section 4.5). Therefore the fractional vertical betatron tune for all further simulations will be

$$[Q_y^{\text{sim}}] \approx 0.286 \tag{5.18}$$

which is slightly above ${}^2\!/_7$. Figure 5.32 shows the resonance lines $\kappa = [kQ_y]$ which are inside the range $0.27 \leq [Q_y] \leq 0.305$ and $0.4 \leq \kappa \leq 0.6$ up to order 20 (which does not appear in this range). Note the region free of resonance conditions indicated by the “diamond” in the middle of figure 5.32 around $Q_y = {}^2\!/_7$. If $\nu_0 = {}^1\!/_2$ and the influence of longitudinal and horizontal motion is neglected, then the maximum allowable $\Delta_{p0}^{\text{sym}}(\nu)$ is given by

$$\Delta_{p0}^{\text{sym}}(\nu) < \frac{1}{2} - [kQ_y] \,,\ 1 \leq k \leq 20 \quad , \tag{5.19}$$

where the closest by resonance orders are k =5, 12 and 19. Table 5.2 contains the fractional vertical tunes $[Q_y]$ at which the maximum allowable $\Delta_{p0}^{\text{sym}}(\nu)$ around $\nu_0 = {}^1\!/_2$ is 0.06, 0.05 and 0.04 when the closest by resonance of order 19, 12 and 5 is taken into account. The higher the order of the resonance which is not to be touched, the closer must $[Q_y]$ be to ${}^2\!/_7$. In the 5-th column of table 5.2 the maximum allowable symmetrised spin tune spread is given for $[Q_y] = 0.286$ and k =19, 12 and 5.

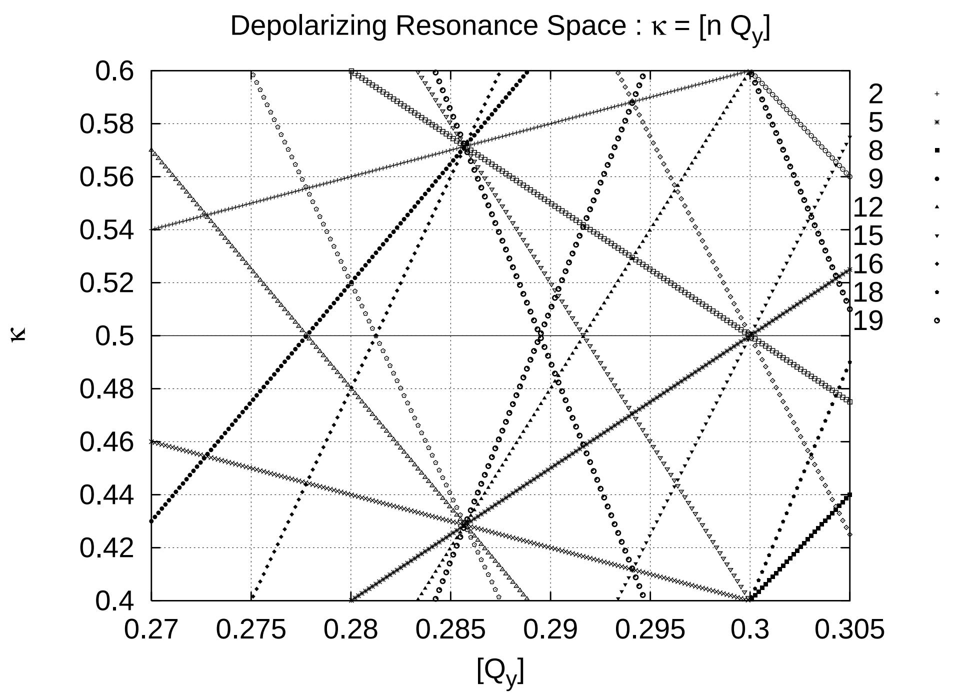

Figure 5.32: The spin–orbit resonance conditions $\kappa = [kQ_y]$ with $|k| \leq 19$ and in the vicinity of $[Q_y] \approx {}^2/_7$ and $\kappa \approx {}^1/_2$.

$\Delta^{\mathrm{sym}}_{p_0}(\nu)$:	0.06	0.05	0.04	$[Q_y]$ =0.286
k		$[Q_y]$		$\Delta^{\mathrm{sym}}_{p_0}(\nu)$:
19	0.2863	0.2868	0.2874	0.066
12	0.287	0.2875	0.2883	0.068
5	0.288	0.290	0.292	0.070

Table 5.2: Column 2 to 4 : Maximal $[Q_y]$ to allow $\Delta^{\mathrm{sym}}_{p_0}(\nu)$ =0.06, 0.05 and 0.04 around $[Q_y] \tilde{>} {}^2/_7$. Column 5: The maximum allowable symmetrised spin tune spread at $[Q_y] = 0.286$.

Another constraint on the tunes is that the dynamic aperture be sufficiently large. In HERA-p the beam loss rates are lowest when the machine is operated close to the difference resonance $Q_y - Q_x = \in \mathbb{Z}$. In practice $|[Q_y] - [Q_x]| \approx 0.005$ has been adopted for the ramp and storage in HERA–p. Therefore, and in order that $[Q_x]$, at least, does not deviate too far from the optimal region $0.292 \leq [Q_x] \leq 0.297$, the setting

$$[Q_x^{\mathrm{sim}}] \approx 0.291 \tag{5.20}$$

will be used in the following.

In the standard HERA–p ramp procedure of 1996 the injection optics hp96inj40 is remains unchanged until 150 GeV and then as the acceleration continues linear interpolation of the magnet currents steers the parameters to those of the intermediate optics hp96zw300 at 300 GeV. From 300 GeV to 670 GeV the hp96zw300 is linearly interpolated to the separation optics hp96se820, which is then kept unchanged until 820 GeV. Then, after the $e^{\pm}$–ring has been filled and ramped, the luminosity optics hp96lu820 is obtained by linear interpolation of the magnet currents from hp96se820 to hp96lu820 at constant energy. The complete proton ramp procedure from hp96inj40 to hp96se820, without injection optimisation and filling takes 25 to 30 minutes. In order to make such changes to the optics while simulating acceleration, the `Rampable Optics System` was developed[4] and incorpo-

[4]The `Rampable Optics System` was neither taken from the optics code `PETROS` nor from the spin tracking code `SITROS`.

step	p_i GeV	$Q_{z,i}$ 10^{-3}	source lattice	target lattice	trigger points	p_f GeV	Δp GeV	$\delta E/$ turn KeV
1	40	0.65894	hp96inj40	hp96inj40–90	–	90	50	3.0
2	90	0.91489	hp96inj40–90	hp96inj40–150	–	150	60	3.0
3	150	0.93635	hp96inj40–150	hp96zw230	8	230	80	6.3
4	230	0.83537	hp96zw230	hp96zw300	7	300	70	6.3
5	300	0.78714	hp96zw300	hp96zw400	4	400	100	16.5
6	400	0.77252	hp96zw400	hp96zw550	6	550	150	16.5
7	550	0.76020	hp96zw550	hp96se820–650	4	650	100	16.5
8	650	0.75513	hp96se820–650	hp96se820	–	820	170	22.3
9	820	0.62379	hp96se820	hp96lu820	–	820	0	0.0
END	820	0.62511	hp96lu820	—	–	—	Aver=	8.8

Table 5.3: The modified ramp table for HERA–p

rated in SPRINT. The ROS modules not only implement the linear interpolation between two lattices at given reference momenta but moreover allow to set trigger points at which the rates of variations of the strengths of various elements are increased or decreased. This feature is particularly useful since the orbital tunes are *not* linear functions of the quadrupole strengths and the transverse tunes would actually cross the quarter integer resonance when naively interpolating between hp96inj40 and hp96zw300. Thus the focusing strengths of certain quadrupoles (QP40 and QP42) have to be steered explicitly to keep the transverse tunes close to their specified values. In addition 3 more "intermediate" optics, hp96zw230, hp96zw400 and hp96zw550 have been generated to allow for a sufficient number of possible break points on the ramp between 40 and 820 GeV. It should be noted that these additional intermediate optics were obtained by linear interpolation between the reference files hp96inj40, hp96zw300 and hp96se820 and by subsequent tune correction. They were *not* explicitly matched to minimise β- and dispersion–beat.

An attempt was made to mimic the real behaviour of the synchrotron tune during acceleration as closely as possible — with the exception that from 650 to 820 GeV the synchrotron tune Q_z was *reduced* instead of increased in order to move possible low order synchrotron sidebands of the spin–orbit resonances as close as possible to their parent resonances. Note that the effective strength of synchrotron sidebands is enhanced for decreasing Q_z [LB96]. Again, as in section 5.3.2 the 6 adjacent cavities in HERA–p have been substituted with a single cavity at the centre of the positions of the 208 Mhz systems.

Table 5.3 shows the modified ramp table to be used in the following. The ramp table consists of 9 steps. During steps 3 to 7 up to 8 trigger points, modifying the rates of variation of the focusing strengths of the QP40 and QP42 magnets, have been used to stabilise the transverse tunes. The suffixes –90, –150 and –650 on the optics names indicate that the cavity strength was adjusted to produce the correct synchrotron tune at the reference momenta of 90, 150 and 650 GeV respectively. Columns 2, 7 and 8 contain the initial and final reference momenta and the total momentum increase of the ramp step. The last column (9) contains the approximate energy gain per turn of the *real* HERA ramp procedure of 1998/1999. The last entry in column 9 is the average energy gain per turn. Although the ROS modules in SPRINT are able to interpolate between two lattices at constant reference momentum, the last step from the hp96se820 to the hp96lu820 optics will not be discussed here. This would only make sense if an optimal momentum for polarised $e^{\pm}$–p collisions had been found.

Figure 5.33 shows the evolution of the orbital tunes during momentum variation according to the modified ramp table 5.3. Q_x and Q_y are displayed to the left and Q_z is shown to the right. Both plots

Neither of these programs is capable of simulating the effect of acceleration on orbit and spin — even without lattice interpolation!

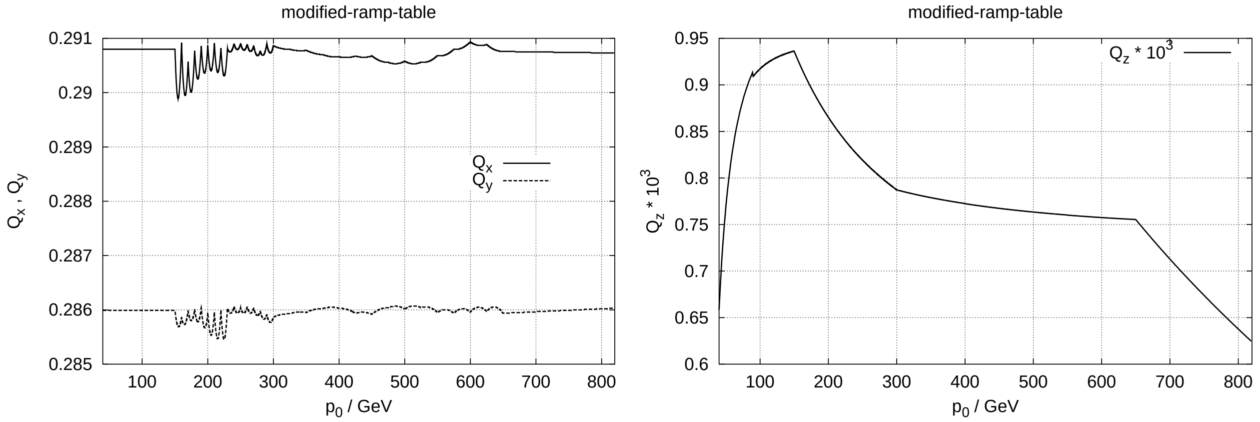

Figure 5.33: The evolution of the orbital tunes during the ramp procedure with the modified ramp table.

show the behaviour of the tunes from 40 GeV with the optics hp96inj40 to 820 GeV with the optics hp96se820. The 15 trigger points from 150 to 300 GeV can clearly be identified as cusps of the curve $Q_{x,y}(p_0)$ at which the vertical tunes come back to their "nominal" values. In between the cusps the tunes drift away because of the non–linear dependence of the tunes on the lattice parameters. Note that it is *not* yet possible to control the transverse tunes as exactly as in this simulation during a *real* HERA ramp.

All further simulations were performed using the 3e1b snake scheme. The scheme was not only obtained by linear long range filtering with the lattice hp96se820, but it also appeared most promising during the simulations described in sections 5.3.2 and 5.3.3. The final reference momentum was chosen to be 820 GeV although the discussions in sections 5.3.1, 5.3.2 and 5.3.3 did not really suggest this momentum for luminosity operation with polarised protons. The main purpose of the ramp studies in section 5.4.2 will be to ascertain the maximum momentum that can be reached with the optimised tunes and the filtered 4–snake scheme.

5.4.1 Static evaluation of HERA with modified orbital tunes

In this section the Fourier based analysis of $P_{\rm lim}$ and ν that was employed in section 5.3.3 is repeated for the modified ramp table. The `ROS` modules are not only able to control interpolation between various optics during real acceleration but also during static scans of the reference momentum.

Figure 5.34 shows the static polarisation limit $P_{\rm lim}$ and the amplitude dependent spin tune ν computed with the `SODOM-2` algorithm over the complete momentum range of the HERA–p ramp procedure. As in section 5.3.3 $P_{\rm lim}$ and ν for the same vertical amplitude are displayed one above the other. The vertical amplitudes are 1 σ (upper two left), 1.5 σ (upper two right), 2 σ (lower two left) and 2.5 σ (lower two right). It can be observed in all 8 plots, that around 40 GeV the spin motion in HERA–p with 4 filtered snakes is quite well behaved. $P_{\rm lim}$ is close to 100% even at 2.5 σ and the residual resonance structures (RRSs) are narrow and isolated. Even at the RRSs, at low energy the symmetrised spin tune spread is small, for example $\Delta^{\rm sym}_{p_0}(\nu) < 0.01$ for $p_0 < 180$ GeV. Note that owing to the modified vertical tune no resonance conditions up to 19–th order occur in the plotted range of ν. With increasing momentum the oscillations of $P_{\rm lim}$ increase and hence $P_{\rm lim}$ averaged over the regions *between* the RRSs decreases. Nevertheless globally $\langle P_{\rm lim}\rangle_{p_0}$ is higher than with the original tunes in figure 5.31. This is true for all amplitudes and even above 803.5 GeV. We note that because of the modified tunes, with 2.5 σ vertical amplitude the region between the strong RRS at 720 GeV and the RRS at 803.5 GEV is *not* filled with deep minima of $P_{\rm lim}$ in contrast to figure 5.31. There is only one region where the `SODOM-2` algorithm did not converge. That is inside the RRS around 803.5 GeV with

$2.5\,\sigma$ vertical amplitude. The non–convergence was verified with `SODOM-2` using 128 Fourier harmonics and stroboscopic averaging with more than 10^5 turns! There are two possibilities for the failure of both algorithms in this parameter range. Either the effect of resonances of much higher order than 19 is so strongly enhanced that both algorithms fail for finite numbers of averaging turns or Fourier harmonics respectively, or the spin motion in this region is *not* integrable or not even approximately integrable at all. Nevertheless there is a momentum range directly *below* 800 GeV where $\Delta_{p_0}^{\rm sym}(\nu)$ is small and $P_{\rm lim}$ has maxima close to 99% for all vertical amplitudes. Therefore the combined effect of the optimised 4–snake scheme and the optimised ramp tunes seems to provide the possibility of high beam polarisation at high energy in HERA–p, as long as the horizontal and longitudinal motions are not taken into account.

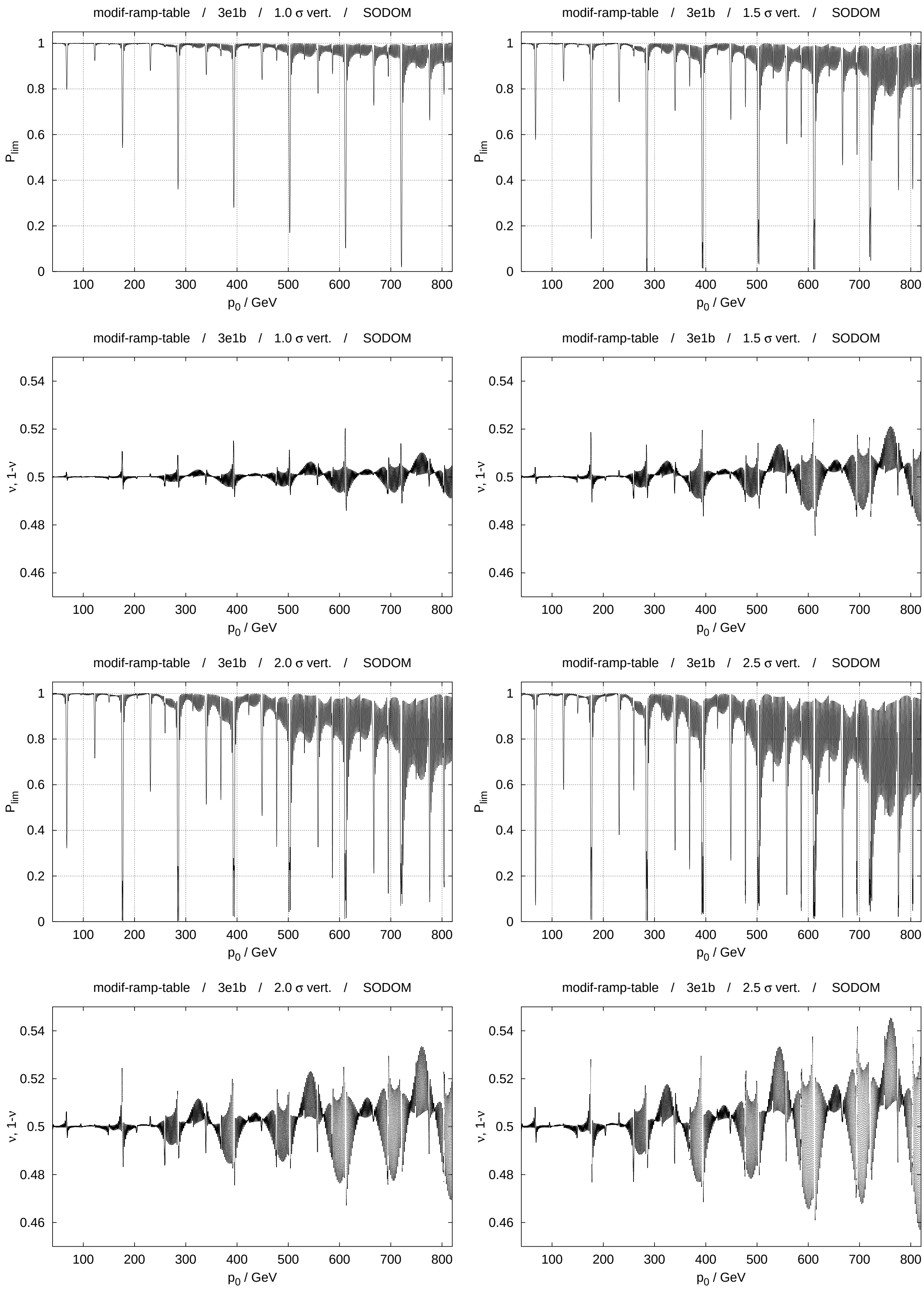

Figure 5.34: Modified ramp table : `SODOM-2` scans of $P_{\lim}(p_0)$ and $\nu(p_0)$ for 1, 1.5, 2 and 2.5 σ vertical amplitude.

5.4.2 Ramp studies for the modified orbital tunes

In section 5.4.1 we have demonstrated that for 2.5 σ of purely vertical motion, with the snake scheme 3e1b obtained by linear long range filtering and with the modified tunes $[Q_x^{\rm sim}] \approx 0.291$ and $[Q_y^{\rm sim}] \approx 0.286$, the symmetrised spin tune spread from 40 GeV to about 800 GeV is sufficiently small to avoid the crossing of, or even closeness to, all kinetic higher order resonances up to 19-th order during the HERA–p ramp procedure. Since our simulations were restricted to purely vertical motion we must test the modified ramp table with *all* three orbital modes being excited at the same time. The only method which is practically feasible for such a test over the whole momentum range with 6–dimensional orbital motion is straightforward tracking, or to be more precise, acceleration with simultaneously varying lattice parameters via the `ROS` modules of `SPRINT` .

While discussing the simulations presented in section 5.3.2 we have seen that acceleration studies with just one particle and just a few momentum steps are relatively hard to interpret. On the contrary tracking many particles and computing $P_{\rm rmp}$ at many momentum steps with sufficient accuracy is quite time consuming. In this section we will use an intermediate approach. The HERA ramp procedure was simulated with various particle ensembles on various invariant tori and with different ramp speeds. Let now $(M_x \times M_y \times M_z)$ denote the number of initial orbital phases uniformly distributed in the range $[0, 2\pi)$ for the "horizontal', "vertical" and "longitudinal" eigenplanes respectively. The complete momentum range was simulated with

1. 5 times the original ramp speed as defined in table 5.3 and an ensemble of $(1 \times 2 \times 2) = 4$ particles,
2. 10 times the original ramp speed and
   (a) $(1 \times 3 \times 3) = 9$ particles and
   (b) $(2 \times 2 \times 2) = 8$ particles,
3. constantly 200 keV per turn and
   (a) $(1 \times 3 \times 3) = 9$ particles and
   (b) $(2 \times 2 \times 2) = 8$ particles,
4. 200 keV per turn up to 300 GeV and then with 5 times the original ramp speed and
   (a) $(1 \times 9 \times 1) = 9$ particles for purely vertical motion and
   (b) $(2 \times 2 \times 2) = 8$ particles.

The spins of the particle ensemble were set parallel to the $\hat{n}$–axis at 40 GeV momentum and the initial orbital phases.

Three particular regions around strong residual resonance structures, namely from 600 to 625 GeV, 710 to 740 GeV and 790 to 820 GeV were studied with the original ramp speed, i.e. 16.5 keV/turn below 650 GeV and 22.3 GeV beyond 650 GeV. These regions were studied with $(3 \times 3 \times 2) = 18$ particles all on the same invariant torus and with 10 or 11 particles all at the same orbital phase but placed on 10 (11) invariant tori so that the initial orbital amplitude linearly increases from torus 1 to 10 (11). In all simulations $P_{\rm rmp}$ was calculated after every 100 to 1000 turns with initially 200 turns for adaptive averaging (i.e. starting with $T = 200$ in (5.14)). Note that 4 to 18 particles are still not enough to completely eliminate the artifacts from "few particle tracking" described in section 5.3.2, but it should be taken into account that one such ramp simulation from 40 to 820 GeV took up to *2 weeks* of CPU–time! In any case, the artificial effect of an apparent *increase* of the polarisation during resonance crossing instead of the expected *decrease* is already averaged away to a greater extent with 4 particles than with just 1 particle.

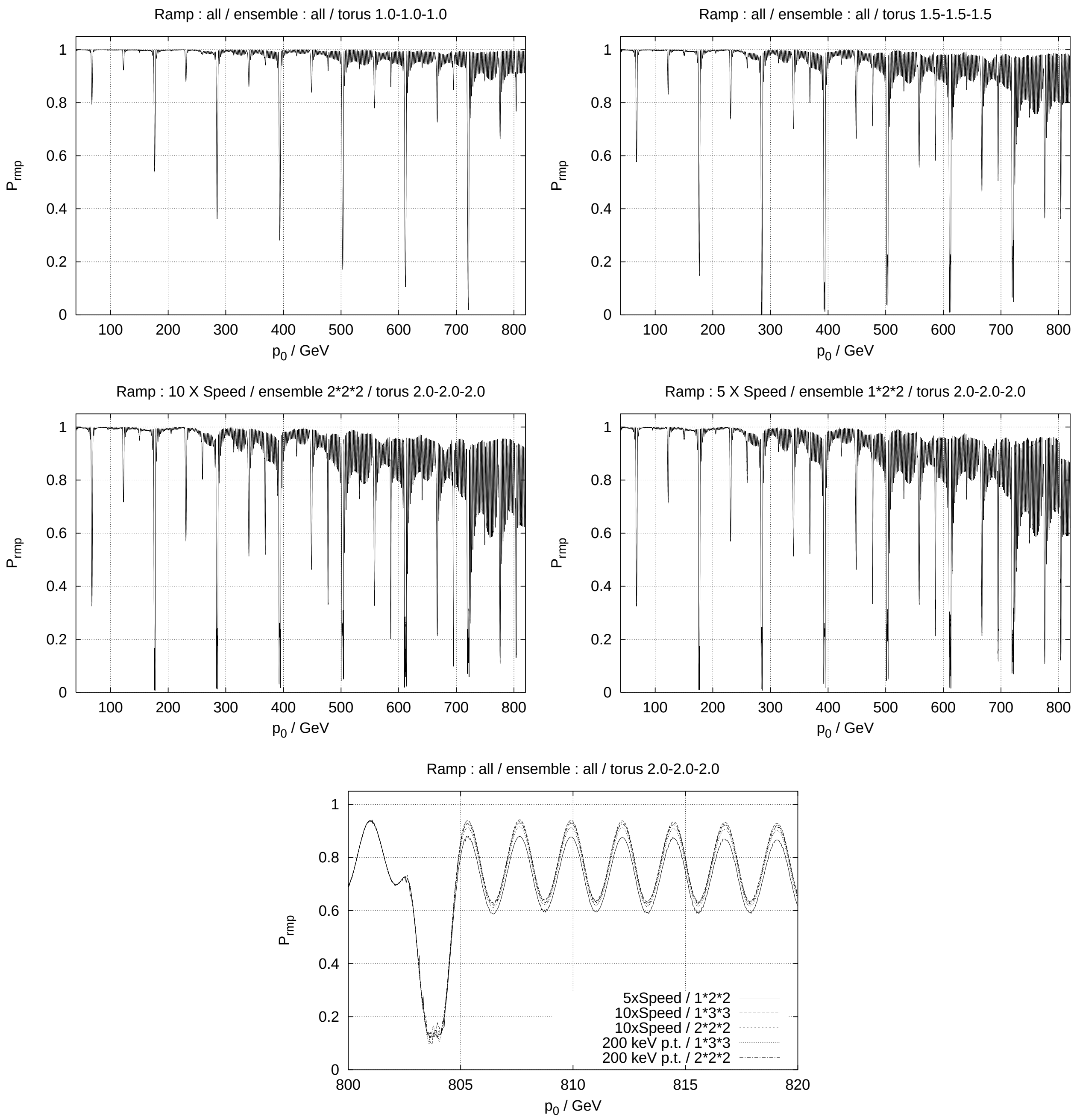

Figure 5.35: Ramp simulations with the modified ramp table on the $(1,1,1)\sigma$, $(1.5,1.5,1.5)\sigma$ and $(2,2,2)\sigma$ invariant tori.

Figure 5.35 shows the results of ramp simulations on the invariant tori with $(1,1,1)\sigma$ (top left), $(1.5,1.5,1.5)\sigma$ (top right) and $(2,2,2)\sigma$ orbital amplitudes (all three plots below). On the $(1,1,1)\sigma$ torus no polarisation is lost w.r.t. P_{lim} for all ramp speeds and all ensembles. Comparison with figure 5.34 (topmost left) shows that although figure 5.34 was produced with purely vertical motion, P_{lim} of figure 5.34 is almost identical to P_{rmp} of figure 5.35 (top left). In figure 5.25 we have seen that as long as all orbital amplitudes, in particular the vertical amplitude, are *small*, the horizontal and longitudinal amplitudes have an almost negligible impact on the invariant spin field compared to the vertical amplitude. Comparison of the P_{rmp} on the $(1.5,1.5,1.5)\sigma$ torus with P_{lim} at $(0,1.5,0)\sigma$ in figure 5.34 (topmost right) shows that P_{rmp} is still very close to P_{lim}. Nevertheless, difference $P_{\text{lim}} - P_{\text{rmp}}$ increases continuously with momentum, namely up to 2% at top energy. This difference is not surprising since at high energy and the further we go outwards in phase space the more important are the horizontal and longitudinal amplitudes which were zero in figure 5.34. Moreover there are no sudden drops of P_{rmp} w.r.t. P_{lim}. Since $P_{\text{rmp}}(p_0)$ is the same for all simulated ramp speeds and ensembles, it is very likely that the smooth decay of P_{dyn} w.r.t. figure 5.34 is caused by the enhanced opening of the invariant spin field with increasing momentum once longitudinal and horizontal motion are introduced. The middle row of figure 5.35 shows two representative examples of the simulation on the $(2,2,2)\sigma$ torus. With these orbital amplitudes we expect that the horizontal and longitudinal amplitudes significantly decrease P_{lim} w.r.t. the case of purely vertical motion. In the plot to the left the ramp was simulated with 10 times the original ramp speed and an ensemble of 8 particles. Compared to P_{lim} in figure 5.34 (3-rd row left), the ramped polarisation P_{rmp} drops almost smoothly with energy indicating a static effect of the increasing spread of the $\hat{n}$–axis rather than lack of adiabaticity. The plot to the right was obtained with 4 particles and 5 times the original ramp speed. It shows a sudden drop of P_{rmp} by about 5% at the RRS around 803.5 GeV. This drop clearly indicates that some kinetic resonance has been crossed in a not completely adiabatic way. We note that the static `SODOM-2` scans in figure 5.34 showed neither any obvious resonance crossings nor any candidates for non–integrability of the spin motion up to 2 σ of *purely* vertical amplitude. Therefore it is very likely that the average spin action was decreased during the crossing of a kinetic resonance which includes the horizontal and/or longitudinal orbital modes. The fact that the final P_{rmp} is larger with larger ramp speed indicates that a kinetic resonance which is weak compared to the acceleration rate was crossed. The picture at the bottom of figure 5.35 puts together the various curves of P_{rmp} with different ramp speeds and ensembles on the $(2,2,2)\sigma$ torus in the zoomed momentum range from 800 to 820 GeV. Obviously before entering the RRS around 803.5 GeV, all 5 curves are identical, but on exit they have a spread of 5%. This clearly demonstrates that the resonance around 803.5 GeV is not crossed adiabatically. Note that the bottom picture of figure 5.35 was obtained by zooming the last 20 GeV of complete ramp simulations starting at 40 GeV. Therefore the fact that the 5 curves are identical up to the graphical resolution *before* entering the RRS indicates the absence of depolarisation up to about 800 GeV on this invariant torus!

In [BG98b] similar simulations were performed with a model of HERA–p without vertical bends around the O–IP, flattened vertical bend sections around the N- and S–IP and 4 main snakes, namely a longitudinal snake at O and 3 radial snakes at S, W and N. The tunes were *not* modified. In these simulations the polarisation on the (1,1,0) and $(1,1,1)\sigma$ tori was preserved during acceleration to 820 GeV but on the (0,2,0) and $(2,2,0)\sigma$ tori polarisation was lost completely around 750 and 600 GeV respectively. This is consistent with the assumption that filtered snake schemes and modified orbital tunes improve the preservation of polarisation on tori with large orbital amplitudes.

Figure 5.36 shows the results of the ramp simulations with the original ramp speed in momentum ranges around the strong RRSs at 612, 721 and 803.5 GeV. The lattice parameters were interpolated to the starting momenta of 600, 710 and 790 GeV. Then the spins of the particle ensemble were set parallel to the $\hat{n}$–axis at this momentum and the initial orbital phases and ramped through the corresponding parameter range of the modified HERA ramp table. Figure 5.36 shows not only P_{rmp} defined in equation (5.14), but also the vertical component of the unit vector pointing in the direction

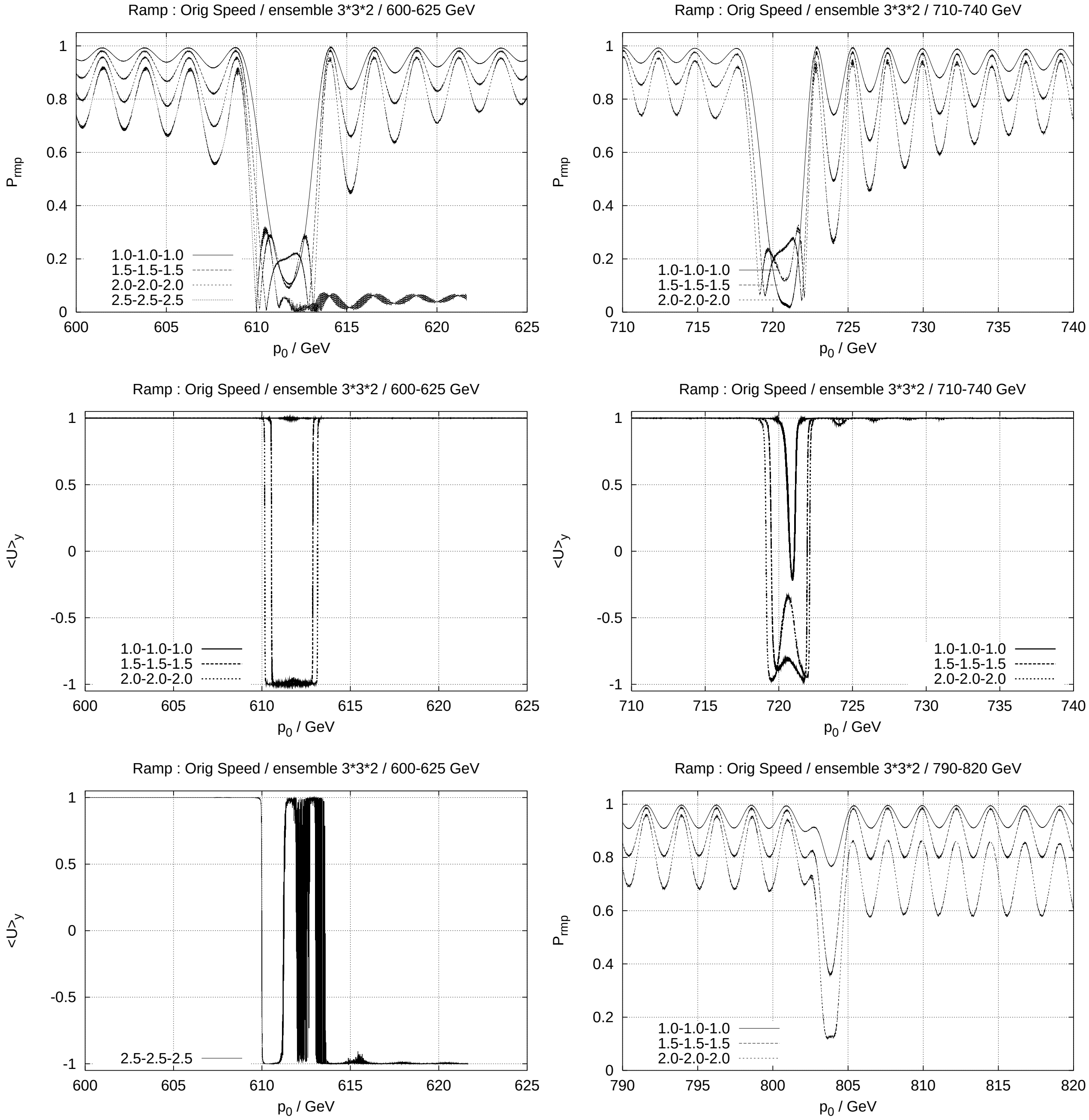

Figure 5.36: Ramp simulations with the modified ramp table and the original ramp speed on various invariant tori around the RRSs at 612, 721 and 803.5 GeV.

of the ramped polarisation

$$u_y^{\langle\xi\rangle}(\vec{J}_k,\theta_k;N,T) \equiv \frac{1}{P_{\rm rmp}(\vec{J}_k,\theta_k;N,T)}\,\frac{1}{N}\sum_{l=1}^{N}\frac{1}{T}\sum_{j=1}^{T}\hat{y}\cdot\hat{\xi}_l^k(\theta_k+j2\pi) \quad . \tag{5.21}$$

Here we assume that $P_{\rm rmp}(\vec{J}_k,\theta_k;N,T)\neq 0$. Far away from any RRS $|u_y^{\langle\xi\rangle}|$ is approximately 1 and according to the adiabatic limit of equation (4.104) it should change sign during adiabatic resonance crossing. Figure 5.36 (top left) shows $P_{\rm rmp}(p_0)$ during ramping from 600 to 625 GeV with 16.5 KeV per turn. The 4 curves correspond to invariant tori of (1,1,1), (1.5,1.5,1.5), (2,2,2) and (2.5,2.5,2.5)σ orbital amplitudes. The fact that on all tori up to (2,2,2)σ the ramped polarisation $P_{\rm rmp}$ has maxima of between 90 and 99% and that these maxima have approximately the same height *before* and *after* passing the RRS around 612 GeV, obviously indicates that on these tori the spin motion stays adiabatic. On the (2.5,2.5,2.5)σ torus the polarisation vanishes almost completely close to the centre of the RRS at 612 GeV. The curve of $P_{\rm rmp}$ becomes extremely wiggly since for an ensemble of spins almost completely perpendicular to their local $\hat{n}$–axis , an enormous number T of tracking turns for averaging $P_{\rm rmp}$ is in principle required but could not be provided in the simulation run for the sake of computational speed. Moreover since the polarisation was definitely lost after passage through the RRS, the simulation on the (2.5,2.5,2.5)σ torus was stopped manually before 625 GeV were reached. Figure 5.36 (middle left) shows $u_y^{\langle\xi\rangle}(p_0)$ in the same momentum range and for the (1,1,1), (1.5,1.5,1.5), (2,2,2)σ tori. On the (1,1,1)σ torus $u_y^{\langle\xi\rangle}$ stays always positive and close to 1 with the exception of some fluctuations around 612 GeV. On both the (1.5,1.5,1.5)σ and (2,2,2)σ tori $u_y^{\langle\xi\rangle}$ changes its sign twice, namely at the zeros of $P_{\rm rmp}$ displayed in the plot directly above. This together with the apparent preservation of the spin action demonstrates that actually two kinetic resonances are crossed adiabatically. Two remarks are needed here. First, we have seen in earlier sections that inner tori, due to their lower $\Delta_{p_0}^{\rm sym}(\nu)$ are less likely to meet resonances than outer tori. The danger is of course that, even if all kinetic resonances can be crossed adiabatically on all tori, on some tori the number of adiabatically crossed resonances is *odd* whereas on others it might be *even*. Adiabatic crossing of each such resonance implies that the spin moves from one hemisphere defined by the North pole $\hat{u}_{\langle n\rangle}$ into the other. In other words, if we choose the sign of $\hat{n}_{\vec{J}}(p_0)$ such that it fulfils $\lim_{\vec{J}\to\vec{0}}\hat{n}_{\vec{J}}=\hat{n}_0=+\hat{y}$, then the spin action I changes its sign at the crossing of the kinetic resonance. Therefore, when adding up the contributions of all tori to the beam polarisation, those tori on which an *odd* number of resonances was crossed, contribute with a negative sign relative to those tori on which an even number of resonances was crossed. Second, we have seen for example in figure 4.7 and in the `SODOM-2` scans in sections 5.3.3 and 5.4.1 that the amplitude dependent spin tune oscillates as a function of p_0 around some mean value close to ν_0. If the symmetrised spin tune spread $\Delta_{p_0}^{\rm sym}(\nu)$ is small enough to avoid resonance conditions except for certain momenta inside the strong RRSs, then one might expect that resonance crossings occur in *pairs*, i.e. "up" and "down". These pairs are then typically (figure 4.7) separated by less than 1 GeV, whereas the kinetic resonance strengths change on a scale of some tens of GeV as can be seen in figures 5.26 to 5.31. If the two resonances of such a pair are close enough so that their kinetic resonance strengths are approximately the same, and if the ramp speed provides adiabatic passage through the first resonance, it is most likely to provide adiabaticity at the second resonance of the pair also. Moreover the number of spin flips after complete passage through a sequence of RRSs is even. Therefore the hope is that outside the RRSs the spin action has the same sign on all tori. Nevertheless this has to be verified by suitable simulations. They will be presented in figure 5.37. Figure 5.36 (bottom left) shows $u_y^{\langle\xi\rangle}(p_0)$ during acceleration through the RRS around 612 GeV on the (2.5,2.5,2.5)σ torus. Here $u_y^{\langle\xi\rangle}$ changes sign already twice before the centre of the RRS at 612 GeV. Beyond 612 GeV $u_y^{\langle\xi\rangle}$ starts to oscillate violently but the modulations of these oscillations indicate 2 or even 3 more resonance crossings. On exiting the RRS $u_y^{\langle\xi\rangle}$ has become negative, but there is almost no dynamical polarisation left on the torus. Figure 5.36 (top and middle right) show

$P_{\mathrm{rmp}}(p_0)$ and $u_y^{\langle\xi\rangle}(p_0)$ on the tori up to $(2,2,2)\sigma$ during acceleration from 710 to 740 GeV. In this momentum range the lattice interpolation has already been completed except for variations of the cavity voltage. Again we see that the maxima of P_{rmp} before and after passage through the RRS around 721 GeV are approximately of the same height on all tori, indicating adiabatic acceleration in the complete region. Directly below (middle right) $u_y^{\langle\xi\rangle}(p_0)$ is displayed. On all three tori $u_y^{\langle\xi\rangle}$ strongly deviates from $+1$ during acceleration through the RRS around 721 GeV. In other words, the unit vector of the ramped polarisation is strongly tilted from the vertical. On the $(1,1,1)\sigma$ torus $u_y^{\langle\xi\rangle}$ has a narrow isolated minimum of about -0.2 close to 721 GeV. On the (1.5,1.5,1.5) and $(2,2,2)\sigma$ tori $u_y^{\langle\xi\rangle}$ almost approaches -1, but in contrast to the RRS around 612 GeV, $u_y^{\langle\xi\rangle}$ is not constant between the two spin flips. Note that inside the strong RRSs in a ring like HERA–p which is *not* mid–plane symmetric, even the unit vector in the direction of the average $\hat{n}$–axis , $\hat{u}_{\langle n\rangle}$ can have a significant deviation from the vertical. Therefore the signal for double resonance crossing is not so clear as it was in the case of the RRS around 612 GeV. In figure 5.36 (bottom right) $P_{\mathrm{rmp}}(p_0)$ during acceleration through the RRS around 803.5 GeV is displayed. On the (1,1,1) and $(1.5,1.5,1.5)\sigma$ tori P_{dyn} is preserved, but on the $(2,2,2)\sigma$ torus the maxima of P_{rmp} below the RRS are about 10% higher than the maxima beyond 803.5 GeV. This indicates a drop of P_{dyn} by about 10% during passage of the RRS. Comparing the depolarisation with different acceleration rates from figures 5.35 and 5.36 we find that simulations with *lower* acceleration rates provide a slightly *higher* degree of depolarisation. Therefore we can conclude that a kinetic resonance is crossed in the non–adiabatic limit of the generalised Froissart–Stora formula rather than in the adiabatic limit. We do not know the derivative $\mathrm{D}_{p_0}\,\tilde{\nu}$ of the non–resonant contribution $\tilde{\nu}$ to the amplitude dependent spin tune at the position of the resonance. Therefore the actual kinetic resonance strength cannot be estimated from the dependence of P_{dyn} on the acceleration rate. But we assume that the width of the resonant dip of P_{lim} w.r.t. p_0, corresponding to the observed depolarising resonance, is small compared to the momentum range in which the non–resonant approximation $\widetilde{P}_{\mathrm{lim}}$ changes more than the approximate 10 % polarisation loss. As we have seen in figures 4.20 and 4.21, the non–adiabatic limit of the Froissart–Stora formula is valid only if $\widetilde{P}_{\mathrm{lim}}$ is almost constant over the width of the resonance.

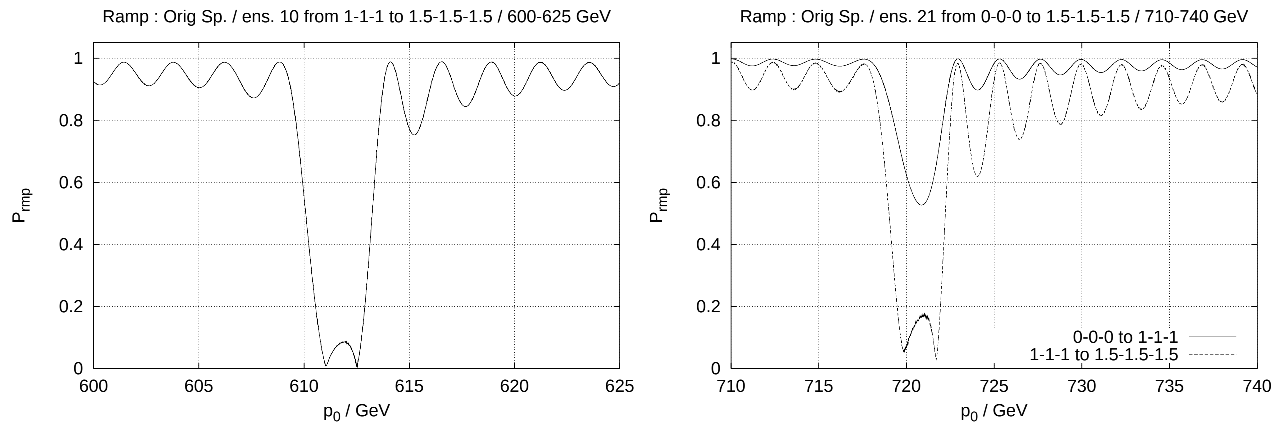

Figure 5.37: Ramp simulations around the residual resonance structures at 612 and 721 GeV. Left: 11 particles with linearly increasing orbital amplitudes from (1,1,1) to $(1.5,1.5,1.5)\sigma$. Right 10 and 11 particles with linearly increasing orbital amplitudes from (0.1,0.1,0.1) to $(1,1,1)\sigma$ and from (1,1,1) to (1.5,1.5,1.5) σ.

We have observed in figure 5.36 that the polarisation on certain tori may change its sign while passing through a strong RRS. Owing to our general experience on the dependence of the amplitude dependent spin tune on the reference momentum we have presumed that whenever kinetic resonances are crossed because of an isolated strong swing of ν away from and back to ν_0, they are crossed in pairs with approximately the same level of adiabaticity. In figure 5.37 this hypothesis is tested in more detail during acceleration through the RRSs around 612 and 721 GeV. Figure 5.37 (left) shows P_{rmp}

of an ensemble of 11 spins on a sequence of 11 invariant tori with orbital amplitudes of $(1.0,1.0,1.0)\sigma$, $(1.05,1.05,1.05)\sigma,\ldots,$ $(1.45,1.45,1.45)\sigma$ and $(1.5,1.5,1.5)\sigma$ during acceleration from 600 to 625 GeV with 16.5 keV per turn.

In figure 5.36 (middle left) we have seen that $u_y^{\langle\xi\rangle} \approx$ const. $= 1$ on the $(1,1,1)\sigma$ torus whereas $u_y^{\langle\xi\rangle}$ changes its sign twice on the $(1.5,1.5,1.5)\sigma$ torus. On both tori the acceleration process was almost adiabatic. We therefore have to test if the acceleration stays adiabatic in the whole range of amplitudes from 1 to 1.5 σ and if the spin is flipped an even number of times in the whole range.

For figure 5.37 (left), all 11 spins were located on a straight line in the amplitude domain defined by $(1,1,1)\sigma + x\ (0.5,0.5,0.5)\sigma$, $0 \le x \le 1$. If an isolated range in x of width larger than $^1/_{10}$ exists such that the spin action of a particle inside this range is changed from initially $+1$ to I_f and if all other spin actions remain unchanged ($I_f = 1$) during the ramp, then the final P_{rmp} from the ensemble of 11 particles is equal to $\langle P_{\mathrm{lim}}(p_{0,f})\rangle_x\,(10 + I_f)/11$. Thus a range of x of width $^1/_{10}$ in which the particle is partially (e.g. $I_f \approx 0.8$) or completely ($I_f \approx 0$) depolarised or flipped an odd number of times ($I_f \approx -1$) gives $P_{\mathrm{rmp}}/\langle P_{\mathrm{lim}}\rangle_x \approx 0.98$, 0.9 or 0.8 respectively. Thus any effect leading to a change of I by more than 20% for at least one particle should be clearly observable from the data. There is no drop of P_{rmp}, i.e. the maxima of P_{rmp} are close to 99% before as well as after the RRS has been passed. Therefore we conclude that none of the 11 spins flipped an odd number of times and none of them suffered any decrease of I by more than 20%. In figure 5.37 (right) the same type of simulation has been performed for the RRS around 721 GeV. Here two ensembles of 10 and 11 particles with linearly increasing amplitudes from (0.1,0.1,0.1) to $(1,1,1)\sigma$ and from (1,1,1) to $(1.5,1.5,1.5)\sigma$ respectively have been used in order not to bury the effect of each single particle in a too large ensemble. With both ensembles the maxima of P_{rmp} before and after acceleration through the RRS are about the same, namely 99% and 97%, showing that none of the particles suffered from a change of I by more 10%

This simulation, like all the others in this thesis, does *not* provide any kind of strict proof for the absence of depolarising effects during the complete ramp procedure or in the whole phase space *included* in the chosen tori. It is still possible that at each of some singular energies some rather small, possibly disjunct, subsets of tori get noticeably depolarised one after the other, or that the polarisation direction in these regions is reversed w.r.t. the other tori. The parameter space defined by the direct product of the momentum and the amplitude domain is 4–dimensional and the dependence of the invariant spin field and the amplitude dependent spin tune on these parameters, even with fixed orbital tunes, is in general too complicated for one to even try to sample it sufficiently densely with static and ramp simulations. Nevertheless it seems unlikely that kinetic resonances that contribute to depolarisation at *one* energy in *one* region of phase space stay confined to that region for all *other* energies. Therefore *long range* scans of the reference momentum and *long range* ramp simulations using a limited set of tori should provide a reasonably secure answer to the question of whether or not depolarisation occurs *inside* the torus with the maximal amplitudes.

Figure 5.38 shows the results of ramp simulations with the modified ramp table on the $(2.5,2.5,2.5)\sigma$ torus for various ramp speeds and ensembles. The top row of plots was obtained by ramping the ensembles with $(1 \times 3 \times 3)$ (left) and $(2 \times 2 \times 2)$ particles (right) and for a constant energy gain of 200 keV per turn. The middle row displays P_{rmp} for the same ensembles but with 10 times the original ramp speed from table 5.3. The bottom picture shows P_{rmp} for the $(1 \times 2 \times 2)$ ensemble and 5 times the original ramp speed. Obviously the spin motion can only be stabilised by means of the chosen snake scheme and orbital tunes below the RRS around 390 GeV. Comparison with P_{lim} in figure 5.34, which is of course over optimistic since it does not contain the effect of the horizontal and longitudinal amplitudes, and the sudden drops of P_{rmp} itself suggest that on passage through this RRS P_{rmp} makes in all but one simulation a sudden drop by 5 to 15%. For the ensemble with $(1\times3\times3)$ particles ramped with 10 times the real acceleration rate no visible drop of P_{rmp} occurs. The next drop occurs at the RRS around 580 GeV. Here almost all polarisation is lost with the $(1 \times 2 \times 2)$ ensemble which is closest to the original ramp speed. We note that the positions of obvious changes of $|P_{\mathrm{dyn}}|$ are the same for *all* 5 simulation runs. With increasing momentum further non–adiabatic changes of $|P_{\mathrm{dyn}}|$

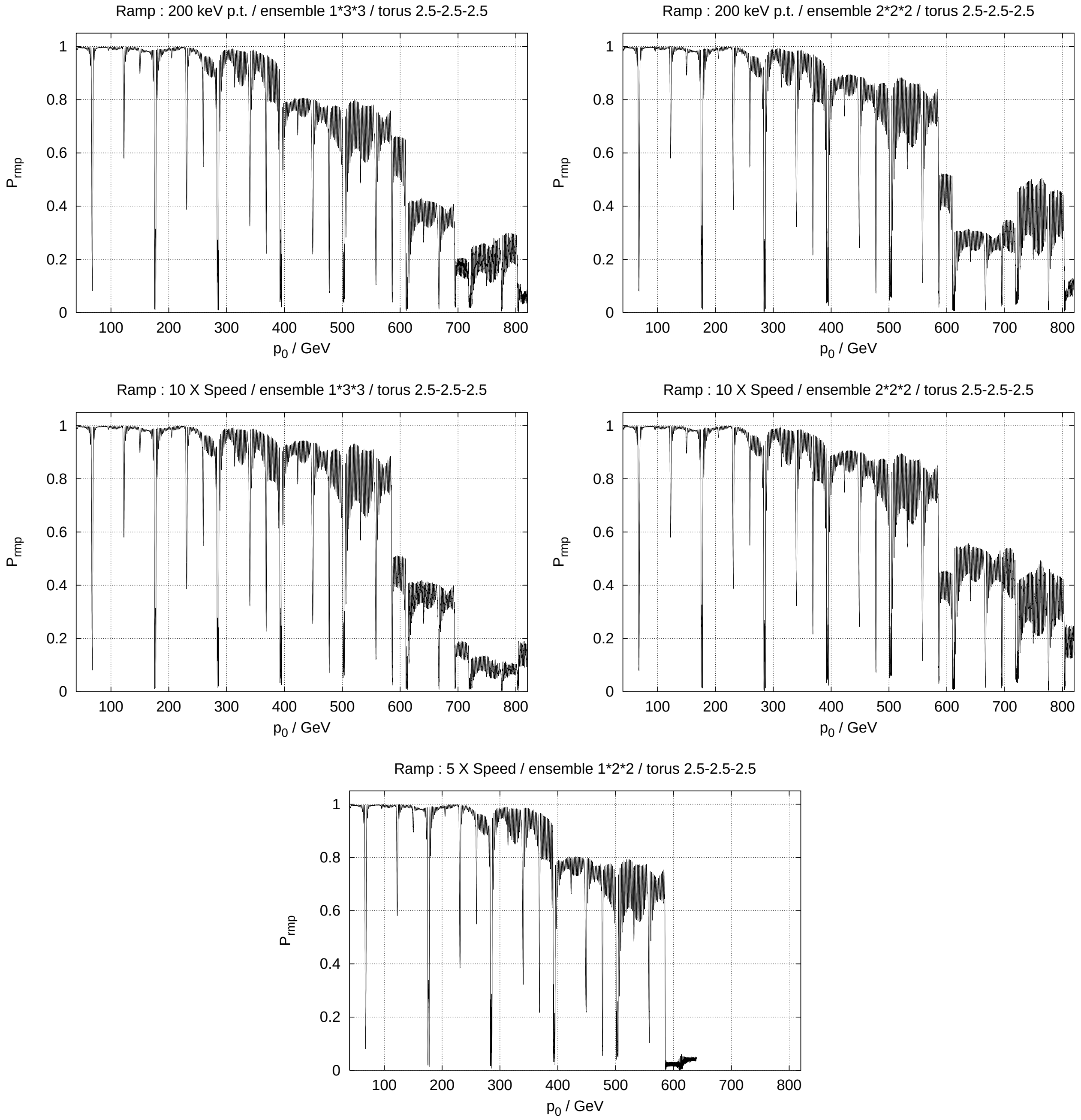

Figure 5.38: Ramp simulations with the modified ramp table on the $(2.5,2.5,2.5)\sigma$ invariant torus.

occur only at the RRSs around 612, 690, 720 and 803.5 GeV. The more the ensemble is depolarised, i.e. $|P_{\rm dyn}|$ is reduced, the more likely it is that artifacts of "few particle tracking" show up. This means that the apparent increases of $P_{\rm rmp}$ must be corrected in the sense that for each sudden change $\Delta P \equiv |P^f_{\rm rmp} - P^i_{\rm rmp}|$,

$$P^{f,{\rm corr}}_{\rm rmp} = \max\{0, P^{i,{\rm corr}}_{\rm rmp} - \Delta P\} \tag{5.22}$$

rather than $P^f_{\rm rmp}$ should be used as a conservative estimate of the beam polarisation after passage through the RRS. Here $P^i_{\rm rmp}$ and $P^f_{\rm rmp}$ are the uncorrected few particle multi–turn polarisations directly before and after the RRS. We find that $P^{\rm corr}_{\rm rmp} \approx 0$ and hence $|P_{\rm dyn}| \approx 0$ after the RRS at 721 GeV in all 5 cases! We therefore conclude that on the (2.5,2.5,2.5)σ torus the spin action $I = \widehat{S} \cdot \hat{n}$ is *not* preserved up to high energy. The actual level of depolarisation cannot be computed to a high accuracy with this method, but nevertheless the above results imply a strong restriction on the possible beam average of the polarisation. Imagine that $P_{\rm lim} = 1$ at some high energy working point for polarised $e^{\pm}$–p collisions at HERA–p. If $P_{\rm dyn} = 1$ at this working point for all tori with *all* amplitudes less than 2.0 σ, and $P_{\rm dyn} = 0$ for all tori with *one* amplitude greater than 2.0 σ, then the fraction of the beam which remains polarised is $F_3(2,2,2) \approx 65\%$. Thus with an initial polarisation of about 80% from the source and no losses in the pre–accelerator chain we find $P \approx 0.8\,F_3(2,2,2) \approx 50\%$. If we assume $P_{\rm dyn} = 1$ on all tori with *all* amplitudes less than 2.5 σ, and $P_{\rm dyn} = 0$ for all tori with *one* amplitude greater than 2.5 σ we obtain a beam average of $P \approx 0.8\,F_3(2.5, 2.5, 2.5) \approx 70\%$. Both estimates are valid only within the simplification of linearised orbital motion and without inclusion of depolarising effects driven by the closed orbit perturbations. In HERA–p rms horizontal and vertical orbit distortions are typically 2 mm. In a flat model of HERA for this rms closed orbit the imperfection resonance strengths at the positions $\kappa_0 \in \mathbb{N}$ have been estimated to reach up to about 3 in [AC96]. Ramp simulations [BG98b, NG99] assuming a horizontal and vertical rms closed orbit deviation of 0.5 mm after applying the MICADO correction method, show noticeable loss of polarisation around 400 GeV already on the (1,1,0)σ torus.

In fact the assumption that polarisation is lost whenever *any* of the orbital amplitudes exceeds 2 or 2.5 σ is surely too pessimistic. Already in section 5.3.2 we have seen that the vertical amplitudes up to which no polarisation is lost can be increased if the longitudinal and horizontal amplitudes are decreased and furthermore that rather large horizontal and longitudinal amplitudes do not imply depolarisation, provided that the vertical amplitude is sufficiently small. Recall that the `SODOM-2` scans in figure 5.34 did *not* show any visible kinetic resonances or regions of non–integrability below 803.5 GeV. Figure 5.39 shows the results of ramp simulations with particles distributed on tori with either purely vertical amplitudes, namely 2.5 and 3σ or just a small vertical amplitude (1σ) and large horizontal and longitudinal amplitudes, namely 2.5σ. The ramp speed was 200 keV/turn until a reference momentum of 300 GeV was reached. Then the ramp speed was reduced to 5 times the original value given in table 5.3. For figure 5.39 (top left) an ensemble of 9 particles uniformly distributed on the 2.5 σ ellipse in the vertical eigenplane was ramped from 40 to 820 GeV according to the modified ramp table. Here a comparison with the corresponding static scan of $P_{\rm lim}(p_0)$ in figure 5.34 shows that for $p_0 < 803$ GeV, $P_{\rm rmp} = P_{\rm lim}$ up to the graphical resolution. This tracking result verifies the assumption that whenever the spin–orbit system is integrable ($\hat{u}_1$, $\hat{n}$ and $\hat{u}_2$ exist), or almost integrable (the spin motion is well approximated by (4.25)), *and* no spin–orbit resonances are crossed, the ramp procedure is adiabatic in the sense of theorem 4.8. In particular *static* scans of $P_{\rm lim}$ and ν w.r.t. p_0 suffice to decide if integrability and absence of resonances can be guaranteed!

At the RRS around 803.5 GeV the polarisation on the (0,2.5,0)σ torus is almost completely lost. Recall that with 2.5 σ vertical motion (figure 5.34 lower two right) there was a region inside this RRS in which neither the `SODOM-2` method even with 128 Fourier harmonics included nor the `SPRINT` method with more than 10^5 averaging turns seemed to converge, although there was no kinetic resonance of moderate order within the symmetrised spin tune spread in that momentum range. The sudden death of polarisation exactly during passage through this region indicates that the non–convergence of the

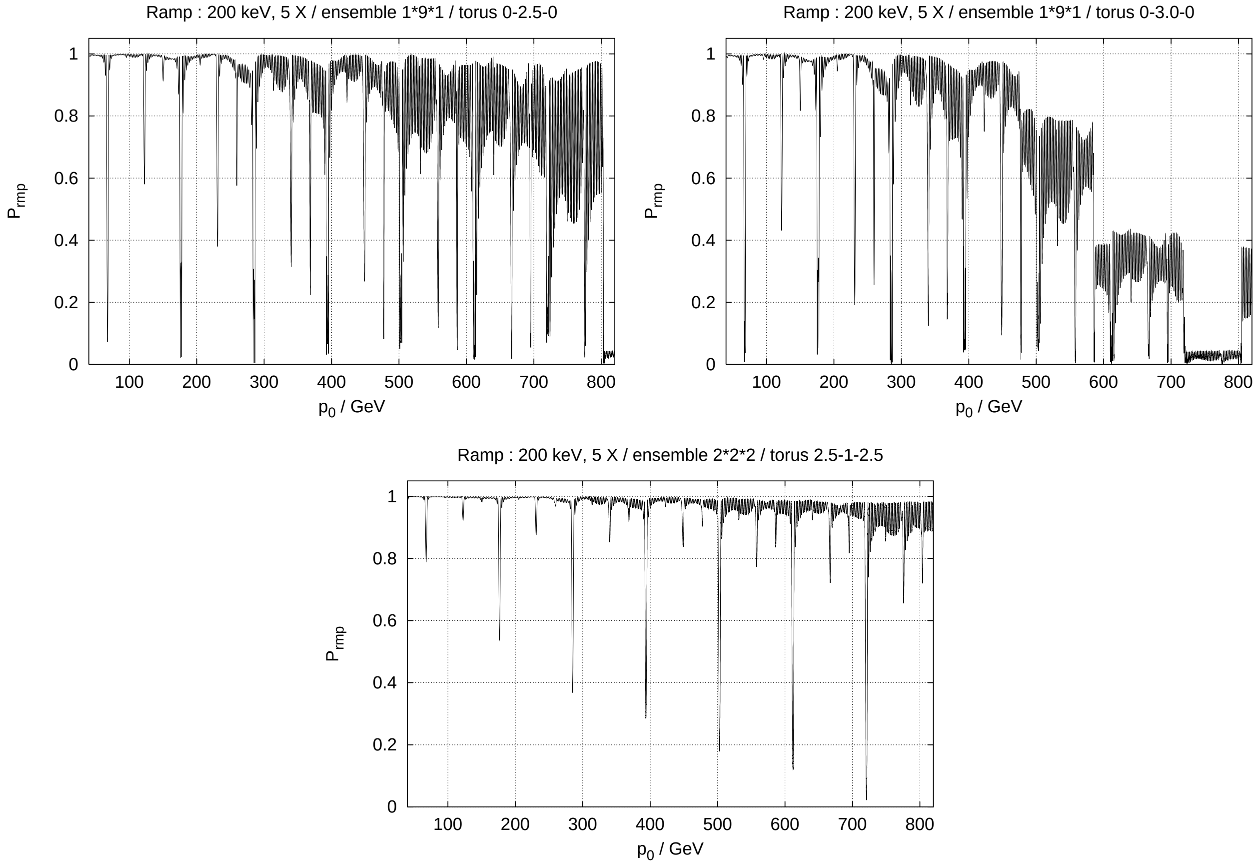

Figure 5.39: Ramp simulations with the modified ramp table on the invariant tori with $(0,2.5,0)\sigma$, $(0,3,0)\sigma$ and $(2.5,1,2.5)\sigma$

`SPRINT` and the `SODOM-2` methods is *not* caused by any inadequacy of the algorithms used but either by a pathological invariant spin field or even the non–integrability of spin motion in this parameter range. Figure 5.39 (top right) shows $P_{\mathrm{rmp}}(p_0)$ for an ensemble of 9 particles distributed uniformly on the 3 σ vertical ellipse. Here polarisation is lost successively during acceleration through the RRSs around 470, 580, 610, 720 and 803.5 GeV. In fact we find $P_{\mathrm{rmp}} \approx 0$ already beyond 720 GeV. In figure 5.39 (bottom) the ramped polarisation $P_{\mathrm{rmp}}(p_0)$ is displayed for an ensemble of $(2 \times 2 \times 2)$ particles on the torus with $(2.5,1,2.5)\sigma$ orbital amplitudes. The polarisation is preserved even up to 820 GeV, but note that only approximately 6% of the particles of the beam that are included in the $(2.5,1,2.5)\sigma$ torus are *not* already in the $(2,2,2)\sigma$ torus which we already know provides high polarisation around 800 GeV.

In principle all tori with horizontal, vertical and longitudinal amplitudes between 2 and at least 3 σ have to be sampled by similar ramp simulations. Even if the discretisation of the amplitudes is held to steps of 0.5 σ, which might still be too crude, there are $2^3 = 8$ such tori to simulate. Due to lack of time these simulations could not be done during the preparation of this thesis. Finally, after the stability of polarisation on various tori is analysed, ramp simulations of large ensembles of spins with a Gaussian distribution in all orbital amplitudes and with approximately the original ramp speed should be done to produce realistic estimates for the polarisation at the chosen working energy. Yet these conditions for simulations seem to be impossible to fulfil with existing computer hardware. Nevertheless figure 5.39 shows that $P \leq 70\%$ might be somewhat pessimistic.The fact that particles on tori with amplitudes up to 2 σ in all three planes can be accelerated to about 800 GeV with 4 main Siberian Snakes is an improvement in comparison with the results from section

5.3.2 where depolarisation already occurred on the (1.5,1.5,1.5)σ torus. The obvious problems during acceleration through the RRS around 803.5 GeV suggest a target momentum of close to 800 GeV but below 803 GeV. At this momentum we find $P_{\rm rmp} \approx P_{\rm lim}$ up to 2 σ in all planes. Let $P_{\rm lim}(a)$ with $P_{\rm lim}(0) = 1$ be the static polarisation limit at some optimal energy on the torus with $(a, a, a)\sigma$ orbital amplitudes. We now assume $P_{\rm lim} \geq P_{\rm lim}(a)$ for all tori (a_x,a_y,a_z) with $a_i \leq a$, $i = x, y, z$. Moreover we assume that $P_{\rm dyn}(a)$ is $P_{\rm initial}$ for all tori with $a_i < a_{\rm max}$ and that $P_{\rm dyn}(a) = 0$ for all tori for which at least one of the $a_i \geq a_{\rm max}$. We know that this is already a pessimistic approximation because it neglects the contribution of tori with, for example, $a_y \approx 0$ and $a_x > a_{\rm max}$. Given a discrete sample $\mathcal{A} = \{a_k | k = 0, \ldots, m; a_0 = 0, a_{m-1} < a_{\rm max} < a_m\}$, of tori with $a_k\sigma$ in all three planes, we can put approximate bounds on the polarisation with the estimate

$$\begin{aligned}\sum_{k=1}^{m-1} P_{\rm lim}(a_k)\Big(F_3(a_k, a_k, a_k) - F_3(a_{k-1}, a_{k-1}, a_{k-1})\Big) \quad &\leq \quad \frac{P}{P_{\rm initial}} \leq \\ \sum_{k=1}^{m} P_{\rm lim}(a_{k-1})\Big(F_3(a_k, a_k, a_k) - F_3(a_{k-1}, a_{k-1}, a_{k-1})\Big) & \end{aligned} \tag{5.23}$$

where F_3 is defined in equation (5.8). The lower bound is given by the approximations $a_{m-1} = a_{\rm max}$ and $P_{\rm lim}(x) = P_{\rm lim}(a_k)$ for $x \in [a_{k-1}, a_k]$ whereas the upper bound is given by the approximations $a_m = a_{\rm max}$ and $P_{\rm lim}(x) = P_{\rm lim}(a_k)$ for $x \in [a_k, a_{k+1}]$. Inserting the maximal values of $P_{\rm rmp}$ shown in figure 5.36 (bottom right) close to 800 GeV as $P_{\rm lim}(1) = 0.99$, $P_{\rm lim}(1.5) = 0.97$, $P_{\rm lim}(2.0) = 0.95$ and extrapolating to $P_{\rm lim}(2.5) = 0.90$, we obtain as a crude approximation for the equilibrium beam polarisation

$$62\% \leq \frac{P}{P_{\rm initial}} \leq 85\% \quad , \tag{5.24}$$

In order to increase the luminosity in HERA electron cooling of the proton beam in PETRA has been proposed [BB99, WB99, GHS99]. In these proposals it is assumed that the counteracting effect of intra–beam scattering prevents the horizontal emittance from being significantly reduced, but it is expected that a reduction of the vertical emittance by a factor of 2 to 5 would be possible. Apart from increasing the maximum luminosity, another effect of the reduced vertical emittance would, of course, be that larger fractions of the beam are contained inside of tori with given amplitudes. If the normalised emittance is reduced from ε^N to ε^N/κ, then the beam size is reduced from σ to $\sigma/\sqrt{\kappa}$. Rescaling our results but keeping the horizontal and longitudinal emittances unchanged we have

$$\begin{aligned}\sum_{k=1}^{m-1} P_{\rm lim}(a_k)\Big(F_3(a_k, a_k\sqrt{\kappa}, a_k) - F_3(a_{k-1}, a_{k-1}\sqrt{\kappa}, a_{k-1})\Big) \quad &\leq \quad \frac{P}{P_{\rm initial}} \leq \\ \sum_{k=1}^{m} P_{\rm lim}(a_k)\Big(F_3(a_k, a_k\sqrt{\kappa}, a_k) - F_3(a_{k-1}, a_{k-1}\sqrt{\kappa}, a_{k-1})\Big) & \end{aligned} \tag{5.25}$$

and

$$71\% \leq \frac{P}{P_{\rm initial}} \leq 89.1\% \ \text{ for } \ \kappa = 2 \quad \text{and} \quad 72\% \leq \frac{P}{P_{\rm initial}} \leq 89.4\% \ \text{ for } \ \kappa = 5 \quad , \tag{5.26}$$

showing that decreasing the vertical emittance by more than a factor of 2 does not have any significant effect on this crude estimate. If in addition the horizontal and the longitudinal emittances could be reduced by a factor of approximately 1.5 in PETRA and the intra–beam scattering would not blow–up the emittances before the ramp had completed in HERA, then polarisations of 86 to 96% of $P_{\rm initial}$ could be achieved. In any case electron cooling in PETRA seems to be helpful for providing the highest polarisation at high energy.

Chapter 6

Summary and conclusion

The keys to the analysis of proton spin dynamics in high energy accelerators are the invariant spin field $\hat{n}$, the amplitude dependent spin tune ν and the adiabatic invariance of the spin action $I \equiv \widehat{S} \cdot \hat{n}$. With these concepts the polarisation state of a stored beam can be decomposed into a static property of the lattice and the energy, called the static polarisation limit $P_{\rm lim}$ and a history dependent dynamic property of the beam, namely $P_{\rm dyn}$. In particular for an asymmetric lattice like HERA–P at high energy where all first order intrinsic spin–orbit resonances are excited and many of them have a large strength, simple models and their predictions based either on perturbation theory or on the assumption of *isolated* resonances must fail.

In collaboration with Dr. G. H. Hoffstaetter and Prof. Dr. K. Yokoya, who supplied the core routines for the revised `SODOM-2` algorithm, a computer code for simulating spin dynamics, `SPRINT` , was developed. Besides linear modules for the computation of intrinsic resonance strengths, the linear $P^{(1)}_{\rm lim}$ and linear filtering of snake schemes, and modules for straightforward tracking and acceleration, `SPRINT` offers the non–perturbative tools for computation of the $\hat{n}$–axis and the amplitude dependent spin tune, explained in sections 4.3, 4.5, 4.6 and 4.10.3. These tools, Fourier analysis, stroboscopic averaging, averaging of the pseudo spin tune, and anti–damping allow numerical approximations of $\hat{n}$ and ν to be computed in the domains in which spin–orbit motion is integrable. In their domains of applicability all methods agree to a high level of accuracy. For the first time ever the complicated structure of the invariant spin field in a ring like HERA–p at high energy could be simulated and demonstrated.

In section 2.2.2 we have seen that at high energy when the spin enhancement factor $G\gamma$ is sufficiently large, the major non–linear contributions to the flow of the spin precession equation are caused by multiple iteration of the *linear* part of the source term in the precession equation and *not* by the non–linear part of the source term. The non–linearities caused by the iteration of the linear part of the source term, which are induced by the structure of the precession equation and not by the explicit form of the source term were named *kinetic* non–linearities. In contrast to this the much weaker non–linearities due to higher order contributions to the source term were named *dynamical* non–linearities. It was shown that in a *mid–plane symmetric* ring, the horizontal component of the source term can only have odd harmonics in the vertical orbital phase. Therefore in such a ring all dynamical spin–orbit resonant spin tunes must contain an odd multiple of the vertical tune.

With the help of the formalism of unit–quaternions described in section 2.2.1 terse and intuitive expressions for one–turn spin maps of simple models of rings were derived. Moreover it could be shown that in a mid–plane symmetric ring without any (in chapter 2), or with an even number of horizontal Siberian Snakes (in chapter 3), the components of the one–turn map have a definite mirror symmetry w.r.t. the mid–plane. Then in chapter 4 the perturbative spin normal form method was employed to show that "resonances" with the on–orbit spin tune, at which the algorithm fails due to the large denominator problem, arise in mid–plane symmetric rings with or without an even number of horizontal snakes only when the closed orbit spin tune ν_0 is an integer combination of the radial and longitudinal orbital tunes plus an *odd* integer multiple of the vertical orbital tune. By this means the so–called "snake resonances" that appear in the traditional literature were demystified and the question of how, and in which order, they contribute to spin dynamics was clarified. In particular the apparent contradiction between the fact that resonances of even order in Q_y appear in simulations of spin motion in HERA–p, which is *not* mid–plane symmetric, and the popular opinion that resonances of even order in Q_y should not occur, which is motivated by simulation of mid–plane symmetric models, could be resolved.

The implications of the these results for the HERA–p accelerator are obvious. HERA–p contains sections of interleaved vertical and horizontal bends around three of the four straight sections. The effect of these vertical bend sections can be compensated completely by means of flattening snakes *only* for spin motion on the design orbit. With finite orbital amplitudes the absence of the mid–plane symmetry induces a variety of *even* order spin–orbit resonances.

In addition, a heuristic model was invented to motivate the observation that, whenever the amplitude dependent spin tune has a symmetric discontinuity of height $2\epsilon_\kappa$ around an integer combination κ of the orbital tunes, $P_{\lim}$ has a pronounced local minimum of characteristic width ϵ_κ. In particular κ has to contain an *odd* integer times the vertical tune if the ring is mid–plane symmetric. This heuristic model was verified with various numerical simulations using the single resonance model with snakes as well as with various models of the HERA–p lattice. Moreover the evolution of the spin action during continuous variation of the system parameters, so that ν crosses a resonance position κ, was simulated for various types of parameters. It turned out that the degree of adiabaticity of such a process is described well by the Froissart–Stora formula (4.104) with the definition of the resonance strength generalised to kinetic resonances and with a rate parameter that reflects the actual slope of ν in the vicinity of κ. The concepts of the invariant spin field and the amplitude dependent spin tune allow higher order spin–orbit resonances to be identified and classified in a rather rigorous way.

The simple existence of flattened or non–flattened vertical bend sections around *three out of four* straight sections implies that HERA–p has only the minimal superperiodicity $P = 1$. The distribution of arcs and straight sections requires the number of main Siberian Snakes to be N_s =2, 4 or 8. If results from the single resonance model can with any safety be generalised to an asymmetric ring with strongly overlapping resonances like HERA–p, then they suggest N_s =2, 6 or 10. However, even if HERA–p had the superperiodicity $P = 4$ with either *all* or *none* of the straight sections being surrounded by vertical bend sections and all of the straight sections being identical, it would still not be amenable to 6 or 10 main snakes.

Simulations show that, in general, schemes with 4 and 8 main snakes can provide a tightly bundled $\hat{n}$–axis only at certain energies and inside some finite region of phase space. In particular at energies around those where the strongest linear intrinsic resonances of the HERA–p lattice *without snakes* are located, $P_{\lim}$ oscillates violently and has an explicitly low average value. Moreover around these *residual resonance structures* the oscillations of the amplitude dependent spin tune produce the largest deviation from its nominal value of $\nu_0 = {}^1\!/_2$.

With the help of the linear filtering algorithm performed over large energy ranges, 4- and 8–snake schemes were found that improve the average $P_{\lim}$ outside as well inside the residual resonance structures to some extent. In non–perturbative scans of $P_{\lim}$ and ν w.r.t. the beam reference momentum p_0 and during ramp simulations, it turned out that the schemes obtained by linear filtering are, by far, more efficient than schemes based on naive rules of thumb. In particular all schemes tested with maximum possible snake periodicity $P_s = {}^{N_s}\!/_2$ could not provide sufficient stability of the polarisation even with small and purely vertical orbital excitation. On the contrary the schemes obtained by long range filtering *all* have a $P_s = 1$ but an odd mirror symmetry w.r.t. the East–West axis.

Nevertheless even with the optimised snake schemes the fraction of beam in which polarisation survived the ramp procedure in the standard setup of HERA–p from 1996 and with normalised 1σ

emittances of $4\,\pi$ mm mrad in both transverse planes and $1.8\cdot10^{-2}$ m rad in the longitudinal plane was about 6 to 30% with 4, and 30 to 65%, with 8 snakes. Therefore the orbital tunes were moved closer to the 7–th order orbital resonance $7[Q_y]=2$ at which the maximum allowed spin tune spread has a local maximum. Simulations, employing the capability of `SPRINT` to interpolate between two different beam optics during the acceleration, have shown that with these modified tunes the fraction of the beam in which the polarisation is conserved during the whole modified HERA–p ramp procedure is increased to about 62 to 85% with 4 snakes. Under the restrictions of the chosen model, i.e. linear unperturbed orbital motion, a linear source term in the spin precession equation and the absence of beam–beam interaction and any sources of noise, this result means that between 62 and 85% of the *initial* beam average of the polarisation, i.e. of the polarisation of the beam injected into HERA–p at 40 GeV, will be available at high energy close to 800 GeV. The working energy of 1996, namely 820 GeV and the current working energy of 920 GeV do not seem realistic without further improvement. One source of improvement may be the proposed [BB99, WB99, GHS99] electron cooling in PETRA.

Ramp simulations which included the effects of a perturbed closed orbit [BG98b, NG99] seem to indicate that misalignment is a serious source of depolarisation even with moderate orbital amplitudes. In the future the studies must be extended to include closed orbit perturbations and non–linear orbital motion, at least in so far as the effect of orbital chromatic tune spread and the beam–beam effect has to be included. Moreover the effects of the major sources of noise, i.e. intra–beam scattering and power supply noise have to be studied in order to estimate the polarisation lifetime at the top energy. However all of these additional complications can only be analysed seriously if the theoretical concepts underlying spin dynamics are unambiguously defined and the stationary polarisation on the level described in this thesis can be controlled.

In the near future, first experimental results on acceleration and storage of polarized protons in RHIC will be available. RHIC will be operated at less than a third of the top energy of HERA–p, is flat and has a higher superperiodicity (P=6). It will be interesting to see in how far the effects on polarisation, e.g. partial depolarisation due to crossing of higher order kinetic resonances, as predicted by the theory of chapter 4 and found numerically for the HERA–p ring in chapters 4 and 5, can already be clearly resolved experimentally in RHIC.

Appendix A

Introduction to the orbital motion in circular accelerators

Classical spin motion in accelerators is driven by the electromagnetic fields observed by the particles on their trajectories. The Stern–Gerlach forces that deflect the orbit, on the other hand, can normally be neglected at high energy. So to sufficient accuracy the spin can be seen as a kind of "spectator" travelling with the particle but *not* affecting the trajectory. Therefore spin motion in the electromagnetic fields of accelerators can only be understood starting from the orbital dynamics.

In this appendix we will briefly summarize the principles of Hamiltonian motion in circular accelerators. The first section is a review on some definitions and basic rules of classical Hamiltonian dynamics [VA88, ems3, LM88, GH94, MH92]. It is meant to be fairly general and in particular does *not* implicitly assume that the Hamiltonian system describes a particle in an accelerator. Many of the concepts and results of the first section can be extended to systems without an explicit or implicit Hamiltonian structure. The second section reviews the basic concepts of Hamiltonian orbital dynamics in circular accelerators. It is meant to give the reader from outside the accelerator physics community a notion of the standard concepts.

We will work in the approximation that there are no mutual interactions between particles.

A.1 Hamiltonian dynamics

Hamiltonian dynamics is usually defined via the concept of exterior forms on even dimensional symplectic manifolds. This concept is mathematically rigorous and ensures a wide applicability of Hamiltonian theory. In this appendix the concept of symplectic maps is emphasised which allows to derive formulae which can be easily embedded in numerical codes [MB90, GH94, MB92, MH92]. The subset of Hamiltonian theory which is presented here is essential for orbital tracking, for the concept of the invariant spin field and for the amplitude dependent spin tune.

A.1.1 Hamiltonian equations of motion and symplectic maps

The basic equations of motion (EOM) in a Hamiltonian system for the generalised coordinates q and the corresponding canonical momenta p take the form $\mathrm{D}_t\, q' = \partial_p\, H$, $\mathrm{D}_t\, p = -\partial_q\, H$ with the Hamiltonian $H(q,p,t)$. Here and in the following t is the free "time–like" parameter but *not* necessarily a "physical" time. It will be more convenient to rewrite these EOM more compactly using the "symplectic unit matrix" $\underline{J}$. We will assume that all functions have the required smoothness. The coordinates q of a solution will be assumed to be generally continuous and piecewise differentiable w.r.t. t. The canonical momenta p will only be assumed to be piecewise continuous and piecewise differentiable w.r.t. t. A Hamiltonian function H is supposed to be continuously differentiable w.r.t the canonical coordinates and momenta, and piecewise differentiable w.r.t. t. The symbol $\mathbb{K}$ refers either to the field of real numbers, $\mathbb{R}$ or the field of complex numbers, $\mathbb{C}$. For a system with 1 degree of freedom, i.e. with a 2–dimensional phase space, we define $\underline{J}_2$

$$\underline{J}_2 \equiv \begin{pmatrix} 0 & 1 \\ -1 & 0 \end{pmatrix} \ . \tag{A.1}$$

For n degrees of freedom we define $\underline{J}_{2n} \in \mathbf{SL}(2n, \mathbb{K})$ as the $2n$–dimensional block diagonal matrix

$$\underline{J}_{2n} \equiv \underline{\operatorname{diag}}(\underline{J}_2, \ldots, \underline{J}_2) \ . \tag{A.2}$$

For this definition, pairs of conjugate variables have adjacent indices in the orbit vectors $\vec{z}$, i.e. $z_{2i-1} \equiv q_i$ and $z_{2i} \equiv p_i$. Later, when dealing with canonical transformations we will occasionally reorder the components of $\vec{z}$ such that all configuration coordinates have indices $1 \leq i \leq n$ and all momenta have indices $n+1 \leq i \leq 2n$ to obtain

$$\tilde{\underline{J}}_{2n} \equiv \begin{pmatrix} \underline{0}_n & \underline{1}_n \\ -\underline{1}_n & \underline{0}_n \end{pmatrix} \ . \tag{A.3}$$

From now on we will suppress the subscript $2n$ for $\underline{J}$ and assume that the correct dimensional $\underline{J}$ is used.

Definition A.1 (Hamiltonian system) *A continuous dynamical system is called a Hamiltonian system if it consists of a singly connected phase space $\mathcal{P} \subseteq \mathbb{K}^{2n}, n \in \mathbb{N}$, a "time"– domain $\mathbb{R}$, a vector field $\vec{F} : \mathcal{P} \times \mathbb{R} \to \mathcal{P}$, $(\vec{z}, t) \mapsto \vec{F}(\vec{z}, t)$ with the EOM*

$$\mathrm{D}_t \vec{\xi}(t) = \vec{F}(\vec{\xi}(t), t) \tag{A.4}$$

and if the Jacobian of $\underline{J}\vec{F}$ is symmetric

$$\left(\partial_{\vec{z}} \, (\underline{J}\vec{F})^{\mathrm{T}}\right)^{\mathrm{T}} = \partial_{\vec{z}} \, (\underline{J}\vec{F})^{\mathrm{T}} \tag{A.5}$$

We will call a function $\vec{\xi} : \mathbb{R} \to \mathcal{P}$, $t \mapsto \vec{\xi}(t)$ a trajectory of that system if it is a solution of equation (A.4). We will call $\mathcal{P}^\star = \mathcal{P} \times \mathbb{R}$ the "extended" phase space.

Theorem A.1 *For all functions $H : \mathcal{P}^\star \to \mathbb{R}$, $(\vec{z}, t) \mapsto H(\vec{z}, t)$ the vector field $\vec{F}_H \equiv \underline{J}\,\partial_{\vec{z}}\, H$ satisfies equation (A.5).*

The proof is simple : $\partial_{\vec{z}}\, \underline{J}\,\underline{J}\,\partial_{\vec{z}}^{\mathrm{T}}\ H = -\partial_{\vec{z}}\,\partial_{\vec{z}}^{\mathrm{T}}\ H = (-\partial_{\vec{z}}\,\partial_{\vec{z}}^{\mathrm{T}}\ H)^{\mathrm{T}}$. □

With the help of the theory of potentials it can be shown that for each $\vec{F}$ which satisfies equation (A.5) one can find a Hamiltonian H such that $\vec{F} \equiv \underline{J}\,\partial_{\vec{z}}\ H$. From now on we will always assume that this H is known and use the symbol $(\mathcal{P}^\star, H)$ to specify a Hamiltonian system.

Note that generally there is an infinite number of trajectories $\vec{\xi}(t)$ that correspond to different initial value problems defined by equation (A.4) and by different initial conditions $\vec{\xi}(t_0) = \vec{z}_0$.

Definition A.2 (Flow of a Hamiltonian system) *A map $\vec{T} : \mathcal{P} \times \mathbb{R}^2 \to \mathcal{P}$, $(\vec{z}; t, t_0) \mapsto \vec{T}(\vec{z}; t, t_0)$ such that*

$$\partial_t \vec{T}(\vec{z}_0; t, t_0) \;=\; \underline{J}\,\partial_{\vec{z}}\ H(\vec{T}(\vec{z}_0; t, t_0), t) \tag{A.6a}$$

$$\vec{T}(\vec{z}_0, t_0, t_0) \;=\; \vec{z}_0 \tag{A.6b}$$

for all $(\vec{z}_0, t_0) \in \mathcal{P}^\star$ and $t \in \mathbb{R}$ is called the flow of the Hamiltonian system $(\mathcal{P}^\star, H)$.

It can be shown [VA88, ems3, LM88, MH92] that the following two identities hold:

$$\vec{T}\Big|_{t_2,t_1} \circ \vec{T}\Big|_{t_1,t_0} = \vec{T}\Big|_{t_2,t_0} \quad , \quad \vec{T}\Big|_{t_0,t_1} \circ \vec{T}\Big|_{t_1,t_0} = \vec{Id} \quad . \tag{A.7}$$

Definition A.3 (Symplecticity) *A matrix $\underline{M} \in \mathbb{K}^{2n\times 2n}$ is called symplectic with multiplier $\kappa \in \mathbb{R}\backslash\{0\}$ if*

$$\underline{M}\,\underline{J}\,\underline{M}^{\mathrm{T}} = \kappa\,\underline{J} \quad . \tag{A.8}$$

A matrix $\underline{M} \in \mathbb{K}^{2n\times 2n}$ is called symplectic if $\kappa = +1$. A map $\vec{M} : \mathcal{P} \subseteq \mathbb{K}^{2n} \to \mathbb{K}^{2n}$, $\vec{z} \mapsto \vec{M}(\vec{z})$ is called symplectic (with multiplier κ) if its Jacobian $\underline{M}(\vec{z})$ with $\underline{M}_{ij}(\vec{z}) \equiv \partial_j \vec{M}_i\Big|_{\vec{z}}$ is symplectic (with multiplier κ) for all $\vec{z} \in \mathcal{P}$.

Lemma A.1 *Let $\underline{M}$, $\underline{N} \in \mathbb{K}^{2n\times 2n}$ be symplectic then:*

1. *the products $\underline{M}\,\underline{N}$ and $\underline{N}\,\underline{M}$ are symplectic*
2. *the inverse always exists and is given by $\underline{M}^{-1} = \underline{J}\,\underline{M}^{\mathrm{T}}\,\underline{J}^{\mathrm{T}} = -\,\underline{J}\,\underline{M}^{\mathrm{T}}\,\underline{J}$,*
3. *$\underline{M}^{\mathrm{T}}$ and $\underline{M}^{-1}$ are symplectic.*

Using definition A.3, $\underline{J}^{-1} = -\,\underline{J} = \underline{J}^{\mathrm{T}}$, $\det(\underline{J}) = 1$ and $\underline{J}^2 = -\,\underline{1}$, we conclude that

1. $(\underline{M}\,\underline{N})\,\underline{J}(\underline{M}\,\underline{N})^{\mathrm{T}} = \underline{M}\,\underline{N}\,\underline{J}\,\underline{N}^{\mathrm{T}}\,\underline{M}^{\mathrm{T}} = \underline{M}\,\underline{J}\,\underline{M}^{\mathrm{T}} = \underline{J}$.
2. $\underline{M}\,\underline{J}\,\underline{M}^{\mathrm{T}}\,\underline{J}^{\mathrm{T}} = \underline{1} \Rightarrow \underline{M}^{-1}$ exists and $\underline{M}^{-1} = \underline{J}\,\underline{M}^{\mathrm{T}}\,\underline{J}^{\mathrm{T}} = -\,\underline{J}\,\underline{M}^{\mathrm{T}}\,\underline{J}$.
3. $-\,\underline{J}\,\underline{M}^{\mathrm{T}}\,\underline{J}\,\underline{M} = \underline{1} \Rightarrow$
   $\underline{M}^{\mathrm{T}}\,\underline{J}\,\underline{M} = \underline{J}$ and $\underline{M}^{-1}\,\underline{J}\,\underline{M}^{-\mathrm{T}} = (\underline{M}^{\mathrm{T}}\,\underline{J}^{-1}\,\underline{M})^{-1} = -(\underline{M}^{\mathrm{T}}\,\underline{J}\,\underline{M})^{-1} = -\,\underline{J}^{-1} = \underline{J}$,

which proves the lemma A.1. □

Therefore (and because $\underline{1}$ is trivially symplectic) the symplectic $2n \times 2n$–matrices form a group, which is denoted by the symbol $\mathbf{SP}(2n, \mathbb{K})$ or, if it is clear which field $\mathbb{K}$ is meant, just $\mathbf{SP}(2n)$.

Lemma A.2 *Let $\underline{M} \in \mathbb{K}^{2n\times 2n}$ be symplectic then:*

1. *if λ is an eigenvalue of $\underline{M}$ of multiplicity l then $1/\lambda$ is also an eigenvalue of multiplicity l,*
2. *the determinant is $\det(\underline{M}) = +1$,*
3. *if $\lambda_i \neq 1/\lambda_j$, then the corresponding eigenvectors $\vec{v}_i$, $\vec{v}_j$ are skew–orthogonal in the sense that $\vec{v}_i^{\mathrm{T}}\,\underline{J}\vec{v}_j = 0$, for $i \neq j$*
4. *if $\underline{M}$ is furthermore non–degenerate, there is a symplectic possibly complex transformation $\underline{C}$ such that $\underline{C}\,\underline{M}\,\underline{C}^{-1} = \underline{\mathrm{diag}}(\lambda_1, \ldots, \lambda_{2n})$,*
5. *if $\underline{M}$ is real and diagonalisable, then the eigenvalues come in*
   (a) *quadruples : λ,λ^*,$1/\lambda$,$1/\lambda^*$ if $|\lambda| \neq 1$ and $\Im\lambda \neq 0$*
   (b) *or in real pairs: $\lambda = \lambda^*$, $1/\lambda = 1/\lambda^*$*
   (c) *or in pairs on the unit circle $\lambda = 1/\lambda^*$, $\lambda^* = 1/\lambda$.*

Since $\underline{M}^{-1} = \underline{J}\,\underline{M}^{\mathrm{T}}\,\underline{J}^{-1}$, $\underline{M}^{\mathrm{T}}$ and $\underline{M}^{-1}$ are similar. Let $p_{\underline{A}}(\lambda)$ be the characteristic polynomial of $\underline{A}$. Then $p_{\underline{M}} = p_{\underline{M}^{\mathrm{T}}} = p_{\underline{M}^{-1}}$. Since the eigenspace to a zero of $p_{\underline{M}}$ is never empty, a $\vec{v}$ exists with $\underline{M}\vec{v} = \lambda\vec{v}$. Since $\underline{M}$ is regular, λ is not 0 and we obtain $1/\lambda\vec{v} = \underline{M}^{-1}\vec{v}$. Hence if λ is an eigenvalue of $\underline{M}$, then $1/\lambda$ is an eigenvalue of $\underline{M}^{-1}$. But $p_{\underline{M}} = p_{\underline{M}^{-1}}$ and therefore λ and $1/\lambda$ are both eigenvalues of $\underline{M}$ and $\underline{M}^{-1}$ and the multiplicity is the same. This implies part 1. Every matrix $\underline{M} \in \mathbb{K}^{2n\times 2n}$ can be transformed by a similarity transform to $\underline{S}\,\underline{M}_{\mathrm{J}}\,\underline{S}^{-1}$ where $\underline{S} \in \mathbf{GL}(2n, \mathbb{C})$ is a regular, generally complex matrix and $\underline{M}_{\mathrm{J}} \in \mathbb{R}^{2n\times 2n}$ is the Jordan normal form of $\underline{M}$. The Jordan normal form of a matrix is in particular triangular with the eigenvalues on the diagonal. Since the determinant of a triangular matrix is the product of the diagonal elements, since the eigenvalues of $\underline{M}$ come in pairs $(\lambda, 1/\lambda)$ and since the determinant is invariant under similarity transforms, we obtain $\det(\underline{M}) = +1$. Part 3 follows from the relation $(\lambda_i\lambda_j - 1)\vec{v}_i^{\mathrm{T}}\,\underline{J}\vec{v}_j = \vec{v}_i^{\mathrm{T}}(\underline{M}^{\mathrm{T}}\,\underline{J}\,\underline{M} - \underline{J})\vec{v}_j = 0$. If we assume that $\underline{M}$ is non–degenerate, then the eigenvectors $\vec{v}_i$ are linearly independent. We can then normalise the eigenvectors to λ_{2i} and sort them so that $\lambda_{2i-1} \equiv 1/\lambda_{2i}$ to give $\vec{v}_{2i-1}^{\mathrm{T}}\,\underline{J}\vec{v}_{2i} = 1$. Then $\underline{C} = (\vec{v}_1, \ldots, \vec{v}_{2n})$ is symplectic and diagonalises $\underline{M}$, which proves part 4 for diagonalisable symplectic matrices. Note for later use that this normalisation still leaves the freedom of n complex conjugate pairs of phase factors for the n pairs $\vec{v}_{2i-1}\ \vec{v}_{2i}$. Part 5 follows from part 1 and from the well known fact that the zeros of a polynomial with real coefficients are real or come in complex conjugate pairs. □

A 2×2–matrix $\underline{M}_2$ is symplectic if and only if its determinant is 1, since for an arbitrary 2×2–matrix we have

$$\underline{M}_2\,\underline{J}_2\,\underline{M}_2^{\mathrm{T}} \equiv \begin{pmatrix} 0 & \det(\underline{M}_2) \\ -\det(\underline{M}_2) & 0 \end{pmatrix} \quad . \tag{A.9}$$

This result can easily be generalised to $2n\times 2n$ matrices with $n\times n$–block structure if one chooses the basis of equation (A.3). A matrix

$$\underline{M}_{2n} \equiv \begin{pmatrix} \underline{A}_n & \underline{B}_n \\ \underline{C}_n & \underline{D}_n \end{pmatrix} \tag{A.10}$$

is symplectic w.r.t $\underline{\tilde{J}}$ if and only if

$$\underline{A}_n\,\underline{B}_n^{\mathrm{T}} - \underline{B}_n\,\underline{A}_n^{\mathrm{T}} = \underline{0}_n \qquad (\underline{A}_n\,\underline{B}_n^{\mathrm{T}} \text{ is symmetric}) \tag{A.11a}$$

$$\underline{C}_n\,\underline{D}_n^{\mathrm{T}} - \underline{D}_n\,\underline{C}_n^{\mathrm{T}} = \underline{0}_n \qquad (\underline{C}_n\,\underline{D}_n^{\mathrm{T}} \text{ is symmetric}) \tag{A.11b}$$

$$\underline{A}_n\,\underline{D}_n^{\mathrm{T}} - \underline{B}_n\,\underline{C}_n^{\mathrm{T}} = \underline{1}_n \quad . \tag{A.11c}$$

Theorem A.2 *The flow $\vec{T}(\vec{z}; t_f, t_i)$ of a Hamiltonian system $(\mathcal{P}, \mathbb{R}, H)$ is a symplectic map for all $t_f, t_i \in \mathbb{R}$.*

To prove this we introduce the Jacobians of $\vec{T}$ and $\vec{F} \equiv \underline{J}\partial_{\vec{z}} H$

$$(\underline{T})_{ij}(\vec{z}; t, t_0) \equiv (\partial_{\vec{z}}\vec{T}^{\mathrm{T}})_{ji}\,|_{\vec{z};t,t_0} = \partial_j\,(\vec{T})_i\,|_{\vec{z};t,t_0} \tag{A.12a}$$

$$(\underline{F})_{ij}(\vec{z}; t) \equiv (\partial_{\vec{z}}\vec{F}^{\mathrm{T}})_{ji}\,|_{\vec{z};t} = \partial_j\,(\vec{F})_i\,|_{\vec{z};t} \quad . \tag{A.12b}$$

Then, assuming $\vec{T}$ to be sufficiently smooth we obtain

$$\begin{aligned} \partial_t\,\underline{T}(\vec{z}; t, t_0)_{ij} &= \partial_t\,\partial_j\,\vec{T}(\vec{z}; t, t_0)_i = \partial_j\,\partial_t\,\vec{T}(\vec{z}; t, t_0)_i \\ &= \partial_j\,\vec{F}(\vec{T}(\vec{z}; t, t_0), t)_i \\ &= \underline{F}(\vec{T}(\vec{z}; t, t_0), t)_{il}\,\underline{T}(\vec{z}; t, t_0)_{lj} \end{aligned} \tag{A.13a}$$

$$\partial_t\,\underline{T}(\vec{z}; t, t_0) = \underline{F}(\vec{T}(\vec{z}; t, t_0), t)\,\underline{T}(\vec{z}; t, t_0) \quad . \tag{A.13b}$$

Now we define the matrix $\underline{K} \equiv \underline{T}\,\underline{J}\,\underline{T}^{\mathrm{T}}$. Obviously, since $\underline{T}(\vec{z}; t_0, t_0) = \underline{1}$ we have $\underline{K}(\vec{z}; t_0, t_0) = \underline{J}$ and

$$\partial_t\,\underline{K}(\vec{z}; t, t_0) = \underline{F}(\vec{T}(\vec{z}; t, t_0), t)\,\underline{K}(\vec{z}; t, t_0) + \underline{K}(\vec{z}; t, t_0)\,\underline{F}(\vec{T}(\vec{z}; t, t_0), t)^{\mathrm{T}} \quad . \tag{A.14}$$

For each fixed $\vec{z} \in \mathcal{P}$ and $t_0 \in \mathbb{R}$ this is just a linear ODE which has a unique solution around $t = t_0$. Since $\vec{F}$ is a Hamiltonian vector field, i.e. $\underline{J}\,\underline{F} = (\underline{J}\,\underline{F})^{\mathrm{T}}$

$$\underline{F}(\vec{T}(\vec{z};t,t_0),t)\,\underline{J} + \underline{J}\,\underline{F}(\vec{T}(\vec{z};t,t_0),t)^{\mathrm{T}} = 0 \quad . \tag{A.15}$$

Therefore $\underline{K} = \underline{J}$ is a solution of (A.14). Since (A.14) is a linear ODE $\underline{K} = \underline{J}$ is the *unique* solution for all t. $\square$

A.1.2 Canonical transformations and integrability

When working with Hamiltonian systems it is useful to have methods for manipulating the EOM without destroying their canonical structure.

Definition A.4 (Canonical transformation) *A possibly time dependent transformation $\vec{A} : \mathcal{P}_1 \times \mathbb{R} \to \mathcal{P}_2$, $(\vec{z}, t) \mapsto \vec{A}(\vec{z}, t)$ is called canonical with multiplier κ if for all $t \in \mathbb{R}$ the transformation $\vec{a}_t : \mathcal{P}_1 \to \mathcal{P}_2$, $\vec{z} \mapsto \vec{A}(\vec{z}, t)$ is symplectic with multiplier κ. It is called a canonical transformation if $\kappa = 1$.*

Lemma A.3 (Scale transformations) *The constant scale transformations*

$$\begin{pmatrix} z_{2i-1} \\ z_{2i} \end{pmatrix} \mapsto \begin{pmatrix} z_{2i-1} \\ x_{2i} = a z_{2i} \end{pmatrix} \ \forall 1 \le i \le n \tag{A.16a}$$

$$\begin{pmatrix} z_{2i-1} \\ z_{2i} \end{pmatrix} \mapsto \begin{pmatrix} x_{2i-1} = a z_{2i-1} \\ z_{2i} \end{pmatrix} \ \forall 1 \le i \le n \tag{A.16b}$$

with $1 \le i \le n$ and $a = \mathrm{const.} \in \mathbb{K}$, $a \ne 0$ are canonical transformations with multiplier a, and

$$\begin{aligned} \begin{pmatrix} z_{2j-1} \\ z_{2j} \end{pmatrix} &\mapsto \begin{pmatrix} x_{2j-1} = a z_{2j-1} \\ x_{2j} = z_{2j}/a \end{pmatrix} \ \textit{for some } 1 \le j \le n \\ \begin{pmatrix} z_{2i-1} \\ z_{2i} \end{pmatrix} &\mapsto \begin{pmatrix} z_{2i-1} \\ z_{2i} \end{pmatrix} \ \forall 1 \le i \le n,\ i \ne j \end{aligned} \tag{A.17}$$

with $1 \le i \le n$ and $a = \mathrm{const.} \in \mathbb{K}$, $a \ne 0$ is a canonical transformation.

All three transformations are block–diagonal with 2×2–blocks. By direct calculation one easily verifies that $\left(\begin{smallmatrix}1&0\\0&a\end{smallmatrix}\right)\underline{J}_2\left(\begin{smallmatrix}1&0\\0&a\end{smallmatrix}\right) = \left(\begin{smallmatrix}1&a\\0&1\end{smallmatrix}\right)\underline{J}_2\left(\begin{smallmatrix}1&a\\0&1\end{smallmatrix}\right) = a\,\underline{J}_2$ proving that (A.16a) and (A.16b) are canonical with multiplier a. The only 2×2–block in (A.17) which is not the identity, i.e. the j-th block, has determinant 1 which proves its symplecticity. $\square$

A widely used class of canonical transformations are those given in terms of *generating functions*. In this context it is useful to define for the "old" coordinates ($\vec{z}$) and the "new" coordinates ($\vec{x}$)

$$\vec{q} = \underline{P}_{\mathrm{odd}}\vec{z} \ , \ \vec{p} = \underline{P}_{\mathrm{even}}\vec{z} \ , \ \vec{\Psi} = \underline{P}_{\mathrm{odd}}\vec{x} \ , \ \vec{J} = \underline{P}_{\mathrm{even}}\vec{x} \tag{A.18}$$

where $\underline{P}_{\mathrm{odd/even}}$ is the projector from the $2n$–dimensional phase space $\mathcal{P}$ to the n–dimensional configuration/momentum space. Note that at this stage $\vec{J}$ and $\vec{\Psi}$ don't necessarily mean "action" and "angle"!

Theorem A.3 (Generating functions) *Any of the functions $F(\vec{q}, \vec{\Psi}, t)$, $F(\vec{q}, \vec{J}, t)$, $F(\vec{p}, \vec{\Psi}, t)$ or $F(\vec{p}, \vec{J}, t)$ whereby the corresponding equation of*

$$\vec{p} = +\partial_{\vec{q}} F(\vec{q}, \vec{\Psi}, t) \quad , \quad \vec{J} = -\partial_{\vec{\Psi}} F(\vec{q}, \vec{\Psi}, t) \tag{A.19a}$$

$$\text{or} \quad \vec{p} = +\partial_{\vec{q}} F(\vec{q}, \vec{J}, t) \quad , \quad \vec{\Psi} = +\partial_{\vec{J}} F(\vec{q}, \vec{J}, t) \tag{A.19b}$$

$$\text{or} \quad \vec{q} = -\partial_{\vec{p}} F(\vec{p}, \vec{\Psi}, t) \quad , \quad \vec{J} = -\partial_{\vec{\Psi}} F(\vec{p}, \vec{\Psi}, t) \tag{A.19c}$$

$$\text{or} \quad \vec{q} = -\partial_{\vec{q}} F(\vec{p}, \vec{J}, t) \quad , \quad \vec{\Psi} = +\partial_{\vec{J}} F(\vec{p}, \vec{J}, t) \tag{A.19d}$$

can be solved in the form

$$\begin{pmatrix}\vec{\Psi}\\ \vec{J}\end{pmatrix} = \vec{A}_F(\vec{q},\vec{p},t) \;\;,\;\; \begin{pmatrix}\vec{q}\\ \vec{p}\end{pmatrix} = \vec{A}_F^{-1}(\vec{\Psi},\vec{J},t) \tag{A.20}$$

generates a canonical transformation $\vec{A}_F(\vec{q},\vec{p},t)$*.*

We will prove this only for the first case of $F(\vec{q},\vec{\Psi},t)$. Definition A.4 implies that it suffices to show that the generated transformation is symplectic for all t. By the premises of the theorem we can solve equation (A.19a) and obtain

$$\begin{pmatrix}\vec{\Psi}\\ \vec{J}\end{pmatrix} = \begin{pmatrix}\vec{\Psi}\\ -\partial_{\vec{\Psi}}\,F(\vec{q},\vec{\Psi},t)\end{pmatrix} \equiv \begin{pmatrix}\vec{\Psi}\\ -\vec{F}_{\vec{\Psi}}(\vec{q},\vec{\Psi},t)\end{pmatrix} \equiv \vec{f}(\vec{q},\vec{\Psi},t) \tag{A.21a}$$

$$\begin{pmatrix}\vec{q}\\ \vec{p}\end{pmatrix} = \begin{pmatrix}\vec{q}\\ +\partial_{\vec{q}}\,F(\vec{q},\vec{\Psi},t)\end{pmatrix} \equiv \begin{pmatrix}\vec{q}\\ \vec{F}_{\vec{q}}(\vec{q},\vec{\Psi},t)\end{pmatrix} \equiv \vec{g}(\vec{q},\vec{\Psi},t) \tag{A.21b}$$

$$\begin{pmatrix}\vec{\Psi}\\ \vec{J}\end{pmatrix} = \vec{f}(\vec{g}^{-1}(\vec{q},\vec{p},t),t) \equiv \vec{A}(\vec{q},\vec{p},t) \equiv \begin{pmatrix}\vec{A}_{\vec{\Psi}}(\vec{q},\vec{p},t)\\ \vec{A}_{\vec{J}}(\vec{q},\vec{p},t)\end{pmatrix} \tag{A.21c}$$

$$\begin{pmatrix}\vec{q}\\ \vec{p}\end{pmatrix} = \vec{g}(\vec{f}^{-1}(\vec{\Psi},\vec{J},t),t) \equiv \vec{A}^{-1}(\vec{\Psi},\vec{J},t) \equiv \begin{pmatrix}\vec{A}_{\vec{q}}^{-1}(\vec{\Psi},\vec{J},t)\\ \vec{A}_{\vec{p}}^{-1}(\vec{\Psi},\vec{J},t)\end{pmatrix} \;. \tag{A.21d}$$

Showing that the Jacobian $\underline{A}$ of $\vec{A}$ is symplectic w.r.t $\underline{\tilde{J}}$ can be enormously simplified [GH98] by using the result of lemma A.1 for the inverse of a symplectic matrix. We want to show that

$$\underline{\tilde{J}}\,\underline{A}^{\mathrm{T}}|_{\vec{q},\vec{p},t} = \underline{A}^{-1}|_{\vec{A}(\vec{q},\vec{p},t),t}\,\underline{\tilde{J}} \;\;, \tag{A.22}$$

where $\underline{A}$ and $\underline{A}^{-1}$ are given by

$$\underline{A}|_{\vec{q},\vec{p},t} = \underline{f}|_{\vec{g}^{-1}(\vec{q},\vec{p},t)}\,\underline{g}^{-1}|_{\vec{q},\vec{p},t} \;\;,\;\; \underline{A}^{-1}|_{\vec{A}(\vec{q},\vec{p},t),t} = \underline{g}|_{\vec{f}^{-1}(\vec{A}(\vec{q},\vec{p},t),t)}\,\underline{f}^{-1}|_{\vec{A}(\vec{q},\vec{p},t)} \;. \tag{A.23}$$

The Jacobians of $\vec{f}$, $\vec{g}$ and their inverses are

$$\underline{f} = \begin{pmatrix} \underline{0} & \underline{1} \\ -\underline{F}_{\vec{q}\vec{\Psi}} & -\underline{F}_{\vec{\Psi}\vec{\Psi}} \end{pmatrix} \;\;,\;\; (\underline{f})^{-1} = \begin{pmatrix} -\underline{F}_{\vec{q}\vec{\Psi}}^{-1}\,\underline{F}_{\vec{\Psi}\vec{\Psi}} & -\underline{F}_{\vec{q}\vec{\Psi}}^{-1} \\ \underline{1} & \underline{0} \end{pmatrix} \tag{A.24a}$$

$$\underline{g} = \begin{pmatrix} \underline{1} & \underline{0} \\ \underline{F}_{\vec{q}\vec{q}} & \underline{F}_{\vec{\Psi}\vec{q}} \end{pmatrix} \;\;,\;\; (\underline{g})^{-1} = \begin{pmatrix} \underline{1} & \underline{0} \\ -\underline{F}_{\vec{\Psi}\vec{q}}^{-1}\underline{F}_{\vec{q}\vec{q}} & \underline{F}_{\vec{\Psi}\vec{q}}^{-1} \end{pmatrix} \;\;, \tag{A.24b}$$

where $\underline{F}_{\vec{q}\vec{\Psi}} \equiv \partial_{\vec{\Psi}}\,\partial_{\vec{q}}^{\mathrm{T}}\,F$, $\underline{F}_{\vec{\Psi}\vec{q}} \equiv \partial_{\vec{q}}\,\partial_{\vec{\Psi}}^{\mathrm{T}}\,F$, $\underline{F}_{\vec{q}\vec{q}} \equiv \partial_{\vec{q}}\,\partial_{\vec{q}}^{\mathrm{T}}\,F$ and $\underline{F}_{\vec{\Psi}\vec{\Psi}} \equiv \partial_{\vec{\Psi}}\,\partial_{\vec{\Psi}}^{\mathrm{T}}\,F$. Now by simple matrix multiplication one obtains

$$\underline{A} = \begin{pmatrix} -\underline{F}_{\vec{\Psi}\vec{q}}^{-1}\underline{F}_{\vec{q}\vec{q}} & \underline{F}_{\vec{\Psi}\vec{q}}^{-1} \\ -\underline{F}_{\vec{q}\vec{\Psi}} + \underline{F}_{\vec{\Psi}\vec{\Psi}}\,\underline{F}_{\vec{\Psi}\vec{q}}^{-1}\underline{F}_{\vec{q}\vec{q}} & -\underline{F}_{\vec{\Psi}\vec{\Psi}}\,\underline{F}_{\vec{\Psi}\vec{q}}^{-1} \end{pmatrix} \tag{A.25a}$$

$$\underline{A}^{-1} = \begin{pmatrix} -\underline{F}_{\vec{q}\vec{\Psi}}^{-1}\,\underline{F}_{\vec{\Psi}\vec{\Psi}} & -\underline{F}_{\vec{q}\vec{\Psi}}^{-1} \\ \underline{F}_{\vec{\Psi}\vec{q}} - \underline{F}_{\vec{q}\vec{q}}\underline{F}_{\vec{q}\vec{\Psi}}^{-1}\,\underline{F}_{\vec{\Psi}\vec{\Psi}} & -\underline{F}_{\vec{q}\vec{q}}\underline{F}_{\vec{q}\vec{\Psi}}^{-1} \end{pmatrix} \;\;, \tag{A.25b}$$

and finally by using the relation $\underline{F}_{\vec{q}\vec{\Psi}}^{\mathrm{T}} = \underline{F}_{\vec{\Psi}\vec{q}}$ and the symmetry of $\underline{F}_{\vec{q}\vec{q}}$ and $\underline{F}_{\vec{\Psi}\vec{\Psi}}$ we find that indeed the Jacobian of $\vec{A}$ is symplectic everywhere in phase space where the defining equation (A.19a) can be solved :

$$\underline{\tilde{J}}\,\underline{A}^{\mathrm{T}} = \begin{pmatrix} \underline{F}_{\vec{q}\vec{\Psi}}^{-1} & -\underline{F}_{\vec{q}\vec{\Psi}}^{-1}\,\underline{F}_{\vec{\Psi}\vec{\Psi}} \\ \underline{F}_{\vec{q}\vec{q}}\underline{F}_{\vec{q}\vec{\Psi}}^{-1} & \underline{F}_{\vec{\Psi}\vec{q}} - \underline{F}_{\vec{q}\vec{q}}\underline{F}_{\vec{q}\vec{\Psi}}^{-1}\,\underline{F}_{\vec{\Psi}\vec{\Psi}} \end{pmatrix} = \underline{A}^{-1}\,\underline{\tilde{J}} \;\;. \tag{A.26}$$

This proves the symplecticity of $\vec{A}$. $\square$

The other cases (A.19b), (A.19c) and (A.19d) can be proved in analogous ways. It should be noted that this proof can be somewhat simplified if one has introduced the concept of differential forms as in [VA88, ems3].

We will now restrict ourselves to origin preserving periodic Hamiltonian systems, i.e. Hamiltonian systems where the EOM are of the form

$$\begin{aligned} \mathrm{D}_t\,\vec{z} &= \vec{F}(\vec{z},t) && \text{(A.27a)}\\ \text{with}\quad \vec{F}(\vec{z},t+\tau) &\equiv \vec{F}(\vec{z},t)\ \ \forall(\vec{z},t)\in\mathcal{P}^\star && \text{(A.27b)}\\ \text{and}\quad \vec{F}(\vec{0},t) &\equiv \vec{0}\ \ \forall t\in\mathbb{R}\ . && \text{(A.27c)} \end{aligned}$$

This implies that $H(\vec{z},t)$ is periodic with period τ and has, seen as a formal series in $\vec{z}$, no contribution linear in $\vec{z}$. In case of periodic systems it is convenient to rescale the independent variable t to $\theta = 2\pi\frac{t}{\tau}$ so that the Hamiltonian EOM are

$$\begin{aligned} \mathrm{D}_\theta\,\vec{z} &= \underline{J}\partial_{\vec{z}}\,H_\theta(\vec{z},\theta) && \text{(A.28a)}\\ \text{with}\quad H_\theta(\vec{z},\theta) &= \frac{\tau}{2\pi}H(\vec{z},\frac{\tau}{2\pi}\theta)\ . && \text{(A.28b)} \end{aligned}$$

In accelerator physics the parameter θ is called the *(generalised) azimuth*. From now on we will omit the index θ for Hamiltonians in the new free "time" parameter θ. For *linear periodic*, not necessarily Hamiltonian, systems

$$\mathrm{D}_\theta\,\vec{z} = \underline{F}(\theta)\vec{z} \tag{A.29}$$

the following theorem holds [ems1]:

Theorem A.4 (Floquet's theorem) *There is a change of variables $\vec{z} = \underline{C}(\theta)\vec{x}$, which is linear in $\vec{z}$ and where $\underline{C}(\theta)$ is 2π–periodic in θ, which transforms the system equation (A.29) into a linear system with constant coefficients $\mathrm{D}_\theta\,\vec{x} = \underline{\Lambda}\vec{x}$ and correspondingly the flow of equation (A.29) is given by*

$$\underline{T}(\theta,\theta_0) = \underline{C}(\theta)\exp\left((\theta-\theta_0)\,\underline{\Lambda}\right)\,\underline{C}^{-1}(\theta_0)\ . \tag{A.30}$$

It is clear that periodicity of the Hamiltonian does *not* imply periodic motion. In fact the motion is not even necessarily bounded.

Definition A.5 (One–turn map) *For a 2π–periodic not necessarily Hamiltonian system we call the map $\vec{T}_{\mathrm{otm}}:\ \mathcal{P}^\star\to\mathcal{P},\ (\vec{z},\theta)\mapsto\vec{T}_{\mathrm{otm}}(\vec{z};\theta)$*

$$\vec{T}_{\mathrm{otm}}(\vec{z};\theta)\equiv\vec{T}(\vec{z};\theta+2\pi,\theta)\ , \tag{A.31}$$

with $\vec{T}$ being the flow of that system, the one–turn map (OTM) of the system.

Often we will distinguish between one–turn map and flow just by the number of azimuth parameters, i.e. we will use $\vec{T}(\vec{z};\theta)\equiv\vec{T}_{\mathrm{otm}}(\vec{z};\theta)$ for the one–turn map and $\vec{T}(\vec{z};\theta_f,\theta_i)$ for the flow. The OTM is of course 2π–periodic in θ. The one–turn matrix of the linear periodic Hamiltonian system of equation (A.29) is given by $\underline{T}(\theta) = \underline{C}(\theta)\exp(2\pi\,\underline{\Lambda})\,\underline{C}^{-1}(\theta)$.

Definition A.6 (Incommensurability) *We call the components Q_i of a vector $\vec{Q}\in\mathbb{R}^n$ incommensurable if $\vec{k}\cdot\vec{Q}\neq 0$ for all $\vec{k}\in\mathbb{Z}^n$, $\vec{k}\neq\vec{0}$.*
We call the components Q_i of a vector $\vec{Q}\in\mathbb{R}^n$ incommensurable with 1 if $\vec{k}\cdot\vec{Q}\neq k_0$ for all $\vec{k}\in\mathbb{Z}^n$, $\vec{k}\neq\vec{0}$, $k_0\in\mathbb{Z}$.
We call the components strongly incommensurable if there are positive real numbers c, ρ so that for all $\vec{k}\in\mathbb{Z}^n$, $\vec{k}\neq\vec{0}$ the inequality $|\vec{k}\cdot\vec{Q}| > c\|\vec{k}\|^{-\rho}$ holds.
We call the components strongly incommensurable with 1 if the components of $(1,\vec{Q})\in\mathbb{R}^{n+1}$ are strongly incommensurable.

For non–linear origin preserving Hamiltonian systems where the Jacobian $\underline{T}(\vec{0},\theta)$ of the OTM is diagonalisable with eigenvalues $\lambda_i \equiv e^{i2\pi Q_i}$ on the unit circle and with strongly incommensurable *tunes* Q_i, one can show [ems1, ems3] that in some neighbourhood of $\vec{z}=\vec{0}$ there is a biholomorphic change of variables that transforms the non–linear system to the linearised one. For $\rho > n-1$ the number of points $\vec{Q}$ for which one cannot find such a c is of zero measure [ems3, LM88]. Therefore for almost all systems with diagonalisable Jacobian of the one–turn map the "qualitative" properties of the exact flow can be derived from the linearised flow in some neighbourhood of $\vec{z}=\vec{0}$. While discussing the tunes of a non–autonomous system which is 2π–periodic in θ and which is origin preserving we will often abbreviate "(strong) incommensurability with 1" to "(strong) incommensurability".

Definition A.7 (Stability) *An origin preserving map $\vec{M}: \mathcal{P}\to\mathcal{P}$, $\vec{z}\mapsto\vec{M}(\vec{z})$, $\vec{M}(\vec{0})=\vec{0}$ is called stable if for each $\epsilon>0$ there is a $\delta>0$ so that for all $\|\vec{z}\|<\delta$ and all $N\in\mathbb{N}^+$ the N–times iterated composition of the map is bounded by $\|\vec{M}^N\vec{z}\|<\epsilon$.*

Definition A.8 (Strong stability of a linear symplectic map) *A linear map $\vec{M}:\mathbb{K}^{2n}\to\mathbb{K}^{2n}$, $\vec{z}\mapsto\vec{M}(\vec{z})\equiv\underline{M}\vec{z}$ is called strongly stable if it is stable and there is an $\epsilon>0$ so that all real symplectic matrices $\underline{N}$ with $\max_{1\le k,l\le 2n}|(\underline{M})_{kl}-(\underline{N})_{kl}|<\epsilon$ are stable.*

Theorem A.5 *[VA88] A real linear symplectic matrix $\underline{M}$ is strongly stable if all its eigenvalues are non–degenerate and are on the unit circle.*

If all eigenvalues λ_i of $\underline{M}$ are non–degenerate, then the eigenvectors $\vec{v}_i$ can be normalised to form an skew–orthonormal basis $\{\hat{v}_i\}_{1\le i\le 2n}$ of $\mathbb{K}^{2n}$, i.e. $\hat{v}_i^{\mathrm{T}}\underline{J}\hat{v}_j=0$ for $\lambda_i\ne 1/\lambda_j$ and $\|\hat{v}_i\|=1$. Hence stability follows directly from the relation $\|\underline{M}\hat{v}_i\|=|\lambda_i|\,\|\hat{v}_i\|\equiv 1$. Since the λ_i are non–degenerate one can find pair–wise disjunct circular neighbourhoods in the complex plane around them. The eigenvalues from the characteristic polynomial are continuous functions of the matrix coefficients. Therefore we can choose ϵ sufficiently small, so that if $\underline{N}\ne\underline{M}$ belongs to the ϵ–neighbourhood of $\underline{M}$ in the sense of definition A.8, there is exactly one of the $2n$ eigenvalues ρ_i of $\underline{N}$ in one of these circular neighbourhoods (conclusion A). Since $\underline{N}$ is real with ρ_i also ρ_i^* is an eigenvalue. Therefore if $|\rho_i|\ne 1$, i.e. $\rho_i^*\ne 1/\rho_i$, there is another eigenvalue in this circular neighbourhood — which is in contradiction to conclusion A. □

We conclude that for real periodic linear Hamiltonian systems

Lemma A.4 *If the one–turn matrix $\underline{T}(\theta)$ is stable/strongly stable for some θ_0, then it is stable/strongly stable for all $\theta\in\mathbb{R}$.*

Since $\underline{T}(\theta)=\underline{T}(\theta,\theta_0)\,\underline{T}(\theta_0)\,\underline{T}(\theta_0,\theta)=\underline{T}(\theta,\theta_0)\,\underline{T}(\theta_0)\,\underline{T}^{-1}(\theta,\theta_0)$ the N–turn map is $\underline{T}^N(\theta)=\underline{T}(\theta,\theta_0)\,\underline{T}^N(\theta_0)\,\underline{T}^{-1}(\theta,\theta_0)$. Therefore the linearity and periodicity of the flow implies its boundedness for all θ, thereby proving the lemma. □

Unfortunately in the case of non–linear periodic Hamiltonian systems with origin preserving one–turn maps, statements about stability cannot be made in general. Integrable non–linear systems as described below are stable. But although a wide range of non–linear systems have been proved to be integrable and even stable under small perturbations, a general theorem for integrability and is not known. In accelerator physics the domain in which the one–turn map is stable is called the *dynamic aperture* of the accelerator.

We will now give a convenient definition of action–angle representations of t–periodic Hamiltonians. There are more general definitions [GH94] but we are interested mainly in two special properties, namely invariance of the action variable $\vec{J}=\mathrm{const.}$ and periodicity of the canonical coordinates of $\mathcal{P}$ w.r.t the angle: $\vec{z}(\vec{J},\vec{\Psi}+2\pi\vec{k})=\vec{z}(\vec{J},\vec{\Psi})\ \forall\vec{k}\in\mathbb{N}^n$.

Definition A.9 (Action–angle variables) *The phase space coordinates of a Hamiltonian system* $(\mathcal{P}^\star, H_{\mathrm{AA}})$ *are action–angle variables if the EOM read like*

$$\begin{aligned} \mathrm{D}_\theta\, z_{2i-1} \equiv \mathrm{D}_\theta\, \Psi_i &= \partial_{2i}\, H_{\mathrm{AA}} \equiv \kappa_i(\vec{J}) & \text{(A.32a)} \\ \mathrm{D}_\theta\, z_{2i} \equiv \mathrm{D}_\theta\, J_i &= -\partial_{2i-1}\, H_{\mathrm{AA}} \equiv 0 \ . & \text{(A.32b)} \end{aligned}$$

Note that from the definition of $\vec{\kappa} = \partial_{\vec{J}} H$ it follows that the Jacobian of $\vec{\kappa}$ is symmetric.

$$\partial_{\vec{J}} \vec{\kappa}^{\mathrm{T}} \equiv \partial_{\vec{J}} \partial_{\vec{J}}^{\mathrm{T}} H_{\mathrm{AA}} = (\partial_{\vec{J}} \partial_{\vec{J}}^{\mathrm{T}} H_{\mathrm{AA}})^{\mathrm{T}} \equiv (\partial_{\vec{J}} \vec{\kappa}^{\mathrm{T}})^{\mathrm{T}} \ . \tag{A.33}$$

The flow $\vec{T}_{\mathrm{AA}}$ is affine linear in $\theta_f - \theta_i$

$$\begin{aligned} \vec{J}(\vec{\Psi}_0, \vec{J}_0; \theta_f, \theta_i) &= \text{const.} = \vec{J}_0 & \text{(A.34a)} \\ \vec{\Psi}(\vec{\Psi}_0, \vec{J}_0; \theta_f, \theta_i) &= \vec{\Psi}_0 + (\theta_f - \theta_i)\, \vec{\kappa}(\vec{J}_0) \ . & \text{(A.34b)} \end{aligned}$$

Definition A.10 (Integrability) *We will call a periodic origin preserving Hamiltonian system* $(\mathcal{P}_1^\star, H)$ *integrable if there is a canonical transformation* $\vec{A}:\ \mathcal{P}_1 \times \mathbb{R} \to \mathcal{P}_2,\ (\vec{z}, \theta) \mapsto (\vec{\Psi}, \vec{J})$ *so that*

1. $\vec{A}$ *transforms* $(\mathcal{P}_1, H)$ *to action–angle variables, i.e.* $\mathrm{D}_\theta\, \vec{\Psi} = \vec{Q}(\vec{J})$, $\mathrm{D}_\theta\, \vec{J} = 0$ *and*
2. $\vec{A}^{-1}(\vec{\Psi} + 2\pi\vec{K}, \vec{J}, \theta) = \vec{A}^{-1}(\vec{\Psi}, \vec{J}, \theta)$ *for* $\vec{K} \in \mathbb{N}^n$.

For an integrable system the phase space is foliated into different n–dimensional submanifolds. $\vec{A}$ maps these submanifolds onto *invariant n–dimensional tori* $\mathcal{T}^n$ which can be parametrised by the vector of the actions. Each trajectory transformed by $\vec{A}$ winds itself uniformly around the torus defined by its starting value of $\vec{J}$. The rate of winding w.r.t. θ is fully determined by the value of $\vec{Q}$. The Q_i are called *tunes* in accelerator physics. If we consider for example an integrable system with 2 degrees of freedom, then the invariant tori are defined by 2 parameters J_1, J_2 and the winding rate of a trajectory is given by $Q_1(J_1, J_2)$ and $Q(J_1, J_2)$. Now consider the case that both tunes are independent of $\vec{J}$ and have values $Q_1 = 5^1\!/_4$ and $Q_2 = 7^1\!/_3$, and $\vec{\Psi}_0 = \vec{0}$, $\theta_0 = 0$. Then $\Psi_1 \bmod 2\pi$ traverses the interval $[0, 2\pi)$ $5^1\!/_4$ times for each 2π period in θ. After 4 periods it comes back to 0 when $\theta \bmod 2\pi = 0$. Therefore the motion in the phase space plane corresponding to (J_1, Ψ_1) is 8π–periodic. After 3 periods $\Psi_2 \bmod 2\pi$ has traversed the interval $[0, 2\pi)$ 22 times and therefore the motion in the phase space plane corresponding to (J_2, Ψ_2) is 6π–periodic. The vector $\vec{\Psi} \bmod 2\pi$ is regained after 12 periods and with these tunes the motion is 24π–periodic. If one tune were irrational, the trajectories would never close on the torus and if they were incommensurable, the set of points $\mathcal{L} \equiv \{\vec{\Psi}_0 + \mathbb{R}^+\vec{Q}\}$ would be a dense subset of of the torus $\mathcal{T}^2$. In the 24π–periodic example the trajectory is a closed curve on the torus.

Theorem A.6 *A real Hamiltonian system* $(\mathcal{P}_1^\star, H)$ *with a flow* $\vec{T}$ *that is linear in* $\vec{z}$ *and* 2π*–periodic in* θ

$$\begin{aligned} \vec{T}(\vec{z}; \theta, \theta_0) &\equiv \underline{T}(\theta, \theta_0)\vec{z} & \text{(A.35a)} \\ \underline{T}(\theta + 2\pi, \theta_0 + 2\pi) &= \underline{T}(\theta, \theta_0) & \text{(A.35b)} \end{aligned}$$

is integrable in the sense of definition A.10 if the one–turn map $\underline{T}(\theta) \equiv \underline{T}(\theta + 2\pi, \theta)$ *can be diagonalised and all its eigenvalues* λ_i *are on the unit circle* $|\lambda_i| = 1$

Let $\underline{C}(\theta)$ be the complex 2π–periodic transformation that diagonalises $\underline{T}$

$$\underline{C}(\theta)^{-1}\, \underline{T}(\theta)\, \underline{C}(\theta) = \underline{\mathrm{diag}}(\lambda_1, 1/\lambda_1, \ldots, \lambda_n, 1/\lambda_n) \equiv \underline{D} \tag{A.36}$$

with $\lambda_i = e^{i2\pi[Q_i]}$, $[Q_i] \in [0,1)$. The complex functions $\vec{\xi}(\theta) \equiv \underline{C}^{-1}(\theta)\vec{z}(\theta)$ are called *complex normal forms*. They transform under the OTM like $\vec{xi}_f = \underline{D}\vec{xi}_i$. The λ_i are azimuth independent since

$$\begin{aligned}
\underline{T}(\theta') \equiv \underline{T}(\theta'+2\pi,\theta') &= \underline{T}(\theta'+2\pi,\theta+2\pi)\,\underline{T}(\theta+2\pi,\theta)\,\underline{T}(\theta,\theta') && \text{(A.37a)}\\
&= \underline{T}(\theta',\theta)\,\underline{T}(\theta)\,\underline{T}(\theta,\theta') && \text{(A.37b)}\\
&= \underline{T}(\theta',\theta)\,\underline{T}(\theta)\,\underline{T}(\theta',\theta)^{-1} && \text{(A.37c)}
\end{aligned}$$

is a similarity transform which does not change the eigenvalues. In accelerator physics the $[Q_i]$ are called the *fractional tunes* of the system and $2\pi[Q_i]$ the corresponding phase advances per turn. Note that these fractional tunes $[\vec{Q}]$ from the eigenvalues of the one–turn map do not constrain the integer part of $\vec{Q}$. Since $\underline{T}(\theta)$ is real, the eigenvectors, which are the column vectors of $\underline{C}$, form complex conjugate pairs $\vec{c}_{2j-1} = \vec{c}^{\,*}_{2j}$. The real and imaginary parts $\vec{b}_{2j-1}(\theta) = \Re\{\vec{c}_{2j-1}(\theta)\} = \Re\{\vec{c}_{2j}(\theta)\}$, $\vec{b}_{2j}(\theta) = \Im\{\vec{c}_{2j-1}(\theta)\} = -\Im\{\vec{c}_{2j}(\theta)\}$ are transformed by $\underline{T}$ like

$$\underline{T}\vec{c}_{2j-1} = \underline{T}(\vec{b}_{2j-1}+i\vec{b}_{2j}) = \left(\cos 2\pi[Q_j]\,\vec{b}_{2j-1} - \sin 2\pi[Q_j]\,\vec{b}_{2j}\right) + i\left(\cos 2\pi[Q_j]\,\vec{b}_{2j} + \sin 2\pi[Q_j]\,\vec{b}_{2j-1}\right) \ . \tag{A.38}$$

Since $\underline{T}$ was assumed to be diagonalisable, the $\vec{b}_i$ can be chosen to be a skew–orthogonal basis of $\mathbb{R}^{2n}$ and can be normalised to $\vec{b}^{\mathrm{T}}_{2j-1}\,\underline{J}\vec{b}_{2j} = 1$. This can be seen as follows: first $\vec{b}^{\mathrm{T}}_{2j-1}\,\underline{J}\vec{b}_{2k} = 0$ for $j \neq k$ since $\vec{c}_{2j+1}$ and $\vec{c}_{2j}$ belong to eigenvalue λ_j but $\vec{c}_{2k+1}$ and $\vec{c}_{2k}$ belong to eigenvalue λ_k which we have assumed to be different. Moreover we have $4\vec{b}^{\mathrm{T}}_{2j-1}\,\underline{J}\vec{b}_{2j-1} = \vec{c}^{\,\mathrm{T}}_{2j-1}\,\underline{J}\vec{c}_{2j-1} + \vec{c}^{\,\mathrm{T}}_{2j-1}\,\underline{J}\vec{c}_{2j} + \vec{c}^{\,\mathrm{T}}_{2j}\,\underline{J}\vec{c}_{2j-1} + \vec{c}^{\,\mathrm{T}}_{2j}\,\underline{J}\vec{c}_{2j} = 0$ and analogously find $\vec{b}^{\mathrm{T}}_{2j}\,\underline{J}\vec{b}_{2j} = 0$. Finally we obtain $4i\vec{b}^{\mathrm{T}}_{2j-1}\,\underline{J}\vec{b}_{2j} = \vec{c}^{\,\mathrm{T}}_{2j-1}\,\underline{J}\vec{c}_{2j-1} - \vec{c}^{\,\mathrm{T}}_{2j-1}\,\underline{J}\vec{c}_{2j} + \vec{c}^{\,\mathrm{T}}_{2j}\,\underline{J}\vec{c}_{2j-1} - \vec{c}^{\,\mathrm{T}}_{2j}\,\underline{J}\vec{c}_{2j} = 2\vec{c}^{\,\mathrm{T}}_{2j-1}\,\underline{J}\vec{c}_{2j}$ so that we can choose a normalisation for the $\vec{c}_i$ so that the real matrix $\underline{B}^{(1)}$ with column vectors $\vec{b}_i$ is symplectic with multiplier 1. Note that we have normalised the $\vec{c}_i$ so that $\underline{C}$ is no longer symplectic with multiplier 1. Moreover the normalisation of the $2n$ complex eigenvectors $\vec{c}_i(\theta)$ has still n free phase factors $e^{\pm i\psi_i(\theta)}$. The periodicity constraint on $\underline{C}$ only requires that $\psi_i(\theta) = \psi_i^{\mathrm{per.}}(\theta) + k_i\theta$ where $\psi_i^{\mathrm{per.}}$ is 2π periodic and k_i is an integer. Since the system system $(\mathcal{P}^*_1, H)$ is linear and 2π–periodic its flow can be written according to theorem A.4 as $\underline{T}(\theta,\theta_0) = \underline{\widetilde{C}}(\theta)\exp\left((\theta-\theta_0)\,\underline{\Lambda}\right)\underline{\widetilde{C}}(\theta_0)^{-1}$ where $\underline{\widetilde{C}}(\theta)$ is 2π–periodic in θ and $\underline{\Lambda}$ has constant coefficients. In particular the OTM is $\underline{T}(\theta) = \underline{\widetilde{C}}(\theta)\exp(2\pi\,\underline{\Lambda})\,\underline{\widetilde{C}}(\theta)^{-1}$. Thus $\exp(2\pi\,\underline{\Lambda}) = \text{const.} = \underline{\widetilde{C}}(\theta)^{-1}\,\underline{C}(\theta)\ \underline{D}\ \underline{C}(\theta)^{-1}\underline{\widetilde{C}}(\theta)$ and therefore $\underline{\widetilde{C}}(\theta)^{-1}\,\underline{C}(\theta) =$ is the product of a constant matrix and a θ–dependent matrix $\underline{P}$ that commutes with the constant diagonal $\underline{D}$ for all theta. In other words $\underline{P}$ is diagonal itself. Since the flow of a linear ODE is unique, and the choice of the $\vec{c}_i$ in order to make $\underline{B}^{(1)}$ symplectic is unique up to the phase factors $e^{i\psi_j(\theta)}$, we conclude that there are phase functions $\psi_i(\theta)$ such that if we absorb them in the in the normalization of the complex conjugate pairs $\vec{c}_{2j-1}$, $\vec{c}_{2j}$ the transformation $\underline{C}(\theta)$ has a form such that $\underline{T}(\theta,\theta_0) = \underline{C}(\theta)\underline{\widetilde{D}}(\Delta)\,\underline{C}^{-1}(\theta_0)$ with $\underline{\widetilde{D}} \equiv \underline{\mathrm{diag}}(\ldots, e^{i\Delta([Q_i]+k_i)}, e^{-i\Delta([Q_i]+k_i)}, \ldots)$. Here we have defined $\Delta \equiv \theta - \theta_0$. We now set $Q_i = [Q_i] + k_i$. Then the column matrix of the real eigenvectors $\underline{B}^{(1)}$ transforms under the flow $\underline{T}(\theta,\theta_0)$ like $\underline{T}(\theta,\theta_0)\,\underline{B}^{(1)}(\theta) = \underline{B}^{(1)}(\theta)\,\underline{R}(\Delta)$ with block diagonal

$$\underline{R} \equiv \underline{\mathrm{diag}}(\,\underline{r}_1,\ldots,\underline{r}_n) \ \ , \ \ \underline{r}_i \equiv \begin{pmatrix} \cos\Delta Q_i & \sin\Delta Q_i \\ -\sin\Delta Q_i & \cos\Delta Q_i \end{pmatrix} \ . \tag{A.39}$$

An arbitrary vector $\vec{z} \in \mathbb{R}^{2n}$ can be written as $\vec{z}(\theta) = \underline{B}^{(1)}(\theta)\vec{x}(\theta)$ with some coefficient vector $\vec{x}(\theta)$. Since $\underline{B}^{(1)}(\theta)$ is symplectic, the inverse $\underline{A}^{(1)}(\theta) \equiv (\,\underline{B}^{(1)})^{-1}(\theta) = -\,\underline{J}\,\underline{B}^{(1)}(\theta)^{\mathrm{T}}\,\underline{J}$ always exists and is symplectic. Therefore the transformation $\vec{A}^{(1)} : \mathbb{R}^{2n+1} \to \mathbb{R}^{2n}$, $(\vec{z},\theta) \mapsto \vec{x} \equiv \underline{A}^{(1)}(\theta)\vec{z}$ to *linear real normal form coordinates* is a canonical transformation. In the normal form coordinates the flow is just a set of rotations, or in other words $\underline{T}$ restricted on the subspace spanned by $\vec{b}_{2i-1}$ and $\vec{b}_{2i}$ is a rotation by the angle ΔQ_i. Note that in the normal form coordinates the motion is fully decoupled. Moreover, the actions

$$J_i \equiv \frac{1}{2}(x_{2i-1}(\theta)^2 + x_{2i}(\theta)^2) \tag{A.40}$$

are invariants of the system and the angles

$$\Psi_i \equiv \arctan\left(\frac{x_{2i-1}(\theta)}{x_{2i}(\theta)}\right) \tag{A.41}$$

advance linearly with azimuth

$$\vec{\Psi}(\theta) = \vec{\Psi}_0 + (\theta - \theta_0)\,[\vec{Q}] \ . \tag{A.42}$$

The transformation $\vec{A}^{(2)}: \ \mathbb{R}^{2n} \to \mathbb{R}^n \times \mathbb{R}^{+,n}, \ \vec{x} \mapsto (\vec{\Psi}, \vec{J}) \equiv \vec{A}^{(2)}(\vec{x})$ is symplectic since its block diagonal Jacobian

$$\left(\partial_{\vec{x}}\, \vec{A}^{(2)\mathrm{T}}\Big|_{\vec{x}_0}\right)^{\mathrm{T}} = \underline{\mathrm{diag}}(\underline{A}_1^{(2)}, \ldots, \underline{A}_n^{(2)}) \tag{A.43a}$$

$$\underline{A}_i^{(2)} = \begin{pmatrix} \frac{x_{2i}}{x_{2i-1}^2 + x_{2i}^2} & -\frac{x_{2i-1}}{x_{2i-1}^2 + x_{2i}^2} \\ x_{2i-1} & x_{2i} \end{pmatrix} \tag{A.43b}$$

is a symplectic matrix. The inverse transformation $\vec{B}^{(2)} \equiv (\vec{A}^{(2)})^{-1}$

$$x_{2i-1} = \sqrt{2J_i}\sin\Psi_i \tag{A.44a}$$

$$x_{2i} = \sqrt{2J_i}\cos\Psi_i \tag{A.44b}$$

is not only symplectic but indeed periodic in the Ψ_i. Therefore the transformation $\vec{A} \equiv \vec{A}^{(2)} \circ \vec{A}^{(1)}$: $\mathbb{R}^{2n+1} \to \mathbb{R}^n \times \mathbb{R}^{+,n}, \ (\vec{z}, \theta) \mapsto \vec{A}^{(2)}(\,\underline{A}^{(1)}(\theta)\vec{z})$ is symplectic, since its Jacobian $\underline{A}(\vec{z}, \theta) = \underline{A}^{(2)}(\vec{x})\,\underline{A}^{(1)}(\theta)$ is. Also the inverse $\vec{B} = \vec{B}^{(1)} \circ \vec{B}^{(2)}$ is periodic in $\vec{\Psi}$ since $\vec{B}^{(2)}$ is periodic and $\vec{B}^{(1)}$ is linear in $\vec{x}$. Therefore we have proved the integrability of the system. $\Box$

Two remarks are now in order. First, the transformation $\vec{C}$ to *complex normal forms* can always be made if the flow is diagonalisable, which is true at least for non–degenerate eigenvalues — whether or not the eigenvalues are on the unit circle. In the case of a pair of eigenvalues $\lambda_i, 1/\lambda_i$ with $|\lambda_i| \neq 1$ one can then find real normal forms that transform under the one–turn map like a rotation combined with a dilation. One can even construct an action–angle pair $\tilde{J}_i = {}^1\!/_2(x_{2i-1}^2 - x_{2i}^2)$, $\widetilde{\Psi}_i = \mathrm{arctanh}({}^{x_{2i-1}}\!/_{x_{2i}})$ but the back transformation $\vec{B}^{(2)}$ is not periodic since the motion is unbounded. Second, although $\vec{B}$ is periodic in $\vec{\Psi}$, and the one–turn map of the original system $\underline{T}(\theta)$ is periodic in θ, the trajectories $\vec{\xi}(\theta)$ are generally *not* periodic in θ.

$$\vec{\xi}(\vec{z}_0; \theta + 2\pi N, \theta_0) = \underline{B}^{(1)}(\theta + 2\pi N)\vec{B}^{(2)}(\vec{\Psi}_0 + (\theta + 2\pi N - \theta_0)\,[\vec{Q}], \vec{J}_0) \tag{A.45a}$$

$$= \underline{B}^{(1)}(\theta)\vec{B}^{(2)}\left(\vec{\Psi}_0 + (\theta - \theta_0)\,[\vec{Q}] + 2\pi N[\vec{Q}], \vec{J}_0\right) \tag{A.45b}$$

which is equal to $\underline{B}^{(1)}(\theta)\vec{B}^{(2)}\left(\vec{\Psi}_0 + (\theta - \theta_0)\,[\vec{Q}], \vec{J}_0\right) \equiv \vec{\xi}(\vec{z}_0; \theta, \theta_0)$ for some $N = N_{\vec{k}}$ only if the tunes $[Q_i]$ are *commensurable with 1*, i.e.

$$\exists \vec{k} \in \mathbb{N}^n, \vec{k} \neq \vec{0} \ : \ \vec{k} \cdot [\vec{Q}] = 0 \bmod 1 \ . \tag{A.46}$$

The period is $2\pi N_{\vec{k}}$ with $N_{\vec{k}}$ being the least common multiple of the $\{l_i \equiv |\vec{k}_i|\}_{1 \leq i \leq n}$. The condition implied by equation (A.46) is called orbital resonance. If the orbital motion is *not* on resonance the motion is called *pseudo–periodic.*

A.1.3 Pseudo–periodic functions

Definition A.11 *We will call a function* $f: \ \mathbb{R} \to \mathbb{C}, \ \theta \mapsto f(\theta)$ *elementarily pseudo-periodic with tune* Q *if* $f(\theta + 2\pi) = e^{i2\pi Q} f(\theta)$ *for some arbitrary non–integer real* Q, *i.e. with* $[Q] \in (0, 1)$. *We call a vector function* $\vec{f}: \ \mathbb{R} \to \mathbb{C}^n, \ \theta \mapsto \vec{f}(\theta)$ *elementarily pseudo-periodic if all its components* f_i *are elementarily pseudo-periodic and the tunes are incommensurable.*

Since $g(\theta) \equiv e^{-iQ\theta} f(\theta)$ is 2π–periodic and therefore has a Fourier series decomposition $g(\theta) = \sum_{k=-\infty}^{\infty} f_k\, e^{ik\theta}$, one can decompose f into different harmonics.

Definition A.12 *For an elementarily pseudo–periodic f with tune Q we define the generalised Fourier series*

$$f(\theta) = \sum_{k=-\infty}^{+\infty} f_k\, e^{i(k+Q)\theta} \tag{A.47}$$

where the coefficients are given by

$$f_k = \frac{1}{2\pi} \int_0^{2\pi} f(\theta) e^{-i(k+Q)\theta}\, d\theta \quad . \tag{A.48}$$

Note that the Fourier monomials $e^{i(k+Q)\theta}$ for *different* Q are orthogonal over $\mathbb{R}$ but not over $[0, 2\pi]$ as in the case of $e^{ik\theta}$. Also note that the monomials $e^{i(k+Q)\theta}$ and $e^{i(k'+Q')\theta}$ are orthonormal in the sense that

$$\lim_{T\to\infty} \frac{1}{2T} \int_{-T}^{+T} e^{i(k+Q)\theta}\, e^{-i(k'+Q'))\theta}\, d\theta = \delta_{k+Q,k'+Q'} \tag{A.49}$$

where the Kronecker symbol $\delta_{x,y}$ is 1 for $x = y$ and 0 otherwise. Whereas the ordinary Fourier monomials $\{e^{ik\theta}\}_{k\in\mathbb{Z}}$ are a complete basis of the (integrable) 2π–periodic functions, the generalised monomials $\{e^{i(k+Q)\theta}\}_{k\in\mathbb{Z}}$ are a complete basis of the elementarily pseudo–periodic functions with tune Q.

In the following we will occasionally meet functions of the extended phase space $\vec{f}: \mathbb{C}^{2n} \times \mathbb{R} \to \mathbb{C}^m$, $(\vec{z}, \theta) \mapsto \vec{f}(\vec{z}, \theta)$ that are 2π–periodic in θ and analytic or even simple polynomials in $\vec{z}$. For a linear Hamiltonian integrable system there is a 2π–periodic canonical transformation matrix $\underline{C}$, as defined in the proof of theorem A.6, so that $\vec{z}(\theta) = \underline{C}(\theta)\vec{\xi}(\theta)$ with $\vec{\xi}(\theta) = (\xi_{0,1}e^{iQ_1\theta}, \ldots, \xi_{0,2n}e^{iQ_{2n}\theta})$ with $\xi_{0,2j-1} = \sqrt{J_j}e^{i\Psi_{j,0}} = \xi^*_{0,2j}$. The components of $\vec{\xi}$ are elementarily pseudo–periodic functions with tunes $\{q_i\}_{1\le i\le 2n}$. If the system is real, then the tunes can be ordered in pairs $Q_i \equiv q_{2i-1} = -q_{2i}$, $1 \le i \le n$. So the problem of finding the spectrum of the components of $\vec{z}$ boils down to finding the spectrum of a linear combination of elementarily pseudo–periodic functions. Let

$$\vec{z}(\theta) = \underline{C}(\theta)\vec{\xi}(\theta) \;\; , \;\; C_{ij}(\theta) = \sum_{\mu=-\infty}^{+\infty} C_{ij,\mu}\, e^{i\mu\theta} \;\; , \;\; \xi_j(\theta) = \xi_{0,j}\, e^{iq_j\theta} \quad . \tag{A.50}$$

Then we obtain for each component of $\vec{z}$

$$z_i(\theta) = \sum_{j=1}^{2n} \sum_{\mu=-\infty}^{+\infty} C_{ij,\mu}\xi_{0,j}\, e^{i(\mu+q_j)\theta} \equiv \sum_{j=1}^{2n} \sum_{\mu=-\infty}^{+\infty} z_{ij,\mu}(\vec{\xi}_0)\, e^{i(\mu+q_j)\theta} \tag{A.51}$$

where $q_{2i} = -q_{2i-1} = Q_i$, $1 \le i \le n$. We conclude that linear combinations of elementarily pseudo–periodic functions are generally not *elementarily* pseudo–periodic but contain *all* the q_i. Now let $\vec{f}^{(1)}$ be a linear form in $\vec{z}$ with a 2π–periodic matrix $\underline{F}$

$$\begin{aligned} \vec{f}^{(1)}(\theta) &= \underline{F}(\theta)\vec{z}(\theta) && \text{(A.52a)} \\ f_i^{(1)}(\theta) &= \sum_{j=1}^{2n} \sum_{\mu=-\infty}^{+\infty} F_{ij,\mu} \sum_{k=1}^{2n} \sum_{\nu=-\infty}^{+\infty} z_{jk,\nu}\, e^{i(\nu+\mu+q_k)\theta} \\ &= \sum_{k=1}^{2n} \sum_{\mu=-\infty}^{+\infty} \left(\sum_{j=1}^{2n} \sum_{\nu=-\infty}^{+\infty} F_{ij,\nu} z_{jk,\mu-\nu} \right) e^{i(\mu+q_k)\theta} \end{aligned}$$

$$\equiv \sum_{k=1}^{2n} \sum_{\mu=-\infty}^{+\infty} \tilde{f}_{ik,\mu}\, e^{i(\mu+q_k)\theta} \tag{A.52b}$$

$$\equiv \sum_{\vec{k}} \sum_{\mu=-\infty}^{+\infty} f_{i,\vec{k},\mu}\, e^{i(\mu+\vec{k}\cdot\vec{Q})\theta} \quad , \tag{A.52c}$$

with $\vec{k} \in \mathbb{Z}^n, |\vec{k}| = 1$ and provided that the sum in brackets converges. Now let $\vec{f}^{(2)}$ be quadratic in $\vec{z}$ with a periodic $\underline{\underline{F}}(\theta)$

$$\begin{aligned}
\vec{f}^{(2)}(\theta) &= \underline{\underline{F}}(\theta)\vec{z}(\theta)\vec{z}(\theta) && \text{(A.53a)}\\
f_i^{(2)}(\theta) &= \sum_{j=1}^{2n}\sum_{k=1}^{2n} F_{ijk} z_j z_k \\
&= \sum_{l,m=1}^{2n} \sum_{j,k=1}^{2n} \sum_{\mu=-\infty}^{+\infty} \sum_{\nu=-\infty}^{+\infty} \sum_{\rho=-\infty}^{+\infty} F_{ijk,\mu} z_{jl,\nu} z_{km,\rho}\, e^{i(\mu+\nu+\rho+q_l+q_m)\theta} \\
&= \sum_{l,m=1}^{2n} \sum_{\phi=-\infty}^{+\infty} \left(\sum_{j,k=1}^{2n} \sum_{\mu+\nu+\rho=\phi} F_{ijk,\mu} z_{jl,\nu} z_{km,\rho} \right) e^{i(\phi+q_l+q_m)\theta} \\
&\equiv \sum_{l,m=1}^{2n} \sum_{\phi=-\infty}^{+\infty} \tilde{f}_{ilm,\phi}\, e^{i(\phi+q_l+q_m)\theta} && \text{(A.53b)}\\
&\equiv \sum_{\vec{k}} \sum_{\mu=-\infty}^{+\infty} f_{i,\vec{k},\mu}\, e^{i(\mu+\vec{k}\cdot\vec{Q})\theta} \quad , && \text{(A.53c)}
\end{aligned}$$

with $\vec{k} \in \mathbb{Z}^n, |\vec{k}| = 0, 2$ and again provided that the sum over μ,ν and ρ converges. Therefore a quadratic form in $\vec{z}$ contains all integer combinations of order $|\vec{k}| = 0, 2$ of the tunes $\vec{Q}$. Similarly for every $\vec{f}^{(m)}$ which is m–multi–linear in $\vec{z}$ and has 2π–periodic coefficients we find

$$\begin{aligned}
f_i^{(m)}(\theta) &= \sum_{j_1,\ldots,j_m=1}^{2n} F_{ij_1\cdots j_m}(\theta) \prod_{l=1}^{m} z_{j_l}(\theta) && \text{(A.54a)}\\
&= \sum_{j_1,\ldots,j_m=1}^{2n} \sum_{\mu=-\infty}^{+\infty} \tilde{f}_{ij_1\cdots j_m,\mu}\, e^{i(\mu+\sum_{l=1}^{m} q_{j_l})\theta} && \text{(A.54b)}\\
&= \sum_{|\vec{k}|\le m} \sum_{\mu=-\infty}^{+\infty} f_{i,\vec{k},\mu}\, e^{i(\mu+\vec{k}\cdot\vec{Q})\theta} \quad . && \text{(A.54c)}
\end{aligned}$$

We can now define general pseudo–periodic functions over a *vector* of tunes.

Definition A.13 (Pseudo–periodic function) *Let $\vec{f} : \mathbb{R}^{n+1} \to \mathbb{R}^l$, $(\theta_1, \ldots, \theta_{n+1}) \mapsto \vec{f}(\theta_1, \ldots, \theta_{n+1})$ be 2π–periodic in the θ_i and the tunes $(Q_1, \ldots, Q_n)$ be incommensurable with 1. Then we call $\vec{g}$: $\mathbb{R} \to \mathbb{R}^l$, $\theta \mapsto \vec{f}(Q_1\theta, \ldots, Q_n\theta, \theta)$ pseudo-periodic with the tunes $(Q_1, \ldots, Q_n)$.*

It is clear that if the tunes are commensurable with 1, $\vec{g}$ is periodic rather then pseudo–periodic. If $\vec{f}(\vec{\xi}, \theta)$ is a function of the normal form coordinates $\vec{\xi}$ and the azimuth θ, then the function $\tilde{f}_{\vec{\xi}_0}(\theta_1, \ldots, \theta_n, \theta) \equiv \vec{f}(\xi_{0,1}e^{i\theta_1}, \xi_{0,2}e^{-i\theta_1}, \ldots, \xi_{0,2n-1}e^{i\theta_n}, \xi_{0,2n}e^{-i\theta_n}, \theta)$ generates a pseudo–periodic function $\vec{g}_{\vec{\xi}_0}(\theta) \equiv \tilde{f}_{\vec{\xi}_0}(Q_1\theta, \ldots, Q_n\theta, \theta)$.

Theorem A.7 *Let $(\mathcal{P}^\star, H)$ be real, linear and integrable with tunes $\vec{Q} \in \mathbb{R}^n$ incommensurable with 1. If $\vec{f} : \mathcal{P}^\star \subset \mathbb{C}^l \times \mathbb{R} \to \mathbb{C}^{2n}$, $(\vec{\xi}, \theta) \mapsto \vec{f}(\vec{\xi}, \theta)$ is analytic in the complex normal form coordinates $\vec{\xi}$ around the origin $\vec{\xi} = \vec{0}$ and 2π–periodic in θ, bounded and piecewise continuous in θ, i.e. the Taylor coefficients are 2π–periodic, then there exists a domain $\mathcal{D} \subseteq \mathcal{P}$ with $\vec{0} \in \mathcal{D}$ such that the pseudo–periodic function $\vec{g}_{\vec{\xi}_0} : \mathbb{R} \to \mathbb{C}^l$, $(\vec{J}, \vec{\Psi}_0, \theta) \mapsto \vec{f}(\sqrt{J_1} e^{+i(\Psi_{0,1}+Q_1\theta)}, \sqrt{J_1} e^{-i(\Psi_{0,1}+Q_1\theta)} \ldots, \theta)$ can be decomposed into a generalised Fourier series*

$$\vec{g}_{\vec{\xi}_0}(\theta) = \sum_{\vec{k}\in\mathbb{Z}^n} \sum_{k_0=-\infty}^{+\infty} \vec{g}_{k_0,\vec{k}}\, e^{i(k_0+\vec{k}\cdot\vec{Q})\theta} \tag{A.55}$$

with

$$\vec{g}_{k_0,\vec{k}} = \lim_{T\to\infty} \frac{1}{2T} \int_{-T}^{+T} \vec{g}_{\vec{\xi}_0}(\theta)\, e^{-i(k_0+\vec{k}\cdot\vec{Q})\theta}\, d\theta \tag{A.56}$$

for $\vec{z}(\vec{\xi}_0) \in \mathcal{D}$

There is an open ball $\mathcal{B} \equiv \{\vec{\xi} : \|\vec{\xi}\| < a, a > 0\}$ such that for $\vec{\xi} \in \mathcal{B}$ the Taylor series

$$\vec{f}(\vec{\xi}, \theta) = \sum_{\vec{l}\in\mathbb{N}^{2n}} \vec{F}_{\vec{l}}(\theta)\, \vec{\xi}^{\vec{l}} \;\; , \;\; \vec{\xi}^{\vec{l}} \equiv \prod_{i=1}^{2n} \xi_i^{l_i} \tag{A.57}$$

converges absolutely and uniformly. In the complex normal form coordinates the motion is described by a uniform rotation in phase space and therefore $\vec{\xi}(\theta)$ stays in $\mathcal{B}$ whenever $\vec{\xi}_0 \in \mathcal{B}$. For this paragraph we define $\vec{Q}^\pm \equiv (+Q_1, -Q_1, \ldots, +Q_n, -Q_n)$. The normal form trajectory $\vec{\xi}(\vec{\xi}_0; \theta) = \exp(i\, \underline{\mathrm{diag}}(\vec{Q}^\pm)\theta)\vec{\xi}_0$ is elementarily pseudo–periodic with $\vec{Q}^\pm$. Therefore the (scalar) monomials

$$\vec{\xi}^{\vec{l}}(\vec{\xi}_0; \theta) = e^{i\theta\vec{l}\cdot\vec{Q}^\pm} \prod_{i=1}^{2n} \xi_{0,i}^{l_i} \tag{A.58}$$

are elementarily pseudo–periodic with tune $\vec{k}'(\vec{l}) \cdot \vec{Q}$ where $\{k'_i(\vec{l}) = l_{2i-1} - l_{2i}\}_{1\le i\le n}$. The Fourier integral $\vec{g}_{k_0,\vec{k}}$ as in equation (A.56) exists since $\vec{g}$ and the generalised Fourier monomials are bounded and piecewise continuous. The corresponding integral for $\vec{F}_{\vec{l}}(\theta)\, \vec{\xi}^{\vec{l}}$ exists because of the same argument. Moreover the Taylor series converges absolutely and uniformly in $\mathcal{B}$ so that we can interchange integration and summation. The generalised Fourier monomials are orthonormal for incommensurable tunes and hence the $e^{-i(k_0+\vec{k}\cdot\vec{Q})\theta}$ in (A.55) projects out a sub series of the Taylor series of $g_{\vec{\xi}_0}$

$$\vec{g}_{k_0,\vec{k}} = \lim_{T-\infty} \frac{1}{2T} \int_{-T}^{+T} \vec{G}_{\vec{k}}(\theta)\, e^{-ik_0\theta}\, d\theta \;\; , \;\; \vec{G}_{\vec{k}}(\theta) \equiv \sum_{\vec{k}'(\vec{l})=\vec{k}} \vec{F}_{\vec{l}}(\theta) \vec{\xi}_0^{\vec{l}} \;\; . \tag{A.59}$$

Since the series (A.57) converges absolutely, $\vec{G}_{\vec{k}}(\theta)$ is well defined. The series

$$\widetilde{G}_{\vec{k}}(\theta) \equiv \sum_{k_0=-\infty}^{+\infty} \vec{g}_{k_0,\vec{k}}\, e^{ik_0\theta} \tag{A.60}$$

converges in the quadratic mean to $\vec{G}_{\vec{k}}(\theta)$, i.e. $\widetilde{G}_{\vec{k}}$ and $\vec{G}_{\vec{k}}$ are the same except for a set of zero measure. Since the union of countably many sets of zero measure has zero measure, the series

$$\tilde{g}(\theta) \equiv \sum_{\vec{k}\in\mathbb{Z}^n} \widetilde{G}_{\vec{k}}(\theta)\, e^{i\vec{k}\cdot\vec{Q}} \tag{A.61}$$

converges in the quadratic mean to $\vec{g}_{\vec{\xi}_0}$. Finally we set $\mathcal{D} = \vec{C}^{-1}(\mathcal{B}, 0)$ where $\vec{C}$ is the normal form transformation and have proved that $\vec{g}_{\vec{\xi}_0}$ can be expanded in a generalised Fourier series with coefficients $\vec{g}_{k_0,\vec{k}}$ as in (A.55) and (A.56). □

In integrable Hamiltonian systems we can replace the average over the surface of a torus $\mathcal{T}^n$ with incommensurable tunes by the long term average along a trajectory with arbitrary $\vec{\Psi}_0$.

Theorem A.8 *[VA88] Let $f : \mathcal{T}^n \to \mathbb{K}$ be bounded and piecewise continuous and $\vec{\Psi}(\theta) = \vec{Q}(\vec{J})\theta$ with incommensurable tunes $\vec{Q}$ then*

$$(2\pi)^{-n} \int_{\mathcal{T}^n} f(\vec{\Psi})\, d\vec{\Psi}^n = \lim_{T\to\infty} \frac{1}{T} \int_0^T f(\vec{\Psi}_0 + \theta\vec{Q})\, d\theta \ . \tag{A.62}$$

A proof for this theorem is in [VA88]

A.1.4 Averaging of perturbations

We will now consider the effect of small perturbations on integrable Hamiltonian systems and find approximate solutions by the method of averaging. We suppose that the unperturbed Hamiltonian H_0 has already been transformed to action–angle variables in a phase space $\mathcal{P} = \mathcal{T}^n \times \mathbb{R}^n$. The perturbed Hamiltonian H is given by

$$H(\vec{J}, \vec{\Psi}, \epsilon) = H_0(\vec{J}) + \epsilon H_1(\vec{J}, \vec{\Psi}, \epsilon) \tag{A.63}$$

where we will generally assume the parameter ϵ to be small. It is clear from the definition of $\mathcal{P}$ that H_1 has to be periodic in $\vec{\Psi}$. The EOM are

$$\mathrm{D}_\theta\, \vec{\Psi} = \vec{Q}(\vec{J}) + \epsilon\partial_{\vec{J}} H_1(\vec{J}, \vec{\Psi}, \epsilon) \tag{A.64a}$$
$$\mathrm{D}_\theta\, \vec{J} = -\epsilon\partial_{\vec{\Psi}}\, H_1(\vec{J}, \vec{\Psi}, \epsilon) \ . \tag{A.64b}$$

Note that although the perturbation in the above system is autonomous, we can easily include non–autonomous systems with $H_1(\vec{\Psi}, \vec{J}, \theta, \epsilon)$ being 2π–periodic in θ. We define $\vec{J}' \equiv (\vec{J}, J_\theta)$, $\vec{Q}' \equiv (\vec{Q}, 1)$ and $\vec{\Psi}' \equiv (\vec{\Psi}, \vec{\Psi}_\theta \equiv \theta)$, and therefore obtain a system in the standard form of equations (A.64a), (A.64b) with two extra EOM $\mathrm{D}_\theta\, \Psi_\theta = 1$ and $\mathrm{D}_\theta\, J_\theta = -\epsilon\partial_\theta\, H_1$.

In the unperturbed system $\epsilon = 0$ the actions are constant and the angles are linear in θ. The main idea of averaging is to approximate the above system by replacing equation (A.64b) with the averaged equation

$$\mathrm{D}_\theta\, \vec{K} = -\epsilon\vec{F}(\vec{K}) \ \ , \ \ \vec{F}(\vec{K}) \equiv (2\pi)^{-n} \int_{\mathcal{T}^n} \partial_{\vec{\Psi}}\, H_1(\vec{K}, \vec{\Psi}, 0)\, d\vec{\Psi}^n \ \ , \tag{A.65}$$

which is considerably simpler since the new variable $\vec{K}$ is actually constant:

Theorem A.9 *In the averaged system of equation (A.65) $\vec{K}$ is constant.*

The proof, as in [ems3] is easy. When calculating the integral of each of the $\partial_{\Psi_i} H_1$ over the torus $\mathcal{T}^n$ we can first integrate over Ψ_i :

$$\int_0^{2\pi} \partial_{\Psi_i} H_1\, d\Psi_i = H_1(\vec{K}, \Psi_1, \ldots, \Psi_i = 2\pi, \ldots, \Psi_n, 0) - H_1(\vec{K}, \Psi_1, \ldots, \Psi_i = 0, \ldots, \Psi_n, 0) = 0 \ \ , \tag{A.66}$$

since H_1 is 2π–periodic in each Ψ_i. □

In systems $\mathrm{D}_\theta\, \vec{\Psi} = \vec{Q}(\vec{J}) + \epsilon\vec{g}(\vec{J}, \vec{\Psi}, \epsilon)$, $\mathrm{D}_\theta\, \vec{J} = \epsilon\vec{f}(\vec{J}, \vec{\Psi}, \epsilon)$ where the perturbations are not Hamiltonian the theorem does not hold, but still the EOM in the averaged system are much simplified since the new "slow" variables $\vec{K}$ are decoupled from the "fast" variables $\vec{\Psi}$. It is clear that the combined system of equations (A.64a),(A.65) is generally *not* Hamiltonian any more. However Kolmogorov, Arnold and Moser [ems3] have developed a method of successively applying canonical changes of coordinates $(\vec{J}_i, \vec{\Psi}_i, H_0^{(i)}, H_1^{(i)}) \to (\vec{J}_{i+1}, \vec{\Psi}_{i+1}, H_0^{(i+1)}, H_1^{(i+1)})$, $(\vec{J}_0, \vec{\Psi}_0, H_0^{(0)}, H_1^{(0)}) \equiv (\vec{J}, \vec{\Psi}, \vec{J}, H_0, H_1)$ so that in the n-th step the Hamiltonian is

$$H^{(n)}(\vec{J}_n, \vec{\Psi}_n, \epsilon) \equiv H_0^{(n)}(\vec{J}_n) + \epsilon^{2^n} H_1^{(n)}(\vec{J}_n, \vec{\Psi}_n, \epsilon) \tag{A.67}$$

in the case of strongly incommensurable $\vec{Q}(\vec{J})$.

For $\partial_{\vec{J}} \vec{Q}^{\mathrm{T}} = \underline{0}$, i.e. for linear systems and strongly incommensurable $\vec{Q}$ the difference between the original slow variables $\vec{J}$ and the averaged slow variables $\vec{K}$ is bounded over intervals $\Delta\theta < 1/\epsilon$.

Theorem A.10 *If the tunes $\vec{Q}$ of the unperturbed motion are independent of $\vec{J}$ and strongly incommensurable, the perturbation is analytic in its variables, periodic in θ (but not necessarily Hamiltonian) and if $\vec{J}(\theta_i) = \vec{K}(\theta_i)$, then there is a $c > 0$ such that*

$$|\vec{J}(\theta_f) - \vec{K}(\theta_f)| < c\epsilon, \quad 0 \le \theta_f - \theta_i \le 1/\epsilon \ . \tag{A.68}$$

For the proof, as given in [ems3], we start with a change of variables $(\vec{J}, \vec{\Psi}) \to (\vec{K}, \vec{\Phi})$ defined by a formal series of which we will only need terms up to $O(\epsilon)$. This proof includes a description of the complete procedure of first order canonical perturbation theory. The EOM in the old variables are

$$\begin{aligned} \mathrm{D}_\theta \vec{J} &= \epsilon \vec{f}(\vec{J}, \vec{\Psi}, \epsilon) = \epsilon \vec{f}(\vec{J}, \vec{\Psi}, 0) + O(\epsilon^2) \\ \mathrm{D}_\theta \vec{\Psi} &= \vec{Q} + \epsilon \vec{g}(\vec{J}, \vec{\Psi}, \epsilon) = \vec{Q} + \epsilon \vec{g}(\vec{J}, \vec{\Psi}, 0) + O(\epsilon^2) \ . \end{aligned} \tag{A.69}$$

We choose an ansatz for the change of variables analytic in ϵ and close to a unit transform

$$\begin{aligned} \vec{J} &= \vec{K} + \epsilon \vec{u}(\vec{K}, \vec{\Phi}) + O(\epsilon^2) \\ \vec{\Psi} &= \vec{\Phi} + \epsilon \vec{v}(\vec{K}, \vec{\Phi}) + O(\epsilon^2) \ . \end{aligned} \tag{A.70}$$

The ansatz for the EOM in the new variables which is constructed to contain the new fast variable $\vec{\Phi}$ only in $O(\epsilon^2)$ is

$$\begin{aligned} \mathrm{D}_\theta \vec{K} &= \epsilon \vec{F}(\vec{K}) + O(\epsilon^2) \\ \mathrm{D}_\theta \vec{\Phi} &= \vec{Q} + \epsilon \vec{G}(\vec{K}) + O(\epsilon^2) \ . \end{aligned} \tag{A.71}$$

Taking the derivative of the transformation (A.70), inserting the transformation into the EOM (A.69) and keeping only terms up to $O(\epsilon)$ we obtain up to first order in ϵ

$$\begin{aligned} \epsilon \vec{f}(\vec{K}, \vec{\Phi}, 0) &=_1 \mathrm{D}_\theta \vec{K} + \epsilon \left((\partial_{\vec{K}} \vec{u}^{\mathrm{T}})^{\mathrm{T}} \mathrm{D}_\theta \vec{K} + (\partial_{\vec{\Phi}} \vec{u}^{\mathrm{T}})^{\mathrm{T}} \mathrm{D}_\theta \vec{\Phi} \right) \\ \vec{Q} + \epsilon \vec{g}(\vec{K}, \vec{\Phi}, 0) &=_1 \mathrm{D}_\theta \vec{\Phi} + \epsilon \left((\partial_{\vec{K}} \vec{v}^{\mathrm{T}})^{\mathrm{T}} \mathrm{D}_\theta \vec{K} + (\partial_{\vec{\Phi}} \vec{v}^{\mathrm{T}})^{\mathrm{T}} \mathrm{D}_\theta \vec{\Phi} \right) \ . \end{aligned} \tag{A.72}$$

Finally by inserting the ansatz for the new EOM into equation (A.72) and again disregarding terms in $O(\epsilon)$ we get the following relations:

$$\begin{aligned} \vec{F}(\vec{K}) &= \vec{f}(\vec{K}, \vec{\Phi}, 0) - (\partial_{\vec{\Phi}} \vec{u}^{\mathrm{T}}(\vec{K})^{\mathrm{T}}, \vec{\Phi}) \, \vec{Q} \\ \vec{G}(\vec{K}) &= \vec{g}(\vec{K}, \vec{\Phi}, 0) - (\partial_{\vec{\Phi}} \vec{v}^{\mathrm{T}})^{\mathrm{T}}(\vec{K}, \vec{\Phi}) \, \vec{Q} \ . \end{aligned} \tag{A.73}$$

To solve the equation (A.73) we make use of the periodicity *and* analyticity of $\vec{f}$ and $\vec{g}$. We define the Fourier coefficients $\vec{h}_0$ and $\vec{h}_{\vec{l}}$ for $\vec{h}$ representing either $\vec{f}$ or $\vec{g}$, so that

$$\vec{h}(\vec{K}, \vec{\Phi}) = \vec{h}_0(\vec{K}) + \sum_{\vec{l} \in \mathbb{Z}, \vec{l} \neq \vec{0}} \vec{h}_{\vec{l}}(\vec{K}) e^{i\vec{l}\cdot\vec{\Phi}} \ . \tag{A.74}$$

Moreover we define

$$\vec{A}_h \equiv \vec{h}_0(\vec{K}) \qquad \text{(the average of } \vec{h} \text{ w.r.t } \vec{\Phi}) \tag{A.75a}$$

$$\vec{I}_h \equiv \sum_{\vec{l}\in\mathbb{Z},\vec{l}\neq\vec{0}} \frac{\vec{h}_{\vec{l}}}{i\,\vec{l}\cdot\vec{Q}}\, e^{i\vec{l}\cdot\vec{\Phi}} \quad \text{(the incomplete integral of } \vec{h} \text{ w.r.t. } \vec{\Phi}). \tag{A.75b}$$

The tunes are assumed to be incommensurable. Therefore the denominators in the series I_f and I_g cannot identically vanish. Since $\vec{f}$ and $\vec{g}$ are analytic functions of $\vec{\Phi}$, their Fourier coefficients $\vec{f}_{\vec{l}}$ and $\vec{g}_{\vec{l}}$ decay [LM88] exponentially with $|\vec{l}|$, i.e. $\|\vec{f}_{\vec{l}}\|, \|\vec{g}_{\vec{l}}\| < c_{f,g}e^{-r_{f,g}|\vec{l}|}$. The tunes are *strongly* incommensurable. Hence the denominators decay only like a power of $|\vec{l}|$. Therefore the series expansions of I_f and I_g converge. One easily verifies that

$$(\partial_{\vec{\Phi}}\, \vec{I}_h^{\mathrm{T}})^{\mathrm{T}}\, \vec{Q} = \vec{h} - \vec{A}_h \ . \tag{A.76}$$

We can now solve equation (A.73) to give $\vec{F}$ and $\vec{G}$ independent of $\vec{\Psi}$

$$\vec{F}(\vec{K}) = A_{\vec{f}(\vec{K},\vec{\Phi},0)} \quad , \quad \vec{G}(\vec{K}) = A_{\vec{g}(\vec{K},\vec{\Phi},0)} \tag{A.77a}$$

$$\vec{u}(\vec{K},\vec{\Phi}) = I_{\vec{f}(\vec{K},\vec{\Phi},0)} \quad , \quad \vec{v}(\vec{K},\vec{\Phi}) = I_{\vec{g}(\vec{K},\vec{\Phi},0)} \ . \tag{A.77b}$$

Therefore we have obtained a change in variables that transforms the exact EOM to the averaged EOM (A.71) plus a perturbation of $O(\epsilon^2)$ (A.70) and that differs from the unit transform by a quantity of $O(\epsilon)$. Over an interval $\Delta\theta \le 1/\epsilon$ the deviation of the value of the slow variable $\vec{K}$ from the its value in the unperturbed averaged system is at most of $O(\epsilon)$. The inverse transformation differs from unity by a quantity of $O(\epsilon)$ Hence $|\vec{J}(\theta_f) - \vec{K}(\theta_f)| < c\epsilon$ over $\Delta\theta \le 1/\epsilon$. This proves the theorem. □

Note that $\mathrm{D}_\theta\, \vec{K} = \epsilon A_{\vec{f}(\vec{K},\vec{\Phi},0)}$ is up to $O(\epsilon^2)$ the averaged system that we wanted.

For non–linear integrable systems $\partial_{\vec{J}}\vec{Q}^{\mathrm{T}} \neq \underline{0}$ and thus the incommensurability condition cannot hold for all values of $\vec{Q}$. The tori where the tunes are incommensurable are called *non–resonant*. The behaviour of the perturbed actions $\vec{J}$ is described by Kolmogorov's theorem.

Definition A.14 *An integrable system is called non–degenerate if the tunes are functionally independent, i.e.*

$$\det\left(\partial_{\vec{J}}\vec{Q}^{\mathrm{T}}\right) \equiv \det\left(\partial_{\vec{J}}\partial_{\vec{J}}^{\mathrm{T}}\, H_0\right) \neq 0 \ . \tag{A.78}$$

It is called isoenergetically non–degenerate if

$$\det\begin{pmatrix} \partial_{\vec{J}}\vec{Q}^{\mathrm{T}} & \vec{Q} \\ \vec{Q}^{\mathrm{T}} & 0 \end{pmatrix} \neq 0 \tag{A.79}$$

In a non–degenerate system the non–resonant tori form a set of full Lebesgue measure on $\{\vec{J}\} \subset \mathbb{R}^n$. Without proof I give here a version of Kolmogorov's theorem [ems3].

Theorem A.11 (Kolmogorov's theorem) *If the unperturbed system is non–degenerate or isoenergetically non–degenerate, then for a sufficiently small Hamiltonian perturbation "most" non–resonant tori do not vanish even on long scales $\Delta\theta$ but are only slightly deformed, so that in the phase space of the perturbed system there are invariant tori densely filled with pseudo–periodic trajectories winding around them with incommensurable tunes. "Most" tori means that the Lebesgue measure of the complement of their union is small when the perturbation is small. In the case of isoenergetically non–degenerate systems the measure has to be taken w.r.t. each submanifold* $H = \mathrm{const.}$.

A.1.5 Adiabatic invariants

We have seen that in the case of a linearly integrable system with perturbations periodic in θ the actions of the unperturbed system change by only $O(\epsilon)$ over time scales of $O(1/\epsilon)$. Now we will touch on the case where we have a Hamiltonian $H(\vec{z},\lambda)$ where the parameter λ is a slowly varying, generally non–periodic, function $\lambda:\ \mathcal{L}\subseteq\mathbb{R}\to\mathbb{R},\ \theta\mapsto\lambda(\epsilon\theta)$. For simplicity we set $\theta_i\equiv 0$.

Definition A.15 (Adiabatic invariance) *A function $I:\ \mathcal{P}\times\mathbb{R}\to\mathbb{K},\ (\vec{z},\lambda)\mapsto I(\vec{z},\lambda)$ is called an adiabatic invariant if there is some positive constant c such that for an arbitrary trajectory $\vec{\xi}(\vec{z}_0;\theta)$*

$$|I(\vec{\xi}(\vec{z}_0;\theta),\lambda(\epsilon\theta))-I(\vec{z}_0,\lambda(0))|<c\epsilon \quad \text{for}\quad 0\le\theta<{}^1/_\epsilon\ . \tag{A.80}$$

We call the function I an almost adiabatic invariant if for each $\kappa>0$ the Lebesgue measure of the set of initial conditions $\vec{z}$ for which the variation of I along a trajectory exceeds κ over a time scale ${}^1/_\epsilon$ tends to 0 as ϵ tends to 0.

We assume now that the Hamiltonian system is integrable for *all* fixed $\lambda(\epsilon\theta)$ with $\theta\in\mathcal{L}$ and has the form

$$H(\vec{z},\lambda(\epsilon\theta))=H_0(\vec{J},\lambda(0))+\epsilon H_1(\vec{\Psi},\vec{J},\lambda(\epsilon\theta))\ , \tag{A.81}$$

where H_1 is periodic in $\vec{\Psi}$ so that averaging can be applied. As we have seen above the actions are constant in the averaged system. I will now without proof state two theorems [ems3]

Theorem A.12 *If the Hamiltonian system (A.81) is non–degenerate, then the action variables $\vec{J}$ are almost adiabatic invariants*

Theorem A.13 *If H_0 in the Hamiltonian system (A.81) is linear, i.e. $\partial_{\vec{J}}\vec{Q}^{\mathrm{T}}=\underline{0}$ and if the tunes $Q_i(\lambda(\epsilon\theta))\neq 0$ are distinct for all $\theta\in\mathcal{L}$, then there are as many independent adiabatic invariants as there are degrees of freedom. The adiabatic invariants are quadratic functions of the $z_i(\theta)$ whose coefficients depend on λ and are 2π–periodic in θ.*

A.2 Application to circular accelerators

In circular accelerators the particles are guided around the ring by electric and magnetic fields. In particular, dipole fields keep the particles on globally circular orbits and combinations of focusing and defocusing quadrupoles ensure that the beam cross section remains bounded. Acceleration and longitudinal stability is provided by time dependent electromagnetic fields in RF cavities. In addition to these "design" fields there are non-negligible field errors due to positional misalignment, iron yoke saturation, field nonlinearities etc. Thus correction coils and extra multipole fields are provided for corrective beam steering and correction of higher order effects. This thesis covers only effects of spin–orbit motion related to the unperturbed particle motion in a machine without any misalignment and field errors. The closed trajectory of the *reference particle* in storage mode, i.e. the trajectory of a particle with just the right momentum and initial conditions to be a fixed point of the unperturbed one–turn map is called the *design orbit.* The Lagrangian for a relativistic particle with charge e and rest mass m, using time in the laboratory frame t, the 3–vectors $\vec{r}$ and $\vec{\beta}\equiv\mathrm{D}_t\,\vec{r}$, and the scalar and vector potentials ϕ and $\vec{A}$ is [HG89, HM96]

$$L(\vec{r},\vec{\beta},t)=-m\sqrt{1-\|\vec{\beta}\|^2}-e\left(\phi(\vec{r},t)-\vec{\beta}\cdot\vec{A}(\vec{r},t)\right)\quad . \tag{A.82}$$

This Lagrangian can be transformed to the curvilinear coordinate system [HR87, GH94, GH99b, CW98] introduced in chapter 2. Then the Hamiltonian is generated by $\tilde{H}(\vec{q},\vec{p},t)=[\vec{\beta}\cdot\vec{p}-L(\vec{r},\vec{\beta},t)]\circ$

$[\vec{r}, \vec{\beta}](\vec{q}, \vec{p})$. A change of variables [CS58, BH94a, MB90, HM96] leads to the Hamiltonian $H(\vec{z}, \theta)$ in its standard form in the field of accelerator physics, where $\vec{z}$ is defined in equation (2.6) and θ is the generalised azimuth. The Hamiltonian is origin preserving and has a critical point at $\vec{z} = \vec{0}$, i.e. $H(\vec{0}, \theta) = 0$ and $\partial_{\vec{z}} H(\vec{0}, \theta) = \vec{0}\ \forall\theta$ so that $\vec{z} = \vec{0}$ is a closed periodic solution. The coordinates $\vec{z}$ can normally be regarded as small so that terms of higher order in $\vec{z}$ have less impact on particle motion then low order terms. Nevertheless higher order terms can significantly decrease the dynamic aperture (section A.1.2) so that the *life time* of a particle with a sufficiently large orbital amplitude is small.

The methods developed in section A.1 can be directly applied to the Hamiltonian system defined by $(\mathcal{P}^\star, H(\vec{z}, \theta))$ with $(\vec{0}, \theta) \in \mathcal{P}^\star \subseteq \mathbb{R}^6\ \forall\theta$.

A.2.1 Hill's equation and Courant–Snyder parameters

In this section we will analyse the linear transverse motion in the absence of coupling of the transverse planes and for a particle with $\delta = \tau = 0$. We only have to take into account the effects of dipoles and quadrupoles. In the fully decoupled case the linearised EOM for (x, a) and (y, b) are analogous. The second order equation of motion for x is

$$\mathrm{D}_{\theta\theta}\, x + k(\theta) x = 0 \tag{A.83}$$

where $k \equiv \frac{L^2}{4\pi^2}(K + \kappa^2)$, $K = e/p_0 \partial_x B_y$ is the field gradient normalised by the magnetic rigidity of the reference particle, κ is the horizontal curvature κ_x defined in equation (2.7), and k is periodic $k(\theta + 2\pi) = k(\theta)$. This type of oscillator equation with periodically varying k is called *Hill's equation*. We will only treat the case of horizontal motion here and note that we can obtain the vertical EOM from the horizontal by replacing K with $-K$ as dictated by the Maxwell's equations and take $\kappa = \kappa_y$ instead of $\kappa = \kappa_x$. In a flat unperturbed ring κ_y vanishes identically. The canonical version of (A.83) is

$$\mathrm{D}_\theta \begin{pmatrix} x \\ a \end{pmatrix} = \begin{pmatrix} 0 & \frac{L}{2\pi} \\ -\frac{2\pi}{L} k(\theta) & 0 \end{pmatrix} \begin{pmatrix} x \\ a \end{pmatrix} \tag{A.84}$$

and this has a principal solution of the Floquet type (A.30). We note that x and $\mathrm{D}_\theta\, x$ have the dimension of a length whereas a and $\mathrm{D}_\theta\, a$ are dimensionless. The factors $L/(2\pi)$ and $2\pi/L$ are caused by $\mathrm{D}_\theta = (2\pi/L)\mathrm{D}_s$ where s is the arc length of the reference trajectory. The next step would be to perform one more canonical transformation with multiplier $2\pi/L$ to change from $\vec{z} = (x, a, y, b, \tau, \delta)$ to the dimensionless phase space vector $\tilde{z} \equiv (\tilde{x} \equiv (2\pi/L)x, a, \tilde{y} \equiv (2\pi/L)y, b, \tilde{\tau} \equiv (2\pi/L)\tau, \delta)$. Moreover the statement whether or not a quantity is "small" makes only sense for a dimensionless quantity. Here $\Lambda = 2\pi/L$ has been used to obtain a transparent connection between the formalism used in this section and the standard formalism of accelerator physics in which the arc length s is taken as the independent variable instead of θ. But in principle one has to introduce a *physical* scale Λ with the same dimension first. Then $\tilde{x} \equiv x/\Lambda$ is dimensionless and thus independent of the system of units used. In order for the truncated Taylor expansion of the EOM in the coordinates to make sense, the physical scale Λ has to be chosen so that for $x \ll \Lambda$ the contributions of higher order neglected terms in x are small compared to the terms included into the truncated expansion. The results presented in this section were obtained with x, y, τ, β and D having the dimension of a length whereas a, b, δ, θ, α and being dimension less and with γ having the dimension of an inverse length. The quantities β, α, γ and D are to be defined later. Either changing from θ to s or performing the scale transform $\vec{z} \mapsto \tilde{z}$ defined above would eliminate the many factors $(2\pi/L)^n$ and reduce the formulae to their standard forms well known in accelerator physics.

We will assume that the linear motion is bounded and treat it in a way [HW93a] that is slightly different to the methods described in section A.1 but introduces the *Courant–Snyder functions*. Inserting the ansatz

$$x(\theta) = \sqrt{\tilde{\varepsilon}\beta(\theta)} \cos(\psi(\theta) - \psi_0) \quad , \tag{A.85}$$

where β is assumed positive and 2π–periodic and $\tilde{\varepsilon}$ is some positive constant, into equation (A.83) we obtain two conditions

$$\begin{aligned} \beta'\psi' + \beta\psi'' \equiv (\beta\psi')' &= 0 && \text{(A.86a)} \\ \beta\beta'' - 1/2\beta'^2 - 2\beta^2\psi'^2 + 2\beta^2 k &= 0 && \text{(A.86b)} \end{aligned}$$

where $'$ denotes differentiation w.r.t. θ. Equation (A.86a) can formally be integrated giving

$$\psi(\theta) - \psi_0 = \int_{\theta_0}^{\theta} \frac{cL}{2\pi\beta(\theta)} d\theta \tag{A.87}$$

with some positive constant c which is normally chosen to be 1. Choosing $c = 1$ is an arbitrary normalisation condition on β that fixes $\tilde{\varepsilon}$ as a function of $x(\theta_0)$. Inserting (A.87) into equation (A.86b) we finally obtain a non–linear second order differential equation for β

$$\frac{1}{2}\beta\beta'' - \frac{1}{4}\beta'^2 + \beta^2 k = \frac{L^2}{4\pi^2} \ . \tag{A.88}$$

Introducing $\alpha \equiv -\beta'\pi/L$ and $\gamma \equiv (1+\alpha^2)/\beta$ we can rewrite equation (A.88) as

$$\alpha' \frac{L}{2\pi} = k\beta - \frac{L^2}{4\pi^2}\gamma \ . \tag{A.89}$$

The functions β, α and γ are called the *Courant–Snyder functions* of the lattice. The ansatz (A.85) is consistent for the real coordinate x only if β, once chosen positive at θ_0, can never change its sign. Inserting $f(\theta) = \sqrt{\beta(\theta)2\pi/L}$ into equation (A.86b) we find

$$f'' + kf - \frac{1}{f^3} = 0 \ . \tag{A.90}$$

Now let $1/\sqrt[4]{k} \gg f_0 > 0$ and the derivative $g \equiv f'$ with $g_0 \equiv f_0' < 0$ be finitely negative. Then $g' = 1/f^3 + O(f) > 0$ for sufficiently small $|f|$ and it approaches infinity as f approaches 0. Since g_0 was assumed finitely negative, g changes sign before f approaches 0. Hence f and therefore β with $f_0 \equiv \sqrt{2\pi/L\beta_0} > 0$ does not change sign.

In general one cannot solve equation (A.88) analytically but with the help of the *Courant–Snyder functions* one can elegantly parametrise the trajectory (A.85), the flow and the integral of motion $\tilde{\varepsilon}$. By introducing

$$c \equiv \frac{x_i}{\sqrt{\beta_i}} \ , \quad s \equiv a_i\sqrt{\beta_i} + \frac{x_i\alpha_i}{\sqrt{\beta_i}} \quad \Rightarrow \quad x(\theta) = c\sqrt{\beta}\cos\psi + s\sqrt{\beta}\sin\psi \tag{A.91}$$

and by setting $\Delta = \psi_f - \psi_i$ we obtain

$$\begin{pmatrix} x_f \\ a_f \end{pmatrix} = \begin{pmatrix} \sqrt{\frac{\beta_f}{\beta_i}}(\cos\Delta + \alpha_i\sin\Delta) & \sqrt{\beta_f\beta_i}\sin\Delta \\ \frac{\alpha_i-\alpha_f}{\sqrt{\beta_f\beta_i}}\cos\Delta - \frac{1+\alpha_i\alpha_f}{\sqrt{\beta_f\beta_i}}\sin\Delta & \sqrt{\frac{\beta_i}{\beta_f}}(\cos\Delta - \alpha_f\sin\Delta) \end{pmatrix} \begin{pmatrix} x_i \\ a_i \end{pmatrix} \ . \tag{A.92}$$

The periodic linear one–turn matrix can be parametrised in terms of the Courant–Snyder functions as

$$\underline{T}_{2\times 2}(\theta) = \begin{pmatrix} \cos\mu + \alpha(\theta)\sin\mu & \beta(\theta)\sin\mu \\ -\gamma(\theta)\sin\mu & \cos\mu - \alpha(\theta)\sin\mu \end{pmatrix} \tag{A.93}$$

where we have used $\mu = \psi(\theta + 2\pi) - \psi(\theta)$. One immediately verifies $\det(\underline{T}_{2\times 2}) = 1$ and

$$\text{trace}\left(\underline{T}_{2\times 2}\right) = 2\cos\mu = \lambda + \frac{1}{\lambda} = e^{i2\pi[Q]} + e^{-i2\pi[Q]} \ . \tag{A.94}$$

Therefore the matrix is symplectic and stable in agreement with our assumption that the linear motion is bounded. Note that in general solutions of Hill's equation are not necessarily bounded, but a real ring is never operated with such an optic. Moreover the OTM is strongly stable if $[Q] \equiv [\mu/2\pi] \neq 0$. From theorem A.10 we conclude that if $[Q]$ is strongly incommensurable with 1 the invariant tori (circles) are stable for a sufficiently small perturbation. In addition, if the one–turn matrix of equation (A.84) is stable it can be expressed in terms of Courant–Snyder functions α, β, γ and the phase advance μ. So once we are given the one–turn matrix for all θ we can easily compute the Courant–Snyder functions. In the case of piecewise constant fields we can in principle even compute the OTM analytically. Let $\chi_i \equiv 2\pi l_i/L \equiv \theta_{i+1} - \theta_i$ be the azimuth range of the ring that the i–the beam line element occupies. For $\theta_{i+1} > \theta > \theta_i$ we have $k_i = \text{const}$. Hill's equation is then piecewise equivalent to the equation of a simple harmonic oscillator. Then the single element transfer matrix is

$$\begin{aligned}
\underline{T}_i^{\text{foc}} &= \begin{pmatrix} \cos\left(\sqrt{|k_i|}\chi_i\right) & \frac{L}{2\pi}\frac{\sin\left(\sqrt{|k_i|}\chi_i\right)}{\sqrt{|k_i|}} \\ -\frac{2\pi}{L}\sqrt{|k_i|}\sin\left(\sqrt{|k_i|}\chi_i\right) & \cos\left(\sqrt{|k_i|}\chi_i\right) \end{pmatrix} \\
\underline{T}_i^{\text{drf}} &= \begin{pmatrix} 1 & l_i \\ 0 & 1 \end{pmatrix} \\
\underline{T}_i^{\text{def}} &= \begin{pmatrix} \cosh\left(\sqrt{|k_i|}\chi_i\right) & \frac{L}{2\pi}\frac{\sinh\left(\sqrt{|k_i|}\chi_i\right)}{\sqrt{|k_i|}} \\ \frac{2\pi}{L}\sqrt{|k_i|}\sinh\left(\sqrt{|k_i|}\chi_i\right) & \cosh\left(\sqrt{|k_i|}\chi_i\right) \end{pmatrix} \qquad \text{(A.95)}
\end{aligned}$$

for focusing ($k > 0$), drift ($k = 0$) and defocusing ($k < 0$) elements respectively. Quadrupoles focus in one plane and defocus in the other with the sign of $k = \frac{L^2}{4\pi^2}K$ depending on their polarity. Sector bends focus in the plane of deflection with $k = \frac{L^2}{4\pi^2}\kappa^2$ and behave drift–like in the perpendicular plane. Sector combined function magnets focus in the plane of deflection with $k = \frac{L^2}{4\pi^2}(K + \kappa^2)$ and in the other with $k = -\frac{L^2}{4\pi^2}K$. The focusing with κ^2 is called *weak* and that with K is called *strong*. Rectangular bends introduce extra *edge* focusing because the entry and exit boundaries are not in the plane defined by the normal and co–normal vector of the reference trajectory. The one–turn map at the entrance of the element with index 1 of a ring with m elements (including drifts!) is then just $\underline{T}(\theta_1) = \underline{T}_m\,\underline{T}_{m-1}\cdots\underline{T}_2\,\underline{T}_1$.

When proving the integrability of stable linear systems we have shown before equation (A.39) that $\underline{T}(\theta) = \underline{B}^{(1)}(\theta)\,\underline{R}\,\underline{B}^{(1)-1}(\theta)$, where $\underline{R}$ describes a phase space rotation by μ and $\underline{B}^{(1)} \equiv (\vec{b}_1, \vec{b}_2)$ is the real symplectic and periodic matrix made from the real *column* "eigenvectors" $\vec{b}_i$ that are transformed by $\underline{T}$ like $\underline{T}\,\underline{B}^{(1)} = \underline{B}^{(1)}\,\underline{R}$. In the 2–dimensional case we have

$$\begin{aligned}
\underline{T}_{2\times 2}(\theta) &= \begin{pmatrix} b_{11} & b_{21} \\ b_{12} & b_{22} \end{pmatrix}\begin{pmatrix} \cos\mu & \sin\mu \\ -\sin\mu & \cos\mu \end{pmatrix}\begin{pmatrix} b_{22} & -b_{21} \\ -b_{12} & b_{11} \end{pmatrix} \\
&= \begin{pmatrix} \cos\mu - (b_{11}b_{12} + b_{21}b_{22})\sin\mu & (b_{11}^2 + b_{21}^2)\sin\mu \\ -(b_{12}^2 + b_{22}^2)\sin\mu & \cos\mu + (b_{11}b_{12} + b_{21}b_{22})\sin\mu \end{pmatrix} \qquad \text{(A.96)}
\end{aligned}$$

where we have used $\det(\underline{B}^{(1)}) = \det(\underline{B}^{(1)-1}) = 1$ in the second step. Comparison with equation (A.93) yields

$$b_{11}^2(\theta) + b_{21}^2(\theta) = \beta(\theta),\;\; b_{12}^2(\theta) + b_{22}^2(\theta) = \gamma(\theta),\;\; b_{11}(\theta)b_{12}(\theta) + b_{21}(\theta)b_{22}(\theta) = -\alpha(\theta)\;. \qquad \text{(A.97)}$$

Equation (A.85) together with

$$a =_1 \frac{2\pi}{L}\mathrm{D}_\theta\, x = -\sqrt{\frac{\tilde{\varepsilon}}{\beta}}\left(\alpha\cos(\psi - \psi_0) - \sin(\psi - \psi_0)\right) \qquad \text{(A.98)}$$

enables us to eliminate the phase $\psi - \psi_0$ and find the *Courant–Snyder invariant*

$$\gamma x^2 + 2\alpha x a + \beta a^2 = \tilde{\varepsilon} = \text{const.} \tag{A.99}$$

Equation (A.99) is the equation of an ellipse in the (x, a) plane with area $A_{\text{ellipse}} = \pi\tilde{\varepsilon} \equiv \varepsilon$. Note that the area is independent of θ but the shape and orientation of the ellipse vary 2π–periodically with θ. Comparing equations (A.97) and the ansatz (A.85) with the transformation to action–angle variables

$$\begin{pmatrix} x(\theta) \\ a(\theta) \end{pmatrix} = \begin{pmatrix} b_{11}(\theta) & b_{21}(\theta) \\ b_{12}(\theta) & b_{22}(\theta) \end{pmatrix} \begin{pmatrix} \sqrt{2J}\sin\psi \\ \sqrt{2J}\cos\psi \end{pmatrix} \tag{A.100}$$

we find

$$\tilde{\varepsilon} = \frac{\varepsilon}{\pi} = 2J \ . \tag{A.101}$$

The Courant–Snyder invariant is defined as a property of a single torus. It is a common property of all particles whose trajectories wind around the torus with $J = \tilde{\varepsilon}/2$. In the next subsection we will introduce another property of $\tilde{\varepsilon}$.

Until now we have treated only fully decoupled motion, i.e. motion where any coupling of the two transverse planes due to rotated quadrupoles and solenoids is absent and where we have neglected the effect of off–momentum trajectories. Rotated quadrupoles and solenoids might be avoidable from the theoretical point of view, but a mono–energetic beam is as impossible as a beam without betatron oscillations. In the absence of vertical bends and vertical orbit distortions the relative energy offset δ feeds into the horizontal motion.

$$\mathrm{D}_{\theta\theta}\, x + k(\theta)x =_1 \xi(\theta)\delta \ . \tag{A.102}$$

Here we have introduced $\xi = \frac{L}{2\pi}\kappa \left.\frac{d\delta_p}{d\delta}\right|_{\delta=0}$ with the relative momentum offset $\delta_p \equiv (p - p_0)/p_0$. If we assume δ to be constant, as in a ring without RF–cavities, this is an inhomogeneous equation of the Hill type. We can find a particular solution by means of a Green's function

$$G(\theta_2, \theta_1) \equiv S(\theta_2)C(\theta_1) - C(\theta_2)S(\theta_1), \ \ C(\theta) = T_{11}(\theta, \theta_0), \ \ S(\theta) = T_{12}(\theta, \theta_0) \tag{A.103}$$

where $\underline{T}(\theta, \theta_0)$ is the flow of the homogeneous Hill's equation (A.83). Using the relation $C\mathrm{D}_\theta\, S - S\mathrm{D}_\theta\, C = 1$ one easily verifies [HW93a] that $\delta D(\theta, \theta_0)$ where

$$D(\theta, \theta_0) \equiv \int_{\theta_0}^{\theta} G(\theta, \theta_1)\xi(\theta_1)\, d\theta_1 \tag{A.104}$$

is a particular solution of equation (A.102). Therefore we obtain for a given δ

$$\vec{x}(\theta) \equiv \begin{pmatrix} x(\theta) \\ a(\theta) \end{pmatrix} =_1 \underline{T}(\theta, \theta_0)\vec{x}(\theta_0) + \vec{D}(\theta, \theta_0)\delta \ , \ \ \vec{D}(\theta, \theta_0) \equiv \begin{pmatrix} D(\theta, \theta_0) \\ \frac{2\pi}{L}\mathrm{D}_\theta\, D(\theta, \theta_0) \end{pmatrix} \ . \tag{A.105}$$

The constant energy offset leads to a new periodic reference trajectory $\vec{x}_\delta =_1 \vec{x}_D\delta$ where

$$\vec{x}_D(\theta) = (\underline{1} - \underline{T}(\theta))^{-1}\, \vec{D}(\theta) \tag{A.106}$$

is the 2π–periodic solution of $\vec{x} = \underline{T}\vec{x} + \vec{D}\delta$ whereby $\underline{T}(\theta)$ is the one–turn matrix and $\vec{D}(\theta) \equiv \vec{D}(\theta + 2\pi, \theta)$ and $\underline{T}(\theta)$ and $\vec{D}(\theta)$ being the linear one–turn matrix and the one–turn dispersion respectively. The trajectory $\vec{x}_D(\theta)$ is called the *periodic dispersion trajectory* and is well defined whenever $\underline{1} - \underline{T}$ is regular, i.e. whenever the tune is *not* an integer. The spatial component $x_D \equiv (\vec{x}_D)_1$ is called the *periodic dispersion.* Usually the dispersion $\widetilde{D}$ and periodic dispersion $\tilde{x}_D$ are defined in an analogous way but by substituting the relative momentum offset $\delta_p \equiv (p - p_0)/p_0$ and $\frac{L}{2\pi}\kappa$ for the canonical momentum $\delta \equiv (K - K_0)/K_0$ (see 2.7) and ξ in equation (A.104).

In addition the transverse variables feed into the longitudinal plane due to the path lengthening resulting from the the transverse displacement and angles.

The longitudinal motion in the linear decoupled case can be shown [WR88, HW93a, HW93b] to be also governed by a Hill type equation and therefore the one–turn map can be written in terms of longitudinal Courant–Snyder parameters. Nevertheless it might be more instructive to look at the longitudinal transfer maps of different elements. If we totally neglect the coupling of transverse and longitudinal motion all elements except the RF–cavities behave like drifts:

$$\underline{T}^{(\mathrm{drf})}_{\tau\delta,i} = \begin{pmatrix} 1 & \frac{l_i}{(\gamma_0+1)^2} \\ 0 & 1 \end{pmatrix} \quad , \quad \underline{T}^{(\mathrm{cav})}_{\tau\delta,i} = \begin{pmatrix} 1 & 0 \\ -\frac{4\pi^2 f_{\mathrm{rf}} U_{\mathrm{rf}} p_0}{L K_0^2} & 1 \end{pmatrix} \quad , \tag{A.107}$$

where K_0 is the "kinetic energy" of the synchronous particle ($\delta = 0$), f_{rf} and U_{rf} are the RF–frequency and RF–voltage respectively and where the sign of $(\underline{T}^{(\mathrm{cav})}_{\tau\delta,i})_{21}$ has been chosen to be focusing for positive RF–voltage. The transport matrix for a cavity has been computed in the thin lens approximation ($\chi \to 0$). The first order approximation for the influence of the magnetic elements on the path length is integral $\Delta L = \frac{L}{2\pi}\int_0^{2\pi}(\kappa_x x + \kappa_y y)d\theta$ along the dispersive orbit $x_D\delta$. We assume for simplicity that the ring is flat ring with $\kappa_y = 0$. One then obtains [HW93a] for the relative change of the path length to first order as

$$\frac{\Delta L}{L_0} =_1 \alpha_p\delta_p = \alpha_K\delta \quad , \quad \alpha_p \equiv \frac{1}{2\pi}\int_0^{2\pi}\kappa\tilde{x}_D(\theta)\,d\theta \quad , \quad \alpha_K \equiv \frac{1}{2\pi}\int_0^{2\pi}\kappa x_D(\theta)\,d\theta \quad , \tag{A.108}$$

where we have introduced the well known momentum compaction factor α_p and the equivalent kinetic energy compaction factor α_K. The relative time of flight difference can be computed to first order

$$\frac{t-t_0}{t_0} =_1 \frac{\Delta L}{L_0} - \frac{\Delta\beta}{\beta_0} \quad =_1 \quad -(\gamma_0^{-2} - \alpha_p)\delta_p \tag{A.109a}$$

$$=_1 \quad -(\gamma_0^{-2} - \alpha_p)\left.\frac{d\delta_p}{d\delta}\right|_{\delta=0}\delta =_1 -\left(\frac{\gamma_0 - 1}{\beta_0^2\gamma_0^3} - \alpha_K\right)\delta \quad . \tag{A.109b}$$

Since ${}^{(t-t_0)}/_{t_0} = {}^{-p_0\tau}/_{K_0 t_0}$, $\alpha_K =_1 \alpha_p{}^{(\gamma_0-1)}/_{\gamma_0\beta_0^2}$ and t_0 is the inverse revolution frequency f_0, the change of τ after one turn is then

$$\Delta\tau =_1 (\gamma_0^{-2} - \alpha_p)\frac{(\gamma_0-1)^2}{f_0\gamma_0^2\beta_0^3}\,\delta =_1 \frac{\gamma_0 - 1}{f_0\beta_0\gamma_0}\left(\frac{\gamma_0-1}{\beta_0^2\gamma_0^3} - \alpha_K\right)\,\delta \equiv \eta\delta \quad . \tag{A.110}$$

As expected $\lim_{p_0\to\infty} {}^{\alpha_K}/_{\alpha_p} = 1$. Therefore the combined linear effect of the dispersion in the whole ring except for the cavities can be written as a longitudinal transfer matrix $\begin{pmatrix} 1 & \eta \\ 0 & 1 \end{pmatrix}$.

The most striking consequence of (A.110) is that for $\alpha_p > 0$ there is a $\gamma_t \equiv 1/\sqrt{\alpha_p}$ such that for $\gamma_0 < \gamma_t$ a particle with $\delta > 0$ gains relatively more speed than relative additional path length so that it arrives *early* ($\Delta\tau > 0$) whereas at $\gamma_0 > \gamma_t$ the lengthening of the path over–compensates the gain in speed and a particle with more kinetic energy arrives *late*. This effect is called transition and γ_t is called "γ–transition". Therefore in order that $\tau = \delta = 0$ is an elliptic fixed point the RF–phase must be adjusted so that below/above transition a late particle gains/looses energy.

A.2.2 Fully 6–dimensional motion

We return now to the fully coupled motion. The transfer maps for the most important beam line elements as used in `SPRINT` are derived in [CW98]. The 6×6 one–turn map for the unperturbed machine, i.e. without any misalignment, has the following 3×3 block structure

$$\underline{T}(\theta) = \begin{pmatrix} \underline{H} & \underline{C}_{hv} & \underline{D}_h \\ \underline{C}_{vh} & \underline{V} & \underline{D}_v \\ \underline{L}_h & \underline{L}_v & \underline{L} \end{pmatrix} \quad . \tag{A.111}$$

The 2×2 matrices $\underline{H}$, $\underline{V}$ and $\underline{L}$ describe, as in the uncoupled case, the dependence of the horizontal, vertical and longitudinal variable on themselves. $\underline{D}_h$ and $\underline{D}_v$ includes the effect of horizontal and vertical dispersion, whereas $\underline{L}_h$ and $\underline{L}_v$ describe mainly the effect of transverse excitation on the time of flight variable τ. In completely mid–plane symmetric rings, particularly in rings without vertical bending dipoles, $\underline{D}_v$, $\underline{L}_v$, $\underline{C}_{vh}$ and $\underline{C}_{hv}$ vanish and in rings without RF–cavities the first column of the $\underline{D}_i$ and the second row of the $\underline{L}_i$ vanish. The coupling between the horizontal and the vertical plane is described by the matrices $\underline{C}_{hv}$ and $\underline{C}_{vh}$. Rotated quadrupoles as well as solenoids introduce so–called linear coupling and destroy the mid–plane symmetry even in a ring without vertical bends. In a rotated quadrupole the EOM take the form

$$\mathrm{D}_{\theta\theta}\, x + kx + \tilde{k}y = 0 \ \ , \ \ \mathrm{D}_{\theta\theta}\, y - ky + \tilde{k}x = 0 \tag{A.112}$$

where $k = 0$ is the special case of *skew* quadrupoles, i.e. quadrupoles rotated by $\pi/4$. In rings with horizontal *and* vertical bends and cavities, and even in the absence of solenoids and rotated quadrupoles, a small transverse coupling arises from the cross talk between horizontal, vertical and longitudinal degrees of freedom. Any horizontal offset in a region with non–vanishing horizontal curvature creates a lengthening of the closed orbit and therefore feeds into the time of flight variable τ. The same argument applies to vertical offsets in regions with vertical curvature. But the cavities change the particle energy according to the arrival time at the azimuth of the cavity. Thus, if there is horizontal and vertical curvature in the ring and from the view point θ_0 to the azimuth of the cavity both dispersions $\vec{D}_x(\theta_{\rm cav}, \theta_0)$ and $\vec{D}_y(\theta_{\rm cav}, \theta_0)$ do not vanish identically, then $\underline{C}_{vh} \neq \underline{0} \neq \underline{C}_{hv}$ even without solenoids and rotated quadrupoles.

If the linear motion is bounded, i.e. if the all the eigenvalues λ_i of the one–turn map fulfil $|\lambda_i| = 1$, then we can transform the system to normal form coordinates in which the different eigenplanes are decoupled. Each plane has its own tune Q_i and if the tunes are mutually different, then, according to theorem A.13 the invariant tori are stable under small perturbations of $O(\epsilon)$ over a time scale $O(1/\epsilon)$. If coupling between the transverse degrees of freedom is weak and dispersion is small in both the horizontal and the vertical planes, then the eigenplanes are almost parallel to the (x, a), (y, b) and (τ, δ) planes in Cartesian phase space. In mid–plane symmetric rings the vertical plane is almost decoupled from the other two planes, at least if misalignments are ignored. Due to the dispersion being mainly in the horizontal plane the horizontal and the longitudinal planes in phase space cannot normally be seen as decoupled.

In analogy to the Courant–Snyder functions of the uncoupled case one can define the Mais–Ripken lattice functions [MR82, FI92] through the normalised "eigenvectors" according to equation (A.38)

$$\begin{aligned} \beta_{i,j} &= b^2_{2i-1,2j-1} + b^2_{2i,2j-1} \\ \gamma_{i,j} &= b^2_{2i-1,2j} + b^2_{2i,2j} \\ -\alpha_{i,j} &= b_{2i-1,2j-1} b_{2i-1,2j} + b_{2i,2j-1} b_{2i,2j} \end{aligned} \tag{A.113}$$

where $1 \leq i \leq 3$ refers to the eigenplane and $1 \leq j \leq 3$ refers to the plane in Cartesian phase space. In the case of a block diagonal one–turn map, i.e. in the absence of any inter–plane coupling this reduces to $\beta_{i,j} = \delta_{ij}\beta_j$, $\gamma_{i,j} = \delta_{ij}\gamma_j$ and $\alpha_{i,j} = \delta_{ij}\alpha_j$. Even with fully coupled 6–dimensional motion it is in general possible to associate each eigenplane spanned by ($\vec{b}_{2i-1}$ and $\vec{b}_{2i}$) as in equation (A.38) with the Cartesian plane (x, a), (y, b) or (τ, δ) on which the projection of $\vec{b}_{2i-1}$ and $\vec{b}_{2i}$ is maximal. It is therefore convenient to denote the planes by x, y and z as in the uncoupled case.

Let $\tilde{\rho}(\vec{J}, \vec{\Psi}, \theta)$ be the *normalised* particle density in phase space, which evolves under the Liouville equation $\partial_\theta\, \tilde{\rho} + \vec{Q} \cdot \partial_{\vec{\Psi}}\, \tilde{\rho} = 0$. If $\tilde{\rho}$ is stationary, i.e. $\partial_\theta\, \tilde{\rho} = 0$, then $\tilde{\rho}(\vec{J}, \vec{\Psi}, \theta)$ is independent of $\vec{\Psi}$ and can be written as $\tilde{\rho} = (2\pi)^{-3}\rho(\vec{J})$. Since the normal form coordinates of the i-th eigenplane $\vec{x}_i \equiv (\sqrt{2J_i}\cos\Psi_i, \sqrt{2J_i}\sin\Psi_i)$ are monotonic functions of the J_i for constant θ we can define the particle content *inside* of a torus under stationary conditions as

$$N_{\vec{\varepsilon}} = N_{\rm tot} \int_{J_i < \varepsilon_i/(2\pi)} \int_{\mathcal{T}^3} \rho(\vec{J})\, d\vec{J}^3 \tag{A.114}$$

where $N_{\rm tot}$ is the total number of particles. In this context $\varepsilon \equiv \pi\tilde{\varepsilon}$ which describes a volume in phase space is called *emittance*. We assume now that ρ can be factorised as $\rho(\vec{J}) = \prod_i \rho_i(J_i)$, so that the normalised densities ρ_i for each eigenplane are double Gaussians in the normal form coordinates x_{2i-1} and x_{2i} of that plane. Then we obtain with $J_i = {}^1\!/_2(x_{2i-1}^2 + x_{2i}^2)$

$$\rho_i(J_i) = \frac{1}{2J_{\sigma,i}} e^{-\frac{J_i}{2J_{\sigma,i}}} \tag{A.115}$$

where $\int_{\mathbb{R}^+} J_i \rho_i(J_i) dJ_i = 2J_{\sigma,i}$. The action J_i is given by half of the Courant–Snyder invariant $\tilde{\epsilon}_i$ which is the the area enclosed by the invariant ellipse in the i-th eigenplane divided by π

In fact various versions of the emittance — as a parameter characterising the particle distribution of a proton beam — are in use. The most common definitions for the emittance are:

1. either 2π times the orbital action $\widetilde{J}_i$ for which $\int_{\mathbb{R}^{2+}} \int_0^{\widetilde{J}_i} \rho(\vec{J})\, d\vec{J} = 1 - e^{-\widetilde{J}_i/(2J_{\sigma,i})} = 95\%$. Therefore we find $\widetilde{J}_i = J_{\sigma,i} \ln(1/(1-.95)^2) \approx 6J_{\sigma,i}$. $2\pi\widetilde{J}_i$ is called the *95%–emittance*,

2. or 2π times the orbital action $J_{\sigma,i}$ ($J_{2\sigma,i}$) for which the trajectories have a maximum projection on configuration space of 1 (2) standard deviations σ of the beam profile. These emittances are called the *1-σ (2–σ) emittances*. Since $J_{s\sigma,i} = s^2 J_{\sigma,i} = s^2$, the integral $\int_{\mathbb{R}^{2+}} \int_0^{J_{s\sigma,i}} \rho(\vec{J})\, d\vec{J}$ is $1 - e^{-s^2/2}$. Therefore, if all other degrees of freedom are already integrated out, then the circle in the normal form coordinates whose maximum projection on configuration space is 1 (2) σ contains about 39% (87%) of the beam, and the 2.45 σ circle contains 95%.

In this thesis "emittance" **always** means the **1-σ emittance** ! Note that $\int_0^{J_{s_x\sigma,x}} \int_0^{J_{s_y\sigma,y}} \int_0^{J_{s_z\sigma,z}} \rho(\vec{J})\, d\vec{J} = (1-e^{-s_x^2/2})(1-e^{-s_y^2/2})(1-e^{-s_z^2/2})$ and thus, for example, that the torus with $(s_x, s_y, s_z) = (1,1,1)$ contains only 6% of the beam.

A.2.3 Adiabatic phase space shrinking

In the previous sections we have only treated the case of constant reference momentum p_0. The coordinates (2.7) have been obtained by a rescaling process $(x, p_x, y, p_y, -\Delta t, \Delta K) \to (x, a, y, b, \tau \equiv -K_0/p_0 \Delta t, \delta \equiv \Delta K/K_0)$ which is according to lemma A.3 a canonical transformation only if p_0, $K_0 =$ const. In a synchrotron the reference momentum is only changed in RF–cavities. It is *not* changed in the rest of the ring, which makes up almost the whole lattice. Therefore the acceleration process can be described as a composition of symplectic maps, describing the motion between cavities and non–symplectic maps, describing the motion inside the cavities. In thin lens approximation the linear transfer map of a cavity increasing the energy by ΔE is

$$\underline{T}_{\Delta E}^{\rm acc/cav} = \begin{pmatrix} 1 & 0 & 0 & 0 & 0 & 0 \\ 0 & \frac{p_1}{p_2} & 0 & 0 & 0 & 0 \\ 0 & 0 & 1 & 0 & 0 & 0 \\ 0 & 0 & 0 & \frac{p_1}{p_2} & 0 & 0 \\ 0 & 0 & 0 & 0 & \frac{p_1 K_2}{K_1 p_2} & 0 \\ 0 & 0 & 0 & 0 & -\frac{4\pi^2 f_{\rm rf} U_{\rm rf} p_1}{L K_1 K_2} & \frac{K_1}{K_2} \end{pmatrix} \quad \text{with} \quad \begin{array}{rcl} K_2 & \equiv & K_1 + \Delta E \\ p_2 & \equiv & \sqrt{(K_1 + \Delta E + m)^2 - m^2} \end{array} . \tag{A.116}$$

This matrix has a determinant $\det(\underline{T}_{\Delta E}^{\mathrm{acc/cav}}) = \frac{p_1^3}{p_2^3}$ and the three sub–blocks acting on the three planes (x, a), (y, b), and (τ, δ) have determinant $\frac{p_1}{p_2}$. Therefore $\det(\underline{T}_{\Delta E}^{\mathrm{acc/cav}})$ with positive/negative ΔE causes the phase space volume to shrink/expand. It has been shown [CS58] that in the case of linear orbital motion which is integrable all along the ramp, even in the case of an additional continuous change of the lattice parameters, the *normalised* actions $\beta_0\gamma_0 J_i,\ i = 1, 2, 3$ in the 3 eigenplanes are adiabatic invariants of motion. One often calls the $\varepsilon_i^{\mathrm{nrm}} = 2\pi\beta_0\gamma_0 J_i$ the normalised or invariant emittances.

Appendix B

Conventions

- We use rationalised units in which $\hbar = c = 1$. Nevertheless, numerical values except for particle momenta are given in the mKsA system.

mksA–System	rationalised units
1 m	$5.067728\ 10^{15}$ GeV^{-1}
$1.973271\ 10^{-16}$ m	1 GeV^{-1}
1 kg	$1.782663\ 10^{-27}$ GeV
1 s	$1.519266\ 10^{24}$ GeV^{-1}
$6.582122\ 10^{-25}$ s	1 GeV^{-1}
1 A	1.244367^{-5} GeV
$e \approx 1.602\ 10^{-19}$ As	$\approx \sqrt{4\pi/137}$

- Sets in general are denoted by "caligraphic" $\mathcal{S}$.
- Sets of "numbers" are denoted by "blackboard style" $\mathbb{F}$. In particular $\mathbb{Z}$ is the ring of the signed integers, $\mathbb{N}$ and $\mathbb{N}^*$ are the sets of the non–negative and positive integers respectively, $\mathbb{Q}$ and $\mathbb{R}$ are the fields of the rationals and the reals respectively and $\mathbb{H}$ is the skew–field of the quaternions.
- Closed intervals $\{x \in \mathbb{R} a \leq x \leq b\}$ are denoted by $[a, b]$, the open intervals by (a, b), semi–open intervals by $[a, b)$ and $(a, b]$.
- For real numbers $[x]$ means the positive *non*–integer part, i.e. $x - [x] \in \mathbb{Z}$ and $0 \leq [x] < 1$.
- The equality up to order n is indicated by $=_n$, i.e. $a(x) =_n b(x)$ implies $a - b = O(x^{n+1})$.
- Groups are denoted in "bold" and uppercase $\mathbf{G}$, their corresponding Lie–algebras with the same letter in "bold" but lowercase $\mathbf{g}$.
- Vectors are denoted with an "arrow": $\vec{x}$, in particular $\vec{Id}$ is the identity map.
- The Euclidean norm of a *real or complex* vector is denoted by $\|\vec{x}\| \equiv \sqrt{\sum_i |x_i|^2}$.
- For every n–tuple $\vec{k}$ of integers $k_i \in \mathbb{Z}$, $1 \leq i \leq n$ we define $|\vec{k}| \equiv \sum_{i=1}^n |k_i|$.
- *Unit* vectors are denoted with a "hat": $\hat{x}$ so that $\|\hat{x}\|$ is identically 1.
- Spinors are denoted with a "check": $\check{x}$.

- Matrices are denoted with an "underline": $\underline{X}$. Normally 6×6 and 3×3 matrices are written in uppercase and 2×2 matrices in lowercase. In particular $\underline{1}$ is the identity matrix. We will often identify *linear* maps with their matrix representation w.r.t. a given coordinate system.
- Unit quaternions are denoted with a "bar": $\bar{x}$.
- Let $\bar{r}$ be a spin transport quaternion, then $\underline{r}$ is the corresponding $\mathbf{SU(2)}$- and $\underline{R}$ the corresponding $\mathbf{SO(3)}$ map.
- The "tilde": $\tilde{x}$ and the "prime": x' have *no* predefined meaning. Their meaning is explained wherever they are used.
- Complex conjugation is denoted with an "asterisk": x^*.
- Transposition is denoted with a "roman T" superscript : $\underline{X}^{\mathrm{T}}$.
- Hermitian conjugation is denoted with a "dagger" : $\underline{x}^\dagger$ and $\check{x}^\dagger$.
- $\vec{J}$ and $\vec{\Psi}$ are usually the orbital action–angle variables.
- I and Φ are usually the spin action–angle variables.
- The equations of motion in the accelerator are given w.r.t. the independent variable $\theta \equiv 2\pi\frac{l}{L}$.
- The total derivative w.r.t. x is symbolised by D_x .
- Analogously the total *second* derivative w.r.t. x is symbolised by D_{xx} .
- The partial derivative is denoted by ∂_x and the gradient w.r.t. $\vec{x}$ is denoted by $\partial_{\vec{x}}$.
- The Jacobian of a vector function $\vec{f}(\vec{x})$ is denoted by $\underline{f} \equiv (\partial_{\vec{x}}\, \vec{f}^{\mathrm{T}})^{\mathrm{T}}$.
- The space of n–times continuously partially differentiable functions is denoted by $\mathcal{C}^n$.
- The commutative product is symbolised by $\prod_{i=\min}^{\max}$ whereas the "$\bigodot$" symbolises a non–commutative product in the sense that the indexed operator starts at the *right* and stops at the left. Example:

$$\bigodot_{i=1}^{n} \underline{A}_i \equiv \underline{A}_n\, \underline{A}_{n-1} \cdots \underline{A}_2\, \underline{A}_1 \quad .$$

- $\sim$ means proportional.
- $\equiv$ indicates that new symbols are being defined

Appendix C

Key to the snake scheme coding

code	ϕ/deg.	θ/deg.	α/deg.	remark
1	0.0	0	0	rad.
a	22.5	0	45	
b	45.0	0	90	$\rightarrow$ RHIC
c	67.5	0	135	
3	90.0	0	180	long.
d	112.5	0	-135	
e	135.0	0	-90	$\rightarrow$ RHIC
f	157.5	0	-45	
2	0.0	90	—	vert.

Table C.1: Table of types of Siberian Snakes used in snake arrangements for simulations of spin motion in HERA–p. ϕ is the horizontal angle between the snake axis and the radial direction, α is the Steffen–angle 2ϕ but taking into account that ϕ and $\frac{\pi}{2} - \phi$ are equivalent, and θ is the polar angle between the snake axis and vertical direction. Snakes with $\phi = \pm 45°$ are being built for the RHIC polarised proton project.

- All snake schemes start at the East interaction point (O–IP).
- The ordering of the snakes is *clockwise* around the ring — as in the lattice files.
- nX means that the sequence following is repeated n times. This convention is particularly useful for highly periodic schemes with 6 or more snakes. For HERA this notation was *not* used to "abbreviate" 4–snake schemes, i.e. 1b1b was used instead of 2X1b etc.
- For snake pairs of $\pm nn°$, $\pm mm.m°$ or $\pm ll.ll°$ so that the snake angles do *not* fit into the scheme of table C.1, the abbreviations pmnn, pmmmm, pm$llll$ are used.
- If not noted explicitly, the HERA–p snake schemes have as default 6 flattening snakes in the vertical bend sections at the beginning of the arc octants OL, OR, SL, SR, NL and NR. [GH99b].

Bibliography

[AC79] A. W. Chao, *J.Appl.Phys.* **50(2)**, 595-598 (1979).

[AC80] A. W. Chao, *Nucl.Instr.Meth.* **180**, 29-36 (1980).

[AC96] V. A. Anferov, E. D. Courant, Ya. S. Derbenev and A. D. Krisch in University of Michigan report UM-HE-96-20 (1996).

[AK96a] V. A. Anferov and A. D. Krisch, in University of Michigan report UM-HE-96-20 (1996).

[AK96b] V. A. Anferov, A. D. Krisch and R. A. Phelps, in University of Michigan report UM-HE-96-20 (1996).

[AL95] A. Luccio, BNL formal report BNL-52461 (1995).

[AL96] A. Luccio, BNL spin note AGS/RHIC/SN No. 003 (1996).

[AL99] A. Lehrach, in the proceedings of the Workshop on Polarized Protons at High Energies, DESY-PROC-1999-03 (1999).

[AP97] V. A. Anferov and R. A. Phelps, *Nucl.Instr.Meth.* **A389**, 423 (1997).

[BB95] D. P. Barber, M. Böge, et. al., *Phys.Lett.* **B343**, 436-443 (1995).

[BB99] K. Balewski, R. Brinkmann, Ya. S. Derbenev, K. Flöttman, et. al., in the proceedings of ECOOL–99, Uppsala (1999).

[BD97] J. Blümlein, A. De Roerk, T. Gehrmann and W.-D. Nowak (editors), proceedings of the Workshop on Deep Inelastic Scattering off Polarised Targets, DESY report 97-200 (1997).

[BG80] R. L. Bishop and S. I. Goldberg, Tensor Analysis on Manifolds, Dover Publications Inc. 1980.

[BG92] V. V. Balandin and N. I. Golubeva, in proceedings od the 1992 HEAC conference, published in *Int.J.Mod.Phys.* **A 2** (Proc. Suppl.) (1992).

[BG93] V. V. Balandin and N. I. Golubeva, hand written notes, unpublished (1993).

[BG96] V. V. Balandin, N. I. Golubeva and D. P. Barber, DESY internal report M-96-04 (1998).

[BG98a] V. V. Balandin and N. I. Golubeva, DESY report 98-016 (1998).

[BG98b] V. V. Balandin, N. I. Golubeva and D. P. Barber, DESY internal report M-98-03 (1998).

[BH92] D. P. Barber, K. Heinemann and G. Ripken, DESY internal report M-92-04 (1992), second revised version September 1999.

[BH94a] D. P. Barber, K. Heinemann and G. Ripken, *Z.f.Phys.* **C 64**, 117–142 (1994).

[BH94b] D. P. Barber, K. Heinemann and G. Ripken, *Z.f.Phys.* **C 64**, 143–167 (1994).

[BH96a] D. P. Barber, K. Heinemann, G. H. Hoffstaetter, and M. Vogt, Proceedings of SPIN96, Amsterdam (1996), World Scientific, Singapore (1997).

[BH96b] D. P. Barber, K. Heinemann, G. H. Hoffstaetter, and M. Vogt, in proceedings of the Workshop on Future Physics at HERA, Volume 2, DESY (1996).

[BH96c] D. P. Barber, K. Heinemann, G. H. Hoffstaetter, and M. Vogt, DESY internal report HERA 96-07 and in University of Michigan report UM-HE-96-20 (1996).

[BH96d] D. P. Barber, K. Heinemann, G. H. Hoffstaetter, and M. Vogt, DESY internal report M-96-14 and Proceedings of the European Particle Accelerator Conference EPAC96 (1996).

[BH98a] D. P. Barber, G. H. Hoffstaetter, and M. Vogt, Proceedings of EPAC98 (1998).

[BH98b] D. P. Barber, G. H. Hoffstaetter, and M. Vogt, Proceedings of SPIN98, Protvino (1998), World Scientific, Singapore (1999).

[BH98c] D. P. Barber et al., five articles in proceedings of the ICFA Workshop on Quantum Aspects ofBeam Physics, Monterey, U.S.A., 1998, edited by P. Chen, World Scientific (1999) and DESY report 98-096 (1998).

[BH99a] D. P. Barber, G. H. Hoffstaetter and M. Vogt, in the proceedings of the Workshop on Polarized Protons at High Energies, DESY-PROC-1999-03 (1999).

[BH99b] D. P. Barber, G. H. Hoffstaetter, and M. Vogt, in University of Michigan report UM-HE-99-05 (1999).

[BM59] V. Bargmann, L. Michel and V. L. Telegdi, *Phys.Rev.Lett.* **2**(10), 435-436, (1959).

[BM65] N. N. Bogoljubov, J. A. Mitropolski, Asymptotische Methoden in der Theorie der nichtlinearen Schwingungen, Akademie–Verlag GmbH, Berlin (1965).

[BM84] B. W. Montague, *Phys.Rep.* **113**, 1 (1984).

[BN95] J. Blümlein and W.-D. Nowak (editors), proceedings of the Workshop on the Prospects of Spin Physics at HERA, DESY report 95-200 (1995).

[BR99a] D. P. Barber and G. Ripken, articles in Handbook of Accelerator Physics and Engeneering, Eds.: A. W. Chao and M. Tigner, World Scientific, 1999 and DESY report 99–095.

[BR99b] D. P. Barber and A. De Roerk (editors), proceedings of the Workshop on Physics with polarised protons at high energies, DESY-PROC-1999-03 (1999).

[BS99] D. P. Barber, V. Ptitsin and Yu. M.Shatunov, in DESY-PROC-1998-01, 151-162 (1999).

[BV98] D. P. Barber, M. Vogt, and G. H. Hoffstaetter, in DESY 97-200 (1997) and DESY-PROC-1998-01 (1998).

[CM93] C. Montag, diploma thesis, Phillips–Universität, Marburg (1993).

[CN96] M. Conte, B. E. Norum, A. Penzo, M. Pusterla and R. Rossmanith, DESY internal report HERA-96-01 (1996).

[CP95] M. Conte, A. Penzo and M. Pusterla, *Nuovo Cimento* **108 A** (1), 127–136 (1995).

[CR80] E. D. Courant and R. D. Ruth, BNL report 51270 and UC-28 (Particle Accelerators and High Voltage Machines). ISA 80-5 (1980).

[CS58] E. D. Courant and H. S. Snyder, Theory of the alternating gradient synchrotron, *Ann.Phys.* **3**, 1-48 (1958).

[CW98] Ch. Weißbäcker, Diploma thesis, Technical University of Darmstadt, (1998).

[CY81] A. W. Chao and K. Yokoya, KEK Report KEK 81-7 (1981).

[DB95a] D. P. Barber, in "The Spin Structure of the Nucleon" Erice 1995, World Scientific, ISBN 981-02-3323-X (1996).

[DB95b] D. P. Barber, in proceedings of the Workshop on Prospects of Future Physics at HERA, DESY 95-200 (1995).

[DG98] A. De Roerk and T. Gehrmann (editors), proceedings of the Workshop on Physics with polarised protons at HERA, DESY-PROC-1998-01 (1998).

[DK72] Ya. S. Derbenev and A. M. Kondratenko, *Sov.Phys. JETP* **35**(2), 230 (1972).

[DK73] Ya. S. Derbenev and A. M. Kondratenko, *Sov.Phys. JETP* **37**(6), 968 (1973).

[DK75] Ya. S. Derbenev and A. M. Kondratenko, *Sov.Phys.Dokl.* **20**(8), 562 (1975).

[DK78] Ya. S. Derbenev, A. M. Kondratenko, S. I. Serednyakov, A. N. Skrinsky, G. M. Tumaikin and Yu. M. Shatunov, *Part.Acc.* **8**, 115 (1978).

[DK79] Ya. S. Derbenev and A. M. Kondratenko, *Sov.Phys.Dokl.* **24**(5), 366 (1979).

[DK89] Ya. S. Derbenev and A. M. Kondratenko, *Sov.Phys.Tech.Phys.* **34**(10), 1152 (1989).

[E880] T. Roser, Polarized Proton Beams *Proceedings of the 1995 IEEE Particle Accelerator Conference and International Conference on High-Energy Accelerators*, 3154 (1996) ;
M. Bai, et al., *Phys.Rev.* **E**, 5 (1997).

[EC94] E. D. Courant, BNL spin note AGS/RHIC/SN No. 004 (1994).

[EC96] E. D. Courant, BNL spin note AGS/RHIC/SN No. 010 (1996).

[EMC88] The EMC collaboration, J. Ashman et al., *Phys.Lett.* **B 206**, 364 (1998).

[ems1] D. V. Anosov and V. I. Arnold (Ed.), Encycl. of math. sciences V, Dynamical Systems I, Springer New York (1988).

[ems2] Ya. G. Sinai (Ed.), Encycl. of math. sciences V, Dynamical Systems II, Springer New York (1989).

[ems3] V. I. Arnold (Ed.), Encycl. of math. sciences V, Dynamical Systems III, Springer New York (1988).

[FI92] F. Ch. Iselin, The MAD (vs 8.13) Physics Methods Manual, `http://wwwslap.cern.ch/~fci/mad/mad8/phys_guide.ps.gz`, CERN (1992).

[FP95] F. Pilat, BNL spin note AGS/RHIC/SN No. 007 (1996)

[FS60] M. Froissart and R. Stora, *Nucl.Instr.Meth.*, **7**, 297-305 (1960).

[GB99] G. Bunce, in the proceedings of the Workshop on Polarized Protons at High Energies, DESY-PROC-1999-03 (1999).

[GH94] G. H. Hoffstaetter, PhD Thesis, DESY report 94-242 (1994).

[GH96] G. H. Hoffstaetter, transparencies of a talk given at the Workshop on Mathematical Aspects of Accelerator Physics in Bad Honnef, Dec.1996, unpublished.

[GH98] G. H. Hoffstaetter, private communication (1998).

[GH99a] G. H. Hoffstaetter Proceedings of NUCLEON–99, INFN Frascati (1999).

[GH99b] G. H. Hoffstaetter, Habilitation Thesis, Technical University of Darmstadt (1990).

[GH99c] G. H. Hoffstaetter, in University of Michigan report UM-HE-99-05 (1999).

[GHS99] M. Gentner, D. Husmann, C. Steier, R. Brinkmann and Ya. Derbenev, *Nucl.Instr.Meth.* **A 424**, (1999).

[HC93] The HERMES Collaboration, Technical design report, DESY report 93-015 (1993).

[HC00] The HERMES Collaboration, A. Airapetian et al, *Phys.Rev.Lett.* **84** (2000).

[JF26] J. Frenkel, *Z.f.Phys* **37**, 243-262 (1926).

[JJ76] J. D. Jackson, *Rev.Mod.Phys.* **48** (3), 417 (1976).

[JJ83] J. D. Jackson, Klassische Eleoktrodynamik, de Gruyter Berlin, New York (1983).

[HG89] H. Goldstein, Klassische Mechanik, 10-th edition, AULA–Verlag Wiesbaden (1989).

[HH96] K. Heinemann and G. H. Hoffstaetter, *Phys.Rev.* **E 54** (4), 4240 (1996) and DESY report 96-078 (1996).

[HM94] C. J. Horowitz and H. O. Meyer, *Phys.Rev.Lett.* **72** (25), 3981 (1994).

[HM96] H. Mais, DESY report 96-119, (1996).

[HN91] J. Hilgert and K.–H, Neeb, Lie–Gruppen und Lie–Algebren, F. Vieweg & Sohn Verlags–GmbH Braunschweig, Wiesbaden (1991).

[HPlb] G. H. Hoffstaetter and M. Vogt, entry in HERA–Logbook $\overline{\underline{XXXX}}$ (19.10.1999 to 09.12.1999) p. 60–62 from 25.10.1999.

[HR87] H. Rose, *Nucl.Instr.Meth.* **A 258** 374-401 (1987).

[HV99] G. H. Hoffstaetter, M. Vogt, and D. P. Barber, *Phys.Rev.* **ST-AB2** 114001 (1999) and DESY report 97-161 (1997).

[HV01] G. H. Hoffstaetter, M. Vogt, The `SPRINT` manual, in preparation.

[HW93a] H. Wiedemann, Particle Accelerator Physics, Basic Principles and Linear Beam Dynamics, Springer Berlin, Heidelberg (1993).

[HW93b] H. Wiedemann, Particle Accelerator Physics, Nonlinear and Higher–Order Beam Dynamics, Springer Berlin, Heidelberg (1995).

[ID96] G. Ingelman, A. De Roeck, R. Klanner (editors), proceedings of the Workshop on Future Physics at HERA, `http://www.desy.de/~heraws96`, DESY (1996)

[KB82] K. L. Brown, *Adv.Part.Phys.* **1**, 71-134 (1968) and SLAC preprint SLAC-75,Rev.4, UC-28 (1982).

[KH96] K. Heinemann, DESY report 96-229 (1996) and `http://xxx.lanl.gov/list/physics/9611/9611001`

[KS88a] K. Steffen, DESY report DESY-88-068 (1988) and *Part.Accel.* **24**, 45 (1988).

[KS88b] K. Steffen, DESY internal report HERA-88-12 (1988).

[KY86] K. Yokoya, DESY report 86-57 (1986).

[KY88] K. Yokoya, SSC CDG report SSC-189 (1988).

[KY92] K. Yokoya, KEK report 92-6 (1992).

[KY99] K. Yokoya, DESY report 99-006 (1999).

[LB96] S. Y. Lee and M. Berglund, *Phys.Rev.* **E 54** (1) (1996).

[LM88] P. Lochak and C. Meunier, Multiphase Averaging for Classical Systems, Springer New York, Berlin, Heidelberg (1988).

[LR94] A. Luccio and T. Roser (editors), Third Workshop on Siberian Snakes and Spin Rotators, BNL formal report BNL-52453 (1994).

[LT27] L. H. Thomas, *Phil.Mag.* **3** (13), 1-20, (1927).

[LT86] S. Y. Lee and S. Tepikian, *Phys.Rev.Lett.* **56** (16), 1635 (1986).

[MB90] M. Berz, *Nucl.Instr.Meth.* **A 298**, 473-479 (1990).

[MB92] M. Berz, in "The Physics of Particle Accelerators", M. Month and M. Dienes (editors), *AIP Conf.Proc.* **249**, AIP New York (1992).

[MB99] M. Bai, PhD Thesis, Indiana University, Bloomington (1999).

[MC55] H. Mendlowitz and K. M. Case, *Phys.Rev.* **97**, 33 (1955).

[MH92] K. R. Meyer and G. R. Hall, Introduction to Hamiltonian Dynamical Systems and the N–Body Problem, Springer NY 1992.

[MR82] H. Mais and G. Ripken, DESY internal report M-82-05 (1982).

[MS70] A. D. Martin and T. D. Spearman, Elementary Particle Theory, North–Holland Publishing Company, Amsterdam (1970).

[MS96a] M. J. Syphers, BNL spin note AGS/RHIC/SN No. 016 (1996).

[MS96b] M. J. Syphers, BNL spin note AGS/RHIC/SN No. 020 (1996).

[NG99] N. Golubeva, in DESY-PROC-1999-03, 130-136 (1999).

[OF84] O. Forster, Analysis 2, Differentialrechnung im $\mathbb{R}^n$ Gewöhnliche Differentialgleichungen, Friedr. Vieweg & Sohn Braunschweig, Wiesbaden (1984).

[pdg94] Particle Data Group, Particle Physics Booklet, LBL or CERN (1994).

[PS96] V. Ptitsin and Yu. M. Shatunov, Proceedings of SPIN96, Amsterdam (1996), World Scientific, Singapore (1997).

[RM93] F. Rathmann, C. Montag, et.al., *Phys.Rev.Lett.* **71** (9), 1379–1382 (1993).

[SL88] S. Y. Lee, in proceedings of SPIN-88, Minneapolis, *AIP Conf.Proc.* **187**, 1105-1153, AIP New York (1988).

[SL97] S. Y. Lee, Spin Dynamics and Snakes in Synchrotrons, World Scientific Singapore, New Jersey, London, Hong Kong (1997).

[SM86a] S. R. Mane, *Phys.Rev. A* **36** (1) part I, 105-119 (1986).

[SM86b] S. R. Mane, *Phys.Rev. A* **36** (1) part II, 120-130 (1986).

[SM88] S. R. Mane, FNAL technical report TM-1515 (1988).

[SM92] S. R. Mane, *Nucl.Instr.Meth.* **A 321**, 21-41 (1992).

[SM93] S. R. Mane, RHIC Note 93-04 (1993).

[SPC96] The Spin Collaboration, University of Michigan report UM-HE-96-20 (1996).

[SPC99] The Spin Collaboration, University of Michigan report UM-HE-99-05 (1999).

[ST64] A. A. Sokolov and I. M. Ternov, *Sov.Phys.Dokl.* **8**, 1203 (1964).

[ST86] S. Tepikian, PhD Thesis, State University of New York at Stony Brook (1986).

[TR94] T. Roser, *Nucl.Instr.Meth.* **A 342**, 343-347 (1994).

[TR99] T. Roser, in the proceedings of the Workshop on Polarized Protons at High Energies, DESY-PROC-1999-03 (1999).

[VA88] V .I. Arnold, Mathematische Methoden der Klassischen Mechanik, VEB Verlag der Wissenschaften (1988).

[VA98] V. A. Anferov, *Phys.Rev.* **ST-AB1** 071001 (1998).

[VA99] V. A. Anferov, in DESY-PROC-1999-03, 144-150 (1999).

[VB98] M. Vogt, D. P. Barber, and G. H. Hoffstaetter, HERA annual report (1998).

[VP94] V. Ptitsin, BNL spin note AGS/RHIC/SN No. 005 (1996).

[VW97] V. Wünsch, Differentialgeometrie, Kurven und Flächen, Teubner Verlagsgesellschaft Stuttgart, Leipzig (1997).

[WF96] W. Fischer, BNL spin note AGS/RHIC/SN No. 017 (1996).

[WB99] P. Wesolowski, K. Balewski, R. Brinkmann, Ya. Derbenev and K. Flöttman, in the proceedings of ECOOL–99, Uppsala (1999).

[WH90] W. Hein, Struktur- und Darstellungstheorie der klassischen Gruppen, Springer New York (1997).

[WR88] F. Willeke and G. Ripken, DESY report DESY 88-114 (1988)

[YD90a] Ya. S. Derbenev, University of Michigan preprint UM HE 90-30 (1990).

[YD90b] Ya. S. Derbenev, University of Michigan preprint UM HE 90-32 (1990).

[YD97] Ya. S. Derbenev, University of Michigan preprint UM HE 97-07 (1997).

[ZL96] C. D. P. Levy, P. Schwandt and A. N. Zelenski, in University of Michigan report UM-HE-96-20 (1996).

[ZL99] C. D. P. Levy and A. N. Zelenski, in University of Michigan report UM-HE-99-05 (1999).

Acknowledgements

This thesis would never been possible without the guidance, collaboration and friendship of many people from DESY and all over the world. In particular I am very much in debt to my teachers Dr. Desmond Barber and Dr. Georg Hoffstätter, who not only introduced me to spin dynamics but in addition contributed so much to my education in the fields of accelerator physics and non–linear dynamics in general. Their deep understanding and ongoing willingness to discuss and help solving problems of every kind enabled me, who started off as a total newcomer in this field, to perform the study presented here. I cannot emphasise enough my gratefulness to them.

I want to thank Prof. G. Kramer and Prof. J. Bartels for making it possible that this study was accepted as the topic of an external PhD thesis.

I owe a lot of thanks to so many people from the DESY M–division who contributed many fruitful discussions on accelerator physics and information on the HERA–p ring. In particular I want to mention Dr. K. Balewski, Dr. D. Barber, Dr. M. Bieler, Dr. F. Brinker, Dr. R. Brinkmann, Dr. E. Gianfelice–Wendt, Dr. G. Hoffstätter, Dr. B. Holzer, Dr. K. Kleffner, Dr. D. Kohaupt, Dr. J. Maidment, Dr. H. Mais, Dr. C. Montag, Dr. I. Reyzl, Dr. J. Rossbach, Dr. T. Sen, Dr. D. Trines, Dr. R. Wanzenberg and Dr. F. Willeke. Moreover I very much appreciated the warm atmosphere at DESY–MPY.

The computer code `SPRINT` which was used for all simulations presented here was developed together with Dr. G. Hoffstätter. I want to thank him again for the very pleasant and professional collaboration. I am grateful to Prof. K. Yokoya who supplied the core routines for the `SODOM-2` algorithm.

I would like to thank Prof. J. Ellison who introduced me to many of the mathematical concepts necessary for this work.

I thank M. Berglund, K. Heinemann and G. Ripken who are also members of the DESY polarisation team and contributed many ideas and fruitful discussions on spin dynamics. I also want to thank Dr. V. Balandin, Prof. Ya. Derbenev and Dr. N. Golubeva who collaborated in this project and who contributed many new ideas and additional simulation data.

During my visit at BNL I not only learned much about the practical issues of accelerating a “real” beam of polarised protons but moreover enjoyed the warm hospitality at BNL, in particular I want to mention Dr. A. Luccio, Dr. M. Syphers and Dr. T. Roser.

I also want to thank the other (ex-) PhD students with whom I shared the office during the years and who not only contributed interesting physics discussions but are also responsible to a great extent for the great time I had at DESY: M. Berglund, Dr. R. Glantz, Dr. C. Montag, Š. Stres and Dr. M.–P. Zorzano.

I thank K. Desler, K. Dietel, Dr. F. Hars, Dr. A. Kabel, C. Kluth, M. Marx and S. Wipf for the many interesting discussions on computational issues.

Last but not least I want to thank my family and friends for their support and and patience. In particular, I am very much in debt to my parents Dr. Helmut Vogt and Renate Stark without whose love, support and understanding I would have never been able to finish this thesis. I want to dedicate this thesis to my parents.

Hamburg, May 18, 2000